

The Handbook of Environmental Chemistry 61
Series Editors: Damià Barceló · Andrey G. Kostianoy

Minghua Zhou
Mehmet A. Oturan
Ignasi Sirés *Editors*

Electro- Fenton Process

New Trends and Scale-Up

 Springer

The Handbook of Environmental Chemistry

Founded by Otto Hutzinger

Editors-in-Chief: Damià Barceló • Andrey G. Kostianoy

Volume 61

Advisory Board:

**Jacob de Boer, Philippe Garrigues, Ji-Dong Gu,
Kevin C. Jones, Thomas P. Knepper, Alice Newton,
Donald L. Sparks**

More information about this series at <http://www.springer.com/series/698>

Electro-Fenton Process

New Trends and Scale-Up

Volume Editors: Minghua Zhou · Mehmet A. Oturan ·
Ignasi Sirés

With contributions by

A.A. Alvarez-Gallegos · M. Bechelany · E. Brillas · M. Cretin ·
A. Hasanzadeh · A.J. Karabelas · A. Khataee · T.X.H. Le · L. Liang ·
H. Lin · L. Ma · E. Mousset · J.L. Nava · P.V. Nidheesh ·
H. Olvera-Vargas · M.A. Oturan · N. Oturan · M. Panizza ·
K.V. Plakas · C. Ponce de León · G. Ren · M.A. Rodrigo ·
O. Scialdone · S. Silva-Martínez · I. Sirés · C. Trelu · Y. Wang ·
J. Wu · W. Yang · F. Yu · H. Zhang · Y. Zhang · L. Zhou ·
M. Zhou · S. Zuo

Editors

Minghua Zhou
College of Environmental Science & Eng.
Nankai University
Tianjin, China

Mehmet A. Oturan
Laboratoire Géomaériaux et Environnement
Université Paris-Est
Champs sur Marne, France

Ignasi Sirés
Departament de Química Física
Universitat de Barcelona
Barcelona, Spain

ISSN 1867-979X ISSN 1616-864X (electronic)
The Handbook of Environmental Chemistry
ISBN 978-981-10-6405-0 ISBN 978-981-10-6406-7 (eBook)
<https://doi.org/10.1007/978-981-10-6406-7>

Library of Congress Control Number: 2017959330

© Springer Nature Singapore Pte Ltd. 2018

This work is subject to copyright. All rights are reserved by the Publisher, whether the whole or part of the material is concerned, specifically the rights of translation, reprinting, reuse of illustrations, recitation, broadcasting, reproduction on microfilms or in any other physical way, and transmission or information storage and retrieval, electronic adaptation, computer software, or by similar or dissimilar methodology now known or hereafter developed.

The use of general descriptive names, registered names, trademarks, service marks, etc. in this publication does not imply, even in the absence of a specific statement, that such names are exempt from the relevant protective laws and regulations and therefore free for general use.

The publisher, the authors and the editors are safe to assume that the advice and information in this book are believed to be true and accurate at the date of publication. Neither the publisher nor the authors or the editors give a warranty, express or implied, with respect to the material contained herein or for any errors or omissions that may have been made. The publisher remains neutral with regard to jurisdictional claims in published maps and institutional affiliations.

Printed on acid-free paper

This Springer imprint is published by Springer Nature
The registered company is Springer Nature Singapore Pte Ltd.
The registered company address is: 152 Beach Road, #21-01/04 Gateway East, Singapore 189721, Singapore

Editors-in-Chief

Prof. Dr. Damià Barceló

Department of Environmental Chemistry
IDAEA-CSIC

C/Jordi Girona 18–26
08034 Barcelona, Spain
and

Catalan Institute for Water Research (ICRA)

H20 Building
Scientific and Technological Park of the
University of Girona

Emili Grahit, 101
17003 Girona, Spain
dbcqam@cid.csic.es

Prof. Dr. Andrey G. Kostianoy

P.P. Shirshov Institute of Oceanology
Russian Academy of Sciences

36, Nakhimovsky Pr.
117997 Moscow, Russia
kostianoy@gmail.com

Advisory Board

Prof. Dr. Jacob de Boer

IVM, Vrije Universiteit Amsterdam, The Netherlands

Prof. Dr. Philippe Garrigues

University of Bordeaux, France

Prof. Dr. Ji-Dong Gu

The University of Hong Kong, China

Prof. Dr. Kevin C. Jones

University of Lancaster, United Kingdom

Prof. Dr. Thomas P. Knepper

University of Applied Science, Fresenius, Idstein, Germany

Prof. Dr. Alice Newton

University of Algarve, Faro, Portugal

Prof. Dr. Donald L. Sparks

Plant and Soil Sciences, University of Delaware, USA

The Handbook of Environmental Chemistry Also Available Electronically

The Handbook of Environmental Chemistry is included in Springer's eBook package *Earth and Environmental Science*. If a library does not opt for the whole package, the book series may be bought on a subscription basis.

For all customers who have a standing order to the print version of *The Handbook of Environmental Chemistry*, we offer free access to the electronic volumes of the Series published in the current year via SpringerLink. If you do not have access, you can still view the table of contents of each volume and the abstract of each article on SpringerLink (www.springerlink.com/content/110354/).

You will find information about the

- Editorial Board
- Aims and Scope
- Instructions for Authors
- Sample Contribution

at springer.com (www.springer.com/series/698).

All figures submitted in color are published in full color in the electronic version on SpringerLink.

Aims and Scope

Since 1980, *The Handbook of Environmental Chemistry* has provided sound and solid knowledge about environmental topics from a chemical perspective. Presenting a wide spectrum of viewpoints and approaches, the series now covers topics such as local and global changes of natural environment and climate; anthropogenic impact on the environment; water, air and soil pollution; remediation and waste characterization; environmental contaminants; biogeochemistry; geoecology; chemical reactions and processes; chemical and biological transformations as well as physical transport of chemicals in the environment; or environmental modeling. A particular focus of the series lies on methodological advances in environmental analytical chemistry.

Series Preface

With remarkable vision, Prof. Otto Hutzinger initiated *The Handbook of Environmental Chemistry* in 1980 and became the founding Editor-in-Chief. At that time, environmental chemistry was an emerging field, aiming at a complete description of the Earth's environment, encompassing the physical, chemical, biological, and geological transformations of chemical substances occurring on a local as well as a global scale. Environmental chemistry was intended to provide an account of the impact of man's activities on the natural environment by describing observed changes.

While a considerable amount of knowledge has been accumulated over the last three decades, as reflected in the more than 70 volumes of *The Handbook of Environmental Chemistry*, there are still many scientific and policy challenges ahead due to the complexity and interdisciplinary nature of the field. The series will therefore continue to provide compilations of current knowledge. Contributions are written by leading experts with practical experience in their fields. *The Handbook of Environmental Chemistry* grows with the increases in our scientific understanding, and provides a valuable source not only for scientists but also for environmental managers and decision-makers. Today, the series covers a broad range of environmental topics from a chemical perspective, including methodological advances in environmental analytical chemistry.

In recent years, there has been a growing tendency to include subject matter of societal relevance in the broad view of environmental chemistry. Topics include life cycle analysis, environmental management, sustainable development, and socio-economic, legal and even political problems, among others. While these topics are of great importance for the development and acceptance of *The Handbook of Environmental Chemistry*, the publisher and Editors-in-Chief have decided to keep the handbook essentially a source of information on "hard sciences" with a particular emphasis on chemistry, but also covering biology, geology, hydrology and engineering as applied to environmental sciences.

The volumes of the series are written at an advanced level, addressing the needs of both researchers and graduate students, as well as of people outside the field of

“pure” chemistry, including those in industry, business, government, research establishments, and public interest groups. It would be very satisfying to see these volumes used as a basis for graduate courses in environmental chemistry. With its high standards of scientific quality and clarity, *The Handbook of Environmental Chemistry* provides a solid basis from which scientists can share their knowledge on the different aspects of environmental problems, presenting a wide spectrum of viewpoints and approaches.

The Handbook of Environmental Chemistry is available both in print and online via www.springerlink.com/content/110354/. Articles are published online as soon as they have been approved for publication. Authors, Volume Editors and Editors-in-Chief are rewarded by the broad acceptance of *The Handbook of Environmental Chemistry* by the scientific community, from whom suggestions for new topics to the Editors-in-Chief are always very welcome.

Damià Barceló
Andrey G. Kostianoy
Editors-in-Chief

Preface

Even though the existence and performance appraisal of Fenton's reaction dates back to almost 150 years, the feasibility of full-scale environmental applications has become nowadays a very hot topic. Among the large variety of existing processes whose reactivity is pre-eminently determined by the metal-catalyzed transformation of a mild oxidizing reagent like H_2O_2 into the second strongest oxidant known ($\cdot\text{OH}$), electro-Fenton (EF) process has become one of the most successful, especially for destroying organic pollutants. The origins of EF can be found in organic electrosynthesis in the 1970s, but soon it was adopted as a promising system in the environmental electrochemistry field. EF combines simplicity with outstanding performance in terms of degradation rate and decontamination percentage, overcoming the major drawbacks of conventional Fenton process such as significant sludge generation and need of continuous H_2O_2 addition.

The main feature of EF, that is to say, the one that allows making the difference between this and other Fenton-based processes for water decontamination and disinfection, is the electrogeneration of H_2O_2 on site from the two-electron reduction of oxygen, thus avoiding the cost and risks associated with production, mobilization, storage, and use of industrially synthesized H_2O_2 . In addition, the continuous regeneration of Fe(II) catalyst from cathodic reduction of Fe(III) ensures a permanent catalytic activity and minimizes sludge management.

This book is dedicated to the EF process, embracing from its first steps to the newest trends and scale-up, in 15 chapters. Despite the lack of a strict division between the various aspects that are presented, the chapters could be considered as grouped into four different parts: the first four chapters list and describe the alternative EF setups, from conventional to the most recent ones; then, there appear three chapters on advances in cathode materials; reactor engineering and modeling are explained in the subsequent four chapters; the book concludes with four chapters that deal with applications in soil and water treatment.

In the first chapter, Profs. Sirés and Brillas make a very thorough description of EF fundamentals and reactivity, including up to 50 reactions to unravel the complexity of such systems. Then, Dr. Olvera-Vargas and coworkers give all details on

a new combined process called bio-electro-Fenton. Prof. Wang focuses on the so-called electro-peroxone technology, which combines cathodic H_2O_2 production with conventional ozonation to upgrade the latter process thanks to $\cdot\text{OH}$ generation. Dr. Nidheesh and coworkers describe the fundamentals of heterogeneous EF process, which relies on the use of insoluble solid catalysts to promote the removal of organic pollutants from water with the possibility to recover the catalyst.

The three chapters devoted to cathode modification for enhancing the H_2O_2 electrogeneration are presented by Profs. A. Khataee and A. Hasanzadeh (use of carbon-based nanomaterials like carbon nanotubes, graphene, and mesoporous carbon), Dr. Le and coworkers (use of carbon felt), and Prof. Zhou and coworkers (use of modified graphite felt and composites with carbon black or graphene). These chapters include characterization of modified materials as well as performance assessment regarding pollutant destruction.

Reactor engineering and modeling is first addressed in the chapter of Profs. Scialdone and Panizza, experts in either microreactors or conventional reactors. The flow-through reactor for EF treatment is described by Prof. Zhou and coworkers, who explain the enhanced mass transport and electron transfer upon use of such configuration. Profs. Nava and Ponce de León introduce in a detailed manner the principles of reactor design and comment on the modeling of a solar photoelectro-Fenton flow plant. To sum up with this part, Profs. Álvarez Gallegos and Silva Martínez focus on the elucidation of a semiempirical chemical model to predict the time course of organic pollutants in EF treatments.

The last chapters contain different applications of EF and related processes. First, Prof. Brillas shows the great performance of solar photoelectro-Fenton process for wastewater treatment. Then, Drs. Plakas and Karabelas summarize the state of the art of pilot, demonstration, and full-scale EF systems, including a patent survey. Dr. Lin and coworkers show the results of EF treatment of artificial sweeteners (aspartame, sucralose, saccharin, and acesulfame) in aqueous medium. And finally, Dr. Mousset and coworkers discuss the feasibility of soil remediation by EF.

We believe that this book, which has been written by world leading experts, constitutes a timely milestone for scientists and engineers alike. It constitutes a platform for addressing the most challenging issues and future prospects of EF process. From the excellent results that have been obtained so far, we aim to foster the gradual scale-up and implementation of this electrochemical technology in the public and private sector. We would like to acknowledge very warmly all the authors, who are kindly involved in this project and committed to clearly explain the pros and cons of EF technology. We are also thankful to Springer for their support in publishing this book.

Nankai, China
Champs-sur-Marne, France
Barcelona, Spain

M. Zhou
M.A. Oturan
I. Sirés

Contents

Electro-Fenton Process: Fundamentals and Reactivity	1
Ignasi Sirés and Enric Brillas	
Bio-electro-Fenton: A New Combined Process – Principles and Applications	29
Hugo Olvera-Vargas, Clément Trelu, Nihal Oturan, and Mehmet A. Oturan	
The Electro-peroxone Technology as a Promising Advanced Oxidation Process for Water and Wastewater Treatment	57
Yujue Wang	
Heterogeneous Electro-Fenton Process: Principles and Applications . . .	85
P.V. Nidheesh, H. Olvera-Vargas, N. Oturan, and M.A. Oturan	
Modified Cathodes with Carbon-Based Nanomaterials for Electro-Fenton Process	111
Alireza Khataee and Aliyeh Hasanzadeh	
Advances in Carbon Felt Material for Electro-Fenton Process	145
Thi Xuan Huong Le, Mikhael Bechelany, and Marc Cretin	
Cathode Modification to Improve Electro-Fenton Performance	175
Minghua Zhou, Lei Zhou, Liang Liang, Fangke Yu, and Weilu Yang	
Conventional Reactors and Microreactors in Electro-Fenton	205
Marco Panizza and Onofrio Scialdone	
Cost-Effective Flow-Through Reactor in Electro-Fenton	241
Minghua Zhou, Gengbo Ren, Liang Ma, Yinqiao Zhang, and Sijin Zuo	
Reactor Design for Advanced Oxidation Processes	263
José L. Nava and Carlos Ponce de León	

Modeling of Electro-Fenton Process	287
A.A. Alvarez-Gallegos and S. Silva-Martínez	
Solar-Assisted Electro-Fenton Systems for Wastewater Treatment . . .	313
Enric Brillas	
Electro-Fenton Applications in the Water Industry	343
Konstantinos V. Plakas and Anastasios J. Karabelas	
The Application of Electro-Fenton Process for the Treatment of Artificial Sweeteners	379
Heng Lin, Nihal Oturan, Jie Wu, Mehmet A. Oturan, and Hui Zhang	
Soil Remediation by Electro-Fenton Process	399
Emmanuel Mousset, Clément Trelleu, Nihal Oturan, Manuel A. Rodrigo, and Mehmet A. Oturan	
Index	425

Electro-Fenton Process: Fundamentals and Reactivity

Ignasi Sirés and Enric Brillas

Abstract This chapter is conceived as the gateway to more specific sections in the book. Its main aim is to introduce all the reactions of interest for fully understanding further development and applications of the EF process. The 50 reactions provided condense all the phenomena occurring in such a complex system and serve as the platform to justify the need of different devices and setups when treating water matrices of very different nature. In addition, all the key operation parameters for H₂O₂ electrogeneration and water decontamination are discussed. Subsections devoted to explaining the effect of the electrolyte composition, cell design, cathode and anode nature, catalyst source, hydrodynamic conditions, solution pH, and operation mode (potentiostatic or galvanostatic) are set out in summarized form, in order to present all the crucial information without intending to duplicate ideas that will be already given in subsequent chapters.

Keywords Catalyst source for electro-Fenton, Cathode and anode nature in electro-Fenton treatment, Electrolytic cells for electro-Fenton, Influence of electrolyte composition on degradation kinetics in electro-Fenton, Operation modes in electro-Fenton, Reactions occurring in electro-Fenton process

Contents

1	Introduction	2
2	Conventional Fenton Process	3
3	Hydrogen Peroxide Electrogeneration	6
	3.1 Cathode Materials	7
	3.2 Divided Cells	8

I. Sirés (✉) and E. Brillas

Laboratori d'Electroquímica dels Materials i del Medi Ambient, Departament de Química Física, Facultat de Química, Universitat de Barcelona, Martí i Franquès 1-11, 08028 Barcelona, Spain

e-mail: i.sires@ub.edu; brillas@ub.edu

M. Zhou et al. (eds.), *Electro-Fenton Process: New Trends and Scale-Up*,
Hdb Env Chem (2018) 61: 1–28, DOI 10.1007/698_2017_40,

© Springer Nature Singapore Pte Ltd. 2017, Published online: 31 May 2017

3.3 Undivided Cells	13
4 Electro-Fenton Process	15
4.1 Cell Configuration	17
4.2 Iron Catalysts	18
4.3 Anode Behavior and Electrolyte Composition	20
4.4 Operation Variables	22
5 Conclusions	25
References	25

1 Introduction

In 1876, the destruction of tartaric acid using a mixture of H_2O_2 and Fe^{2+} signaled the dawn of Fenton process and all the related Fenton's reaction chemistry [1]. Nowadays, after more than a century of thorough investigation, several issues are still subjected to vivid discussion: do the pure aquacomplex models explain in a correct manner the reactivity between iron ions and H_2O_2 [2]? Is hydroxyl radical ($\cdot\text{OH}$) or a high-valent oxoiron (i.e., ferryl) species the main oxidant [3]? Despite these mechanistic controversies, much progress has been gained regarding the optimization, scale-up, and implementation of the classical (i.e., conventional or dark) Fenton process, with multiple existing alternatives born from its combination with physical, (photo)(electro)chemical, and biological treatments. Currently, the Fenton process has an extraordinary impact in many research fields. For example, Fenton-based $\cdot\text{OH}$ can be used to activate methane bond scission to form methanol, being useful for energy storage/conversion [4]. The occurrence of Fenton's reaction is also very relevant in medicine, since free radicals have a negative impact on cells and organs as they trigger the lipid peroxidation [5]. In humans, mitochondria are the main source of H_2O_2 , inducing oxidative damage of macromolecules in the presence of iron and copper ions. Conversely, $\cdot\text{OH}$ can also serve as a therapeutic agent to remove malignant tumors [6]. Fenton's reaction is also useful in the development of new materials such as Zn-doped carbon dots employed as biosensors for detecting H_2O_2 by fluorescence [7]. Nonetheless, the flagship applications are found in environmental chemistry, where the great oxidation power of $\cdot\text{OH}$ (and/or ferryl and other concomitant reactive species) can be used to inactivate microorganisms, degrade organic contaminants, and transform metal ions in water, sludge, or soil [8, 9].

The electro-Fenton (EF) process finds its origins in the 1970s within the field of organic electrosynthesis, when several pioneer studies reported the oxidative transformation of benzene and other molecules with electrogenerated Fenton's reagent [10]. At that time, Hg cathode was the material of choice. Later, in the mid-1970s, carbonaceous cathodes were introduced to overcome the limitations due to the toxicity of Hg. However, their first use in EF systems for wastewater treatment did not appear until the mid-1980s [11]. This work, reporting the degradation of phenol solutions in a Pt/graphite electrolytic cell, fired the starting gun on a vast plethora of

successive applications of EF and combined EF processes, which include (photo) peroxi-coagulation, heterogeneous EF, photoelectro-Fenton with UVA light or sunlight (PEF and SPEF, respectively), sonoelectro-Fenton, and bioelectro-Fenton. Forthcoming chapters of this book focus their attention on some of these upgraded EF systems, which favor process intensification.

The most characteristic feature of all the mentioned Fenton-based electrochemical processes is the in situ electrogeneration of H_2O_2 from the two-electron reduction of O_2 , either sparged into the solution or pumped into a gas diffusion device, at a carbonaceous cathode. Thus, the industrial production, transportation, storage, and handling of synthetic H_2O_2 can be avoided, eventually minimizing the costs and risks. This key feature does not exist in processes like Fered-Fenton, electrochemical peroxidation, or anodic Fenton treatment, where H_2O_2 is added to the solution as a chemical reagent [1]. As a collateral but crucial effect, in EF-based systems that incorporate large surface area cathodes, the simultaneous regeneration of Fe^{2+} can occur continuously, which clearly enhances the performance of the processes because of the longer availability of $\cdot\text{OH}$ in the bulk.

2 Conventional Fenton Process

The Fenton process is based on the use of H_2O_2 and Fe^{2+} , so-called Fenton's reagent, with notorious application to the removal of organic pollutants from water. H_2O_2 is a green chemical since it gives rise to oxygen gas and water as by-products. It is a weak oxidant with $E^\circ(\text{H}_2\text{O}_2/\text{H}_2\text{O}) = 1.763 \text{ V/SHE}$ in acidic solution and $E^\circ(\text{H}_2\text{O}_2/\text{OH}^-) = 0.88 \text{ V/SHE}$ in alkaline medium. H_2O_2 can only attack reduced sulfur compounds, cyanides, and certain organics such as aldehydes, formic acid, and some nitro-organic and sulfo-organic compounds [1]. Its reaction with Fe^{2+} originates the very oxidizing and unstable species hydroxyl radical ($\cdot\text{OH}$) as predominant oxidant, thereby being the Fenton process considered as an advanced oxidation process (AOP). As a result of its short mean lifetime, estimated in the range of few nanoseconds in water, it has to be generated in situ in the reaction medium to nonselectively oxidize organic compounds. It is the second strongest oxidizing agent known, with a standard reduction potential $E^\circ(\cdot\text{OH}/\text{H}_2\text{O}) = 2.8 \text{ V/SHE}$, which allows the overall mineralization of organic and organometallic pollutants, i.e., transformation into CO_2 , water, and inorganic ions.

There are three possible attack modes of $\cdot\text{OH}$ onto organic molecules:

1. Dehydrogenation or abstraction of a hydrogen atom to form water, as occurs for alkanes and alcohols, with absolute rate constants (k_2) in the range $10^7\text{--}10^9 \text{ M}^{-1} \text{ s}^{-1}$
2. Hydroxylation or electrophilic addition to a double bond or aromatic ring, with higher k_2 -values of $10^8\text{--}10^{10} \text{ M}^{-1} \text{ s}^{-1}$ [12]
3. Electron transfer or redox reactions

Table 1 collects the main reactions and their k_2 -values for Fenton's chemistry reported in the literature [1, 13]. The generally accepted mechanism of the Fenton

Table 1 Absolute second-order rate constants for the main reactions involved in a Fenton system at pH ~3

Reaction	k_2 ($M^{-1} s^{-1}$)	Number
<i>Initiation</i>		
$H_2O_2 + Fe^{2+} \rightarrow Fe^{3+} + \cdot OH + OH^-$	55	(1)
<i>Catalysis: Fe^{2+} regeneration</i>		
$H_2O_2 + Fe^{3+} \rightarrow Fe^{2+} + HO_2\cdot + H^+$	3.1×10^{-3}	(2)
$Fe^{3+} + HO_2\cdot \rightarrow Fe^{2+} + O_2 + H^+$	2×10^4	(3)
$Fe^{3+} + O_2^{\cdot-} \rightarrow Fe^{2+} + O_2$	5×10^7	(4)
$Fe^{3+} + O_2^{\cdot-} + 2H_2O \rightarrow Fe^{2+} + 2H_2O_2$	1.0×10^7	(5)
<i>Propagation</i>		
$H_2O_2 + \cdot OH \rightarrow H_2O + HO_2\cdot$	3.3×10^7	(6)
$HO_2\cdot \rightleftharpoons H^+ + O_2^{\cdot-}$	4.8 ^a	(7)
$RH + \cdot OH \rightarrow R\cdot + H_2O$	10^7-10^9	(8)
$Ar + \cdot OH \rightarrow ArOH\cdot$	10^8-10^{10}	(9)
<i>Inhibition/termination</i>		
$Fe^{2+} + \cdot OH \rightarrow Fe^{3+} + OH^-$	4.3×10^8	(10)
$Fe^{2+} + HO_2\cdot + H^+ \rightarrow Fe^{3+} + H_2O_2$	1.2×10^6	(11)
$O_2^{\cdot-} + HO_2\cdot + H^+ \rightarrow H_2O_2 + O_2$	9.7×10^7	(12)
$HO_2\cdot + HO_2\cdot \rightarrow H_2O_2 + O_2$	8.3×10^5	(13)
$HO_2\cdot + \cdot OH \rightarrow H_2O + O_2$	7.1×10^9	(14)
$O_2^{\cdot-} + \cdot OH \rightarrow OH^- + O_2$	1.0×10^{10}	(15)
$O_2^{\cdot-} + \cdot OH + H_2O \rightarrow H_2O_2 + OH^- + \frac{1}{2} O_2$	9.7×10^7	(16)
$\cdot OH + \cdot OH \rightarrow H_2O_2$	5.2×10^9	(17)

^aEquilibrium constant

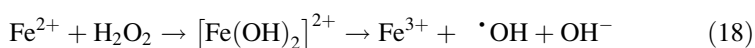
process is initiated by the formation of $\cdot OH$ in accordance with classical Fenton's reaction (1), which has been well proven by means of chemical probes and spectroscopic techniques such as spin-trapping. The Fenton process becomes operative at optimum pH of 2.8–3.0, where Fenton's reaction (1) is propagated by the catalytic behavior of the Fe^{3+}/Fe^{2+} couple with a high number of cycles, up to 2,200 as maximal [14]. It is expected that Fe^{2+} can be slowly regenerated from the so-called Fenton-like reaction (2) between Fe^{3+} and H_2O_2 yielding hydroperoxyl radical ($HO_2\cdot$). This species exhibits such a low oxidation power compared to $\cdot OH$ that, in practice, it is quite unreactive toward organic matter [1]. However, Fe^{2+} can be regenerated more rapidly upon reduction of Fe^{3+} with $HO_2\cdot$ from reaction (3) and/or with superoxide ion ($O_2^{\cdot-}$) from reactions (4) and (5).

The propagation of Fenton's reaction (1) involves the generation of $HO_2\cdot$ by reaction (6) and $O_2^{\cdot-}$ by reaction (7), as well as the attack of $\cdot OH$ to saturated (RH) or aromatic (Ar) organics giving dehydrogenated or hydroxylated derivatives via reaction (8) or (9), respectively. It is noteworthy that reaction (2) and, primarily, reaction (6) play a scavenging role with H_2O_2 destruction, and, hence, they are parasitic reactions competing with Fenton's reaction (1).

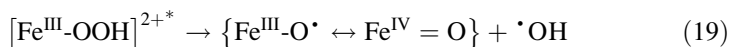
The inhibition reactions (10)–(17) promote the removal of reactive oxygen species (ROS), thus competing with the destruction of organic substrate and

eventually restricting the range of several experimental parameters. The existence of reaction (10), for example, has huge importance since it determines the optimum Fe^{2+} content in the medium in order to minimize the consumption of $\cdot\text{OH}$. It should also be stated that reactions (12)–(17) play a relatively minor role despite their quite high k_2 -values, because of the low concentration of radical ROS in the bulk. This limits their occurrence compared to that of other reactions involving the participation of some non-radical species, like reactions (10) and (11).

It has been described that the rate of Fenton's reaction (1) depends strongly on the presence of inorganic ions like chloride, sulfate, nitrate, carbonate, and hydrogencarbonate [15], which is mainly due to their scavenging role. On the other hand, the experimental tests in favor of the free radical theory are not always satisfactory and convincing, and, in fact, some experimental evidence has been found by means of electron paramagnetic resonance measurements for the presence of hypervalent iron complexes such as ferryl or Fe(IV) ions. From this, Kremer [16] proposed the formation of a mononuclear Fe(IV) oxo complex as follows:



Unlike $\cdot\text{OH}$, the ferryl ion $[\text{Fe}(\text{OH})_2]^{2+}$ is only able to oxidize organic molecules by electron transfer. Several researchers have proposed that both the "classical" (based on hydroxyl radicals) and the "nonclassical" (based on ferryl ion) mechanisms coexist, with predominance of one or another depending on the operation conditions [8, 17]. Pignatello et al. [18] demonstrated the cogeneration of both, $\cdot\text{OH}$ and a high-valent oxoiron complex, by time-resolved laser flash photolysis spectroscopy:



where $[\text{Fe}^{\text{III}}\text{-OOH}]^{2+*}$ denotes an excited state and reaction (19) can be interpreted as an intraligand reaction. These results suggested to the authors that secondary ferryl formation under classical Fenton conditions cannot be ruled out.

The regeneration of Fe^{2+} from Fe^{3+} produced during the Fenton process is a key factor with high impact on the treatment efficiency. An accurate control of experimental variables like pH, temperature, and H_2O_2 and catalyst concentrations is crucial [1]. The catalytic activity of iron species is mainly determined by the solution pH, which is optimal at pH 2.8 since it allows the maximum available Fe^{2+} concentration and, consequently, yields the highest rate of Fenton's reaction (1). Conversely, the use of $\text{pH} < 2$ enhances the formation of the inert protonated form H_3O_2^+ , whereas at $\text{pH} > 5$ Fe(III) species precipitate as $\text{Fe}(\text{OH})_3$, and hence, the quantity of catalyst in solution diminishes and H_2O_2 is split into O_2 and H_2O . The temperature is also a relevant parameter, whose influence needs to be ascertained for each case study. In general, the reaction kinetics is upgraded upon heating, although this accelerates the chemical H_2O_2 decomposition to O_2 and H_2O . As for the concentration of both

Fenton's reagents, it has to be optimized on the basis of the $[\text{Fe}^{2+}]/[\text{H}_2\text{O}_2]$ ratio utilized, instead of treating them independently.

The main advantages of Fenton process for wastewater treatment are [8] (1) simple and flexible operation with easy implementation in industrial plants, (2) easy-to-handle chemicals, and (3) no need for energy input. The following disadvantages have been reported:

1. Relatively high cost and risks related to the storage, transportation, and handling of H_2O_2 .
2. High quantities of chemicals for acidifying effluents to pH 2–4 and for neutralizing treated solutions before disposal.
3. Accumulation of iron sludge that needs to be managed at the end of the treatment.
4. Overall mineralization is not feasible because of the formation of Fe(III) complexes with generated carboxylic acids that cannot be destroyed with $\cdot\text{OH}$.

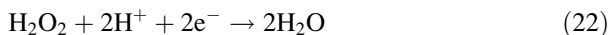
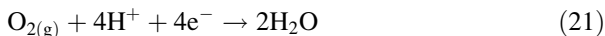
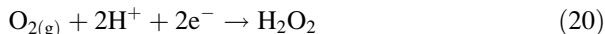
Minimum amounts of H_2O_2 may be utilized if its concentration is optimized, whereas the massive formation iron sludge may be prevented by using heterogeneous catalysis, with solid iron-containing supports like zeolites, alumina, clays, mesoporous molecular sieves, natural oxides, ion-exchange resins, and ion-exchange Nafion membranes that can be easily separated from treated solutions. The intensification of the Fenton process is also feasible by combination or integration with other technologies, as reviewed by Pliego et al. [19]. With this aim, the EF process represents a major milestone in the course of Fenton process development, using the electrochemical technology for its significant upgrade.

3 Hydrogen Peroxide Electrogeneration

The main difference between the EF process and the classical Fenton one is the on-site electrogeneration of H_2O_2 in an electrochemical reactor in EF, which entails a reduction of costs and drawbacks related to its production, transportation, storage, and handling. The pioneer work of Traube in 1882 described the cathodic reduction of dissolved O_2 in aqueous NaOH to generate H_2O_2 [1]. In the mid-1970s, Dow Chemical along with Huron Technologies Inc. developed a system for the reduction of O_2 at a carbon-polytetrafluoroethylene (PTFE) gas diffusion electrode (GDE) using a trickle bed reactor, being employed in the pulp and paper industry. Currently, the leading procedure for industrial H_2O_2 production consists in the catalytic oxidation of anthraquinone, so-called anthraquinone cyclic process, developed by Riedl and Pfeleiderer (BASF) between 1935 and 1945.

In the EF process, H_2O_2 is continuously supplied to an acidic contaminated aqueous solution, typically at pH \sim 3, contained in an electrolytic cell from the two-electron reduction of oxygen gas, directly injected as pure gas or bubbled air, by reaction (20) with $E^\circ = 0.695$ V/SHE. This transformation is easier than its four-electron reduction to water from reaction (21) with $E^\circ = 1.23$ V/SHE [20, 21]. Several

parasitic reactions at the cathode surface slow down its accumulation in solution, preeminently its reduction to water and that of protons to hydrogen gas from reactions (22) and (23), respectively. On the other hand, H_2O_2 disproportionation in the bulk by reaction (24) can also occur to much lesser extent:



The current efficiency for H_2O_2 accumulation, determined from Faraday's law, mainly depends on the cell configuration, which includes the use of divided and undivided cells with two or three electrodes. The cathode material and operation conditions also affect largely the H_2O_2 generation for each setup.

3.1 Cathode Materials

H_2O_2 can be electrosynthesized by dissolving O_2 or air in the solution, thereby being reduced under galvanostatic or potentiostatic conditions at suitable cathode materials, or by directly injecting the gas into GDEs. Smooth carbonaceous electrodes like planar graphite and boron-doped diamond (BDD) thin film produce low amounts of H_2O_2 because of the low solubility of O_2 in water (about 40 or 8 mg L^{-1} upon saturation with pure O_2 or air, respectively, at 1 atm and 25°C). To obtain high rates for reaction (20), 3D carbonaceous electrodes such as carbon felt, activated carbon fiber (ACF), reticulated vitreous carbon (RVC), carbon sponge and carbon nanotubes (NTs), as well as carbon-PTFE GDEs or beds of graphite particles have been used. Note that carbon is a nontoxic material with large overvoltage for H_2 evolution, low catalytic activity for H_2O_2 decomposition and relatively high stability, conductivity, and chemical resistance.

3D electrodes present a high surface/volume ratio and porosity that counteracts the limitations of the low space-time yield and low normalized space velocity that are typically encountered in electrochemical processes with two-dimensional electrodes. Fluidized bed, packed bed, rolling tube, and porous materials can also be used for water treatment. These 3D electrodes possess large specific areas and enhance mass transfer of dissolved O_2 . GDEs have a thin and porous structure allowing the percolation of the injected gas across its pores to contact with the solution at the carbon surface. The large number of active surface sites in GDEs leads to a very fast O_2 reduction with large accumulation of H_2O_2 using high currents. These cathodes commonly incorporate PTFE to bind the carbon particles into a cohesive layer and to give some hydrophobicity to the electrode [1, 21].

A large number of chemically modified cathodes have been prepared for the electrocatalytic enhancement of O_2 reduction with the consequent shift of the reduction potential to more positive values and the acceleration of H_2O_2 formation. For example, the modification of graphite/PTFE with 2-ethylanthraquinone allowed a higher H_2O_2 production. GDEs have been successfully modified with Co and Cu phthalocyanines, metal oxide nanoparticles, and noble metal like Ag, which increases the extent of reaction (21) but enlarges the lifetime of the cathode. The use of NTs has also received attention for H_2O_2 electrogeneration in EF, because of their closed topology, tubular structure, and ability to be functionalized with long-term stability. Chemically modified multiwalled carbon NTs (MWCNTs) with metal oxide and sulfide have been prepared for the same purpose [22, 23].

3.2 Divided Cells

These systems are composed of two solutions called anolyte and catholyte, which are usually separated by a cationic Nafion[®] membrane that only allows the crossing of protons to maintain the electroneutrality of both solutions. In the catholyte, H_2O_2 is generated from O_2 reduction via reaction (20) and the EF process can then be run to destroy organic pollutants. Only the anode is immersed in the anolyte, whereas the catholyte can contain the cathode alone or a reference electrode as well, giving rise to two- and three-electrode cells, respectively. Figure 1a shows a sketch of a typical cylindrical three-electrode cell with two tank reactors as the anodic and cathodic compartments [24], whereas Fig. 1b presents a scheme of a three-electrode flow system operating in batch mode [25]. In contrast, Fig. 1c [26] shows the components of a two-electrode flow cell. In fact, all these systems can operate with two or three electrodes depending on the use or not of a reference electrode. The three-electrode systems tend to operate under potentiostatic conditions by providing a constant potential to the cathode (E_{cath}) against the reference electrode, usually SCE or Ag/AgCl, with a resulting current flow between the anode and cathode. The two-electrode systems work under galvanostatic conditions by directly supplying a constant current (I) or current density (j) to the electrodes.

Table 2 collects selected results for H_2O_2 accumulation in the above systems using different arrangements and electrode materials. As can be seen, high current efficiencies, up to $\sim 100\%$, were obtained in most cases operating up to -1.6 V/SCE or 3 A with 100 cm^2 electrodes under potentiostatic and galvanostatic conditions. An interesting comparative study on the ability of graphite and GDE cathodes to electrogenerate H_2O_2 has been reported by Da Pozzo et al. [24]. They utilized the three-electrode cell of Fig. 1a equipped with a Nafion 324 cationic membrane for the electrolysis of 100 mL of 0.04 M Na_2SO_4 + 0.05 M $NaHSO_4$ as the catholyte. A continuous H_2O_2 accumulation over time was obtained at $E_{\text{cath}} = -0.9$ V/SCE, although with much greater performance, near the ideal behavior, for the O_2 -diffusion cathode compared to graphite. Several electrogeneration trials were made with graphite cathode applying from -0.6 to -1.1 V/SCE, and a maximum

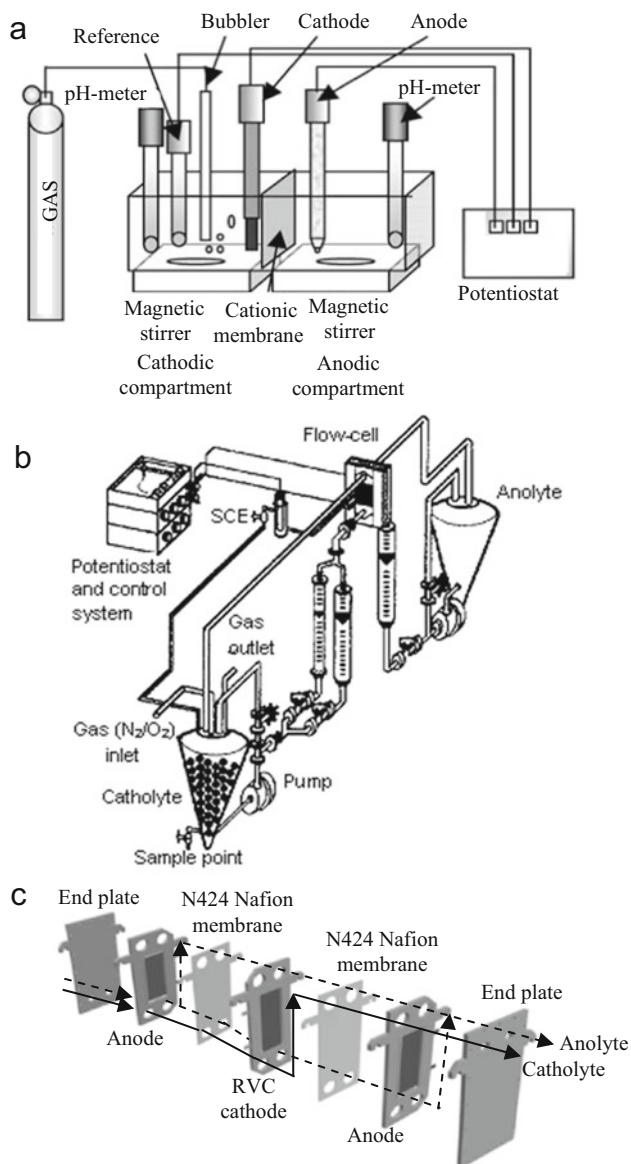


Fig. 1 (a) Scheme of a bench-scale three-electrode divided cell with a Nafion 324 cationic membrane, a 5 cm² Pt anode, a 5 cm² carbon-PTFE GDE or graphite cathode, and a SCE reference electrode. Adapted from [24]. Copyright 2005 Springer Science+Business Media. (b) Experimental setup for H₂O₂ electrogeneration in a flow divided system in batch operation mode. Adapted from [25]. Copyright 1998 Elsevier. (c) Expanded view of a bench-scale divided flow cell in batch operation mode. Two parallel Ti plates coated with (Ta₂O₅)_{0.6}(IrO₂)_{0.4} acted as anodes and a central stainless steel plate coated with RVC on both sides acted as cathode, separated by N424 Nafion membranes, with 150 cm² total area. Adapted from [26]. Copyright 2005 Springer Science+Business Media

Table 2 Selected results for the cathodic generation of H₂O₂ in divided cells

Cell configuration	Operation conditions ^a	[H ₂ O ₂] (mg L ⁻¹)	Efficiency (%) ^b
<i>Three-electrode cell</i>			
Cylindrical tank with cationic membrane, Pt plate anode and 5 cm ² GDE cathode	100 mL of 1 M Na ₂ SO ₄ (catholyte), 25°C; O ₂ supply; E _{cath} = -0.4 to -0.6 V/Ag/AgCl for 5 h	600 ^c	- ^d
Cylindrical tank with cationic membrane, Pt anode and 5 cm ² carbon-PTFE GDE (A) or graphite (B) cathode	100 mL of 0.04 M Na ₂ SO ₄ + 0.05 M NaHSO ₄ (catholyte) at pH 3, room T, and 100 mL of 0.01 M NaClO ₄ (anolyte); O ₂ or air flow rate 130 mL min ⁻¹ ; E _{cath} = -0.9 V/SCE up to 500°C	800 (A) 100 (B)	85 (A) 85 (B)
Cylindrical tank with cationic membrane, Pt anode and 5 cm ² carbon-PTFE GDE cathode	100 mL seawater (catholyte), pH 3 and 100 mL of 0.01 M NaClO ₄ (anolyte); O ₂ flow rate in catholyte 130 mL min ⁻¹ ; E _{cath} = -0.9 V/SCE up to 2,400°C	2,900	70
Flow plant with Nafion 417 cationic membrane, Pt gauze anode (50 × 50 mm) and RVC cathode (50 × 50 × 12 mm)	2.5 L of 1 M NaOH (catholyte) pumped at 0.19 m s ⁻¹ , room T; air saturation; E _{cath} = -0.6 V/SCE (I = 95 mA)	6 ^d	94
Same flow plant equipped with Nafion 450 cationic membrane	2 L of 10 mM HCl + 50 mM NaCl (catholyte) pumped at 0.13 m s ⁻¹ , O ₂ supply; E _{cath} = -0.6 V/SCE up to 6,000°C	0.76–21 ^e	60
Flow plant with two N424 Nafion membranes, two 150 cm ² Ti/(Ta ₂ O ₅) _{0.6} (IrO ₂) _{0.4} anodes and a RVC plate cathode (50 × 150 × 6 mm, gap = 5 mm)	3.5 L of 0.3 M K ₂ SO ₄ (catholyte) pumped at 300 L h ⁻¹ , pH 2.5 or 10, 10°C; O ₂ flow rate 6 L min ⁻¹ ; E _{cath} = -1.6 V/SCE for 300 min	850	65
<i>Two-electrode cell</i>			
H-type reactor with glass frit separator, Pt wire anode and 43 cm ² graphite plate cathode	125 mL (catholyte) and 50 mL (anolyte) of 0.5 M Na ₂ SO ₄ , pH 11, 25°C; O ₂ flow rate in catholyte 5 mL s ⁻¹ ; j = 0.5 mA cm ⁻² up to 200°C	- ^c	92
Cylindrical tank with porous glass diaphragm, Pt wire anode and 6.15 cm ² carbon-PTFE GDE cathode	250 mL (catholyte) and 10 mL (anolyte) of 0.05 M Na ₂ SO ₄ , pH 7, 25°C; air flow rate in catholyte 20 mL s ⁻¹ ; j = 30 mA cm ⁻² for 60 min	8.8 ^d	47
Cylindrical tank with insulating diaphragm, 67 cm ² Ti/RuO ₂ anode and 177 cm ² carbon-felt RVC cathode	5 L of tap water (catholyte) at 20°C; O ₂ or air supply; I = 2,000 mA for 90 min	15	- ^c

(continued)

Table 2 (continued)

Cell configuration	Operation conditions ^a	[H ₂ O ₂] (mg L ⁻¹)	Efficiency (%) ^b
Cylindrical tank with cotton diaphragm, 14 cm ² Ti/IrO ₂ /RuO ₂ anode and carbon-PTFE GDE cathode	100 mL of 0.02 M Na ₂ SO ₄ (catholyte), pH 7; air flow rate in the catholyte 25 mL s ⁻¹ ; $j = 39 \text{ mA cm}^{-2}$ for 100 min	8.3	— ^c
Flow plant with a filter-press cell containing a membrane, 100 cm ² DSA [®] anode and carbon-PTFE GDE cathode	5 L of 0.05 M Na ₂ SO ₄ (catholyte) pumped at 360 L h ⁻¹ , pH 3–13, 25–60°C; O ₂ or air flow rate 30 g h ⁻¹ ; $I = 3,000 \text{ mA}$ for 60 min	1,000	98–100 (at 35 min)

Adapted from [1]. Copyright 2009 ACS Publications

^aApplied current (I), current density (j), and cathodic potential (E_{cat})

^bCurrent efficiency according to Faraday's law

^cConcentration in mM

^dNot reported

^eH₂O₂ generation rate in $\mu\text{mol s}^{-1}$

current efficiency of 85% was found at optimum $E_{\text{cath}} = -0.9 \text{ V/SCE}$. The same efficiency was obtained for the GDE electrode, practically independent of applied charge operating between -0.6 and -0.9 V/SCE . These results demonstrate that GDEs exhibit a higher selectivity for H₂O₂ production, thanks to the direct supply of O₂ to the electrode surface that minimizes the extent of side reactions. In fact, the limited solubility and slow mass transport of O₂ in water impede the production of great concentrations of H₂O₂, whereas the use of GDEs allows overcoming these drawbacks thanks to their porous structure and the coexistence of a triple phase boundary (TPB) [27]. More recently, in 2015, Barazesh et al. [28] also showed the excellent performance of GDEs for H₂O₂ electrogeneration in a three-electrode cell similar to that of Fig. 1a equipped with a DSA[®] anode. Current efficiencies as high as 95% were obtained by these authors by electrolyzing 120 mL of synthetic groundwater, surface water, or urban wastewater with electrodes of 60 cm² area at 3.0 mA cm⁻².

Excellent H₂O₂ electrogeneration has also been obtained using an RVC cathode. Alvarez-Gallegos and Pletcher [25] used it in a three-electrode flow cell in the divided flow system of Fig. 1b to obtain maximum current efficiencies of 56–68% using 10 mM HCl and 10 mM H₂SO₄ (pH ~2) as catholytes at E_{cath} ranging between -0.4 and -0.7 V/SCE , which slightly increased upon addition of NaCl and Na₂SO₄ as background electrolytes, respectively. By adding 1 mM Fe²⁺, a fast disappearance of H₂O₂ due to the action of Fenton's reaction was observed. On the other hand, Badellino et al. [26] utilized a similar flow circuit equipped with the two-electrode cell of Fig. 1c, also with an RVC cathode to electrolyze 3.5 L of 0.3 M K₂SO₄ at pH 10 and liquid flow rate of 300 L h⁻¹. Figure 2a, b highlights that optimum conditions were attained at $E_{\text{cath}} = -1.6 \text{ V/SCE}$ and O₂ flow rate of 6 L min⁻¹ by saturating the solution with 25 mg L⁻¹ of the gas. However, only a 65% current efficiency was obtained because of the large extent of reactions (21), (22), and (24).

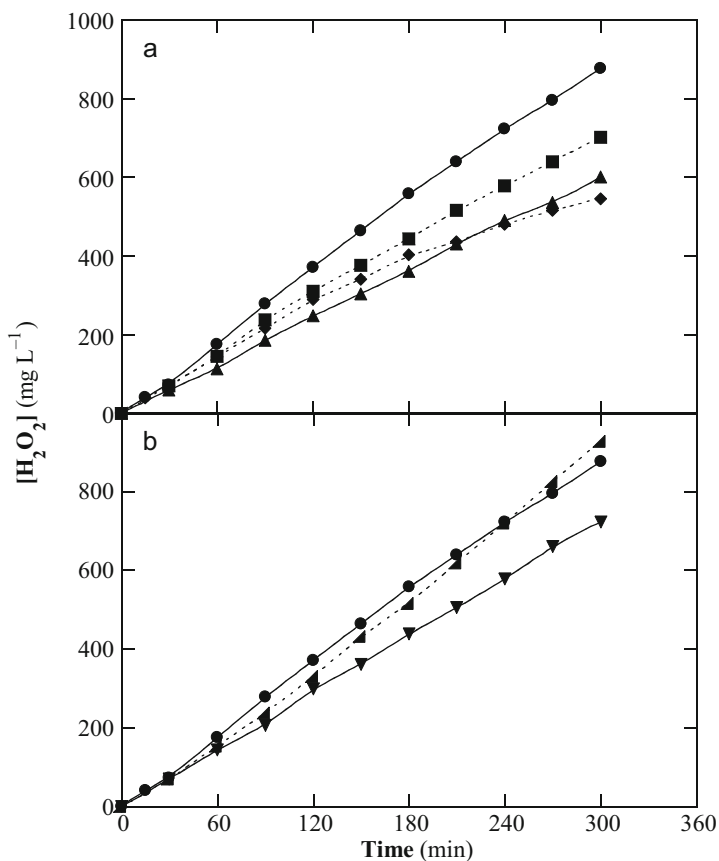
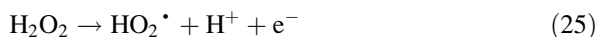


Fig. 2 Accumulated H_2O_2 concentration vs electrolysis time for 3.5 L of 0.3 M K_2SO_4 at pH 10 circulating as catholyte through the cell of Fig. 1c at room temperature. (a) E_{cath} : (triangle) -4 V/SCE, (square) -5 V/SCE, (circle) -6 V/SCE and (diamond) -7 V/SCE, at O_2 flow rate of 6 L min^{-1} (b) $E_{\text{cath}} = -6$ V/SCE at O_2 flow rate of: (inverted triangle) 4 L min^{-1} , (circle) 6 L min^{-1} and (lower right triangle) 8 L min^{-1} . Adapted from [26]. Copyright 2007 Springer Science+Business Media

Similar results were found by electrolyzing the same catholyte at pH 2.5, being rapidly alkalized due to the consumption of protons from reaction (20), thus needing continuous pH regulation. These issues, along with the potential penalty provided by the separator, are inherent drawbacks of divided cells and entail greater costs.

3.3 Undivided Cells

Despite the stable pH solution and lower energy requirements of undivided cells compared with divided ones for H_2O_2 electrogeneration, the former kind of systems is not suitable to obtain large amounts of H_2O_2 since this species is oxidized to O_2 at the anode via HO_2^\bullet as intermediate as follows:



The concomitant anodic oxidation of cathodically generated H_2O_2 in three- and two-electrode undivided cells via reactions (25) and (26) then leads to a remarkably lower steady-state concentration of this compound. Moreover, other weaker oxidants can also be produced at the anode, thus complicating the degradation process of organic pollutants in EF, as will be discussed below.

Figure 3a and 3b show typical bench-scale stirred-tank reactors with GDE [29] and carbon-felt [30] cathodes, respectively, utilized as undivided cells for EF. Figure 4 depicts the experimental setup for a flow plant with a typical filter-press flow cell equipped with a GDE cathode [31]. An example for the profiles for H_2O_2 accumulation in all these systems is given in Fig. 5a and 5b [32], which correspond to the electrolysis of 2.5 L of 0.050 M NaClO_4 at pH 3.0 and 35°C using the flow plant of Fig. 4 with a filter-press cell with 20 cm^2 electrodes at $j = 50 \text{ mA cm}^{-2}$ in the absence and presence of 0.50 mM Fe^{2+} , respectively. As can be seen, the concentration of H_2O_2 always rose with time tending to a quasi-steady value, which is achieved exactly when its generation rate at the air-diffusion cathode from reaction (20) equates its decomposition rate, mainly at the anode surface from reaction (25). The influence of the latter process can be clearly observed in Fig. 5a, where H_2O_2 is destroyed much more rapidly at BDD compared to Pt. In the presence of 0.50 mM Fe^{2+} , Fig. 5b highlights the existence of a much smaller accumulation of H_2O_2 because of its removal via Fenton's reaction. It can also be seen that H_2O_2 destruction at the anode was upgraded in the order: Pt < BDD < DSA[®]-O₂ (IrO₂-based) < DSA[®]-Cl₂ (RuO₂-based). On the other hand, Reis et al. [20] studied the effect of liquid flow rate on H_2O_2 accumulation using a three-electrode undivided flow cell with a DSA[®]-Cl₂ anode and a GDE as cathode fed with O₂ under circulation of 5 L of 0.1 M K₂SO₄ at pH.

Under laminar flow conditions (50 L h^{-1}), H_2O_2 was accumulated up to 414 mg L^{-1} at $E_{\text{cath}} = -2.25 \text{ V/Ag|AgCl}$ for 2 h, whereas under turbulent flow (300 L h^{-1}) this species was more rapidly decomposed at the anode, and a maximal yield of 294 mg L^{-1} was reached at $E_{\text{cath}} = -1.75 \text{ V/Ag|AgCl}$.

Lower H_2O_2 electrogeneration ability has been obtained for other cathodes. For example, Badellino et al. [33] reported a poor current efficiency of 7.8% for H_2O_2 accumulation at 240 min using a cylindrical tank reactor with a Pt anode and a rotating RVC cathode to electrolyze 130 mL of 0.3 M K₂SO₄ solutions at pH 3.5 or 10, 10°C , and $E_{\text{cath}} = -1.6 \text{ V/SCE}$. They also found a drop in H_2O_2 production

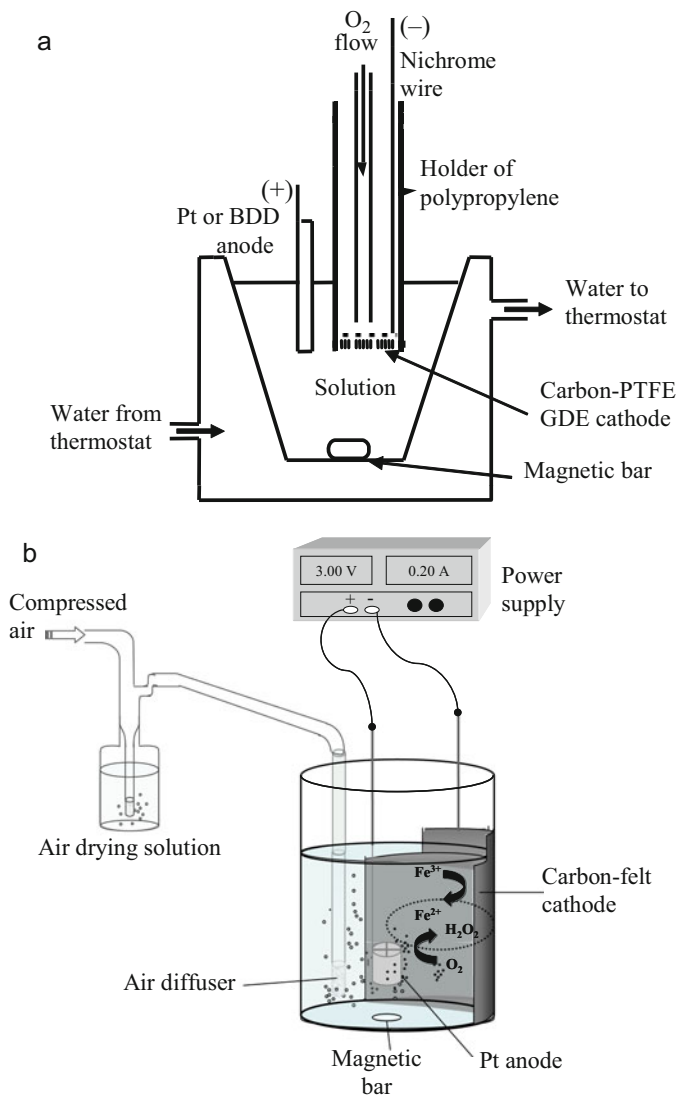


Fig. 3 Schemes of bench-scale open, undivided two-electrode cells. (a) Stirred-tank reactor with a GDE directly fed with pure O₂. Adapted from [29]. Copyright 1995 The Electrochemical Society. (b) Stirred-tank reactor with a carbon-felt cathode and bubbled compressed air. Adapted from [30]. Copyright 2008 Elsevier

with increasing temperature as a result of the lower O₂ solubility in the aqueous solution, without significant pH effect. Wang et al. [34] used a two-electrode tank reactor with 20 cm² Ti/RuO₂ mesh anode to produce 600 or 52 μM of H₂O₂ during the electrolysis of 500 mL of an O₂-saturated 0.05 M Na₂SO₄ solution at pH 3.0 and 0.36 A for 180 min, using a 20 cm² ACF or graphite cathodes, respectively. The

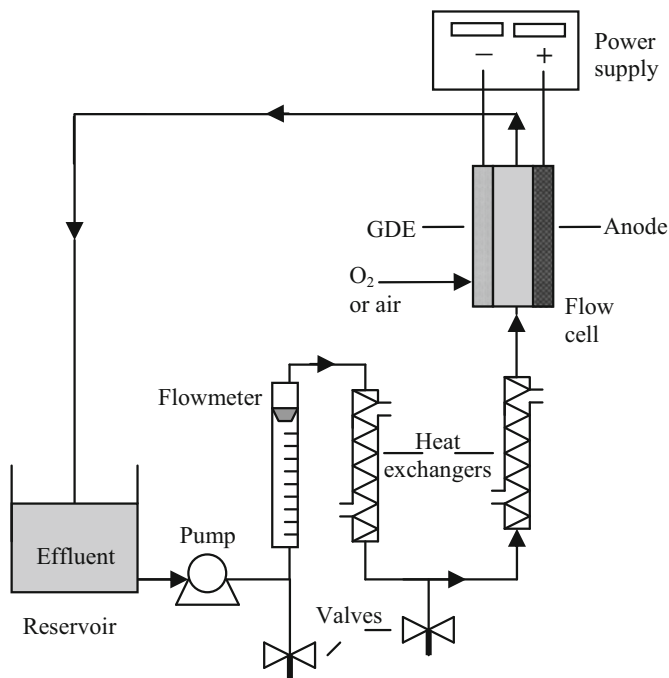


Fig. 4 Experimental setup for a flow plant operating in batch mode and containing a filter-press undivided flow reactor with a GDE cathode. Adapted from [31]. Copyright 2007 Elsevier

superiority of ACF was ascribed to its larger specific area and the great number of mesopores favoring O₂ diffusion. Özcan et al. [35] described that a carbon sponge cathode, with a quite similar structure to ACF, led to the accumulation of nearly three times higher concentration of H₂O₂ than carbon felt. These authors reported that the application of $I > 100$ mA diminished the H₂O₂ accumulation because the reduction of O₂ to H₂O from reaction (21) became preferential.

4 Electro-Fenton Process

The EF process was the first EAOP based on Fenton's reaction chemistry developed to decontaminate toxic and persistent pesticides, organic synthetic dyes, pharmaceuticals and personal care products, and a great deal of industrial pollutants, usually in acidic wastewater. Since Sudoh et al. [11] and the groups of Brillas and Oturan in the mid-1990s described their pioneering works, a large variety of related processes, even coupled or integrated with other techniques to enhance the degradation ability of EF, have been developed and will be extensively detailed in subsequent chapters related to bioelectro-Fenton, heterogeneous EF, and solar photoelectro-Fenton.

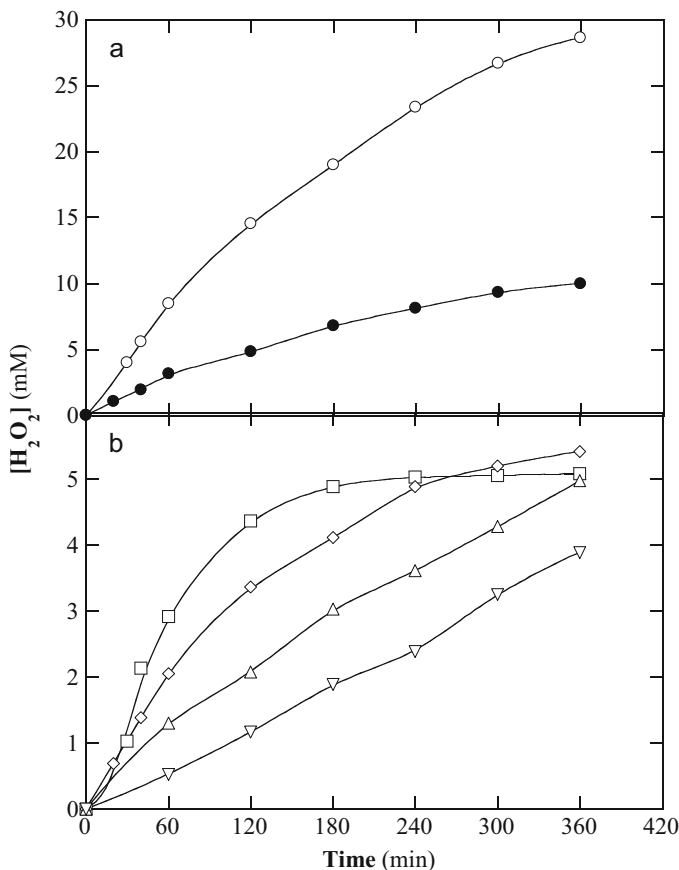


Fig. 5 Change of the accumulated H_2O_2 concentration with electrolysis time for the treatment of 2.5 L of a 0.050 M NaClO_4 solution at pH 3.0 and 35°C using the flow plant of Fig. 4 equipped with a filter-press cell with electrodes of 20 cm^2 at 50 mA cm^{-2} and liquid flow rate of 180 L h^{-1} . A carbon-PTFE air-diffusion cathode was employed. In (a), anode: (open circle) Pt and (filled circle) BDD, in the absence of Fe^{2+} . In (b), 0.50 mM Fe^{2+} was added to the solution using a (square) Pt, (diamond) BDD anode (triangle) IrO_2 -based, and (inverted triangle) RuO_2 -based anode. Adapted from [32]. Copyright 2016 Elsevier

The EF technology is based on the continuous H_2O_2 electrogeneration at a suitable cathode fed with O_2 or air by reaction (20) and the presence or addition of an iron catalyst to generate $\cdot\text{OH}$ in the bulk from Fenton's reaction (1). The major advantages of this indirect electrochemical oxidation method compared to conventional Fenton process are [1]:

1. The on-site production of H_2O_2 , whose concentration and accumulation rate can be simply modulated by adjusting the applied current or potential
2. The control of the degradation kinetics, which allows mechanistic studies

3. The higher degradation rate of organic pollutants because of the continuous regeneration of Fe^{2+} from cathodic Fe^{3+} reduction via reaction (27), with the concomitant minimization of sludge production
4. The feasibility of total mineralization at relatively low cost when operation parameters are optimized, being the costs largely reduced when the electrical supply comes from renewable energy sources



It is noteworthy that the fast regeneration of Fe^{2+} by reaction (27) with $E^{\circ} = 0.77 \text{ V/SHE}$ accelerates the production of $\cdot\text{OH}$ from Fenton's reaction, upgrading the decontamination of organic solutions compared to single conventional Fenton and electrooxidation with electrogenerated H_2O_2 (EO- H_2O_2). Figure 6 highlights the main reactions occurring in the catholyte of a divided cell in EF. This catalytic cycle includes the cathodic H_2O_2 generation, the cathodic Fe^{2+} regeneration, and the attack of $\cdot\text{OH}$ formed from Fenton's reaction onto an unsaturated compound RH and an aromatic pollutant Ar, reaching their conversion into CO_2 [36]. In an undivided cell, the process is much more complex and involves the simultaneous destruction of pollutants with oxidizing species formed at the anode, as will be discussed below.

4.1 Cell Configuration

The EF technology utilizes three- and two-electrode divided and undivided electrolytic cells in which H_2O_2 is continuously electrogenerated at the cathode from reaction (20) using O_2 or air as explained above, usually in batch operation mode. Some examples of divided cells with GDE or RVC cathodes for the EF treatment of organics are shown in Fig. 1. Figure 3a depicts an undivided stirred two-electrode cell, and Fig. 4 presents a recirculation flow plant with an undivided two-electrode filter-press cell, both equipped with a GDE cathode. This setup is commonly employed for research on EF in our group. On the other hand, Fig. 3b shows the typical undivided two-electrode cell with a large surface carbon-felt cathode used in Oturan's group for studies on EF. Anodes such as Pt, BDD, and DSA[®] are the most widely employed in this method. A large number of raw and modified carbonaceous materials are used as cathodes. Detailed information on different electrochemical cells and reactors devised for this technique, as well as the use of modified cathodes with carbon-based materials and other advanced cathodes useful for electro-Fenton, will be described in further chapters of this book.

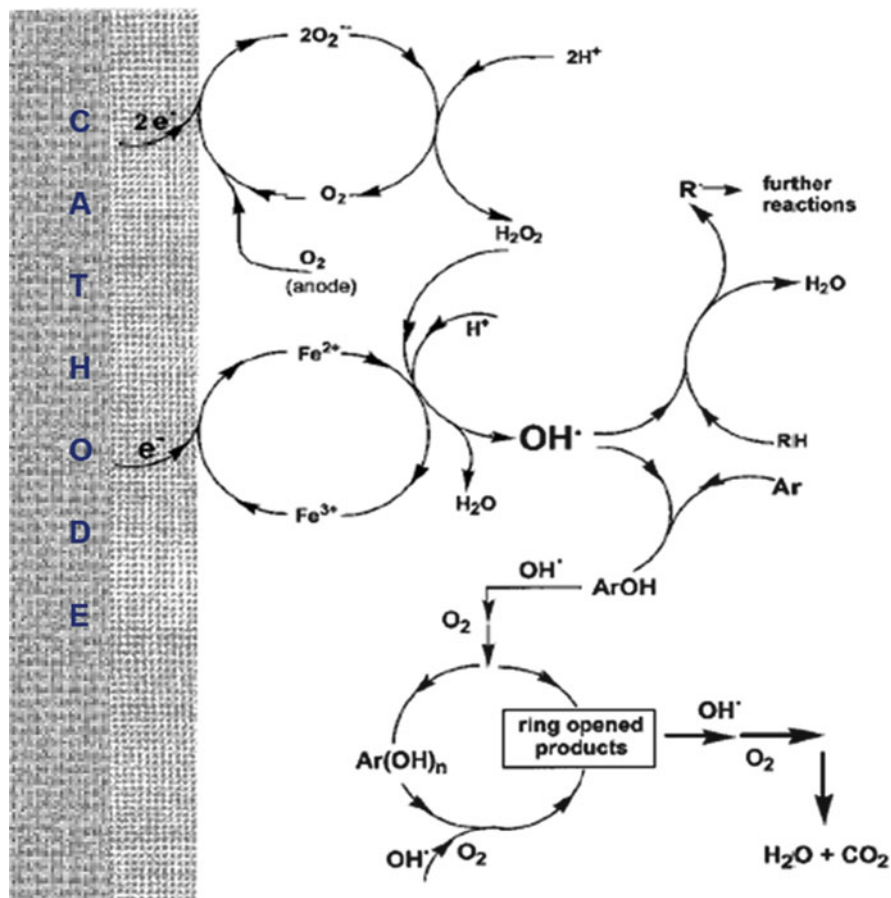


Fig. 6 Schematic representation of the main reactions involved in the EF process of the catholyte of a divided cell. RH is an unsaturated compound that is dehydrogenated, whereas Ar denotes an aromatic pollutant that is hydroxylated. Reproduced with permission from [36]. Copyright 2000 Springer Science+Business Media

4.2 Iron Catalysts

Homogeneous EF involves the catalytic action of the dissolved $\text{Fe}^{3+}/\text{Fe}^{2+}$ couple, considering the possibility of cathodic Fe^{2+} regeneration, as shown in Fig. 6. Qiang et al. [37] claimed the dependence of reaction (27) on factors such as electrode potential and area, pH, temperature, and catalyst content. Using a divided graphite/graphite cell to electrogenerate Fe^{2+} in 0.05 M NaClO_4 solutions at constant potential or constant current density, they found an optimum $E_{\text{cath}} = -0.1$ V/SCE ($j = 43$ mA cm^{-2}) for 500 mg L^{-1} Fe^{3+} in terms of current efficiency, a linear increase of j with initial Fe^{3+} content, and faster Fe^{2+} regeneration at higher cathode surface area and temperature. Regeneration degrees between 75 and 98% were

obtained within the pH range 0–2.5, quickly dropping at greater pH values due to $\text{Fe}(\text{OH})_3$ precipitation. They also observed that Fe^{2+} regeneration was feasible up to $E_{\text{cath}} = -0.8 \text{ V/SCE}$ since higher potentials favored the H_2 evolution from reaction (28) with $E^\circ = -0.83 \text{ V/SHE}$:



The selection of the iron source strongly relies on the cathode nature in homogeneous EF. This was clearly revealed in a work by Sirés et al. [38], where the authors found that, using a GDE cathode in an undivided cell with a BDD or Pt anode, a concentration of 4.0 mM Fe^{3+} in 0.050 M Na_2SO_4 at pH 3.0 was kept practically constant during the electrolysis. This suggests a very rapid transformation of the low quantity of Fe^{2+} , produced at the GDE from reaction (27), into Fe^{3+} by Fenton's reaction. Conversely, a concentration of 0.2 mM Fe^{3+} in the same medium was completely reduced to Fe^{2+} at a 3D carbon-felt cathode, using the same undivided cell with BDD or Pt, with only a slow anodic oxidation of Fe^{2+} to Fe^{3+} as follows:



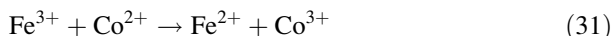
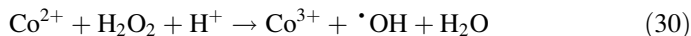
The above findings allow concluding that in systems with a GDE, the use of Fe^{2+} as catalyst is mandatory in order to accelerate the production of $\cdot\text{OH}$ within the early stages of EF, since this ion is gradually removed from the solution. In contrast, either Fe^{3+} or Fe^{2+} ions can be used as iron sources in systems with 3D carbonaceous materials owing to the fast Fe^{2+} regeneration, producing continuously $\cdot\text{OH}$ by reaction with electrogenerated H_2O_2 . Oturan et al. [30] confirmed this behavior when they found that the dye malachite green underwent the same decay using either 0.2 mM Fe^{2+} or 0.2 mM Fe^{3+} as catalyst in an undivided Pt/carbon-felt cell.

The most recent work has been devoted to heterogeneous EF aiming to use natural sources of iron ions, cocatalysts with ability for promoting Fenton-like reaction and modified cathodes that not only electrogenerate H_2O_2 but also yield surface-catalyzed reactions to produce $\cdot\text{OH}$. For example, excellent degradation of organics, even quicker than in homogeneous EF under comparable conditions, has been reported using pyrite [39], alginate gel beads with Mn and Fe [40], and Fe_2O_3 -kaolin [41] as catalysts, which are able to leach iron ions that are subsequently used for Fenton's reaction. Other articles described the good performance of EF systems equipped with cathodes such as composite graphite felt modified with transition metals like Co [42] and hierarchical CoFe-layered double hydroxide modified carbon felt [43]. In the latter case, Acid Orange II was rapidly destroyed at pH 2–7, and this was ascribed to:

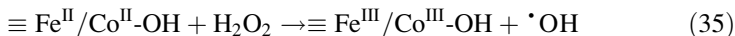
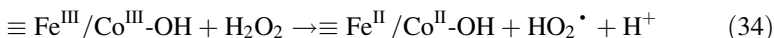
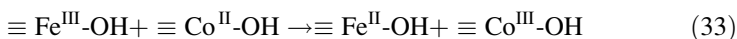
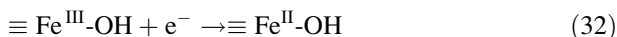
1. The surface-catalyzed reaction occurring at the cathode, which expands the working pH window, avoiding the precipitation of iron sludge as pH increases
2. The enhanced generation of H_2O_2 due to the enhanced electroactive surface area

3. The cocatalyst effect of the Co^{2+} ion that can promote regeneration and additional production of Fe^{2+} and $\cdot\text{OH}$, respectively

This is explained from the Fenton-like reaction (30) with leached Co^{2+} and the reaction of this ion with leached Fe^{3+} according to reaction (31) in the bulk:



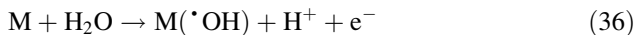
Moreover, at the cathode surface (\equiv), the hydroxylated Fe(III) can be reduced to hydroxylated Fe(II) by reaction (32). Other catalytic reactions involve the heterogeneous formation of hydroxylated Fe(II) and Co(III) from reaction (33), the heterogeneous Fenton-like reaction (34) to produce $\text{HO}_2\cdot$, and reaction (35) generating $\cdot\text{OH}$:



4.3 Anode Behavior and Electrolyte Composition

When an undivided cell is used in EF, organic pollutants are simultaneously destroyed by: (1) oxidants generated at the anode and (2) ROS produced from cathodic reactions, schematized in Fig. 6. The whole process is so-called “paired” or “coupled” electrocatalysis, because of the formation of oxidizing agents from both anode and cathode reactions. The kind and relative proportions of oxidants formed at the anode depend on its nature and the electrolyte composition.

At a large O_2 overvoltage anode, heterogeneous hydroxyl radical ($\text{M}(\cdot\text{OH})$) is produced from water oxidation by reaction (36) regardless of the medium [1, 21]:

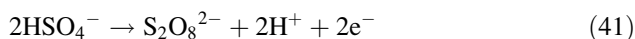
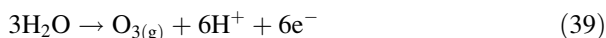
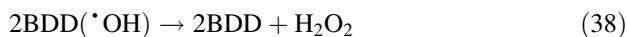


The requirement of a large O_2 overvoltage is needed to minimize the extent of O_2 discharge from reaction (37):

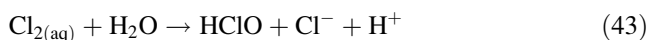


The oxidative action of $\text{M}(\cdot\text{OH})$ is very low for classical active electrodes such as Pt- and IrO_2 -based or RuO_2 -based DSA[®], being much more efficient for BDD

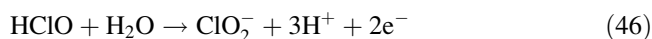
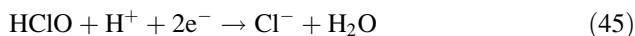
[44]. Operating at high current within the water discharge region, large amounts of reactive BDD($\cdot\text{OH}$) are generated, and these radicals can mineralize to great extent aromatics and carboxylic acids in free-chlorine media [21]. Note that the low adsorption of $\cdot\text{OH}$ on BDD favors its dimerization to H_2O_2 by reaction (38), whereas the high oxidation power of this anode facilitates ozone generation from water oxidation by reaction (39) with $E^\circ = 1.51$ V/SHE. In inert electrolytes such as perchlorate and nitrate, reactions (36)–(39) along with H_2O_2 and Fe^{2+} oxidation via reactions (25) and (27), respectively, predominate at the anode [45]. In contrast, peroxodisulfate ($\text{S}_2\text{O}_8^{2-}$) ion can be obtained from oxidation of SO_4^{2-} and HSO_4^- ions from reactions (40) and (41), respectively, using sulfate medium [1]. It has been proposed that a very strong oxidizing species like $\text{SO}_4^{\cdot-}$ radical with $E^\circ = 2.6$ V/SCE is originated as intermediate of $\text{S}_2\text{O}_8^{2-}$ formation, and then, this radical can attack the organic matter as well:

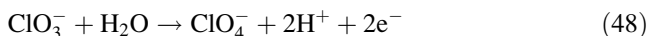
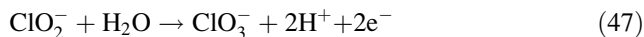


The situation is very different when chlorinated pollutants or chloride-containing medium is employed, since the oxidant Cl_2 is also originated in the bulk from the anodic oxidation of chloride ion by reaction (42). Hydrolysis of this species produces hypochlorous acid (HClO) by reaction (43), which is dissociated to hypochlorite (ClO^-) ion by reaction (44) with $\text{p}K_a = 7.56$ [45, 46]. They act as active chlorine species oxidizing organics. Cl_2 , HClO , and ClO^- predominate at $\text{pH} < 3.0$, $3.0\text{--}8.0$, and > 8.0 , respectively. Consequently, under the best EF conditions of $\text{pH} \sim 3$, organics are preeminently attacked by HClO , which is the most oxidizing active chlorine species:

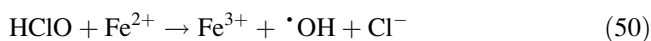
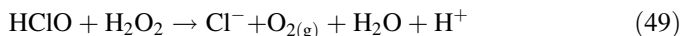


While acting as an oxidant, electrogenerated HClO can be removed by different processes. Cathodic reduction to Cl^- ion via reaction (45) [47] and its consecutive anodic oxidation to ClO_2^- , ClO_3^- and ClO_4^- ions by reactions (46)–(48), respectively, occur regardless of the electrode tested [45, 48]:





Very interestingly, under EF conditions HClO can also attack Fenton's reagent via reactions (49) and (50) [49], causing a loss of treatment efficiency:



A recent work by Thiam et al. [48] reported the degradation of 130 mL of 0.42 mM Ponceau 4R dye in 0.050 M of several electrolytes with 0.50 mM Fe^{2+} by means of EF with a BDD or Pt anode and an air-diffusion cathode. They found much greater decolorization rate using Cl^- ion than ClO_4^- , NO_3^- , and SO_4^{2-} ions, as expected if active chlorine attacks more rapidly the dye than $\text{M}(\cdot\text{OH})$ and $\cdot\text{OH}$. Moreover, the use of BDD instead of Pt accelerated the loss of color, indicating the parallel oxidation of the dye by BDD($\cdot\text{OH}$). For the mineralization of 100 mL of 158 mg L^{-1} methylparaben in 0.025 M Na_2SO_4 + 0.035 M NaCl with 0.50 mM Fe^{2+} at pH 3.0 by EF using different anodes and an air-diffusion cathode, Steter et al. [46] showed the enhancement of total organic carbon (TOC) reduction in the anode sequence: Pt < RuO_2 -based < IrO_2 -based < BDD. Again, the combination of BDD($\cdot\text{OH}$) and active chlorine yielded the best performance regarding organic removal. However, this depends critically on the by-products formed. Figure 7a shows that H_2O_2 is accumulated at similar rate in 2.5 L of either 0.050 M Na_2SO_4 or LiClO_4 at pH 3.0, being much faster than using 0.050 M NaCl , using the flow plant of Fig. 4 with a BDD/air-diffusion cell [45]. The lower H_2O_2 accumulation in NaCl is due to its destruction by reaction (49). In contrast, the attack of active chlorine on 209.3 mg L^{-1} Carmoisine with 0.50 mM Fe^{2+} at pH 3.0 in chloride medium which was much faster than that of BDD($\cdot\text{OH}$) and $\cdot\text{OH}$ in perchlorate and sulfate media, as can be seen in Fig. 7b. As for TOC removal, Fig. 7c depicts a slower mineralization in chloride medium, which can be related to the formation of highly recalcitrant chloroderivatives that are more hardly removed than by-products originated by BDD($\cdot\text{OH}$) and $\cdot\text{OH}$ in perchlorate and sulfate media.

4.4 Operation Variables

The EF degradation of organics in the catholyte of a divided cell involves the attack by ROS, preeminently $\cdot\text{OH}$ formed from Fenton's reaction (1). As explained above, the process becomes much more complicated in an undivided cell using a free-chlorine medium, where organic oxidation can be mainly related to the action of both, $\cdot\text{OH}$ in the bulk and $\text{M}(\cdot\text{OH})$ at the anode surface, along with parallel destruction with weaker oxidizing species such as ROS (HO_2^\cdot , H_2O_2 , O_3), $\text{S}_2\text{O}_8^{2-}$ ion, etc. In

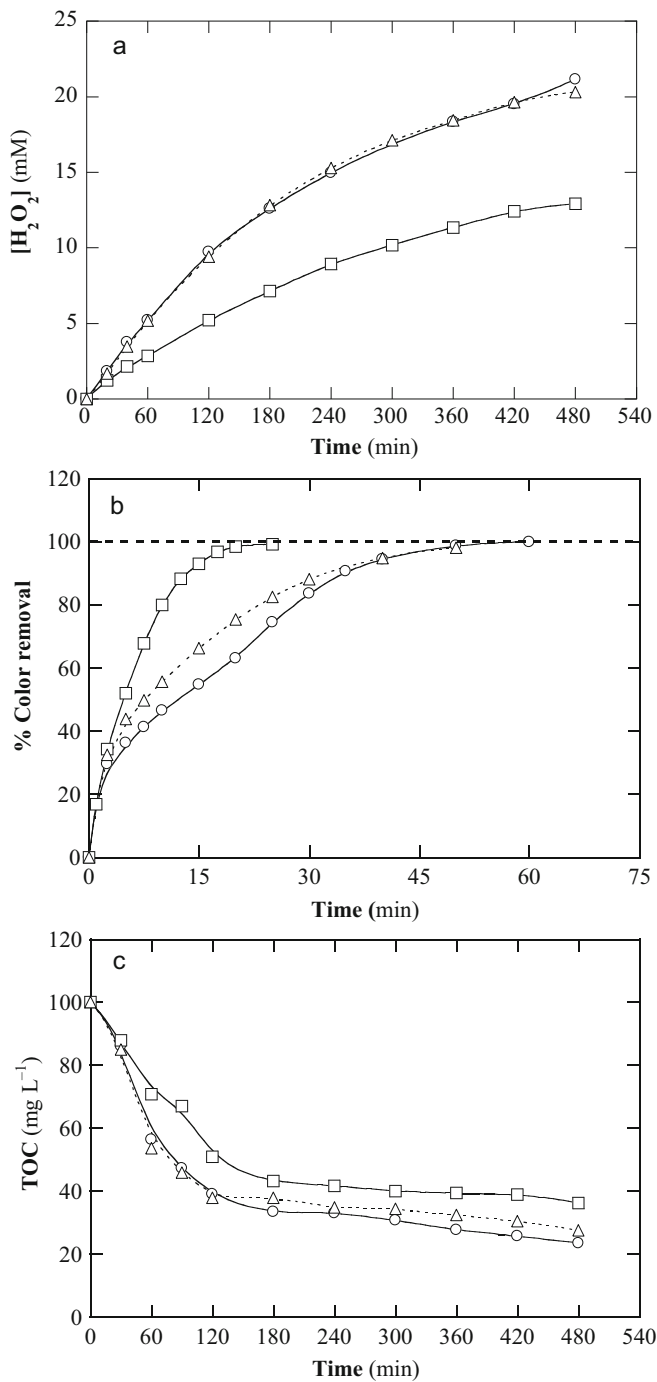


Fig. 7 (a) Time course of H_2O_2 concentration for 2.5 L of solutions with 0.050 M of (circle) Na_2SO_4 , (triangle) LiClO_4 , and (square) NaCl , at pH 3.0 using the flow plant of Fig. 4 with a

chloride medium, the process is even more complex due to the electrogeneration of active chlorine species, other chlorinated ions, and chlorinated by-products. In all cases, the reactivity of the oxidizing species in a given arrangement (i.e., cell configuration, anode, cathode, and electrolyte) is a function of operation variables like temperature, pH, liquid flow rate, j or E_{cath} and catalyst, and pollutant concentrations. The specific assessment of these variables is needed to find the best performance of the process.

Some variables can be easily optimized [1, 21]. Although the EF process is accelerated with raising temperature, values $>35^{\circ}\text{C}$ are not recommended in order to avoid water evaporation that can provoke analytical errors in mineralization measurements. It has been well established that the optimum pH for homogeneous EF is about 3, optimal for Fenton's reaction. Recent efforts in heterogeneous EF allowed the use of catalyst and cathodes that can operate up to neutral or circumneutral pH (see Sect. 4.2), thus expanding the applicability. The stirring rate in tank reactors or the liquid flow rate in recirculation or continuous flow plants is another important variable to ensure the homogenization of solutions and enhance the transport of reactants toward/from the electrodes. The effect of the latter variable on different flow reactors will be discussed in subsequent chapters of this book. The optimum iron catalyst concentration for homogeneous EF is low, usually 0.50 mM Fe^{2+} using GDE as cathode and $0.10\text{--}0.20\text{ mM Fe}^{2+}$ using 3D cathodes like carbon felt. In three-electrode cells, the optimization of E_{cath} is closely related to the maximum production of H_2O_2 , which is assumed to control the degradation process. In contrast, in two-electrode cells, the applied current can be increased up to a maximum value whereupon no higher mineralization is attained. Higher j accelerates slightly the degradation process, but with loss of current efficiency and a strong growth of energy consumption due the larger enhancement of O_2 and/or H_2 evolution and parasitic reactions that cause the destruction of electrogenerated oxidants. Consequently, the optimum j has to be chosen by keeping well balanced the treatment time, the current efficiency, and the energy consumption. Finally, it is well known that the presence of higher organic pollutant concentration upgrades the current efficiency in EF because a relatively greater proportion of oxidants is employed to attack organic molecules instead of being lost in wasting reactions. However, longer times are required to attain a significant mineralization degree, reason for which it is recommended to study the degradation behavior of model pollutants for concentrations $<500\text{ mg L}^{-1}$. Note also that too concentrated solutions have to be avoided because of their highly exothermic degradation, which leads to a poor control of the treatment and safety concerns. This problem becomes crucial for industrial wastewater, where the EF process can

Fig. 7 (continued) BDD/air-diffusion cell at 100 mA cm^{-2} and 35°C . **(b)** Percentage of color removal at 514 nm and **(c)** TOC decay vs electrolysis time during the EF process of 209.3 mg L^{-1} Carmoisine with 0.50 mM Fe^{2+} under the same conditions. Adapted from [45]. Copyright 2015 Elsevier

be very inefficient if they contain very high organic load, thus needing (1) their dilution before electrolysis or (2) sequential treatments that allow a preliminary reduction of the TOC content, as we have recently proposed by combining EF with electrocoagulation [50].

5 Conclusions

EF process and all the methods that have derived from it in recent years are experiencing considerable progress, which can be mainly explained by two reasons:

1. The new awakening of electrochemical technology as a highly versatile, clean and adaptable tool to multiple purposes, from nanoscience to industrial engineering, and
2. The serious concerns related to water scarcity and environmental contamination, which constitutes a major challenge within the framework of an ever-increasing population and a more industrialized society.

EF process is thus a perfect alternative for the electrochemical decontamination of water and soil. A large plethora of devices and setups has appeared since the first application of EF, aiming at both, gradually enhancing the treatment efficiency and offer new solutions to the management of more complex polluted matrices. EF and related technologies can then be considered a hot topic nowadays, as deduced by the important advances that are being reported in all topics of interest: novel modified cathodes with larger selectivity to electrogenerate H_2O_2 and regenerate Fe^{2+} , anodes with higher oxidation power, new reactors with innovative arrangements, and process intensification by combination of EF with other physicochemical and electrochemical technologies. The present is bright for EF, but the future is challenging and further work will be needed.

References

1. Brillas E, Sirés I, Oturan MA (2009) Electro-Fenton process and related electrochemical technologies based on Fenton's reaction chemistry. *Chem Rev* 109:6570–6663
2. Zakharov II, Kudjukov KY, Bondar VV, Tyupalo NF, Minaev BF (2011) DFT-based thermodynamics of Fenton reactions rejects the 'pure' aquacomplex models. *Comput Theoret Chem* 964:94–99
3. Yamamoto N, Koga N, Nagaoka M (2012) Ferryl-oxo species produced from Fenton's reagent via a two-step pathway: minimum free-energy path analysis. *J Phys Chem B* 116:14178–14182
4. Ayodele OB (2016) Structure and reactivity of ZSM-5 supported oxalate ligand functionalized nano-Fe catalyst for low temperature direct methane conversion to methanol. *Energy Conv Manage* 126:537–547
5. Saporito-Magriñá C, Musacco-Sebio R, Acosta JM, Bajicoff S, Paredes-Fleitas P, Boveris A, Repetto MG (2017) Rat liver mitochondrial dysfunction by addition of copper(II) or iron(III) ions. *J Inorg Biochem* 166:5–1

6. Li WP, Su CH, Chang YC, Lin YJ, Yeh CS (2016) Ultrasound-induced reactive oxygen species mediated therapy and imaging using a Fenton reaction activable polymersome. *ACS Nano* 10:2017–2027
7. Xu Q, Liu Y, Su R, Cai L, Li B, Zhang Y, Zhang L, Wang Y, Wang Y, Li N, Gong X, Gu Z, Chen Y, Tan Y, Dong C, Sreepasad TS (2016) Highly fluorescent Zn-doped carbon dots as Fenton reaction-based bio-sensors: an integrative experimental–theoretical consideration. *Nanoscale* 8:17919–17927
8. Pignatello JJ, Oliveros E, MacKay A (2006) Advanced oxidation processes for organic contaminant destruction based on the Fenton reaction and related chemistry. *Environ Sci Technol* 36:1–84
9. Oturan MA, Aaron JJ (2014) Advanced oxidation processes in water/wastewater treatment: principles and applications. A review. *Crit Rev Environ Sci Technol* 44:257–264
10. Tomat R, Vecchi E (1971) Electrocatalytic production of OH radicals and their oxidative addition to benzene. *J Appl Electrochem* 1:185–188
11. Sudoh M, Kodera T, Sakai K, Zhang JQ, Koide K (1986) Oxidative degradation of aqueous phenol effluent with electrogenerated Fenton's reagent. *J Chem Eng Jpn* 19:513–518
12. Buxton GU, Greenstock CL, Helman WP, Ross AB (1988) critical review of rate constants for reactions of hydrated electrons, hydrogen atoms and hydroxyl radicals ($\cdot\text{OH}/\text{O}^-$) in aqueous solution. *J Phys Chem Ref Data* 17:513–886
13. Oturan MA, Oturan N, Aaron JJ (2004) Traitement des micropolluants organiques dans l'eau par des procédés d'oxydation avancée. *Actual Chimique* 277–278:57–63
14. Burns J, Craig P, Shaw T, Ferry A (2010) Multivariate examination of Fe(II)/Fe(III) cycling and consequent hydroxyl radical generation. *Env Sci Technol* 44:7226–7723
15. Bossmann SH, Oliveros E, Göb S, Siegwart S, Dahlen EP, Payawan J, Straub M, Wörner M, Braun AM (1998) New evidence against hydroxyl radicals as reactive intermediates in the thermal and photochemically enhanced Fenton reactions. *J Phys Chem A* 102:5542–5550
16. Kremer ML (1999) Mechanism of the Fenton reaction. Evidence for a new intermediate. *Phys Chem Chem Phys* 1:3595–3605
17. Pang SY, Jiang J, Ma J (2011) Oxidation of sulfoxides and arsenic(III) in corrosion of nanoscale zero valent iron by oxygen: evidence against ferryl ions (Fe(IV)) as active intermediates in Fenton reaction. *Environ Sci Technol* 45:307–312
18. Pignatello JJ, Liu D, Huston P (1999) Evidence for an additional oxidant in the photoassisted Fenton reaction. *Environ Sci Technol* 33:1832–1839
19. Pliego G, Zazo JA, Garcia-Muñoz P, Muñoz M, Casas JA, Rodríguez JJ (2015) Trends in the intensification of Fenton process by wastewater treatment: an overview. *Crit Rev Environ Sci Technol* 45:2611–2692
20. Reis RM, Beati AAGF, Rocha RS, Assumpção MHMT, Santos MC, Bertazzoli R, Lanza MRV (2012) Use of gas diffusion electrode for the in situ generation of hydrogen peroxide in an electrochemical flow-by reactor. *Ind Eng Chem Res* 51:649–654
21. Martínez-Huitle CA, Rodrigo MA, Sirés I, Scialdone O (2015) Single and coupled electrochemical processes and reactors for the abatement of organic water pollutants: a critical review. *Chem Rev* 115:13362–13407
22. Liang Y, Li Y, Wang H, Dai H (2013) Strongly coupled inorganic/nanocarbon hybrid materials for advanced electrocatalysis. *J Amer Chem Soc* 135:2013–2036
23. Faber MS, Dzedzic R, Lukowski MA, Kaiser NS, Ding Q, Jin S (2014) High-performance electrocatalysis using metallic cobalt pyrite (CoS_2) micro- and nanostructures. *J Amer Chem Soc* 136:10053–11006
24. Da Pozzo A, Di Palma L, Merli C, Petrucci E (2005) An experimental comparison of a graphite electrode and a gas diffusion electrode for the cathodic production of hydrogen peroxide. *J Appl Electrochem* 35:413–419
25. Alvarez-Gallegos A, Pletcher D (1998) The removal of low level organics via hydrogen peroxide formed in a reticulated vitreous carbon cathode cell, Part I. The electrosynthesis of hydrogen peroxide in acidic aqueous solutions. *Electrochim Acta* 44:853–886

26. Badellino C, Rodrigues CA, Bertazzoli R (2007) Oxidation of herbicides by in situ synthesized hydrogen peroxide and Fenton's reagent in an electrochemical flow reactor: study of the degradation of 2,4-dichlorophenoxyacetic acid. *J Appl Electrochem* 37:451–459
27. Yu X, Zhou M, Ren G, Ma L (2015) A novel dual gas diffusion electrodes system for efficient hydrogen peroxide generation used in electro-Fenton. *Chem Eng J* 263:92–100
28. Barazesh JM, Hennebel T, Jasper JT, Sedlak DL (2015) Modular advanced oxidation process enabled by cathodic hydrogen peroxide production. *Env Sci Tech* 49:7391–7399
29. Brillas E, Bastida RM, Llosa E, Casado J (1995) Electrochemical destruction of aniline and 4-chloroaniline for waste water treatment using a carbon-PTFE O₂-fed cathode. *J Electrochem Soc* 142:1733–1174
30. Oturan MA, Guivarch E, Oturan N, Sirés I (2008) Oxidation pathways of malachite green by Fe³⁺-catalyzed electro-Fenton process. *Appl Catal B: Environ* 82:244–254
31. Flox C, Garrido JA, Rodríguez RM, Cabot PL, Centellas F, Arias C, Brillas E (2007) Mineralization of herbicide mecoprop by photoelectro-Fenton with UVA and solar light. *Catal Today* 129:29–36
32. Coria G, Sirés I, Brillas E, Nava JL (2016) Influence of the anode material on the degradation of naproxen by Fenton-based electrochemical processes. *Chem Eng J* 304:817–825
33. Badellino C, Rodrigues CA, Bertazzoli R (2006) Oxidation of pesticides by in situ electrogenerated hydrogen peroxide: study for the degradation of 2,4-dichlorophenoxyacetic acid. *J Hazard Mater* 137:856–872
34. Wang A, Qu J, Ru J, Liu H, Ge J (2005) Mineralization of an azo dye Acid Red 14 by electro-Fenton's reagent using an activated carbon fiber cathode. *Dyes Pigments* 65:227–233
35. Özcan A, Şahin Y, Savaş Koparal A, Oturan MA (2008) Carbon sponge as a new cathode material for the electro-Fenton process: comparison with carbon felt cathode and application to degradation of synthetic dye basic blue 3 in aqueous medium. *J Electroanal Chem* 616:71–78
36. Oturan MA (2000) An ecologically effective water treatment technique using electrochemically generated hydroxyl radicals for in situ destruction of organic pollutants: application to herbicide 2,4-D. *J Appl Electrochem* 30:475–482
37. Qiang Z, Chang J-H, Huang C-P (2003) Electrochemical regeneration of Fe²⁺ in Fenton oxidation processes. *Water Res* 37:1308–1319
38. Sirés I, Garrido JA, Rodríguez RM, Brillas E, Oturan N, Oturan MA (2007) Catalytic behavior of the Fe³⁺/Fe²⁺ system in the electro-Fenton degradation of the antimicrobial chlorophene. *Appl Catal B: Environ*. 72:382–394
39. Ammar S, Oturan MA, Labiadh L, Guersalli A, Abdelhedi R, Oturan N, Brillas E (2015) Degradation of tyrosol by a novel electro-Fenton process using pyrite as heterogeneous source of iron catalyst. *Water Res* 74:77–87
40. Iglesias O, Mejjide J, Bocos E, Sanroman MA, Pazos M (2015) New approaches on heterogeneous electro-Fenton treatment of winery wastewater. *Electrochim Acta* 169:134–114
41. Özcan A, Atilir Özcan A, Demirci Y, Sener E (2017) Preparation of Fe₂O₃ modified kaolin and application in heterogeneous electro-catalytic oxidation of enoxacin. *Appl Catal B: Environ* 200:361–337
42. Liang L, Yu F, An Y, Liu M, Zhou M (2017) Preparation of transition metal composite graphite felt cathode for efficient heterogeneous electro-Fenton process. *Environ Sci Pollut Res* 24:1122–1132
43. Ganiyu SO, Le TXH, Bechelany M, Esposito G, van Hullebusch ED, Oturan MA, Cretin M (2017) A hierarchical CoFe-layered double hydroxide modified carbon-felt cathode for heterogeneous electro-Fenton process. *J Mater Chem A* 5:3655–3666
44. Thiam A, Brillas E, Garrido JA, Rodríguez RM, Sirés I (2016) Routes for the electrochemical degradation of the artificial food azo-colour Ponceau 4R by advanced oxidation processes. *Appl Catal B: Environ* 180:227–236
45. Thiam A, Sirés I, Garrido JA, Rodríguez RM, Brillas E (2015) Effect of anions on electrochemical degradation of azo dye Carmoisine (Acid Red 14) using a BDD anode and air-diffusion cathode. *Sep Purif Technol* 140:43–52

46. Steter JR, Brillas E, Sirés I (2016) On the selection of the anode material for the electrochemical removal of methylparaben from different aqueous media. *Electrochim Acta* 222:1464–1474
47. Kodera F, Umeda M, Yamada A (2005) Detection of hypochlorous acid using reduction wave during anodic cyclic voltammetry. *Jpn J Appl Phys* 44:L718–L719
48. Thiam A, Brillas E, Centellas F, Cabot PL, Sirés I (2015) Electrochemical reactivity of Ponceau 4R (food additive E124) in different electrolytes and batch cells. *Electrochim Acta* 173:523–533
49. Aguilar ZA, Brillas E, Salazar M, Nava JL, Sirés I (2017) Evidence of Fenton-like reaction with active chlorine during the electrocatalytic oxidation of Acid Yellow 36 azo dye with Ir-Sn-Sb oxide anode in the presence of iron ion. *Appl Catal B: Environ* 206:44–52
50. Thiam A, Zhou M, Brillas E, Sirés I (2014) Two-step mineralization of Tartrazine solutions: Study of parameters and by-products during the coupling of electrocoagulation with electrochemical advanced oxidation processes. *Appl Catal B: Environ* 150–151:116–125

Bio-electro-Fenton: A New Combined Process – Principles and Applications

Hugo Olvera-Vargas, Clément Trelu, Nihal Oturan,
and Mehmet A. Oturan

Abstract Biological treatments show insufficient removal efficiency in the case of recalcitrant organic compounds. Therefore, the necessity of upgrading wastewater treatment plants (WWTPs) with advanced treatment steps is unequivocal. Advanced oxidation processes (AOPs) are the most effective technologies for the removal of a large range of organic pollutants from water due to the generation of strong oxidizing species like hydroxyl radicals ($\cdot\text{OH}$). However, AOPs often involve high energy and/or reagent consumption and are considered as less cost-effective than biological processes. Hence, the combination of AOPs and biological treatments has been implemented aiming at maximizing efficient removal of recalcitrant organic pollutants while minimizing treatment costs. Among AOPs, electrochemical advanced oxidation processes (EAOPs) have been widely explored during coupled processes, since they possess remarkable advantages, such as high efficiencies, operability at mild conditions, economic feasibility, ease of automation, as well as eco-friendly character. The electro-Fenton process (EF) stands out as one of the most applied EAOPs and the present chapter is devoted to the advances and applications of EF process as a treatment step coupled with biological methods: the so-called bio-electro-Fenton (Bio-EF) process, which brings together the high oxidation power of EF and cost-effectiveness of biological methods.

Keywords Biodegradability, Bio-electro-Fenton, Biological treatment, By-products, Combined process, Electro-Fenton, Hydroxyl radicals, Mineralization, Toxicity, Water treatment

H. Olvera-Vargas, C. Trelu, N. Oturan, and M.A. Oturan (✉)
Laboratoire Géomatériaux et Environnement (LGE), EA 4508, Université Paris-Est, UPEM, 5
bd Descartes, Marne-la-Vallée, Cedex 2 77454, France
e-mail: mehmet.oturan@univ-paris-est.fr

Contents

1	Introduction	30
2	Biological Methods for the Degradation of Organic Emerging Contaminants	31
3	The Coupling of Biological Processes with AOPs	32
	3.1 AOPS as Pre- or Post-treatment for Biological Processes	32
	3.2 Biodegradability Indicators	33
4	The Electro-Fenton Process	34
5	Bio-electro-Fenton Process	36
	5.1 Fundamentals of Bio-EF Process	36
	5.2 Degradation Pathways During the Bio-EF Process	44
	5.3 Experimental Features and Operating Conditions	46
	5.4 Economic Aspects	51
6	Concluding Remarks and Perspectives	52
	References	53

1 Introduction

The worldwide water problem has boosted research in the field of wastewater treatment technologies (WWTT) during last decades since environmentally compatible technological solutions are imperative for providing clean water to the fast-growing population on one hand, and to protect natural water resources on the other.

Traditionally, municipal wastewater treatment plants (WWTP) have been designed for removing different contaminants, which include particles, organic and inorganic compounds, pathogens, and so on. However, they are generally not suitable for the control of the so-called emerging contaminants or micropollutants (pharmaceuticals, pesticides, dyestuff, personal care products, and industrial chemicals), due to their recalcitrance and low biodegradability [1, 2]. The presence of these potentially persistent and harmful substances in different environmental water sources has been extensively documented and they are reported to come from industrial wastewater, agriculture, livestock and aquaculture activity, landfill leachates, as well as domestic and hospital effluents, being the release of contaminated WWTP effluents (especially for pharmaceuticals and personal care products) the main responsible for the discharge of these pollutants in surface water [3]. The noxious effects associated with these contaminants are principally short-term and long-term toxicity, endocrine disrupting effects (even at very low concentration), and antibiotic resistance of microorganisms [4].

In conventional WWTP, wastewater treatment goes through primary, secondary, and sometimes tertiary treatment processes. The aim of primary treatment is the removal of suspended solids by physical methods and it is ineffective in removing dissolved chemicals such as organic micropollutants. Secondary processes comprise mainly biological methods, the most widespread conventional processes. Their cost-effectiveness and well-established operating conditions arise as their most relevant advantages. Biological technologies include activated sludge (AS),

constructed wetland (CW), membrane bioreactor (MBR), sequential batch reactor (SBR), microalgae and fungal bioreactor, trickling filter, nitrification and denitrification, enzyme treatment, and biosorption. Among them, AS and MBR are the most utilized processes for the treatment of refractory contaminants, which are predominately removed via sorption, biodegradation, and/or chemical conversion [5, 6]. Tertiary treatment aims at increasing water quality with defined objectives generally related to public health and environmental purposes. They are normally accompanied by high treatment costs [1].

2 Biological Methods for the Degradation of Organic Emerging Contaminants

When it comes to the degradation of emerging organic contaminants, biological processes present several limitations since these refractory substances are hardly biodegradable due to their toxicity and/or resistance to microbial activities. The main mechanisms through which organic micropollutants are degraded during biological oxidation are: (1) metabolism, in which organics are directly assimilated as a source of carbon through enzymatic reactions for cellular growth and (2) co-metabolism, in which a different substrate is needed as a source of energy to maintain biomass growth, while organic contaminants are degraded by the enzymes or cofactors produced during metabolism of that substrate [7]. Removal efficiencies are governed by physicochemical properties of pollutants under study and the different operating treatment conditions [6]. Several discrepancies exist between the reports on the biological degradation of emerging pollutants and the removal rates are generally low. Luo et al. exhaustively reviewed the fate of some of the most assessed micropollutants in different countries during diverse WWTT, evidencing the large range in the variation of removal efficiencies when applying biological methods. For example, nonsteroidal anti-inflammatory drugs (NSAIDs) like ibuprofen, naproxen, and ketoprofen have moderate to high removal efficiencies (between 52 and 90%), while antibiotics, lipid regulators, and β -blockers present low to moderate degradation rates (between 37 and 73%). The drug carbamazepine and various pesticides have been reported to be highly persistent with insufficient removal rates [4]. Furthermore, removal efficiencies are generally related to the disappearance of starting pollutants, referred only to degradation of parent molecules, while the formation and removal of different intermediates is not taken into consideration, even though numerous studies have stated the generation of toxic by-products as a result of partial degradation [8, 9]. Some other thorough reviews have been focused on the state of the art and perspectives of biological wastewater treatment processes [6, 10, 11].

3 The Coupling of Biological Processes with AOPs

Owing to the limited capability of biological treatments, the application of advanced oxidation processes (AOPs) was implemented for removing persistent organic pollutants from wastewater. AOPs are chemical/photochemical methods based on the production of highly oxidizing species, mainly hydroxyl radicals ($\cdot\text{OH}$), whose oxidizing power ($E^\circ = 2.8 \text{ V/SHE}$) is only overpassed by fluoride (F^-) ion. These technologies comprise conventional Fenton's reagent, ozonation, homogeneous photocatalysis (photo-Fenton), heterogeneous photocatalysis, ferrate oxidation, sonolysis, electrochemical advanced oxidation processes (EAOPs), and diverse combinations of them [1, 2, 12]. They have been applied mainly as pre- or post-treatment of conventional biological methods. When preceding a biological process, the goal is to increase the biodegradability of the treated effluent, whilst removal of refractory micropollutants and their degradation products is the aim of AOPs following biological treatment [13]. In this way, hybrid or integrated processes emerged aiming at enhancing efficiencies of individual techniques by combining their most remarkable features.

3.1 AOPS as Pre- or Post-treatment for Biological Processes

The first steps of oxidation of organic molecules by hydroxyl radicals lead to the formation of degradation by-products that can be more toxic than initial compounds [14] further degradation leads to production of various short-chain carboxylic acids with lower reactivity with $\cdot\text{OH}$ but biodegradable, which provoke an improve of the biodegradability of refractory effluents [13, 15–17]. In this way, AOPs have been used as pre-treatment stages prior to biological treatment with the purpose of producing biodegradable by-products that can be removed in a cost-effective way during the post-biological treatment. The level of biodegradability enhancement depends on the nature of the process, the operating conditions, and the degradation pathways of organic compounds. Most of times, an optimal compromise has to be defined between maximum biodegradability and minimum energy/reagent consumption during the AOP pre-treatment [18]. On the other hand, it is also important to avoid the presence of oxidizing species or catalysts at the end of the pre-treatment, because they might have adverse effects on the biomass. Moreover, depending on the optimal operating conditions of individual AOPs, intermediate steps can also be required between the pre-treatment and the biological treatment, such as pH adjustment (if the applied AOP does not operate at near-neutral pH) or supply of inorganic nutrients necessary for the biomass.

AOPs have also been applied as a post-treatment with the aim of removing refractory organic compounds that could not be removed during the biological process. Thus, AOPs act as a polishing step to achieve higher overall removal

rates [13, 19]. The advantage is that hydroxyl radicals are not wasted for the oxidation of initial easily biodegradable compounds.

Different applications of such combined approaches have been investigated on various industrial effluents and synthetic solutions containing diverse emerging contaminants [2, 13]. The choice of the treatment strategy strongly depends on the nature of the effluent.

3.2 Biodegradability Indicators

When combining AOPs with biological methods, the assessment and monitoring of the biodegradability becomes a crucial parameter. It is performed by measurement of the general parameters: biological oxygen demand after x days (BOD_x), chemical oxygen demand (COD), dissolved organic carbon (DOC), and total organic carbon (TOC), as well as the calculation of the generalized indexes: BOD_5/COD ratio and/or the average oxidation state (AOS). These ratios give an approximation of the proportion of biodegradable substances under aerobic conditions during a determined period of time; 5 days for the BOD_5 , or 28 days for the Zahn-Wellens assays, in which the portion of removed DOC is expressed as the percentage of biodegradation ($Dt(\%)$). In the latter method, biodegradability is considered for biodegradation values above 70%. Quick respirometric measurements based on the amount of oxygen used by bacteria in 20 min-contact are also used for determining the biodegradability. The readily biodegradable fraction of the COD (COD_{rb}) is measured during the tests and the ratio $R = COD_{rb}/COD$ indicates the biodegradability of the sample ($R > 0.1$: biodegradable, $0.1 < R < 0.05$: low biodegradability, and $R < 0.05$: non-biodegradable) [13, 20]. It is important to mention that the nature of the inoculum used for these methods can strongly influence the results. In the case of the AOS, this ratio is related to the mean oxidation state of organic carbon, which ranges from -4 for the most reduced form of carbon (CH_4) to $+4$ for the most oxidized form (CO_2). Positive AOS values evidence the presence of compounds with more oxidized forms of carbon, such as formic acid ($+2$) or oxalic acid ($+3$), which are more biocompatible [21].

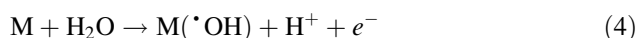
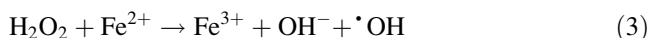
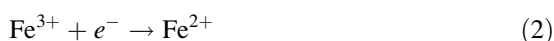
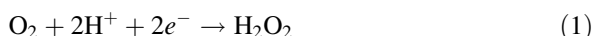
Alternatively, the use of a real biological reactor, which can mimic the operating conditions of a real biological treatment, can be a more reliable method for assessing the feasibility of a biological treatment.

Another crucial aspect when applying AOPs as pre-treatment stage preceding bio-treatment is the evolution of toxicity, as biodegradability is strongly linked with the presence of toxic compounds. A lack of toxicity is hence another important hint of the suitability of the effluents for biological treatment [13]. Among the most utilized methods for ecotoxicological water quality assessment, *in vitro* essays based on the determination of luminescence inhibition of bioluminescent bacteria (such as *Vibrio fischeri* and *Aliivibrio fischeri*) stand out because of their simplicity.

They are good indicators of potential toxicity and are proper starting tools for the analysis of ecotoxicological effects. However, a vast number of approaches for toxicological assessment can be found, and their choice relies on the objectives of the study [5].

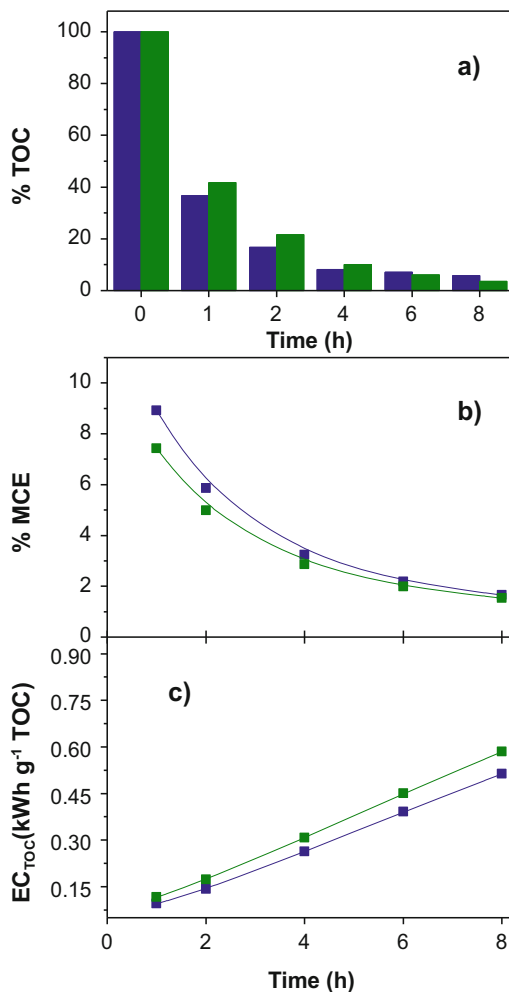
4 The Electro-Fenton Process

The EF process has shown notable advantages among EAOPs and its application for the degradation of persistent/toxic organic contaminants and the remediation of diverse kinds of wastewaters has been exhaustively studied. The process is based on the electrochemical generation of the “Fenton’s reagent”: H_2O_2 by 2-electron reduction of dissolved O_2 (Eq. 1) and Fe^{2+} (catalyst) from 1-electron reduction of externally added Fe^{3+} (Eq. 2) at a “suitable cathode” leading to the continuous formation of $\cdot\text{OH}$ via the Fenton’s reaction (Eq. 3). In this way, organics are efficiently oxidized by the powerful attack of generated $\cdot\text{OH}$, which promote their mineralization to CO_2 , water, and inorganic ions [12, 22, 23]. Furthermore, by using a suitable anode with a high O_2 evolution overpotential (such as boron-doped diamond (BDD), Ti_4O_7 ceramic materials, and PbO_2), additional $\cdot\text{OH}$ can also be produced at the surface of the anode from water discharge (anodic oxidation, AO), Eq. 4, thus enhancing the mineralization rates [24]. The remarkable efficiency and sustainability of the EF process has boosted the development of more effective advanced carbon-based cathode materials [25, 26], as well as catalysts [27, 28] for enhancement of the process. Furthermore, EF has also found a great number of applications in integrated or hybrid systems, in which its outstanding oxidative power is combined with other wastewater treatment technologies during “step-by-step” or “one-step” methodologies [16, 29, 30]. Thorough details on the mechanisms, operating conditions, experimental setups, and advances of the EF process, as well as a wide range of applications, are exhaustively described through the different chapters of the present book.



On the other hand, although the EF process presents numerous advantages when it comes to the degradation of persistent and refractory organic pollutants, there are still some shortcomings that require further development. One of them is related to energetic needs. In fact, the mineralization of organics during electrochemical treatment is generally energy-consuming since the degradation by-products generated throughout the electro-oxidation process tend to be more and more recalcitrant

Fig. 1 Evolution of TOC removal (a), MCE percentage (b) and EC_{TOC} (c) as a function of electrolysis time for the mineralization of 230 mL of 0.1 mM furoseamide (FRSM) (blue filled squares) and ranitidine (RNTD) (green filled squares) aqueous solutions, both in 0.05 M Na_2SO_4 at pH 3.0, room temperature and 500 mA of current, using a BDD/carbon-felt cell with $[Fe^{2+}] = 0.1$ mM. Adapted from [17]



to the oxidative attack of $\cdot OH$, therefore necessitating longer treatment times and increasing electrical energy intake. This fact is illustrated in Fig. 1, from which it can be seen that the specific energy consumption per unit TOC mass (EC_{TOC}) in $kWh (g\ TOC)^{-1}$ importantly rose with increasing the percentage of TOC removal (as a function of treatment time) during the EF treatment of the pharmaceuticals ranitidine and furoseamide, while the mineralization current efficiency (MCE) decreased with treatment time [17]. In this sense, the integration of EF with conventional biological methods results highly beneficial effects, since the application of EF for partial oxidation of refractory organics (to enhance the biodegradability) as pre-treatment step or destruction of recalcitrant pollutants as post-treatment step, considerably reduces EF treatment times and thus operational costs, while mineralization can be completed by means of cheaper biological processes [16].

5 Bio-electro-Fenton Process

5.1 Fundamentals of Bio-EF Process

The first application of a hybrid process between EF and biological treatment can be traced from the work of Lin and Chang, who reported the combination of a sequential “EF – Activated sludge (AS)” process for the treatment of landfill leachate, in which COD removal was significantly enhanced during short-time electrochemical treatment (30 min for 1 L of leachate effluent), while the quality of treated effluent was increased to meet standard parameters for direct discharge or reuse as non-potable water by further application of sequencing batch reactor [31]. The referred “EF” process by the authors was in fact an “electrochemical peroxidation” process, which consisted in electro-coagulation with iron electrodes (total effective area 22.6 cm²) coupled with the Fenton’s reaction by external addition of H₂O₂. However, the bases for the combination of EAOP and biodegradation were established.

As a matter of fact, the increase of biodegradability, which is measured in terms of the BOD₅/COD ratio, is the key factor to be taken into consideration when combining EF with biological degradation. It has been demonstrated that EAOPs, including EF, are capable of rapidly oxidizing refractory organic compounds, generating low-molecular weight products, which can be more easily biodegraded. Accordingly, biodegradability of the treated solutions is risen, attaining BOD₅/COD ratios above the accepted threshold value of 0.4 for applicability of biological treatment [16, 18, 32].

Interestingly, the combined AO-biological approach was successfully explored for the treatment of soil washing (SW) solutions containing phenanthrene and the surfactant Tween 80. The authors reported that the degradation efficiency was enhanced by the synergistic effects of coupling AO (using BDD anode) with aerobic biological treatment (ABT) in both, AO-ABT and ABT-AO sequential processes. Using only ABT, a plateau was rapidly reached and only 44% of COD was removed. In the configuration AO-ABT, AO pre-treatment (3 h at 21 mA cm⁻²) resulted in an increase of biodegradability after which, an overall 80% of COD removal was achieved following 14 days of ABT. It was stated that recalcitrant organics were transformed into biocompatible aliphatic organic acids during AO, which were further metabolized during ABT. The formation of these species along the electrochemical oxidation phase is presented in Fig. 2. Moreover, toxicological tests utilizing bioluminescent *V. fischeri* marine bacteria showed that toxicity was decreased during the AO pre-treatment due to the production of less toxic compounds. For the opposite sequence (ABT-AO), a total 93% of COD removal was obtained when AO was applied as post-treatment (5 h at 500 mA). The efficiency of AO for the degradation of persistent and refractory pollutants from SW solutions into biodegradable compounds was highlighted, while its coupling with a biological method proved to be a cost-effective alternative [18]. In addition, Mousset et al.

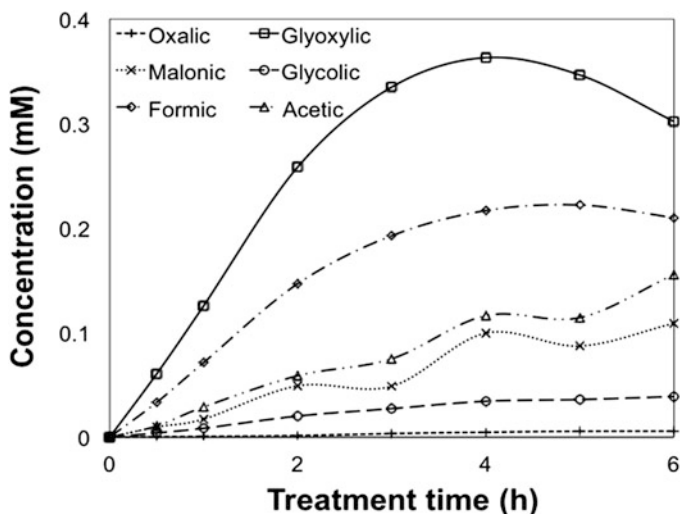


Fig. 2 Time-course of the concentration of the main short-chain carboxylic acids produced during the AO of the soil washing solution ($I = 500$ mA; $[\text{Na}_2\text{SO}_4] = 0.05$ M; $V_T = 330$ mL; BDD anode and stainless steel cathode). Reprinted with permission from [18]. Copyright 2016 Elsevier

also reported the increase of SW solution biodegradability by using EAOPs (AO and EF) [33, 34]. These results are detailed in Mousset et al. [35].

In another study, an increase in the biodegradability index up to 0.39 was reported after the anodic oxidation (AO) of 100 mg L^{-1} tetracycline (TC) solutions using a 3-electrodes divided cell with graphite felt as working electrode during a potential controlled electrolysis, evidencing suitability of the treated sample for biological degradation. AO pre-treatment degraded 97% of TC, but was only able to reach low mineralization rates ($<20\%$) [36]. TC was also used as model contaminant for optimization of the AO process contemplating post-biological treatment. A Pb/PbO₂ anode placed in an undivided cell operating at 13.75 mA cm^{-2} , 40°C , and initial TC concentration of 100 mg L^{-1} was found to rise the BOD₅/COD ratio from an initial value of 0.028–0.41 after 5 h of electrolysis, which permitted further aerobic treatment. The coupled treatment was able to reduce the overall COD by 76% (5 h of AO and 30 days of activated sludge) [37].

Coupling of CW and electrochemical oxidation was also explored. Grafias et al. assessed this hybrid system for the remediation of olive pomace processing leachate. AO with BDD electrodes was applied in two different configurations: post-treatment (CW-AO(BDD)) and pre-treatment (AO(BDD)-CW). In the first case, COD was reduced by 86% in CW (with initial COD of $3,000 \text{ mg L}^{-1}$ and 14.3 mS cm^{-1} of conductivity), while a total of 95% COD removal was achieved after 360 min of post-AO(BDD) treatment. Toxicity assays with *V. fischeri* bacteria revealed absence of hazardousness. Regarding the opposite configuration, only 40% of COD reduction was obtained by AO(BDD) pre-treatment step, and 81% COD removal was the overall result after CW post-treatment. The efficiency drop

of this second configuration was accounted for by the generation of persistent (or toxic) intermediates during the electrochemical phase [38].

As for coupling between EF and biological treatment (Bio-EF), better performance could be expected due to generation of $\cdot\text{OH}$ in the bulk solution in addition to $\text{M}(\cdot\text{OH})$ produced on the anode surface. In this context, EF process was used as pre-treatment step prior to biological treatment (activated sludge) and showed a rise in BOD_5/COD ratio (from 0.14 to 0.45 at 180 min and 0.47 at 300 min of electrolysis, respectively) when treating a pharmaceutical effluent (1 L) containing the antibiotic trimethoprim. Although a total degradation of the drug was obtained after both EF pre-treatment trials, mineralization degree was only 14 and 16% at 180 and 300 min, respectively. After optimization of operational conditions of the EF pre-treatment using synthetic solutions containing trimethoprim, overall 80 and 89% TOC reductions were obtained by the integrated process at the end of 180 and 300 min of EF, respectively, followed by 15 days of AS culture [39].

In a similar way, synthetic solutions of the β -blocker metoprolol (MTPL) were treated by the hybrid Bio-EF process. EF pre-treatment increased the biodegradability index of 0.1 mM MTPL solutions from 0.012 to 0.44 after a short electrolysis time of 1 h using a carbon-felt/BDD cell operating at 300 mA. The evolution of the BOD_5/COD ratio is presented in Fig. 3, from which it can also be seen that the increase of biodegradability was accompanied by a rise of the AOS, another indicator of biocompatibility, which reached a value of 1.0 at 1 h-treatment, evidencing that the remaining organic carbon was present mainly in oxidized forms (biocompatible aliphatic compounds). The initial TOC was reduced by 46% after 1 h EF pre-treatment and it was effectively decreased by 90% following 4 days-incubation under aerobic conditions. Moreover, toxicity tests based on the use of *V. fischeri* bioluminescent bacteria (Microtox[®] test) evidenced that harmful intermediates were formed during the EF treatment, which were also destroyed, as attested by the absence of toxicity after the EF stage [32].

Fig. 3 Evolution of the BOD_5/COD (gray filled squares) ratio and the AOS (-black filled squares-) during the EF-processing of 0.22 L of 0.1 mM of MTPL solution in 0.05 M Na_2SO_4 and 0.1 mM Fe^{2+} at pH 3.0 using an EF-BDD cell at 300 mA and room temperature. Reprinted with permission from [32]. Copyright 2016 Elsevier

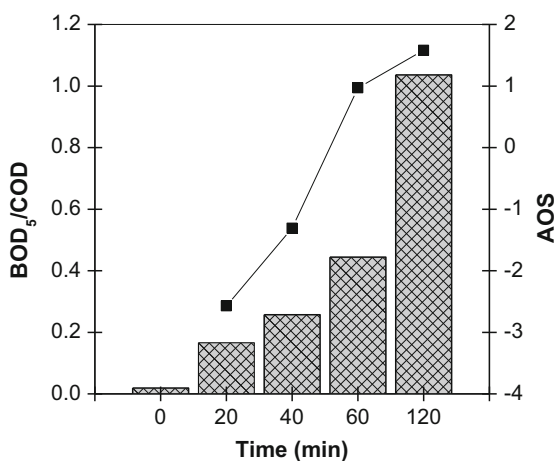


Table 1 Relevant studies on the application of the hybrid Bio-EF process

System setup/reference	Operating conditions		Effluent	BOD ₅ /COD ratio increase	Efficiency		Overall
	EF	Biological process			EF	Biological process	
EF-SBR/SBR-EF [17]	Carbon-felt cathode/BDD anode, 1.4 L in undivided cell 0.2 mM Fe ²⁺ , 500 mA (pre-treatment) and 200 mA (post-treatment), pH 3, 0.05 M Na ₂ SO ₄ 0.5 h – pre-treatment 4 h – post-treatment	Activated sludge from WWTP, sequencing batch reactor (SBR), 1-L sample for post-treatment and 1.5 L sample for pre-treatment 24 h – pre-treatment 48 h – post-treatment	Pharmaceutical wastewater spiked with caffeine and 5-fluorouracil	<0.05–0.33 (in 0.5 h of EF pre-treatment)	Pre-treatment: 60% COD removal Post-treatment: 48% COD removal	Post-treatment: 30% COD removal Pre-treatment: 52% COD removal	90% Total COD removal
EF-AS [39]	Carbon-felt cathode/Pt anode, 1 L-undivided cell 0.69 mM Fe ²⁺ , 466 mA, pH 3, 0.05 M Na ₂ SO ₄ 30 and 60 min electrolysis (synthetic solutions) 180 and 300 min (industrial effluent)	Activated sludge from WWTP 20 days-treatment (for synthetic samples) 15 days-treatment (for industrial)	Synthetic and industrial pharmaceutical wastewater containing trimethoprim (0.2 mM)	For synthetic solution: 0.11–0.32 (in 30 min) 0.11–0.52 (in 50 min) For industrial effluent: 0.4–0.45 (in 180 min) 0.4–0.47 (in 300 min)	Total degradation, 12% and 21% TOC removal at 30 and 60 min, respectively (synthetic sample) 98% degradation, 14 and 18% TOC removal at 180 and 300 min, respectively (industrial effluent)	47 and 59% TOC removal after 30 and 60 min pre-treatment, respectively (synthetic sample) 76% and 87% TOC removal after 180 and 300 min pre-treatment, respectively (industrial effluent)	61 and 80% TOC removal 80 and 89% TOC removal

(continued)

Table 1 (continued)

System setup/ reference	Operating conditions		Effluent	BOD ₅ / COD ratio increase	Efficiency		Overall
	EF	Biological process			EF	Biological process	
AS-Coagulation-SPEF [42]	30 L-flow plant, 20 L conical tank One-compartment-filter-press reactor, GDE-PTFE cathode/Pt anode 200 mA cm ⁻² , 60 mg L ⁻¹ Fe ²⁺ , pH 2.8, 20 °C 147 min-treatment	Activated sludge from WWTP, 12 L-reactor (27 °C), 8 L of raw sample 168 h-treatment	Sanitary landfill leachate	0.07 to 0.2 (at the end of SPEF) Dt (%) = 61% (Zhan-Wellens test)	54.7% (after AS and coagulation)	13–33% DOC removal, total ammonium oxidation, total alkalinity removal	~87.8% (sequence AS-Coagulation-SPEF)
EF-AS [49]	Carbon-felt cathode/Pt anode, 1 L-undivided cell 0.1 mM Fe ²⁺ , 300 mA, pH 3, 0.05 M Na ₂ SO ₄ 2 and 4 h-treatment	Activated sludge from WWTP, 500 mL-reactor at 25 °C, 400 mL of pre-treated solution. 25 days-incubation	Antibiotic tylosin (100 mg L ⁻¹)	0–0.3 (in 2 h) 0–0.5 (in 4 h)	45% TOC removal (at 2 h) 62% TOC removal (at 4 h)	33% (for the 2 h-pre-treated solution) 26% (for the 4 h-pre-treated solution)	78% (for the 2 h-pre-treated solution) 88% (for the 4 h-pre-treated solution)
EF [50]	ACF cathode/ RuO ₂ /Ti anode, 500 mL-undivided cell 1.0 mM Fe ²⁺ , 6.67 mA cm ⁻² , pH 3, 0.05 M Na ₂ SO ₄ 360 min-treatment	–	Antibiotic levofloxacin (200 mg L ⁻¹)	0–0.24 (in 360 min)	Complete removal in 120 min 68% TOC removal (at 360 min)	–	–

EF-AS [41]	Carbon-felt cathode/Pt anode 1 L-undivided cell 0.1 mM Fe ²⁺ , 200 mA, pH 3, 0.05 M Na ₂ SO ₄ , 18 °C 1 h-treatment	Activated sludge from WWTP, 250 mL-reactor at 25 °C, 100 mL of pre-treated solution 13 days-incubation	Antibiotic sulfamethazine (0.36 mM)	0–0.5	80% TOC removal (1 h)	17.3% TOC removal (13 days)	97.3%
EF-AS [51]	Carbon-felt cathode/Pt anode, 1 L-undivided cell 0.5 mM Fe ²⁺ , 500 mA, pH 3, 0.05 M Na ₂ SO ₄ , 18 °C 60 min-treatment	Activated sludge from WWTP, 500 mL-reactor at 25 °C, 200 mL of pre-treated solution 18 days-treatment	Synthetic and industrial pharmaceuticals containing sulfamethazine (0.2 mM)	Synthetic solution: 0.17–0.31 (in 30 min) 0.17–0.51 (in 60 min) Industrial effluent: 0.17–0.32 (in 100 min)	Total degradation in 30 min 2.1% and 18.1% TOC removal at 30 and 60 min, respectively (synthetic sample) Total degradation in 100 min, 7.5% TOC removal at 100 min (industrial effluent)	61.4% TOC removal after 30 min pre-treatment (synthetic sample) 80% TOC removal after 100 min pre-treatment (industrial effluent)	63.5% TOC removal (synthetic sample) 87.4% TOC removal (industrial effluent)
EF [52]	Carbon-felt cathode/RuO ₂ /Ti anode, undivided cell, 500 mL solutions 1 mM Fe ²⁺ , 6.66 mA cm ⁻² , pH 3, 0.05 M Na ₂ SO ₄ 8 h-treatment	–	Cefalexin (200 mg L ⁻¹)	From 0 to: 0.05 (in 2 h) 0.1 (in 4.5 h) 0.26 (in 8 h)	47% TOC removal (at 4.5 h) 72% TOC removal (at 8 h)	–	–

(continued)

Table 1 (continued)

System setup/ reference	Operating conditions		Effluent	BOD ₅ / COD ratio increase	Efficiency		
	EF	Biological process			EF	Biological process	
EC-AS [53]	Fe plate electrodes, undivided cell, 200 mL solutions 8.5 mA cm ⁻² , pH 10, 10 mM H ₂ O ₂ min ⁻¹ 6 min-treatment	Activated sludge from WWTP (acclimatized biomass), bench-scale bioreactor, 150 mL pre-treated sample + 50 mL biomass suspension 16 days-incubation	Formaldehyde (7.5 g L ⁻¹)	–	51% COD removal (at 6 min pre-treatment)	48% COD removal (16 days)	Overall 99% COD removal
EF-Aerobic [32]	Carbon-felt cathode/BDD anode undivided cell, 230 mL solutions 0.1 mM Fe ²⁺ , 300 mA, pH 3, 0.05 M Na ₂ SO ₄ 1 h-treatment	Pure cultures under aerobic conditions, 0.5 L-capacity batch reactor, 200 mL pre-treated sample 4 days-incubation	β-Blocker metoprolol (0.1 mM)	0.02–0.44 (in 1 h-pre-treatment)	47% TOC removal (at 1 h-pre-treatment)	43% TOC removal (at 4 days-treatment)	90% TOC removal
Anaerobic-SPEF [54]	GDE-PTFE cathode/BDD anode undivided cell, 100 mL pre-treated solutions 1 mM Fe ²⁺ , 30 mA cm ⁻² , pH 3, 0.05 M Na ₂ SO ₄ , 35 °C 180 min-treatment	Anaerobic digestion sludge, 500 mL-capacity reactor, 320 mL sample + 80 mL sludge, 35 °C 30 days-incubation	Slaughterhouse wastewater	–	95% COD removal of the initial COD after pre-treatment (7% COD removal of the raw sample)	90% COD removal (at 30 days-treatment)	97% COD removal

EF-Aerobic [17]	Carbon-felt cathode/BDD anode undivided cell, 230 mL solutions 0.1 mM Fe^{2+} , 500 mA, pH 3, 0.05 M Na_2SO_4 1 h-treatment	Pure cultures under aerobic conditions, 0.5 L-capacity batch reactor, 200 mL pre-treated sample 7 days-incubation	Pharmaceuticals furosemide and ranitidine (0.1 mM, separate solutions)	0.03–0.41 (in 1 h-treatment of furosemide) 0.06–0.37 (in 1 h-treatment of ranitidine)	64% TOC removal (at 1 h-treatment of furosemide) 59% TOC removal (at 1 h-treatment of ranitidine)	29% TOC removal (for furosemide solution) 35% TOC removal (for ranitidine solution)	93% TOC removal (for furosemide solution) 94% TOC removal (for ranitidine solution)
--------------------	--	---	--	---	---	---	---

Bio-EF process was also applied for the treatment of pharmaceutical wastewater spiked with the drugs caffeine and 5-fluorouracil. Two sequential systems were investigated: EF as pre- or post-treatment coupled with a biological process (sequencing batch reactor, SBR); EF-SBR and SBR-EF, respectively (referred to Table 1 for the experimental details). For the first configuration, EF was capable of completely removing both drugs in 2 h using 200 mA, while only 60% of COD removal was achieved (1.4 L was the volume treated). The post-SBR treatment removed 30% more of COD in 2 days-incubation, giving an overall 90% of COD removal. It was found that higher EF pre-treatment times at lower current values resulted in higher biodegradability increase, thus highlighting that operating conditions must be optimized for achieving the best compromise in terms of efficiency, biodegradability enhancement, and minimal energy consumption. Regarding the SBR-EF sequence, caffeine and COD were only degraded by 43% and 52%, respectively, after 24 h-treatment using acclimated biomass, while 5-fluorouracil was almost totally removed. Subsequent application of EF (applying 500 mA of current) yielded total degradation of caffeine and COD at 30 min and 4 h, respectively [40].

Form the above mentioned, it can be seen that starting target pollutants are quickly degraded during the first stages of electrochemical treatment, and even if the mineralization rates are generally low, an increase in the biodegradability of the treated influent is highly relevant since the biodegradable by-products formed in the EF pre-treatment can be eliminated by microbial cultures during biological processes. Indeed, it is desirable to have a moderate mineralization rate, since a good fraction of organic matter is needed for sustaining the energy needs of microorganisms during biological treatment.

5.2 Degradation Pathways During the Bio-EF Process

As mentioned in the previous sections, the main goal of combining EF with biological methods is the destruction of refractory contaminants by $\cdot\text{OH}$ produced during the electrochemical process, either in a pre-treatment or a post-treatment stage. When EF precedes biological oxidation, organic pollutants are transformed into smaller molecules as a result of the oxidative attack of $\cdot\text{OH}$. These low-molecular weight species can be then metabolized by the microbial cultures during biological degradation. On the other hand, when EF is applied after biologic oxidation, initial biodegradable organic compounds are bio-transformed by the microbial consortia and the resulting refractory by-products (as well as those refractory pollutants initially present) can be oxidized during post-electrochemical process. These two strategies are depicted in Fig. 4, showing the sequence of the Bio-EF units according to the characteristics of the target effluent.

The oxidation of organics with $\cdot\text{OH}$ occurs through well-known pathways, principally H atom abstraction (mainly from aliphatics) and addition to C = C bonds (mainly with aromatics leading to the formation of hydroxylated aromatic derivatives) [12, 40]. In the latter case, consecutive oxidation reactions lead to ring

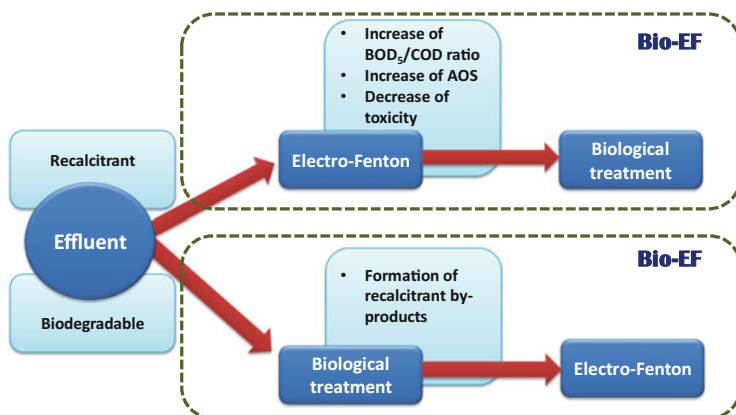


Fig. 4 Schematic representation of the sequence followed by the single units during the Bio-EF integrated system according to the characteristics of the target effluent

cleavage and generation of aliphatic organic acids (short-chain carboxylic acids), which are the final intermediates before complete mineralization into CO_2 , water, and inorganic ions [22]. More detailed discussion of these mechanisms can be found in the previous chapters. As explained in Sect. 2, during biological oxidation, biodegradation of organics occurs by metabolic and co-metabolic routes [7].

In this context, degradation of the β -blocker metoprolol was assessed during the integrated Bio-EF treatment and was reported to follow the pathway presented in Fig. 5. The drug was firstly electro-oxidized during the EF pre-treatment using a carbon-felt/BDD electrolytic cell, forming various aromatic/cycle and aliphatic intermediates, whose progressive oxidation ultimately led to short-chain carboxylic acids (mainly oxalic, oxamic, maleic, malonic, formic, and acetic acid). At this stage of partial electrochemical oxidation (1 h-electrolysis), where most of the remaining TOC pertained to these carboxylic acids (initial TOC was reduced by 47%), the EF process was stopped in order to complete the mineralization process by biological means using different environmental bacterial cultures under aerobic conditions without any previous conditioning step. It was found that the microorganisms were able to mineralize the short-chain organic acids, which was reflected in the 43% removal of the initial TOC content [32]. Thus, the combined process was able to reach almost overall mineralization (>90%) of the initial refractory solution. In a different work, the final short-chain carboxylic acids produced by the EF oxidation of the pharmaceuticals ranitidine and furosemide were incubated under aerobic conditions with biomass composed by different cultures of environmental microorganisms. The concentration of the organic acids was monitored during the biological oxidation and the results pointed out that these species were indeed assimilated by the bacterial consortia, thus highlighting the capacity of biological methods to degrade the intermediates generated during electrochemical advanced oxidation [17].

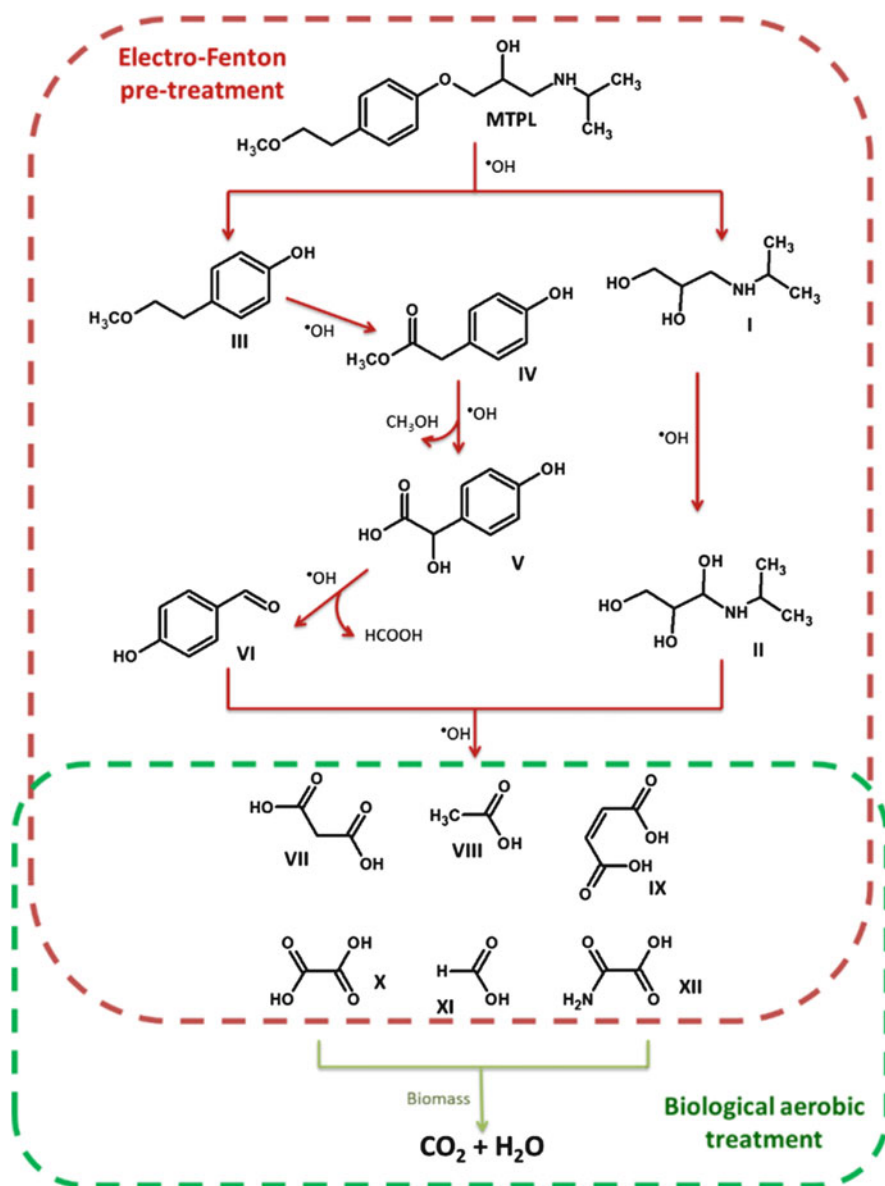


Fig. 5 Reaction pathway for the mineralization of metoprolol during the hybrid Bio-EF process. Reprinted with permission from [32]. Copyright 2016 Elsevier

5.3 Experimental Features and Operating Conditions

The efficiency and potential of the integrated Bio-EF process has been assessed in different wastewater samples, including effluents from the textile, olive mill and

pharmaceutical industries, landfill leachates, as well as synthetic and industrial wastewaters containing dyes, pesticides, pharmaceuticals, and other emerging organic pollutants. The most relevant works on Bio-EF have been summarized in Table 1, in which the system configuration, the operating conditions, as well as the main results are included.

Generally, the efficacy of the EF process for the degradation of organic contaminants is investigated in terms of target pollutant removal, degradation mechanisms, and mineralization degree, with concomitant optimization prior to (or after) biological oxidation (mainly in terms of percentage of mineralization, increase of the BOD₅/COD ratio, and sometimes toxicity assays). Optimization is done taking into consideration both, the rise in biodegradability (strongly linked with the degradation pathways of organics) and the minimum energy consumption. In this sense, EF is remarkably advantageous, since its operating conditions are easily adjustable, which allows for a convenient manipulation of the degradation and mineralization kinetic rates. For example, Olvera-Vargas et al. reported that 500 mA was the optimal current value for an efficient EF treatment of the pharmaceutical metoprolol, with which the best degradation and mineralization rates were achieved. Nonetheless, a lower current value of 300 mA was chosen when EF was used as pre-treatment stage before biological aerobic oxidation, because the lower mineralization rates obtained at 300 mA were preferable for maintaining a good fraction of organic matter as source of carbon for the microorganisms. Moreover, a diminution of the consumed energy was also favored by reduction of the applied current [32]. Likewise, Ganzenko et al. highlighted the importance of optimizing operational conditions of EF so the minimum energy is consumed for the production of a biodegradable effluent. It was found that even if the biodegradability enhancement was higher at increasing current values and longer treatment times, the BOD₅/COD threshold for biodegradability was rapidly reached for all the tested current values (Fig. 6), showing that the use of elevated high-consuming currents can be avoided [19]. In a similar way, Mansour et al. reported that changes in the operating conditions of the pre-EF stage lead to notable changes in the overall results gotten after the activated sludge (AS) process. They reported that under optimal conditions of catalyst and pollutant concentration, applied current, and treatment time, the biodegradability can be importantly increased during EF pre-treatment, therefore entailing higher mineralization rates after the biological stage [41].

Most of the studies on Bio-EF have been conducted applying EF as pre-treatment method. However, EF has also been used to follow the degradation process initiated by a biological approach. Indeed, the establishment of the best sequence strategy relies mostly on the characteristics of the effluent. Just as in the case of the integration of AOPs and biological methods, EF pre-treatment will be preferred when the effluent is charged with high amounts of bio-recalcitrant or toxic compounds, while an EF post-treatment phase will be most adapted for effluents containing biodegradable compounds in large extent (refer to Fig. 4). For example, during a multistage treatment system for remediation of sanitary landfill leachate, the EF, photoelectro-Fenton (PEF), and solar photoelectro-Fenton (SPEF) processes were integrated as post-treatment stage following a first AS treatment and

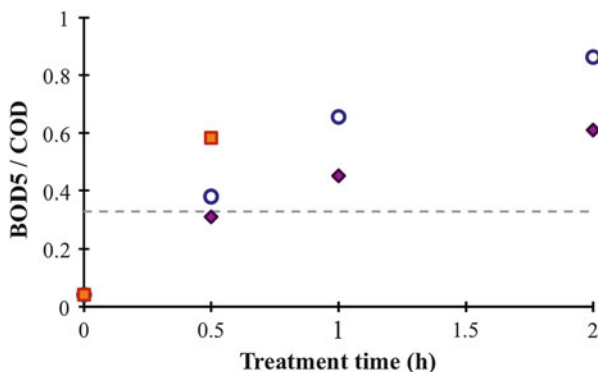


Fig. 6 Biodegradability of the effluent after EF treatment in dependence on treatment duration and applied current intensity (mA): 100 (-purple filled diamonds-); 500 (-blue open circles-); 800 mA (-dark red filled squares-). Dashed line – $BOD_5/COD = 0.33$. Operating conditions: $[Fe^{2+}] = 0.2$ mM, $[Na_2SO_4] = 50$ mM, $V = 1.4$ L. Reprinted with permission from [19]. Copyright 2016 Springer

a second coagulation method [42]. The aim of the electrochemical treatment was to increase the biodegradability of the pre-treated effluent so a possible second biological process could finish the whole treatment procedure. Initially, 13–33% of DOC removal (DOC initial value of 1,222–1,460 $mg L^{-1}$) was obtained at the end of the AS treatment in a 12 L-capacity reactor, along with total ammonium oxidation and total removal of alkalinity. Following coagulation process resulted in 63–65% of DOC abatement. In the subsequent step, 34, 72, and 78% of DOC removal was reached by means of EF, PEF, and SPEF, respectively, after 300 min-electrolysis at 200 $mA cm^{-2}$, pH 2.8 and 20 °C, using 1.18 L of the pre-treated effluent. SPEF was ultimately applied for pilot scale treatment of the pre-treated effluent by AS and coagulation. The resulting COD, BOD_5 , and total nitrogen values were slightly above the Portuguese and European regulations for discharge in the environment [42]. On the other hand, it is noteworthy that an effective step for biomass settling had to be implemented between the biological treatment and the EF post-treatment in order to avoid parasitic reactions between hydroxyl radicals and the biomass.

With regard to the biological treatment, the advantages and disadvantages of individual processes are also applicable for integrated systems (the key point is the removal of recalcitrant compounds prior to bio-treatment). AS has been the preferred choice during the combined Bio-EF setup due to its robustness, low cost, and well-known operability. AS biomass obtained from local WWTP is generally used for the treatment of the biodegradable fraction. Sample conditioning prior to biological degradation is highly relevant, since pH adjustment to a neutral value is crucial, especially after the EF pre-treatment, considering that EF is usually performed at an optimal pH value of 3. Moreover, the generation of short-chain aliphatic acids from the oxidation of higher molecular weight compounds during EF entails a decrease of pH. Additionally, inorganic nutrients are also needed for

maintenance of biomass growth. High sludge retention times of several days are generally needed for the biodegradation process and it depends on the properties of the pre-/post-treated effluents. It has been reported that the acclimation phase can last various days. As an example, Mansour et al. reported that the activated sludge required a 10-days phase of acclimation to the degradation products present in the pre-electrolyzed solution before the TOC began dropping, as illustrated in Fig. 7 [41].

On the contrary, short EF pre-treatment times have been generally reported, as the biodegradability index increases rapidly because of the quick oxidation of organics by $\cdot\text{OH}$, giving more readily biodegradable intermediates. Electrochemical treatment times ranging between 0.5 and 4 h have been communicated when combining EF and biological treatment, as can be observed in Table 1. For example, for the Bio-EF treatment of the drug metoprolol, Olvera-Vargas et al. conducted a 1 h EF pre-treatment before aerobic incubation. An overall 90% TOC removal was achieved after 4 days of biological oxidation, as shown in Fig. 8 [32].

An interesting variant of the Bio-EF process is the utilization of microorganisms to power the EF oxidation of organic contaminants through the generation of “biological electrons” in a microbial fuel cell (MFC). The experimental setup consists in a divided cell in which the microbial metabolism of a substrate in the anodic compartment is responsible for the production of the electrons flowing to the cathode for promotion of the electrochemical reactions leading to the electrogeneration of the “Fenton’s reagent.” Hence, organics are oxidized by the $\cdot\text{OH}$ formed from the Fenton’s reaction during a single integrated Bio-EF-MFC system. During this process,

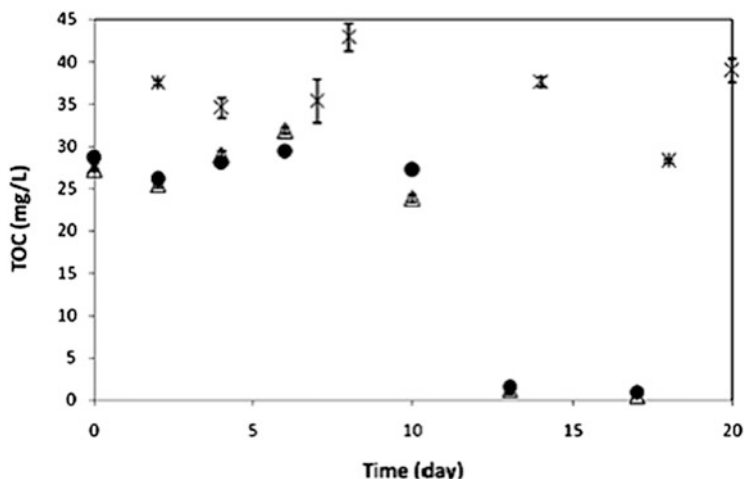
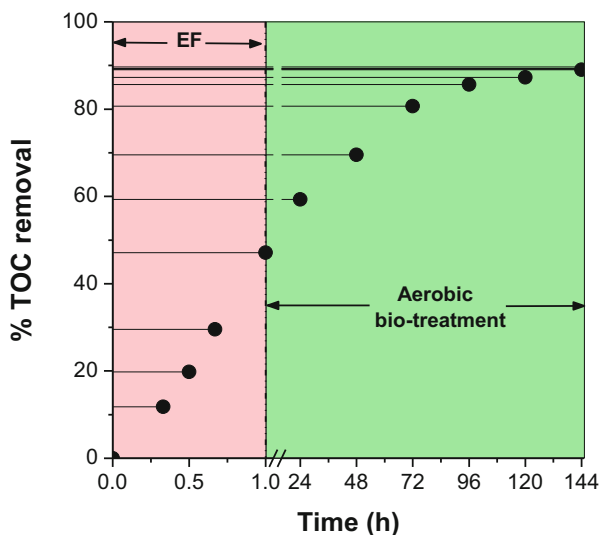


Fig. 7 Mineralization of non-pre-treated (x) and pre-electrolyzed (filled circles and open triangles) solutions of sulfamethazine (SMT) during activated sludge culture. EF pre-treatment conditions: $t = 1$ h, $[\text{SMT}] = 0.36$ mM, $[\text{Fe}^{2+}] = 0.1$ mM, $[\text{Na}_2\text{SO}_4] = 50$ mM, $\text{pH} = 3$, $T = 18$ °C, $I = 200$ mA, $V = 1$ L. Reprinted with permission from [41]. Copyright 2016 Elsevier

Fig. 8 Time-course of the overall TOC removal during the integrated Bio-EF process of a 26.74 mg L⁻¹ MTPL solution. EF stage conditions: 0.22 L of MTPL solution in 0.05 M Na₂SO₄ containing 0.1 mM Fe²⁺ at pH 3.0 and 300 mA, using a carbon-felt-BDD cell at room temperature. Biological phase was conducted at aerobic conditions using biomass composed of 12 pure cultures of microorganisms. Reprinted from [32]. Copyright 2016, Elsevier



microbial cultures do not participate in the degradation of pollutants, instead, their role is to produce the energy to drive the electrochemical treatment for self-sustainability of the process [43, 44].

Bio-EF-MFC process was successfully applied for the degradation of the dye Orange II. A pure culture of *Shewanella decolorationis* S12 was introduced in the anodic chamber containing a carbon-felt cathode and lactate as substrate. A carbon nanotube (CNT)/ γ -FeOOH composite was used as electrode in the cathodic compartment containing a 0.1 mM orange II solution at pH 7. Both chambers had a net volume capacity of 75.6 mL. Total decolorization was achieved in 14 h, whilst almost complete mineralization was attained in 44 h. Remarkably, the electrons necessary for maintaining a current flow throughout the experiment were provided by the bio-electrochemical reactions taking place in the anodic side, thus avoiding the use on any power input. Furthermore, the (CNT)/ γ -FeOOH composite cathode was capable not only of promoting the electrogeneration of H₂O₂, but also of providing the right amount of Fe²⁺ at neutral pH, hence highlighting the eco-friendly character of the system. The setup used in this study is presented in Fig. 9, in which the mechanisms involved in the degradation of the dye are depicted [45]. Similar results were reported by Yong et al. during the degradation of thiphenyltin chloride by means of the MFC-configuration Bio-EF process [46].

This system has also been applied for the remediation of medicinal herbs wastewater, in which 84% of COD removal was achieved after 50 h-treatment using a Fe@Fe₂O₃/graphite composite electrode in the cathodic chamber, operating at pH 3. The anodic chamber was inoculated with anaerobic sludge and the wastewater sample was enriched with different nutrients at pH 7 [47]. Interestingly, the oxidation and removal of arsenite was assessed using a Bio-EF-MFC system using a carbon-felt/ γ -FeOOH cathode in the EF chamber at pH 7. 98.5% of As(III) oxidation to As

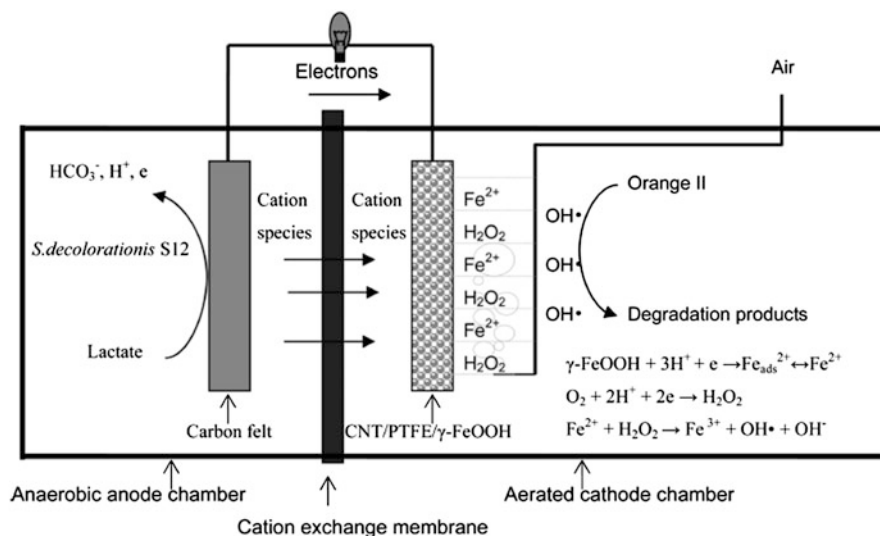


Fig. 9 Schematic representation of the Bio-EF system having an MFC configuration. Reprinted from [45]. Copyright 2010 American Chemical Society

(V) was achieved in 72 h. An important fraction of As(V) was removed by adsorption at the anode surface, while the rest remained in the solution [48].

5.4 Economic Aspects

EAOPs high efficiencies and mild operating conditions are worth the investment costs for full-scale application. In fact, electrochemical technology has been reported to be an economically attractive alternative for the treatment of wastewater that can cost-effectively compete with other AOPs like the classic chemical Fenton and ozonation [1, 55].

Nevertheless, high electric energy requirement is an intrinsic characteristic of EAOPs. In general, the mineralization of polluted effluents requires prolonged treatment times, which clearly represents a substantial increase of energy consumption and therefore of operational costs, a critical drawback for full-scale application. Hence, the utilization of a cheap biological process coupled with short-time EF treatment can significantly decrease the energy consumption. In this way, it was found that the application of an aerobic process as a subsequent step following only 1 h of partial EF treatment of the drug furosemide significantly reduced by a factor of 6 the electric energy costs needed for almost total mineralization during EF (7.66 € kg⁻¹ TOC were needed for achieving 64% of TOC removal in 1 h-treatment, contrasting with the 43.03 € kg⁻¹ TOC required for 94.2% of TOC

removal in 8-h), while the remaining organic matter was removed by cheap biological aerobic oxidation [17].

6 Concluding Remarks and Perspectives

Electrochemical technologies for wastewater treatment, including the EF process, have reached a state of development in which their industrial application for the degradation of refractory organic pollutants is greatly encouraged. Nevertheless, on account of the shortcomings intrinsic to these processes, as well as the unequivocal need for upgrading WWTPs with advanced and sustainable steps, their integration as a part of a multistage treatment systems is more advantageous, inasmuch as the most remarkable features of the individual methods are capitalized into a comprehensive and synergistic one. Accordingly, the main advantages emerging from the hybrid Bio-EF system include:

- Since biological methods are much more cost-effective wastewater treatment technologies, their utilization is always preferred in an economic point of view, as well as in terms of feasibility. Consequently, integration of a biological method in a system where a refractory and/or toxic effluent containing emerging organic pollutants can be pre-treated for biodegradability increase, or post-treated for degradation of the non-biodegradable fraction, always brings economic benefits and it's the only way to reach sufficient removal rates and meet effluent discharge requirements. In this case, the outstanding characteristics of the EF process highlight its advantages as part of an integrated process.
- Reduction of energy consumption related to the EF process. Indeed, as the biodegradability is increased due to the oxidation of recalcitrant organics to biodegradable ones during the EF pre-treatment, electrochemical treatment times can be importantly reduced, which results in a significant depletion of the amount of energy necessitated for higher mineralization degrees. Lower energy consumption is evidently accompanied by an important fall of the overall operating costs. In the opposite sense, when EF is used as post-treatment method, persistent compounds to biodegradation can also be destroyed during short EF treatment times because of the absence of competitive reactions with biodegradable compounds.
- Shorter EF treatment times are also beneficial in terms of the stability of the electrode materials used for electrolysis. In fact, reduced treatment times could increase the lifetime of electrodes, an important benefice in the electrochemical point of view.
- Since only partial mineralization is required during the EF phase, different operating conditions and reactor configurations can be applied with the aim of finding the most advantageous energy-consumption/biodegradability-increase compromise according to the objectives to be attained. For example, the utilization of advanced and expensive electrode materials can be avoided by

augmenting treatment times or on the contrary, they can be used only for short-duration electrolysis.

Despite the advantages presented by this coupled method, there are still some gaps to be filled. The use of electricity to power EF and EAOPs in general, remains a drawback. In this matter, great progress has been done by utilizing solar radiation (photovoltaic technology) as a source of energy for electrochemical technology [56, 57]. However, further exploration in the use of renewable energies as driven forces for electrochemical methods, as well as self-sufficient technologies, needs the attention of researchers and engineers.

On the other hand, the optimal pH value (3.0) for the EF process stands as well an important limitation, since pH adjustment before or after biological oxidation is imperative, thus representing extra operational cost. A potential alternative has been the use of chelating agents that allow Fenton's reaction to take place at circumneutral pH values by the complexation of iron ions, such as tripolyphosphate (TPP) [58]. The use of heterogeneous catalysts increasing the interval of working-pH has also been proposed as an interesting alternative [59]. Other options include the utilization of graphene-based cathodes [60] or hierarchical CoFe-layered double hydroxide modified carbon-felt cathode [26]. These topics are subject of additional research.

Further research is also needed on scaling up and optimization for industrial application. The design of sequential integrated systems in which a comprehensive control of the different parameters affecting the performance of each single unit and that of the whole system is an intricate task demanding the unceasing efforts of the scientific community.

References

1. Ribeiro AR, Nunes OC, Pereira MFR, Silva AMT (2015) An overview on the advanced oxidation processes applied for the treatment of water pollutants defined in the recently launched directive 2013/39/EU. *Environ Int* 75:33–51
2. Uribe IO, Mosquera-Corral A, Rodicio JL, Esplugas S (2015) Advanced technologies for water treatment and reuse. *AIChE J* 61:3146–3158
3. Barbosa MO, Moreira NFF, Ribeiro AR et al (2016) Occurrence and removal of organic micropollutants: an overview of the watch list of EU decision 2015/495. *Water Res* 94:257–279
4. Luo Y, Guo W, Ngo HH et al (2014) A review on the occurrence of micropollutants in the aquatic environment and their fate and removal during wastewater treatment. *Sci Total Environ* 473–474:619–641
5. Prasse C, Stalter D, Schulte-Oehlmann U et al (2015) Spoilt for choice: a critical review on the chemical and biological assessment of current wastewater treatment technologies. *Water Res* 87:237–270
6. Ahmed MB, Zhou JL, Ngo HH et al (2016) Progress in the biological and chemical treatment technologies for emerging contaminant removal from wastewater: a critical review. *J Hazard Mater* 323:274–298

7. Tran NH, Urase T, Ngo HH et al (2013) Insight into metabolic and cometabolic activities of autotrophic and heterotrophic microorganisms in the biodegradation of emerging trace organic contaminants. *Bioresour Technol* 146:721–731
8. Fatta-Kassinos D, Kalavrouziotis IK, Koukoulakis PH, Vasquez MI (2011) The risks associated with wastewater reuse and xenobiotics in the agroecological environment. *Sci Total Environ* 409:3555–3563
9. Picó Y, Barceló D (2015) Transformation products of emerging contaminants in the environment and high-resolution mass spectrometry: a new horizon. *Anal Bioanal Chem* 407:6257–6273
10. Garcia-Rodríguez A, Matamoros V, Fontàs C, Salvadó V (2013) The ability of biologically based wastewater treatment systems to remove emerging organic contaminants – a review. *Environ Sci Pollut Res* 21:11708–11728
11. Pomiès M, Choubert J-M, Wisniewski C, Coquery M (2013) Modelling of micropollutant removal in biological wastewater treatments: a review. *Sci Total Environ* 443:733–748
12. Oturan MA, Aaron J-J (2014) Advanced oxidation processes in water/wastewater treatment: principles and applications. A review. *Crit Rev Environ Sci Technol* 44:2577–2641
13. Oller I, Malato S, Sánchez-Pérez JA (2011) Combination of advanced oxidation processes and biological treatments for wastewater decontamination – a review. *Sci Total Environ* 409:4141–4166
14. Dirany A, Sirés I, Oturan N et al (2012) Electrochemical treatment of the antibiotic sulfachloropyridazine: kinetics, reaction pathways, and toxicity evolution. *Environ Sci Technol* 46:4074–4082
15. Oturan MA, Pimentel M, Oturan N, Sirés I (2008) Reaction sequence for the mineralization of the short-chain carboxylic acids usually formed upon cleavage of aromatics during electrochemical Fenton treatment. *Electrochim Acta* 54:173–182
16. Ganzenko O, Huguenot D, van Hullebusch ED et al (2014) Electrochemical advanced oxidation and biological processes for wastewater treatment: a review of the combined approaches. *Environ Sci Pollut Res* 21:8493–8524
17. Olvera-Vargas H, Oturan N, Buisson D, Oturan MA (2016) A coupled bio-EF process for mineralization of the pharmaceuticals furosemide and ranitidine: feasibility assessment. *Chemosphere* 155:606–613
18. Trellu C, Ganzenko O, Papirio S et al (2016) Combination of anodic oxidation and biological treatment for the removal of phenanthrene and tween 80 from soil washing solution. *Chem Eng J* 306:588–596
19. Ganzenko O, Trellu C, Papirio S et al (2017) Bio-electro-Fenton: evaluation of a combined biological-advanced oxidation treatment for pharmaceutical wastewater. *Environ Sci Pollut Res*. doi:10.1007/s11356-017-8450-6
20. Pulgarin C, Invernizzi M, Parra S et al (1999) Strategy for the coupling of photochemical and biological flow reactors useful in mineralization of biorecalcitrant industrial pollutants. *Catal Today* 54:341–352
21. Contreras S, Rodríguez M, Momani FA et al (2003) Contribution of the ozonation pre-treatment to the biodegradation of aqueous solutions of 2,4-dichlorophenol. *Water Res* 37:3164–3171
22. Brillas E, Sirés I, Oturan MA (2009) Electro-Fenton process and related electrochemical technologies based on Fenton's reaction chemistry. *Chem Rev* 109:6570–6631
23. Moreira FC, Boaventura RAR, Brillas E, Vilar VJP (2017) Electrochemical advanced oxidation processes: a review on their application to synthetic and real wastewaters. *Appl Catal Environ* 202:217–261
24. Sopaj F, Oturan N, Pinson J et al (2016) Effect of the anode materials on the efficiency of the electro-Fenton process for the mineralization of the antibiotic sulfamethazine. *Appl Catal Environ* 199:331–341
25. Mousset E, Ko ZT, Syafiq M et al (2016) Electrocatalytic activity enhancement of a graphene ink-coated carbon cloth cathode for oxidative treatment. *Electrochim Acta* 222:1628–1641

26. Ganiyu SO, Le TXH, Bechelany M et al (2017) Hierarchical CoFe-layered double hydroxide modified carbon-felt cathode: synthesis, characterization and application in heterogeneous electro-Fenton degradation of organic pollutants at circumneutral pH. *J Mater Chem A* 4:17686–17693
27. He Z, Gao C, Qian M et al (2014) Electro-Fenton process catalyzed by Fe₃O₄ magnetic nanoparticles for degradation of C.I. Reactive blue 19 in aqueous solution: operating conditions, influence, and mechanism. *Ind Eng Chem Res* 53:3435–3447
28. Khataee A, Sajjadi S, Hasanzadeh A et al (2017) One-step preparation of nanostructured martite catalyst and graphite electrode by glow discharge plasma for heterogeneous electro-Fenton like process. *J Environ Manage* 199:31–45
29. Ganiyu SO, van Hullebusch ED, Cretin M et al (2015) Coupling of membrane filtration and advanced oxidation processes for removal of pharmaceutical residues: a critical review. *Sep Purif Technol* 156:891–914
30. Martínez-Huitle CA, Rodrigo MA, Sirés I, Scialdone O (2015) Single and coupled electrochemical processes and reactors for the abatement of organic water pollutants: a critical review. *Chem Rev* 115:13362–13407
31. Lin SH, Chang CC (2000) Treatment of landfill leachate by combined electro-Fenton oxidation and sequencing batch reactor method. *Water Res* 34:4243–4249
32. Olvera-Vargas H, Cocerva T, Oturan N et al (2016) Bioelectro-Fenton: a sustainable integrated process for removal of organic pollutants from water: application to mineralization of metoprolol. *J Hazard Mater* 319:13–23
33. Mousset E, Oturan N, van Hullebusch ED et al (2014) Treatment of synthetic soil washing solutions containing phenanthrene and cyclodextrin by electro-oxidation. Influence of anode materials on toxicity removal and biodegradability enhancement. *Appl Catal Environ* 160–161:666–675
34. Mousset E, Oturan N, van Hullebusch ED et al (2014) Influence of solubilizing agents (cyclodextrin or surfactant) on phenanthrene degradation by electro-Fenton process – study of soil washing recycling possibilities and environmental impact. *Water Res* 48:306–316
35. Mousset E et al. (2017) Soil remediation by electro-Fenton process. *Handb Environ Chem*. doi:10.1007/698_2017_38
36. Belkheiri D, Fourcade F, Geneste F et al (2011) Feasibility of an electrochemical pre-treatment prior to a biological treatment for tetracycline removal. *Sep Purif Technol* 83:151–156
37. Yahiaoui I, Aissani-Benissad F, Fourcade F, Amrane A (2013) Removal of tetracycline hydrochloride from water based on direct anodic oxidation (Pb/PbO₂ electrode) coupled to activated sludge culture. *Chem Eng J* 221:418–425
38. Grafias P, Xekoukoulotakis NP, Mantzavinos D, Diamadopoulos E (2010) Pilot treatment of olive pomace leachate by vertical-flow constructed wetland and electrochemical oxidation: an efficient hybrid process. *Water Res* 44:2773–2780
39. Mansour D, Fourcade F, Soutrel I et al (2015) Mineralization of synthetic and industrial pharmaceutical effluent containing trimethoprim by combining electro-Fenton and activated sludge treatment. *J Taiwan Inst Chem Eng* 53:58–67
40. Pignatello JJ, Oliveros E, MacKay A (2006) Advanced oxidation processes for organic contaminant destruction based on the Fenton reaction and related chemistry. *Crit Rev Environ Sci Technol* 36:1–84
41. Mansour D, Fourcade F, Huguet S et al (2014) Improvement of the activated sludge treatment by its combination with electro Fenton for the mineralization of sulfamethazine. *Int Biodeter Biodegr* 88:29–36
42. Moreira FC, Soler J, Fonseca A et al (2015) Incorporation of electrochemical advanced oxidation processes in a multistage treatment system for sanitary landfill leachate. *Water Res* 81:375–387
43. Zhu X, Ni J (2009) Simultaneous processes of electricity generation and p-nitrophenol degradation in a microbial fuel cell. *Electrochem Commun* 11:274–277

44. Huong Le TX, Esmilaire R, Drobek M et al (2016) Design of a novel fuel cell-Fenton system: a smart approach to zero energy depollution. *J Mater Chem A* 4:17686–17693
45. Feng C-H, Li F-B, Mai H-J, Li X-Z (2010) Bio-electro-Fenton process driven by microbial fuel cell for wastewater treatment. *Environ Sci Technol* 44:1875–1880
46. Yong X-Y, Gu D-Y, Wu Y-D et al (2017) Bio-electron-Fenton (BEF) process driven by microbial fuel cells for triphenyltin chloride (TPTC) degradation. *J Hazard Mater* 324:178–183
47. Birjandi N, Younesi H, Ghoreyshi AA, Rahimnejad M (2016) Electricity generation through degradation of organic matters in medicinal herbs wastewater using bio-electro-Fenton system. *J Environ Manage* 180:390–400
48. Wang X-Q, Liu C-P, Yuan Y, Li F (2014) Arsenite oxidation and removal driven by a bio-electro-Fenton process under neutral pH conditions. *J Hazard Mater* 275:200–209
49. Ferrag-Siagh F, Fourcade F, Soutrel I et al (2014) Electro-Fenton pretreatment for the improvement of tylosin biodegradability. *Environ Sci Pollut Res* 21:8534–8542
50. Gong Y, Li J, Zhang Y et al (2016) Partial degradation of levofloxacin for biodegradability improvement by electro-Fenton process using an activated carbon fiber felt cathode. *J Hazard Mater* 304:320–328
51. Mansour D, Fourcade F, Soutrel I et al (2015) Relevance of a combined process coupling electro-Fenton and biological treatment for the remediation of sulfamethazine solutions – application to an industrial pharmaceutical effluent. *Comptes Rendus Chim* 18:39–44
52. Ledezma Estrada A, Li Y-Y, Wang A (2012) Biodegradability enhancement of wastewater containing cefalexin by means of the electro-Fenton oxidation process. *J Hazard Mater* 227:41–48
53. Moussavi G, Bagheri A, Khavanin A (2012) The investigation of degradation and mineralization of high concentrations of formaldehyde in an electro-Fenton process combined with the biodegradation. *J Hazard Mater* 237:147–152
54. Vidal J, Huiliñir C, Salazar R (2016) Removal of organic matter contained in slaughterhouse wastewater using a combination of anaerobic digestion and solar photoelectro-Fenton processes. *Electrochim Acta* 210:163–170
55. Cañizares P, Paz R, Sáez C, Rodrigo MA (2009) Costs of the electrochemical oxidation of wastewaters: a comparison with ozonation and Fenton oxidation processes. *J Environ Manage* 90:410–420
56. Garcia-Segura S, Brillas E (2014) Advances in solar photoelectro-Fenton: decolorization and mineralization of the direct yellow 4 diazo dye using an autonomous solar pre-pilot plant. *Electrochim Acta* 140:384–395
57. Mook WT, Aroua MK, Issabayeva G (2014) Prospective applications of renewable energy based electrochemical systems in wastewater treatment: a review. *Renew Sustain Energy Rev* 38:36–46
58. Wang L, Cao M, Ai Z, Zhang L (2015) Design of a highly efficient and wide pH electro-Fenton oxidation system with molecular oxygen activated by ferrous-tetrapolyphosphate complex. *Environ Sci Technol* 49:3032–3039
59. Zhang C, Zhou M, Yu X et al (2015) Modified iron-carbon as heterogeneous electro-Fenton catalyst for organic pollutant degradation in near neutral pH condition: characterization, degradation activity and stability. *Electrochim Acta* 160:254–262
60. Le TXH, Bechelany M, Lacour S, Oturan N, Oturan MA, Cretin M (2015) High removal efficiency of dye pollutants by electron-Fenton process using a graphene based cathode. *Carbon* 94:1003–1011

The Electro-peroxone Technology as a Promising Advanced Oxidation Process for Water and Wastewater Treatment

Yujue Wang

Abstract The electro-peroxone (E-peroxone) process is a novel electrochemical advanced oxidation process (EAOP) that is enabled by in situ generation of hydrogen peroxide (H_2O_2) from cathodic oxygen (O_2) reduction during conventional ozonation. The electro-generated H_2O_2 can considerably enhance ozone (O_3) transformation to hydroxyl radicals ($\cdot\text{OH}$), thus greatly enhancing pollutant degradation and total organic carbon (TOC) mineralization by the E-peroxone process than by conventional ozonation. Due to its higher kinetics of pollutant degradation, the E-peroxone process can also reduce reaction time and energy consumption required for water and wastewater treatment. In addition, the in situ generated H_2O_2 can effectively reduce bromate formation during the E-peroxone treatment of bromide-containing water compared to conventional ozonation. All oxidants (O_3 , H_2O_2 , and $\cdot\text{OH}$) are produced on site at controllable rates during the E-peroxone process using only clean oxygen and electricity. No chemicals or catalysts are added in the E-peroxone process nor does it produce secondary pollutants. By simply installing low-cost carbon-based cathodes in ozone contactors, conventional ozonation systems that are commonly used in water and wastewater utilities can be easily retrofitted to the E-peroxone process with minimal upgrade work and costs. Therefore, the E-peroxone process can provide a convenient and economical way to significantly improve the performance of existing ozonation systems in many aspects and has thus emerged as a promising EAOP for practical water and wastewater treatment.

Keywords Electrochemical advanced oxidation process, Electro-peroxone, Hydrogen peroxide, Micropollutant, Ozone, Wastewater treatment, Water treatment

Y. Wang (✉)

School of Environment, Tsinghua University, Beijing 100084, China

e-mail: wangyujue@tsinghua.edu.cn

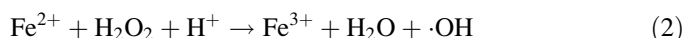
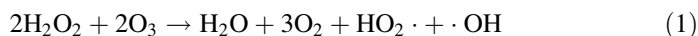
Contents

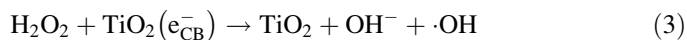
1	Introduction	58
2	Principles and Advantages of the Electro-peroxone Process	61
2.1	Cathodic Reaction Mechanisms During the Electro-peroxone Process	62
2.2	Bulk Reaction Mechanism During the Electro-peroxone Process	65
2.3	Photoelectro-peroxone Process	67
3	Applications of the Electro-peroxone Process for Water and Wastewater Treatment	69
3.1	Electro-peroxone for Wastewater Treatment	69
3.2	Electro-peroxone for Advanced Wastewater Treatment	71
3.3	Electro-peroxone for Drinking Water Treatment	75
3.4	Electro-peroxone Regeneration of Spent Activated Carbon	76
4	Concluding Remarks	77
4.1	Potentials of the Electro-peroxone Process for Water and Wastewater Treatment ..	77
4.2	Future Research Directions	78
	References	81

1 Introduction

Advanced oxidation processes (AOPs) are of great interest in water and wastewater treatment [1–5]. AOPs have been broadly defined as those aqueous phase oxidation processes that are driven by highly reactive oxidants, especially hydroxyl radicals ($\cdot\text{OH}$) [6]. $\cdot\text{OH}$ is just about the strongest oxidant ($E^0 = 2.8 \text{ V}$ [7]) that can be safely applied in water treatment and can nonselectively oxidize most organic pollutants at diffusion-controlled rates ($\sim 10^8\text{--}10^{10} \text{ M}^{-1} \text{ s}^{-1}$) [8]. Therefore, $\cdot\text{OH}$ -based AOPs have been increasingly used in water and wastewater treatment to degrade refractory organic pollutants that are difficult to remove by other conventional treatment technologies.

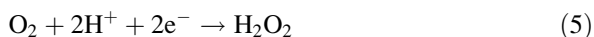
Due to its extremely high reactivity and short lifetime, $\cdot\text{OH}$ has to be produced in situ during AOP treatment of water and wastewater. Hydrogen peroxide (H_2O_2) is one of the most common chemicals used to produce $\cdot\text{OH}$ in a variety of AOPs [9]. H_2O_2 is relatively stable in pure water. However, it can react actively with many chemicals (e.g., ozone (O_3) and ferrous iron (Fe^{2+})) and catalysts (e.g., titanium dioxide and transition metal oxides) or undergo ultraviolet-induced photolysis to produce $\cdot\text{OH}$ (Eqs. 1–4) [1, 7, 10]. Therefore, H_2O_2 has been considered a versatile reagent for $\cdot\text{OH}$ production in many AOPs, for example, the peroxone ($\text{O}_3/\text{H}_2\text{O}_2$), Fenton ($\text{Fe}^{2+}/\text{H}_2\text{O}_2$), and UV/ H_2O_2 processes. In addition, H_2O_2 is also an environmentally friendly oxidant because the only decomposition products of H_2O_2 are water (H_2O) and oxygen (O_2) [9].





Currently, H_2O_2 is manufactured almost exclusively by the anthraquinone oxidation process on an industrial scale, and commercially available as aqueous solutions at concentrations of usually 30, 50, and 70 wt.% [9]. The market price for industrial grade H_2O_2 (30 wt.% solution) is about 0.39–0.5 USD kg^{-1} , equivalent to ~1.2–1.5 USD kg^{-1} on a 100 wt.% basis [11, 12]. Therefore, H_2O_2 is generally considered a costly chemical for water and wastewater treatment [12–14]. Moreover, H_2O_2 stock solutions may decay during storage, leading to a decline in the efficiency of water and wastewater treatment. Furthermore, due to its high reactivity and strong oxidizing properties ($E^0 = 1.78$ V), the transportation, storage, and handling of bulk H_2O_2 solutions involve safety hazards, which has considerably limited the use of H_2O_2 in some water and wastewater utilities [9, 10, 12].

To overcome the drawbacks associated with the use of bulk H_2O_2 solutions, the in situ generation of H_2O_2 from cathodic O_2 reduction (Eq. 5) during water and wastewater treatment has gained increasing interest in recent years [2, 10, 12, 15–17]. Results show that by bubbling air or pure oxygen into an electrolysis reactor that has a carbon-based cathode (e.g., carbon-polytetrafluorethylene (carbon-PTFE), carbon felt, and reticulated vitreous carbon (RVC)), H_2O_2 can be electrochemically produced from cathodic O_2 reduction at controllable rates with high current efficiencies (up to ~100%) [18, 19]. This provides a convenient and flexible way to supply H_2O_2 on demand for water and wastewater treatment. In addition, economic analyses indicate that depending on reaction conditions (e.g., solution conductivities and O_2 sources), H_2O_2 can be produced from cathodic O_2 reduction at comparable or even much lower costs (e.g., 0.1–0.3 USD kg^{-1}) compared to H_2O_2 stocks (e.g., 1.2–1.5 USD kg^{-1}) [12, 20]. Therefore, cathodic O_2 reduction to H_2O_2 can not only eliminate the risks and decay problems associated with the use and storage of bulk H_2O_2 solutions but also reduce the operation costs of AOPs. These promising results indicate that the in situ generation of H_2O_2 from cathodic O_2 reduction can provide an attractive approach to providing the H_2O_2 necessary for the implementation of more traditional AOPs and considerably improve the performance of water and wastewater treatment in many aspects.



Over the past two decades, a variety of electrochemically driven AOPs (EAOPs) have been developed on the basis of the electro-generation of H_2O_2 from cathodic O_2 reduction [10, 12, 15–18, 21]. Among this kind of EAOPs, the electro-Fenton (E-Fenton) process, which was developed in the 1990s by Brillas' and Oturan's groups [18, 22], is probably the most known and popular one. Since its appearance, the E-Fenton process has been extensively investigated and successfully applied to treat a wide range of wastewaters that are polluted by toxic and/or refractory organic

pollutants, such as industrial effluents, landfill leachates, and concentrates from membrane processes (see [4, 5, 10] and references therein).

However, the applications of the E-Fenton process in drinking water treatment have been largely limited because of several reasons. For example, Fenton-related processes usually need to be operated under acidic conditions (e.g., pH of ~ 3), whereas the typical pH values encountered in drinking water treatment are circumneutral (e.g., ~ 7 – 8) [1, 23]. pH adjustment is uneconomical or impractical for large-scale drinking water treatment [1]. Moreover, the addition of Fe^{2+} catalysts and the ensuing formation of iron sludge during Fenton-related processes are problematic for drinking water treatment. Therefore, Fenton-related processes have rarely been applied in drinking water treatment.

To exploit the benefits of in situ H_2O_2 generation in drinking water treatment, we have recently developed a novel EAOP, named as the electro-peroxone (E-peroxone) process, by combining conventional ozonation with cathodic H_2O_2 production from O_2 reduction [16]. Unlike the Fenton process, ozonation is a well-established technology in drinking water treatment with numerous successful experiences of large-scale applications [1]. In addition, ozonation has also been increasingly applied in wastewater treatment in recent years, for example, as pretreatment to improve the biodegradability of wastewater for biological treatment, or as posttreatment to abate refractory organic residuals in biologically treated effluents [1]. Ozone is a strong oxidant ($E^0 = 2.07$ V) and can oxidize a wide range of inorganic and organic pollutants, especially compounds with activated double bonds (e.g., activated aromatic systems, deprotonated amines, and reduced sulfur groups) [1]. In addition, O_3 is also an excellent disinfectant and capable of inactivating a broad variety of waterborne pathogens such as viruses, bacteria, and protozoa [24]. Therefore, O_3 has been commonly used in both water and wastewater treatment as an oxidant and disinfectant.

While ozonation has been working well and applied successfully in full-scale operations, it still has some room for improvement. For example, O_3 is a very selective oxidant. Therefore, ozonation is often inefficient at degrading O_3 -resistant pollutants (such as atrazine, 1,4-dioxane, and ibuprofen) and mineralizing total organic carbon (TOC) [1, 25, 26]. Moreover, while O_3 -reactive pollutants can be readily degraded by ozonation, they may generate some O_3 -resistant transformation products that can accumulate in ozonation effluents and thus still pose threat to the ecosystem and human health [1, 26, 27]. Furthermore, ozonation of bromide (Br^-)-containing water can produce bromate (BrO_3^-) [1, 24], which is a potential human carcinogen and therefore strictly regulated in drinking water with a maximum contaminant level (MCL) of $10 \mu\text{g L}^{-1}$ in many countries [28–30].

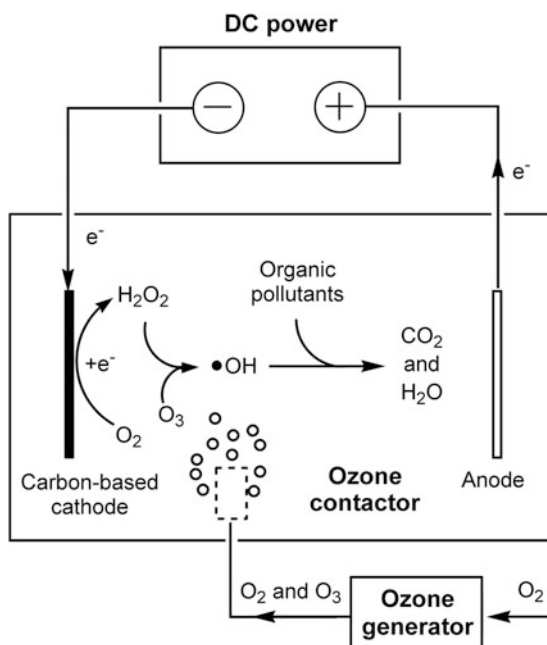
Interestingly, our recent studies have shown that the major limitations of conventional ozonation can be successfully overcome by electrochemically producing H_2O_2 in situ from cathodic O_2 reduction during the E-peroxone process [16, 20, 31–34]. The E-peroxone process has a simple reactor configuration and can be easily

upgraded from conventional ozonation systems by installing a pair of electrodes in existing ozone contactors [32]. Therefore, the E-peroxone process can provide a convenient way to improve the performance of conventional ozonation systems, that are already widely used in numerous water and wastewater utilities, and has emerged as an attractive AOP option for water and wastewater treatment. This chapter will describe the fundamentals of the E-peroxone technology, review its recent progresses, and discuss the issues that need further investigation for this novel technology toward practical applications.

2 Principles and Advantages of the Electro-peroxone Process

The E-peroxone process involves the in situ generation of H_2O_2 from cathodic O_2 reduction during conventional ozonation [16]. A distinct advantage of the E-peroxone process is that it can be easily retrofitted from conventional ozonation system by simply installing a pair of electrodes in existing ozone contactor (see Fig. 1 for the schematic of the E-peroxone process), which requires minimal capital cost and upgrade work [32]. During the E-peroxone process, O_3 is produced from

Fig. 1 Schematic representation of the main reaction mechanisms of the electro-peroxone (E-peroxone) process



an O₂ feed gas using an ozone generator, which is the same as in conventional ozonation. Because ozone generators can convert only a small fraction of O₂ feed gas to O₃, ozone generator effluents that are bubbled into ozone contactors still contain predominantly O₂ (usually >90% V/V) [1]. This part of O₂ has little use for pollutant removal and therefore is wasted during conventional ozonation. However, it provides an ideal O₂ source for cathodic H₂O₂ production during the E-peroxone process. The in situ generated H₂O₂ can then react with sparged O₃ via the so-called peroxone reaction to yield ·OH (Eq. 1), thus greatly improving the degradation of O₃-resistant pollutants and the mineralization of solution TOC [19, 20]. Furthermore, the electro-generated H₂O₂ can significantly reduce the amount of bromate (BrO₃⁻) formed during the treatment of bromide (Br⁻)-containing water [31, 32]. These results indicate that by utilizing O₂ that would otherwise have been wasted in conventional ozonation, the E-peroxone process can significantly improve the performance of water and wastewater treatment in many aspects.

2.1 Cathodic Reaction Mechanisms During the Electro-peroxone Process

Effective production of H₂O₂ from cathodic O₂ reduction plays a vital part in the E-peroxone process. However, several reactions may occur in competition with O₂ reduction to H₂O₂ at the cathode during the E-peroxone process, for example, hydrogen (H₂) evolution, further reduction of electro-generated H₂O₂, and O₃ reduction (see Table 1).

These side reactions can impair H₂O₂ electro-generation and thus affect the performance of the E-peroxone process. Therefore, it is critical to minimize these

Table 1 Possible cathodic reactions that may occur during the E-peroxone process and their standard electrode potentials (E^0)

Reaction ^a	E^0 (vs. SHE) ^b	Reference
$O_2 + 2H_2O + 4e^- \rightarrow 4OH^-$ (6)	0.401	[35]
$O_2 + H_2O + 2e^- \rightarrow HO_2^- + OH^-$ (7)	-0.076	[35]
$HO_2^- + H_2O + 2e^- \rightarrow 3OH^-$ (8)	0.878	[35]
$2H_2O + 2e^- \rightarrow H_2 + 2OH^-$ (9)	-0.828	[35]
$O_3 + H_2O + 2e^- \rightarrow O_2 + 2OH^-$ (10)	1.24	[35]
$O_3 + e^- \rightarrow O_3^- \cdot$ (11)	1.23	[36]

^aThe table lists the cathodic reactions and standard reduction potentials under alkaline conditions, which simulate the high local pH in the cathode diffuse layers

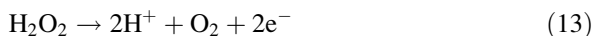
^b E^0 values are presented against standard hydrogen electrode (SHE) at 298.15 K (25°C), and at pressure of 101.325 kPa. The activity of all the soluble species (e.g., OH⁻) is assumed to be 1.000 mol L⁻¹

side reactions during the E-peroxone process by selecting proper electrodes and optimizing the reaction conditions [37].

Due to their high overpotential for H₂ evolution and low catalytic activity for H₂O₂ decomposition, carbon-based electrodes have been commonly used to produce H₂O₂ from cathodic O₂ reduction [10, 38]. Many carbon electrodes can be used for H₂O₂ production, such as graphite, carbon-PTFE, carbon felt, RVC, carbon nanotube, and graphene electrodes [10]. Figure 2 shows that when a pure O₂ gas was sparged into a background electrolyte (0.05 M Na₂SO₄) during electrolysis with a carbon-PTFE cathode, H₂O₂ could be produced with high apparent current efficiencies (~87–96%, calculated according to Eq. 12) over a wide range of current density (5–25 mA cm⁻²) [19]. Considering that some cathodically generated H₂O₂ could be decomposed at the anode (Eq. 13) or undergo self-decomposition (Eq. 14) in the bulk solution during the process, the actual current efficiencies of cathodic H₂O₂ production are expected to be even higher. The high current efficiencies for cathodic H₂O₂ production suggest that when carbon-PTFE cathodes are used in the E-peroxone process, the four-electron reduction of O₂ to OH⁻ (Eq. 6), H₂ evolution (Eq. 9), and H₂O₂ reduction (Eq. 8) are generally negligible cathodic reactions compared to the two-electron reduction of O₂ to H₂O₂ (Eq. 7) [19, 37].

$$\text{CE (\%)} = \frac{nFC_{\text{H}_2\text{O}_2}V}{\int_0^t I \, dt} \times 100 \quad (12)$$

where n is the number of electrons consumed for converting O₂ to H₂O₂ (two electrons), F is the Faraday constant (96,486 C mol⁻¹), $C_{\text{H}_2\text{O}_2}$ is the concentration of H₂O₂ (mol L⁻¹), V is the solution volume (L), I is the current (A), and t is the electrolysis time (s).



However, it should be noted that during the E-peroxone process, an O₂/O₃ mixture (rather than pure O₂) is sparged into the system to electrochemically drive the peroxone reaction for ·OH production. Thermodynamically, O₃ can be preferentially reduced at much more positive potentials than O₂ at the cathodes (see Table 1). Therefore, cathodic O₂ reduction to H₂O₂ would be inhibited if sufficient quantity of O₃ is available in the cathode diffuse layer to accept all the electrons transferred at the cathode, i.e., cathodic O₃ reduction is limited by the applied currents [37]. Under such current limited conditions, the desired electrochemically driven peroxone process (i.e., cathodic O₂ reduction to H₂O₂ and the ensuing peroxone reaction of H₂O₂ with O₃ to ·OH) actually cannot occur during the E-peroxone process [37]. Fortunately, because O₃ accounts for only small fractions of the sparged O₂/O₃ gas mixture (<10% V/V [1]) and can be rapidly consumed in bulk reactions with O₃-reactive water matrix (e.g., natural organic matter (NOM) and compounds with activated double bonds) as well as electro-generated H₂O₂ in the

Fig. 2 Electro-generation of H_2O_2 from sparged O_2 during electrolysis with a carbon-polytetrafluorethylene (carbon-PTFE) cathode at varying currents. Reaction conditions: 400 mL of 0.05 M Na_2SO_4 solution, O_2 gas flow rate of 0.4 L min^{-1} , 20 cm^2 carbon-PTFE cathode, and 2 cm^2 Pt anode. The inset plot shows the concentration of H_2O_2 at 1 h and the apparent current efficiency for H_2O_2 production as a function of the applied current. Reprinted from Ref. [19], Copyright 2015, with permission from Elsevier

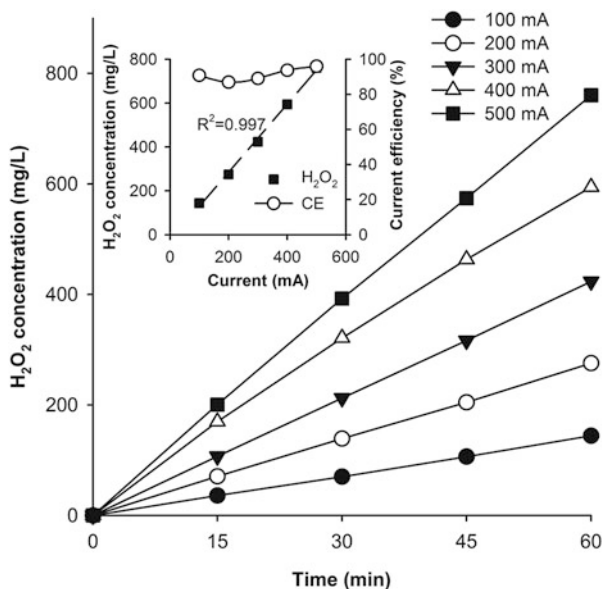
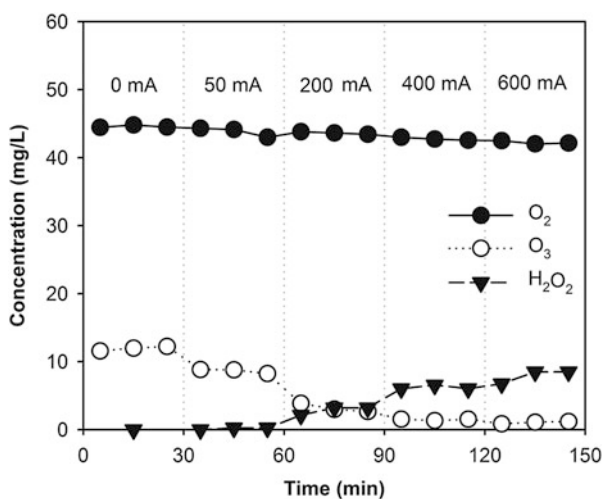


Fig. 3 Evolutions of the concentrations of dissolved O_2 , dissolved O_3 , and H_2O_2 during electrolysis with O_2/O_3 gas mixture sparging. Reaction conditions: 1 L of 0.1 M Na_2SO_4 solution, 24 cm^2 IrO_2/Ti anode, polyacrylonitrile based carbon fiber brush cathode, sparging gas flow rate = 0.4 L min^{-1} , and inlet O_3 gas phase concentration = 45 mg L^{-1} . Reprinted from Ref. [37], Copyright 2017, with permission from Elsevier



solution, the concentrations of dissolved O_3 are usually much lower than dissolved O_2 during the E-peroxone process (see Fig. 3) [37]. Therefore, cathodic O_3 reduction is often limited by the mass transfer of dissolved O_3 to the cathode during the E-peroxone process [37]. Under such O_3 -mass transfer limited conditions, cathodic O_2 reduction to H_2O_2 can occur and often dominate the cathodic reaction mechanisms during the E-peroxone process similarly as during electrolysis with pure O_2 sparging [19, 37].

For example, Fig. 3 shows that as applied currents were stepwise increased during electrolysis with sparging an O₂/O₃ gas mixture, increasing concentrations of H₂O₂ could be detected in the solution at currents higher than 200 mA [37]. This trend suggests that as the applied currents were increased beyond 200 mA, cathodic O₃ reduction changed from current limited to mass transfer limited. Consequently, cathodic O₂ reduction to H₂O₂ occurred. Due to the enhanced H₂O₂ production at higher currents, H₂O₂ concentrations increased progressively in the solution. On the other hand, dissolved O₃ concentrations declined continuously due to the accelerated O₃ decomposition by electro-generated H₂O₂. These results confirm that cathodic O₂ reduction to H₂O₂ can indeed occur during electrolysis with O₂/O₃ sparging, thus enabling the desired E-peroxone process for water and wastewater treatment.

2.2 Bulk Reaction Mechanism During the Electro-peroxone Process

Once electrochemically generated at the cathode, H₂O₂ can diffuse into the bulk solution to react with dissolved O₃ and other water constituents. This can change the bulk reaction mechanisms fundamentally as compared to conventional ozonation.

The observed second-order rate constant for the reaction of H₂O₂ with O₃ is pH dependent (Eq. 15), and ~1,500 M⁻¹ s⁻¹ at pH 7 [1].

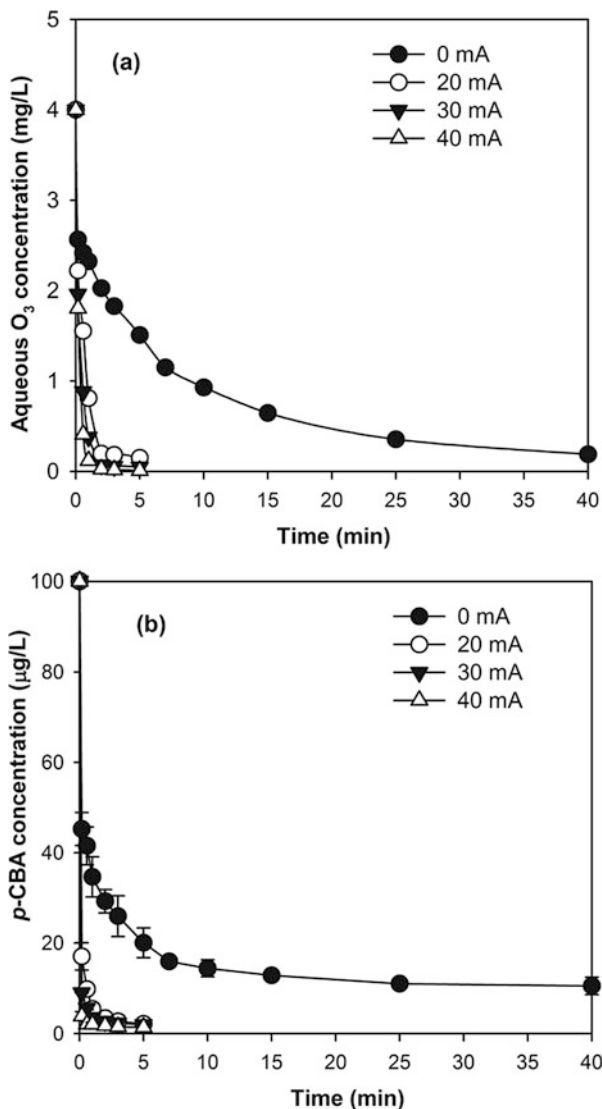
$$k_{\text{obs}} = k(\text{HO}_2^- + \text{O}_3) \times 10^{(\text{pH} - \text{pK}_a)} \quad (15)$$

where $k(\text{HO}_2^- + \text{O}_3) = 9.6 \times 10^6 \text{ M}^{-1} \text{ s}^{-1}$ is the second-rate constant for the reaction of O₃ with HO₂⁻ (conjugate base of H₂O₂); pK_a(H₂O₂) = 11.8 [39].

Therefore, the electro-generated H₂O₂ can considerably accelerate the kinetics of O₃ decomposition to ·OH under typical pH range encountered in water and wastewater treatment [19, 31]. As shown in Fig. 4a, it took more than 40 min for dosed O₃ (~4.7 mg L⁻¹) to decay completely in a surface water during conventional ozonation [31]. In contrast, complete O₃ decay could be attained within 2–5 min of the E-peroxone process operated with varying currents of 20–40 mA. The acceleration of O₃ transformation to ·OH can in turn increase the abatement rates of O₃-resistant pollutants accordingly, as shown for para-chlorobenzoic acid (*p*-CBA) spiked in the surface water (Fig. 4b) [20].

In addition to accelerating O₃ decomposition kinetics, the electro-generated H₂O₂ can also enhance the yield of ·OH production from O₃ decomposition (i.e., moles of ·OH formed per mole of O₃ consumed). As suggested by the overall stoichiometry of the peroxone reaction (Eq. 1), H₂O₂ reacts with O₃ to produce ·OH with an approximately 50% yield (i.e., 0.5 mol ·OH formed per mole O₃ consumed) [1, 40]. This value is generally much higher than those (e.g., 13–41%) that could be obtained from O₃ decomposition with ·OH-producing water constituents (e.g., NOM and electron-rich aromatics) in water and wastewater [1, 40–43]. Therefore, depending on various

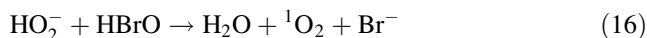
Fig. 4 Evolution of (a) O_3 and (b) para-chlorobenzoic acid (*p*-CBA) as a function of applied current during batch conventional ozonation and the E-peroxone treatment of a surface water (dissolved organic carbon (DOC) = 2.35 mg L^{-1}). Experimental conditions: solution volume = 260 mL, 6 cm^2 Pt anode, 10 cm^2 carbon-PTFE cathode, specific ozone dose = $2 \text{ mg } O_3/\text{mg DOC}$, pH = 8.0, and temperature = $23 \pm 1^\circ\text{C}$. Adapted from Ref. [31], Copyright 2017, with permission from Elsevier



process and water parameters (e.g., O_3 and H_2O_2 doses, reaction time, pH, the reactivity of water matrix with O_3 , and the nature and concentrations of $\cdot OH$ scavenger), the E-peroxone process can usually enhance the $\cdot OH$ yields from O_3 decomposition to varying extents compared to conventional ozonation [31]. As the $\cdot OH$ yields are closely related to the extents of abatement efficiencies of O_3 -resistant pollutants in ozone-based AOPs [1, 43, 44], the E-peroxone process can usually improve the abatement efficiencies of O_3 -resistant pollutants than conventional ozonation when the same O_3 doses are applied in the two processes [20, 31, 34].

In addition to enhancing pollutant degradation, the E-peroxone process can significantly reduce bromate (BrO_3^-) formation during the treatment of bromide (Br^-)-containing water as compared to conventional ozonation [31, 32]. It is well-known that natural waters usually contain a certain amount of Br^- ranging from 10 to 1,000 $\mu\text{g L}^{-1}$ [24]. During ozonation, Br^- can be oxidized to BrO_3^- via a multistep oxidation mechanism involving O_3 , $\cdot\text{OH}$, or their combination [1, 45]. For waters containing more than 50 $\mu\text{g L}^{-1}$ of bromide, bromate formation may exceed the drinking water standard of 10 $\mu\text{g L}^{-1}$ during ozonation, which represents a major concern of conventional ozonation for drinking water treatment [24]. In contrast, by in situ producing H_2O_2 from cathodic O_2 reduction, the E-peroxone process can successfully inhibit BrO_3^- formation [31, 32].

As shown in Fig. 5a, considerable fractions of Br^- (initial concentration of 150 $\mu\text{g L}^{-1}$) in a synthetic solution could be transformed to BrO_3^- during a pilot-scale conventional ozonation treatment (current = 0 mA) [32]. However, with step-wise increasing applied currents to enhance H_2O_2 electro-generation (Fig. 5b), BrO_3^- formation could be decreased to undetectable levels during the E-peroxone process. This improvement can be mainly attributed to the fact that: (a) the reaction of electro-generated H_2O_2 with O_3 leads to a decline in the residual concentration of O_3 (Fig. 5b), which is an indispensable reactant in $\cdot\text{OH}$ -induced BrO_3^- formation mechanism [1, 24], and (b) HO_2^- (the conjugate base of H_2O_2) can rapidly reduce hypobromous acid, a decisive intermediate for BrO_3^- formation in ozone-induced process, back to Br^- (Eq. 16, $k = 7.6 \times 10^8 \text{ M}^{-1} \text{ s}^{-1}$) and thus impede the formation pathways of BrO_3^- [1, 45, 46].



Besides reacting with O_3 and HBrO , H_2O_2 can react actively with many species (e.g., transition metals and free chlorine) that may exist in water and wastewater [47]. These reactions can have complex effects on the performance of water and wastewater treatment by the E-peroxone process (e.g., pollutant degradation and by-product formation). Due to the complex effects of water matrix and interactions between the bulk and electrode reactions, more studies are needed to better understand the reaction mechanisms involved in the E-peroxone process.

2.3 Photoelectro-peroxone Process

To further enhance pollutant degradation and TOC mineralization kinetics, the E-peroxone process can be combined with UV irradiation to form the so-called photoelectro-peroxone (PE-peroxone) process as shown in Fig. 6 [17]. During the PE-peroxone process, significant amounts of $\cdot\text{OH}$ can be produced via multiple reaction pathways, e.g., UV photolysis of the sparged O_3 (Eq. 17) and the electro-generated H_2O_2 (Eq. 4), as well as the peroxone reaction of O_3 with H_2O_2 (Eq. 1).

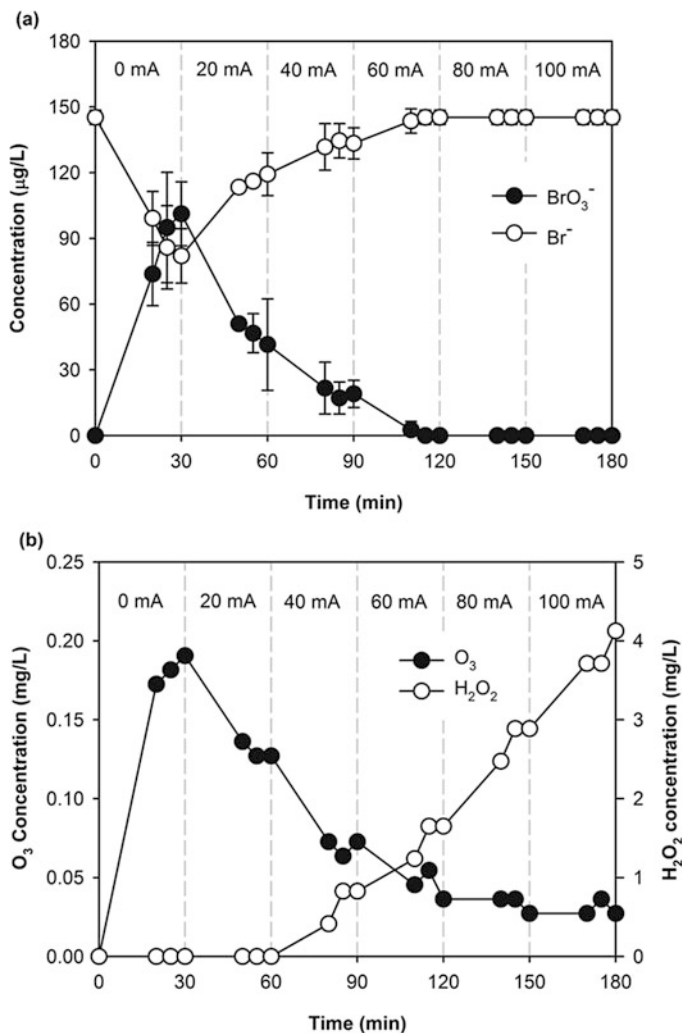


Fig. 5 Evolution of (a) Br^- and BrO_3^- , and (b) O_3 and H_2O_2 in the effluent during ozonation (i.e., current = 0 mA) and E-peroxone treatment of synthetic water that contained $150 \mu\text{g L}^{-1}$ Br^- and 3mg L^{-1} total organic carbon (TOC). Reaction conditions: hydraulic retention time = 20 min; O_3 dose = 5.2mg L^{-1} . Error bars represent the standard deviation of duplicate experiments. Reprinted from Ref. [32], Copyright 2015, with permission from Elsevier

Due to the enhanced $\cdot\text{OH}$ production, the PE-peroxone process can considerably improve the kinetics of pollutant degradation and TOC mineralization compared to the single process (O_3 , UV, and electrolysis), as well as their binary combinations (UV/ O_3 , UV/ H_2O_2 , and the E-peroxone process). For example, it took less than 30 min for the PE-peroxone process to completely mineralize TOC from a mixture solution of substituted benzene (nitrobenzene, chlorobenzene, and benzaldehyde), whereas it took ~ 90 min for

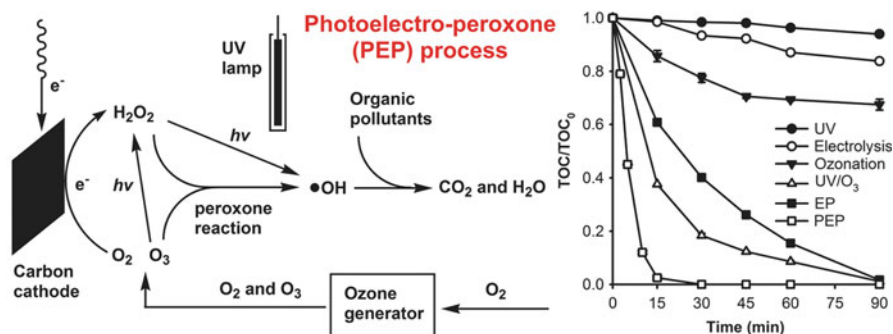
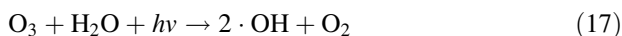


Fig. 6 Schematic representation of the main reaction mechanisms of the photoelectro-peroxone process and TOC mineralization from substituted benzene mixture solution by ozonation, UV, electrolysis, UV/O₃, E-peroxone, and photoelectro-peroxone (PE-peroxone) processes. Reaction conditions: initial concentration of nitrobenzene, chlorobenzene, and benzaldehyde = 10 mg L⁻¹, solution volume = 700 mL, sparging gas flow rate = 0.25 L min⁻¹, inlet O₃ gas phase concentration = 110 mg L⁻¹, current = 400 mA, UV fluence rate = 0.87 mW cm⁻². Reprinted from Ref. [17], Copyright 2016, with permission from Elsevier

the E-peroxone and UV/O₃ processes to achieve the similar extents of TOC mineralization. In addition, due to the multiple ways of ·OH generation and pollutant degradation (e.g., oxidation with O₃ and ·OH, anodic oxidation, and UV photolysis), the PE-peroxone process can maintain high kinetics and energy efficiencies for pollutant degradation under a variety of reaction conditions that may be unfavorable for other AOPs (e.g., low pH for O₃/H₂O₂ and high color and turbidity for UV/H₂O₂ processes) [17, 48–50]. Therefore, although the PE-peroxone process would require a more complex system design and higher capital investment than the more traditional AOPs such as O₃/H₂O₂, UV/O₃, and UV/H₂O₂, it may serve as a robust and effective option to treat wastewaters (e.g., landfill leachate and industrial effluents) that are problematic to treat by other AOPs.



3 Applications of the Electro-peroxone Process for Water and Wastewater Treatment

3.1 Electro-peroxone for Wastewater Treatment

O₃ is a highly selective oxidant and reacts preferentially with conjugated double bonds (e.g., N = N, C = O, and C = C) that are often the chromophores of dye molecules. Therefore, O₃ has been commonly used in dye wastewater treatment for decolorization purpose [1, 34]. As an ozone-based EAOP, the E-peroxone process

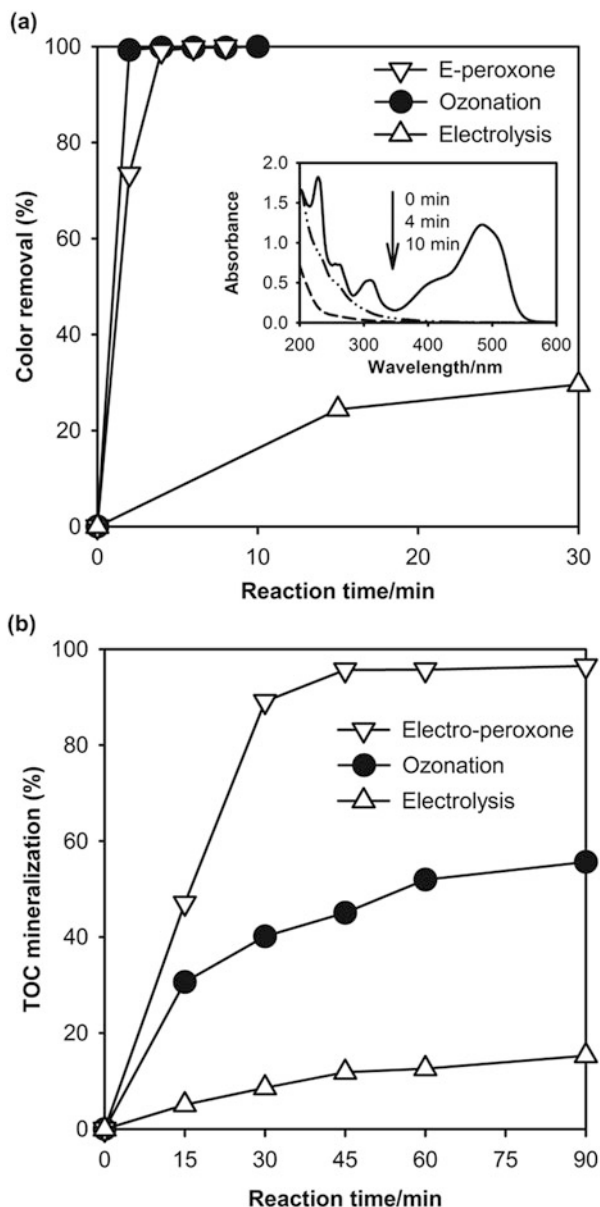
is also very effective at color removal. Figure 7a shows that similar to conventional ozonation, the E-peroxone process is capable of completely removing the color of a synthetic Orange II dye wastewater in a short reaction time (4 min) [34].

Due to the selective oxidation characteristics of O_3 , conventional ozonation is usually ineffective at TOC mineralization and can generate a variety of O_3 -resistant transformation products from the oxidative degradation of parent pollutants [1]. On the other hand, electrolysis usually needs long reaction time to completely mineralize pollutants from wastewater because the rate of pollutant degradation can be limited by the mass transfer of pollutants to the electrodes, and this limitation becomes increasingly severe as the pollutant concentrations decrease [3]. In contrast, by electrochemically producing H_2O_2 to enhance O_3 transformation to aqueous $\cdot OH$, which can then nonselectively and rapidly oxidize most organic pollutants in the bulk solution, the E-peroxone process can greatly enhance TOC mineralization as compared to conventional ozonation and electrolysis [19]. As Fig. 7b shows, only ~15% and ~56% TOC could be removed from the Orange II wastewater after 90 min of electrolysis and conventional ozonation treatment, respectively. In contrast, more than 95% TOC was removed after only 45 min of the E-peroxone process [34]. These results indicate that the E-peroxone process is very effective at both decolorization and TOC mineralization and can therefore provide a suitable technology for dye wastewater treatment.

Similar enhancement in TOC mineralization has also been observed during the E-peroxone treatment of a wide variety of wastewaters, such as landfill leachate [33], and wastewaters containing pharmaceuticals [26, 27, 47, 51], 1,4-dioxane [25, 48], aromatics [17, 52], and phenols [53, 54]. These results highlight that the E-peroxone process can successfully overcome the inherent limitations of conventional ozonation and electrolysis for pollutant degradation, i.e., the selective oxidation with O_3 and the limitation of pollutant mass transfer on their electrode degradation kinetics, and thus greatly improve the performance of wastewater treatment for pollutant degradation and TOC mineralization (Table 2).

Due to its high kinetics of pollutant degradation, the E-peroxone process can often reduce the energy consumption for water and wastewater treatment compared to conventional ozonation and electrolysis [20, 25, 55]. Figure 8 shows that after 2 h treatment, conventional ozonation and electrolysis with a boron-doped diamond (BDD) anode removed ~6% and 27% TOC from 1,4-dioxane solutions with a specific energy consumption (SEC) of 2.43 and 0.558 kWh g^{-1} $TOC_{removed}$, respectively. It is note that because O_3 is essentially unreactive with saturated carboxylic acids formed from 1,4-dioxane degradation, the SEC for ozonation increased sharply after 60 min. In contrast, the E-peroxone process almost completely removed the solution TOC (~97%) with a lower SEC of 0.376 kWh g^{-1} $TOC_{removed}$ [25]. In addition, because pollutants can be effectively oxidized by aqueous $\cdot OH$ generated primarily from the cathodically induced peroxone reaction, the E-peroxone process does not require potent but expensive anodes (e.g., BDD) to enhance pollutant degradation by anodic oxidation [19]. Therefore, cheap anode materials such as dimensionally stable anode (DSA) can be used to reduce the capital cost for the E-peroxone process [25, 47].

Fig. 7 (a) Decolorization and (b) TOC mineralization of synthetic Orange II wastewater by electrolysis, ozonation, and E-peroxone treatment. Reaction conditions: 400 mL of 0.05 M Na_2SO_4 electrolyte, 1 cm^2 Pt anode, 10 cm^2 carbon-PTFE cathode, current of 400 mA, sparging gas flow rate = 0.4 L min^{-1} , and inlet O_3 gas phase concentration = 118 mg L^{-1} . The *inset* plot shows the UV-vis spectral changes of Orange II solution with reaction time in the E-peroxone process. Reprinted from Ref. [34], Copyright 2013, with permission from Elsevier



3.2 Electro-peroxone for Advanced Wastewater Treatment

Over the past two decades, increasing emerging contaminants such as pharmaceuticals, pesticides, and industrial chemicals have been detected in the aquatic environment worldwide, which has raised considerable international concerns [56]. Municipal wastewater

Table 2 Examples of the E-peroxone and PE-peroxone process for water and wastewater treatment

Pollutants	Solutions	Processes	Reaction conditions	Comments	References
Methylene blue	0.05 M Na ₂ SO ₄	Ozonation ^a Electrolysis E-peroxone ^a	Volume = 0.4 L, C ₀ = 180 mg L ⁻¹ , O ₂ /O ₃ gas flow rate = 0.4 L min ⁻¹ , inlet O ₃ gas concentration = 75 mg L ⁻¹ , current = 500 mA, and carbon-PTFE cathode	TOC abatement of 93%, 22%, and 10% after 2 h of E-peroxone, ozonation, and electrolysis treatment, respectively	[16]
Orange II	0.05 M Na ₂ SO ₄	Ozonation ^a Electrolysis E-peroxone ^a	Volume = 0.4 L, C ₀ = 200 mg L ⁻¹ , O ₂ /O ₃ gas flow rate = 0.4 L min ⁻¹ , inlet O ₃ gas concentration = 118 mg L ⁻¹ , current = 400 mA, and carbon-PTFE cathode	Complete decolorization was obtained after 4 min of E-peroxone treatment; TOC abatement of 96%, 45%, and 12% after 45 min E-peroxone, ozonation, and electrolysis treatment, respectively	[34]
Ibuprofen	0.05 M Na ₂ SO ₄	Ozonation ^a Electrolysis E-peroxone ^a	Volume = 0.3 L, C ₀ = 20 mg L ⁻¹ , O ₂ /O ₃ gas flow rate = 0.25 L min ⁻¹ , inlet O ₃ gas concentration = 40 mg L ⁻¹ , current = 300 mA, carbon-PTFE cathode	Complete ibuprofen degradation was achieved after 7 and 30 min of E-peroxone and ozonation, respectively; TOC abatement of 100%, 42%, and 11% after 2 h of E-peroxone, ozonation, and electrolysis treatment, respectively	[26]
Venlafaxine	0.05 M Na ₂ SO ₄ , NaCl, or NaClO ₄	Ozonation ^a Electrolysis E-peroxone ^a	Volume = 0.3 L, C ₀ = 20 mg L ⁻¹ , O ₂ /O ₃ gas flow rate = 0.25 L min ⁻¹ , inlet O ₃ gas concentration = 20 mg L ⁻¹ , current = 200 mA, and carbon-PTFE cathode	Complete venlafaxine degradation and TOC mineralization after 3 and 120 min of the E-peroxone treatment; Faster venlafaxine degradation and TOC mineralization were obtained in the order of Na ₂ SO ₄ > NaCl > NaClO ₄ during the E-peroxone process	[27]
Oxalic acid	0.05 M Na ₂ SO ₄	Ozonation ^a Electrolysis E-peroxone ^a	Volume = 0.4 L, C ₀ = 2 mM, O ₂ /O ₃ gas flow rate = 0.4 L min ⁻¹ , inlet O ₃ gas concentration = 100 mg L ⁻¹ , current = 400 mA, carbon-PTFE cathode	TOC abatement of 95%, 3%, and 18% after 1 h of E-peroxone, ozonation, and electrolysis treatment, respectively	[19]
1,4-Dioxane	0.05 M Na ₂ SO ₄	Ozonation ^a Electrolysis E-peroxone ^a	Volume = 0.4 L, C ₀ = 200 mg L ⁻¹ , O ₂ /O ₃ gas flow rate = 0.3 L min ⁻¹ , inlet O ₃ gas concentration = 118 mg L ⁻¹ ,	After 2 h treatment, E-peroxone abated 97% TOC with a specific energy consumption (SEC) of 0.376 kWh g ⁻¹ TOC _{removed} , whereas ozonation and	[25]

Diethyl phthalate (DEP)	0.05 M Na ₂ SO ₄	E-peroxone with different cathodes ^a	current = 400 mA, and carbon-PTFE cathode Volume = 0.4 L, C ₀ = 20 mg L ⁻¹ , O ₂ /O ₃ gas flow rate = 0.4 L min ⁻¹ , inlet O ₃ gas concentration = 104 mg L ⁻¹ , current = 400 mA, carbon-PTFE, reticulated vitreous carbon, or carbon felt cathode Volume = 1.0 L, C ₀ = 200 mg L ⁻¹ , O ₂ /O ₃ gas flow rate = 0.4 L min ⁻¹ , inlet O ₃ gas concentration = 45 mg L ⁻¹ , current = 400 mA, pH = 7.8, and carbon brush cathode	electrolysis abated 6% and 27% TOC with SEC of 2.43 and 0.558 kWh g ⁻¹ TOC _{removed} , respectively TOC abatement of 92%, 85%, and 76% after 1 h of E-peroxone treatment with carbon-PTFE, reticulated vitreous carbon, and carbon felt cathode, respectively	[52]
Phenol	0.1 M Na ₂ SO ₄		Volume = 0.7 L, C ₀ = 10 mg L ⁻¹ for each compound, O ₂ /O ₃ gas flow rate = 0.25 L min ⁻¹ , inlet O ₃ gas concentration = 110 mg L ⁻¹ , current = 400 mA, UV fluence rate = 0.87 mW cm ⁻² , and carbon-PTFE cathode	Complete phenol degradation was similarly obtained after 30 min of E-peroxone and ozonation treatment; TOC abatement of 89% and 57% after 2 h of E-peroxone and ozonation treatment, respectively	[37]
Chlorobenzene Nitrobenzene Benzaldehyde	0.05 M Na ₂ SO ₄	UV/O ₃ ^a E-peroxone ^a PE-peroxone ^a	Volume = 0.6 L, C ₀ = 200 mg L ⁻¹ , O ₂ /O ₃ gas flow rate = 0.25 L min ⁻¹ , inlet O ₃ gas concentration = 85 mg L ⁻¹ , current = 400 mA, UV fluence rate = 0.87 mW cm ⁻² , and carbon-PTFE cathode	Complete TOC mineralization was obtained after 15 min of PE-peroxone treatment with a specific energy consumption (SEC) of 0.66 kWh g ⁻¹ TOC _{removed} , and after 90 min of E-peroxone and UV/O ₃ treatment with SEC of 1.07 and 3.56 kWh g ⁻¹ TOC _{removed} , respectively	[17]
1,4-Dioxane	0.05 M Na ₂ SO ₄ or 0.1 M NaCl	UV/O ₃ ^a E-peroxone ^a PE-peroxone ^a	Volume = 0.2 L, TOC ₀ = 1,650 mg L ⁻¹ , O ₂ /O ₃ gas flow rate = 0.3 L min ⁻¹ , inlet O ₃ gas concentration = 157 mg L ⁻¹ , current = 350 mA, and carbon-PTFE cathode	After 45 min treatment, PE-peroxone abated 98% TOC with an SEC of 0.30 kWh g ⁻¹ TOC _{removed} , whereas E-peroxone and UV/O ₃ abated 37% and 70% TOC with SEC of 0.22 and 0.38 kWh g ⁻¹ TOC _{removed} , respectively	[48]
Humic acid Fulvic acid	Landfill leachate	Ozonation ^a Electrolysis E-peroxone ^a		TOC abatement of 92%, 55%, and 20% after 6 h of E-peroxone, ozonation, and electrolysis treatment, respectively	[33]

(continued)

Table 2 (continued)

Pollutants	Solutions	Processes	Reaction conditions	Comments	References
Clofibric acid	Secondary effluent	E-peroxone with different anodes (Pt and BDD) ^a	Volume = 0.4 L, $C_0 = 1 \text{ mg L}^{-1}$, $\text{Cl}^- = 1.90 \text{ mM}$, O_2/O_3 gas flow rate = 0.25 L min^{-1} , inlet O_3 gas concentration = 38 mg L^{-1} , current density = 32 mA cm^{-2} , and carbon-PTFE cathode	Complete clofibric acid abatement was obtained after 1 h of E-peroxone with both anodes; E-peroxone with BDD anodes generated significantly more perchlorate (0.46 mM) than that with Pt anodes (undetectable) during the treatment	[47]
Diclofenac Gemfibrozil Bezafibrate Clofibric acid Ibuprofen	Secondary effluents	Ozonation ^a E-peroxone ^a	Volume = 0.4 L, $C_0 = 0.4 \text{ mg L}^{-1}$ for each pharmaceutical, O_2/O_3 gas flow rate = 0.25 L min^{-1} , inlet O_3 gas concentration = 6 mg L^{-1} , current = 80 mA , and carbon-PTFE cathode	E-peroxone reduced the reaction time and energy consumption required to abate >90% of all spiked pharmaceuticals from four secondary effluents compared to conventional ozonation	[20]
Methylisoborneol Geosmin	Surface water	Ozonation ^b E-peroxone ^b	Volume = 0.26 L , $C_0 = 10 \text{ } \mu\text{g L}^{-1}$ for each compound, bromide = $150 \text{ } \mu\text{g L}^{-1}$, specific ozone dose = $2 \text{ mg O}_3/\text{mg DOC}$, current = 40 mA , and carbon-PTFE cathode	E-peroxone significantly accelerated methylisoborneol and geosmin abatement (5 min) and moderately increased their abatement efficiencies by ~10% compared to conventional ozonation (40 min); Significantly less bromate was generated during E-peroxone ($8.2 \text{ } \mu\text{g L}^{-1}$) than during ozonation ($76.1 \text{ } \mu\text{g L}^{-1}$)	[31]
Natural organic matter (NOM)	Surface water	Ozonation ^c E-peroxone ^c	$\text{DOC}_0 = 6.1 \text{ mg L}^{-1}$, bromide = $150 \text{ } \mu\text{g L}^{-1}$, hydraulic retention time of 20 min, and carbon-PTFE cathode	E-peroxone decreased DOC to 3.1 mg L^{-1} and completely inhibited bromate formation compared to ozonation (5 mg L^{-1} DOC and ~60 $\text{ } \mu\text{g L}^{-1}$ bromate); Energy consumption was 0.190 and 0.117 kWh m^{-3} for E-peroxone and ozonation, respectively	[32]

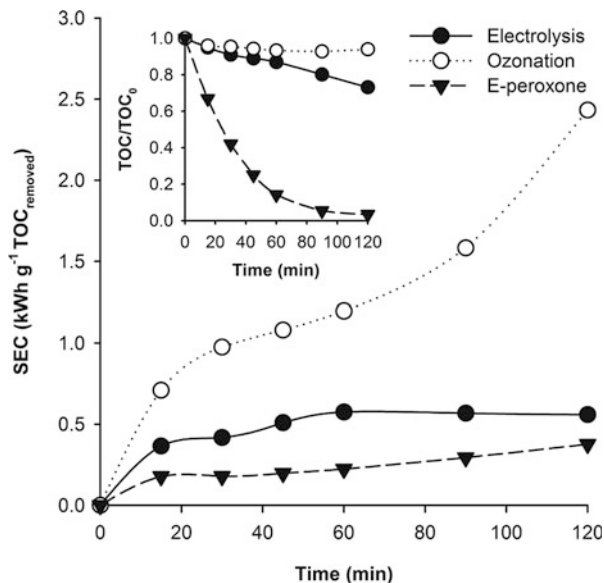
^aSemi-batch reactor with continuous O_2/O_3 gas sparging^bBatch reactor with addition of O_3 stock solutions^cContinuous flow reactor (simulating real ozone reactor)

treatment plants (WWTPs) have been identified as hotspots for the release of these emerging contaminants into the environment [1, 57]. To protect the aquatic environment, ozonation has been extensively investigated as a promising advanced wastewater treatment option for the removal of emerging contaminants from secondary effluents of WWTPs [1]. However, due to the selective oxidation characteristics of O_3 , conventional ozonation often cannot ensure the effective removal of O_3 -resistant pollutants, although a non-negligible removal degree can still be obtained for these compounds via indirect oxidation with $\cdot OH$ formed from O_3 decomposition with water matrix such as effluent organic matter (EfOM) [1]. Figure 9 shows that while ozone-reactive pollutants (e.g., diclofenac and gemfibrozil) could be rapidly oxidized by O_3 from a secondary effluent within 2 min of conventional ozonation, ozone-resistant pollutants (e.g., clofibric acid and ibuprofen) required much longer reaction time (~ 15 min) to be removed [20]. In comparison, by in situ producing H_2O_2 from cathodic O_2 reduction to enhance O_3 transformation to $\cdot OH$, the E-peroxone process significantly reduced the reaction time required to effectively remove the O_3 -resistant pollutants (< 10 min). This result suggests that shorter reaction time can be used during advanced wastewater treatment by the E-peroxone process than by conventional ozonation. In addition, due to the acceleration of O_3 -resistant pollutant removal, the E-peroxone process actually reduced the energy consumption required to remove 90% of all (or most) pharmaceuticals from secondary effluents (i.e., electrical energy per log-order removal (EEO), $kWh\ m^{-3}\text{-log}$) as compared to conventional ozonation (see Table 3) [20, 55]. These promising results indicate that the E-peroxone process may provide a convenient and effective way to improve the performance of existing ozonation systems for advanced wastewater treatment in WWTPs.

3.3 *Electro-peroxone for Drinking Water Treatment*

During algal bloom episodes, high concentrations of taste and odor (T&O) compounds such as 2-methylisoborneol (MIB) and geosmin can often be found in surface waters that serve as drinking water sources. To adequately abate T&O compounds, higher ozone doses than those typically used in routine drinking water treatment (e.g., 0.5–1.0 mg O_3 /mg dissolved organic carbon (DOC)) are required during algal bloom periods. However, the increase of ozone doses may lead to exceeding bromate formation even if the source water contains moderate concentrations of bromide (e.g., $> 50\ \mu g\ L^{-1}$) [1, 24, 58]. As shown in Fig. 10, while increasing applied ozone doses enhanced MIB and geosmin abatement in a surface water by conventional ozonation, this approach resulted in significant bromate formation beyond the drinking water standard ($10\ \mu g\ L^{-1}$) [31]. In comparison, by electrochemically producing H_2O_2 to enhance the transformation of O_3 to $\cdot OH$ and the reduction of $HBrO$ to Br^- [32], the E-peroxone process allowed higher ozone doses (3.8–5.1 mg O_3 /mg DOC) to be used to enhance MIB and geosmin abatement while still keeping BrO_3^- formation at much lower levels (Fig. 10c). The in situ electro-generation of H_2O_2 provides a convenient and simple way to supply H_2O_2 on demand during

Fig. 8 TOC mineralization and specific energy consumption (SEC) for TOC mineralization during ozonation, electrolysis (using 12.5 cm² BDD anode), and E-peroxone (using 20 cm² Pt/Ti anode) processes. Reaction conditions: 20 cm² carbon-PTFE cathode, inlet O₃ gas phase concentration = 118 mg L⁻¹, sparging gas flow rate = 0.3 L min⁻¹, and current = 400 mA. Reprinted from Ref. [25], Copyright 2015, with permission from Elsevier



ozonation. Therefore, the E-peroxone process may serve as an attractive backup for conventional ozonation to improve the performance of pollutant degradation and bromate control, e.g., during emergency situations and seasonal events such as chemical spills and algal blooms, when high ozone doses are required to enhance the abatement of pollutants of concern.

3.4 *Electro-peroxone Regeneration of Spent Activated Carbon*

In addition to directly treating water and wastewater, the peroxone process may also provide an attractive way to regenerate spent activated carbon saturated with organic pollutants [53, 54]. In recent years, electrochemical regeneration has been proposed as a promising way to regenerate organic-saturated activated carbon [59, 60]. However, the desorbed pollutants cannot be effectively mineralized during the electrochemical regeneration, whose effluents thus still require further treatment. For example, Fig. 11 shows that while the cathodic regeneration could effectively restore ~95% of the adsorption capacity of a *p*-nitrophenol (PNP) saturated activated carbon fiber (ACF) by cathodically induced desorption, the desorbed pollutants accumulated in the solution, resulting in a high residual TOC at the end of the cathodic regeneration. In contrast, the E-peroxone process successfully coupled the cathodically induced desorption and the peroxone-driven mineralization together and thus achieved simultaneous regeneration of saturated adsorbent (regeneration efficiency (RE) >90%) and mineralization of desorbed pollutants [53]. Notably, during the E-peroxone

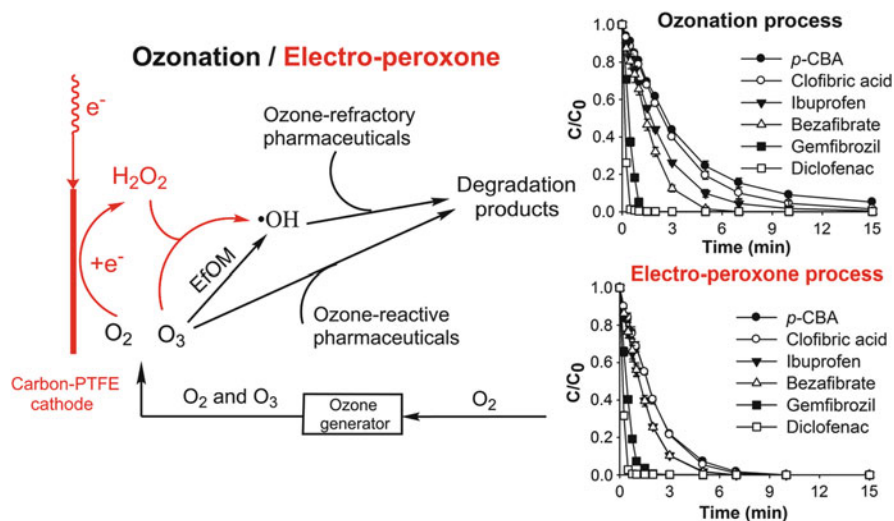


Fig. 9 Mechanisms and kinetics for pharmaceutical removal from a secondary effluent ($\text{DOC} = 3.2 \text{ mg L}^{-1}$) by conventional ozonation and the E-peroxone process. Reaction conditions: solution volume = 400 mL, 6 cm^2 Pt anode, 10 cm^2 carbon-PTFE cathode, current = 80 mA, inlet O_3 gas phase concentration = 6 mg L^{-1} , and sparging gas flow rate = 250 mL min^{-1} . Reprinted from Ref. [20], Copyright 2016, with permission from Elsevier

regeneration, the cathode can provide a cathodic protection for the ACF to resist O_3 and $\cdot\text{OH}$ oxidation, which occurred significantly during ozone-regeneration [53, 54]. Therefore, in contrast to ozone-regeneration, the E-peroxone regeneration did not cause considerable modifications to the structural and chemical properties of ACF. As a result, the E-peroxone regenerated ACF could still retain more than 90% of the adsorption capacity of the virgin control after 12 cycles of PNP adsorption and E-peroxone regeneration [53]. These promising results suggest that the E-peroxone process may provide an attractive alternative to regenerate spent activated carbon and extend the lifetime of valuable adsorbent materials for water and wastewater treatment.

4 Concluding Remarks

4.1 Potentials of the Electro-peroxone Process for Water and Wastewater Treatment

The E-peroxone process is a new EAOP that has only been developed for several years. However, it has exhibited great potentiality for practical applications because it can considerably improve the performance of water and wastewater treatment in many aspects. Overall, the following features of the E-peroxone process make it an attractive option for oxidative water and wastewater treatment:

Table 3 Energy consumption required to remove 90% of all spiked pharmaceuticals (diclofenac, gemfibrozil, bezafibrate, ibuprofen, clofibrac acid, and *p*-CBA) from four secondary effluents (SE) by conventional ozonation and the E-peroxone process [20]

Sample	Water quality parameters				Energy consumption (kWh m ⁻³)	
	pH	DOC (mg L ⁻¹)	HCO ₃ ⁻ (mg L ⁻¹)	Total OH scavenging rate (s ⁻¹)	Ozonation	E-peroxone
SE-1	8.09	3.2	257	1.25 × 10 ⁵	0.62	0.30
SE-2	8.19	5.8	151	1.74 × 10 ⁵	0.41	0.33
SE-3	8.15	7.6	339	2.52 × 10 ⁵	0.68	0.55
SE-4	8.2	15.4	272	4.68 × 10 ⁵	2.59	2.49

- Easy upgrade from conventional ozonation
By simply installing low-cost electrodes in ozone contactors, existing ozonation systems that are widely used in water and wastewater utilities can be conveniently retrofitted for the E-peroxone system with minimal upgrade work and costs.
- High kinetics and energy efficiency for pollutant degradation
Compared with conventional ozonation, the E-peroxone process can significantly accelerate the kinetics of pollutant degradation and TOC mineralization and thus considerably reduce reaction time and energy consumption required for water and wastewater treatment.
- Reduced bromate formation
By in situ generating H₂O₂ from cathodic O₂ reduction, the E-peroxone process can significantly reduce bromate formation during the treatment of bromide-containing water, which is a major concern associated with conventional ozonation for drinking water treatment.
- Easy operation and automation
As an electricity-driven process, the E-peroxone process can produce all oxidants (e.g., O₃, H₂O₂, and ·OH) on site at controllable rates according to the requirement of water and wastewater treatment.
- Environmental friendliness
The E-peroxone process needs only clean oxygen and electricity to operate. No chemicals or catalysts that may cause secondary pollution are added in the E-peroxone process.

4.2 Future Research Directions

While many promising results have been shown for the E-peroxone process, as a new AOP, it still needs much research before its real applications in water and wastewater treatment. Several important issues that have yet to be investigated for the E-peroxone process include:

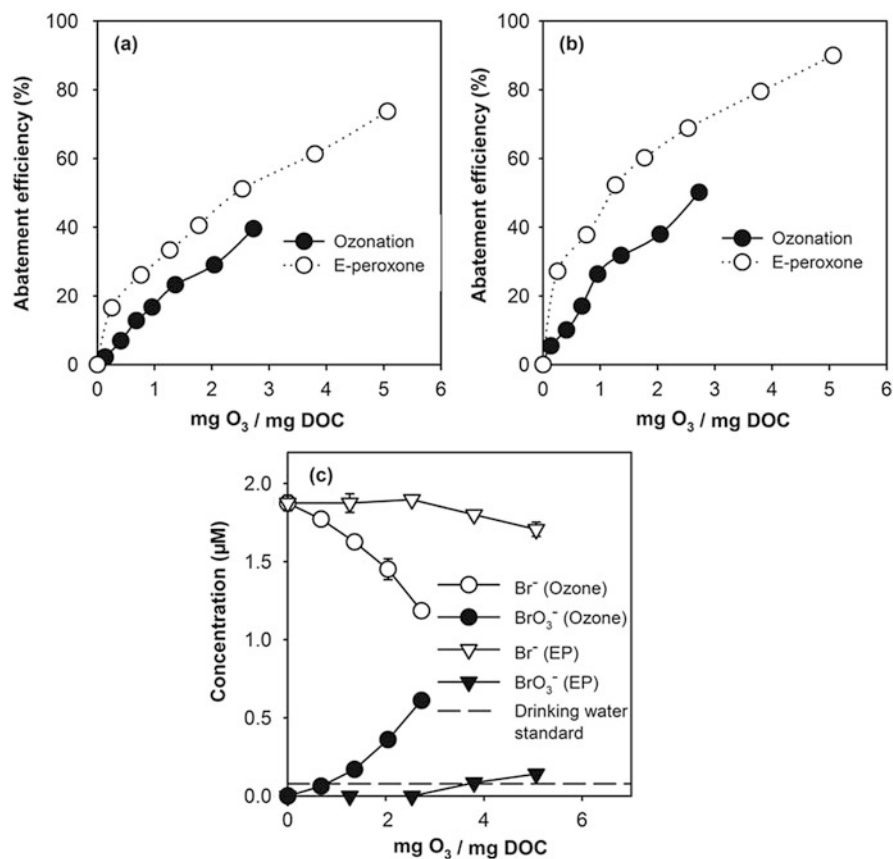


Fig. 10 Abatement of (a) 2-methylisoborneol (MIB) and (b) geosmin and (c) transformation of Br⁻ to BrO₃⁻ as a function of ozone dose during semi-batch conventional ozonation and E-peroxone treatment of a surface water (DOC = 2.35 mg L⁻¹). Reaction conditions: solution volume = 260 mL, 6 cm² Pt anode, 10 cm² carbon-PTFE cathode, pH = 8.1, temperature = 23 ± 1°C, inlet O₃ gas phase concentration = 3 mg L⁻¹, sparging gas flow rate = 0.17 L min⁻¹, and current = 40 mA. Reprinted from Ref. [31], Copyright 2017, with permission from Elsevier

- Disinfection performance

Ozone can be used as both oxidant and disinfectant in water and wastewater treatment. While the electro-generation of H₂O₂ can enhance O₃ transformation to ·OH, thus improving the oxidation capacity of the E-peroxone process, it decreases O₃ concentrations in the solution. This may lead to a reduction in the disinfection efficiency of the E-peroxone process as compared to conventional ozonation, similar to the findings previously reported for conventional peroxone (O₃/H₂O₂) process [24]. Therefore, more studies are needed to evaluate and optimize the disinfection performance of the E-peroxone process if disinfection is of concern in some applications.

- Formation and control of chloride-derived by-products

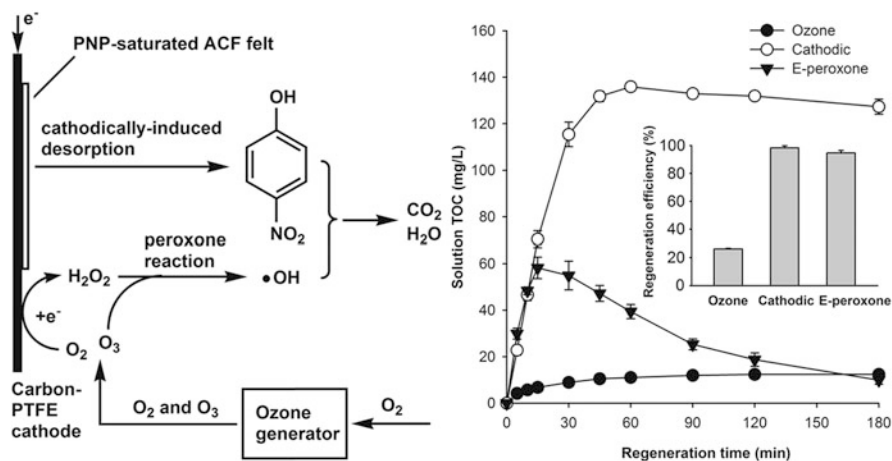


Fig. 11 Schematic representation of the main mechanisms involved in the E-peroxone regeneration of *p*-nitrophenol (PNP) saturated activated carbon fiber (ACF), and comparison of TOC evolution and regeneration efficiencies for the ozone, cathodic, and E-peroxone regeneration. Reaction conditions: 400 mL of 0.05 M Na_2SO_4 electrolyte, 4 cm^2 Pt anode, 20 cm^2 carbon-PTFE cathode, 0.25 g ACF, current = 400 mA, inlet O_3 gas phase concentration = 65 $mg L^{-1}$, sparging gas flow rate = 0.4 $L min^{-1}$, and regeneration time = 3 h. Adapted from Ref. [53], Copyright 2016, with permission from Elsevier

While the E-peroxone process can effectively reduce the formation of bromate compared to conventional ozonation, it may increase the formation of chloride-derived by-products. Chloride (Cl^-) is ubiquitously present in various source waters. During conventional ozonation, the formation of undesired chloride-derived by-products is usually negligible because neither O_3 nor $\bullet OH$ can practically convert Cl^- [24]. However, Cl^- can be electrochemically oxidized to oxychlorine species (e.g., ClO^- , ClO_2^- , and ClO_3^-) at the anode during electrolytic water treatment, which may lead to the formation of chlorinated organic by-products from the ensuing reaction of ClO^- with organic solutes (e.g., NOM) [3]. Due to the complex effects of water matrix and interactions between the electrode and bulk reactions involved in the E-peroxone process [47], more works are needed to systematically evaluate the formation mechanisms and control strategies of chloride-derived by-products during the E-peroxone process.

- Pilot-scale evaluation of the E-peroxone process

Up to date, most studies on the E-peroxone process have been conducted at laboratory scale. Although these laboratory works can provide important information regarding reaction kinetics and mechanisms, effects of water matrix, energy efficiency, etc., pilot-scale studies have yet to be conducted under more realistic conditions of water and wastewater treatment to better evaluate the long-term performance and economic feasibility (e.g., the stability of electrodes and cost-effectiveness) of the E-peroxone process for real applications.

References

1. von Sonntag C, von Gunten U (2012) Chemistry of ozone in water and wastewater treatment. From basic principles to applications, vol EPFL-BOOK-181142. IWA Publishing, London
2. Brillas E, Martínez-Huitle CA (2015) Decontamination of wastewaters containing synthetic organic dyes by electrochemical methods. An updated review. *Appl Catal Environ* 166–167 (0):603–643. doi:[10.1016/j.apcatb.2014.11.016](https://doi.org/10.1016/j.apcatb.2014.11.016)
3. Panizza M, Cerisola G (2009) Direct and mediated anodic oxidation of organic pollutants. *Chem Rev* 109(12):6541–6569. doi:[10.1021/Cr9001319](https://doi.org/10.1021/Cr9001319)
4. Oturan MA, Aaron JJ (2014) Advanced oxidation processes in water/wastewater treatment: principles and applications. A review. *Crit Rev Environ Sci Technol* 44(23):2577–2641. doi:[10.1080/10643389.2013.829765](https://doi.org/10.1080/10643389.2013.829765)
5. Sires I, Brillas E, Oturan MA, Rodrigo MA, Panizza M (2014) Electrochemical advanced oxidation processes: today and tomorrow. A review. *Environ Sci Pollut R* 21(14):8336–8367. doi:[10.1007/s11356-014-2783-1](https://doi.org/10.1007/s11356-014-2783-1)
6. Glaze WH (1987) Drinking-water treatment with ozone. *Environ Sci Technol* 21(3):224–230. doi:[10.1021/es00157a001](https://doi.org/10.1021/es00157a001)
7. Legrini O, Oliveros E, Braun AM (1993) Photochemical processes for water-treatment. *Chem Rev* 93(2):671–698. doi:[10.1021/cr00018a003](https://doi.org/10.1021/cr00018a003)
8. Buxton GV, Greenstock CL, Helman WP, Ross AB (1988) Critical review of rate constants for reactions of hydrated electrons, hydrogen atoms and hydroxyl radicals ($\cdot\text{OH}/\text{O}^-$) in aqueous solution. *J Phys Chem Ref Data Monogr* 17(2):513–886. doi:[10.1063/1.555805](https://doi.org/10.1063/1.555805)
9. Campos-Martin JM, Blanco-Brieva G, Fierro JLG (2006) Hydrogen peroxide synthesis: an outlook beyond the anthraquinone process. *Angew Chem Int Ed* 45(42):6962–6984. doi:[10.1002/anie.200503779](https://doi.org/10.1002/anie.200503779)
10. Brillas E, Sires I, Oturan MA (2009) Electro-Fenton process and related electrochemical technologies based on Fenton's reaction chemistry. *Chem Rev* 109(12):6570–6631. doi:[10.1021/Cr900136g](https://doi.org/10.1021/Cr900136g)
11. Zhu X, Logan BE (2013) Using single-chamber microbial fuel cells as renewable power sources of electro-Fenton reactors for organic pollutant treatment. *J Hazard Mater* 252–253:198–203. doi:[10.1016/j.jhazmat.2013.02.051](https://doi.org/10.1016/j.jhazmat.2013.02.051)
12. Barazesh JM, Hennebel T, Jasper JT, Sedlak DL (2015) Modular advanced oxidation process enabled by cathodic hydrogen peroxide production. *Environ Sci Technol* 49(12):7391–7399. doi:[10.1021/acs.est.5b01254](https://doi.org/10.1021/acs.est.5b01254)
13. Rosenfeldt EJ, Linden KG, Canonica S, von Gunten U (2006) Comparison of the efficiency of OH radical formation during ozonation and the advanced oxidation processes $\text{O}_3/\text{H}_2\text{O}_2$ and $\text{UV}/\text{H}_2\text{O}_2$. *Water Res* 40(20):3695–3704. doi:[10.1016/j.watres.2006.09.008](https://doi.org/10.1016/j.watres.2006.09.008)
14. Katsoyiannis IA, Canonica S, von Gunten U (2011) Efficiency and energy requirements for the transformation of organic micropollutants by ozone, $\text{O}_3/\text{H}_2\text{O}_2$ and $\text{UV}/\text{H}_2\text{O}_2$. *Water Res* 45 (13):3811–3822. doi:[10.1016/j.watres.2011.04.038](https://doi.org/10.1016/j.watres.2011.04.038)
15. Frangos P, Shen WH, Wang HJ, Li X, Yu G, Deng SB, Huang J, Wang B, Wang YJ (2016) Improvement of the degradation of pesticide deethylatrazine by combining UV photolysis with electrochemical generation of hydrogen peroxide. *Chem Eng J* 291:215–224. doi:[10.1016/j.cej.2016.01.089](https://doi.org/10.1016/j.cej.2016.01.089)
16. Yuan S, Li ZX, Wang YJ (2013) Effective degradation of methylene blue by a novel electrochemically driven process. *Electrochem Commun* 29:48–51. doi:[10.1016/j.elecom.2013.01.012](https://doi.org/10.1016/j.elecom.2013.01.012)
17. Frangos P, Wang HJ, Shen WH, Yu G, Deng SB, Huang J, Wang B, Wang YJ (2016) A novel photoelectro-peroxone process for the degradation and mineralization of substituted benzenes in water. *Chem Eng J* 286:239–248. doi:[10.1016/j.cej.2015.10.096](https://doi.org/10.1016/j.cej.2015.10.096)
18. Brillas E, Mur E, Casado J (1996) Iron(II) catalysis of the mineralization of aniline using a carbon-PTFE O_2 -fed cathode. *J Electrochem Soc* 143(3):L49–L53

19. Wang HJ, Yuan S, Zhan JH, Wang YJ, Yu G, Deng SB, Huang J, Wang B (2015) Mechanisms of enhanced total organic carbon elimination from oxalic acid solutions by electro-peroxone process. *Water Res* 80:20–29. doi:[10.1016/j.watres.2015.05.024](https://doi.org/10.1016/j.watres.2015.05.024)
20. Yao WK, Wang XF, Yang HW, Yu G, Deng SB, Huang J, Wang B, Wang YJ (2016) Removal of pharmaceuticals from secondary effluents by an electro-peroxone process. *Water Res* 88:826–835. doi:[10.1016/j.watres.2015.11.024](https://doi.org/10.1016/j.watres.2015.11.024)
21. Li XZ, Liu HS (2005) Development of an E-H₂O₂/TiO₂ photoelectrocatalytic oxidation system for water and wastewater treatment. *Environ Sci Technol* 39(12):4614–4620. doi:[10.1021/es048276k](https://doi.org/10.1021/es048276k)
22. Oturan MA, Peiroten J, Chartrin P, Acher AJ (2000) Complete destruction of p-nitrophenol in aqueous medium by electro-Fenton method. *Environ Sci Technol* 34(16):3474–3479
23. von Gunten U (2003) Ozonation of drinking water: part I. Oxidation kinetics and product formation. *Water Res* 37(7):1443–1467. doi:[10.1016/S0043-1354\(02\)00457-8](https://doi.org/10.1016/S0043-1354(02)00457-8)
24. von Gunten U (2003) Ozonation of drinking water: part II. Disinfection and by-product formation in presence of bromide, iodide or chlorine. *Water Res* 37(7):1469–1487. doi:[10.1016/S0043-1354\(02\)00458-X](https://doi.org/10.1016/S0043-1354(02)00458-X)
25. Wang HJ, Bakheet B, Yuan S, Li X, Yu G, Murayama S, Wang YJ (2015) Kinetics and energy efficiency for the degradation of 1,4-dioxane by electro-peroxone process. *J Hazard Mater* 294:90–98. doi:[10.1016/j.jhazmat.2015.03.058](https://doi.org/10.1016/j.jhazmat.2015.03.058)
26. Li X, Wang YJ, Yuan S, Li ZX, Wang B, Huang J, Deng SB, Yu G (2014) Degradation of the anti-inflammatory drug ibuprofen by electro-peroxone process. *Water Res* 63:81–93. doi:[10.1016/j.watres.2014.06.009](https://doi.org/10.1016/j.watres.2014.06.009)
27. Li X, Wang YJ, Zhao J, Wang HJ, Wang B, Huang J, Deng SB, Yu G (2015) Electro-peroxone treatment of the antidepressant venlafaxine: operational parameters and mechanism. *J Hazard Mater* 300:298–306. doi:[10.1016/j.jhazmat.2015.07.004](https://doi.org/10.1016/j.jhazmat.2015.07.004)
28. WHO G (2011) Guidelines for drinking water quality. World Health Organization, Geneva
29. USEPA (1998) National primary drinking water regulations: disinfectants and disinfection byproducts – final rule. Federal Register, vol 63
30. European Union (1998) Council directive 98/83/EC of 3 November 1998 on the quality of water intended for human consumption. European Union, Brussels
31. Yao W, Qu Q, von Gunten U, Chen C, Yu G, Wang Y (2017) Comparison of methylisoborneol and geosmin abatement in surface water by conventional ozonation and an electro-peroxone process. *Water Res* 108:373–382. doi:[10.1016/j.watres.2016.11.014](https://doi.org/10.1016/j.watres.2016.11.014)
32. Li YK, Shen WH, SJ F, Yang HW, Yu G, Wang YJ (2015) Inhibition of bromate formation during drinking water treatment by adapting ozonation to electro-peroxone process. *Chem Eng J* 264:322–328. doi:[10.1016/j.cej.2014.11.120](https://doi.org/10.1016/j.cej.2014.11.120)
33. Li ZX, Yuan S, Qiu CC, Wang YJ, Pan XJ, Wang JL, Wang CW, Zuo JA (2013) Effective degradation of refractory organic pollutants in landfill leachate by electro-peroxone treatment. *Electrochim Acta* 102:174–182. doi:[10.1016/j.electacta.2013.04.034](https://doi.org/10.1016/j.electacta.2013.04.034)
34. Bakheet B, Yuan S, Li ZX, Wang HJ, Zuo JN, Komarneni S, Wang YJ (2013) Electro-peroxone treatment of Orange II dye wastewater. *Water Res* 47(16):6234–6243. doi:[10.1016/j.watres.2013.07.042](https://doi.org/10.1016/j.watres.2013.07.042)
35. Haynes WM (2014) CRC handbook of chemistry and physics, 95th edn. CRC Press, Boca Raton, FL
36. Kishimoto N, Morita Y, Tsuno H, Oomura T, Mizutani H (2005) Advanced oxidation effect of ozonation combined with electrolysis. *Water Res* 39(19):4661–4672. doi:[10.1016/j.watres.2005.09.001](https://doi.org/10.1016/j.watres.2005.09.001)
37. Xia G, Wang Y, Wang B, Huang J, Deng S, Yu G (2017) The competition between cathodic oxygen and ozone reduction and its role in dictating the reaction mechanisms of an electro-peroxone process. *Water Res* 118:26–38. doi:[10.1016/j.watres.2017.04.005](https://doi.org/10.1016/j.watres.2017.04.005)
38. Šljukić B, Banks C, Compton R (2005) An overview of the electrochemical reduction of oxygen at carbon-based modified electrodes. *J Iran Chem Soc* 2(1):1–25

39. Sein MM, Golloch A, Schmidt TC, von Sonntag C (2007) No marked kinetic isotope effect in the peroxone ($\text{H}_2\text{O}_2/\text{D}_2\text{O}_2+\text{O}_3$) reaction: mechanistic consequences. *ChemPhysChem* 8 (14):2065–2067. doi:[10.1002/cphc.200700493](https://doi.org/10.1002/cphc.200700493)
40. Fischbacher A, von Sonntag J, von Sonntag C, Schmidt TC (2013) The $\cdot\text{OH}$ radical yield in the $\text{H}_2\text{O}_2+\text{O}_3$ (peroxone) reaction. *Environ Sci Technol* 47(17):9959–9964. doi:[10.1021/es402305r](https://doi.org/10.1021/es402305r)
41. Nöthe T, Fahlenkamp H, CV S (2009) Ozonation of wastewater: rate of ozone consumption and hydroxyl radical yield. *Environ Sci Technol* 43(15):5990–5995. doi:[10.1021/es900825f](https://doi.org/10.1021/es900825f)
42. Flyunt R, Leitzke A, Mark G, Mvula E, Reisz E, Schick R, von Sonntag C (2003) Determination of $\cdot\text{OH}$, $\text{O}_2^{\cdot-}$, and hydroperoxide yields in ozone reactions in aqueous solution. *J Phys Chem B* 107(30):7242–7253. doi:[10.1021/jp022455b](https://doi.org/10.1021/jp022455b)
43. Lee Y, Kovalova L, McArdell CS, von Gunten U (2014) Prediction of micropollutant elimination during ozonation of a hospital wastewater effluent. *Water Res* 64(0):134–148. doi:[10.1016/j.watres.2014.06.027](https://doi.org/10.1016/j.watres.2014.06.027)
44. Pocostales JP, Sein MM, Knolle W, von Sonntag C, Schmidt TC (2010) Degradation of ozone-refractory organic phosphates in wastewater by ozone and ozone/hydrogen peroxide (peroxone): the role of ozone consumption by dissolved organic matter. *Environ Sci Technol* 44 (21):8248–8253. doi:[10.1021/es1018288](https://doi.org/10.1021/es1018288)
45. von Gunten U, Hoigne J (1994) Bromate formation during ozonation of bromide-containing waters: interaction of ozone and hydroxyl radical reactions. *Environ Sci Technol* 28(7):1234–1242. doi:[10.1021/es00056a009](https://doi.org/10.1021/es00056a009)
46. von Gunten U, Oliveras Y (1997) Kinetics of the reaction between hydrogen peroxide and hypobromous acid: implication on water treatment and natural systems. *Water Res* 31 (4):900–906. doi:[10.1016/s0043-1354\(96\)00368-5](https://doi.org/10.1016/s0043-1354(96)00368-5)
47. Lin ZR, Yao WK, Wang YJ, Yu G, Deng SB, Huang J, Wang B (2016) Perchlorate formation during the electro-peroxone treatment of chloride-containing water: effects of operational parameters and control strategies. *Water Res* 88:691–702. doi:[10.1016/j.watres.2015.11.005](https://doi.org/10.1016/j.watres.2015.11.005)
48. Shen W, Wang Y, Zhan J, Wang B, Huang J, Deng S, Yu G (2017) Kinetics and operational parameters for 1,4-dioxane degradation by the photoelectro-peroxone process. *Chem Eng J* 310(Part 1):249–258. doi:[10.1016/j.cej.2016.10.111](https://doi.org/10.1016/j.cej.2016.10.111)
49. Bessegato GG, Cardoso JC, da Silva BF, Zanoni MVB (2016) Combination of photoelectrocatalysis and ozonation: a novel and powerful approach applied in acid yellow 1 mineralization. *Appl Catal Environ* 180:161–168. doi:[10.1016/j.apcatb.2015.06.013](https://doi.org/10.1016/j.apcatb.2015.06.013)
50. Mena E, Rey A, Acedo B, Beltran FJ, Malato S (2012) On ozone-photocatalysis synergism in black-light induced reactions: oxidizing species production in photocatalytic ozonation versus heterogeneous photocatalysis. *Chem Eng J* 204:131–140. doi:[10.1016/j.cej.2012.07.076](https://doi.org/10.1016/j.cej.2012.07.076)
51. Guo WQ, QL W, Zhou XJ, Cao HO, JS D, Yin RL, Ren NQ (2015) Enhanced amoxicillin treatment using the electro-peroxone process: key factors and degradation mechanism. *RSC Adv* 5(65):52695–52702. doi:[10.1039/c5ra07951a](https://doi.org/10.1039/c5ra07951a)
52. Hou MF, Chu YF, Li X, Wang HJ, Yao WK, Yu G, Murayama S, Wang YJ (2016) Electro-peroxone degradation of diethyl phthalate: cathode selection, operational parameters, and degradation mechanisms. *J Hazard Mater* 319:61–68. doi:[10.1016/j.jhazmat.2015.12.054](https://doi.org/10.1016/j.jhazmat.2015.12.054)
53. Zhan JH, Wang HJ, Pan XJ, Wang JL, Yu G, Deng SB, Huang J, Wang B, Wang YJ (2016) Simultaneous regeneration of p-nitrophenol-saturated activated carbon fiber and mineralization of desorbed pollutants by electro-peroxone process. *Carbon* 101:399–408. doi:[10.1016/j.carbon.2016.02.023](https://doi.org/10.1016/j.carbon.2016.02.023)
54. Zhan JH, Wang YJ, Wang HJ, Shen WH, Pan XJ, Wang JL, Yu G (2016) Electro-peroxone regeneration of phenol-saturated activated carbon fiber: the effects of irreversible adsorption and operational parameters. *Carbon* 109:321–330. doi:[10.1016/j.carbon.2016.08.034](https://doi.org/10.1016/j.carbon.2016.08.034)
55. Yao W, Lin Z, von Gunten U, Yang H, Yu G, Wang Y. Pilot-scale evaluation of an electro-peroxone process for pharmaceutical abatements (in preparation)
56. Schwarzenbach RP, Escher BI, Fenner K, Hofstetter TB, Johnson CA, von Gunten U, Wehrli B (2006) The challenge of micropollutants in aquatic systems. *Science* 313(5790):1072–1077. doi:[10.1126/science.1127291](https://doi.org/10.1126/science.1127291)

57. Michael I, Rizzo L, McArdell CS, Manaia CM, Merlin C, Schwartz T, Dagot C, Fatta-Kassinos D (2013) Urban wastewater treatment plants as hotspots for the release of antibiotics in the environment: a review. *Water Res* 47(3):957–995. doi:[10.1016/j.watres.2012.11.027](https://doi.org/10.1016/j.watres.2012.11.027)
58. Mizuno T, Ohara S, Nishimura F, Tsuno H (2011) O₃/H₂O₂ process for both removal of odorous algal-derived compounds and control of bromate ion formation. *Ozone Sci Eng* 33 (2):121–135. doi:[10.1080/01919512.2011.548200](https://doi.org/10.1080/01919512.2011.548200)
59. Narbaitz RM, Cen JQ (1994) Electrochemical regeneration of granular activated carbon. *Water Res* 28(8):1771–1778. doi:[10.1016/0043-1354\(94\)90250-X](https://doi.org/10.1016/0043-1354(94)90250-X)
60. Berenguer R, Marco-Lozar JP, Quijada C, Cazorla-Amoros D, Morallon E (2010) Electrochemical regeneration and porosity recovery of phenol-saturated granular activated carbon in an alkaline medium. *Carbon* 48(10):2734–2745. doi:[10.1016/j.carbon.2010.03.071](https://doi.org/10.1016/j.carbon.2010.03.071)

Heterogeneous Electro-Fenton Process: Principles and Applications

P.V. Nidheesh, H. Olvera-Vargas, N. Oturan, and M.A. Oturan

Abstract Electro-Fenton (EF) process has received much attention among the various advanced oxidation process, due to its higher contaminant removal and mineralization efficiencies, simplicity in operation, in situ generation of hydrogen peroxide, etc. Heterogeneous EF process rectifies some of the drawbacks of conventional EF process by using solid catalyst for the generation of reactive hydroxyl radicals in water medium. The efficiency of various heterogeneous EF catalysts such as iron oxides, pyrite, iron supported on zeolite, carbon, alginate beads, etc. was tested by various researchers. All of these catalysts are insoluble in water; and most of them are stable and reusable in nature. Depending on the iron leaching characteristics, hydroxyl radicals are generated either in the solution or over the catalyst surface. Catalysts with higher leaching characteristics exhibit the first radical generation mechanism, while the stable catalyst with insignificant leaching exhibits the second radical generation mechanism. Adsorption of the pollutant over the surface of the catalyst also enhances the pollutant degradation. Overall, heterogeneous EF process is very potent, powerful, and useful for the pollutant decontamination from the water medium.

Keywords Advanced oxidation process, Electro-Fenton, Heterogeneous EF, Hydroxyl radicals, Solid catalyst, Water treatment

P.V. Nidheesh (✉)

CSIR-National Environmental Engineering Research Institute, Nagpur, Maharashtra, India
e-mail: nidheeshpv129@gmail.com

H. Olvera-Vargas, N. Oturan, and M.A. Oturan

Laboratoire Géomatériaux et Environnement, Université Paris-Est, UPEMLV 77454, Marne-la-Vallée EA 4508, France

M. Zhou et al. (eds.), *Electro-Fenton Process: New Trends and Scale-Up*,
Hdb Env Chem (2018) 61: 85–110, DOI 10.1007/698_2017_72,

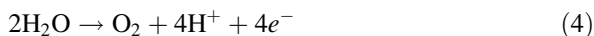
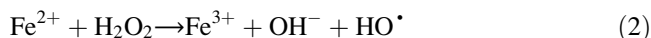
© Springer Nature Singapore Pte Ltd. 2017, Published online: 16 Aug 2017

Contents

1	Introduction	86
2	Importance of Heterogeneous EF Process	87
3	Heterogeneous Electro-Fenton Catalysts	88
3.1	Magnetite (Fe ₃ O ₄)	89
3.2	Zero-Valent Iron	90
3.3	Pyrite	92
3.4	Sludge Containing Iron	99
3.5	Iron-Loaded Alginate Beads	99
3.6	Iron-Loaded Carbon	101
3.7	Iron-Loaded Zeolite	102
3.8	Iron-Loaded Sepiolite	103
4	Pollutant Degradation Mechanism	104
5	Conclusions and Perspectives	107
	References	108

1 Introduction

Electro-Fenton (EF) process is an indirect electrochemical advanced oxidation process, initially explained by Brillas and Oturan groups [1–5]. EF process utilizes in situ generated hydrogen peroxide by the two-electron reduction of oxygen molecules over the cathodic surface in acidic medium as in Eq. (1) [2, 3, 6]. The electrolytically generated hydrogen peroxide reacts with ferrous ions, which are added externally in the electrolytic cell, resulting in Fenton's reactions and in the subsequent generation of highly reactive hydroxyl radicals as in Eq. (2). The ferric ions generated from the Fenton's reactions undergo cathodic reduction (Eq. 3) and regenerate ferrous ions, apart from conventional Fenton's chain reactions [2, 3, 6–8]. Increase in solution pH with increase in reaction time is the main operating problem of conventional Fenton's process. This is mainly due to the generation of hydroxyl ions in water during the Fenton's reactions [9]. This increase in solution pH during the Fenton's reactions counterbalanced in EF process by the generation of protons by the water oxidation at anode (Eq. 4) and by the generation of carboxylic acids by the degradation of pollutants [10, 11].



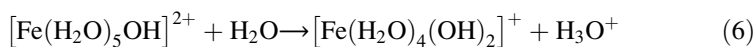
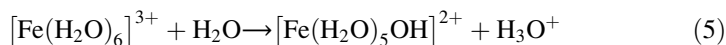
EF process is a world widely accepted process, due to its higher efficiency, in situ generation of hydrogen peroxide, negligible or absence of sludge production, higher ferrous ion regeneration rate, etc. [7, 9, 12]. Based on the physical nature of catalyst, EF process can divide into two: homogeneous EF process and heterogeneous EF

process. In homogeneous EF process, the soluble forms of iron are used as the source of catalyst. The most commonly used homogeneous Fenton catalysts are the salts of iron such as ferrous sulfate, ferric chloride, etc. These salts generate ferrous or ferric ions in water medium and undergo Fenton's reaction with in situ generated hydrogen peroxide.

Heterogeneous EF process uses heterogeneous catalysts, which are generally very slightly soluble or insoluble in water. That is, in heterogeneous EF process, solid catalysts are used as the source of iron. The solid catalysts contain iron, generally in its stable form. The most commonly used heterogeneous Fenton catalysts are the oxides of iron.

2 Importance of Heterogeneous EF Process

Even though, there are several advantages for homogeneous EF process, some of its drawbacks retard its industrial-level applications. One of the main drawbacks of homogeneous EF is its narrow optimal operating pH interval. The optimal pH condition for the effective Fenton's reaction is near to 3. Iron exhibits in various hydroxide forms in solution, and the concentration of these hydroxides also depends on the solution pH. In water medium, these compounds form hexa-coordinated complexes. For example, ferric ions exist in aqueous solution as $\text{Fe}(\text{H}_2\text{O})_6^{3+}$ [13]. Six molecules of water have a covalent bond with the iron species located at the center. For the formation of bond, water molecule uses one of the lone electron pairs of oxygen. This ferric complex undergoes further hydrolysis as in Eqs. 5 and 6 [14]. Similarly, ferrous ions also undergo complex formation. Among the various hexa-aqua complex species of iron, Fe^{2+} (i.e., $\text{Fe}(\text{H}_2\text{O})_6^{2+}$) and Fe^{3+} (i.e., $\text{Fe}(\text{H}_2\text{O})_6^{3+}$) are the predominant forms of iron at solution pH less than 3 [15–17]. With increase in solution pH from 3, these complexes convert into insoluble complexes like $[\text{Fe}(\text{H}_2\text{O})_8(\text{OH})_2]^{4+}$, $[\text{Fe}_2(\text{H}_2\text{O})_7(\text{OH})_3]^{3+}$, $[\text{Fe}_2(\text{H}_2\text{O})_7(\text{OH})_4]^{5+}$, etc. [14]. At these conditions, pollutant removal by coagulation predominates the degradation. It has been experimentally proved that the electrocoagulation of organic pollutants using iron anode has the optimal values at pH between 6 and 8. Also, in the presence of oxygen, oxidation of ferrous ions to ferric ions occurs at pH greater than 4 as in Eq. 7 [13, 18]. This retards the rate of Fenton's reaction at pH values higher than 4. Therefore, the Fenton's reaction occurs in higher rates at pH 3, due to the predominant concentrations of ferrous and ferric ions. This pH is maintained near to the initial condition in EF process by the anodic oxidation of water.





Generally, the pH of wastewater generated from the industries is either alkaline or neutral. Therefore, the pH of wastewater should bring down to 3 for the effective operation of homogeneous EF process. This problem can be avoided in heterogeneous EF process. Fenton's reaction occurs on the catalyst surface rather than in the aqueous medium. Thus, the solid catalysts are effective in wide range of pH conditions. The ferrous or ferric ions present in the catalysts are highly stable. Thus, ferrous or ferric ions do not form their complexes by the hydrolysis process.

Another problem with the homogeneous EF process is the inability of recycling the Fenton catalyst. The iron salts which are used as the source of iron ions (catalyst) are soluble in water. Therefore, it is very difficult to reuse/recycle the catalyst. As a result, these ions come along with the effluent and act as a pollutant. Therefore, the treatment of effluent containing iron is required after the homogeneous EF process. This problem can be avoided in heterogeneous EF process very easily. Since the source of catalyst is solid, its separation from treated solution is very easy. Moreover, experiments have proven that heterogeneous catalysts can be reused [19, 20].

Overall, the differences between homogeneous and heterogeneous EF processes can be summarized as in Table 1, given below.

3 Heterogeneous Electro-Fenton Catalysts

Various heterogeneous Fenton catalysts used in Fenton's process and related processes for the degradation of persistent organic pollutants are shown in Fig. 1. Electro-Fenton activity of a few catalysts was tested among these catalysts and its catalytic properties are discussed below.

Table 1 Differences between homogeneous and heterogeneous EF processes

No.	Item	Homogeneous EF process	Heterogeneous EF process
1	Solubility of catalyst	Soluble	Insoluble
2	Physical nature of catalyst during reaction	Liquid phase	Solid
3	Optimal operating pH	Acidic, specifically near to 3	Wide range
4	Reusability of catalyst	Not possible/difficult	Possible
5	Separation of catalyst from aqueous phase	Difficult	Easy
6	Reactions	Occurs in liquid phase	Generally occurs on the surface of catalyst

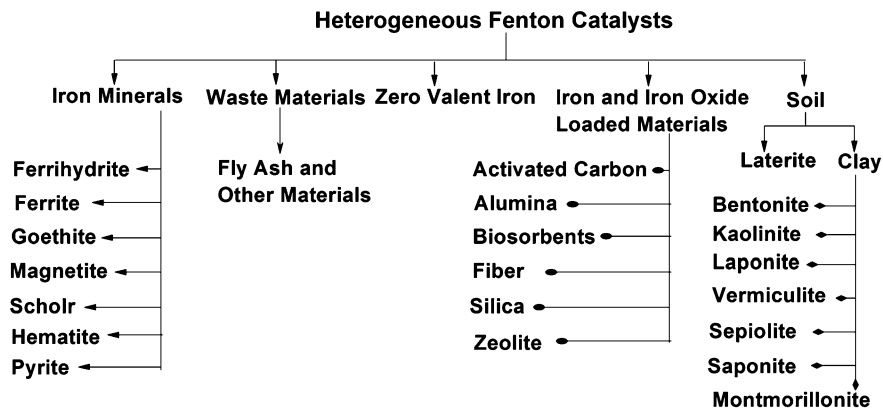


Fig. 1 Various heterogeneous Fenton catalysts. Reprinted from Ref. [21] with permission. Copyright 2015 RSC

3.1 Magnetite (Fe_3O_4)

Iron oxides are present in our earth crust abundantly. The octahedron structure of iron oxide consists of ferric ion surrounded by six numbers of oxygen or oxygen and hydroxyl ions. The major forms of iron oxides are goethite, ferrihydrate, hematite, magnetite, maghemite, etc. The oxidation activity of these oxides depends mainly on its crystallinity, surface area, particle size, iron content, oxidation states of iron, etc. Magnetite is a well-tested iron oxide, which contains ferric and ferrous ions in its structure. Magnetite has both octahedral and tetrahedral units in which ferric ions are placed in both units while ferrous ions are placed only in its octahedral unit. The catalytic activity of magnetite is mainly due to the presence of octahedral cations and the higher surface exposure of octahedral cations compared to tetrahedral cations [20–22]. In a theoretical manner, magnetite contains ferrous and ferric ions in the ratio 1:2. The following properties of magnetite gave much attention to this iron oxide in the field of heterogeneous Fenton catalysis [22–25].

1. Magnetite is one of the iron oxides present in earth crust in abundant form. The presence of ferrous ions in magnetite is very helpful for the initiation of Fenton's reactions. The ferrous ions in the octahedral unit are very efficient for the Fenton's reaction initiation via Haber-Weiss mechanism.
2. Magnetite is easily separable from the reaction medium because of its higher magnetic property.
3. Electron mobility in the spinal structure of magnetite is very high.
4. The dissolution rate of iron is very high in magnetite, compared to other iron oxides.
5. Substitution of other transition metals instead of iron is very easy in magnetite structure. This enhances the Fenton activity of the catalyst in a significant manner.

Nidheesh et al. [20] tested the efficiency of magnetite as heterogeneous EF catalyst by considering rhodamine B as a model pollutant. The authors prepared the magnetite by chemical precipitation method. Ferrous and ferric ion solutions were taken in different molar ratios and mixed together in a conical flask. The authors prepared mixed solutions with various ferrous to ferric molar ratios such as 1:0, 0:1, 1:1, 2:1, 1:2, 1:4, and 4:1. A total iron concentration (both ferrous and ferric) of 0.075 M was considered for the magnetite preparation. This solution kept under continuous mixing, and 8–10 mL of 8 M sodium hydroxide solution was added slowly till the precipitation of magnetite. The authors observed specific changes in the characteristics of magnetite with changes in the concentration of both ferrous and ferric ions in the solution. Increase in ferric ion concentration (indirectly decrease in ferrous ion concentration) altered the color of magnetite from black to brown. Magnetite was not precipitated only in the presence of ferric ion. All the magnetite particles prepared were highly amorphous, except in the case of 0:1 ratio. The average particle size increased from 13.6 to 30.9 nm with increase in ferric ion concentration.

The authors tested the catalytic efficiency of prepared magnetite for the degradation of 10 mg L⁻¹ rhodamine B solution in the presence of graphite electrodes. The first-order rate constant for the dye degradation was in between 0.014 and 0.019 min⁻¹. Total dye removal efficiency after 3 h of electrolysis varied from 86 to 93%. Among these catalysts, magnetite with ferrous to ferric ratio 1:2 and 2:1 showed higher dye removal efficiency and rate. Thus magnetite prepared with 2:1 ratio was selected for the further studies.

The efficiency of magnetite depends on the concentration of dye, electrolysis time, inner electrode gap, electrode area, catalyst dosage, applied voltage, solution pH, etc. Efficiency of magnetite decreased with increase in dye concentration. But, the absolute dye removal increased with increase in initial dye concentration. At the optimal conditions (pH 3, catalyst dosage 10 mg L⁻¹, clear electrode spacing 4 cm, and applied voltage 8 V), a total of 97% of dye reduction was observed after 3 h of electrolysis. The comparison of rhodamine B degradation efficiency of magnetite with other EF catalysts is given in Table 2. The dye removal efficiency of magnetite is comparable with that of homogeneous Fenton catalysts, and the rate of removal of dye by heterogeneous Fenton catalysts is only slightly lower compared to homogeneous catalysts. Removal rate and efficiency of magnetite is very high compared to locally available iron oxide. Apart from this, the reusable nature of magnetite is highly impressive (Fig. 2). The dye removal efficiency of magnetite remains the same even after five cycles [20].

3.2 Zero-Valent Iron

Zero-valent iron (ZVI) received much attention in the field of heterogeneous catalysis due to its higher catalytic efficiency, large surface area, low cost, etc. The dual surface property of ZVI, i.e., core and shell of ZVI covering with iron and

Table 2 Comparison of dye removal efficiency of magnetite with other EF catalysts

Catalyst	Removal efficiency (%)	First-order rate constant (min^{-1})
Magnetite [20]	97.3	0.023
Fe^0 [26]	94.5	0.039
Fe^{2+} [26]	93.2	0.032
Fe^{3+} [26]	88.4	0.031
Cu^{2+} [26]	92.2	0.027
Mn^{2+} [26]	91.7	0.035
Commercial iron oxide [20]	60	0.013

Experimental conditions: pH 3, catalyst dosage 10 mg L^{-1} , applied voltage 8 V, and inner electrode spacing 4 cm

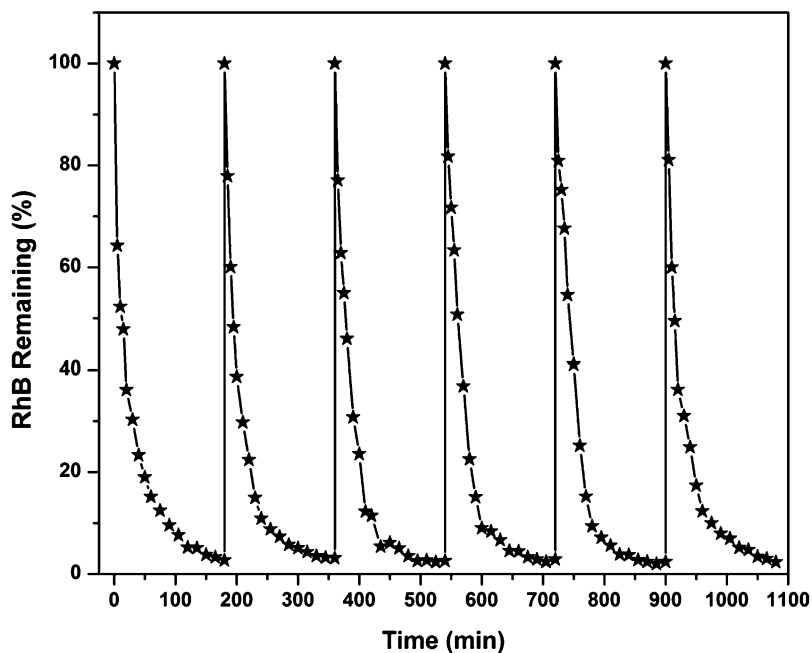


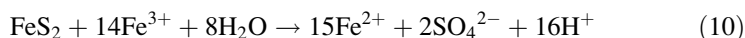
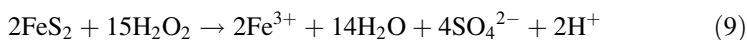
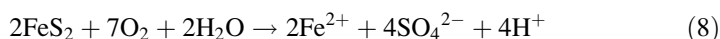
Fig. 2 Reusability of magnetite for the degradation of dye (experimental conditions: clear electrode spacing 4 cm, applied voltage 8 V, catalyst dosage 10 mg L^{-1} , and initial pH 3) Reprinted from Ref. [20] with permission. Copyright 2014 RSC

iron oxides, respectively, enhanced the catalytic performance of ZVI significantly [27]. Babuonpusami and Muthukumar [28] tested the efficiency of ZVI to decompose hydrogen peroxide and consequent removal of phenol in Fenton, EF, and photo-EF processes. Performance of ZVI in Fenton system was slightly less than that in EF process. Phenol removal after 60 min was observed as 65% and 87% for Fenton and EF processes, respectively. This increased performance of ZVI was further improved by the addition of light energy. Complete removal of phenol was

observed after 30 min in photo-assisted EF process. But the efficiency of ZVI was less than homogeneous EF catalysts with ferrous and ferric ions [29]. After 180 min of electrolysis, the authors observed the salicylic acid removals as 47%, 43%, and 23%, respectively for ferrous ion, ferric ion, and ZVI, for an initial pollutant concentration of 100 mg L⁻¹ operated at an initial solution pH 3. In contrary to this, Nidheesh and Gandhimathi [26] observed higher textile dye degradation rate in the presence of ZVI than homogeneous EF catalysts (ferrous and ferric ions) and homogeneous EF-like catalysts (copper and manganese). The removal efficiency of ZVI is also higher than homogeneous EF catalysts as given in Table 2.

3.3 Pyrite

Another alternative that has been explored for homogeneously catalyzing the EF process is the utilization of pyrite (FeS₂), the most abundant sulfide mineral found in the earth's crust. Pyrite participates in many environmental and geochemical processes of relevance, such as the formation of acid mine drainage, the metal cycle in sediments, the degradation of pollutants, and so on [30]. This mineral is a natural source of Fe²⁺ ions according to its oxidation by dissolved oxygen in aqueous solutions (Eq. 8). Furthermore, in the presence of H₂O₂ and Fe³⁺, reactions (9) and (10) occur, which results in a self-regulated process for Fe²⁺ ions production [31].



The generation of H⁺ from the series of reactions (8–10) is noteworthy, since it promotes acidification of the medium, a remarkable fact for the EF process that allows the acidic optimal pH value for the Fenton's reaction (2).

As background, pyrite was used as heterogeneous catalyst for the chemical Fenton treatment applied in the degradation of refractory pollutants. It was reported that pyrite considerably enhanced the efficiency of the process compared to classic homogeneous Fenton's process, which is illustrated in Fig. 3. This trend was explained by the continuous formation of [•]OH from Fenton's reaction, which was ensured by the constant release of Fe²⁺ ions, whose amount was regulated by the presence of H₂O₂ (Eq. 9), and the reduction of Fe³⁺ ions at the surface of the catalyst (Eq. 10) to generate ferrous iron required by Fenton's reaction (2). In this way, the catalytic system was capable of maintaining a favorable H₂O₂/Fe²⁺ molar ratio for Fenton's reaction, which prevented detrimental quenching reactions. Moreover, the solution pH was kept in optimal acidic values due to the intrinsic deprotonation of pyrite.

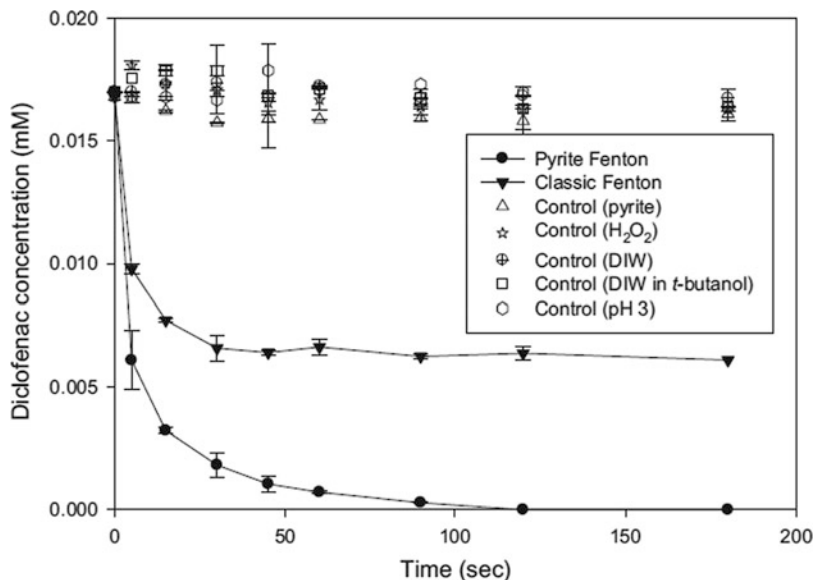


Fig. 3 Degradation kinetics of diclofenac under different experimental conditions (five types of controls, classical Fenton, and pyrite-Fenton processes). Experimental boundary conditions: $[\text{Diclofenac}]_0 = 0.017 \text{ mM}$, $[\text{pyrite}]_0 = 0.5 \text{ mM}$, $[\text{H}_2\text{O}_2]_0 = 1.0 \text{ mM}$, initial pH 4.0, and temperature = 25 °C. Reprinted with permission from Ref. [32]. Copyright 2013 Elsevier

In this scenario, the pyrite-Fenton oxidation of the pharmaceutical diclofenac resulted in 100% of removal efficiency, while only 65% was achieved by classic Fenton under comparable experimental conditions. The authors pointed out that the degradation of the drug by $\cdot\text{OH}$ formed from the Fenton's reaction in the bulk solution was the predominant mechanism (accounting for 90% of diclofenac removal), while the reported surface-catalyzed pathway taking place in heterogeneous iron oxides, such as magnetite, goethite, and hematite at circumneutral pH, had little contribution [32]. Similarly, the chlorinated pollutant trichloroethylene was successfully degraded by the pyrite-Fenton method, with 97% of removal efficiency, which contrasted with the 77% obtained during classic Fenton [33]. Pyrite was also used as catalyst for the Fenton treatment of synthetic surfactant-aided soil washing wastewater contaminated with pyrene; 96% removal efficiency was obtained by pyrite-Fenton, while only 32% removal was observed for the equivalent homogeneous Fenton's process. Besides, the solution TOC was decreased in 87% when using pyrite, which represented a good mineralization rate [34]. Pyrite-Fenton was similarly used for degrading off-gas toluene in a continuous system, in which classical Fenton resulted to be less efficient. Moreover, from a model based on the concentration profile of Fe(II), Fe(III), and sulfate ions, the authors estimated that the pyrite-Fenton continuous system could operate for 28.9

days without further charge of pyrite, thus highlighting the stability/durability of the pyrite as catalyst [35].

On the other hand, cyclic/aromatic intermediates were concomitantly degraded during pyrite-Fenton process, which demonstrated the capacity of this homogeneously catalyzed process to degrade hazardous by-products normally formed during the classical Fenton treatment [32, 34]. Accordingly, shortcuts associated with classic Fenton were overcome by the use of pyrite as catalyst, including the slow and incomplete oxidation of organics, the early termination of Fenton's reaction, and the formation of toxic by-products. Additionally, acidic pH was maintained.

More recently, the utilization of pyrite as heterogeneous catalyst for the EF process, the so-called EF-pyrite, whose schematic representation is depicted in Fig. 4, has been proposed. As in the case of chemical pyrite-Fenton, it was found that the pyrite can release and regulate the appropriate amount of Fe^{2+} ions and pH in the solution necessary for the Fenton's reaction (2) in accordance with Eqs. (8–10). Moreover, the continuous electrochemical production of the Fenton's reagent (H_2O_2 and Fe^{2+} ions) enhances the efficiency of the process, since H_2O_2 accelerates reaction (9), while the electro-regeneration of Fe^{2+} ions at the cathode contributes to the $\text{Fe}^{2+}/\text{Fe}^{3+}$ regulation cycle.

The profile of total iron, Fe^{2+} , and Fe^{3+} ions during the EF-pyrite treatment of an azo textile dye (AHPS) is illustrated in Fig. 5. It can be seen from this figure that Fe^{2+} ions are quickly oxidized into Fe^{3+} through Fenton's reaction, while the reduction of Fe^{3+} by Eqs. (3) and (10) takes place at slower kinetic rates.

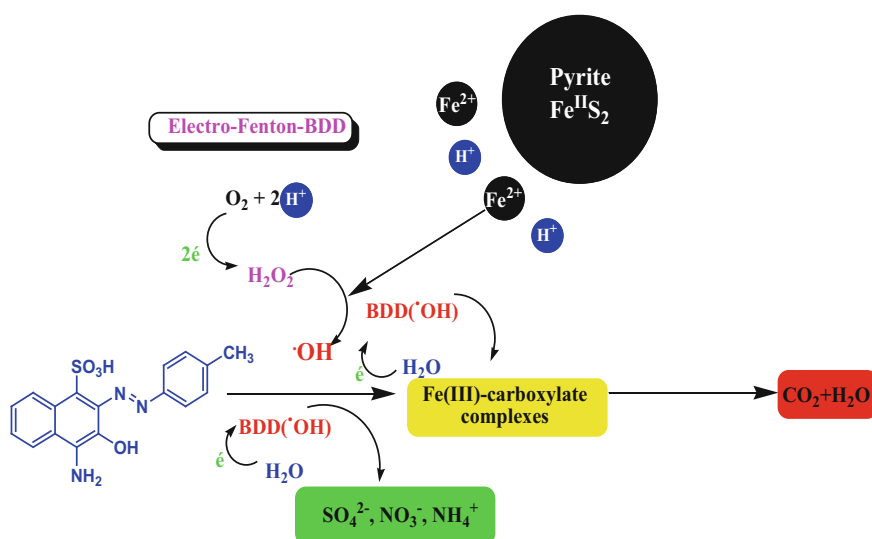


Fig. 4 Schematic representation of the heterogeneous EF-Pyrite process with a BDD anode applied to the degradation of the synthetic dye 4-amino-3-hydroxy-2-p-tolylazo-naphthalene-1-sulfonic acid (AHPS). Reprinted with permission from Ref. [36]. Copyright 2015 Elsevier

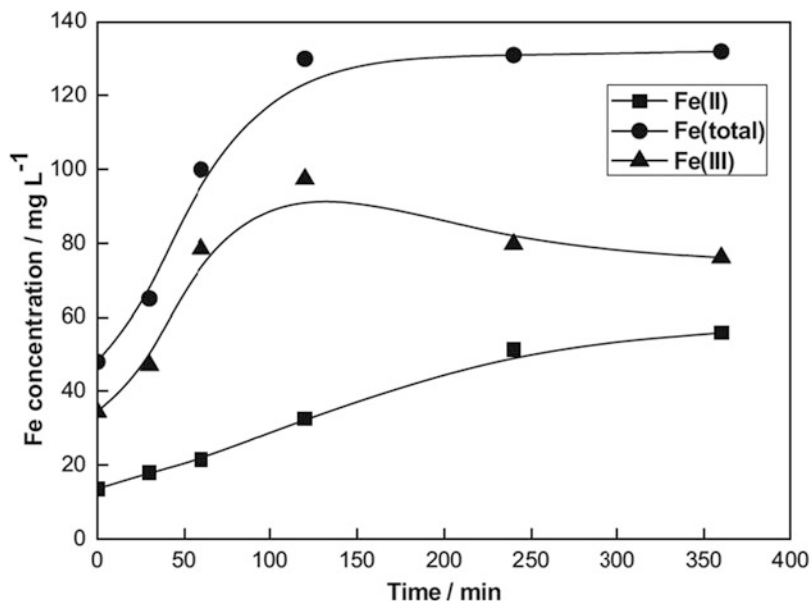


Fig. 5 Concentration profile of aqueous Fe^{2+} , Fe^{3+} , and total Fe during the degradation of AHPS textile dye solution by EF-pyrite process. Experimental conditions: $[\text{ADPS}]_0 = 175 \text{ mg L}^{-1}$, $I = 300 \text{ mA}$, $[\text{pyrite}]_0 = 2 \text{ g L}^{-1}$, $[\text{Na}_2\text{SO}_4]_0 = 50 \text{ mM}$. Reprinted with permission from Ref. [36]. Copyright 2015 Elsevier

On the other hand, pyrite also demonstrated its ability to provide an acid medium since the first stages of electrolysis, keeping it along the treatment. This behavior is accounted for by the release of protons from the mineral surface according to Eqs. (8–10). This is of significant relevance because the EF process optimally operates at pH values around 3 [12]. For example, Labiadh et al. [36] reported that the solution pH during the EF-pyrite degradation of a synthetic dye progressively decreased from 6.0 to about 4.0/3.0 (depending on the amount of catalyst) within the 10 first minutes of electrolysis, remaining without significant change throughout the experiment [36]. The main parameters affecting the effectiveness of the process, which include current intensity, pyrite dosage, initial concentration of the pollutant, and the nature of the anode material used, have been investigated. Degradation and mineralization rates were increased with rising current up to an optimal value, from which kinetic rates did not rise any further, which was due to the acceleration of waste reactions not consuming OH or electrical energy, a general trend that was constant with the reported behavior of the classic EF process [12, 37]. For the initial concentration of the substrate, it was found that the TOC removal efficiency dropped with increasing initial substrate concentration. On the contrary, the mineralization current efficiency (MCE) was increased, while the energy consumption per unit removed TOC mass ($\text{EC} (\text{g TOC})^{-1}$) decreased. These tendencies were in total agreement with the typical behavior of classic homogeneous EF [12, 37]. With respect to the amount of pyrite catalyst, it was

reported that performance of the process increased with rising the concentration of pyrite in suspension from 0.5 to 2 g L⁻¹. Further increase in the amount of catalyst resulted detrimental, since an excess of Fe²⁺ ions released from the catalyst's surface consumes $\cdot\text{OH}$ according to the Eq. (11), thus decreasing efficiency.



Table 3 summarizes the main results obtained during the EF-pyrite treatment of the abovementioned contaminants. In all cases, degradation of organics obeyed a pseudo-first-order kinetic reaction, and almost complete mineralization was obtained, whereby highlighting the power of the process for mineralizing refractory organics. Furthermore, the comparison assessment with classic EF with homogeneous Fe²⁺ ions under equivalent operating conditions revealed a slight superiority of EF-pyrite, which has been ascribed to the remarkable Fe(II)-self-regulation ability of pyrite and its pH-controller character.

On the other hand, it was demonstrated that the use of a BDD electrode enhances the mineralization efficiencies. This phenomenon has been explained by the combined action of homogeneous $\cdot\text{OH}$ formed from Fenton's reaction (2) and heterogeneous BDD($\cdot\text{OH}$) produced at the anode surface from the discharge of water, following Eq. (12) [37, 38]. For example, Barhoumi et al. [39] reported that the use of a BDD anode during EF-pyrite increased the TOC removal rate in 9% with respect to Pt electrode: 95% of TOC removal was achieved by EF-pyrite-BDD, while only 86% was obtained when utilizing Pt [40]. Noteworthy is the fact that the EF-pyrite process with a Pt anode gave comparable results to those obtained by means of classic EF-BDD with homogeneous Fe(II) catalyst, since the utilization of expensive BDD anodes can be avoided when making use of pyrite as catalyst, which represents a significant decrease of operational costs [39]. This behavior can

Table 3 TOC removal efficiencies obtained during the EF-pyrite treatment of different refractory contaminants and the comparison with classic homogeneous EF

Contaminant	Cell configuration	% TOC removal (EF-pyrite)	%TOC removal (Classic EF)
Levofloxacin [40]	BDD-carbon felt undivided cell (300 mA)	95 in 8-h treatment	–
	1 g L ⁻¹ of pyrite		
Tyrosol [41]	BDD-carbon felt undivided cell (300 mA)	89 in 6-h treatment	88 in 6-h treatment
	1 g L ⁻¹ of pyrite		
Synthetic dye (AHPS) [36]	BDD-carbon felt undivided cell (450 mA)	>90 in 5-h treatment	70 in 5-h treatment
	2 g L ⁻¹ of pyrite		
Sulfamethazine [39]	BDD-carbon felt undivided cell (300 mA)	95 in 8-h treatment	90 in 8-h treatment
	2 g L ⁻¹ of pyrite		

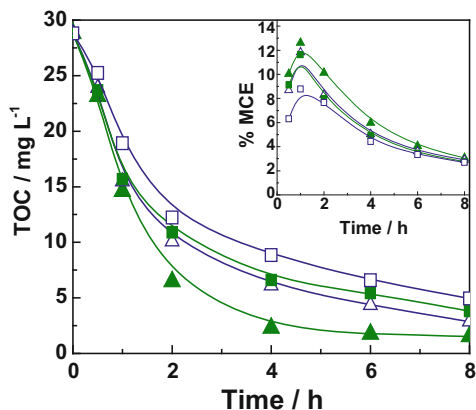


Fig. 6 Removal of solution's TOC vs. electrolysis time for the mineralization of 200 mL of 0.2 mM sulfamethazine solution in 0.05 M Na₂SO₄ at pH 3.0, 300 mA, and room temperature, using an undivided (*filled triangle, open triangle*) BDD/carbon-felt and (*filled square, open square*) Pt/carbon-felt cell. The inset panel presents the corresponding MCE curves for (*filled triangle, filled square*) EF-pyrite with 2.0 g L⁻¹ pyrite and (*open triangle, open square*) EF with 0.2 mM Fe²⁺. Reprinted with permission from Ref. [39]). Copyright 2016 Elsevier

be observed in Fig. 6, which also exemplifies the superiority of EF-pyrite over the classic EF process.

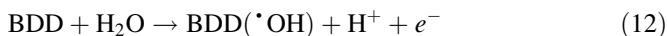
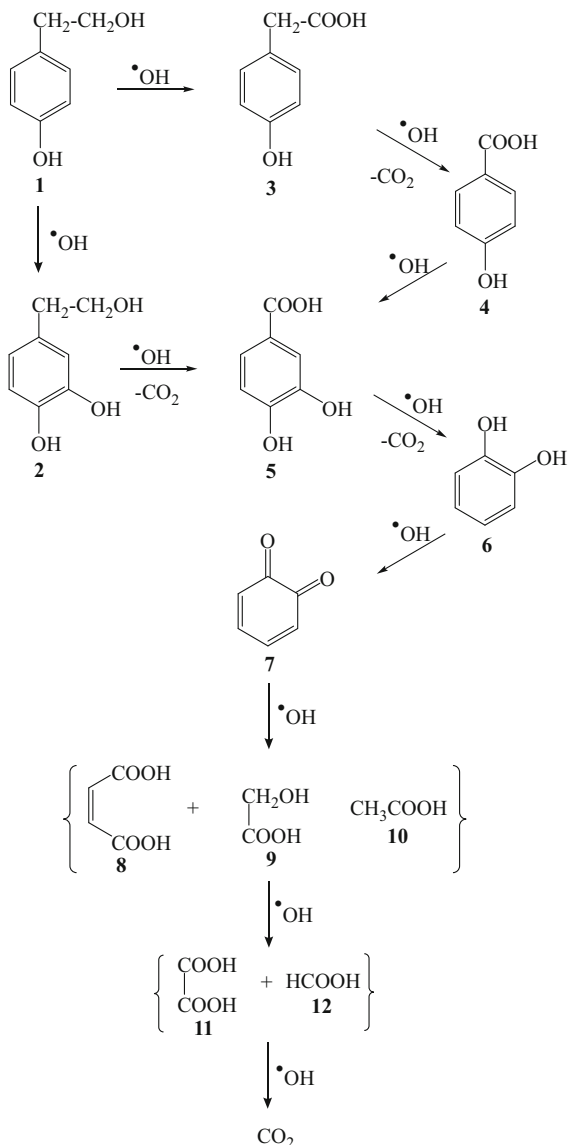


Figure 7 depicts the proposed degradation pathway for the mineralization of tyrosol by $\cdot\text{OH}$ during EF-pyrite oxidation, which is based on the identification of aromatic intermediates and short-chain aliphatic acids. A series of hydroxylation and decarboxylation reactions progressively succeeded until breakage of the aromatic cycles, which yielded low-molecular-weight carboxylic acids. Oxalic and formic acids were the most persistent species at prolonged electrolysis times and the ultimate by-products before complete mineralization until CO₂ and water. This behavior is in agreement of with the known reaction mechanisms reported for the incineration of organics by $\cdot\text{OH}$ [11, 12].

Barhoumi et al. [39] also assessed the evolution of toxicity during the EF-Pyrite treatment of sulfamethazine by means of a bioluminescence-based method using *V. fischeri* marine bacteria (Microtox[®]). They found that under optimal conditions of EF-pyrite, toxic intermediates produced during the first stages of electrolysis were also destroyed during treatment, thereby demonstrating the efficiency of the heterogeneous EF-pyrite for detoxifying aqueous solutions of antibiotics.

Overall, it was demonstrated that the utilization of pyrite as heterogeneous catalyst is a potential alternative for performing the EF process. Several advantages emerged using this natural mineral as solid catalyst, which are listed below:

Fig. 7 Proposed reaction pathway for tyrosol mineralization by the EF-pyrite process in a BDD/ carbon-felt cell. Reprinted with permission from Ref. [41]. Copyright 2015 Elsevier



- Release and regulation of appropriate amounts of Fe^{2+} ions throughout electrolysis, which are necessary for the Fenton's reaction
- Avoidance of external addition of mineral acids for pH adjustment, since the catalyst can provide an optimal acid medium for EF and maintain it during the treatment
- Slightly superior performance than classic homogeneous EF, which is due to the self-regulation system of Fe^{2+} ions and solution pH provided by the mineral

- High environmental compatibility, which is related to its reusable character and its pH-controlling ability, which prevents utilization of corrosive acids

3.4 *Sludge Containing Iron*

Nidheesh and Gandhimathi [42] used sludge produced after the peroxi-coagulation of real textile wastewater as a heterogeneous EF catalyst for the treatment of the same textile wastewater. The sludge contains higher amount of iron in the form of $\text{Fe}(\text{OH})_3$, iron(III) oxide-hydroxide ($\text{FeO}(\text{OH})$), FeCl_2 , Fe_2O_3 , and $\delta\text{-FeOOH}$. After the peroxi-coagulation process, the sludge generated in the electrolytic system was filtered, washed, and dried in oven at $100\text{ }^\circ\text{C}$ for 24 h. The sludge was found as an effective catalyst at the acidic condition. After the completion of 1 h electrolysis, 97% of color, 47% of COD, and 33% of TOC were removed from the textile wastewater effectively. Mineralization efficiency of this heterogeneous catalyst is slightly less than that of homogeneous catalyst, even the color removal efficiency of homogeneous EF process using ferric ion and the heterogeneous EF process is the same. Color, COD, and TOC removal efficiencies of homogeneous EF process were observed as 97%, 64%, and 47%, respectively, under the following experimental conditions: Initial pH 3, applied voltage 7 V, working volume 500 mL, electrode area 25 cm^2 , electrode spacing 3 cm, and ferric ion concentration 10 mg L^{-1} . The lesser mineralization efficiency of heterogeneous EF process compared to homogeneous EF process may be due to the lower iron concentration in heterogeneous EF system compared to homogeneous EF system. In both the cases, catalyst dosage was considered as 10 mg L^{-1} and was found to be the optimal value in homogeneous system. But, in the case of heterogeneous EF system, the effective iron concentration should be less than 10 mg L^{-1} as the solid catalyst contains other ions along with iron. Thus the dosage added into the solution is insufficient for the effective mineralization of textile wastewater.

3.5 *Iron-Loaded Alginate Beads*

Alginate beads are highly porous material, normally in spherical shapes. This material contains higher concentration of carboxylic groups and can able to form cross-links with ferric or ferrous ion, when it contacts with iron solution. The make use of iron-loaded alginate beads is found to be an efficient EF catalyst for the abatement of indole, a malodorous compound from the aqueous solution [19]. The porosity of alginate beads was $9.32\text{ m}^2\text{ g}^{-1}$ and can able to hold 320 mg g^{-1} of iron by cross-linking. By the cross-linking with iron, alginate beads converted to its egg-box structure. Absolute target pollutant removal was observed by the researchers at the optimal conditions (catalyst dosage of 200 mg L^{-1} , initial pH of 3.0, electrolysis time of 60 min, and a current intensity of 0.53 mA cm^{-2}). At the

same condition and after 7 h of electrolysis, 90% of mineralization efficiency was also observed. The prepared catalyst was highly reusable and stable in nature. The authors reused the material for four cycles without iron leaching.

Iglesias et al. [43] tested the efficiency of iron-loaded alginate beads for the abatement of dyes in continuous flow mode. An airlift glass reactor with a working volume of 1.5 L was used for the entire study. Reactive Black 5 and Lissamine Green B dyes were considered as the model dyes. Based on the energy consumption and dye removal efficiency, applied voltage of 3 V and solution pH of 2 were considered as optimal and operated the reactor at the same conditions. The working of the reactor was similar to a continuously stirred tank reactor. Based on the hydrodynamic and kinetic studies, authors developed a prediction model as given below:

$$D = \frac{k\tau}{1 + k\tau} \quad (13)$$

where D is the dye removal efficiency, k is the first-order kinetic rate constant (min^{-1}), and τ is the residence time (min).

The predicted model showed a good fit with the experimental data [43]. The standard deviations between theoretical and experimental data were below 6%.

de Dios et al. [44] prepared manganese-loaded alginate beads and verified its heterogeneous EF catalytic performance by considering several persistent organic pollutants like Reactive Black 5, imidacloprid, di-2-ethylhexyl phthalate, and 4-nitrophenol. Major studies were carried out by considering Reactive Black 5 as the target compound. The researchers evaluated the competence of homogeneous system with heterogeneous system and found that heterogeneous EF-like oxidation with Mn-loaded alginate beads is more efficient than the homogeneous EF-like oxidation in the presence of soluble Mn ions. The main problem with homogeneous system was the insoluble hydroxide formation at the cathode surface. The supplement of chelating compounds rectifies this drawback of homogeneous EF system to an indicative extent. Citric acid was found to be a good chelating agent due to its ability to stabilize hydrogen peroxide, to increase the desorption rate of entrapped pollutant, and to form the complex with metals. The complex formation enhances the regeneration rate of Fenton catalyst. Authors observed an entire target pollutant removal; and the prepared catalyst was highly stable and reusable as stated above. The authors also tested the efficiency of Mn-loaded alginate beads for the degradation of other pollutants such as imidacloprid, di-2-ethylhexyl phthalate, and 4-nitrophenol [44]. After 180 min of electrolysis, 80% of di-2-ethylhexyl phthalate degradation, complete removal of 4-nitrophenol, and 80% of imidacloprid degradation were observed.

3.6 Iron-Loaded Carbon

Carbon, especially activated carbon, is a well-known adsorbent widely used for the removal of dyes, heavy metals, phenols, pesticides, etc. Higher surface area, sorption capacity, porosity, etc. of activated carbon made the material as popular adsorbent. The ability of activated carbon for the sorption of heavy metals leads to the preparation of iron-supported activated carbon catalyst for the abatement of various organic pollutants via Fenton's reactions. Nidheesh and Rajan [45] prepared this heterogeneous Fenton catalyst and found that the iron sorption capacity of activated carbon is in the range of 2.66 g g^{-1} . The iron concentration in the catalysts was around 62.3%. Bounab et al. [46] used this catalyst for the electrolytic generation of hydroxyl radicals and for the degradation of m-cresol and tert-butylhydroquinone. The authors used catalyst with iron concentrations 28 and 46 mg L^{-1} . The authors observed higher catalytic efficiency for the catalyst with lower iron concentration. The catalyst with iron concentration 28 mg L^{-1} took 40 min for the complete reduction of m-cresol, while the other catalyst took 120 min for reaching the same efficiency. TOC removal efficiency and energy consumption also followed the same trend. TOC removal efficiency of the catalyst with 46 mg L^{-1} iron after 120 min of electrolysis was 67.3%, while that of catalyst with 28 mg L^{-1} of iron was 83%. The energy consumptions for the catalyst with 46 mg L^{-1} iron and 28 mg L^{-1} of iron were found as 29.7 kWh kg^{-1} and 15.1 kWh kg^{-1} , respectively. The rate of degradation of tert-butylhydroquinone was higher than that of m-cresol. Complete removal of tert-butylhydroquinone was observed in 20 min of electrolysis.

Zhang et al. [47] used the modified iron-carbon catalyst for the EF oxidation of 2,4-dichlorophenol. Iron-carbon catalysts were dipped in ethanol and carried out the sonication for 30 min. Then the catalyst was washed twice with ethanol and dipped in solution containing various concentrations of polytetrafluoroethylene (PTFE). The modified catalyst was filtered and dried 2 h at $100 \text{ }^\circ\text{C}$ with N_2 protection. After the PTFE treatment, the surface of the catalyst becomes more compacted with few pores. This was mainly due to the uniform distribution of PTFE over the surface of catalyst and PTFE reduces the iron leaching from the catalyst. Iron was distributed over the surface of catalyst in the form of zero-valent iron and magnetite. The efficiency of the modified catalyst was changed insignificantly after the electrolysis time of 120 min, compared to the original catalyst. The addition of PTFE reduced the iron leaching from the synthesized catalyst noticeably. The iron leaching ratio of raw catalyst was 1.32% after 120 min of electrolysis, while that of the catalysts modified with 20% PTFE was around 0.29%, after the similar electrolysis time. More than 95% degradation of 2,4-dichlorophenol was observed after 120 min of electrolysis at initial pH 6.7, current intensity 100 mA, catalyst loading 6 g L^{-1} .

The authors [47] also monitored the H_2O_2 and $\cdot\text{OH}$ production during the process and compared with other related processes such as anodic oxidation and homogeneous EF process. Compared to other processes, the accumulation of H_2O_2

in the anodic oxidation was very high. The concentrations of H_2O_2 after 120 min of anodic oxidation, homogeneous EF process, and heterogeneous EF process were found as 517.3 mg L^{-1} , 330 mg L^{-1} , and 370 mg L^{-1} , respectively. The generation of $\cdot\text{OH}$ in the anodic oxidation process was very less. The values of H_2O_2 and $\cdot\text{OH}$ concentrations indicate the ineffective decomposition of H_2O_2 in anodic oxidation process. The concentration of $\cdot\text{OH}$ was very high in homogeneous EF process compared to other processes, which indicates the effective decomposition of H_2O_2 . But, an insignificant change in the amount of $\cdot\text{OH}$ was observed between 60 and 120 min of electrolysis. Compared to homogeneous EF process, the generation of $\cdot\text{OH}$ in heterogeneous EF process was less after 60 min of electrolysis, but it was very high after 120 min of electrolysis.

The authors [47] tested the application of heterogeneous EF process in real condition by spiking 120 mg L^{-1} of 2,4-dichlorophenol in two different wastewater, which are generated from a chemical industry plant and from an oil treatment factory. The TOC concentrations of chemical industry and oil treatment factory wastewater were observed as 81 mg L^{-1} and 277 mg L^{-1} , respectively. The reduction of 2,4-dichlorophenol was less in oil treatment factory wastewater compared to chemical industry wastewater. This may be due to the higher competitive reactions in oil treatment factory wastewater compared to chemical industry wastewater.

3.7 Iron-Loaded Zeolite

Like activated carbon, zeolite is extensively used as an adsorbent and ion exchange material. Zeolite can accommodate varieties of cations like potassium, sodium, calcium, etc. in its structure. Iglesias et al. [48] prepared iron supported Y-zeolite and investigated its imidacloprid and chlorpyrifos degradation efficiencies. Initial acid treatment for Y-zeolite was carried out using $0.1 \text{ M H}_2\text{SO}_4$ and used for the sorption of iron. The iron concentration in zeolite after the sorption process was found to be 52.21 mg g^{-1} . The prepared catalyst was found to be very effective for the degradation of pesticides. Initially the authors tested for the degradation of imidacloprid having initial concentration of 100 mg L^{-1} at an applied voltage of 5 V and various catalyst dosages. For all conditions, 98% of pesticide removal was observed after 120 min of electrolysis. Based on the energy consumption, authors selected lowest catalyst dosage for testing the degradation of chlorpyrifos and observed 96% removal after 5 min of electrolysis. Sorption of pesticide over the prepared catalyst was also checked and found the absence of pesticide on the surface of prepared catalyst.

Inadequacy of pH adjustment for the effective performance is one of the advantages of this catalyst over other heterogeneous Fenton catalyst. Fenton's process is very effective at pH 3, and most of the case external addition of acid is required for adjusting the required pH. By the action of acid-treated Y-zeolite

catalyst, pH control is not required. The authors observed a reduction in solution pH from 6 to 3 with the addition of prepared catalyst.

The authors [48] embedded the prepared catalyst in alginate gel and tested its electro-Fenton activity. Previous studies reported that the poor mechanical properties of alginate beads restricted its application in EF system. The mechanical properties of these gels can be improved by the combination with clay minerals. The authors did not observe any increase in the catalytic activity of iron-loaded Y-zeolite after embedment in alginate gel.

3.8 Iron-Loaded Sepiolite

Sepiolite is a complex clay mineral containing magnesium. The fibrous structure of sepiolite provides larger surface area to this clay mineral and thus, extensively tested for the sorption process. The iron-loaded sepiolite clay was found to be a competent heterogeneous EF catalyst for the deletion of Reactive black B [49]. The prepared catalyst was very effective at acidic conditions. Significant removal of dye in alkaline condition was also observed by the authors. A maximum decolorization of 97.3% after 90 min of electrolysis was found at pH 2.

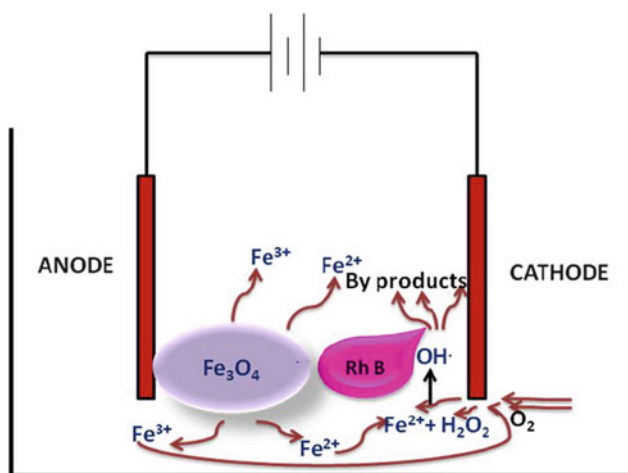


Fig. 8 Magnetite catalyzed rhodamine B (RhB) abatement mechanism of EF process. Reprinted from Ref. [20] with permission. Copyright 2014 RSC

4 Pollutant Degradation Mechanism

Hydroxyl radicals are generated in the heterogeneous EF system in two ways: (1) in the solution and (2) on the surface of solid catalyst. In the first mode of radical formation, ferrous or ferric ion leached into the solution during the electrolysis and undergoes Fenton's reaction as in the case of homogeneous system. Degradation of rhodamine B by magnetite (Fig. 8) is an example for this [20]. The authors monitored the concentration of ferrous and ferric ions in the solution during the electrolysis. Modified 1,10-phenanthroline method and ferric-salicylic acid complex method were used for finding the concentrations of ferrous and ferric ions, respectively. The concentration of ferric ion in the solution increased with electrolysis time and reached a maximum value of 3.85 mg L^{-1} after 135 min of electrolysis. Similar manner, the concentration of ferrous ions increased up to 1.63 mg L^{-1} after 30 min of electrolysis and then decreased with the electrolysis time as shown in the Fig. 9. This indicates that the presence of electric field enhanced the leaching of iron species from iron oxides [22].

The iron species leached from the surface of magnetite are positively charged and thus attracts toward the cathode surface. At the same time, the pollutant is also cationic in nature and attracts toward the same electrode. H_2O_2 generated at the

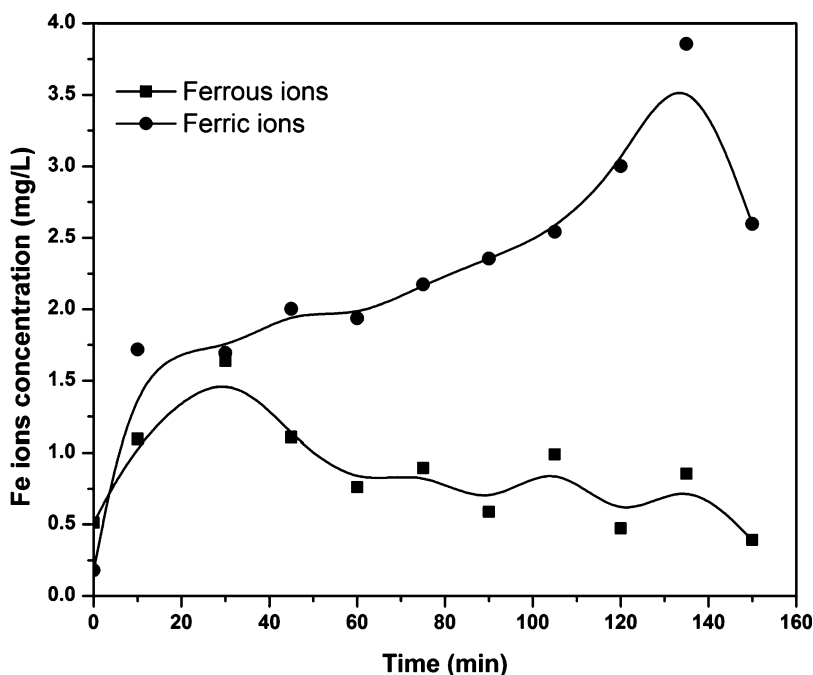


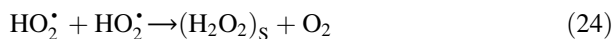
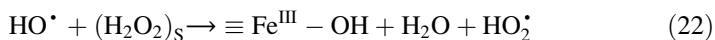
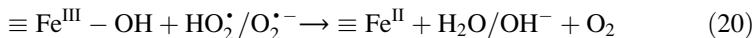
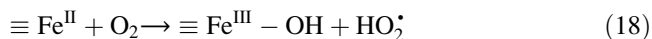
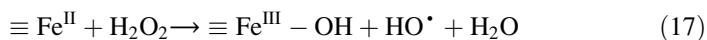
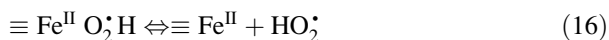
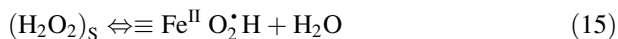
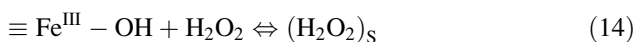
Fig. 9 Changes in ferrous and ferric ion concentrations with electrolysis time, during the rhodamine B degradation by heterogeneous EF process. Reprinted from Ref. [20] with permission. Copyright 2014 RSC

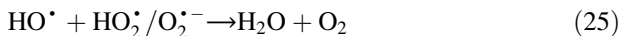
surface of cathode reacts with the leached iron species and produces $\cdot\text{OH}$ in the solution. These radicals degrade the organic pollutants present in the water.

In the second mode of degradation mechanism, the radicals are generated at the surface of catalyst. In this case, the leaching of the catalyst is insignificant. Thus the surface of the catalyst is covered with iron species. The H_2O_2 produced at the cathode surface dissolves in water and contacts with the catalyst due to the external mixing. Thus the Fenton's reaction occurs at the surface of catalyst and produces $\cdot\text{OH}$.

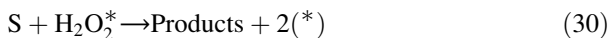
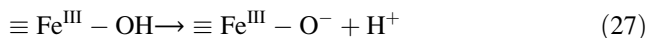
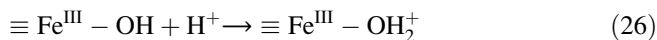
The degradation of persistent organic pollutants by the second method (reactions occur on the surface of catalyst) may take place in two ways. Researchers proposed two ways of pollutant degradation mechanism: radical and non-radical mechanisms. Take goethite as an example of heterogeneous Fenton catalyst. Based on the studies, Lin and Gurol [50] proposed the radical mechanism and Andreozzi et al. [51] proposed the non-radical mechanism.

According to the radical mechanism of goethite, formation of a precursor surface complex of hydrogen peroxide on the surface of goethite is the initial reaction (Eq. 14). Then the surface hydrogen peroxide undergoes a reversible electron transfer reaction (Eq. 15), which results in the formation of the excited state of ligands. This excited state is unstable and deactivated by the generation of hydroperoxyl radical and ferrous ion (Eq. 16). The ferrous ions generated from the above reactions react with either hydrogen peroxide (Eq. 17) or oxygen (Eq. 18). The reaction of surface ferrous ion with oxygen is too slow and can be neglected. The hydroperoxyl radical decomposes and forms oxygen radicals (Eq. 19). The hydroperoxyl radical and hydroxyl radicals generated in the system react with surface ferrous ion (Eq. 20), ferric ion (Eq. 21), and hydrogen peroxide (Eqs. 22 and 23). Finally these radicals react with each other as termination reactions (Eqs. 24 and 25).





Based on the results obtained from 3,4-dihydroxybenzoic acid degradation by goethite, Andreozzi et al. [51] proposed a non-radical mechanism in heterogeneous Fenton system. Goethite is in two forms according to the solution pH (Eqs. 26 and 27). Superficial sites of goethite are very effective for the sorption of hydrogen peroxide and organic pollutant (Eqs. 28 and 29), where (*) indicates free catalyst active sites and “S” indicates the pollutant. The adsorbed pollutant and hydrogen peroxide react at the surface of catalyst (Eq. 30), which results in the regeneration of active sites and the production reaction products.



Optimal pH of the EF reactions has an indirect relationship for the degradation mechanism. If the degradation of organic pollutant by heterogeneous EF process has an optimal pH, especially at pH 3, the process follows always the first degradation mechanism because the leached iron species are in their form only at pH near to 3. Increase in solution pH converts the ferrous and ferric form to their insoluble hydroxide complex form as mentioned above. These compounds have inability to enhance the decomposition of hydrogen peroxide and the subsequent generation of hydroxyl radicals. If the catalyst is effective at all the pH conditions, it follows the second radical formation reaction. The surface of the catalyst is always covered with the ferrous and ferric ions in every pH conditions and undergoes Fenton's reactions as explained above.

Adsorption plays an important role in the catalytic activity of heterogeneous Fenton catalyst [22]. The solubility of iron species decreases with increase in solution pH and is very less at neutral pH. At this condition the interaction between the pollutant and the catalyst surface controls the pollutant degradation. Pollutants are first sorbed on the surface of catalyst and undergo degradation by the in situ generated radicals. Bounab et al. [46] checked this hypothesis by conducting the adsorption and desorption studies. The prepared heterogeneous catalyst (iron-loaded activated carbon) was very efficient for the degradation of m-cresol. Therefore, the authors conducted adsorption studies in the presence of catalyst and found a complete pollutant removal after 120 min. At the same time, the pollutant was removed completely after 45 min in EF process. This indicates that the removal of pollutant occurs faster in EF process than in adsorption process and the pollutant removal in EF process is not due to the sorption process. In order to check the coupled adsorption and degradation process during EF oxidation, the authors carried out desorption study for the catalyst after 90 min of electrolysis and found

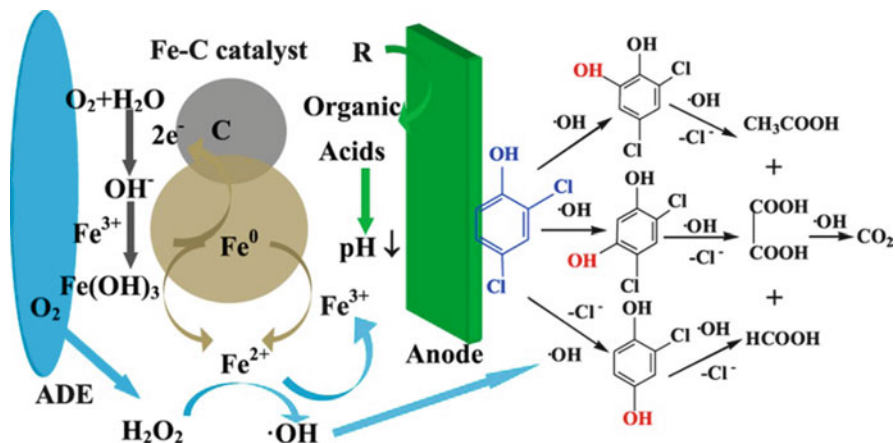


Fig. 10 2,4-Dichlorophenol degradation mechanism and pathway in the presence of modified iron-carbon catalyst. In figure ADE air diffusion electrode. Reprinted with permission from reference Zhang et al. [47], Copyright 2015 Elsevier

the pollutant concentration nearly 1% of its initial concentration. These results indicate that the degradation of pollutant occurs after the sorption process in heterogeneous EF process.

Zhang et al. [47] observed a two-stage degradation mechanism for the degradation of 2,4-dichlorophenol in the presence of PTFE modified iron-loaded carbon (Fig. 10). The authors used carbon-PTFE air diffusion electrode as cathode and Ti/IrO₂-RuO₂ as anode. The anode is able to produce hydroxyl radicals in the solution via anodic oxidation process. This process controls the degradation rate at the initial stages of electrolysis, especially at higher initial pH conditions. The pH of the solution having the initial pH greater than 5 reduced near to 3 after the electrolysis. This lowered pH condition enhances the EF and Fe-C micro-electrolysis process and results in the faster degradation of pollutant at later stages of electrolysis.

5 Conclusions and Perspectives

Heterogeneous EF process utilizes solid catalysts for the generation of hydroxyl radicals in the aqueous medium. The insoluble, reusable, and stable natures of heterogeneous EF catalysts nullify some of the drawbacks of homogeneous EF process. Heterogeneous EF catalysts like magnetite, pyrite, and iron loaded on carbon, zeolite, alginate beads, etc. are found to be very efficient for the decontamination of water and wastewater, which are contaminated by organic pollutants. Hydroxyl radical generation and contaminant abatement mechanism by these solid catalysts depend more on its iron leaching characteristics. Adsorption of pollutants

over the surface of solid catalysts also plays the major role for the effective degradation of organic pollutants.

Even though, these solid catalysts are very efficient for the removal/mineralization of persistent organic pollutants in synthetic water medium, although real field application of these catalysts are not yet tested in detail. Since, these catalysts are solid in nature, real field implementation of heterogeneous EF process is a great challenge. Real field water and wastewater contain several ions other than the target pollutants. These ions may cause the deactivation of catalyst and reduce the efficiency in a significant manner. Deactivation of heterogeneous catalyst in water medium occurs mainly via poisoning, thermal degradation, fouling, etc. These deactivation mechanisms reduced the effective active sites of heterogeneous catalyst. In some of the cases, the adsorbed or deposited ions over the heterogeneous catalysts may act as a barrier for the effective contact between catalyst and hydrogen peroxide.

Leaching of iron ions is one of the radical formation mechanisms as in the case of magnetite. This continuous leaching of ions in the presence of electric field is responsible for the higher reusability nature of magnetite as observed in Fig. 2. Due to the higher leaching of ferrous and ferric ions to the water medium, the magnetite surface is always active and fresh during the reaction and after the reactions as that of newly prepared magnetite. Thus, these types of catalyst are highly reusable with a reduction in its initial weight. But, in the real field application, the adsorbed or deposited ions over the surface of the heterogeneous catalyst prevent the effective leaching of ions.

References

1. Oturan MA, Pinson J (1995) Hydroxylation by electrochemically generated OH radicals. Mono – and polyhydroxylation of benzoic acid: products and isomers distribution. *J Phys Chem* 99:13948–13954
2. Oturan MA, Peiroten J, Chartrin P, Acher AJ (2000) Complete destruction of p-nitrophenol in aqueous medium by electro-Fenton method. *Environ Sci Technol* 34:3474–3479
3. Oturan MA (2000) Ecologically effective water treatment technique using electrochemically generated hydroxyl radicals for in situ destruction of organic pollutants: application to herbicide 2,4-D. *J Appl Electrochem* 30:475–482
4. Brillas E, Mur E, Casado J (1996) Iron(II) catalysis of the mineralization of aniline using a carbon-PTFE O₂-Fed cathode. *J Electrochem Soc* 143:L49–L53
5. Brillas E, Calpe JC, Casado J (2000) Mineralization of 2,4-D by advanced electrochemical oxidation processes. *Water Res* 34:2253–2262
6. Oturan MA, Oturan N, Lahitte C, Trevin S (2001) Production of hydroxyl radicals by electrochemically assisted Fenton's reagent: application to the mineralization of an organic micropollutant, pentachlorophenol. *J Electroanal Chem* 507:96–102
7. Nidheesh PV, Gandhimathi R (2012) Trends in electro-Fenton process for water and wastewater treatment: an overview. *Desalination* 299:1–15
8. Nidheesh PV, Gandhimathi R, Sanjini NS (2014) NaHCO₃ enhanced Rhodamine B removal from aqueous solution by graphite-graphite electro Fenton system. *Sep Purif Technol* 132:568–576

9. Nidheesh PV, Gandhimathi R, Ramesh ST (2013) Degradation of dyes from aqueous solution by Fenton processes: a review. *Environ Sci Pollut Res* 20:2099–2132
10. El-Desoky HS, Ghoneim MM, El-Sheikh R, Zidan NM (2010) Oxidation of Levafix CA reactive azo-dyes in industrial wastewater of textile dyeing by electro-generated Fenton's reagent. *J Hazard Mater* 175:858–865
11. Oturan MA, Aaron J-J (2014) Advanced oxidation processes in water/wastewater treatment: principles and applications. A review. *Crit Rev Environ Sci Technol* 44:2577–2641
12. Brillas E, Sirés I, Oturan MA (2009) Electro-Fenton process and related electrochemical technologies based on Fenton's reaction chemistry. *Chem Rev* 109:6570–6631
13. Pignatello JJ, Oliveros E, MacKay A (2006) Advanced oxidation processes for organic contaminant destruction based on the Fenton reaction and related chemistry. *Crit Rev Environ Sci Technol* 36:1–84
14. Neyens E, Baeyens J (2003) A review of classic Fenton's peroxidation as an advanced oxidation technique. *J Hazard Mater* 98:33–50
15. Benefield LD, Judkins JF, Weand BL (1982) Process chemistry for water and wastewater treatment. Prentice-Hall, Englewood Cliffs, NJ
16. Wells CF, Salam MA (1965) Hydrolysis of ferrous ions: a kinetic method for the determination of the Fe(II) species. *Nature* 205:690–692
17. Wells CF, Salam MA (1968) The effect of pH on the kinetics of the reaction of iron(II) with hydrogen peroxide in perchlorate media. *J Chem Soc A Inorganic Phys Theor* 24–29
18. Magario I, García Einschlag FS, Rueda EH et al (2012) Mechanisms of radical generation in the removal of phenol derivatives and pigments using different Fe-based catalytic systems. *J Mol Catal A Chem* 352:1–20
19. Hammouda SB, Fourcade F, Assadi A et al (2016) Effective heterogeneous electro-Fenton process for the degradation of a malodorous compound, indole, using iron loaded alginate beads as a reusable catalyst. *Appl Catal B Environ* 182:47–58
20. Nidheesh PV, Gandhimathi R, Velmathi S, Sanjini NS (2014) Magnetite as a heterogeneous electro Fenton catalyst for the removal of Rhodamine B from aqueous solution. *RSC Adv* 4:5698–5708
21. Costa RCC, Lelis MFF, Oliveira LC et al (2006) Novel active heterogeneous Fenton system based on $\text{Fe}_{3-x}\text{M}_x\text{O}_4$ (Fe, Co, Mn, Ni): the role of M^{2+} species on the reactivity towards H_2O_2 reactions. *J Hazard Mater* 129:171–178
22. Nidheesh PV (2015) Heterogeneous Fenton catalysts for the abatement of organic pollutants from aqueous solution: a review. *RSC Adv* 5:40552–40577
23. Munoz M, de Pedro ZM, Casas JA, Rodriguez JJ (2015) Preparation of magnetite-based catalysts and their application in heterogeneous Fenton oxidation – a review. *Appl Catal B Environ* 176–177:249–265
24. Rahim Pouran S, Abdul Raman AA, Wan Daud WMA (2014) Review on the application of modified iron oxides as heterogeneous catalysts in Fenton reactions. *J Clean Prod* 64:24–35
25. Dhakshinamoorthy A, Navalon S, Alvaro M, Garcia H (2012) Metal nanoparticles as heterogeneous Fenton catalysts. *ChemSusChem* 5:46–64
26. Nidheesh PV, Gandhimathi R (2014) Comparative removal of Rhodamine B from aqueous solution by electro-Fenton and electro-Fenton-like processes. *Clean Soil Air Water* 42(6):779–784
27. Sun Y-P, Li X, Cao J et al (2006) Characterization of zero-valent iron nanoparticles. *Adv Colloid Interf Sci* 120:47–56
28. Babuponnusami A, Muthukumar K (2012) Removal of phenol by heterogenous photo electro Fenton-like process using nano-zero valent iron. *Sep Purif Technol* 98:130–135
29. George SJ, Gandhimathi R, Nidheesh PV, Ramesh ST (2014) Electro-fenton oxidation of salicylic acid from aqueous solution: batch studies and degradation pathway. *Clean Soil Air Water* 42(12):1701–1711
30. Bonnissel-Gissingner P, Alnot M, Ehrhardt JJ, Behra P (1998) Surface oxidation of pyrite as a function of pH. *Environ Sci Technol* 32:2839–2845

31. Pham HT, Kitsuneduka M, Hara J et al (2008) Trichloroethylene transformation by natural mineral pyrite: the deciding role of oxygen. *Environ Sci Technol* 42:7470–7475
32. Bae S, Kim D, Lee W (2013) Degradation of diclofenac by pyrite catalyzed Fenton oxidation. *Appl Catal B Environ* 134–135:93–102
33. Che H, Bae S, Lee W (2011) Degradation of trichloroethylene by Fenton reaction in pyrite suspension. *J Hazard Mater* 185:1355–1361
34. Choi K, Bae S, Lee W (2014) Degradation of pyrene in cetylpyridinium chloride-aided soil washing wastewater by pyrite Fenton reaction. *Chem Eng J* 249:34–41
35. Choi K, Bae S, Lee W (2014) Degradation of off-gas toluene in continuous pyrite Fenton system. *J Hazard Mater* 280:31–37
36. Labiadh L, Oturan MA, Panizza M et al (2015) Complete removal of AHPS synthetic dye from water using new electro-fenton oxidation catalyzed by natural pyrite as heterogeneous catalyst. *J Hazard Mater* 297:34–41
37. Brillas E, Martínez-Huitle CA (2015) Decontamination of wastewaters containing synthetic organic dyes by electrochemical methods. An updated review. *Appl Catal B Environ* 166:603–643
38. Sopaj F, Oturan N, Pinson J et al (2016) Effect of the anode materials on the efficiency of the electro-Fenton process for the mineralization of the antibiotic sulfamethazine. *Appl Catal B Environ* 199:331–341
39. Barhoumi N, Oturan N, Olvera-Vargas H et al (2016) Pyrite as a sustainable catalyst in electro-Fenton process for improving oxidation of sulfamethazine. Kinetics, mechanism and toxicity assessment. *Water Res* 94:52–61
40. Barhoumi N, Labiadh L, Oturan MA et al (2015) Electrochemical mineralization of the antibiotic levofloxacin by electro-Fenton-pyrite process. *Chemosphere* 141:250–257
41. Ammar S, Oturan MA, Labiadh L et al (2015) Degradation of tyrosol by a novel electro-Fenton process using pyrite as heterogeneous source of iron catalyst. *Water Res* 74:77–87
42. Nidheesh PV, Gandhimathi R (2014) Effect of solution pH on the performance of three electrolytic advanced oxidation processes for the treatment of textile wastewater and sludge characteristics. *RSC Adv* 4:27946–27954
43. Iglesias O, Rosales E, Pazos M, Sanromán MA (2013) Electro-Fenton decolourisation of dyes in an airlift continuous reactor using iron alginate beads. *Environ Sci Pollut Res* 20:2252–2261
44. Fernández de Dios MÁ, Rosales E, Fernández-Fernández M et al (2015) Degradation of organic pollutants by heterogeneous electro-Fenton process using Mn-alginate composite. *J Chem Technol Biotechnol* 90:1439–1447
45. Nidheesh PV, Rajan R (2016) Removal of rhodamine B from a water medium using hydroxyl and sulphate radicals generated by iron loaded activated carbon. *RSC Adv* 6:5330–5340
46. Bounab L, Iglesias O, Gonzalez-Romero E et al (2015) Effective heterogeneous electro-Fenton process of m-cresol with iron loaded activated carbon. *RSC Adv* 5:31049–31056
47. Zhang C, Zhou M, Ren G et al (2015) Heterogeneous electro-Fenton using modified iron-carbon as catalyst for 2,4-dichlorophenol degradation: influence factors, mechanism and degradation pathway. *Water Res* 70:414–424
48. Iglesias O, de Dios MAF, Tavares T et al (2015) Heterogeneous electro-Fenton treatment: preparation, characterization and performance in groundwater pesticide removal. *J Ind Eng Chem* 27:276–282
49. Iglesias O, Fernández de Dios MA, Pazos M, Sanromán MA (2013) Using iron-loaded sepiolite obtained by adsorption as a catalyst in the electro-Fenton oxidation of reactive black 5. *Environ Sci Pollut Res* 20:5983–5993
50. Lin S-S, Gurol MD (1998) Catalytic decomposition of hydrogen peroxide on iron oxide: kinetics, mechanism, and implications. *Environ Sci Technol* 32:1417–1423
51. Andreozzi R, Caprio V, Marotta R (2002) Oxidation of 3,4-dihydroxybenzoic acid by means of hydrogen peroxide in aqueous goethite slurry. *Water Res* 36:2761–2768

Modified Cathodes with Carbon-Based Nanomaterials for Electro-Fenton Process

Alireza Khataee and Aliyeh Hasanzadeh

Abstract Electro-Fenton (EF) process is based on the continuous in situ production of hydrogen peroxide (H_2O_2) by a two-electron reduction of oxygen on cathode and the addition of ferrous ion to generate hydroxyl radical ($\cdot OH$) at the solution through Fenton's reaction in acidic condition. Hence, cathode material has prominent effects on the H_2O_2 electro-generation efficiency and regeneration of ferrous ion. Carbonaceous materials are applied as suitable cathode in virtue of being highly conductive, stable, nontoxic, and commercially available. Besides, modification of cathode electrode with carbon-based nanomaterials (e.g., carbon nanotubes (CNTs), graphene, mesoporous carbon) can improve the electroactive surface area and the rate of oxygen mass transfer to the electrode, which increases the H_2O_2 electro-generation in the EF process. This chapter is to summarize the recent progress and advances in the modification of cathode electrode with carbon-based nanomaterials for EF process. The ability of different carbon-based nanomaterials to electro-generate H_2O_2 and degradation of pollutants is also discussed briefly.

Keywords Carbon nanomaterials, Carbon nanotubes, Electro-Fenton, Graphene, Graphene oxide, Hydrogen peroxide, Mesoporous carbon, Reduced graphene oxide

Contents

1	Introduction	112
2	Modification of Cathodes with Carbon-Based Nanomaterials for EF Process	115
	2.1 Carbon Nanotubes	115
	2.2 Graphene Family	120
	2.3 Mesoporous Carbons	130

A. Khataee (✉) and A. Hasanzadeh

Research Laboratory of Advanced Water and Wastewater Treatment Processes, Department of Applied Chemistry, Faculty of Chemistry, University of Tabriz, Tabriz, Iran
e-mail: a_khataee@tabrizu.ac.ir

M. Zhou et al. (eds.), *Electro-Fenton Process: New Trends and Scale-Up*,
Hdb Env Chem (2018) 61: 111–144, DOI 10.1007/698_2017_74,

111

© Springer Nature Singapore Pte Ltd. 2017, Published online: 17 Oct 2017

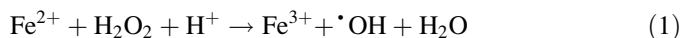
3 Conclusion	137
References	138

Abbreviations

ACF	Activated carbon fiber
AQS	Anthraquinone monosulfonate
BDD	Boron-doped diamond
CF	Carbon felt
CNT	Carbon nanotube
CTAB	Cetyl trimethyl ammonium bromide
DETA	3-(Trimethoxysilylpropyl) diethylenetriamine
EF	Electro-Fenton
ERGO	Electrochemical reduction of graphene oxide
GDE	Gas diffusion electrode
GO	Graphene oxide
HPC	Hierarchically porous carbon
MOF	Metal-organic framework
MWCNTs	Multiwalled carbon nanotubes
OMC	Ordered mesoporous carbons
PTFE	Polytetrafluoroethylene
rGO	Reduced graphene oxide
Rh B	Rhodamine B
RVC	Reticulated vitreous carbon
SEM	Scanning electron microscopy
SWNTs	Single-walled nanotubes
TEM	Transmission electron microscopy
TOC	Total organic carbon

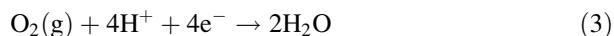
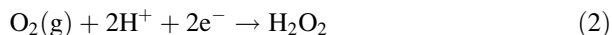
1 Introduction

Electro-Fenton (EF) process is based on the continuous in situ production of hydrogen peroxide (H_2O_2) and the addition of Fe^{2+} ion as a catalyst to generate hydroxyl radical ($\cdot\text{OH}$) at the solution through Fenton's reaction in acidic condition as the following reaction:



H_2O_2 can be continuously produced in an electrolytic cell from the two-electron reduction of oxygen gas at the cathode electrode by reaction (2) ($E^\circ = 0.695 \text{ V/SHE}$),

which occurs more easily than its four-electron reduction to water from reaction (3) ($E^\circ = 1.23$ V/SHE) [1]:



In EF process, Fe^{2+} can be regenerated via cathodic reduction (reaction (4)), which accelerates the generation of $\cdot\text{OH}$ from Fenton's reaction (1):



Cathode material has prominent effects on the oxidation power of the EF process and H_2O_2 electro-generation efficiency. Carbonaceous materials are subject of great interest as cathode electrodes for the two-electron reduction of O_2 to H_2O_2 and the favorable options for electrocatalyst support in virtue of being nontoxic and stable and having high overpotential for H_2 evolution and relatively good chemical resistance and conductivity [2]. In the 1970s, Oloman and Watkinson [3, 4] firstly investigated the application of graphite particles in the trickle-bed electrochemical reactors for the cathodic reduction of O_2 to H_2O_2 . Especially worth noting are the researches reporting the use of planar (2D) cathodes such as graphite [5–9], gas diffusion electrodes (GDEs) [10–13], three-dimensional (3D) electrodes such as activated carbon fiber (ACF) [14], carbon felt (CF) [15–19], carbon sponge [20, 21], reticulated vitreous carbon (RVC) [22–24], O_2 -fed carbon polytetrafluoroethylene (PTFE) [25, 26], and boron-doped diamond (BDD) [27, 28].

Due to the poor solubility of O_2 in aqueous solution (about 40 or 8 mg L^{-1} in contact with pure O_2 or air, respectively, at 1 atm and 25°C), GDEs and 3D electrodes of high specific surface area are favored as cathodes to supply reasonable current densities for practical applications. GDEs have a thin and porous structure preferring the percolation of the injected gas across its pores to contact the solution at the carbon surface. These electrodes have a great amount of active surface sites leading to a very fast O_2 reduction and large production of H_2O_2 [1]. Figure 1 provides a schematic diagram of structure and function of GDE.

In the last three decades, carbon-based nanomaterials have attracted substantial attention due to their superior electronic, photonic, electrocatalytic, chemical, and mechanical features that remarkably depend on their nanoscale properties [29]. Carbon-based nanomaterials can be classified into two groups: nanosized and nanostructured carbons [30]. Many more types of carbon materials, including graphene family (e.g., graphene, graphene oxide (GO), and reduced graphene oxide (rGO)), carbon nanotubes (CNTs), nanofibers, nanodiamonds, nanocoils, nanoribbon, and fullerene belonging to nanosized class, because the shell size and thickness of these carbon materials are on the nanometer scale [29]. New carbon materials such as carbon fibers and ordered mesoporous carbons are classified as nanostructured carbons, because their nanostructure is controlled in their construction through various processes [30]. Figure 2 provides a schematic illustration of some nanocarbons. Carbon blacks are constructed of nanosized particles, but they

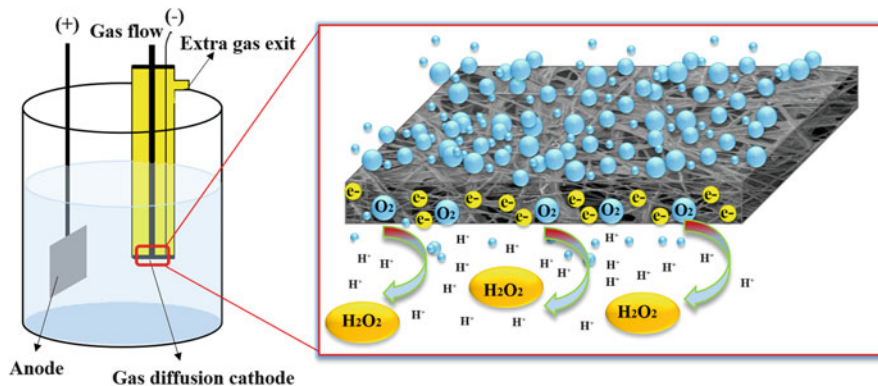


Fig. 1 Schematic diagram of structure and function of GDE

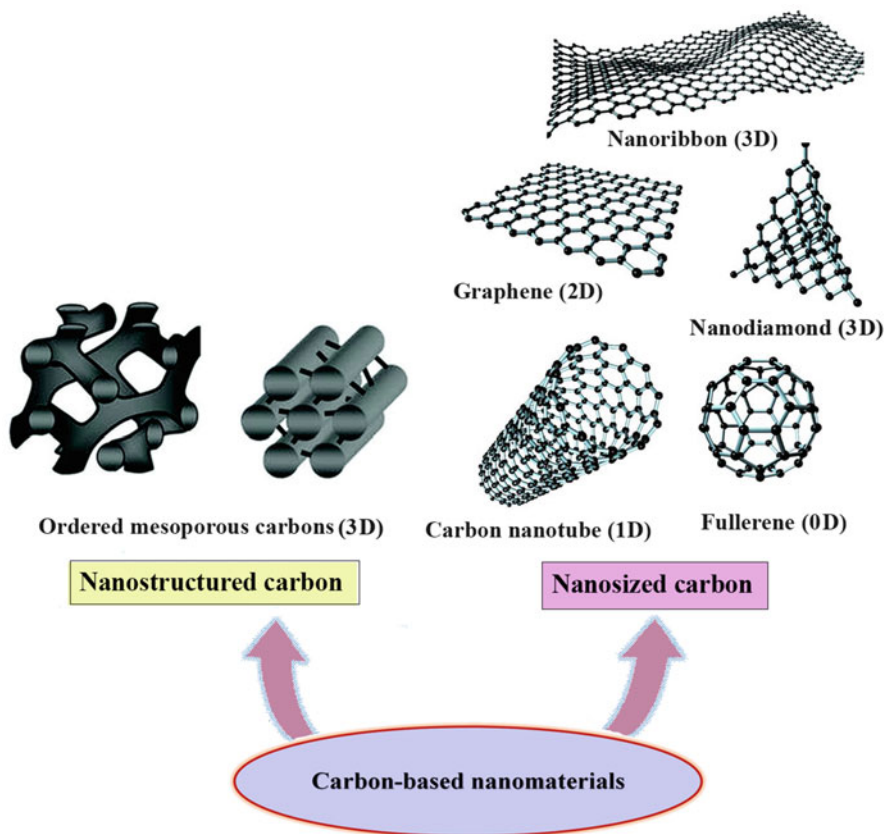


Fig. 2 Schematic illustration of some carbon-based nanomaterials

do not usually belong to nanocarbons due to their various applications as a mass and not in their distinctive form of nanosized particles [31].

In addition, doping carbon nanomaterials with heteroatoms, especially nitrogen, can enhance the performance of oxygen reduction activity by improving the surface chemical reactivity, conductivity, catalytic sites, and stability [32]. Among different possible dopants, nitrogen doping could either enhance the current of oxygen reduction or diminish the onset overpotential through (1) increasing chemically active sites, (2) improving the O₂ chemisorption, and (3) enhancing the hydrophilicity of surface [33].

Therefore, there are many investigations focused on the modification of cathode electrode by carbon-based nanomaterials [5, 34–36]. In these studies, the performance of EF process has been enhanced through improving the mass transfer characteristics of cathode. The novel EF electrode materials should possess several properties as follows: high selectivity for two-electron reduction of oxygen, good mass transfer performance, high electrochemical active reaction area, and high electrical conductivity.

The purpose of this chapter is to review the attempts in surface modification of cathode electrodes with carbon-based nanomaterials, e.g., CNTs, graphene family, and mesoporous carbons for EF process.

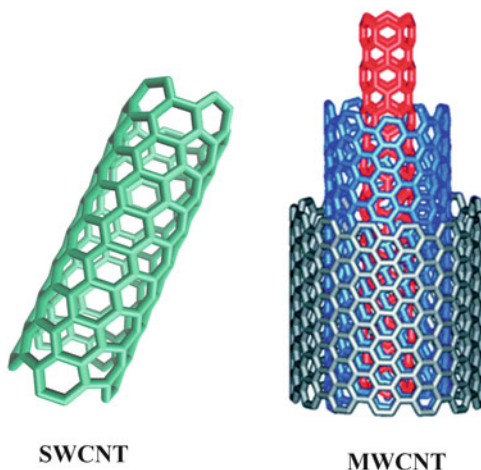
2 Modification of Cathodes with Carbon-Based Nanomaterials for EF Process

2.1 Carbon Nanotubes

The discovery of CNTs by Iijima in 1991 [37] has created a revolution in nanotechnology and material science. CNTs have attracted substantial consideration from the scientific community as one of the main members of carbon nanomaterials with unique optoelectronic, electrochemical, and electronic features [38]. The carbon atoms in CNTs are ordered in hexagons with sp² hybridization (one-dimensional (1D) system) [29]. A single-walled CNT (SWCNT) is produced by the rolling of a graphite layer into a nanoscale tube form which has an approximate diameter of 1 nm. Multiwalled CNTs (MWCNTs) can be constituted of two or more numbers of coaxial SWCNTs with expanding diameters that are separated from each other by a distance of around 0.34 nm (see Fig. 3) [33].

CNTs can be semiconducting or metallic in their electronic properties with an electrical conductivity up to 5,000 S cm⁻¹ [38]. Their conductivity is highly dependent on their chirality of the graphitic hexagonal array and diameter. The highly conductive nature of the CNTs confirms their high charge transport ability [29]. Experimental specific surface area of SWCNTs is in the range between 370 and 1,587 m² g⁻¹ with micropore volume of 0.15–0.3 cm³ g⁻¹ [39]. The MWCNT has a specific surface area between 180.9 and 507 m² g⁻¹ with mesopore

Fig. 3 The structure of SWCNT and MWCNT



volume of $0.5\text{--}2\text{ cm}^3\text{ g}^{-1}$ [39]. The tensile modulus and strength of SWCNTs are usually in the range of 320–1,740 GPa and 13–52 GPa, respectively, while being 270–950 GPa and 11–63 GPa in MWCNTs [29, 38]. Besides the huge specific surface area and electrical conductivity, CNTs also have a great thermal conductivity of $6,000\text{ W mK}^{-1}$ [38]. Due to these interesting properties, CNTs are promising nanomaterials for different applications such as in hydrogen-storage systems, sensors, organic photovoltaic cells, supercapacitors, fuel cells, batteries, and solar cells [29, 38, 39]. The applications of CNTs and their derivatives as electrocatalysts for two-electron reduction of O_2 in EF system will be discussed.

During the last years, a number of researches have been focused on the modification of cathode electrode with CNTs to improve its performance for in situ H_2O_2 generation in EF oxidation process. Table 1 summarizes some of the recent reported that modified cathode with CNTs and their derivatives in EF process.

Zarei et al. [52–54] coated the surface of carbon paper as a GDE cathode with CNTs and compared its efficiency for in situ H_2O_2 generation with activated carbon/GDE. PTFE was used to bind the carbon materials into a cohesive layer and convey some hydrophobic feature to the electrode surface. The scanning electron microscopy (SEM) images of the uncoated GDE and CNTs/GDE are shown in Fig. 4. As it can be seen from SEM images, coating of CNTs on GDE electrode improves the specific surface area of the cathode. The results demonstrated that the amount of produced H_2O_2 on the CNTs/GDE electrode (14.3 mmol L^{-1}) was approximately three times higher than that of activated carbon/GDE electrode (5.9 mmol L^{-1}) (Fig. 4c). The degradation efficiency of Basic Yellow 2 (BY2) in peroxi-coagulation process reached 62% and 96% in the first 10 min using activated carbon/GDE and CNTs/GDE electrodes at 100 mA, respectively [52]. The different abilities of H_2O_2 electro-generation of activated carbon/GDE and CNTs/GDE electrodes are attributed to the huge surface area and good electrical conductivity of CNTs [52–54].

Table 1 Selected results reported for modified cathodes with carbon nanotubes

Modified cathode	Process	Pollutant	Operational parameters	Maximum efficiency reported	Ref.
Oxidized MWCNT/ GDE	EF	Methyl orange (MO)	250 mL reaction compartment, Pt wire anode, 0.05 mol L ⁻¹ Na ₂ SO ₄ (electrolyte), pH 3.0, 400 mL min ⁻¹ O ₂ flow rate, 0.2 mmol L ⁻¹ [Fe ²⁺], 1.0 V voltage	95% removal efficiency for 100 mg L ⁻¹ MO, 4.38 mmol L ⁻¹ [H ₂ O ₂] after 90 min electrolysis and 81% current efficiency for CNT-15 (15 min plasma treated time)/GDE	[40]
MWCNT/graphite felt	EF	Rhodamine B (Rh B)	500 mL reaction compartment, 0.06 cm ² Pt sheet anode, 0.05 mol L ⁻¹ [Na ₂ SO ₄] (electrolyte), pH 3.0, 1,000 mL min ⁻¹ air flow rate, 0.5 mmol L ⁻¹ [Fe ²⁺], 5 mA cm ⁻² current density	98.49% removal efficiency for 50 mg L ⁻¹ Rh B and 9.58 mmol L ⁻¹ [H ₂ O ₂] after 360 min electrolysis	[41]
PTFE@MWCNT	EF	<i>m</i> -cresol	200 mL reaction compartment, 38 cm ² Ti/SnO ₂ -Sb ₂ O ₅ -IrO ₂ anode, 0.1 mol L ⁻¹ [Na ₂ SO ₄] (electrolyte), pH 3.0, 1,000 mL min ⁻¹ air flow rate, 0.4 mmol L ⁻¹ [Fe ²⁺], 2.9 mA cm ⁻² current density	99% removal efficiency for 100 mg L ⁻¹ <i>m</i> -cresol and 4.76 mmol L ⁻¹ [H ₂ O ₂] after 150 min electrolysis	[42]
MWCNT/graphite	Photocatalytic- EF	AY36	1000 mL reaction compartment, 11.5 cm ² Pt anode, 0.05 mol L ⁻¹ [Na ₂ SO ₄] (electrolyte), pH 3.0, 2500 mL min ⁻¹ air flow rate, 0.1 mmol L ⁻¹ [Fe ²⁺], 2.7 mA cm ⁻² current density	82.24% removal efficiency for 20 mg L ⁻¹ AY36 and 0.12 mmol L ⁻¹ [H ₂ O ₂] after 180 min electrolysis	[43]
MWCNT/GDE	Photo-EF	Acid Blue 5 (AB5)	2000 mL recirculation reactor with UV lamp, 1.0 cm ² Pt anode, 0.05 mol L ⁻¹ [Na ₂ SO ₄] (electrolyte), pH 3.0, 1000 mL min ⁻¹ solution flow rate, 0.2 mmol L ⁻¹ [Fe ²⁺], 2.9 mA cm ⁻² current density	23% and 98.25% removal efficiency of EF and photo-EF processes for 20 mg L ⁻¹ AB5, respectively, after 60 min reaction time	[44]
		Direct Red 23 (DR23)		94.29% removal efficiency for 30 mg L ⁻¹ DR23 (after 60 min reaction time)/c	[45]

(continued)

Table 1 (continued)

Modified cathode	Process	Pollutant	Operational parameters	Maximum efficiency reported	Ref.
MWCNT-surfactant/graphite	EF	Acid Red 14 (AR14) and Acid Blue 92 (AB92)	1000 mL continuous reactor, 26 cm ² graphite anode, 0.05 mol L ⁻¹ [Na ₂ SO ₄] (electrolyte), pH 3.0, 5.5 mL min ⁻¹ solution flow rate, 0.1 mmol L ⁻¹ [Fe ³⁺], 6.92 mA cm ⁻² current density	99% and 95% removal efficiency for 50 mg L ⁻¹ AR14 and AB92, respectively, after 220 min reaction time	[46]
	Heterogeneous-EF		250 mL reaction compartment, 26 cm ² graphite anode, 0.05 mol L ⁻¹ [Na ₂ SO ₄] and [NaCl] (electrolyte), pH 3.0, 1.0 g L ⁻¹ Fe ₃ O ₄ NPs, 6.92 mA cm ⁻² current density	100% removal efficiency for 50 mg L ⁻¹ AR14 and AB92 in NaCl electrolyte solution after 120 min reaction time	[47]
Fe-CNT/GDE	EF	-	250 mL reaction compartment, 11.4 cm ² graphite anode, 0.05 mol L ⁻¹ [Na ₂ SO ₄] (electrolyte), pH 3.0, 400 mL min ⁻¹ O ₂ flow rate, 0.1 mmol L ⁻¹ [Fe ²⁺], -0.85 V voltage	3.23 mmol L ⁻¹ [H ₂ O ₂] after 90 min electrolysis and 58% current efficiency	[48]
N-doped carbon nanotubes (NCNT)/nickel foam (NF)/CNT	EF	<i>p</i> -Nitrophenol	200 mL reaction compartment, 2.25 cm ² Pt anode, 0.05 mol L ⁻¹ [Na ₂ SO ₄] (electrolyte), pH 3.0, 400 mL min ⁻¹ air flow rate, 0.4 mmol L ⁻¹ [Fe ³⁺], 20 mA cm ⁻² current density	99% removal efficiency for 50 mg L ⁻¹ <i>p</i> -nitrophenol and 0.62 mmol L ⁻¹ [H ₂ O ₂] after 180 min electrolysis	[49]
Polypyrrole@MWCNT/graphite	EF	Basic Blue 41 (BB 41)	100 mL reaction compartment, 10.0 cm ² Pt anode and cathode, 0.1 mol L ⁻¹ [Na ₂ SO ₄] (electrolyte), pH 3.0, 300 mL min ⁻¹ air flow rate, 2.0 mmol L ⁻¹ [Fe ³⁺], -0.55 V (vs. SCE) voltage	About 94% removal efficiency for 15 mg L ⁻¹ BB 41, 0.16 mmol L ⁻¹ [H ₂ O ₂] after 10 min electrolysis	[50]
N-CNTs-PTFE	EF	MO	250 mL reaction compartment, Pt wire anode, 0.05 mol L ⁻¹ Na ₂ SO ₄ (electrolyte), pH 3.0, 400 mL min ⁻¹ O ₂ flow rate, 0.2 mmol L ⁻¹ [Fe ²⁺], -0.85 V voltage	100% removal efficiency for 50 mg L ⁻¹ MO, 4.28 mmol L ⁻¹ [H ₂ O ₂] after 60 min electrolysis and 62% current efficiency	[51]

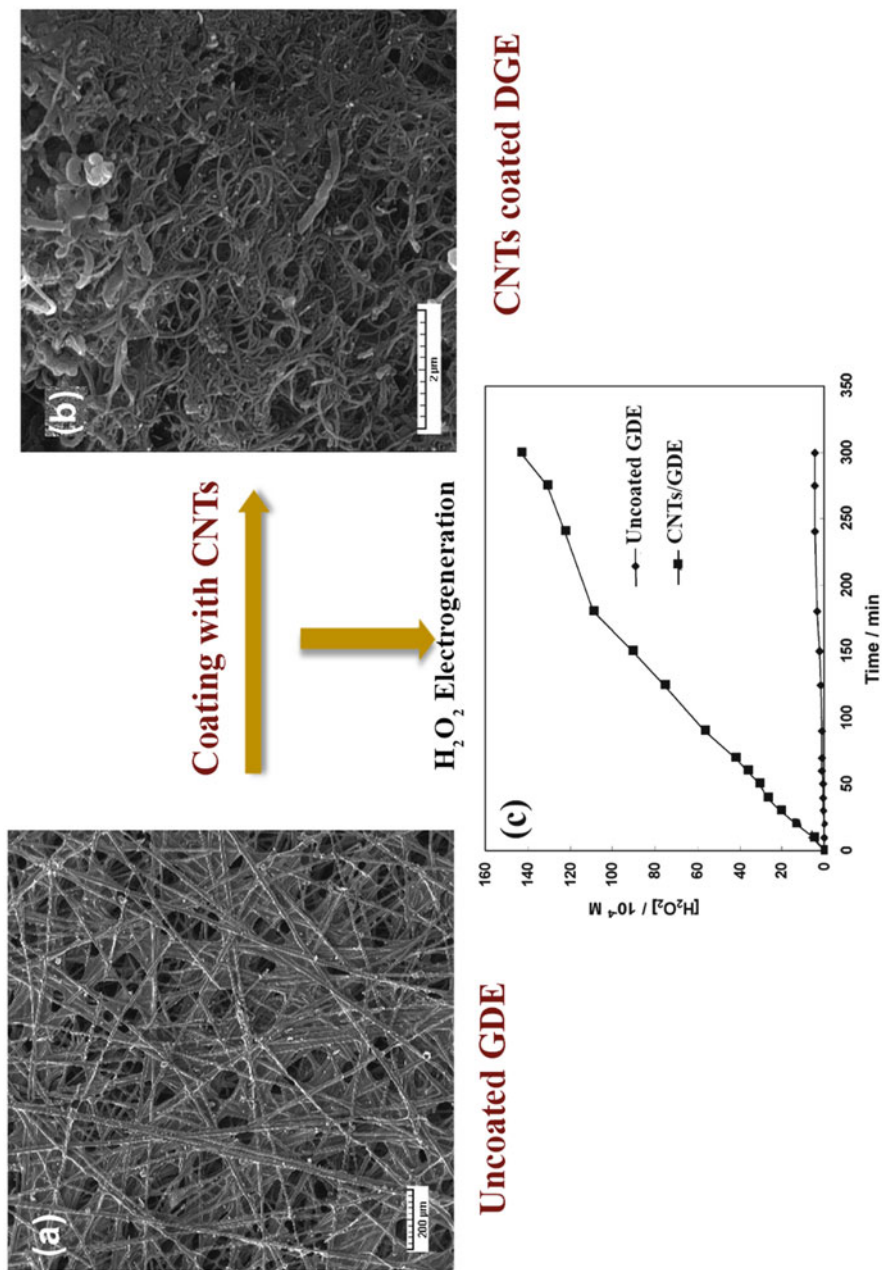


Fig. 4 SEM image of surface of cathodes: (a) uncoated GDE, (b) CNTs/GDE, and (c) the amount of electro-generated H_2O_2 at the uncoated GDE and CNTs/GDE cathodes after 300 min electrolysis (Adapted from [52] with permission from publisher, Elsevier. License Number: 4054120708166)

In another study, graphite electrode was modified by CNTs for treatment of Acid Yellow 36 (AY36) by photo-EF process [5]. The electro-generated H_2O_2 concentration using the CNTs/graphite cathode was approximately seven times greater than that of bare graphite cathode. The decolorization efficiency of AY36 was 31.07 and 70.98% after 120 min of photo-EF treatment for bare graphite and CNTs/graphite, respectively [5]. Also, graphite electrode was modified with MWCNTs accompanied by a cationic surfactant (cetyl trimethyl ammonium bromide (CTAB)) and used as a cathode to degrade two acid dyes by homogeneous and heterogeneous EF processes [46, 47]. The electrodeposition method was used to modify the graphite electrode surface, which was performed by applying the DC voltage to the MWCNTs and CTAB solution. High dye removal efficiency was achieved when MWCNT/graphite was as the cathode compared to the graphite electrode (92% against 64% for 50 mg L^{-1} of dyes), due to the higher electro-generation of H_2O_2 on the surface of the MWCNT/graphite cathode [46, 47].

Recently, some studies revealed that the introduction of nitrogen atoms to the pristine CNT structure can lead to promote the chemical and electrochemical reactivity of surface for oxygen reduction reaction by the generation of extra electron density in the graphite lattice [33, 38]. Zhang et al. [51] prepared the nitrogen functionalized CNT (N-CNT) electrode as a GDE cathode in EF process. In this study, pulsed high voltage discharge was applied to functionalize MWCNTs in a liquid-gas reactor. The results showed that among three electrodes including graphite, CNTs, and N-CNTs, the N-CNT electrode indicated the highest yield of H_2O_2 formation and faster color removal in EF process. The amount of generated H_2O_2 on the graphite, CNT, and N-CNT electrodes were 2.72, 3.06, and 4.28 mmol L^{-1} , respectively. Furthermore, the N-CNT electrode had the greater current efficiency compared to that of CNT electrode. The results confirmed that the nitrogen functionalization did facilitate the electron transfer to improve the production of H_2O_2 .

Nitrogen-doped MWCNTs (N-CNTs) was also used as the catalyst layer on the GDE cathode, which was prepared by immobilizing MWCNTs as the diffusion layer on the surface of nickel foam (NF) as the supporting material [49]. Results showed that the N-CNT/NF/CNT GDE exhibited higher H_2O_2 production amount and greater current efficiency in comparison with the CNT/NF/CNT GDE, consequently, the EF degradation level and total organic carbon (TOC) removal efficiency were higher.

2.2 Graphene Family

Graphene and its derivatives, such as GO, rGO, and few-layer GO, have been thoroughly investigated since their discovery because of their special physical-chemical properties [55]. Graphene, GO, and rGO have different morphological and chemical characteristics as shown in Fig. 5. Pristine graphene consists of a carbon monoatomic layer, 2D planar sheet of carbon atoms in the sp^2 hybridization state, which are densely organized into a honeycomb array (Fig. 5a) [56]. It was first

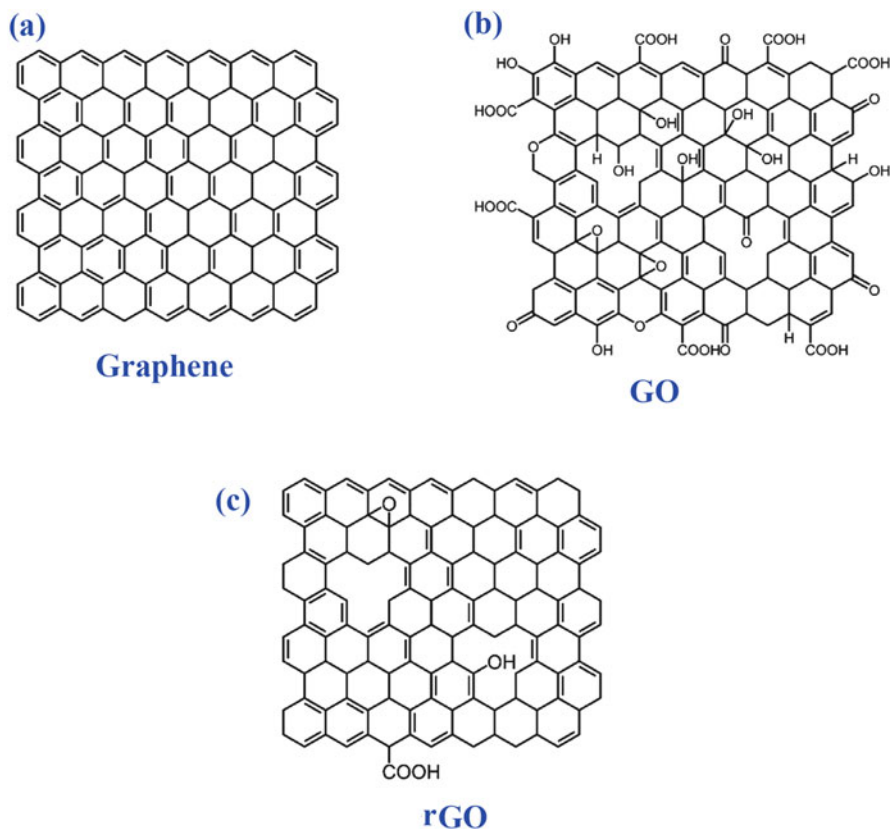


Fig. 5 Schematic illustrating the chemical structure of a single sheet of (a) graphene, (b) GO, and (c) rGO

achieved in 2004 by Novoselov and Geim [57], who prepared graphene sheets by micro-mechanical splitting of oriented pyrolytic graphite and definitively recognized using microscopy. In recognition of the enormous significance of graphene for different applications, its discovery was awarded the 2010 Nobel Prize in Physics. Theoretical and experimental investigations have evidenced that graphene has numerous outstanding properties, comprising a huge specific area (around $2,630 \text{ m}^2 \text{ g}^{-1}$) [55], exceptional mechanical strength (tensile strength of 130 GPa and Young's modulus of 1,000 GPa) [58], high thermal conductivity (in the range of $4,840\text{--}5,300 \text{ W m}^{-1} \text{ K}^{-1}$) [59], high electrical conductivity (up to $6,000 \text{ S cm}^{-1}$) [60], great charge-carrier mobility at room temperature ($2 \times 10^5 \text{ cm}^2 \text{ V}^{-1} \text{ s}^{-1}$) [61], and chemical inertness [62]. Consequently, it is not surprising that graphene has attracted great interest for using in a plethora of various applications, such as supercapacitors, batteries, solar cells, fuel cells, etc. [33, 38].

In general, graphene can be produced either by bottom-up or top-down techniques. The bottom-up method comprises epitaxial growth and chemical vapor

deposition (CVD), including the direct preparation of defect-free graphene from hydrocarbon precursors on solid substrates (Ni or Cu) [38, 63]. Top-down methods, such as electrochemical exfoliation and reduction of GO, refer to the mechanical cleaving of graphite layers for the mass fabrication of graphene sheets. Top-down methodologies present the opportunity to economically synthesize graphene, but it is difficult to obtain high-purity graphene sheets because of the introduction of defects through exfoliation process [29, 38].

The GO is another member of the graphene family, which is an oxygen-functionalized graphene that is fabricated by exfoliation of graphite oxide [64]. The GO is viewed mainly as the precursor to generate graphene [38]. On the GO surface, there are plentiful oxygen-based groups, including epoxy (1,2-ether) (C-O-C) and hydroxyl ($-OH$) groups, located on the hexagonal array of carbon plane, and carbonyl ($-C=O$) and carboxyl ($-COOH$) groups, located at the sheet edges (see Fig. 5b) [56].

The rGO, graphene-like, can be prepared via top-down methods including thermal, chemical, and electrochemical reduction of GO to decrease its oxygen content, with the ratio of C/O rising from 2:1 to up to 246:1 (Fig. 5c) [65]. Although the rGO possesses more defects and thus has less conductivity than pristine graphene, it is enough conductive for use as the electrode material for numerous applications [66]. As graphene, the rGO has also received great attention for different applications in electrochemical devices due to its high specific surface area, functional groups containing oxygen, and hydrophilicity [38]. The oxygen functionalities are opening an adjustable bandgap which is responsible for particular electronic and optical properties [56].

According to the mentioned properties, graphene and its derivatives are alternative candidates for potential use as carbon-based nanomaterials for improving the efficiency of cathode materials employed in EF system. Various scientific reports on applications of graphene family for modification of the cathodes in EF process is summarized in Table 2.

Recently, Mousset and co-workers [76] studied the efficiency of pristine graphene (in the forms of monolayer (G_{mono}), multilayer (G_{multi}), and foam (G_{foam})) as the cathode material in EF process for phenol treatment. It was found that the generated H_2O_2 concentration on the G_{foam} ($0.250 \text{ mmol L}^{-1}$) cathode was 5–50 times more than that on the G_{multi} ($0.055 \text{ mmol L}^{-1}$) and G_{mono} ($0.005 \text{ mmol L}^{-1}$), respectively. The degradation efficiency of 1 mmol L^{-1} phenol was 10.1%, 20.1%, and 62.7% for G_{mono} , G_{multi} , and G_{foam} electrodes, respectively. Therefore, the higher performance of G_{foam} cathode was attributed to its greater electroactive surface area and its higher electrical conductivity than other forms of pristine graphene. Therefore, G_{foam} cathode showed higher phenol degradation and mineralization efficiency than other graphene-based cathodes due to greater rates of $\cdot OH$ formation over Fenton's reaction. Furthermore, less energy consumption and higher mineralization efficiency were achieved by using G_{foam} cathode in comparison with carbon felt cathode, because of the higher electrical conductivity of G_{foam} . The G_{foam} cathode displayed excellent stability as degradation occurred after 10 EF runs.

Table 2 Results reported for modified cathodes with graphene family in EF process

Modified cathode	Process	Pollutant	Operational parameters	Maximum efficiency reported	Ref.
Graphene/graphite-PTFE	EF	Reactive brilliant blue (KN-R)	200 mL three-electrode undivided cell, 6.0 cm ² Pt sheet counter, SCE reference, 0.05 mol L ⁻¹ Na ₂ SO ₄ (electrolyte), pH 3, 333 mL min ⁻¹ O ₂ flow rate, 0.75 mmol L ⁻¹ [Fe ²⁺], 2.0 mA cm ⁻² current density	33.3% TOC decay for 50 mg L ⁻¹ KN-R, 5.5 mmol L ⁻¹ [H ₂ O ₂] after 180 min reaction time, 40% current efficiency (for graphite, G, and PTFE solution with the mass ratio of 8:1:2)	[67]
Graphene/glassy carbon	EF	MB	100 mL three-electrode undivided cell, Pt foil counter, SCE reference, 0.1 mol L ⁻¹ [Na ₂ SO ₄] (electrolyte), pH 3, 11.2 mmol L ⁻¹ [Fe ²⁺], -1.0 V voltage	97% removal efficiency for 12 mg L ⁻¹ MB after 160 min reaction time	[36]
ErGO/carbon felt	EF	AO7	30 mL reaction compartment, 2 cm ² Pt anode, 2 cm ² cathode surface, 0.05 mol L ⁻¹ [Na ₂ SO ₄] (electrolyte), pH 3, 0.2 mmol L ⁻¹ [Fe ²⁺], 20 mA cm ⁻² current density	100% removal efficiency for 100 mg L ⁻¹ AO7 and 94.3% TOC removal after 20 min EF process	[68, 69]
Graphene-PPy/polyester filter cloth/fabric membrane	EF-cathodic membrane filtration	MB	50 mL reaction compartment, stainless iron mesh anode, 0.05 mol L ⁻¹ [Na ₂ SO ₄] (electrolyte), pH 4, 200 mL min ⁻¹ air flow rate, 0.2 mmol L ⁻¹ [Fe ²⁺], -1.0 V voltage, 99 L m ⁻² membrane flux	95% removal efficiency for 5 mg L ⁻¹ MB in 90 min	[70]
ErGO/GDE	Cathodic electrochemical oxidation	BPA	30 mL electrochemical reactor, 1.0 cm ² Pt anode, 0.05 mol L ⁻¹ [Na ₂ SO ₄] (electrolyte), pH 6.5, 2.86 mA cm ⁻² current density, 60 min electrolysis for rGO	100% removal efficiency for 20 mg L ⁻¹ BPA and 74.6% TOC removal in 30 min and 1.17 mmol L ⁻¹ [H ₂ O ₂] in 60 min electrolysis time	[71]
Graphene @Fe ₃ O ₄ /Ni foam	Heterogeneous-EF	MB	150 mL reaction compartment, 8.0 cm ² Pt anode, 0.05 mol L ⁻¹ [Na ₂ SO ₄] (electrolyte), pH 2.0, 0.5 mA cm ⁻² current density	97% removal efficiency for 10 mg L ⁻¹ MB in 24 min	[72]

(continued)

Table 2 (continued)

Modified cathode	Process	Pollutant	Operational parameters	Maximum efficiency reported	Ref.
Graphene@PTFE	EF	2,4-Dichlorophenol (2,4-DCP) and Rh B	50 mL reaction compartment, 1.0 cm ² Pt anode, 0.07 mol L ⁻¹ [Na ₂ SO ₄] (electrolyte), pH 3.0, 2.0 mmol L ⁻¹ [Fe ²⁺], 40 mA cm ⁻² current density	100% and 97.6% removal efficiency for Rh B and 2,4-DCP, respectively, 0.17 mmol L ⁻¹ [H ₂ O ₂] in 150 min electrolysis and 58% current efficiency	[73]
Pd@rGO/carbon felt	EF	EDTA-Ni	450 mL reaction compartment, 54 cm ² graphite tube anode, 35 cm ² cathode surface/ 0.05 mol L ⁻¹ [Na ₂ SO ₄] (electrolyte), pH 4.0, 1.0 mmol L ⁻¹ [Fe ²⁺], 5.7 mA cm ⁻² current density	83.8% removal efficiency for 10 mg L ⁻¹ EDTA-Ni in 100 min treatment	[74]
AQ@ErGO/Ni screen	Heterogeneous-EF	Rh B	200 mL reaction compartment, Pt wire anode, 0.5 mol L ⁻¹ [Na ₂ SO ₄] and [MgSO ₄] (electrolyte), pH 3.4 and 11.3, 600 mL min ⁻¹ O ₂ flow rate, 100 g L ⁻¹ FeOOH- γ -Al ₂ O ₃ , -0.5 V voltage	100% removal efficiency for 10 mg L ⁻¹ Rh B, 4.83 mmol L ⁻¹ [H ₂ O ₂] in 120 min reaction time and 83.4% and 67.5% current efficiency for Na ₂ SO ₄ and MgSO ₄ as electrolytes, respectively	[75]
3D graphene foam	EF	Phenol	150 mL reaction compartment, 30 cm ² Pt anode, 20 cm ² cathode surface area, 0.05 mol L ⁻¹ [K ₂ SO ₄] (electrolyte), pH 3.0, 200 mL min ⁻¹ air flow rate, 0.1 mmol L ⁻¹ [Fe ²⁺], -0.6 V voltage	78% removal efficiency for 1.0 mmol L ⁻¹ phenol and 0.25 mmol L ⁻¹ [H ₂ O ₂] in 120 min electrolysis	[76]
Graphene/carbon cloth			80 mL reaction compartment, 15 cm ² Pt anode, 24 cm ² cathode surface area, 0.05 mol L ⁻¹ [K ₂ SO ₄] (electrolyte), pH 3.0, 200 mL min ⁻¹ air flow rate, 0.1 mmol L ⁻¹ [Fe ²⁺], 1.25 mA cm ⁻² current density	80% removal efficiency for 1.4 mmol L ⁻¹ phenol and 40% TOC removal and 2.00 mmol L ⁻¹ [H ₂ O ₂] in 120 min electrolysis	[34]
N-doped graphene@MWC-NT/stainless steel	EF	Dimethyl phthalate (DMP)	100 mL reaction compartment, 4 cm ² Pt foil anode, 0.05 mol L ⁻¹ [Na ₂ SO ₄] (electrolyte), pH 3.0, 450 mL min ⁻¹ air flow rate, 0.5 mmol L ⁻¹ [Fe ²⁺], -0.2 V voltage	99% removal efficiency for 50 mg L ⁻¹ DMP and 9.03 mmol L ⁻¹ [H ₂ O ₂] after 120 min electrolysis	[77]

CeO ₂ /rGO	EF	Ciprofloxacin (CIP)	250 mL reaction compartment, 0.5 cm ² Pt anode, 24 cm ² cathode surface area, 0.05 mol L ⁻¹ [Na ₂ SO ₄] (electrolyte), pH 3.0, 100 mL min ⁻¹ O ₂ flow rate, 0.1 mmol L ⁻¹ [Fe ²⁺], 53.3 mA cm ⁻² current density	90.97% removal efficiency for 50 mg L ⁻¹ CIP in 6.5 h treatment 100% removal efficiency for 50 mg L ⁻¹ CIP in 5 h treatment	[78] [79]
Ce _{0.75} Zr _{0.25} O ₂ /rGO					
Quinone@graphene@Fe ₃ O ₄ /carbon cloth	Heterogeneous-EF	BPA	60 mL undivided cylindrical cell, 10.0 cm ² Pt anode, 10.0 cm ² cathode surface area, Ag/AgCl reference electrode, 0.05 mol L ⁻¹ [Na ₂ SO ₄] (electrolyte), pH 3.0, 1000 mL min ⁻¹ air flow rate, -2.4 V voltage	100% removal efficiency for 5 mg L ⁻¹ BPA in 90 min treatment and 4.37 mmol L ⁻¹ [H ₂ O ₂] at pH 3	[80]

In another study by this group [34], high purity of graphene was prepared by electrochemical exfoliation. Synthesized graphene was combined with Nafion as a binder to make a conductive ink which was then employed to modify the carbon cloth electrode [34]. The optimal amounts of graphene and Nafion in the ink were found to be 1.0 mg mL^{-1} and 0.025% (w/v), respectively, with a graphene mass loading of 0.27 mg cm^{-2} on the carbon cloth surface. A graphical illustration of preparation of graphene-modified carbon cloth electrode is depicted in Fig. 6. The results showed that the graphene-modified carbon cloth cathode improves electrochemical properties, such as the 97% decline of the charge transfer resistance and an 11.5-fold increment of the electroactive surface area compared with raw carbon cloth [34]. As illustrated in Fig. 6, the maximum electro-generated H_2O_2 concentrations were 1.01 mmol L^{-1} and 1.99 mmol L^{-1} for the uncoated and graphene-coated carbon cloth cathodes, respectively [34]. The superior electrochemical behaviors of the graphene-coated carbon cloth cathode were further proved by the improved performance in EF process for degradation of phenol. Thus, the pseudo-first-order kinetic rate constant (k_{app}) values of phenol degradation on the uncoated and graphene-coated carbon cloth cathodes were 0.0051 and 0.0157 min^{-1} , respectively, a 3.08-fold increase.

Le et al. [68, 69] modified CF electrode with rGO, which was prepared by an electrophoretic deposition of GO and was reduced with the different methods including electrochemical, chemical, and thermal. Among the used reduction methods, the electrochemical reduction of GO under a constant potential (-0.45 V vs. SCE) without addition of any binder or reductant demonstrated remarkable advantages. The schematic of preparation of electrochemically reduced GO (ErGO)/CF electrode and SEM images of ERGO/CF and raw CF were presented in Fig. 7. The ErGO/CF cathode demonstrated significant electrochemical behaviors, such as the enhancement of electroactive surface area and the decline in charge transfer resistance compared to the raw CF cathode. This improvement accelerated the O_2 reduction rate on the cathode surface, which significantly increased the H_2O_2 accumulation in the solution. Consequently, the destruction rate of Acid Orange 7 (AO7) by the EF process was two times greater on the ErGO/CF cathode compared to uncoated CF. TOC removal after 2 h degradation was 73.9% on the ErGO/CF electrode, and this was 18.3% greater than on the unmodified CF (Fig. 7c). Moreover, the ErGO/CF cathode presented good stability over ten runs of EF process for mineralization of AO7.

Chen et al. [36] modified the glassy carbon electrode and studied the effect of annealing temperature of GO (250 and $1,000^\circ\text{C}$) on the electro-generated H_2O_2 efficiency in EF process. The results indicated that the thermally reduced GO annealed at 250°C (G250) was more efficient for mineralization of methylene blue (MB) by the EF method. The oxygen functionalities in G250 were responsible for the high two-electron oxygen reduction selectivity and highest formation rate of H_2O_2 [36].

The results of studies obviously indicated that modification of carbon-based electrode surface with quinone functional groups could remarkably improve the redox activity of the electrode and facilitate the two-electron reduction of O_2 to H_2O_2 reaction on the cathode [75, 80–82]. Zhang and co-worker [75] studied the

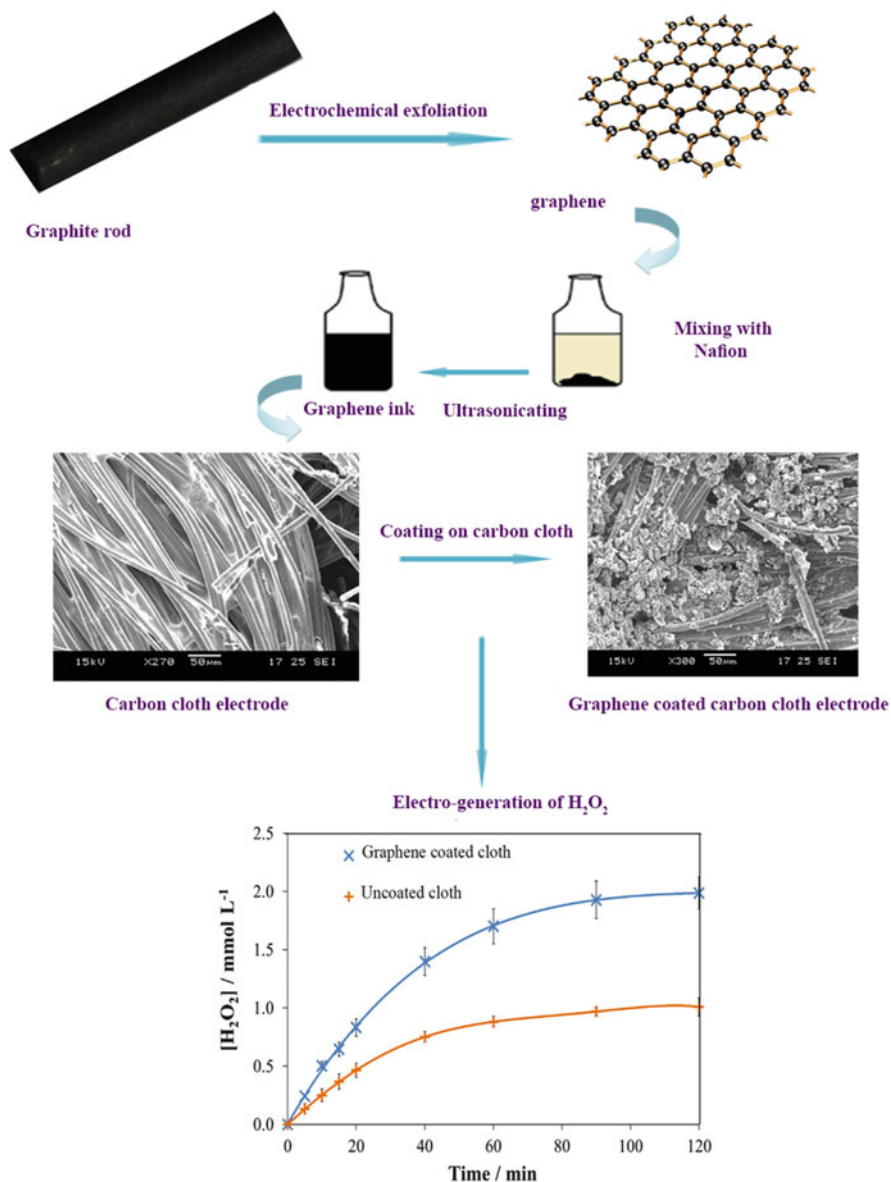


Fig. 6 Schematic steps of preparation of graphene-coated carbon cloth cathode and H₂O₂ accumulation yield of uncoated and graphene-coated carbon cloth cathodes (SEM images and H₂O₂ accumulation yield curves adapted from [34], with permission from Elsevier. License Number: 4047601289247)

electro-generation of H₂O₂ on anthraquinone@ErGO (AQ@ErGO) coated on nickel screen surface cathode and its performance for degradation of Rh B by FeOOH-catalyzed heterogeneous EF process. The strong interfacial connections of

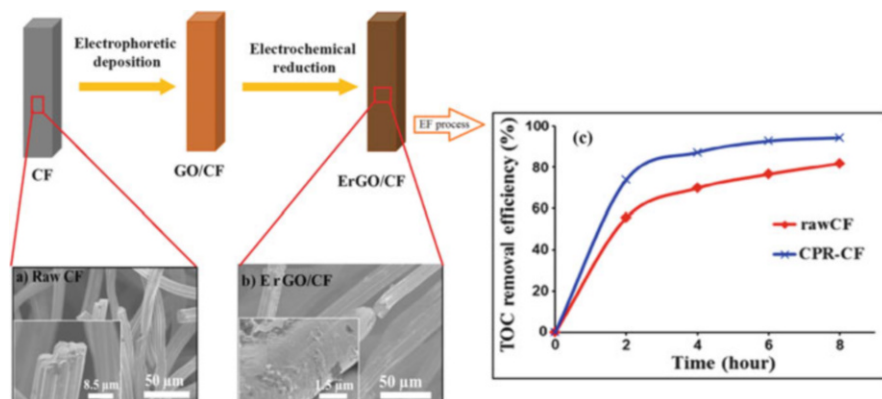
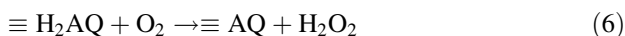
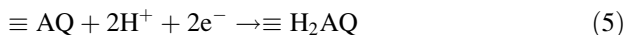


Fig. 7 Schematic steps of preparation of ErGO/CF cathode, SEM images of (a) raw CF, (b) ErGO/CF, and (c) TOC removal after 8 h EF process using raw CF and ErGO/CF cathodes. (Adapted from [68], with permission from Elsevier. License Number: 4036640134966)

ErGO and AQ molecules led to the efficient production of H_2O_2 at the cathode. The AQ@ErGO cathode can efficiently catalyze the two-electron reduction of O_2 to produce H_2O_2 (reactions (5) and (6)) on the cathode/bulk solution interface:



The accumulated concentration of H_2O_2 was obtained at 4.01 and 4.86 mmol L^{-1} in 0.5 mol L^{-1} MgSO_4 and Na_2SO_4 electrolyte, respectively, after 120 min of electrolysis. Then, electro-generated H_2O_2 molecules are catalytically converted into $\cdot\text{OH}$ by the FeOOH nanoparticles, and the dissolved iron ions in MgSO_4 catholyte. Since, no dissolved iron ions were detected in Na_2SO_4 catholyte, the high yield of the hetero-EF process is ascribed generally to the H_2O_2 activation through the surface of FeOOH nanoparticles to form $\cdot\text{OH}$ and $\text{HO}_2\cdot$ ($\text{O}_2\cdot^-$).

Zhao et al. [70] synthesized the graphene/polypyrrole (PPy) modified conductive cathode membrane for the EF filtration treatment of MB as a model pollutant. The better performance of membrane cathode for treatment of MB was obtained by doping with anthraquinone monosulfonate (AQS). The observed performance enhancement can be attributed to the electrical conductivity improvement, resulted by doping with AQS [70].

In recent years, researchers studied the several carbon nanocomposites with metal/metal oxide for modification of electrodes in EF process. Magnetite (Fe_3O_4) seems to be promising candidate for this purpose owing to its reversible redox nature and stability. These modified electrodes revealed extraordinary mechanical stability, making them noteworthy as stable materials for in situ generation of H_2O_2 and $\cdot\text{OH}$, diminishing the iron sludge formation, exhibiting much higher activity than homogenous EF systems under a neutral pH.

Shen et al. [72] synthesized graphene- Fe_3O_4 (G-FeO) hollow hybrid microspheres by a simple aerosolized spray drying method by using ferric ion and GO with various contents (e.g., 0, 5, 15, 30 wt%) as the precursor materials. Subsequently, the obtained composites were coated on the surface of Ni foam cathode. The results of electrochemical studies obviously indicated that the G-FeO composite with graphene content of 30 wt% (30G-FeO) exhibited higher conductivity and lower charge transfer resistance. Also, the two-electron pathway was the dominated process for O_2 reduction on the 30G-FeO electrode. The yield of H_2O_2 generation notably increased when 30G-FeO was applied as the cathode in EF process. The MB degradation rate constant value of 30G-FeO coated Ni foam cathode at pH 2 was 0.140 min^{-1} , which was nearly 8.75 times greater than that for the uncoated Ni foam cathode (0.016 min^{-1}). Figure 8 shows the schematic illustration of EF system and mechanism for MB degradation process on the 30G-FeO cathode.

Researches revealed that palladium (Pd) nanoparticles could interact with graphene-based materials and exhibited extraordinary electrocatalytic ability. Zhang et al. [74] modified CF cathode with Pd@rGO composite and Nafion as a binder. Pd@rGO/CF cathode exhibited high electrocatalytic activity and stability for the elimination of ethylenediaminetetraacetic acid (EDTA)-Ni complex solution by the EF method.

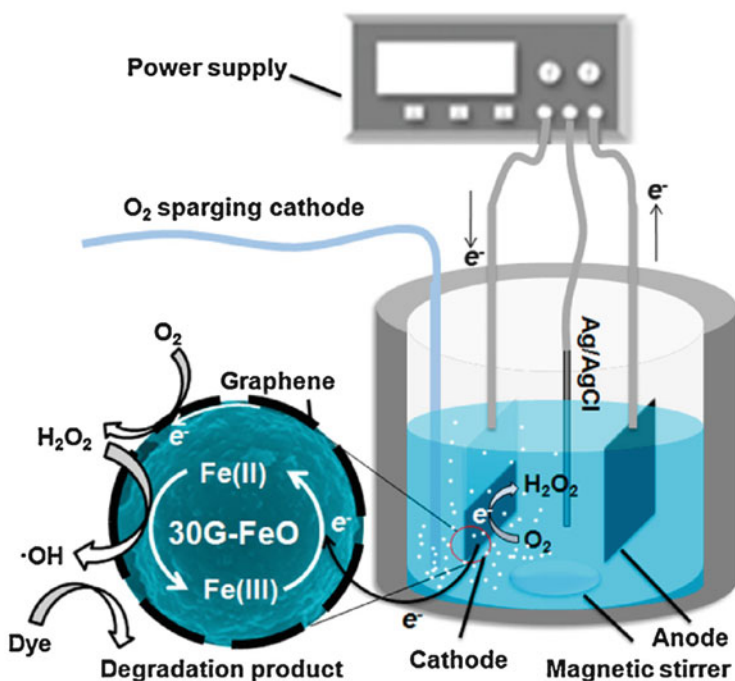


Fig. 8 Schematic illustration of EF system and mechanism for MB degradation process on the 30G-FeO cathode (Reprinted from [72], with permission from Elsevier. License Number: 4037580393197)

Govindaraj et al. [80] synthesized a quinone-functionalized graphene by the electrochemical exfoliation approach (QEEG) followed by prepared QEEG@Fe₃O₄ nanocomposite. Then, QEEG and prepared nanocomposite were used for modifying the surface of the noncatalyzed carbon cloth (NCC) electrode. The SEM images of the NCC and the modified NCC are shown in Fig. 9a. The obtained results demonstrated that the produced H₂O₂ concentration at the QEEG electrode was approximately nine times higher than that at the NCC electrode at pH 3.0 and four times greater at natural pH (see Fig. 9b), which can be attributed to the presence of the quinone functional group and high electroactive surface area in the QEEG structure. Substantial improvement in the electro-generation of [•]OH radicals was observed with QEEG@Fe₃O₄ modified cathodes. Complete degradation of Bisphenol A (BPA) by EF process was achieved using the QEEG@Fe₃O₄ modified electrode in 90 min at pH 3. Also, 98% degradation yield was obtained at neutral condition with less than 1% of iron leaching. Schematic illustration of the overall mechanisms relating to QEEG@Fe₃O₄ modified cathode in the EF treatment of BPA is shown in Fig. 9c.

2.3 Mesoporous Carbons

In the past two decades, mesoporous carbons (with pore size distribution in the range 2–50 nm) have attracted great consideration for use as electrode materials in various applications [29]. These carbon-based nanomaterials have delivered noteworthy advantages such as high specific surface areas for a huge number of surface-active sites, good electrical conductivity for facile electron transport, large accessible space for fast mass transport, high mechanical and chemical durability for powerful electrode longevity, and low density [83]. The synthetic approaches comprising hard and soft templates have established to be the most effective methods for the construction of mesoporous carbons with distinct pore structures and narrow distribution of pore sizes [29]. In these preparation methods, mesoporous carbon structures can be obtained after curing of carbonaceous precursor, elimination of template, and carbonization. In the hard templating method, inorganic templates (hard templates), including metal-organic frameworks (MOFs), zeolites, silicas, and MgO, were employed to synthesize ordered mesoporous carbons (OMC) [29, 83]. Silica templates with ordered mesoporous framework were prepared by templating self-formation of surfactants, such as SBA-15, MCM-48, and MCM-41 [83]. Schematic graphic of the preparation of OMC by silica hard templates is shown in Fig. 10. On the other hand, in the soft templating technique, phenolic resin and some block copolymer surfactants were mainly used as organic templates to produce highly OMC through organic-organic assembly of surfactants and phenolic resins [29]. Additionally, by incorporating soft and hard templating approaches, hierarchically porous carbon (HPC), sometimes described as carbon nanoarchitecture, with organized porosity on multiple levels can be achieved [29, 84].

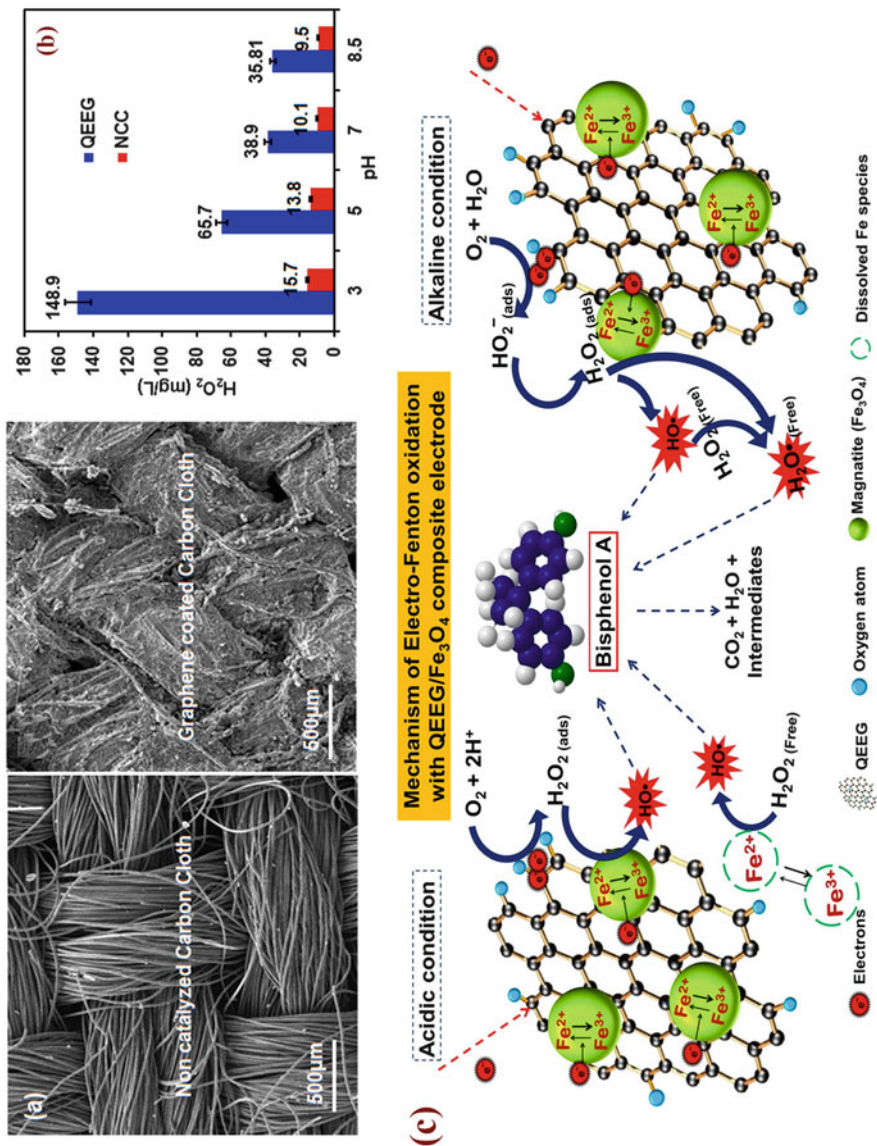


Fig. 9 (a) SEM images of NCC and QEEG coated carbon cloth, (b) difference in H_2O_2 formation with NCC and QEEG modified cathodes, and (c) schematic illustration of the overall mechanisms relating to QEEG/ Fe_3O_4 modified cathode in the EF treatment of BPA (Reprinted from [80], with permission from Elsevier. License Number: 4047001318719)

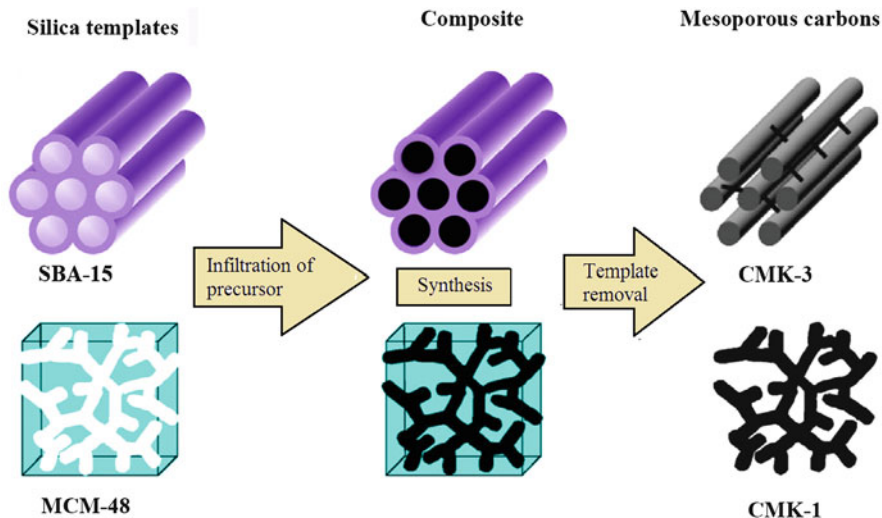


Fig. 10 Schematic graphic of the preparation of OMC by silica hard templates

Recently, mesoporous carbons have been considered to be exceptional candidates for modification of cathode electrode in EF process, which can facilitate the diffusion and transformation of O_2 at the cathode surface and enhance the electro-generation yield of H_2O_2 [85–88]. Table 3 summarizes the main reported modified cathode with CNTs and their derivatives in EF process. Hu et al. [85] grafted the surface of activated carbon fiber (ACF) cathode with OMC, which was prepared by soft templating method. For comparison, ACF was also modified with a layer of disordered mesoporous carbon (DMC). The results demonstrated that the production rate of $\cdot OH$ radicals pursued the order of $OMC/ACF > DMC/ACF > ACF$, which was in accordance with the H_2O_2 generation rate and Brilliant Red X3B (X3B) degradation rate. A graphical illustration of preparation of OMC modified ACF cathode is depicted in Fig. 11.

As previously mentioned, heteroatom (e.g., sulfur and nitrogen) doping of carbon materials can improve their surface attributes, specifically the electrical conductivity and the polarity of surface. For this aim, nitrogen-doped mesoporous carbons were prepared by nitrogenous precursors. For instance, nitrogen-doped OMC (N-OMC) was prepared by dicyandiamide ($C_2H_4N_4$) and was coated onto the surface of ACF cathode (N-OMC/ACF), which showed more electrocatalytic activity and lower overpotential for O_2 reduction compared to OMC/ACF cathode in the EF process [86].

Perazzolo et al. [91, 92] synthesized nitrogen- and sulfur-doped or co-doped mesoporous carbons (N-MC, S-MC, and N,S-MC) by means of a hard template method and used them for modifying glassy carbon electrode for the in situ formation of H_2O_2 and degradation of MO by the EF system. The N-MC modified

Table 3 Results reported for modified cathodes with mesoporous carbons in EF process

Modified cathode	Process	Pollutant	Operational parameters	Carbon mesoporous characteristics	Maximum efficiency reported	Ref.
OMC/ACF	EF	X3B	200 mL reaction compartment, 12 cm ² Pt, 9.0 cm ² cathode surface, 0.1 mol L ⁻¹ [Na ₂ SO ₄] (electrolyte), pH 3.0, 1.0 mmol L ⁻¹ [Fe ²⁺], 600 mL min ⁻¹ air flow rate, 6.2 V voltage	S _{BET} = 722 m ² g ⁻¹ Mesopore volume = 0.19 cm ³ g ⁻¹	The EF degradation rate constant value of X3B in OMC/ACF cathode (0.055 min ⁻¹) was larger than in ACF cathode (0.018 min ⁻¹), 80.6% of TOC depletion was found within 60 min when using OMC/ACF cathode. The maximum H ₂ O ₂ concentration was of 9.4 μmol L ⁻¹ and 7.1 μmol L ⁻¹ in OMC/ACF and ACF cathode, respectively	[85]
N-doped OMC/ACF			250 mL reaction compartment, 9.0 cm ² graphite anode, 9.0 cm ² cathode surface, 0.1 mol L ⁻¹ [Na ₂ SO ₄] (electrolyte), pH 3.0, 1.0 mmol L ⁻¹ [Fe ²⁺], 600 mL min ⁻¹ air flow rate, 3.0 V voltage	Mass of dicyandiamide = 1.0 g S _{BET} = 501 m ² g ⁻¹ Pore volume = 0.35 cm ³ g ⁻¹ Mean pore size = 3.5 nm	The degradation rate of X3B by using of N (1.0)-OMC/ACF cathode was 50% higher than that of the OMC/ACF cathode. The maximum H ₂ O ₂ concentration was of 40.93 μmol L ⁻¹ and 21.75 μmol L ⁻¹ in N(1.0)-OMC/ACF and OMC/ACF cathode, respectively	[86]
OMC-5.4/ACF	EF	Rh B	200 mL reaction compartment, 12 cm ² Pt anode, 9.0 cm ² cathode surface, 0.1 mol L ⁻¹ [Na ₂ SO ₄] (electrolyte), pH 3.0, 1.0 mmol L ⁻¹ [Fe ²⁺], 600 mL min ⁻¹ air flow rate, -0.1 V voltage	S _{BET} = 486 m ² g ⁻¹ Pore volume = 0.45 cm ³ g ⁻¹ Mean pore size = 5.4 nm	100% of Rh B was degraded by OMC-5.4/ACF within 45 min, whereas the degradation rate of Rh B in the presence of OMC-3.7/ACF and OMC-2.6/ACF decreased to 93.2% and 71.2%, respectively. The concentration of	[87]

(continued)

Table 3 (continued)

Modified cathode	Process	Pollutant	Operational parameters	Carbon mesoporous characteristics	Maximum efficiency reported	Ref.
rGO@OMC/ ACF	EF	Dimethyl phthalate (DMP)	200 mL reaction compartment, 12 cm ² Pt anode, 9.0 cm ² cathode surface, 0.1 mol L ⁻¹ [Na ₂ SO ₄] (electrolyte), pH 3.0, 1.0 mmol L ⁻¹ [Fe ²⁺], 600 mL min ⁻¹ air flow rate, -0.7 V voltage	Dosage of rGO = 30 mg S _{BET} = 533.3 m ² g ⁻¹ Mean pore size = 3.8 nm	H ₂ O ₂ was 2.02 mmol L ⁻¹ in OMC-5.4/ACF, while it was 1.79 mmol L ⁻¹ in OMC-3.7/ACF as cathode materials	[35]
CMK-3/ GDE	EF	DMP	200 mL three-electrode undivided cell, Pt foil counter, SCE reference, 4.0 cm ² cathode surface, 0.1 mol L ⁻¹ [Na ₂ SO ₄] (electrolyte), pH 3.0, 300 mL min ⁻¹ O ₂ flow rate, 0.5 mmol L ⁻¹ [Fe ²⁺], -0.5 V voltage	S _{BET} = 992 m ² g ⁻¹ Pore volume = 0.45 cm ³ g ⁻¹ Mean pore size = 4.3 nm	The accumulative H ₂ O ₂ concentrations obtained at the CMK-3/GDE, graphite GDE, and carbon paper were increased to 1.29, 0.41, and 0.29 mmol L ⁻¹ , respectively. The apparent rate constant values of DMP degradation at the CMK-3/GDE, graphite GDE, and carbon paper cathode were 0.300, 0.034, and 0.026 min ⁻¹ , respectively	[89]

Fe-GMCA ^a / Ni foam	Heterogeneous- EF	MB	100 mL three-electrode undivided cell, 8.0 cm ² Pt sheet counter, Ag/AgCl reference, 8.0 cm ² cathode surface, 0.05 mol L ⁻¹ [Na ₂ SO ₄] (electrolyte), pH 3.0, 400 mL min ⁻¹ O ₂ flow rate, 15 mA applied current	S _{BET} = 479.8 m ² g ⁻¹ Pore volume = 0.74 cm ³ g ⁻¹ Mean pore size = 3.1 nm	The concentrations of generated H ₂ O ₂ at the GMCA/Ni foam and Ni foam cathodes were 1.26 and 0.51 mmol L ⁻¹ , respectively. The degradation rate constant values of MB were 0.072 min ⁻¹ , 0.043 min ⁻¹ , and 0.030 min ⁻¹ for Fe-GMCA, Fe-GCA, and Fe-MCA, respectively	[90]
N, S-doped MC/glassy carbon	Electrochemical oxidation	Methyl orange (MO)	100 mL three-electrode undivided cell, graphite rod counter, SCE reference, 6.0 cm ² cathode surface, 0.05 mol L ⁻¹ [Na ₂ SO ₄] (electrolyte), pH 2.4, 400 mL min ⁻¹ O ₂ flow rate, -0.5 V vs. SCE voltage	S _{BET} (N-doped MC) = 881 m ² g ⁻¹ Mean pore size (N-doped MC) = 3.7 nm S _{BET} (S-doped MC) = 1,103 m ² g ⁻¹ Mean pore size (S-doped MC) = 3.7 nm S _{BET} (N, S-doped MC) = 855 m ² g ⁻¹ Mean pore size (N,S-doped MC) = 3.7 nm	Degradation efficiencies of MO were around 100%, 70%, and 60% when N-MC, S-MC, and N,S-MC were applied as electrode material, respectively	[91, 92]
HPC/carbon paper	EF	Perfluorooctanoate (PFOA)	60 mL three-electrode undivided cell, 6.0 cm ² Pt sheet counter, SCE reference, 10 cm ² cathode surface, 0.05 mol L ⁻¹ [Na ₂ SO ₄] (electrolyte), pH 2.0, 1.0 mmol L ⁻¹ [Fe ²⁺], -0.4 V vs. SCE voltage	Hydrothermal time: 24 h S _{BET} = 2,130 m ² g ⁻¹ Pore size distribution: 1.0–10.0 nm	The electro-generated H ₂ O ₂ concentration on the modified cathode with HPC was 142.5 mmol L ⁻¹ with current efficiency of 91.2%. PFOA was degraded with removal efficiency of 94.3% in 120 min	[88, 93]

^aIron oxide containing graphene/carbon nanotube based carbon aerogel

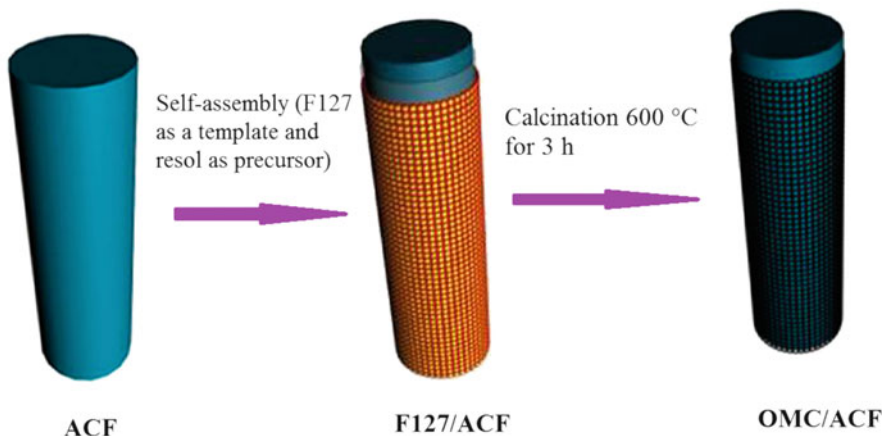


Fig. 11 A graphical illustration of preparation of OMC modified ACF cathode

electrode showed higher performance in EF process compared with S-MC and N, S-MC modified electrodes.

The correlation between mesoporous structure and efficiency of cathode materials in the EF method was investigated [87]. In this research, OMCs with average pore size of 2.6, 3.6, and 5.4 nm were prepared by means of boric acid as the expanding agent and coated on the surface of ACF. Figure 12a, b show TEM images of OMC-3.7/ACF and OMC-5.4/ACF. H_2O_2 accumulation and degradation profiles of Rh B in EF system in the as-prepared cathodes is illustrated in Fig. 12c, d, respectively. It was found that the large pore size (5.4 nm) promotes the mass transfer of O_2 on the surface of the modified cathode, which then results in high generation of H_2O_2 and consequently enhances the degradation efficiency. After ten consecutive EF runs, the reactivity of OMC-5.4/ACF cathode remained approximately unchanged.

In another research, rGO was employed to fabricate rGO@OMC/ACF cathode with lower impedance and better electroactive surface area compared with OMC/ACF, which improved the H_2O_2 production and current efficiency of the EF process. The observed electrochemical performance enhancement can be attributed to the electrical conductivity improvement, resulted by coating of rGO.

Wang and co-workers [89] synthesized CMK-3-type OMC with a pore size of around 4.3 nm by applying the SBA-15 as a hard template. Then, carbon paper was covered by as-prepared CMK-3 to fabricate the GDE cathode with high porosity and large surface area. Using this electrode, the side reaction of H_2 evolution is minimized at a low cathodic potential; thus the H_2O_2 formation is increased to rapidly degrade organic pollutant such as dimethyl phthalate (DMP) by EF process.

Recently, Liu et al. [88, 93] coated the carbon paper surface with HPC which was prepared by hydrothermal synthesis of MOF-5 as a hard template, and then its carbonization resulted HPC to exhibit high amount of sp^3 carbon hybridization and defects, huge surface area ($2,130 \text{ m}^2 \text{ g}^{-1}$), and rapid O_2 mass transport. The modified carbon paper presented a high selectivity for the O_2 reduction to H_2O_2

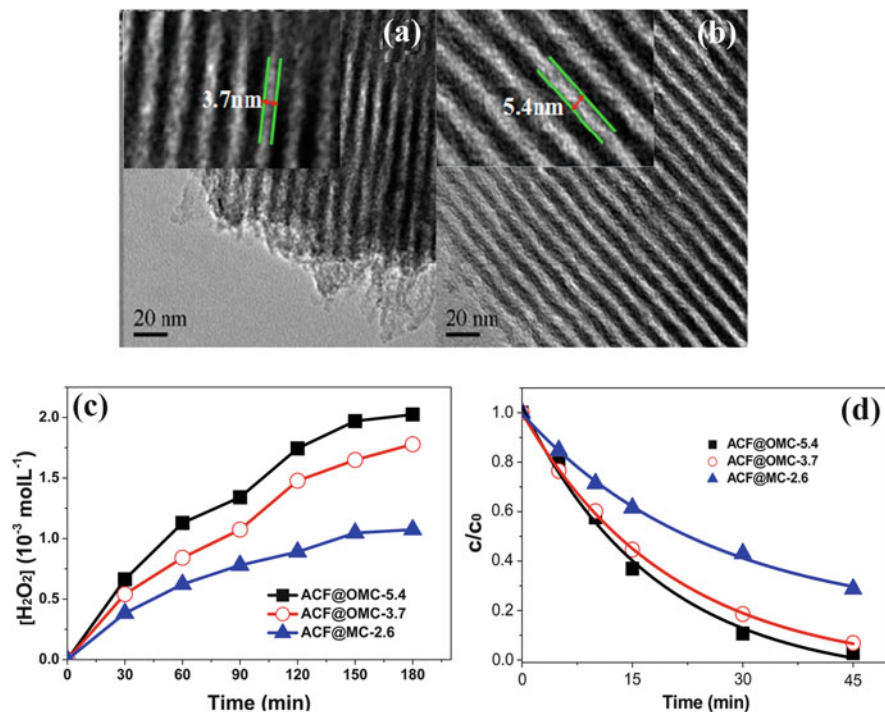


Fig. 12 TEM images of (a) OMC-3.7/ACF, (b) OMC-5.4/ACF, (c) H₂O₂ accumulation, and (d) degradation profiles of Rh B in EF system in the as-prepared cathodes (Reprinted with the permission from [87], Copyright 2015 American Chemical Society)

in a broad range of pH (1–7). Perfluorooctanoate (PFOA) was efficiently treated by using HPC modified cathode at low potential (−0.4 V). The superior efficiency of this EF process can be ascribed to high H₂O₂ generation at the modified cathode at low energy consumption, demonstrating their promising application for efficient treatment of recalcitrant pollutants in wastewater.

3 Conclusion

The main concern with the EF process is to improve the generation of H₂O₂ and enhance the reduction rate of ferric ions on the cathode for effective destruction of pollutants. Thus, it is worthwhile to further develop the performance of cathode with its surface modification. Recently, carbon-based nanomaterials have attracted substantial attention due to their superior physicochemical properties including high specific surface area, good electronic conductivity, chemical inertness, and facile surface modification capability. This chapter discussed the modified cathodes with carbon-based nanomaterials, e.g., CNTs, graphene family, and mesoporous

carbons, for EF system. Progress in the modification of cathodes with these nanomaterials for performance development of EF process has been tremendous in recent years, opening novel alternatives in the degradation of recalcitrant pollutants in wastewater.

Despite the extensive research on the modification of cathodes in EF processes, several challenges still need to be addressed to optimize the design of these cathodes for industrial applications at a large scale. First, a technique for better coating or condensing of carbon nanomaterials needs to be further explored. Due to the fact that nanomaterials may be leached from the coated bed, the efficient coating approaches should be developed. Second, carbon nanomaterials generally have a strong tendency to agglomerate owing to their nanosize and high surface energy. Therefore, their applications are limited due to the difficulty in dispersing them in a solvent (water or organic agent) for coating on the electrode. Improved dispersion of carbon nanomaterials could be achieved by modifying their surfaces or optimizing the coating process. Also, this matter could be resolved by preparing of spongelike or aerogel structure of carbon nanomaterials as an electrode and in situ synthesis of nanomaterials on the electrode surface. In this case, the durability of modified cathode electrodes could be improved. Third, considering the potential effects of leached carbon nanomaterials to the environment, nanomaterial leakage and its environmental toxicity also need to be systematically evaluated. Finally, there are many laboratory-scale researches on the application of modified cathodes with carbon nanomaterials in EF processes, but the industrial application of these cathodes is still not developed. More studies are needed to investigate the cost-effectiveness of large-scale modified cathode fabrication including the supply of carbon nanomaterials and to monitor the long-term stability of modified cathodes under practical application conditions.

Acknowledgment The authors thank the University of Tabriz (Iran) for all the support provided. We also acknowledge the support of Iran Science Elites Federation.

References

1. Brillas E, Sirés I, Oturan MA (2009) Electro-Fenton process and related electrochemical technologies based on fenton's reaction chemistry. *Chem Rev* 109(12):6570–6631
2. Nidheesh PV, Gandhimathi R (2012) Trends in electro-Fenton process for water and wastewater treatment: an overview. *Desalination* 299:1–15
3. Oloman C, Watkinson AP (1975) The electroreduction of oxygen to hydrogen peroxide on fluidized cathodes. *Can J Chem Eng* 53(3):268–273
4. Oloman C, Watkinson AP (1979) Hydrogen peroxide production in trickle-bed electrochemical reactors. *J Appl Electrochem* 9(1):117–123
5. Khataee AR, Safarpour M, Zarei M, Aber S (2011) Electrochemical generation of H₂O₂ using immobilized carbon nanotubes on graphite electrode fed with air: investigation of operational parameters. *J Electroanal Chem* 659(1):63–68

6. Scialdone O, Galia A, Sabatino S (2013) Electro-generation of H_2O_2 and abatement of organic pollutant in water by an electro-Fenton process in a microfluidic reactor. *Electrochem Commun* 26:45–47
7. Leng WH, Zhu WC, Ni J, Zhang Z, Zhang JQ, Cao CN (2006) Photoelectrocatalytic destruction of organics using TiO_2 as photoanode with simultaneous production of H_2O_2 at the cathode. *Appl Catal A* 300(1):24–35
8. Scialdone O, Galia A, Gattuso C, Sabatino S, Schiavo B (2015) Effect of air pressure on the electro-generation of H_2O_2 and the abatement of organic pollutants in water by electro-Fenton process. *Electrochim Acta* 182:775–780
9. Santana-Martínez G, Roa-Morales G, Martín del Campo E, Romero R, Frontana-Uribe BA, Natividad R (2016) Electro-Fenton and electro-Fenton-like with in situ electrogeneration of H_2O_2 and catalyst applied to 4-chlorophenol mineralization. *Electrochim Acta* 195:246–256
10. Flox C, Ammar S, Arias C, Brillas E, Vargas-Zavala AV, Abdelhedi R (2006) Electro-Fenton and photoelectro-Fenton degradation of indigo carmine in acidic aqueous medium. *Appl Catal B* 67(1-2):93–104
11. Liang L, An Y, Zhou M, Yu F, Liu M, Ren G (2016) Novel rolling-made gas-diffusion electrode loading trace transition metal for efficient heterogeneous electro-Fenton-like. *J Environ Chem Eng* 4(4):4400–4408
12. Wang Z-X, Li G, Yang F, Chen Y-L, Gao P (2011) Electro-Fenton degradation of cellulose using graphite/PTFE electrodes modified by 2-ethylanthraquinone. *Carbohydr Polym* 86(4):1807–1813
13. Flores N, Cabot PL, Centellas F, Garrido JA, Rodríguez RM, Brillas E, Sirés I (2017) 4-Hydroxyphenylacetic acid oxidation in sulfate and real olive oil mill wastewater by electrochemical advanced processes with a boron-doped diamond anode. *J Hazard Mater* 321:566–575
14. Wang A, Qu J, Ru J, Liu H, Ge J (2005) Mineralization of an azo dye Acid Red 14 by electro-Fenton's reagent using an activated carbon fiber cathode. *Dyes Pigments* 65(3):227–233
15. Hammami S, Oturan N, Bellakhal N, Dachraoui M, Oturan MA (2007) Oxidative degradation of direct orange 61 by electro-Fenton process using a carbon felt electrode: application of the experimental design methodology. *J Electroanal Chem* 610(1):75–84
16. Pimentel M, Oturan N, Dezotti M, Oturan MA (2008) Phenol degradation by advanced electrochemical oxidation process electro-Fenton using a carbon felt cathode. *Appl Catal B* 83(1-2):140–149
17. Zhou M, Tan Q, Wang Q, Jiao Y, Oturan N, Oturan MA (2012) Degradation of organics in reverse osmosis concentrate by electro-Fenton process. *J Hazard Mater* 215-216:287–293
18. Zhou L, Zhou M, Zhang C, Jiang Y, Bi Z, Yang J (2013) Electro-Fenton degradation of p-nitrophenol using the anodized graphite felts. *Chem Eng J* 233:185–192
19. Yahya MS, Oturan N, El Kacemi K, El Karbane M, Aravindakumar CT, Oturan MA (2014) Oxidative degradation study on antimicrobial agent ciprofloxacin by electro-Fenton process: kinetics and oxidation products. *Chemosphere* 117:447–454
20. Özcan A, Şahin Y, Savaş Koparal A, Oturan MA (2008) Carbon sponge as a new cathode material for the electro-Fenton process: comparison with carbon felt cathode and application to degradation of synthetic dye basic blue 3 in aqueous medium. *J Electroanal Chem* 616(1-2):71–78
21. Trellu C, Péchaud Y, Oturan N, Mousset E, Huguenot D, van Hullebusch ED, Esposito G, Oturan MA (2016) Comparative study on the removal of humic acids from drinking water by anodic oxidation and electro-Fenton processes: mineralization efficiency and modelling. *Appl Catal B* 194:32–41
22. Alvarez-Gallegos A, Pletcher D (1998) The removal of low level organics via hydrogen peroxide formed in a reticulated vitreous carbon cathode cell, part 1. The electrosynthesis of hydrogen peroxide in aqueous acidic solutions. *Electrochim Acta* 44(5):853–861

23. Alvarez-Gallegos A, Pletcher D (1999) The removal of low level organics via hydrogen peroxide formed in a reticulated vitreous carbon cathode cell. Part 2: the removal of phenols and related compounds from aqueous effluents. *Electrochim Acta* 44(14):2483–2492
24. Martínez SS, Bahena CL (2009) Chlorbromuron urea herbicide removal by electro-Fenton reaction in aqueous effluents. *Water Res* 43(1):33–40
25. Thiam A, Sirés I, Garrido JA, Rodríguez RM, Brillas E (2015) Decolorization and mineralization of Allura Red AC aqueous solutions by electrochemical advanced oxidation processes. *J Hazard Mater* 290:34–42
26. Thiam A, Zhou M, Brillas E, Sirés I (2014) Two-step mineralization of Tartrazine solutions: study of parameters and by-products during the coupling of electrocoagulation with electrochemical advanced oxidation processes. *Appl Catal B* 150–151:116–125
27. Cruz-González K, Torres-Lopez O, García-León AM, Brillas E, Hernández-Ramírez A, Peralta-Hernández JM (2012) Optimization of electro-Fenton/BDD process for decolorization of a model azo dye wastewater by means of response surface methodology. *Desalination* 286:63–68
28. Cruz-González K, Torres-López O, García-León A, Guzmán-Mar JL, Reyes LH, Hernández-Ramírez A, Peralta-Hernández JM (2010) Determination of optimum operating parameters for Acid Yellow 36 decolorization by electro-Fenton process using BDD cathode. *Chem Eng J* 160(1):199–206
29. Su DS, Perathoner S, Centi G (2013) Nanocarbons for the development of advanced catalysts. *Chem Rev* 113(8):5782–5816
30. Hassani A, Khataee AR (2017) Activated carbon fiber for environmental protection. In: Chen JY (ed) *Activated carbon fiber and textiles*. Woodhead Publishing, Oxford, pp 245–280
31. Inagaki M, Kang F (2014) *Fundamental science of carbon materials. Materials science and engineering of carbon: fundamentals* 2nd edn. Butterworth-Heinemann, Oxford, pp 17–217
32. Wei Q, Tong X, Zhang G, Qiao J, Gong Q, Sun S (2015) Nitrogen-doped carbon nanotube and graphene materials for oxygen reduction reactions. *Catalysts* 5(3):1574
33. Wang D-W, Su D (2014) Heterogeneous nanocarbon materials for oxygen reduction reaction. *Energy Environ Sci* 7(2):576–591
34. Mousset E, Ko ZT, Syafiq M, Wang Z, Lefebvre O (2016) Electrocatalytic activity enhancement of a graphene ink-coated carbon cloth cathode for oxidative treatment. *Electrochim Acta* 222:1628–1641
35. Ren W, Tang D, Lu X, Sun J, Li M, Qiu S, Fan D (2016) Novel multilayer ACF@rGO@OMC cathode composite with enhanced activity for electro-Fenton degradation of phthalic acid esters. *Ind Eng Chem Res* 55(42):11085–11096
36. Chen C-Y, Tang C, Wang H-F, Chen C-M, Zhang X, Huang X, Zhang Q (2016) Oxygen reduction reaction on graphene in an electro-Fenton system: in situ generation of H₂O₂ for the oxidation of organic compounds. *ChemSusChem* 9(10):1194–1199
37. Iijima S (1991) Helical microtubules of graphitic carbon. *Nature* 354(6348):56–58
38. Dai L, Xue Y, Qu L, Choi H-J, Baek J-B (2015) Metal-free catalysts for oxygen reduction reaction. *Chem Rev* 115(11):4823–4892
39. Popov VN (2004) Carbon nanotubes: properties and application. *Mater Sci Eng R Rep* 43(3):61–102
40. Zhang X, Lei L, Xia B, Zhang Y, Fu J (2009) Oxidation of carbon nanotubes through hydroxyl radical induced by pulsed O₂ plasma and its application for O₂ reduction in electro-Fenton. *Electrochim Acta* 54(10):2810–2817
41. Tian J, Olajuyin AM, Mu T, Yang M, Xing J (2016) Efficient degradation of rhodamine B using modified graphite felt gas diffusion electrode by electro-Fenton process. *Environ Sci Pollut Res* 23(12):11574–11583
42. Chu Y, Zhang D, Liu L, Qian Y, Li L (2013) Electrochemical degradation of m-cresol using porous carbon-nanotube-containing cathode and Ti/SnO₂-Sb₂O₅-IrO₂ anode: kinetics, byproducts and biodegradability. *J Hazard Mater* 252-253:306–312

43. Khataee AR, Safarpour M, Zarei M, Aber S (2012) Combined heterogeneous and homogeneous photodegradation of a dye using immobilized TiO_2 nanophotocatalyst and modified graphite electrode with carbon nanotubes. *J Mol Catal A Chem* 363–364:58–68
44. Khataee AR, Vahid B, Behjati B, Safarpour M, Joo SW (2014) Kinetic modeling of a triarylmethane dye decolorization by photoelectro-Fenton process in a recirculating system: nonlinear regression analysis. *Chem Eng Res Des* 92(2):362–367
45. Khataee AR, Vahid B, Behjati B, Safarpour M (2013) Treatment of a dye solution using photoelectro-fenton process on the cathode containing carbon nanotubes under recirculation mode: investigation of operational parameters and artificial neural network modeling. *Environ Prog Sustain Energy* 32(3):557–563
46. Pajootan E, Arami M, Rahimdokht M (2014) Discoloration of wastewater in a continuous electro-Fenton process using modified graphite electrode with multi-walled carbon nanotubes/surfactant. *Sep Purif Technol* 130:34–44
47. Es'haghzade Z, Pajootan E, Bahrami H, Arami M (2017) Facile synthesis of Fe_3O_4 nanoparticles via aqueous based electro chemical route for heterogeneous electro-Fenton removal of azo dyes. *J Taiwan Inst Chem Eng* 7:91–105
48. Fu J, Zhang X, Lei L (2007) Fe-modified multi-walled carbon nanotube electrode for production of hydrogen peroxide. *Acta Phys Chim Sin* 23(8):1157–1162
49. Tang Q, Wang D, Yao DM, Yang CW, Sun YC (2016) Highly efficient electro-generation of hydrogen peroxide using NCNT/NF/CNT air diffusion electrode for electro-Fenton degradation of p-nitrophenol. *Water Sci Technol* 73(7):1652–1658
50. Babaei-Sati R, Basiri Parsa J (2017) Electrogeneration of H_2O_2 using graphite cathode modified with electrochemically synthesized polypyrrole/MWCNT nanocomposite for electro-Fenton process. *J Ind Eng Chem* 52:270–276
51. Zhang X, Fu J, Zhang Y, Lei L (2008) A nitrogen functionalized carbon nanotube cathode for highly efficient electrocatalytic generation of H_2O_2 in electro-Fenton system. *Sep Purif Technol* 64(1):116–123
52. Zarei M, Salari D, Niaei A, Khataee AR (2009) Peroxi-coagulation degradation of C.I. Basic Yellow 2 based on carbon-PTFE and carbon nanotube-PTFE electrodes as cathode. *Electrochim Acta* 54(26):6651–6660
53. Zarei M, Niaei A, Salari D, Khataee AR (2010) Application of response surface methodology for optimization of peroxi-coagulation of textile dye solution using carbon nanotube-PTFE cathode. *J Hazard Mater* 173(1–3):544–551
54. Zarei M, Khataee AR, Ordikhani-Seyedlar R, Fathinia M (2010) Photoelectro-Fenton combined with photocatalytic process for degradation of an azo dye using supported TiO_2 nanoparticles and carbon nanotube cathode: neural network modeling. *Electrochim Acta* 55(24):7259–7265
55. Geim AK, Novoselov KS (2007) The rise of graphene. *Nat Mater* 6(3):183–191
56. Kiew SF, Kiew LV, Lee HB, Imae T, Chung LY (2016) Assessing biocompatibility of graphene oxide-based nanocarriers: a review. *J Control Release* 226:217–228
57. Novoselov KS, Geim AK, Morozov SV, Jiang D, Zhang Y, Dubonos SV, Grigorieva IV, Firsov AA (2004) Electric field effect in atomically thin carbon films. *Science* 306(5696):666–669
58. Lee C, Wei X, Kysar JW, Hone J (2008) Measurement of the elastic properties and intrinsic strength of monolayer graphene. *Science* 321(5887):385–388
59. Balandin AA, Ghosh S, Bao W, Calizo I, Teweldebrhan D, Miao F, Lau CN (2008) Superior thermal conductivity of single-layer graphene. *Nano Lett* 8(3):902–907
60. Marinho B, Ghislandi M, Tkalya E, Koning CE, de With G (2012) Electrical conductivity of compacts of graphene, multi-wall carbon nanotubes, carbon black, and graphite powder. *Powder Technol* 221:351–358
61. Novoselov KS (2009) Graphene: the magic of flat carbon. *ECS Trans* 19(5):3–7
62. Chen D, Tang L, Li J (2010) Graphene-based materials in electrochemistry. *Chem Soc Rev* 39(8):3157–3180

63. Lee HC, Liu W-W, Chai S-P, Mohamed AR, Lai CW, Khe C-S, Voon CH, Hashim U, Hidayah NMS (2016) Synthesis of single-layer graphene: a review of recent development. *Proc Chem* 19:916–921
64. Shao G, Lu Y, Wu F, Yang C, Zeng F, Wu Q (2012) Graphene oxide: the mechanisms of oxidation and exfoliation. *J Mater Sci* 47(10):4400–4409
65. Perreault F, Fonseca de Faria A, Elimelech M (2015) Environmental applications of graphene-based nanomaterials. *Chem Soc Rev* 44(16):5861–5896
66. Liu L, Qing M, Wang Y, Chen S (2015) Defects in graphene: generation, healing, and their effects on the properties of graphene: a review. *J Mater Sci Technol* 31(6):599–606
67. Xu X, Chen J, Zhang G, Song Y, Yang F (2014) Homogeneous electro-Fenton oxidative degradation of reactive brilliant blue using a graphene doped gas-diffusion cathode. *Int J Electrochem Sci* 9:569–579
68. Le TXH, Bechelany M, Lacour S, Oturan N, Oturan MA, Cretin M (2015) High removal efficiency of dye pollutants by electron-Fenton process using a graphene based cathode. *Carbon* 94:1003–1011
69. Le TXH, Bechelany M, Champavert J, Cretin M (2015) A highly active based graphene cathode for the electro-Fenton reaction. *RSC Adv* 5(53):42536–42539
70. Zhao F, Liu L, Yang F, Ren N (2013) E-Fenton degradation of MB during filtration with Gr/PPy modified membrane cathode. *Chem Eng J* 230:491–498
71. Dong H, Su H, Chen Z, Yu H, Yu H (2016) Fabrication of electrochemically reduced graphene oxide modified gas diffusion electrode for in-situ electrochemical advanced oxidation process under mild conditions. *Electrochim Acta* 222:1501–1509
72. Shen J, Li Y, Zhu Y, Hu Y, Li C (2016) Aerosol synthesis of graphene-Fe₃O₄ hollow hybrid microspheres for heterogeneous Fenton and electro-Fenton reaction. *J Environ Chem Eng* 4 (2):2469–2476
73. Zhao X, Liu S, Huang Y (2016) Removing organic contaminants by an electro-Fenton system constructed with graphene cathode. *Toxicol Environ Chem* 98(3-4):530–539
74. Zhang Z, Zhang J, Ye X, Hu Y, Chen Y (2016) Pd/RGO modified carbon felt cathode for electro-Fenton removing of EDTA-Ni. *Water Sci Technol* 74(3):639–646
75. Zhang G, Zhou Y, Yang F (2015) FeOOH-catalyzed heterogeneous electro-Fenton system upon anthraquinone@graphene nanohybrid cathode in a divided electrolytic cell: catholyte-regulated catalytic oxidation performance and mechanism. *J Electrochem Soc* 162(6):H357–H365
76. Mousset E, Wang Z, Hammaker J, Lefebvre O (2016) Physico-chemical properties of pristine graphene and its performance as electrode material for electro-Fenton treatment of wastewater. *Electrochim Acta* 214:217–230
77. Liu T, Wang K, Song S, Brouzgou A, Tsiakaras P, Wang Y (2016) New electro-Fenton gas diffusion cathode based on nitrogen-doped graphene@carbon nanotube composite materials. *Electrochim Acta* 194:228–238
78. Li Y, Han J, Xie B, Li Y, Zhan S, Tian Y (2017) Synergistic degradation of antimicrobial agent ciprofloxacin in water by using 3D CeO₂/RGO composite as cathode in electro-Fenton system. *J Electroanal Chem* 784:6–12
79. Li Y, Li Y, Xie B, Han J, Zhan S, Tian Y (2017) Efficient mineralization of ciprofloxacin using a 3D Ce_xZr_{1-x}O₂/RGO composite cathode. *Environ Sci Nano* 4(2):425–436
80. Govindaraj D, Nambi IM, Senthilnathan J (2017) An innate quinone functionalized electrochemically exfoliated graphene/Fe₃O₄ composite electrode for the continuous generation of reactive oxygen species. *Chem Eng J* 316:964–977
81. Golabi SM, Raof JB (1996) Catalysis of dioxygen reduction to hydrogen peroxide at the surface of carbon paste electrodes modified by 1,4-naphthoquinone and some of its derivatives. *J Electroanal Chem* 416(1):75–82
82. Jürmann G, Schiffrin DJ, Tammeveski K (2007) The pH-dependence of oxygen reduction on quinone-modified glassy carbon electrodes. *Electrochim Acta* 53(2):390–399

83. Walcarius A (2013) Mesoporous materials and electrochemistry. *Chem Soc Rev* 42 (9):4098–4140
84. Sun M-H, Huang S-Z, Chen L-H, Li Y, Yang X-Y, Yuan Z-Y, Su B-L (2016) Applications of hierarchically structured porous materials from energy storage and conversion, catalysis, photocatalysis, adsorption, separation, and sensing to biomedicine. *Chem Soc Rev* 45 (12):3479–3563
85. Hu J, Sun J, Yan J, Lv K, Zhong C, Deng K, Li J (2013) A novel efficient electrode material: activated carbon fibers grafted by ordered mesoporous carbon. *Electrochem Commun* 28:67–70
86. Peng Q, Zhang Z, Za H, Ren W, Sun J (2014) N-doped ordered mesoporous carbon grafted onto activated carbon fibre composites with enhanced activity for the electro-Fenton degradation of Brilliant Red X3B dye. *RSC Adv* 4(104):60168–60175
87. Ren W, Peng Q, Huang Z, Zhang Z, Zhan W, Lv K, Sun J (2015) Effect of pore structure on the electro-Fenton activity of ACF@OMC cathode. *Ind Eng Chem Res* 54(34):8492–8499
88. Liu Y, Chen S, Quan X, Yu H, Zhao H, Zhang Y (2015) Efficient mineralization of perfluorooctanoate by electro-Fenton with H₂O₂ electro-generated on hierarchically porous carbon. *Environ Sci Technol* 49(22):13528–13533
89. Wang Y, Liu Y, X-Z L, Zeng F, Liu H (2013) A highly-ordered porous carbon material based cathode for energy-efficient electro-Fenton process. *Sep Purif Technol* 106:32–37
90. Chen W, Yang X, Huang J, Zhu Y, Zhou Y, Yao Y, Li C (2016) Iron oxide containing graphene/carbon nanotube based carbon aerogel as an efficient E-Fenton cathode for the degradation of methyl blue. *Electrochim Acta* 200:75–83
91. Perazzolo V, Durante C, Gennaro A (2016) Nitrogen and sulfur doped mesoporous carbon cathodes for water treatment. *J Electroanal Chem* 782:264–269
92. Perazzolo V, Durante C, Pilot R, Paduano A, Zheng J, Rizzi GA, Martucci A, Granozzi G, Gennaro A (2015) Nitrogen and sulfur doped mesoporous carbon as metal-free electrocatalysts for the in situ production of hydrogen peroxide. *Carbon* 95:949–963
93. Liu Y, Quan X, Fan X, Wang H, Chen S (2015) High-yield electrosynthesis of hydrogen peroxide from oxygen reduction by hierarchically porous carbon. *Angew Chem* 127(23):6941–6945

Advances in Carbon Felt Material for Electro-Fenton Process

Thi Xuan Huong Le, Mikhael Bechelany, and Marc Cretin

Abstract In electro-Fenton process, carbon-based materials, particularly 3D carbon felt, are the best choices for the cathodic electrodes because of several advantages such as low cost, excellent electrolytic efficiency, high surface area, and porosity. In this chapter, various aspects of this material are discussed in detail. This chapter is divided into three main sections, including (1) characterization of carbon felt (CF), (2) modification of CF, and (3) application of CF in electro-Fenton (EF) process to remove biorefractory pollutants. First of all, the typical characteristics of CF such as morphology, porosity, and conductivity are discussed. Next, in the modification section, we introduce different methods to improve the performance of CF. We especially focus on the surface area and electrochemical activity toward electrodes applications. Finally, both modified and non-modified CF is used as cathode materials for EF systems like homogeneous, heterogeneous, hybrid, or pilot-scale types.

Keywords Carbon felt, Conductivity, Electrochemical activity, Electro-Fenton process, Hydrogen peroxide production, Modification, Surface area

Contents

1	Introduction	147
2	Characterization of CF Material	148
3	Method to Modify CF Material	148
3.1	Chemical Treatment	148
3.2	Thermal and Plasma Treatment	150
3.3	Graphene Based Modification	151

T.X.H. Le, M. Bechelany (✉), and M. Cretin (✉)

Institut Européen des membranes (IEM UMR-5635, ENSCM, CNRS), Université de Montpellier, Place Eugène Bataillon, 34095 Montpellier Cedex 5, France
e-mail: mikhael.bechelany@umontpellier.fr; Marc.Cretin@umontpellier.fr

3.4	Carbon Nanotube-Based Modification	152
3.5	Polymer-Based Modification	153
3.6	Zeolite-Based Modification	155
4	Carbon Felt-Based Material for Wastewater Treatment by EF Process	156
4.1	Carbon Felt for EF Process	156
4.2	Modified EF Systems Using Carbon Felt Cathodes	159
5	Conclusion	165
	References	166

Abbreviations

AHPS	4-Amino-3-hydroxy-2-p-tolylazo-naphthalene-1-sulfonic acid
ALD	Atomic Layer Deposition
AO7	Acid orange 7
APPJ	Atmospheric Pressure Plasma Jet
AQDS	Anthraquinone-2,6-disulfonate
BDD	Boron-doped diamond
BEF	Bio-electro-Fenton
CF	Carbon felt
CNT	Carbon nanotube
CTAB	Cetyl trimethylammonium bromide
CV	Cyclic voltammogram
CVD	Chemical vapor deposition
DCF	Diclofenac
DMF	<i>N,N</i> -dimethyl formamide
DO 61	Direct orange 61
EC	Energy efficiency
EF	Electro-Fenton
ENXN	Enoxacin
EPD	Electrophoretic deposition
FeAB	Iron alginate gel beads
GF	Graphite felt
GO	Graphene oxide
LDH	Layered double hydroxide
MCE	Mineralization current efficiency
MCF	Microbial fuel cell
MO	Methyl orange
N-doped	Nitrogen-doped
ORR	Oxygen reduction reaction
PAH	Polycyclic aromatic hydrocarbon
PAN-CF	PolyAcryloNitrile-Carbon Felt
PAN-GF	Polyacrylonitrile-graphite felt
PANi	Polyaniline
PB	Prussian blue
PCOC	4-Chloro-2-methylphenol

PEM	Proton Exchange Membrane
POP	Persistent Organic Pollutant
PPy	Polypyrrole
RF	Radiofrequency
rGO	Reduced graphene oxide
RTD	Residence Time Distribution
SCEs	Saturated calomel electrode
SEM	Scanning Electron Microscopy
SPEF	Solar Photo-electro-Fenton
SWCNT	Single-walled carbon nanotube
TOC	Total organic carbon
TT	Thermal treatment
VRFE	Vanadium redox flow battery
XPS	X-ray photoelectron spectroscopy
ZIF	Zeolitic Imidazolate Framework
ZME	Zeolite-modified electrode

1 Introduction

Owing to impressive properties such as low cost, excellent electrolytic efficiency, high surface area, and porosity and the ability to provide abundant redox reaction sites and mechanical stability [1–4], carbon felts (CF) are commonly used as electrodes. However, they simultaneously have some disadvantages relevant to their inadequate wettability and electrochemical activity in aqueous solutions because of their hydrophobic surface nature and poor kinetics for reduction and oxidation reactions. This partly declines the performance of pristine felts when they are applied at electrodes [5, 6]. In the effort to make the felt electrodes more active, several modification methods have been adopted at various conditions. Chakrabarti et al. [7] reported for instance some modification methods to improve the catalytic properties and the conductivity of CF electrodes such as deposition of metals and addition of functional groups by chemical and thermal treatments on the electrode surface. Several methods to produce vapor grown carbon fibers, carbon nanotubes (CNTs), or nitrogenous groups on the carbon fiber surface of CF electrodes were discussed [7]. After these modification processes, the electrochemical activity of CF could be remarkably enhanced [6, 8]. For wastewater treatment, CF was used widely as cathode materials for the removal of Persistent Organic Pollutants (POPs) in aqueous medium by electro-Fenton (EF) process. According to the review of Brillas et al., carbon electrodes present many advantages like nontoxicity, good stability, conductivity, and chemical resistance [9]. The efficiency of EF system using felt cathodes was studied in comparison with other materials like activated carbon fiber, reticulated vitreous carbon, carbon sponge, etc. [10–12]. In order to present a holistic overview about CF-based material for EF process, we will discuss in this chapter some important aspects of this material, including (1) the fabricating

methods and specific properties of pristine felt materials, (2) the various ways to modify felt electrodes, and (3) the application of CF-based cathodes for the removal of biorefractory pollutants by EF treatment. Importantly, modified EF systems using electrons produced from a green power source in fuel cell as well as EF pilot were investigated. These new technologies open new gates for application of felt materials in industrial areas toward zero-energy depollution.

2 Characterization of CF Material

CF is often observed under long smooth fibers dispersed randomly with homogeneous large void spaces between them (Fig. 1). Each fiber has cylinder-like shape with shallow grooves along the long axis which was formed by the combination of thinner fibers, melted together lengthways as reported by González-García et al. [14]. The addition or cutting of thinner sheets from the original one can change the thickness of the three-dimensional felt electrode. The geometrical shape of fibers is quite different from other materials, partly leading to various values for structural as well as physical parameters as shown in Table 1.

3 Method to Modify CF Material

3.1 Chemical Treatment

To activate the surface of felt materials, chemical treatment of CF is useful. Micropores could be generated by surface etching with KOH at high temperature ($\sim 800^{\circ}\text{C}$) leading to oxygen-containing functional groups. Furthermore, the activation by KOH improved remarkably the electrochemical activity of polyacrylonitrile-graphite felt (PAN-GF) (*Gansu Haoshi Carbon Fiber Co., Ltd.*) via the formation of these oxygen groups and the edge carbon sites [16]. The samples could be also treated by refluxing/

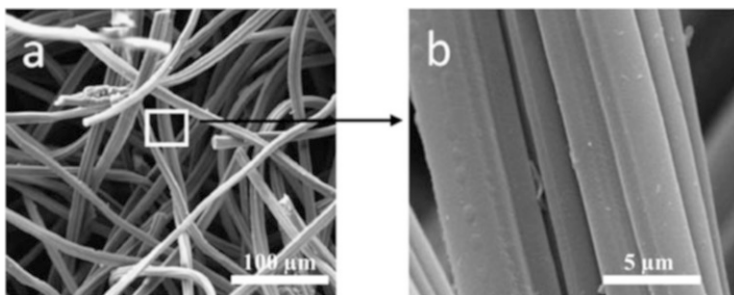


Fig. 1 (a, b) Scanning Electron Microscopy (SEM) images of CF at various magnifications. Reprinted from Deng et al. [13]. Copyright (2010), with permission from *Elsevier*

Table 1 Properties of CF electrodes according to the manufacturer [14, 15]

Company	Type	Porosity	Mean pore diameter	Specific surface area	Apparent electrical resistivity
		Value	Value (m)	Value ($\text{m}^2 \text{m}^{-3}$) excepted when mentioned	Value (Ωm)
Carbone-Lorraine	RVG 2000	0.95	–	–	3.5×10^{-3}
	RVC 1000	–	1.19×10^{-4}	31,000 ^a	–
	RVC 2000	–	2.57×10^{-4}	15,000 ^a	–
	RVC 4000	–	1.60×10^{-4}	23,500 ^a	–
	RVC 4002	0.84	2.94×10^{-4}	33,684 ^b	2.4×10^{-1d}
				3,369 ^c	
	0.984	0.12×10^{-4}	22,100–22,700 ^a ($0.067\text{--}6$) $\times 10^{7a}$	2.7×10^{-3e}	
SiGRI	Sigratherm GFD 5	0.95	1.52×10^{-4}	24,000–60,000 ^a	–
Fiber Materials	CH (0.175)	0.86	1.56×10^{-4}	11,000 ^a	–
	CH (0.25)	0.90	2.04×10^{-4}	8,800 ^a	–
Amoco Thornel Mat VMA		0.98	6.37×10^{-4}	–	7.14×10^{-3}
Shanghai Energy Carbon Limited Co., China	–	–	–	$0.33 (\text{m}^2 \text{g}^{-1})^f$	–

– Not determined

^aCalculated from Filamentary analog^bCalculated from mercury porosimetry^cCalculated from Residence Time Distribution (RTD) modeling^dValue for the short direction^eValue for the long direction^fCalculated from Physical gas adsorption isotherm

boiling either in sulfuric or nitric acid or in their mixture in order to fabricate felts with a large amount of chemisorbed oxygen on the surface [17, 18]. In fact, the better electrochemical property of GF was observed in the higher acid concentration [19]. The increased electrocatalytic activity of the treated GF was thus attributed to the increased concentration of C–O and C=O functional groups on the surface. The combination between thermal and chemical treatments is sometimes necessary to improve the efficiency of the treatment [20]. Electrochemistry is also an interesting route for the growth of functional group. It requires the application of constant current or potential in acidic solutions like $1 \text{ mol L}^{-1} \text{H}_2\text{SO}_4$. The modification following the electrochemical oxidation was successfully applied to improve the properties of different felts like GF (*Shanghai Energy Carbon Limited Co., China* [15] or *Sanye Carbon Co., Ltd.* [21]). Apart from acidic treatments, low-cost chemical reagents like ethanol and hydrazine hydrate were applied to chemically modify the graphite. Interestingly, after modification, some carbon nanoparticles and oxygen/ nitrogen-containing functional groups appeared simultaneously on the cathode surface, which

greatly improved the hydrophilicity of the surface and the electrocatalytic activity. Contact angles decreased gradually from 141°, to 123°, to 110° for bare GF (*Shanghai Qijie Carbon Material Co., LTD*), GF-ethanol, and GF-ethanol/hydrazine, respectively [22, 23].

3.2 Thermal and Plasma Treatment

The thermal treatment under gas flow containing oxygen and/or nitrogen is a simple way for felt modification to improve the electrochemical properties and the hydrophilicity [8]. In the study of Zhong et al. [24], a significant enhancement of the electrochemical activity was observed on GF, based on rayon or PAN precursors after thermal treatment under air. It was found that the electrical conductivity of the PAN-based felts was superior to that of its rayon-based counterpart. X-ray photoelectron spectroscopy (XPS) analysis pointed out that the rayon-based felts reacted more easily with oxygen and forms C=O groups, while the PAN-based felts were more resistant to oxidation and preferentially form C–O groups. The more extensive oxygen interaction in the rayon felts was thought to be due to its microcrystalline structure. Thermal treatment of GF electrodes was carried out under NH₃ atmosphere at 600°C and 900°C. The nitrogen-doped (N-doped) felt was fabricated with high electrochemical performance attributed to the increased electrical conductivity, the increase of active sites amount, and the improved wettability provided by the introduction of the nitrogenous groups on the surface of GF [25, 26]. Interestingly, the thermal treatment under air can also improve the surface area of the pristine electrodes: after treatment in air at 400°C, the surface area of the modified felts increased by more than ten times in comparison to the pristine one based on rayon (*SGL*, thickness 3 mm) [27]. This value was 1,344% higher than bare PAN-CF (*Nippon Chem*, thickness 3 mm) [5]. In the same way, thermal treatment under a flux of N₂/O₂ with 1% of oxygen at 1,000°C for 1 h could also increase the S_{BET} of commercial felts (*Johnson Matthey Co., Germany*, thickness 1.27 cm) up to 64 m² g⁻¹, i.e., around 700 times higher than raw samples. As further benefit, the crystalline size was also ameliorated due to the selective etching of amorphous carbon by thermal treatment [28].

Plasma treatments are also carried out to perform the growth of oxygen-containing functional groups or/and nitrogen doping on the surface of fibers. Oxygen plasma treatment was conducted in a radiofrequency (RF) plasma set-up controlling treatment time, power of the RF generator, and oxygen pressure. In 2015, Chen et al. [29] reported the modification of felts (*COS1011, CeTech, Taiwan*, thickness 6 mm) with Atmospheric Pressure Plasma Jets (APPJs). The APPJ treatment was performed on the felts under the single spot and scanning modes with the presence of N₂ flow rates. The formation of specific oxygen functional groups was observed after the plasma treatment. XPS revealed that this method rather favored the formation of C–O groups than C=O groups [27]. However, the plasma treatment process only often increases the amount of functional groups on

felts and not remarkably the surface area. Apart from oxygen-containing functional groups, nitrogenous groups can also improve electrocatalytic activity of carbon electrode materials for redox reactions. This comes from the reason that carbon atoms neighboring nitrogen dopants present a high positive charge density improving their electrocatalytic activity [30]. Furthermore, nitrogen doping can also make CF materials more hydrophilic which increases the electrochemically active sites [25]. Briefly, the increased amount of surface-active oxygen and nitrogenous groups by thermal or plasma treatment can enhance electrochemical performance of the modified material through facilitating charge transfer between felt electrodes and electrolytes [27, 31].

3.3 Graphene Based Modification

Graphene has received extensive attention due to its remarkable electrical, physical, thermal, optical, high specific surface area, and mechanical properties [32, 33], and it is then widely applicable for electrochemical applications [34]. Dip-coating, electrophoretic deposition (EPD), or voltamperometric techniques are methods often used separately or combined together for the coating of graphene-based materials on felt electrodes. For example, the coating of reduced graphene oxide (rGO) on CF (*Shanghai Qijie Carbon Co., Ltd.*) was performed using different steps: (1) Graphene oxide (GO) suspension was prepared by sonication in water for 1 h to exfoliate graphite. (2) GO was loaded on the CF surface by the dipping-drying process. (3) The GO was then electrochemically reduced by applying a constant voltage in 0.5 M Na₂SO₄ for 10 min. By comparing the response of cyclic voltammograms (CVs) curves in 0.5 M Na₂SO₄ solution, the rGO/CF electrode has overall a higher current density than the bare CF over the scanned voltage range (−0.6 to 0.6 V), suggesting a larger electrode surface area and better conductivity after modification [35].

In addition, the EPD shows several advantages for obtaining homogeneous films on felt electrodes from suspensions containing well-dispersed charged particles like GO solution, with high deposition rates, simple operation, easy scalability, and all that by avoiding the use of binders [36]. A graphene-modified GF was synthesized using EPD method by applying a voltage of 10 V for 3 h. The negative GO sheets were moved toward the positive GF electrode. The electrode showed graphene-like sheets on the fiber surface either in a wrinkled configuration or anchored between them. These sheets consisted of partially rGO with oxygen content decreasing from 13 at.% in the initial GO to 3.84 at.%. To compare with other modification methods, the chemical treatment by electrochemical oxidation in 1 M H₂SO₄ (GF-H₂SO₄) for 3 h or thermal treatment (TT-GF) at 450°C with the same time, 3 h, under air flow in a tubular furnace was done. The electrochemical performance of graphene modification was even higher than GF-H₂SO₄ or TT-GF [37]. Because of the excellent electrochemical properties of graphene-based materials, they have still a promising future for applications in the modification of CF electrode.

3.4 Carbon Nanotube-Based Modification

Felt electrodes were attractively modified by carbon nanotubes because of their excellent electrical and thermal conductivities, mechanical flexibility, and significantly large surface area [38]. The coating of single-walled carbon nanotube (SWCNT) was performed by a simple way where CF was immersed into the SWCNT suspension. The CF was then dried at 80°C for 5 h. The SWCNT (2 wt% relative to the amount of carbon felt) was ultrasonically dispersed previously in *N,N*-dimethyl formamide (DMF). The process was repeated until all the SWCNT suspension adsorbed into the CF. The modified electrode showed a better catalytic performance with higher electron transfer rate compared to the raw one [39]. On the other hand, the carbon nanotubes (CNTs) could be directly grown on the surface of felts by chemical vapor deposition (CVD) method without binding agent. For this purpose, the felt sample was placed in the center of a quartz tube and heated at high temperature (around 800°C) under Ar gas flow, followed by the injection of the carbon precursor source. Toluene or ethylenediamine was applied as source solution for the growth of CNTs or nitrogen-CNTs on GF. The small size (~30 nm in diameter) of CNTs created a significant increase of the electrochemical surface area of the felt materials. In addition, the N-doping could further improve the electrode performance because of the modified electronic and surface properties of CNTs on GF [40]. The CNTs/CF electrode was also obtained by growing CNTs via CVD of methanol on cobalt and manganese metallic particles deposited on CF. The specific surface area of CF loaded with 37.8 mg of CNTs was found to be 148 m² g⁻¹ instead of 1.0 m² g⁻¹ for non-modified one [41].

Growth of multi-walled carbon nanotubes (MWCNTs) on CF was investigated by CVD using ferrocene in toluene as precursor (Fe(C₅H₅)₂ at 20 g L⁻¹ in C₇H₈). CNTs with high aspect ratio were grown from the iron sites, generated by the decomposition and the subsequent nucleation of the iron species from the ferrocene precursor deposited on the CF substrate. The specific surface area successively increases with an increase in CNT loading and reaches 150 m² g⁻¹ for a CNT weight intake of 98%. A significant enhancement of mechanical strength and electrical conductivity along with the effective surface area was observed. The residual iron catalyst was removed by an acid treatment (HNO₃, 65%, at 80°C for 2 h), which caused the formation of oxygenated functional groups on the CNT surface [42]. Other CNTs/CF electrodes were prepared using the decomposition of methanol on different metallic catalysts, including cobalt, manganese, and lithium, supported on CF [43]. Bamboo-like structures were identified in good agreement with the study of Rosolen et al. [44].

EPD shows noticeable advantages as a low-cost and simple method compared to CVD [45, 46]. The first step is the dispersion of CNTs in isopropyl alcohol for 3 h in ultrasonic bath at 1.6 g L⁻¹. Applying a constant voltage of 40 V for 60 s, 1.05 wt% CNTs were deposited uniformly on CF with no obvious agglomeration or acutely curly body [47]. The studies have been enlarged with CNTs functionalized with carboxyl and hydroxyl groups. The carboxyl MWCNTs were adhered onto the CF

(Shenhe Carbon Fibre Materials Co. Ltd., thickness 4 mm) by immersing in a mixture solution of COOH-MWCNTs containing 0.02 wt.% Nafion as a binder to guarantee the stability of the MWCNTs/CF electrode. Not only the hydrophilicity but also the number of active sites of CF was upgraded, depending on the carboxyl groups of MWCNTs [48]. Similarly, the COOH-MWCNTs were ultrasonically dispersed in dimethyl formamide and then the CF was immersed in this solution. COOH-MWCNTs/CF was obtained by drying the electrode in the oven at 100°C for 24 h [49].

3.5 Polymer-Based Modification

Polyaniline (PANi) and polypyrrole (PPy) are the most common conducting polymers for electrode modification because of their high electrical conductivity, ease of preparation, and environmental stability [50, 51]. The coating of conductive polymer film on the surface of CF is usually conducted by the electropolymerization process in solution containing monomers. Interestingly, electropolymerized materials have unique properties which are not peculiar to the corresponding monomers [52, 53]. The PPy/anthraquinone-2,6-disulfonate (AQDS) conductive film was coated on CF (Liaoyang Jingu Carbon Fiber Sci-Tech Co., Ltd., China) (Fig. 2c) in a basic three-electrode electrochemical cell. The polymer film was formed on the CF surface by applying a constant potential of 0.8 V vs saturated calomel electrode (SCE), controlling the thickness with the coulometry. The modified electrode resulted in larger current responses when compared to the unmodified electrode (Fig. 2e) due to the enhanced surface area and conductivity of the PPy/AQDS-modified electrode [54]. Besides electropolymerization method, the polymer-modified felts could be prepared in a simple way by submerging CF in HCl solution adding aniline monomer and ammonium persulfate. The polymerization was conducted for 8 h by continuously stirring in order to coat PANi on the surface of CF [56].

In order to improve the physicochemical and electrochemical properties of the conducting organic films, many copolymers were prepared and investigated. The electrochemical activity of poly(aniline-co-*o*-aminophenol) was about four times as high as that of PANi 0.3 mol L⁻¹ Na₂SO₄ solution of pH 5. The copolymer had a good stability and a high reversibility [57]. A poly(aniline-co-*o*-aminophenol) film with average mass at 1.17 ± 0.1 g was deposited on CF by Cui et al. [39] through electrochemical synthesis in solution containing simultaneously aniline and *o*-aminophenol. What's more, the biocompatibility of felt electrodes was increased significantly when they were coated by the co-polymers containing nitrogen/oxygen functional groups. The hydrophilic conductive co-polymers like poly (aniline-co-*o*-aminophenol), poly (aniline-co-2, 4-diaminophenol), and poly (aniline-1, 8-diaminonaphthalene) acted as the bridge or mediator, playing the role of bonding bacteria and CF cathode more tightly, and facilitated or improved the electron transfer process from cathode to bacteria for microbial fuel cell application [56]. In terms of the increase of surface area, electronic conductivity, biocompatibility, and

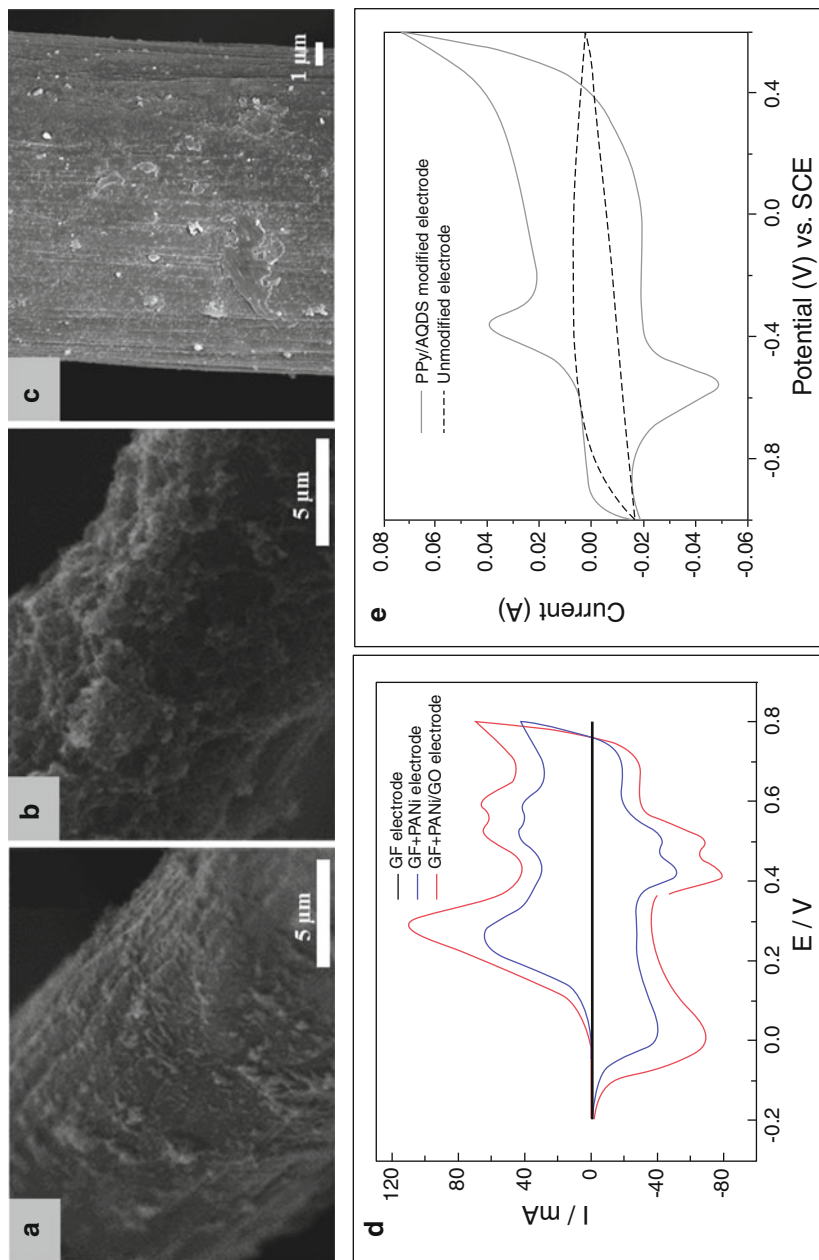


Fig. 2 SEM images of (a) PANi/GF; (b) PANi/GO-GF, (c) PPy/AQDS-CF; CVs of the modified electrodes in (d) 1.0 mol L⁻¹ H₂SO₄ solution (Scan rate of 5 mV s⁻¹), and (e) 0.1 mol L⁻¹ phosphate buffered solution (pH 7.0) (Scan rate of 10 mV s⁻¹). Reprinted from Feng et al. and Jiang et al. [54, 55]. Copyright (2010, 2015), with permission from *E/sevier*

stability, PPy was simultaneously covered on the GF (Beijing Sanye Co. Ltd., thickness 5 mm) with GO. The growth of PPy/GO on GF electrode was carried out in one step by electropolymerization of pyrrole (Py) in the solution containing simultaneously the GO. The functional groups of GO like $-OH$ and $-COOH$ play the role of external dopant for PPy formation. The new electrode exhibited improved performance compared with PPy alone when it could increase significantly the power density of Microbial Fuel Cell (MFC) [58]. In order to overcome the unsatisfactory stability of PANi-modified GF electrode, GO was introduced into PANi/GO composite for the modification of graphite (*Chemshine Carbon CO., China*) by one electrochemical approach [59]. The PANi/GO-GF (Fig. 2b, d) enhanced outstandingly the electrochemical activity as well as the hydrophilicity of GF electrode. The stability of new electrode was actually noticeable when after 1,000 s, the oxidation current of the PANi/GO-modified GF electrode was still higher than that of the PANi-modified GF electrode (Fig. 2a) because of the synergistic effect of PANi and GO [55]. Moreover, conductive polymers have been combined with CNTs to increase the effective surface area and the electrical conductivity of the resulting material. The PANi was electropolymerized on the surface of GF (*Beijing Sanye Carbon, China*, thickness 4 mm) followed by the EPD of CNTs [60]. Using polymer for the modification of GF electrode is convenient and effective method because it is a low-cost approach and improves the electrochemical performance.

3.6 Zeolite-Based Modification

Zeolites are porous crystalline aluminosilicates of SiO_4^{4-} and AlO_4^{5-} tetrahedra connected by oxygen bridges. Zeolite-modified electrodes (ZMEs) have numerous applications in various fields especially in electroanalytical chemistry because of the unique molecular sieving properties of zeolites [61]. NaX zeolite consists of sodalite cages arranged in a three-dimensional open framework leading to a microporous crystalline structure. Cages are linked through double six rings creating a large super cage cavity [62]. NaX zeolite was grown on GF during hydrothermal synthesis at $100^\circ C$ for 3 h in solution containing sodium silicate, sodium aluminate, and sodium hydroxide with a molar composition of 3.5 Na_2O :1 Al_2O_3 :2.1 SiO_2 :1,000 H_2O . Electrode activity was investigated in the presence of bacterial to prove the interest of the approach for microbial biofuel cells. The GF modified with NaX showed a higher electrochemical activity after ex situ acclimatization compared to bare electrodes [62, 63].

Prussian blue (PB, ferric hexacyanoferrate) is another kind of zeolite interesting for electrode modification [64, 65]. PB and its analogues have been known as polynuclear transition metal hexacyanometalates that own the zeolite-like structure [65–67]. Its electrochemical behavior was reported for the first time in 1978 by Neff et al. [68]. Some years later, the PB has attracted extensive attention due to its features relevant to inherent electrochromic [69], electrochemical [70], photophysical [71], as

well as molecular magnetic properties [72]. The electrochemical and chemical depositions were used to modify the GF electrode by PB. Firstly, the conductivity of felt electrode was improved via the electrodeposition of Platinum (Pt) on the surface of GF, which also played the role of catalyst for PB formation. Secondly, the Pt/GF electrode was immersed for 60 min into 20 mL of a solution containing 1.0 mmol L^{-1} FeCl_3 , 1.0 mmol L^{-1} $\text{K}_3\text{Fe}(\text{CN})_6$, 0.1 mol L^{-1} KCl , and 0.025 mol L^{-1} HCl . Next, the washing step was repeated many times before drying the electrode for 2 h at 90°C . This sample was noted as PB@Pt/GF. The SEM images of PB@Pt/GF showed the successful deposition of PB on the GF. PB@Pt/GF electrode showed excellent stability during 150 consecutive voltammetric cycles in 0.5 mol L^{-1} KCl solution as no decrease of the current was observed [4]. On the other hand, GF electrode was modified by a novel PB and ionic liquid 1-butyl-3-methylimidazolium tetrafluoroborate ([Bmim][BF₄]) via simple method involving GF placed in a ultrasound bath of [Bmim][BF₄] and then in a PB precursor solution. In this case, the immobilization of [Bmim][BF₄] supported the anchoring PB nanoparticles on the surface of the GF [73].

Zeolitic Imidazolate Framework (ZIF-8) was recently proposed for modification of CF electrode from Atomic Layer Deposition of Zinc Oxide (ZnO) and its subsequent solvothermal conversion to ZIF-8. After heat treatments under control atmosphere, ZIF-8 conversion leads to microporous carbon structure with enhanced textural and electrochemical properties. The specific surface area of the CF was increased from 0.0915 to $64 \text{ m}^2 \text{ g}^{-1}$ for pristine and modified CF, respectively [74]. To give an overview of the modification methods (Fig. 3), Table 2 summarizes advantages and drawbacks of each one.

4 Carbon Felt-Based Material for Wastewater Treatment by EF Process

4.1 Carbon Felt for EF Process

CF are abundantly used for electrochemical applications and especially for EF process because of their outstanding properties like (1) high specific surface area and high efficiency for both hydrogen peroxide production and cathodic regeneration of Fe^{2+} , good mechanical integrity, and commercial availability, which make them an attractive cathode material for EF process [23, 76]; (2) good adaptability to various EF systems with different shapes and surfaces of electrodes from small (2 cm^2) [28, 77] to large size like 60 cm^2 [78, 79] or 150 cm^2 [80]; and (3) high physicochemical stability allowing a significant decline in the cost for the EF technology, since it can be continuously used for many cycles (at least ten cycles) without any decrease of the treatment efficiency [81].

The application of EF technology for elimination of POPs on CF cathodes has been preceded very early by Oturan and coworkers [82–84]. One of their first papers in 2000s described the EF process in a divided cell allowing almost total

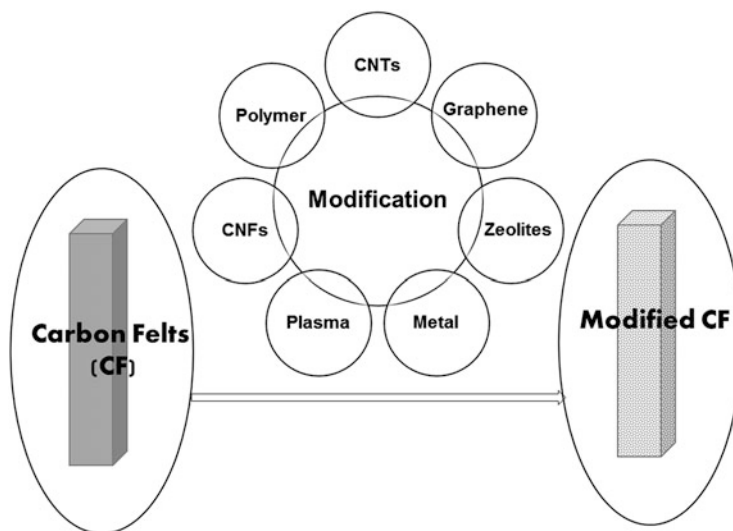


Fig. 3 The schematic for the modification processes of CF

mineralization (>95% total organic carbon (TOC) decay) of 1 mM phenoxyacetic herbicide 2,4-D after consuming 2,000 C [82]. Afterward, they continued developing their research using undivided cells combining CF cathode and Pt anode for the degradation of the herbicide diuron. A very high efficiency of 93% TOC removal at 1,000 C for 125 mL solution containing 40 mg L⁻¹ diuron has been reported [84]. From that, a series of studies using EF technology for water treatment on felt cathodes have been conducted to eliminate many different kinds of POPs in aqueous medium, including:

1. Dye pollutants: 95% TOC of the anthraquinone dye Alizarin Red S was removed in 210 min of electrolysis on GF (*Carbone-Lorraine*, thickness 0.5 cm)/boron-doped diamond (BOD) [85]. A mixture containing four triphenylmethane dyes, namely malachite green, crystal violet, methyl green, and fast green, with initial Chemical Oxygen Demand (COD) ca. 1,000 mg L⁻¹, was totally depolluted with efficiency near 100% at the beginning of the treatment on CF (*Carbone-Lorraine*) [86]. Other dyes were also investigated like malachite green [86], direct orange 61 (DO 61) [78], and acid orange 7 (AO7) [81, 87, 88].
2. Phenolic type compounds: 100% of TOC of aqueous phenol solutions was eliminated by EF process using CF cathode [89]. After 360 min of electrolysis, 95% TOC of the p-coumaric acid (4-hydroxycinnamic acid) was removed on GF (*Carbone-Lorraine*, thick 0.5 cm)/Ti-RuO₂ [90]. Pentachlorophenol [83, 91] and Bisphenol A [92] are also in this group.
3. Pesticides: the EF treatment has also been successfully applied to mineralize the herbicides and pesticides such as chlortoluron [79], 4-chloro-2-methylphenol (PCOC) [93], chlorophenoxy acid [82, 94, 95], and methyl parathion [96].

Table 2 The various modifications of carbon felt electrodes, advantages, and drawbacks of the method

Modification method	Electrode	Surface area increase	Conductivity increase	Stability	Advantages	Drawbacks	Reference
Chemical treatment	CF (SSGL Carbon, Germany)	–	2.5 times ^a	–	Relative low cost	Use of chemicals potentially toxic and not easy to handle	[18]
	GF (Shanghai Energy Carbon Limited Co., China)	1.5 times	–	Energy efficiency (EC) of vanadium redox flow battery (VRFE) above 77% after 20 cycles			[15]
Thermal treatment	CF (<i>Nippon Chem</i>)	1,344%	7% ^b	EC maintained of 75% after 500 cycles	Easy process	High energetically cost, require specific equipment	[5]
Graphene	GF (RVG-2000, Carbon-Lorraine)	–	12.5% ^b	EC maintained of 95% after 20 cycles	Very high efficiency	Stability unknown for long period of use	[37]
	CF	–	2% ^b	EC maintained of 93% after 30 cycles		Task of toxicity due to leaching of CNTs and graphene	[75]
Polymer	CF	–	300% ^a	–	Conductive polymer: high conductivity at room temperature and high stability	Stability unknown for long period of use	[56]
Zeolites	GF (Human Jiuhua Carbon Hi-Tech Co., Ltd., China)	2 times	<2 times ^c	–	Possibility to design different kind of zeolites with surface area	High cost	[62]

– Not determined

^aIncrease of the power density in MFC to raw CF^bIncrease of EC in VRFE to raw CF^cIncrease of the resistance of the electrodes to raw CF

4. Pharmaceuticals: Chlorophene [97], triclosan, and triclocarban [97] were examples for pharmaceutical pollutants which have been degraded efficiently by EF process using felt materials.
5. Hydrocarbons and polycyclic aromatic hydrocarbons (PAHs): EF process was also proposed to enhance the efficiency of soil washing treatment [80, 98, 99].

By the EF process, the pollutants are degraded step by step and eventually mineralized by reacting with hydroxyl radicals. The attack of hydroxyl radicals gives the formation of aromatic intermediate compounds at the beginning of electrolysis. The aromatic ring opening reactions in the next step create aliphatic carboxylic acids (oxalic, acetic, formic acid, etc.) and inorganic ions (i.e., ammonium, nitrate, sulfate, phosphate) as final end products before mineralization [97, 100–102]. Therefore, the EF mineralization also leads to the detoxification of treated solution [88, 91]. In particular, the toxicity of solutions disappeared after 240 min for 220 mL solution with 0.2 mM of sucralose [103], and 60 min for 200 mL solution with 50 mg L⁻¹ of Orange II [100]. The above results allow proposing EF process on CF cathode as an environmentally friendly method for the treatment of wastewater effluents containing toxic and/or persistent organic pollutants. Interestingly, more and more studies are focused now on CF modifications for improving EF processes as described in the following section.

4.2 Modified EF Systems Using Carbon Felt Cathodes

4.2.1 Modified Felt Cathodes for Homogeneous EF

For homogeneous EF process, hydrogen peroxide production and its reaction with catalyst in solution is a crucial factor for the effective destruction of POPs. Aiming to improve the in situ generation of H₂O₂, various attempts have been made to upgrade the electrocatalytic characteristic of CF cathodes. As discussed in Sect. 3.1, chemical modification is a simple and efficient way to ameliorate the electrochemical activity of the felt electrodes by changing their surface functional groups. After treatment in a mixture composed of ethanol and hydrazine hydrate (volume ratio 90/10), the concentration of H₂O₂ after 120 min was 175.8 mg L⁻¹ on the modified felt (CF-B) (*Shang-hai Qijie Carbon material Co., Ltd.*) which was nearly three times higher than 67.5 mg L⁻¹ for commercial CF. The p-nitrophenol TOC removal ratios were then 22.2% and 51.4% for CF and CF-B, respectively, proving that the treated cathode could efficiently promote the degradation efficiency of the pollutants with interesting stability and reusability (after ten cycles, the mineralization ratio was still above 45%) [23]. Anthraquinone-2,6-disulfonate/polypyrrole (AQDS/PPy) composite film was grown on graphite electrodes by electropolymerization of the pyrrole monomer in the presence of anthraquinone-2,6-disulfonic acid. Positive shifts (−0.65, −0.60, and −0.52 V vs SCE for pH 3.0, 4.0, and 6.0, respectively) were recorded indicating a better kinetics for oxygen

Table 3 Mineralization efficiency of homogeneous EF process applying diverse CF cathodes

Cathode material	Pollutant	% TOC removal increase ^a	% TOC removal decrease ^b	Reference
Graphene/CF	AO7	33	6	[77]
Chemically modified CF	p-nitrophenol	29	5	[108]
Thermally treated CF	Paracetamol	31	1	[105]

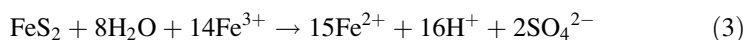
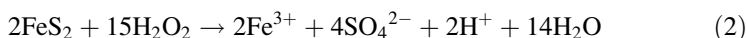
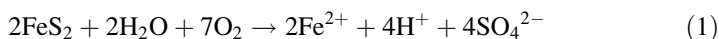
^aCompared to raw cathode after 2 h treatment

^bAfter five cycles

reduction compared to the bare cathode (-0.85 , -0.82 , and -0.77 V vs SCE for pH 3.0, 4.0, and 6.0, respectively), which indicated a better electrocatalytic activity of the AQDS/PPy/GF cathode toward oxygen reduction reaction (ORR). Therefore, the modified cathode resulted in a large accumulation of electrogenerated H_2O_2 which increases the EF degradation of amaranth azo dye [52]. Additionally, the improvement of the H_2O_2 formation rate was found on felt cathode modified by graphene using electrochemical deposition [77, 104], by heat treatment in a tubular furnace, by feeding by a mixture of N_2/O_2 with 1% of oxygen [105], by MWCNTs using the electrodeposition method carried out by applying the voltage of 17.5 V to the solution containing 0.3 g L^{-1} MWCNTs and 0.2 g L^{-1} CTAB [106], and by chemical treatment by electrochemical oxidization which was cyclically polarized in different concentration of H_2SO_4 solution in the range of 0.0 V to +2.0 V at a rate of 10 mV s^{-1} [107] (Table 3).

4.2.2 Modified Felt Cathodes for Heterogeneous EF

Drawbacks of Fenton's reaction are (1) the pH regulation between 2 and 4, (2) the loss of soluble iron catalyst [109, 110], and (3) the post-treatment requirements prior to discharge [111]. Heterogeneous catalyst could overcome these drawbacks. The main advantages of using solid iron sources are self-regulation and electrochemical regeneration of iron [112]. Pyrite is a low-cost and abundant natural iron sulfur mineral, which can provide iron ions and then act as a homogeneous catalyst after its dissolution. It seems to be a good candidate because when used as a suspension in the medium, it self-regulated the Fe^{2+} content and the pH in the solution in the presence of dissolved O_2 through reactions (1)–(3) [113]. Interestingly, the usage of pyrite can be repeated many times by the filtration to collect it from the solution. Therefore, pyrite has been used widely to remove many biorefractory pollutants in aqueous medium such as azo dye – the (4-amino-3-hydroxy-2-p-tolylazo-naphthalene-1-sulfonic acid) (AHPS) on GF (*Carbone Lorraine*, thickness 0.5 cm) [114], antibiotic levofloxacin [113], and tyrosol [113] on CF (*Carbone Lorraine*), etc.



Iron alginate gel beads (FeAB) were also used in suspension as heterogeneous catalyst in the EF treatment in which high imidacloprid removal (90%) was achieved using GF cathode (*Carbon Lorraine, France*) for 4 h [115]. Decolorization of Lissamine Green B and Azure B was 87% and 98%, respectively, after 30 min by using FeAB, maintaining particle shapes throughout the oxidation process [116].

Besides operating with solid catalyst in suspension, in 2017, Özcan et al. [117] prepared a new iron containing Fe_2O_3 -modified kaolin (Fe_2O_3 -KLN) catalyst to develop a heterogeneous EF process with three-dimensional CF cathode for the electrochemical oxidation of enoxacin (ENXN). In the presence of Fe_2O_3 -KLN, mineralization efficiency is increasing and the maximal value was found in the presence of 0.3 g catalyst at 300 mA with a very low iron quantity (~ 0.006 mM) leached in solution, showing that hydroxyl radicals were mainly produced by heterogeneous reactions of surface iron species immobilized on CF [117]. The durability of the catalyst was tested on five runs and a small decrease of around 0.5% was monitored [117]. EF treatment with heterogeneous pyrrhotite catalyst has also shown good stability with a stable color and COD removal of 77% and 78%, respectively, after 45 days. [118]. On the other hand, investigation on hierarchical CoFe-layered double hydroxide (LDH)-modified carbon felt cathode indicated that TOC removal declined 46% compared to fresh electrode after ten cycles, proving that stability has to be improved for this electrode [119].

The performance of the heterogeneous catalysis for the removal of pollutants by EF was also improved compared with homogeneous one. For example, a measured pseudo-first-order rate constant of $2.5 \times 10^{-4} \text{ s}^{-1}$ ($R^2 = 0.990$) was found for EF using pyrite catalyst which was nearly two times higher than the constant determined in electrochemical oxidation ($1.3 \times 10^{-4} \text{ s}^{-1}$ ($R^2 = 0.992$)). In addition, Fe@ Fe_2O_3 [120–122], pyrrhotite [118] γ -FeOOH [123, 124], and (γ - $\text{Fe}_2\text{O}_3/\text{Fe}_3\text{O}_4$ oxides) nanoparticles [125] and chalcopyrite [126] are interesting iron catalyst sources. The stable performance of these heterogeneous iron catalysts open promising perspectives for fast and economical treatment of wastewater polluted by POP contaminants using EF treatment on CF cathodes. In a very recent study, one new kind of heterogeneous catalyst, hierarchical CoFe-Layered Double Hydroxide (CoFe-LDH), was grown on CF by in situ solvothermal method. The CoFe-LDH/CF cathode showed very good stability when after seven cycles of degradation the TOC removal after 2 h was still above 60% [119] (Table 4).

Table 4 CF cathodes for heterogeneous EF process

Cathode	Catalyst/cathodes	Experimental conditions	EF efficiency	Reference
CF	CoFe-LDH	40 mg L ⁻¹ of acid orange 7 (AO7) at pH 3 using Pt mesh at 4.2 mA cm ⁻²	87% TOC removal after 2 h; and 97% after 8 h	[119]
GF (Carbon Lorraine, France)	Iron alginate gel beads (FeAB)	100 mg L ⁻¹ of imidacloprid using BDD anode at constant potential drop of 5 V	90% of imidacloprid removal after 4 h	[115]
CF (Beijing Sanye Carbon Co., Ltd., China)	Pyrrhotite	Real landfill leachate using anodic microbial respiration in MFC system with maximum power density of 4.2 W m ⁻³	77% of color and 78% of COD were removed after 45 days	[118]
CF	γ-FeOOH	Oxidation of arsenite by bio-electro-Fenton process in dual-chamber microbial fuel cell (MFC)	The apparent oxidation current efficiency was 73.1%	[123]
CF (MAST Carbon International Ltd., Great Britain)	γ-Fe ₂ O ₃ /Fe ₃ O ₄	16 μg L ⁻¹ of diclofenac (DCF), applied potential of 2 V using EF filter	The mineralization current efficiency (MCE) was >20%	[125]

4.2.3 Hybrid EF System Using Carbon Felt Cathodes

To boost the degradation efficiency and reduce the treatment cost, many attempts have been made to change the EF reactor. A novel vertical-flow EF reactor, composed of ten cell compartments, was designed to degrade tartrazine, a model azo dye. GF cathode (*Shanghai Qijie carbon material Co., Ltd*) was modified by ultrasonic immersion and coating method, combined with PbO₂/Ti mesh anode. By comparing with the single cell using the parallel-flow EF reactor, the new configuration showed a higher performance. The tartrazine with initial concentration of 100 mg L⁻¹ could reach near 100% degradation but with a TOC removal efficiency of 61.64% [127]. This result came from the reason that the mass transfer rate of the target pollutant molecules is accelerated and the contaminants can be well enriched at the surface in vertical-flow reactor [128].

Rosales et al. [129] fabricated an EF reactor with continuous bubble to treat the wastewater containing synthetic dyes. High decoloration percentages of pollutants were found. On the other hand, methyl orange (MO) degradation was carried in a hemisphere-shaped quartz reactor using dual rotating GF disks (*Shanghai Qijie Carbon Material Co., Ltd*) cathode to supply oxygen. An efficient production of H₂O₂ without oxygen aeration was attributed to the rotation of the cathodic disk, offering a potentially cost-effective EF method for degrading organic pollutants [130].

To further reduce the costs of electricity input, bio-electro-Fenton (BEF) system has been developed. This approach couples the EF process with MCF which

generates electricity directly from organic compounds. Zhang et al. [131] used GF at both cathode and anode without external power supply for bio-electrochemical degradation of paracetamol. In this process, a dual-chamber MFC reactor operated in the anode chamber to release bio-electrons by oxidizing biodegradable pollutants in low-strength real domestic wastewater. In the cathode chamber, $\bullet\text{OH}$ production is possible because the electrons coming from the anode will promote oxygen reduction into hydrogen peroxide and then conversion into radicals in the presence of iron as catalyst. The transfer of iron (III)/iron (II) ($\text{Fe}^{3+}/\text{Fe}^{2+}$) (sourced from $\text{FeSO}_4 \cdot 7\text{H}_2\text{O}$ added directly) from cathode to anode chamber is avoided with the use of a Proton Exchange Membrane (PEM, 6.0 cm \times 5.5 cm cross-sectional area, *Nafion-117, DuPont, USA*) [131].

The BEF system has also been developed toward a clean treatment by using heterogeneous catalysis to avoid iron-soluble salts adding. Birjandi et al. [121] built up a BEF cell through the combination of anaerobic seed sludge as biocatalyst in an anode chamber and $\text{Fe}@\text{Fe}_2\text{O}_3/\text{graphite}$ as cathode (*Entegris, Inc. FCBLK-508305-00004, USA*). This cathode served simultaneously to produce peroxide and as the catalytic iron source. The medicinal herb wastewater degradation was attributed to bio-oxidation by microorganisms at anodic chamber and to the EF process at cathodic one [121]. This BEF system was also performed by Zhuang et al. [132] on CF (4.5 cm \times 4.5 cm, *Liaoyang, China*). The electricity generated by MFC to in situ generate H_2O_2 at a CF cathode for EF process was also investigated to remove p-nitrophenol by Zhu et al. [133]. A power density of 143 mW m^{-2} was generated by the MFC, and p-nitrophenol was completely degraded after 12 h. Similar systems were created to remove biorefractory contaminants in wastewater sources like acid orange 7 dye using CF (5 cm \times 3 cm \times 0.5 cm, *Xinka Co., Shanghai, China*) [134], 17β -estradiol and 17α -ethynyl-estradiol estrogens using $\text{Fe}@\text{Fe}_2\text{O}_3/\text{CF}$ (4.5 cm \times 4.5 cm, *Liaoyang, China*) [120], azo dye (Orange II) [124] using CF anode and CNTs (CNTs)/ γ - FeOOH composite cathode, arsenite (As(III)) using γ - FeOOH/CF (4.4 cm \times 4.4 cm \times 0.5 cm) [123], Rhodamine B using $\text{Fe}@\text{Fe}_2\text{O}_3/\text{carbon felt}$, landfill leachate using CF (5 mm thickness, *Beijing Sanye Carbon Co., Ltd., China*) anode, and pyrrhotite/graphite (5 \times 7 cm^2 , 5 mm thickness) (*grade G10, Hongfeng Carbon Co., Ltd., Shanghai, China*) cathode [122].

Moreover, using modified felts can improve significantly the efficiency of BEF system. The BEF with the modified electrodes, $\text{PPy}/\text{AQDS}-\text{CF}$ (5.0 cm \times 5.0 cm \times 0.6 cm, *Liaoyang Jingu Carbon Fiber Sci-Tech Co., Ltd., China*), resulted in the largest rate of H_2O_2 generation, beneficial for the enhancement in the amount of hydroxyl radicals produced and then the decolorization and mineralization of Orange II at neutral pH [54]. In order to avoid the use of expensive membranes in two-chamber microbial fuel cell (MFC) and to increase the generated power densities, more efficient dual reactor systems were advanced by using a single chamber in a modified electro-Fenton/MFC system. The power source from MFC was transferred directly to EF reactors constituted by CF cathode and iron plate anode as catalyst source. The TOC removal of phenol reached $75 \pm 2\%$ in the EF reactor in one cycle after 22 h treatment [135].

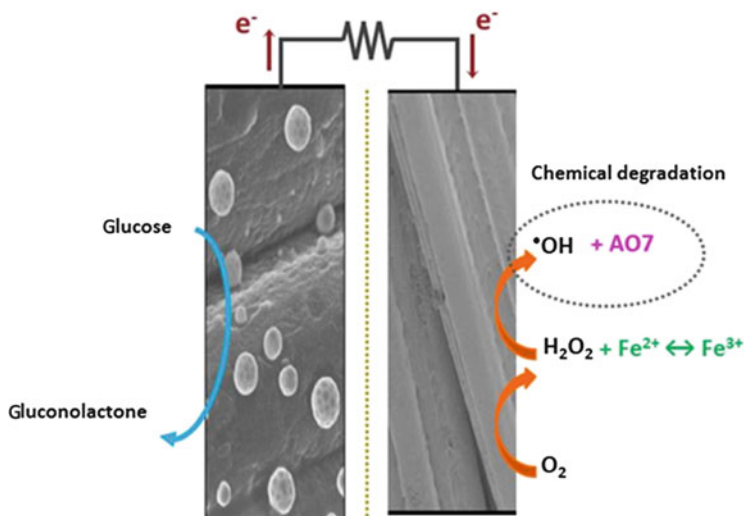


Fig. 4 Schematic diagram of the Fuel Cell-Fenton system. Reprinted from Le et al. [74]. Copyright (2016), with permission from ACS

Very recently, we discussed a Fuel Cell-Fenton system (Fig. 4) to degrade AO_7 in a cell powered by abiotic oxidation of glucose. The cathode (CF/porous Carbon) was supplied by electrical energy of glucose oxidation at a CF electrode modified with gold nanoparticles. The cathode was fabricated by Atomic Layer Deposition (ALD) of ZnO on commercial CF followed by the solvothermal conversion of the metal oxide to a Metal Organic Framework (here ZIF-8). The as-prepared composite material further calcined at high temperature under controlled atmosphere of the material leads to microporous nitrogen-doped carbon. The average power output of the system was 170 mW m^{-2} , and a stability study was carried out for more than 2 months [74].

4.2.4 Industrial Applications

To assess industrial applications, the EF process was set up to treat large volume of contaminated solutions. An organic micropollutant, diclofenac (DCF), was removed from drinking water by a novel EF filter pilot working in continuous flow. The CF was used as material for both anode and cathode. The cathode was fabricated from iron nanoparticles ($\gamma\text{-Fe}_2\text{O}_3/\text{Fe}_3\text{O}_4$ oxides) playing the role of catalyst. Because of CF electrodes high adsorption capacity of DCF, the protocol consisted of a first adsorption step without polarization for CF saturation followed by electrochemical degradation induced by an electrolysis step at 2 V inducing H_2O_2 production for EF process. Multiple cycles of adsorption/oxidation of DCF solutions were investigated at room temperature. In this EF pilot scale, the feed tank

contained 200 L. Satisfactory stability regarding both electrode integrity (no iron leaching) and removal efficiency was attained after multiple filtration/oxidation treatment cycles. The degradation of DCF and TOC removal was steadily achieved 85% and 36%, respectively, showing that efforts should be made to increase mineralization [125].

Sustainable energy sources were also investigated to supply power. There are some recent solar Photo-electro-Fenton (SPEF) systems as interesting examples: A volume of 8.0 L of textile dye solution, acid yellow 42, was treated efficiently by the SPEF process in a lab-scale pilot plant which decreased the energy consumptions [136]. The usage of sunlight as power source was also found in an autonomous solar pre-pilot plant with a capacity of 10 L to mineralize Yellow 4 diazo dye. At 5 A, about 96–97% mineralization was rapidly attained, and a reaction pathway for Direct Yellow 4 was proposed [137]. This solar pre-pilot plant also contributed to mineralize 89% of the antibiotic chloramphenicol [138], or 94% of sulfanilamide [139]. Electrode materials employed in this SPEF process were a boron-doped diamond anode and an air-diffusion cathode. Although this pilot did not use CF electrodes, this system was discussed here as an example of future development for EF pilot scale using sustainable energy sources.

5 Conclusion

Thanks to excellent properties with respect to electronic conductivity, chemical stability, light weight, and low cost, CF is widely applied as electrodes in energy and environmental field, especially water treatment by electrochemical methods. However, for application in aqueous medium, the high hydrophobicity of carbon makes it difficult to apply as electrodes. To overcome this drawback, modification methods can be used resulting in new and various benefits. Plasma, thermal, and chemical treatments change the hydrophobic surface of pristine felts to hydrophilic. They are easy to process but can suffer sometimes of a too high energy cost. Carbon nanotubes and graphene modification improved significantly the conductivity and the electrochemical active surface area; they present a risk of toxicity due to leaching in solution. Besides these modifications, zeolite material modification was also discussed.

Carbon-based modified material is a cheap, non-toxic, and stable cathode for wastewater treatment by EF process. Many toxic biorefractory pollutants were efficiently eliminated in short electrolysis time because of the significant improvement of hydrogen peroxide production, an important issue of EF process. On the other hand, to overcome the disadvantages of soluble catalyst, other solid iron sources were successfully applied for heterogeneous EF process. For industrial applications, new configurations like vertical-flow EF reactor stacked with ten cell compartments and continuous bubble EF process continually improved the efficiency of the treatment. The consumption cost was also considered by zero-energy EF approaches where MFC or abiotic fuel cells supplied clean power. These

hybrid EF systems are cost-effective for recalcitrant contaminants treatment, opening up new development trend for future research in the environmental and energy-related field. Sustainable approach using solar energy with air-diffusion cathodes for EF pre-pilot plants is also an interesting route for the future.

References

1. Smith REG, Davies TJ, Baynes NB, Nichols RJ (2015) The electrochemical characterisation of graphite felts. *J Electroanal Chem* 747:29–38. doi:[10.1016/j.jelechem.2015.03.029](https://doi.org/10.1016/j.jelechem.2015.03.029)
2. Di Blasi A, Di Blasi O, Briguglio N, Aricò AS, Sebastián D, Lázaro MJ, Monforte G, Antonucci V (2013) Investigation of several graphite-based electrodes for vanadium redox flow cell. *J Power Sources* 227:15–23. doi:[10.1016/j.jpowsour.2012.10.098](https://doi.org/10.1016/j.jpowsour.2012.10.098)
3. Wang Y, Hasebe Y (2009) Carbon felt-based biocatalytic enzymatic flow-through detectors: chemical modification of tyrosinase onto amino-functionalized carbon felt using various coupling reagents. *Talanta* 79(4):1135–1141. doi:[10.1016/j.talanta.2009.02.028](https://doi.org/10.1016/j.talanta.2009.02.028)
4. Han L, Tricard S, Fang J, Zhao J, Shen W (2013) Prussian blue @ platinum nanoparticles/graphite felt nanocomposite electrodes: application as hydrogen peroxide sensor. *Biosens Bioelectron* 43:120–124. doi:[10.1016/j.bios.2012.12.003](https://doi.org/10.1016/j.bios.2012.12.003)
5. Kim KJ, Kim Y-J, Kim J-H, Park M-S (2011) The effects of surface modification on carbon felt electrodes for use in vanadium redox flow batteries. *Mater Chem Phys* 131(1–2):547–553. doi:[10.1016/j.matchemphys.2011.10.022](https://doi.org/10.1016/j.matchemphys.2011.10.022)
6. González Z, Sánchez A, Blanco C, Granda M, Menéndez R, Santamaría R (2011) Enhanced performance of a Bi-modified graphite felt as the positive electrode of a vanadium redox flow battery. *Electrochem Commun* 13(12):1379–1382. doi:[10.1016/j.elecom.2011.08.017](https://doi.org/10.1016/j.elecom.2011.08.017)
7. Chakrabarti MH, Brandon NP, Hajimolana SA, Tariq F, Yufit V, Hashim MA, Hussain MA, Lowd CTJ, Aravind PV (2014) Application of carbon materials in redox flow batteries. *J Power Sources* 253:150–166. doi:[10.1016/j.jpowsour.2013.12.038](https://doi.org/10.1016/j.jpowsour.2013.12.038)
8. Sun B, Kazacos MS (1992) Modification of graphite electrode materials for vanadium redox flow battery application – I. Thermal treatment. *Electrochim Acta* 37(7):1253–1260
9. Brillas E, Sirés I, Oturan MA (2009) Electro-Fenton process and related electrochemical technologies based on Fenton's reaction chemistry. *Chem Rev* 109:6570–6631
10. Nidheesh PV, Gandhimathi R (2012) Trends in electro-Fenton process for water and wastewater treatment: an overview. *Desalination* 299:1–15. doi:[10.1016/j.desal.2012.05.011](https://doi.org/10.1016/j.desal.2012.05.011)
11. Rosales E, Pazos M, Sanromán MA (2012) Advances in the electro-Fenton process for remediation of recalcitrant organic compounds. *Chem Eng Technol* 35(4):609–617. doi:[10.1002/ceat.201100321](https://doi.org/10.1002/ceat.201100321)
12. Sires I, Brillas E (2012) Remediation of water pollution caused by pharmaceutical residues based on electrochemical separation and degradation technologies: a review. *Environ Int* 40:212–229. doi:[10.1016/j.envint.2011.07.012](https://doi.org/10.1016/j.envint.2011.07.012)
13. Deng Q, Li X, Zuo J, Ling A, Logan BE (2010) Power generation using an activated carbon fiber felt cathode in an upflow microbial fuel cell. *J Power Sources* 195(4):1130–1135. doi:[10.1016/j.jpowsour.2009.08.092](https://doi.org/10.1016/j.jpowsour.2009.08.092)
14. González-García J, Bonete P, Expósito E, Montiel V, Aldaz A, Torregrasa-Maciá R (1999) Characterization of a carbon felt electrode structural and physical properties. *J Mater Chem* 9:419–426
15. Li XG, Huang KL, Liu SQ, Tan N, Chen LQ (2007) Characteristics of graphite felt electrode electrochemically oxidized for vanadium redox battery application. *Trans Nonferrous Metals Soc China* 17(1):195–199. doi:[10.1016/s1003-6326\(07\)60071-5](https://doi.org/10.1016/s1003-6326(07)60071-5)

16. Zhang Z, Xi J, Zhou H, Qiu X (2016) KOH etched graphite felt with improved wettability and activity for vanadium flow batteries. *Electrochim Acta* 218:15–23. doi:[10.1016/j.electacta.2016.09.099](https://doi.org/10.1016/j.electacta.2016.09.099)
17. Ding C, Zhang H, Li X, Liu T, Xing F (2013) Vanadium flow battery for energy storage: prospects and challenges. *J Phys Chem Lett* 4(8):1281–1294. doi:[10.1021/jz4001032](https://doi.org/10.1021/jz4001032)
18. Hidalgo D, Tommasi T, Bocchini S, Chiolerio A, Chiodoni A, Mazzarino I, Ruggeri B (2016) Surface modification of commercial carbon felt used as anode for microbial fuel cells. *Energy* 99:193–201. doi:[10.1016/j.energy.2016.01.039](https://doi.org/10.1016/j.energy.2016.01.039)
19. Bianting S, Kazacos MS (1992) Chemical modification of graphite electrode materials for vanadium redox flow battery application – Part II: Acid treatments. *Electrochim Acta* 37 (13):2459–2465
20. Flox C, Rubio-García J, Skoumal M, Andreu T, Morante JR (2013) Thermo-chemical treatments based on NH_3/O_2 for improved graphite-based fiber electrodes in vanadium redox flow batteries. *Carbon* 60:280–288. doi:[10.1016/j.carbon.2013.04.038](https://doi.org/10.1016/j.carbon.2013.04.038)
21. Tang X, Guo K, Li H, Du Z, Tian J (2011) Electrochemical treatment of graphite to enhance electron transfer from bacteria to electrodes. *Bioresour Technol* 102(3):3558–3560. doi:[10.1016/j.biortech.2010.09.022](https://doi.org/10.1016/j.biortech.2010.09.022)
22. Zhou L, Hu Z, Zhang C, Bi Z, Jin T, Zhou M (2013) Electrogeneration of hydrogen peroxide for electro-Fenton system by oxygen reduction using chemically modified graphite felt cathode. *Sep Purif Technol* 111:131–136. doi:[10.1016/j.seppur.2013.03.038](https://doi.org/10.1016/j.seppur.2013.03.038)
23. Zhang L, Su Z, Jiang F, Yang L, Qian J, Zhou Y, Li W, Hong M (2014) Highly graphitized nitrogen-doped porous carbon nanopolyhedra derived from ZIF-8 nanocrystals as efficient electrocatalysts for oxygen reduction reactions. *Nanoscale* 6(12):6590–6602. doi:[10.1039/c4nr00348a](https://doi.org/10.1039/c4nr00348a)
24. Zhong S, Padeste C, Kazacos M, Skyllas-Kazacos M (1993) Comparison of the physical, chemical and electrochemical properties of rayon- and polyacrylonitrile-based graphite felt electrodes. *J Power Sources* 45:29–41
25. He Z, Shi L, Shen J, He Z, Liu S (2015) Effects of nitrogen doping on the electrochemical performance of graphite felts for vanadium redox flow batteries. *Int J Energy Res* 39 (5):709–716. doi:[10.1002/er.3291](https://doi.org/10.1002/er.3291)
26. Wu T, Huang K, Liu S, Zhuang S, Fang D, Li S, Lu D, Su A (2011) Hydrothermal ammoniated treatment of PAN-graphite felt for vanadium redox flow battery. *J Solid State Electrochem* 16(2):579–585. doi:[10.1007/s10008-011-1383-y](https://doi.org/10.1007/s10008-011-1383-y)
27. Dixon D, Babu DJ, Langner J, Bruns M, Pfaffmann L, Bhaskar A, Schneider JJ, Scheiba F, Ehrenberg H (2016) Effect of oxygen plasma treatment on the electrochemical performance of the rayon and polyacrylonitrile based carbon felt for the vanadium redox flow battery application. *J Power Sources* 332:240–248. doi:[10.1016/j.jpowsour.2016.09.070](https://doi.org/10.1016/j.jpowsour.2016.09.070)
28. Wang Y, Chen Z, Yu S, Saeed MU, Luo R (2016) Preparation and characterization of new-type high-temperature vacuum insulation composites with graphite felt core material. *Mater Des* 99:369–377. doi:[10.1016/j.matdes.2016.03.083](https://doi.org/10.1016/j.matdes.2016.03.083)
29. Chen JZ, Liao WY, Hsieh WY, Hsu CC, Chen YS (2015) All-vanadium redox flow batteries with graphite felt electrodes treated by atmospheric pressure plasma jets. *J Power Sources* 274:894–898. doi:[10.1016/j.jpowsour.2014.10.097](https://doi.org/10.1016/j.jpowsour.2014.10.097)
30. Shao Y, Wang X, Engelhard M, Wang C, Dai S, Liu J, Yang Z, Lin Y (2010) Nitrogen-doped mesoporous carbon for energy storage in vanadium redox flow batteries. *J Power Sources* 195 (13):4375–4379. doi:[10.1016/j.jpowsour.2010.01.015](https://doi.org/10.1016/j.jpowsour.2010.01.015)
31. Ma K, Cheng JP, Liu F, Zhang X (2016) Co-Fe layered double hydroxides nanosheets vertically grown on carbon fiber cloth for electrochemical capacitors. *J Alloys Compd* 679:277–284. doi:[10.1016/j.jallcom.2016.04.059](https://doi.org/10.1016/j.jallcom.2016.04.059)
32. Rao CN, Sood AK, Subrahmanyam KS, Govindaraj A (2009) Graphene: the new two-dimensional nanomaterial. *Angew Chem Int Ed Engl* 48(42):7752–7777. doi:[10.1002/anie.200901678](https://doi.org/10.1002/anie.200901678)

33. Jang SK, Jeon J, Jeon SM, Song YJ, Lee S (2015) Effects of dielectric material properties on graphene transistor performance. *Solid State Electron* 109:8–11. doi:[10.1016/j.sse.2015.03.003](https://doi.org/10.1016/j.sse.2015.03.003)
34. Chen D, Tang L, Li J (2010) Graphene-based materials in electrochemistry. *Chem Soc Rev* 39(8):3157–3180. doi:[10.1039/b923596e](https://doi.org/10.1039/b923596e)
35. Zhang C, Liang P, Yang X, Jiang Y, Bian Y, Chen C, Zhang X, Huang X (2016) Binder-free graphene and manganese oxide coated carbon felt anode for high-performance microbial fuel cell. *Biosens Bioelectron* 81:32–38. doi:[10.1016/j.bios.2016.02.051](https://doi.org/10.1016/j.bios.2016.02.051)
36. Chavez-Valdez A, Shaffer MS, Boccaccini AR (2013) Applications of graphene electrophoretic deposition. A review. *J Phys Chem B* 117(6):1502–1515. doi:[10.1021/jp3064917](https://doi.org/10.1021/jp3064917)
37. González Z, Flox C, Blanco C, Granda M, Morante JR, Menéndez R, Santamaría R (2016) Outstanding electrochemical performance of a graphene-modified graphite felt for vanadium redox flow battery application. *J Power Sources*. doi:[10.1016/j.jpowsour.2016.10.069](https://doi.org/10.1016/j.jpowsour.2016.10.069)
38. Sehwat P, Julien C, Islam SS (2016) Carbon nanotubes in Li-ion batteries: a review. *Mater Sci Eng B* 213:12–40. doi:[10.1016/j.mseb.2016.06.013](https://doi.org/10.1016/j.mseb.2016.06.013)
39. Cui H, Qian Y, An H, Sun C, Zhai J, Li Q (2012) Electrochemical removal of fluoride from water by PAA-modified carbon felt electrodes in a continuous flow reactor. *Water Res* 46(12):3943–3950. doi:[10.1016/j.watres.2012.04.039](https://doi.org/10.1016/j.watres.2012.04.039)
40. Wang S, Zhao X, Cochell T, Manthiram A (2012) Nitrogen-doped carbon nanotube/graphite felts as advanced electrode materials for vanadium redox flow batteries. *J Phys Chem Lett* 3(16):2164–2167. doi:[10.1021/jz3008744](https://doi.org/10.1021/jz3008744)
41. Rosolen JM, Matsubara EY, Marchesin MS, Lala SM, Montoro LA, Tronto S (2006) Carbon nanotube/felt composite electrodes without polymer binders. *J Power Sources* 162(1):620–628. doi:[10.1016/j.jpowsour.2006.06.087](https://doi.org/10.1016/j.jpowsour.2006.06.087)
42. Wang K, Chizari K, Liu Y, Janowska I, Moldovan SM, Ersen O, Bonnefont A, Savinova ER, Nguyen LD, Pham-Huu C (2011) Catalytic synthesis of a high aspect ratio carbon nanotubes bridging carbon felt composite with improved electrical conductivity and effective surface area. *Appl Catal A Gen* 392(1–2):238–247. doi:[10.1016/j.apcata.2010.11.014](https://doi.org/10.1016/j.apcata.2010.11.014)
43. Mauricio Rosolen J, Patrick Poá CH, Tronto S, Marchesin MS, Silva SRP (2006) Electron field emission of carbon nanotubes on carbon felt. *Chem Phys Lett* 424(1–3):151–155. doi:[10.1016/j.cplett.2006.04.071](https://doi.org/10.1016/j.cplett.2006.04.071)
44. Rosolen JM, Tronto S, Marchesin MS, Almeida EC, Ferreira NG, Patrick Poá CH, Silva SRP (2006) Electron field emission from composite electrodes of carbon nanotubes-boron-doped diamond and carbon felts. *Appl Phys Lett* 88(8):083116. doi:[10.1063/1.2178247](https://doi.org/10.1063/1.2178247)
45. Song Q, Li K, Li H, Fu Q (2013) Increasing the tensile property of unidirectional carbon/carbon composites by grafting carbon nanotubes onto carbon fibers by electrophoretic deposition. *J Mater Sci Technol* 29(8):711–714. doi:[10.1016/j.jmst.2013.05.015](https://doi.org/10.1016/j.jmst.2013.05.015)
46. An Q, Rider AN, Thostenson ET (2012) Electrophoretic deposition of carbon nanotubes onto carbon-fiber fabric for production of carbon/epoxy composites with improved mechanical properties. *Carbon* 50(11):4130–4143. doi:[10.1016/j.carbon.2012.04.061](https://doi.org/10.1016/j.carbon.2012.04.061)
47. Li KZ, Li L, Li HJ, Song Q, Lu JH, Fu QG (2014) Electrophoretic deposition of carbon nanotubes onto carbon fiber felt for production of carbon/carbon composites with improved mechanical and thermal properties. *Vacuum* 104:105–110. doi:[10.1016/j.vacuum.2014.01.024](https://doi.org/10.1016/j.vacuum.2014.01.024)
48. Wei G, Jia C, Liu J, Yan C (2012) Carbon felt supported carbon nanotubes catalysts composite electrode for vanadium redox flow battery application. *J Power Sources* 220:185–192. doi:[10.1016/j.jpowsour.2012.07.081](https://doi.org/10.1016/j.jpowsour.2012.07.081)
49. Li W, Liu J, Yan C (2011) Multi-walled carbon nanotubes used as an electrode reaction catalyst for VO_2^+ for a vanadium redox flow battery. *Carbon* 49(11):3463–3470. doi:[10.1016/j.carbon.2011.04.045](https://doi.org/10.1016/j.carbon.2011.04.045)
50. Chandrasekhar P, Naishadham K (1999) Broadband microwave absorption and shielding properties of a poly(aniline). *Synth Met* 105:115–120
51. Lin Y, Cui X, Bontha J (2006) Electrically controlled anion exchange based on polypyrrole and carbon nanotubes nanocomposite for perchlorate removal. *Environ Sci Technol* 40(12):4004–4009

52. Zhang G, Yang F, Gao M, Liu L (2008) Electrocatalytic behavior of the bare and the anthraquinonedisulfonate/polypyrrole composite film modified graphite cathodes in the electro-Fenton system. *J Phys Chem C* 112:8957–8962
53. Hasebe Y, Wang Y, Fukuoka K (2011) Electropolymerized poly(Toluidine Blue)-modified carbon felt for highly sensitive amperometric determination of NADH in flow injection analysis. *J Environ Sci* 23(6):1050–1056. doi:[10.1016/s1001-0742\(10\)60513-x](https://doi.org/10.1016/s1001-0742(10)60513-x)
54. Feng C, Li F, Liu H, Lang X, Fan S (2010) A dual-chamber microbial fuel cell with conductive film-modified anode and cathode and its application for the neutral electro-Fenton process. *Electrochim Acta* 55(6):2048–2054. doi:[10.1016/j.electacta.2009.11.033](https://doi.org/10.1016/j.electacta.2009.11.033)
55. Jiang X, Lou S, Chen D, Shen J, Han W, Sun X, Li J, Wang L (2015) Fabrication of polyaniline/graphene oxide composite for graphite felt electrode modification and its performance in the bioelectrochemical system. *J Electroanal Chem* 744:95–100. doi:[10.1016/j.jelechem.2015.03.001](https://doi.org/10.1016/j.jelechem.2015.03.001)
56. Li C, Ding L, Cui H, Zhang L, Xu K, Ren H (2012) Application of conductive polymers in biocathode of microbial fuel cells and microbial community. *Bioresour Technol* 116:459–465. doi:[10.1016/j.biortech.2012.03.115](https://doi.org/10.1016/j.biortech.2012.03.115)
57. Mu S (2004) Electrochemical copolymerization of aniline and o-aminophenol. *Synth Met* 143(3):259–268. doi:[10.1016/j.synthmet.2003.12.008](https://doi.org/10.1016/j.synthmet.2003.12.008)
58. Lv Z, Chen Y, Wei H, Li F, Hu Y, Wei C, Feng C (2013) One-step electrosynthesis of polypyrrole/graphene oxide composites for microbial fuel cell application. *Electrochim Acta* 111:366–373. doi:[10.1016/j.electacta.2013.08.022](https://doi.org/10.1016/j.electacta.2013.08.022)
59. Hui J, Jiang X, Xie H, Chen D, Shen J, Sun X, Han W, Li J, Wang L (2016) Laccase-catalyzed electrochemical fabrication of polyaniline/graphene oxide composite onto graphite felt electrode and its application in bioelectrochemical system. *Electrochim Acta* 190:16–24. doi:[10.1016/j.electacta.2015.12.119](https://doi.org/10.1016/j.electacta.2015.12.119)
60. Cui H-F, Du L, Guo P-B, Zhu B, Luong JHT (2015) Controlled modification of carbon nanotubes and polyaniline on macroporous graphite felt for high-performance microbial fuel cell anode. *J Power Sources* 283:46–53. doi:[10.1016/j.jpowsour.2015.02.088](https://doi.org/10.1016/j.jpowsour.2015.02.088)
61. Walcarius A (1999) Zeolite-modified electrodes in electroanalytical chemistry. *Anal Chim Acta* 384:1–16
62. Wu X, Tong F, Yong X, Zhou J, Zhang L, Jia H, Wei P (2016) Effect of NaX zeolite-modified graphite felts on hexavalent chromium removal in biocathode microbial fuel cells. *J Hazard Mater* 308:303–311. doi:[10.1016/j.jhazmat.2016.01.070](https://doi.org/10.1016/j.jhazmat.2016.01.070)
63. Wu X-Y, Tong F, Song T-S, Gao X-Y, Xie J-J, Zhou CC, Zhang L-X, Wei P (2015) Effect of zeolite-coated anode on the performance of microbial fuel cells. *J Chem Technol Biotechnol* 90(1):87–92. doi:[10.1002/jctb.4290](https://doi.org/10.1002/jctb.4290)
64. Haghghi B, Hamidi H, Gorton L (2010) Electrochemical behavior and application of Prussian blue nanoparticle modified graphite electrode. *Sensors Actuators B Chem* 147(1):270–276. doi:[10.1016/j.snb.2010.03.020](https://doi.org/10.1016/j.snb.2010.03.020)
65. Ricci F, Palleschi G (2005) Sensor and biosensor preparation, optimisation and applications of Prussian Blue modified electrodes. *Biosens Bioelectron* 21(3):389–407. doi:[10.1016/j.bios.2004.12.001](https://doi.org/10.1016/j.bios.2004.12.001)
66. Ellis D, Eckhoff M, Neff VD (1981) Electrochromism in the mixed-valence hexacyanides. I. Voltammetric and spectral studies of the oxidation and reduction of thin films of Prussian Blue. *J Phys Chem* 85(9):1225–1231
67. Ricci F, Amine A, Palleschi G, Moscone D (2003) Prussian Blue based screen printed biosensors with improved characteristics of long-term lifetime and pH stability. *Biosens Bioelectron* 18(2–3):165–174
68. Neff VD (1978) Electrochemical oxidation and reduction of thin films of Prussian Blue. *J Electrochem Soc* 125(6):886–887
69. DeLongchamp DM, Hammond PT (2004) High-contrast electrochromism and controllable dissolution of assembled Prussian blue/polymer nanocomposites. *Adv Funct Mater* 14:224–232

70. Itaya K, Uchida I, Neff VD (1986) Electrochemistry of polynuclear transition metal cyanides: Prussian blue and its analogues. *Acc Chem Res* 19:162–168
71. Pyrasch M, Tiede B (2001) Electro- and photoresponsive films of Prussian blue prepared upon multiple sequential adsorption. *Langmuir* 17:7706–7709
72. Zhou P, Xue D, Luo H, Chen X (2002) Fabrication, structure, and magnetic properties of highly ordered Prussian blue nanowire arrays. *Nano Lett* 2:845–847
73. Wang L, Tricard S, Cao L, Liang Y, Zhao J, Fang J, Shen W (2015) Prussian blue/1-butyl-3-methylimidazolium tetrafluoroborate – graphite felt electrodes for efficient electrocatalytic determination of nitrite. *Sensors Actuators B Chem* 214:70–75. doi:[10.1016/j.snb.2015.03.009](https://doi.org/10.1016/j.snb.2015.03.009)
74. Le TXH, Esmilaire R, Drobek M, Bechelany M, Vallicari C, Nguyen DL, Julbe A, Tingry S, Cretin M (2016) Design of novel Fuel Cell-Fenton system a smart approach to zero energy depollution. *J Mater Chem A* 4:17686. doi:[10.1039/C6TA05443A](https://doi.org/10.1039/C6TA05443A)
75. Li W, Liu J, Yan C (2012) The electrochemical catalytic activity of single-walled carbon nanotubes towards VO₂⁺/VO₂²⁺ and V³⁺/V²⁺ redox pairs for an all vanadium redox flow battery. *Electrochim Acta* 79:102–108. doi:[10.1016/j.electacta.2012.06.109](https://doi.org/10.1016/j.electacta.2012.06.109)
76. Petrucci E, Da Pozzo A, Di Palma L (2016) On the ability to electrogenerate hydrogen peroxide and to regenerate ferrous ions of three selected carbon-based cathodes for electro-Fenton processes. *Chem Eng J* 283:750–758. doi:[10.1016/j.cej.2015.08.030](https://doi.org/10.1016/j.cej.2015.08.030)
77. Le TXH, Bechelany M, Lacour S, Oturan N, Oturan MA, Cretin M (2015) High removal efficiency of dye pollutants by electron-Fenton process using a graphene based cathode. *Carbon* 94:1003–1011. doi:[10.1016/j.carbon.2015.07.086](https://doi.org/10.1016/j.carbon.2015.07.086)
78. Hammami S, Oturan N, Bellakhal N, Dachraoui M, Oturan MA (2007) Oxidative degradation of direct orange 61 by electro-Fenton process using a carbon felt electrode: application of the experimental design methodology. *J Electroanal Chem* 610(1):75–84. doi:[10.1016/j.jelechem.2007.07.004](https://doi.org/10.1016/j.jelechem.2007.07.004)
79. Abdessalem AK, Oturan N, Bellakhal N, Dachraoui M, Oturan MA (2008) Experimental design methodology applied to electro-Fenton treatment for degradation of herbicide chlortoluron. *Appl Catal B Environ* 78(3–4):334–341. doi:[10.1016/j.apcatb.2007.09.032](https://doi.org/10.1016/j.apcatb.2007.09.032)
80. Mousset E, Oturan N, van Hullebusch ED, Guibaud G, Esposito G, Oturan MA (2014) Influence of solubilizing agents (cyclodextrin or surfactant) on phenanthrene degradation by electro-Fenton process – study of soil washing recycling possibilities and environmental impact. *Water Res* 48:306–316. doi:[10.1016/j.watres.2013.09.044](https://doi.org/10.1016/j.watres.2013.09.044)
81. Le TXH, Nguyen DL, Yacouba ZA, Zougrana L, Avril F, Petit E, Mendret J, Bonniol V, Bechelany M, Lacour S, Lesage G, Cretin M (2016) Toxicity removal assessments related to degradation pathways of azo dyes: toward an optimization of electro-Fenton treatment. *Chemosphere* 161:308–318. doi:[10.1016/j.chemosphere.2016.06.108](https://doi.org/10.1016/j.chemosphere.2016.06.108)
82. Oturan MA (2000) An ecologically effective water treatment technique using electrochemically generated hydroxyl radicals for in situ destruction of organic pollutants: application to herbicide 2,4-D. *J Appl Electrochem* 30:475–482
83. Oturan MA, Oturan N, Lahitte C, Trevin S (2001) Production of hydroxyl radicals by electrochemically assisted Fenton's reagent application to the mineralization of an organic micropollutant, pentachlorophenol. *J Electroanal Chem* 507:96–102
84. Edelahe MC, Oturan N, Oturan MA, Padellec Y, Bermond A, Kacemi KE (2003) Degradation of diuron by the electro-Fenton process. *Environ Chem Lett* 1(4):233–236
85. Panizza M, Oturan MA (2011) Degradation of alizarin red by electro-Fenton process using a graphite-felt cathode. *Electrochim Acta* 56(20):7084–7087. doi:[10.1016/j.electacta.2011.05.105](https://doi.org/10.1016/j.electacta.2011.05.105)
86. Sires I, Guivarch E, Oturan N, Oturan MA (2008) Efficient removal of triphenylmethane dyes from aqueous medium by in situ electrogenerated Fenton's reagent at carbon-felt cathode. *Chemosphere* 72(4):592–600. doi:[10.1016/j.chemosphere.2008.03.010](https://doi.org/10.1016/j.chemosphere.2008.03.010)
87. Ozcan A, Oturan MA, Oturan N, Sahin Y (2009) Removal of acid Orange 7 from water by electrochemically generated Fenton's reagent. *J Hazard Mater* 163(2–3):1213–1220. doi:[10.1016/j.jhazmat.2008.07.088](https://doi.org/10.1016/j.jhazmat.2008.07.088)

88. Hammami S, Bellakhal N, Oturan N, Oturan MA, Dachraoui M (2008) Degradation of acid Orange 7 by electrochemically generated (*)OH radicals in acidic aqueous medium using a boron-doped diamond or platinum anode: a mechanistic study. *Chemosphere* 73(5):678–684. doi:[10.1016/j.chemosphere.2008.07.010](https://doi.org/10.1016/j.chemosphere.2008.07.010)
89. Pimentel M, Oturan N, Dezotti M, Oturan MA (2008) Phenol degradation by advanced electrochemical oxidation process electro-Fenton using a carbon felt cathode. *Appl Catal B Environ* 83(1–2):140–149. doi:[10.1016/j.apcatb.2008.02.011](https://doi.org/10.1016/j.apcatb.2008.02.011)
90. Elaoud SC, Panizza M, Cerisola G, Mhiri T (2012) Coumaric acid degradation by electro-Fenton process. *J Electroanal Chem* 667:19–23. doi:[10.1016/j.jelechem.2011.12.013](https://doi.org/10.1016/j.jelechem.2011.12.013)
91. Hanna K, Chiron S, Oturan MA (2005) Coupling enhanced water solubilization with cyclodextrin to indirect electrochemical treatment for pentachlorophenol contaminated soil remediation. *Water Res* 39(12):2763–2773. doi:[10.1016/j.watres.2005.04.057](https://doi.org/10.1016/j.watres.2005.04.057)
92. Gözmen B, Oturan MA, Oturan N, Erbatur O (2003) Indirect electrochemical treatment of bisphenol A in water via electrochemically generated Fenton's reagent. *Environ Sci Technol* 37(16):3716–3723
93. Irmak S, Yavuz HI, Erbatur O (2006) Degradation of 4-chloro-2-methylphenol in aqueous solution by electro-Fenton and photoelectro-Fenton processes. *Appl Catal B Environ* 63(3–4):243–248. doi:[10.1016/j.apcatb.2005.10.008](https://doi.org/10.1016/j.apcatb.2005.10.008)
94. Aaron JJ, Oturan MA (2001) New photochemical and electrochemical methods for the degradation of pesticides in aqueous media. *Environmental applications*. *Turk J Chem* 25:509–520
95. Oturan MA, Aaron JJ, Oturan N, Pinson J (1999) Degradation of chlorophenoxyacid herbicides in aqueous media, using a novel electrochemical method. *Pestic Sci* 55:558–562
96. Diagne M, Oturan N, Oturan MA (2007) Removal of methyl parathion from water by electrochemically generated Fenton's reagent. *Chemosphere* 66(5):841–848. doi:[10.1016/j.chemosphere.2006.06.033](https://doi.org/10.1016/j.chemosphere.2006.06.033)
97. Sirés I, Garrido JA, Rodríguez RM, Brillas E, Oturan N, Oturan MA (2007) Catalytic behavior of the Fe³⁺/Fe²⁺ system in the electro-Fenton degradation of the antimicrobial chlorophene. *Appl Catal B Environ* 72(3–4):382–394. doi:[10.1016/j.apcatb.2006.11.016](https://doi.org/10.1016/j.apcatb.2006.11.016)
98. Huguenot D, Mousset E, van Hullebusch ED, Oturan MA (2015) Combination of surfactant enhanced soil washing and electro-Fenton process for the treatment of soils contaminated by petroleum hydrocarbons. *J Environ Manag* 153:40–47. doi:[10.1016/j.jenvman.2015.01.037](https://doi.org/10.1016/j.jenvman.2015.01.037)
99. Mousset E, Huguenot D, van Hullebusch ED, Oturan N, Guibaud G, Esposito G, Oturan MA (2016) Impact of electrochemical treatment of soil washing solution on PAH degradation efficiency and soil respirometry. *Environ Pollut* 211:354–362. doi:[10.1016/j.envpol.2016.01.021](https://doi.org/10.1016/j.envpol.2016.01.021)
100. Lin H, Zhang H, Wang X, Wang L, Wu J (2014) Electro-Fenton removal of Orange II in a divided cell: reaction mechanism, degradation pathway and toxicity evolution. *Sep Purif Technol* 122:533–540. doi:[10.1016/j.seppur.2013.12.010](https://doi.org/10.1016/j.seppur.2013.12.010)
101. Mousset E, Frunzo L, Esposito G, van Hullebusch ED, Oturan N, Oturan MA (2016) A complete phenol oxidation pathway obtained during electro-Fenton treatment and validated by a kinetic model study. *Appl Catal B Environ* 180:189–198. doi:[10.1016/j.apcatb.2015.06.014](https://doi.org/10.1016/j.apcatb.2015.06.014)
102. Oturan MA, Pimentel M, Oturan N, Sirés I (2008) Reaction sequence for the mineralization of the short-chain carboxylic acids usually formed upon cleavage of aromatics during electrochemical Fenton treatment. *Electrochim Acta* 54(2):173–182. doi:[10.1016/j.electacta.2008.08.012](https://doi.org/10.1016/j.electacta.2008.08.012)
103. Lin H, Oturan N, Wu J, Zhang H, Oturan MA (2017) Cold incineration of sucralose in aqueous solution by electro-Fenton process. *Sep Purif Technol* 173:218–225. doi:[10.1016/j.seppur.2016.09.028](https://doi.org/10.1016/j.seppur.2016.09.028)
104. Le TXH, Bechelany M, Champavert J, Cretin M (2015) A highly active based graphene cathode for electro-Fenton reaction. *RSC Adv* 5:42536–42539. doi:[10.1039/C5RA04811G](https://doi.org/10.1039/C5RA04811G)
105. Le TXH, Charmette C, Bechelany M, Cretin M (2016) Facile preparation of porous carbon cathode to eliminate Paracetamol in aqueous medium using electro-Fenton system. *Electrochim Acta* 188:378–384. doi:[10.1016/j.electacta.2015.12.005](https://doi.org/10.1016/j.electacta.2015.12.005)

106. Pajootan E, Arami M, Rahimdokht M (2014) Discoloration of wastewater in a continuous electro-Fenton process using modified graphite electrode with multi-walled carbon nanotubes/surfactant. *Sep Purif Technol* 130:34–44. doi:[10.1016/j.seppur.2014.04.025](https://doi.org/10.1016/j.seppur.2014.04.025)
107. Miao J, Zhu H, Tang Y, Chen Y, Wan P (2014) Graphite felt electrochemically modified in H₂SO₄ solution used as a cathode to produce H₂O₂ for pre-oxidation of drinking water. *Chem Eng J* 250:312–318. doi:[10.1016/j.cej.2014.03.043](https://doi.org/10.1016/j.cej.2014.03.043)
108. Zhou L, Zhou M, Hu Z, Bi Z, Serrano KG (2014) Chemically modified graphite felt as an efficient cathode in electro-Fenton for p-nitrophenol degradation. *Electrochim Acta* 140:376–383. doi:[10.1016/j.electacta.2014.04.090](https://doi.org/10.1016/j.electacta.2014.04.090)
109. Popuri SR, Chang C-Y, Xu J (2011) A study on different addition approach of Fenton's reagent for DCOD removal from ABS wastewater. *Desalination* 277(1–3):141–146. doi:[10.1016/j.desal.2011.04.017](https://doi.org/10.1016/j.desal.2011.04.017)
110. Guo S, Zhang G, Wang J (2014) Photo-Fenton degradation of rhodamine B using Fe₂O₃-Kaolin as heterogeneous catalyst: characterization, process optimization and mechanism. *J Colloid Interface Sci* 433:1–8. doi:[10.1016/j.jcis.2014.07.017](https://doi.org/10.1016/j.jcis.2014.07.017)
111. Hassan H, Hameed BH (2011) Fe-clay as effective heterogeneous Fenton catalyst for the decolorization of Reactive Blue 4. *Chem Eng J* 171(3):912–918. doi:[10.1016/j.cej.2011.04.040](https://doi.org/10.1016/j.cej.2011.04.040)
112. Sánchez-Sánchez CM, Expósito E, Casado J, Montiel V (2007) Goethite as a more effective iron dosage source for mineralization of organic pollutants by electro-Fenton process. *Electrochem Commun* 9(1):19–24. doi:[10.1016/j.elecom.2006.08.023](https://doi.org/10.1016/j.elecom.2006.08.023)
113. Barhoumi N, Labiadh L, Oturan MA, Gadri A, Ammar S, Brillas E (2015) Electrochemical mineralization of the antibiotic levofloxacin by electro-Fenton-pyrite process. *Chemosphere* 141:250–257. doi:[10.1016/j.chemosphere.2015.08.003](https://doi.org/10.1016/j.chemosphere.2015.08.003)
114. Labiadh L, Oturan MA, Panizza M, Hamadi NB, Ammar S (2015) Complete removal of AHPS synthetic dye from water using new electro-Fenton oxidation catalyzed by natural pyrite as heterogeneous catalyst. *J Hazard Mater* 297:34–41. doi:[10.1016/j.jhazmat.2015.04.062](https://doi.org/10.1016/j.jhazmat.2015.04.062)
115. Iglesias O, Gómez J, Pazos M, Sanromán MÁ (2014) Electro-Fenton oxidation of imidacloprid by Fe alginate gel beads. *Appl Catal B Environ* 144:416–424. doi:[10.1016/j.apcatb.2013.07.046](https://doi.org/10.1016/j.apcatb.2013.07.046)
116. Rosales E, Iglesias O, Pazos M, Sanroman MA (2012) Decolourisation of dyes under electro-Fenton process using Fe alginate gel beads. *J Hazard Mater* 213–214:369–377. doi:[10.1016/j.jhazmat.2012.02.005](https://doi.org/10.1016/j.jhazmat.2012.02.005)
117. Özcan A, Atılır Özcan A, Demirci Y, Şener E (2017) Preparation of Fe₂O₃ modified kaolin and application in heterogeneous electro-catalytic oxidation of enoxacin. *Appl Catal B Environ* 200:361–371. doi:[10.1016/j.apcatb.2016.07.018](https://doi.org/10.1016/j.apcatb.2016.07.018)
118. Li Y, Lu A, Ding H, Wang X, Wang C, Zeng C, Yan Y (2010) Microbial fuel cells using natural pyrrhotite as the cathodic heterogeneous Fenton catalyst towards the degradation of biorefractory organics in landfill leachate. *Electrochem Commun* 12(7):944–947. doi:[10.1016/j.elecom.2010.04.027](https://doi.org/10.1016/j.elecom.2010.04.027)
119. Ganiyu SO, Le TXH, Bechelany M, Esposito G, van Hullebusch ED, Oturan MA, Cretin M (2017) A hierarchical CoFe-layered double hydroxide modified carbon-felt cathode for heterogeneous electro-Fenton process. *J Mater Chem A* 5:3655. doi:[10.1039/C6TA09100H](https://doi.org/10.1039/C6TA09100H)
120. Xu N, Zhang Y, Tao H, Zhou S, Zeng Y (2013) Bio-electro-Fenton system for enhanced estrogens degradation. *Bioresour Technol* 138:136–140. doi:[10.1016/j.biortech.2013.03.157](https://doi.org/10.1016/j.biortech.2013.03.157)
121. Birjandi N, Younesi H, Ghoreyshi AA, Rahimnejad M (2016) Electricity generation through degradation of organic matters in medicinal herbs wastewater using bio-electro-Fenton system. *J Environ Manag* 180:390–400. doi:[10.1016/j.jenvman.2016.05.073](https://doi.org/10.1016/j.jenvman.2016.05.073)
122. Zhuang L, Zhou S, Yuan Y, Liu M, Wang Y (2010) A novel bioelectro-Fenton system for coupling anodic COD removal with cathodic dye degradation. *Chem Eng J* 163(1–2):160–163. doi:[10.1016/j.cej.2010.07.039](https://doi.org/10.1016/j.cej.2010.07.039)
123. Wang XQ, Liu CP, Yuan Y, Li FB (2014) Arsenite oxidation and removal driven by a bio-electro-Fenton process under neutral pH conditions. *J Hazard Mater* 275:200–209. doi:[10.1016/j.jhazmat.2014.05.003](https://doi.org/10.1016/j.jhazmat.2014.05.003)

124. Feng CH, Li FB, Mai HJ, Li XZ (2010) Bio-electro-Fenton process driven by microbial fuel cell for wastewater treatment. *Environ Sci Technol* 44(5):1875–1880
125. Plakas KV, Sklari SD, Yiankakis DA, Sideropoulos GT, Zaspalis VT, Karabelas AJ (2016) Removal of organic micropollutants from drinking water by a novel electro-Fenton filter: pilot-scale studies. *Water Res* 91:183–194. doi:[10.1016/j.watres.2016.01.013](https://doi.org/10.1016/j.watres.2016.01.013)
126. Barhoumi N, Olvera-Vargas H, Oturan N, Huguenot D, Gadri A, Ammar S, Brillas E, Oturan MA (2017) Kinetics of oxidative degradation/mineralization pathways of the antibiotic tetracycline by the novel heterogeneous electro-Fenton process with solid catalyst chalcopyrite. *Appl Catal B Environ* 209:637–647. doi:[10.1016/j.apcatb.2017.03.034](https://doi.org/10.1016/j.apcatb.2017.03.034)
127. Ren G, Zhou M, Liu M, Ma L, Yang H (2016) A novel vertical-flow electro-Fenton reactor for organic wastewater treatment. *Chem Eng J* 298:55–67. doi:[10.1016/j.cej.2016.04.011](https://doi.org/10.1016/j.cej.2016.04.011)
128. Smith NAS, Knoerzer K, Ramos ÁM (2014) Evaluation of the differences of process variables in vertical and horizontal configurations of High Pressure Thermal (HPT) processing systems through numerical modelling. *Innovative Food Sci Emerg Technol* 22:51–62. doi:[10.1016/j.ifset.2013.12.021](https://doi.org/10.1016/j.ifset.2013.12.021)
129. Rosales E, Pazos M, Longo MA, Sanromán MA (2009) Electro-Fenton decoloration of dyes in a continuous reactor: a promising technology in colored wastewater treatment. *Chem Eng J* 155(1–2):62–67. doi:[10.1016/j.cej.2009.06.028](https://doi.org/10.1016/j.cej.2009.06.028)
130. Yu F, Zhou M, Zhou L, Peng R (2014) A novel electro-Fenton process with H₂O₂ generation in a rotating disk reactor for organic pollutant degradation. *Environ Sci Technol Lett* 1(7):320–324. doi:[10.1021/ez500178p](https://doi.org/10.1021/ez500178p)
131. Zhang L, Yin X, Li SFY (2015) Bio-electrochemical degradation of paracetamol in a microbial fuel cell-Fenton system. *Chem Eng J* 276:185–192. doi:[10.1016/j.cej.2015.04.065](https://doi.org/10.1016/j.cej.2015.04.065)
132. Zhuang L, Zhou S, Li Y, Liu T, Huang D (2010) In situ Fenton-enhanced cathodic reaction for sustainable increased electricity generation in microbial fuel cells. *J Power Sources* 195(5):1379–1382. doi:[10.1016/j.jpowsour.2009.09.011](https://doi.org/10.1016/j.jpowsour.2009.09.011)
133. Zhu X, Ni J (2009) Simultaneous processes of electricity generation and p-nitrophenol degradation in a microbial fuel cell. *Electrochem Commun* 11(2):274–277. doi:[10.1016/j.elecom.2008.11.023](https://doi.org/10.1016/j.elecom.2008.11.023)
134. Luo Y, Zhang R, Liu G, Li J, Qin B, Li M, Chen S (2011) Simultaneous degradation of refractory contaminants in both the anode and cathode chambers of the microbial fuel cell. *Bioresour Technol* 102(4):3827–3832. doi:[10.1016/j.biortech.2010.11.121](https://doi.org/10.1016/j.biortech.2010.11.121)
135. Zhu X, Logan BE (2013) Using single-chamber microbial fuel cells as renewable power sources of electro-Fenton reactors for organic pollutant treatment. *J Hazard Mater* 252–253:198–203. doi:[10.1016/j.jhazmat.2013.02.051](https://doi.org/10.1016/j.jhazmat.2013.02.051)
136. Espinoza C, Romero J, Villegas L, Cornejo-Ponce L, Salazar R (2016) Mineralization of the textile dye acid yellow 42 by solar photoelectro-Fenton in a lab-pilot plant. *J Hazard Mater* 319:24–33. doi:[10.1016/j.jhazmat.2016.03.003](https://doi.org/10.1016/j.jhazmat.2016.03.003)
137. Garcia-Segura S, Brillas E (2014) Advances in solar photoelectro-Fenton: Decolorization and mineralization of the direct yellow 4 diazo dye using an autonomous solar pre-pilot plant. *Electrochim Acta* 140:384–395. doi:[10.1016/j.electacta.2014.04.009](https://doi.org/10.1016/j.electacta.2014.04.009)
138. Garcia-Segura S, Cavalcanti EB, Brillas E (2014) Mineralization of the antibiotic chloramphenicol by solar photoelectro-Fenton. *Appl Catal B Environ* 144:588–598. doi:[10.1016/j.apcatb.2013.07.071](https://doi.org/10.1016/j.apcatb.2013.07.071)
139. El-Ghenymy A, Cabot PL, Centellas F, Garrido JA, Rodriguez RM, Arias C, Brillas E (2013) Mineralization of sulfanilamide by electro-Fenton and solar photoelectro-Fenton in a pre-pilot plant with a Pt/air-diffusion cell. *Chemosphere* 91(9):1324–1331. doi:[10.1016/j.chemosphere.2013.03.005](https://doi.org/10.1016/j.chemosphere.2013.03.005)

Cathode Modification to Improve Electro-Fenton Performance

Minghua Zhou, Lei Zhou, Liang Liang, Fangke Yu, and Weilu Yang

Abstract A cost-effective cathode is vital for electrochemical production of hydrogen peroxide and its application for organic pollutants degradation by electro-Fenton (EF). Graphite felt is one of the most extensively used cathodes for EF account for its good stability, conductivity, and commercial availability; however, its performance for hydrogen peroxide yield was not so satisfactory, and thus many cathode modification methods were investigated to improve the EF performance. This work systematically summarized our studies on the modification of graphite felt to improve EF performance, including chemical and electrochemical modification. Also, composite graphite felts with carbon black or graphene were reported. The preparation and characterizations of the cathode as well as their application for organic pollutants degradation by EF were described. Further, transition metal doping on the composite graphite felts to fulfill in situ heterogeneous EF was also attempted to overcome some drawbacks of homogeneous EF. Finally, an outlook for cathode modification was proposed. All these progresses would contribute to the application of EF using graphite felt cathode.

Keywords Cathode modification, Electro-Fenton, Graphite felt, Surface characteristics, Transition metal doping

Contents

1	Introduction	176
2	Chemical Modification of Graphite Felt	177
2.1	Chemical Modification Procedure and Performance	177
2.2	Cathode Characterization	179
2.3	Electro-Fenton Application	181

M. Zhou (✉), L. Zhou, L. Liang, F. Yu, and W. Yang
Key Laboratory of Pollution Process and Environmental Criteria, Ministry of Education,
College of Environmental Science and Engineering, Nankai University, Tianjin 300350, China
e-mail: zhoumh@nankai.edu.cn

3	Anodic Oxidation of Graphite Felt	184
3.1	Electrochemical Modification of Cathode	184
3.2	Electrode Characteristics	184
3.3	EF Application	188
4	Graphite Felt Modification with Carbon Black	189
4.1	Cathode Preparation	189
4.2	Cathode Characteristics	191
4.3	EF Application	191
5	Heterogeneous EF	194
5.1	Cathode Preparation	194
5.2	Cathode Characteristics	195
5.3	EF Application	198
6	Summary and Outlook	199
	References	200

1 Introduction

Many phenols, dyes, and pharmaceuticals are common persistent organic contaminants and typical biorefractory organic compounds, and listed as the priority toxic pollutants by the US Environmental Protection Agency [1–3]. The discharge of these compounds into the natural water would cause various severe environmental problems. Therefore, the abatement of these kinds of persistent organic contaminants is very important and has attracted considerable research interests [4–6].

As an efficient and environmentally friendly electrochemical technology, electro-Fenton (EF) is promising in removal of biorefractory pollutants [5, 7]. This process is based on the in situ electro-generation of hydrogen peroxide, eliminating the problem of H₂O₂ storage and shipment, and produces powerful hydroxyl radical ([•]OH) in the presence of iron catalyst through Fenton reaction. Therefore, to improve EF process, it is essential to choose an appropriate cathode material for effective production of H₂O₂.

Carbonaceous materials are the most familiar materials used as cathode due to the advantages such as no toxicity, good stability, high conductivity, and low catalytic activity for H₂O₂ decomposition. Many carbonaceous electrodes have been attempted, including graphite [8–10], carbon or graphite felt [11–13], carbon sponge [14], activated carbon fiber [15], carbon/carbon nanotube with polytetrafluoroethylene (PTFE) composite electrodes [16, 17], and carbon-PTFE air-diffusion electrode [18]. Among them, graphite felt (GF) has been regarded as one of the most widely used cathode materials due to its large 3D active surface, mechanical integrity, commercial availability, easy acquisition, and efficient cathodic regeneration of Fe²⁺ via Eq. (1) [7, 13].



Consequently this graphite felt has been widely applied to the treatment of various wastewaters and soils polluted by persistent organic pollutants such as dyes, phenols,

pesticides, pharmaceuticals and personal care products, landfill, and reverse osmosis concentrates [7, 11–13, 19, 20].

However, the production of H_2O_2 on the original graphite felt was not so satisfactory [21–23]. To further improve the electrocatalytic activity of the cathode, considerable efforts on cathode modification have been devoted, such as heat treatment, plasma pre-treatment, acid treatment [24], chemical and electrochemical oxidation [21–23], and rare-earth-derived compounds doping. It is supposed that the surface modification is an efficient way to improve the electrochemical activity of carbonaceous electrodes by changing their surface physicochemical and catalytic properties. And these changes would not only improve the hydrophilicity of the carbon surface [25, 26] but also result in the introduction of some oxygen- or nitrogen-containing functional groups into carbonaceous materials [27, 28]. Consequently, it is an efficient way to promote the cathodic reduction of H_2O_2 and thus improve the electrochemical performance of EF system.

On the other hand, the homogeneous EF exists some drawbacks, such as a narrow optimum of $\text{pH} = 3$ and the generation of abundant iron sludge after neutralization [29, 30]. Thus, heterogeneous EF oxidation has become prevalent for wastewater treatment, where soluble Fe^{2+} is replaced by Fe containing solids without the adjustment of low pH and production of iron sludge [31–33]. In the past decades, various kinds of iron oxides and iron hydroxides have been attempted, e.g., Fe_3O_4 , $\alpha\text{-Fe}_2\text{O}_3$, and $\alpha\text{-FeOOH}$. However, many of them either show lower catalytic activity than soluble Fe^{2+} or need the aid of ultrasound [29] or UV/visible light irradiation [34], increasing the treatment cost. It is still a great challenge to develop efficient heterogeneous EF catalyst and cathode.

This work reported our progress in series on the modification of graphite felt cathode to improve EF performance [21–23, 35, 36]. The chemical modification with hydrazine, electrochemical oxidation, and composite with carbon black were studied. The preparation/modification of cathode, the change of cathode characteristics (e.g., morphology, surface composition, and electrochemical activity), and the catalytic activity in EF process, using some model target pollutants, were described in detail. Furthermore, some works on transition metal doping on graphite felt to fulfill heterogeneous EF were described. Finally, it summarized our research work and gave a perspective on cathode modification.

2 Chemical Modification of Graphite Felt

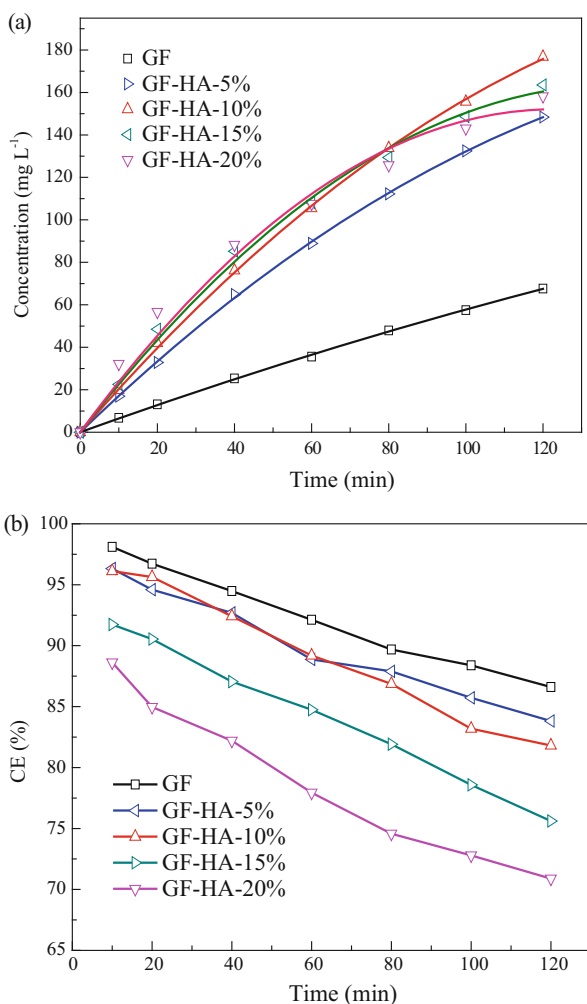
2.1 Chemical Modification Procedure and Performance

The graphite felt used was bought from Shanghai Qijie Carbon material Co., Ltd. with a specific surface area of about $0.6 \text{ m}^2 \text{ g}^{-1}$. Before chemical modification, it was necessary to be pretreated to clean the graphite felt in an ultrasonic bath with acetone and deionized water in sequence, dried at 80°C for 24 h, and then annealed

at 150°C for 2 h. These pretreated materials were marked as GF. A series of modified cathodes were treated by hydrazine hydrate according to the follow procedure: the pretreated graphite felts were immersed in 100 mL mixture of ethanol and hydrazine hydrate, and after refluxing at 60°C for 6 h, the samples were annealed at 150°C for 2 h. Since the volume concentration of the hydrazine hydrate in the mixture were 5%, 10%, 15%, and 20%, the modified electrodes were marked as GF-HA-5%, GF-HA-10%, GF-HA-15%, and GF-HA-20%, respectively.

Figure 1 shows the electro-generated H_2O_2 and current efficiencies on different cathodes modified with different concentrations of hydrazine hydrate. It was observed that the produced H_2O_2 for GF was only 67.6 mg L^{-1} after 120 min, and after modification, the yields of H_2O_2 were all increased, indicating the positive effects on H_2O_2 electro-generation. The GF-HA-10% sample showed the highest yield of H_2O_2 (176.8 mg L^{-1}

Fig. 1 The effects of the concentration of hydrazine hydrate on: (a) the yields of H_2O_2 and (b) current efficiency. Conditions: $E = -0.65 \text{ V}$ (vs. SCE), $0.05 \text{ M Na}_2\text{SO}_4$, $\text{pH} = 6.4$, and O_2 flow rate at 0.4 L min^{-1} . Adapted from Zhou et al. [21], Copyright 2013, with permission from Elsevier



after 120 min), indicating the optimum concentration of hydrazine hydrate for cathode modification. When the concentration of hydrazine hydrate exceeded this optimum value, a little decrease of H_2O_2 was observed. For example, the GF-HA-20% obtained a lower H_2O_2 production of 158.2 mg L^{-1} after the same time.

Figure 1b shows the current efficiency (CE) under the potential of -0.65 V (vs. SCE) for GF, GF-HA-5%, GF-HA-10%, GF-HA-15%, and GF-HA-20%, which were 86.6%, 83.8%, 81.8%, 75.6%, and 70.8%, respectively. The CE was calculated according to the following formula [21]:

$$\text{CE} = \frac{nFCV}{\int_0^t Idt} \times 100\% \quad (2)$$

where n is the number of electrons transferred for oxygen reduction for H_2O_2 , F is the Faraday constant ($96,485 \text{ C mol}^{-1}$), C is the concentration of H_2O_2 (mol L^{-1}), V is the bulk volume (L), I is the current (A), and t is the electrolysis time (s).

It was observed that the current efficiencies declined with the increasing concentration of hydrazine hydrate used in chemical modification. A further cyclic voltammetry characterization indicated that the chemical modification increased the current response, which might contribute to the fast formation of hydrogen peroxide. However, both oxygen reduction reactions (ORRs) (the two-electron transfer for H_2O_2 production and the four-electron transfer for H_2O production) were encouraged, and perhaps the latter improved much, which led to the decrease of CE after chemical modification.

2.2 Cathode Characterization

To explore the effects of chemical modifications on the characteristics of cathode, the cathode modified with absolute ethanol (marked as GF-A), and the cathode modified with the mixture of ethanol and hydrazine hydrate of volume ratio of 90/10 (marked as GF-B) were investigated. Figure 2a–c show the SEM images of the original graphite felt (GF), GF-A, and GF-B. Obviously, GF was composed of an entangled network of carbon microfilaments with diameters around $15 \mu\text{m}$. After chemical modification with absolute ethanol, many nanoscale particles and clusters, with diameters of 100–500 nm, appeared on the fibers surface (Fig. 2b). Since no other substances were involved during modification, the deposition could mostly be composed of carbon, as confirmed by the following XPS studies. The transformation from ethanol to carbon nanoparticles mostly occurred during the heating process (150°C). The special filament-wound structure of the graphite felt rendered the ethanol vapor to be kept within the samples, which made it possible for the nanoparticles forming or depositing on the fiber surface.

Comparing the SEM in Fig. 2b, c, it could be noticed that the carbon nanoparticles deposition on the surface of GF-B was far less than that of GF-A. This result should

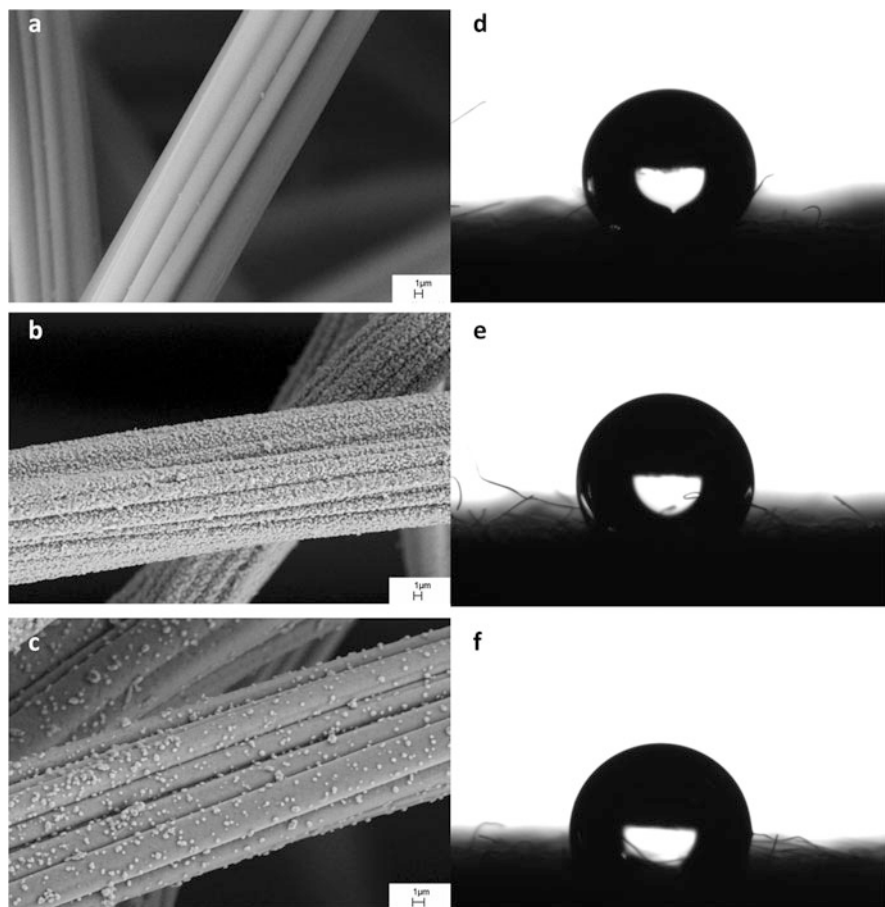


Fig. 2 SEM images and contact angles of GF (a, d), GF-A (b, e), and GF-B (c, f). Reproduced from Zhou et al. [23], Copyright 2014, with permission from Elsevier

be related to the introduction of hydrazine hydrate, indicating a possibility for controllable deposition of carbon nanoparticles on graphite felt. The deposits could increase the gas–liquid contact interface in the modified samples, which would help to improve the catalytic performance.

Figure 2d–f shows the contact angles of the cathode GF, GF-A, and GF-B, which were 141° , 123° , and 110° , respectively. These results confirmed that the modification helps to increase the graphite felt surface hydrophilic property, especially the introduction of hydrazine hydrate could weaken the hydrophobic property more effectively as compared with absolute ethanol. For a highly hydrophobic graphite felt, the improved hydrophilic surfaces could promote the electron transport and the mass transfer between the cathode and electrolyte, resulting in the improvement of the electrochemical performance.

The surface elements and functional groups of graphite felts before and after modification were studied by XPS analysis. As expected, C and O are the main elements, and N element was only detected in GF-B due to the introduction of hydrazine hydrate during modification. It was also observed that the values of the ratio between O and C (O/C) changed in different samples. For GF, the O/C was 0.081, which slightly decreased to 0.064 in GF-A due to the increase of carbon content by the deposition of carbon nanoparticles on the surface, while obviously increased to 0.138 in GF-B.

Figure 3a shows the surface nitrogen-containing groups in GF-B by deconvolution of the high-resolution XPS spectrum of N1s region. The maximum peak centered at 401.1 eV was assigned to quaternary nitrogen, which was known as the “graphitic nitrogen” species [37]. The weaker peaks centered at 398.4 and 404.8 eV could be pyridinic nitrogen and different N-oxide species, respectively [38, 39]. The lone electron pairs of nitrogen atoms could form a delocalized conjugated system with the sp^2 -hybridized carbon frameworks, which resulted in a great improvement of electrocatalytic performance toward the ORR [28].

Figure 3b shows the C1s spectrums of samples GF, GF-A, and GF-B. For GF, the curve fitting of C1s spectrum displayed three binding energy (BE) peaks corresponding to sp^2 carbons ($-C=C-$, $-C-C-$, or $-C-H$, BE = 284.6 eV), carbon coordinated to a single oxygen in hydroxyl groups or ethers ($-C-OH$, $-C-O-R$, BE = 286.2 eV), and carboxyl or ester groups ($-COOH$ or $-COOR$, BE = 289.2 eV) [40]. Compared to GF, the BE of the second peak corresponding to the groups such as $-C-OH$ or $-C-O-R$ in GF-A and GF-B decreased to 285.8 eV. This result indicated that more hydroxyl groups instead of ethers existed on the surface of the modified cathodes, which improved the surface hydrophilicity and behaved as surface-active sites favorable to accelerate electrochemical reactions [25]. The other shoulder peak of GF-B at 287.2 eV was attributed to carbonyl, quinone groups, or carbon–nitrogen single bond ($>C=O$, $-C-N$) [41], and the surface quinone species could behave as surface-active sites to promote the H_2O_2 electro-generation [42]. Besides, the dominant peak in GF-B was shifted to a lower binding energy of 284.2 eV, indicating a more orderly graphitic structure.

2.3 Electro-Fenton Application

The EF performance on the GF, GF-A, and GF-B was evaluated by the degradation of *p*-Nitrophenol (*p*-Np). As shown in Fig. 4, for GF, GF-A, and GF-B, the degradation efficiencies of *p*-Np were 6.6%, 58.3%, and 78.7% after 20 min, respectively. The remarkable improvement in the initial stage met well with the increased H_2O_2 production after modification. The tendency of mineralization ratios in Fig. 4b was consistent with the evolution of *p*-Np, and the total organic carbon (TOC) removal ratios were 22.2%, 31.7%, and 51.4% for GF, GF-A, and GF-B, respectively. These results showed that the modified cathodes could promote the pollutant degradation efficiency as compared with the unmodified one. The GF-B possessed the

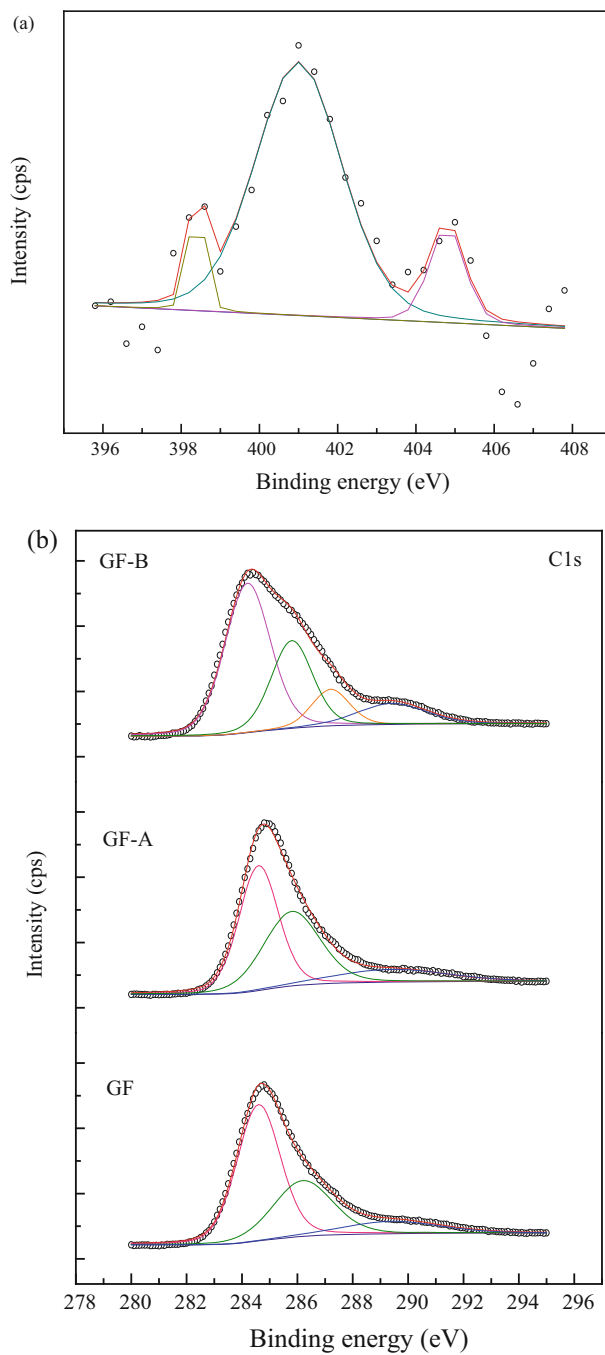
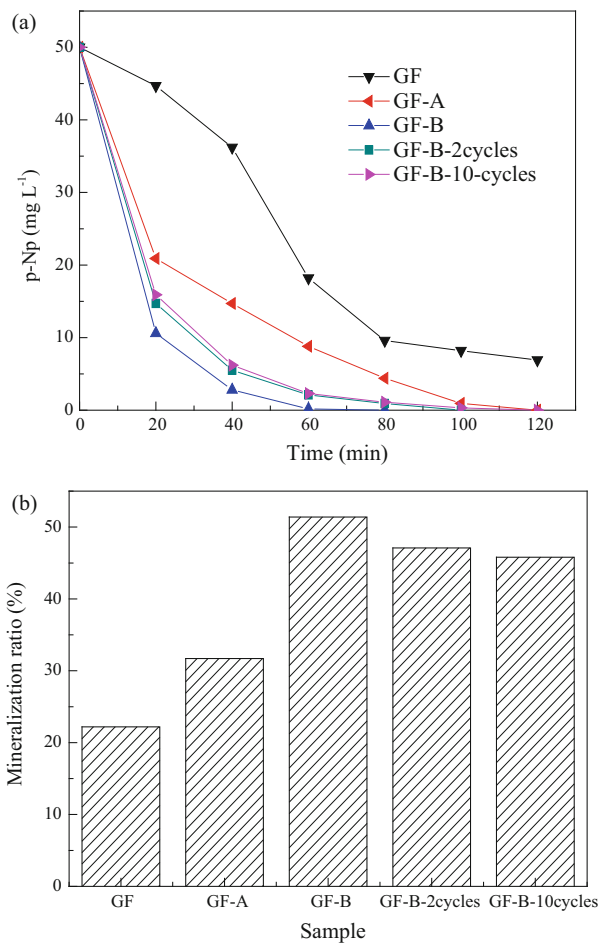


Fig. 3 The high-resolution XPS spectrum of: (a) N1s region and (b) C1s region for the samples GF, GF-A, and GF-B. Adapted from Zhou et al. [23], Copyright 2014, with permission from Elsevier

Fig. 4 (a) The evolution and (b) mineralization ratios of *p*-Np at GF, GF-A, and GF-B used for two and ten cycles. Conditions: $E = -0.65$ V, 50 mg L^{-1} *p*-Np, $0.05 \text{ M Na}_2\text{SO}_4$, 0.2 mM Fe^{3+} , $\text{pH} = 3$, and O_2 flow rate 0.4 L min^{-1} . Adapted from Zhou et al. [23], Copyright 2014, with permission from Elsevier



highest EF performance, which could be ascribed to the change of the surface structures and properties after modification as mentioned above.

Since the cathode stability is important for their practical application, the used GF-B cathode was cleaned with deionized water and then reused for degradation of *p*-Np under the same conditions. A slight decrease in degradation of *p*-Np was observed when the second use of GF-B, and the mineralization ratio after ten cycles was still above 45%, indicating that the modified electrode was stable and reusable.

3 Anodic Oxidation of Graphite Felt

3.1 Electrochemical Modification of Cathode

The same graphite felt was used and pretreated as described above, and these pretreated materials were marked as GF. The pretreated graphite felts were anodized during several successive (0–15) cycles in an undivided three-electrode cell system in 0.05 M Na₂SO₄ aqueous solution. In each cycle, the potential of the working electrode was scanned between 0 and 2 V at a scan rate of 30 mV s⁻¹. After the electrochemical treatment of 5, 10, and 15 successive cycles, the samples were dried at 80°C for 24 h, and the modified electrodes were marked as GF-5, GF-10, and GF-15, respectively.

The effects of the electrochemical modification on electro-generated H₂O₂ were performed at a constant potential of -0.65 V (vs. SCE). Figure 5 shows the accumulations and CE of H₂O₂ production. Obviously, the electrochemical modification greatly improved the H₂O₂ production. For example, after 10 anodizing cycle times, the H₂O₂ increased more than 2.7 times from the pristine one of about 80 mg L⁻¹ at 120 min. However, with more modifying cycles, no significant increase on the accumulation of H₂O₂ was observed. The CEs of H₂O₂ production at GF, GF-5, GF-10, and GF-15, as shown in Fig. 5b, were 87.1%, 85.2%, 79.1%, and 66.9%, respectively, exhibiting a tendency of decline in CE after modification.

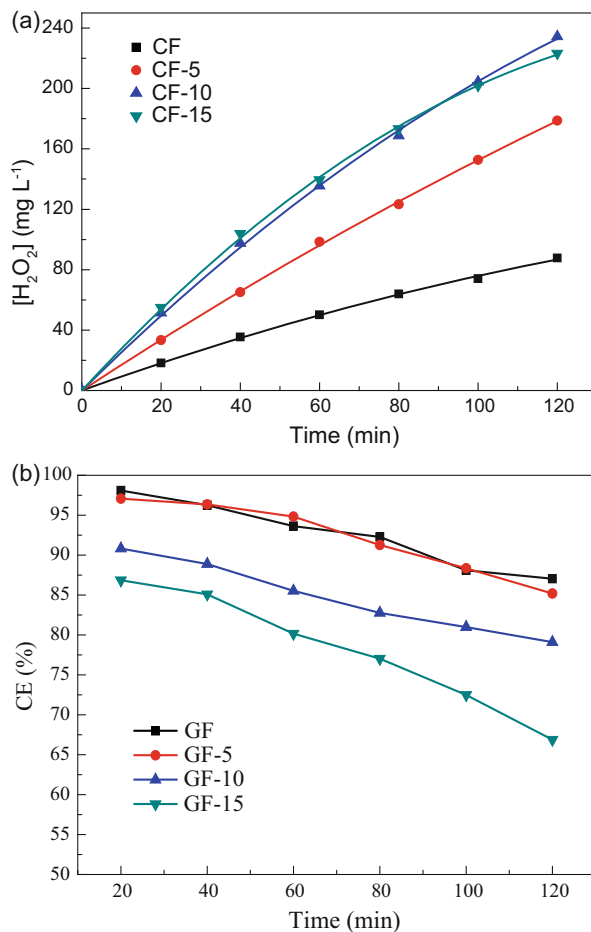
As observed from linear sweep voltammetry (LSV) (see Fig. 8 below), the anodizing modification not only encouraged the two-electron transfer process for H₂O₂ production but also improved the competitive process – the H₂O production. With the positive shift of the current response, especially for the second current peak, the H₂O electro-generation process became more and more significant at the given potential. This would be competitive with the H₂O₂ generation and impeded the accumulation of H₂O₂, and as a result, the yields of H₂O₂ could not proportionally increase with the increasing current response in the system, and then resulted in a drop of current efficiencies for the modified electrodes.

3.2 Electrode Characteristics

Figure 6 shows the SEM picture before and after electrochemical modification, and no obvious difference on surface morphology was observed.

The surface elements and functional groups of graphite felts before and after modification were studied by XPS analysis. It was found that the O/C ratio increased with the anodization cycle times, which were 0.09, 0.22, 0.33, and 0.36 in GF, GF-5, GF-10, and GF-15, respectively, indicating a gradually increasing degree of oxidation with anodizing modification. As shown in Fig. 7, for all electrodes, three peaks of curve fitting for C1s spectrum corresponding to sp² carbons (-C=C-, -C-C-, or -C-H, BE = 284.8 eV), carbon coordinated to a single oxygen in hydroxyl groups or ethers (-C-OH, -C-O-R,

Fig. 5 (a) The accumulations of the H_2O_2 electro-generation and (b) current efficiencies at various cathodes. Conditions: $E = -0.65$ V, 0.05 M Na_2SO_4 , pH = 6.4, and O_2 flow rate 0.4 L min^{-1} . Adapted from Zhou et al. [22], Copyright 2013, with permission from Elsevier

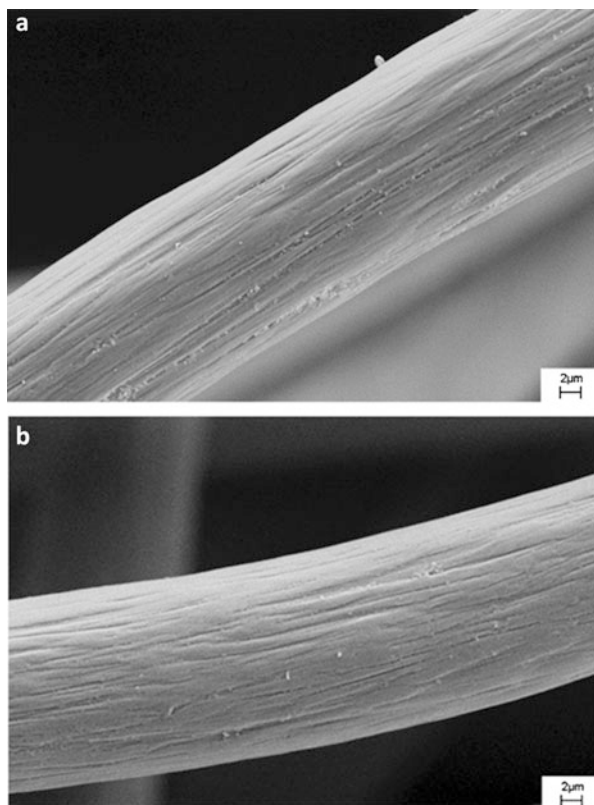


BE = 286.0–286.2 eV), and π - π^* plasmon excitation (BE = 290.4 eV) were observed [38, 43].

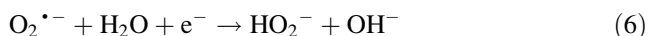
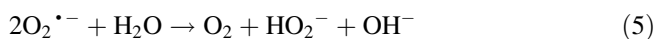
Compared to GF, the BE of the second peak corresponding to the groups such as $-\text{C}-\text{OH}$ or $-\text{C}-\text{O}-\text{R}$ in anodized electrodes were about 0.2 eV lower, which indicated that more hydroxyl groups instead of ethers existed on the surface of cathodes after modification, making a positive effect on the surface hydrophilic property. The other shoulder peaks that attributed to carbonyl, quinone groups ($>\text{C}=\text{O}$, BE = 287.2 eV) and carboxyl or ester groups ($-\text{COOH}$ or $-\text{COOR}$, BE = 289.2 eV) [44] were successively appeared in GF-5, GF-10, and GF-15, which were reasonable to be considered as the production of the electrochemical oxidation.

The oxygen functional groups tended to increase on the carbon surface with the processing cycle times, and this trend slowed down after ten cycle times in our study. The surface oxygen functional groups could improve the electrodes' electrochemical

Fig. 6 SEM images of cathode before (a) and after (b) electrochemical modification

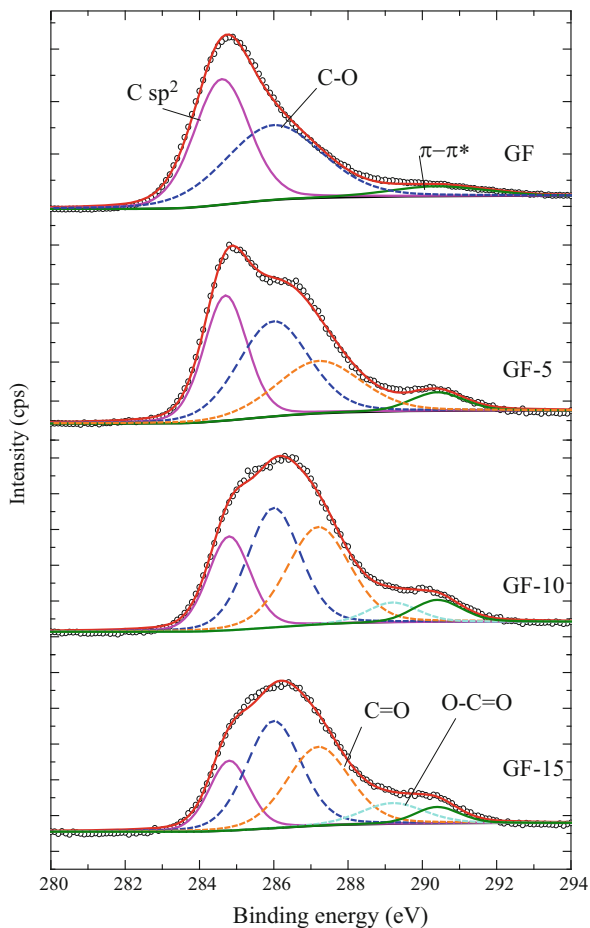


performance in the following way (Eqs. 3–6): the surface quinone species (Q) could behave as surface-active sites to promote the H_2O_2 electro-generation through forming the semiquinone radical anion ($\text{Q}^{\bullet-}$) and the superoxide intermediate ($\text{O}_2^{\bullet-}$) [26].



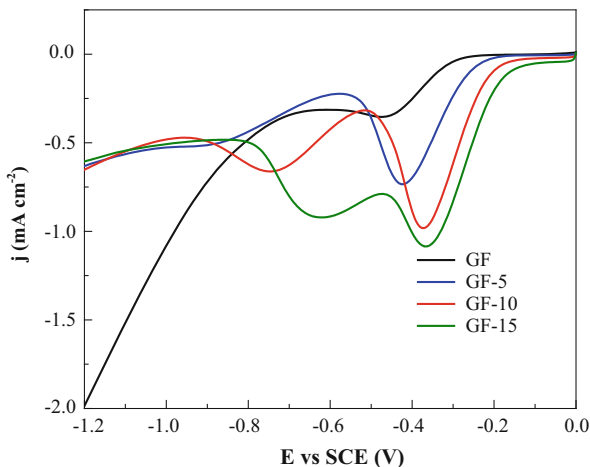
To investigate the effects of the electrochemical modification on the electrocatalytic activity of cathodes toward ORR, LSV was carried out on GF, GF-5, GF-10, and GF-15. As shown in Fig. 8, the current responses dramatically increased with the cycle times of anodization, and the hydrogen evolution potentials of the anodized electrodes were more negative than the pristine one. Moreover, the ORR tended to be triggered at less negative potentials with shift range of about 0.1 V after anodizing modification, and the onset potentials were around -0.2 V, which indicated a much faster electron transfer kinetics for ORR on the anodized electrodes.

Fig. 7 The high-resolution XPS spectrum of C1s region for the electrodes GF, GF-5, GF-10, and GF-15. Adapted from Zhou et al. [22], Copyright 2013, with permission from Elsevier



After electrochemical modification, two obvious oxygen reduction peaks were observed, one corresponding to the two-electron H_2O_2 electrochemical generation and the other one to H_2O formation. It also could be observed that both of the oxygen reduction peaks were shifted to the less negative potentials. When anodizing cycles came to 15 times, the main current response peak corresponding to H_2O_2 production slightly increased and barely shifted, whereas the other peak related to H_2O production still markedly enhanced and positively shifted. These results suggested that the anodizing cycle times could have a significant impact on the H_2O_2 production.

Fig. 8 Linear sweep voltammograms of GF, GF-5, GF-10, and GF-15. Conditions: scanning potential range 0 to -1.2 V, scan rate 10 mV s^{-1} , $0.05 \text{ M Na}_2\text{SO}_4$, $\text{pH} = 6.4$, and oxygen saturation. Adapted from Zhou et al. [22], Copyright 2013, with permission from Elsevier

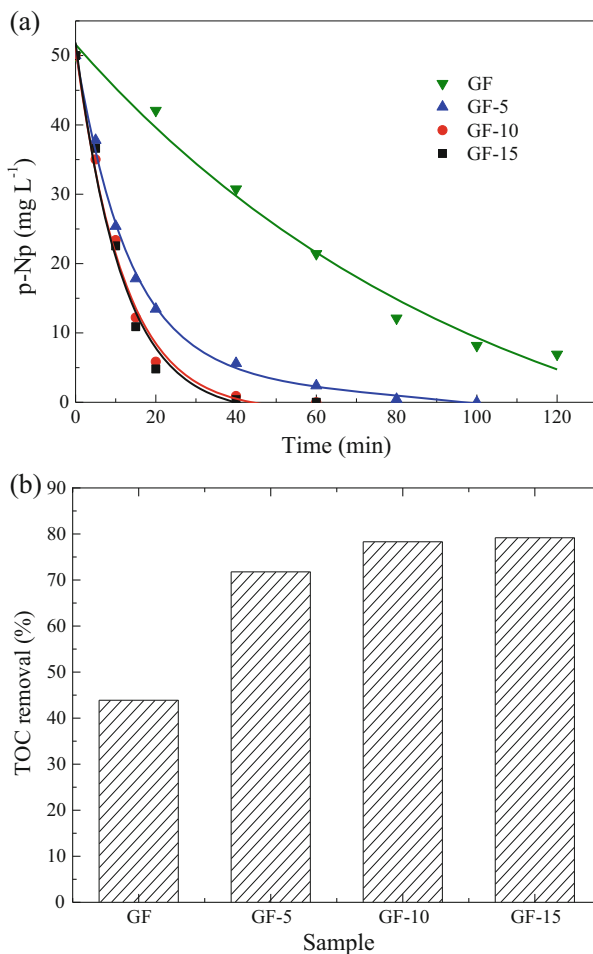


3.3 EF Application

The degradation of *p*-Np by EF at GF, GF-5, GF-10, and GF-15 was compared. As shown in Fig. 9, a fast and complete removal of *p*-Np can be observed in all modified cases. The decay rate underwent a gradual acceleration with the anodizing cycles increasing. It was seen that *p*-Np remained 6.9 mg L^{-1} after 120 min for GF, but completely disappeared in 60 min for GF-10 and GF-15. The effect was related to an increasing quantity of electro-generated H_2O_2 (Fig. 5), and the enhanced current response at the given potential (Fig. 8) which could encourage the regeneration of Fe^{3+} , and hence, the production of hydroxyl radical was improved in the modified cases. After 120 min, the TOC removals for GF, GF-5, GF-10, and GF-15 were 43.9%, 71.8%, 78.3%, and 79.2%, respectively. These results suggested that the anodizing modification could efficiently improve the degradation and mineralization of the contaminants.

To further confirm this statement, *p*-NP degradation on the modified (GF-10) and unmodified electrode (GF) was compared under amperostatic condition (10 and 20 mA). It was observed that at both currents, the modified electrode demonstrated much better performance. When treated at the same current and treatment time, the *p*-NP removal efficiency on GF-10 was found 5–15% higher than that on GF. More importantly, it should be noted that when the same current was applied, the required voltage applied on the system was different, i.e., GF-10 required a much lower voltage. For example, at current of 10 mA, the applied cell voltage with GF was 2.91 V, but with GF-10 it was only 1.87 V. This effect was in agreement with the significant increase in current responses when applied the same potential on the modified electrode. This led to the operation cost (energy consumption) reduced at least by 35.7%. Therefore, both the experiments under potentiostatic and amperostatic condition supported that such a modification on the cathode would help to improve the cost-effectiveness of EF process for *p*-Np degradation.

Fig. 9 Effect of anodizing cycles on: (a) the evolution and (b) mineralization ratios of *p*-Np during the electrolysis of 50 mg L⁻¹ *p*-Np aqueous solution at GF, GF-5, GF-10, and GF-15, respectively. Conditions: $E = -0.65$ V, 0.05 M Na₂SO₄, [Fe³⁺] = 0.4 mM, pH = 3, and O₂ flow rate 0.4 L min⁻¹. Adapted from Zhou et al. [22], Copyright 2013, with permission from Elsevier



4 Graphite Felt Modification with Carbon Black

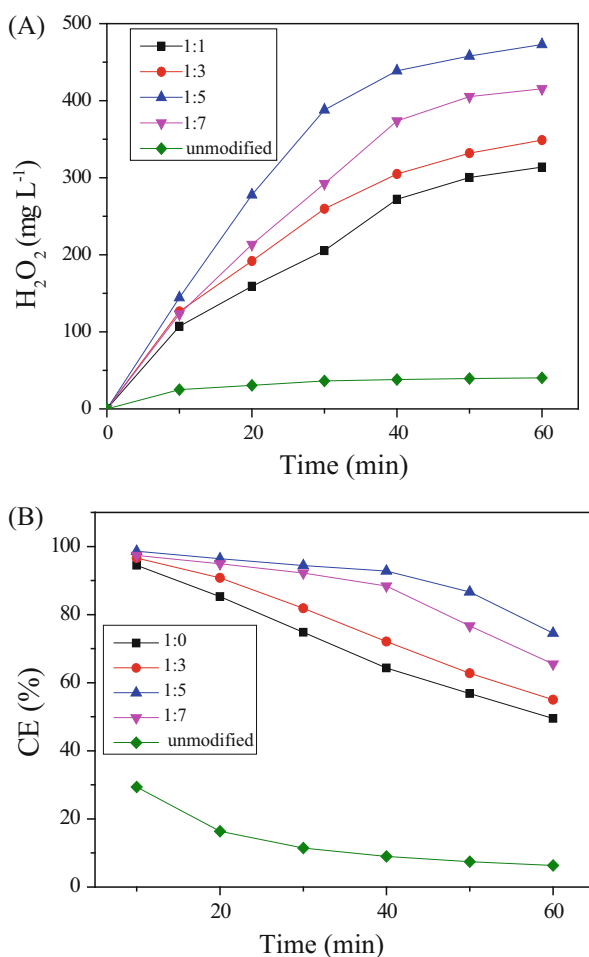
4.1 Cathode Preparation

The commercial graphite felts were marked as the unmodified GF. Appropriate amounts of carbon black (0.3 g), PTFE (0.3–2.1 g), distilled water (30 mL), and *n*-butanol (3%) were mixed in an ultrasonic bath for 10 min to create a highly dispersed mixture. The pretreated graphite felts were immersed into mixture, and after ultrasonication for 0.5 h and dried at 80°C for 24 h, the samples were annealed at 360°C for 1 h. Since the mass ratio of the carbon black to PTFE in the mixture were 1:1, 1:3, 1:5, and 1:7, the modified electrodes were marked as GF-(1:1), GF-(1:3), GF-(1:5), and GF-(1:7), respectively.

Figure 10 shows the electro-generated H_2O_2 and current efficiencies on the cathodes modified with different mass ratio of carbon black to PTFE. After 60 min electrolysis, the concentrations of H_2O_2 for the unmodified GF, GF-(1:1), GF-(1:3), GF-(1:5), and GF-(1:7) were 40.3, 313.9, 348.9, 472.9, and 415.5 mg L^{-1} , respectively. Obviously, after cathode modification, the yield of H_2O_2 was significantly increased, and GF-(1:5) performed the best with an H_2O_2 production 10.7 times higher than that of the unmodified GF.

As shown in Fig. 10b, the CE of GF, GF-(1:1), GF-(1:3), GF-(1:5), and GF-(1:7) was 6.35%, 49.48%, 55.01%, 74.57%, and 65.51%, respectively. With the increase of PTFE, the active sites for electrochemical reaction would increase; however, a higher presence of PTFE made the layer more hydrophobic, reducing the cathode flooding and facilitating oxygen distribution [16]. Therefore, the optimal mass ratio

Fig. 10 The effect of mass ratio of carbon black to PTFE on the yields of H_2O_2 (a) and current efficiency (b). Conditions: current density 50 A m^{-2} , $0.05 \text{ M Na}_2\text{SO}_4$, and initial pH 7. Adapted from Yu et al. [35], Copyright 2015, with permission from Elsevier



of carbon black to PTFE was 1:5, which provided both sufficient active area and oxygen diffusion ability for H_2O_2 production.

4.2 Cathode Characteristics

Figure 11 shows the SEM images of graphite felt (A) before and (B) after modification (GF-(1:5)). Before modification, the graphite felt showed a clear fiber structure with uniform size of about 5–10 μm . After modification, a large number of interconnected particles appeared on graphite felt, which would obviously change the cathode surface characteristics. The BET surface area, pore diameter, and pore volume of the unmodified GF were determined to be $1.565 \text{ m}^2 \text{ g}^{-1}$, 3.005 nm, and 0.004 mL g^{-1} , while for the modified graphite felt, it was $5.320 \text{ m}^2 \text{ g}^{-1}$, 3.405 nm, and 0.087 mL g^{-1} , respectively. Clearly, the cathode modification resulted in about 2.4 times and more than 20 times increase in surface area and pore volume, respectively. This special three-dimensional structure could render oxygen more easily diffusing into the porosity of the porous carbon materials and further react on the inner surface [45]. The dynamic balance of oxygen on the triphase surface of solid, gas, and solution would finally increase the solubility of oxygen in solution. Thus, after modification, the generation of H_2O_2 was significantly enhanced.

To explore the effect of modification on the cathode electrocatalytic activity toward ORR, LSV investigation was carried out. As shown in Fig. 12, all modified cathodes exhibited higher current for ORR, comparing with the unmodified one. This result indicated that the presence of carbon black helped to increase the catalytic activity toward ORR and also higher conductivity. And the GF-(1:5) electrode received the highest current response, while the further addition of PTFE decreased the current response. This trend agreed with the H_2O_2 production, which is reasonable since an electrochemical reaction rate is determined principally by current, so that among the investigated current ranges in this work, the higher the current, the faster the electrochemical generation of H_2O_2 .

4.3 EF Application

The EF performances on the unmodified and modified cathodes were evaluated by degradation of 50 mg L^{-1} methyl orange (MO) under acidic and neutral conditions. As shown in Fig. 13a, higher degradation efficiencies were observed at initial pH 3, which was regarded as the optimum value in EF system [7, 13]. The complete decolorization of MO was achieved within 35 min on the unmodified cathode, but it was only taken 15 min on the modified cathode. Similar phenomena were observed at initial pH 7, in which it took 60 min and 25 min for two cathodes, respectively. The degradation of MO was confirmed following an apparent pseudo-first-order kinetics. At initial pH 3, the rate constant on the unmodified cathode was 0.092 s^{-1} ($R^2 = 0.996$),

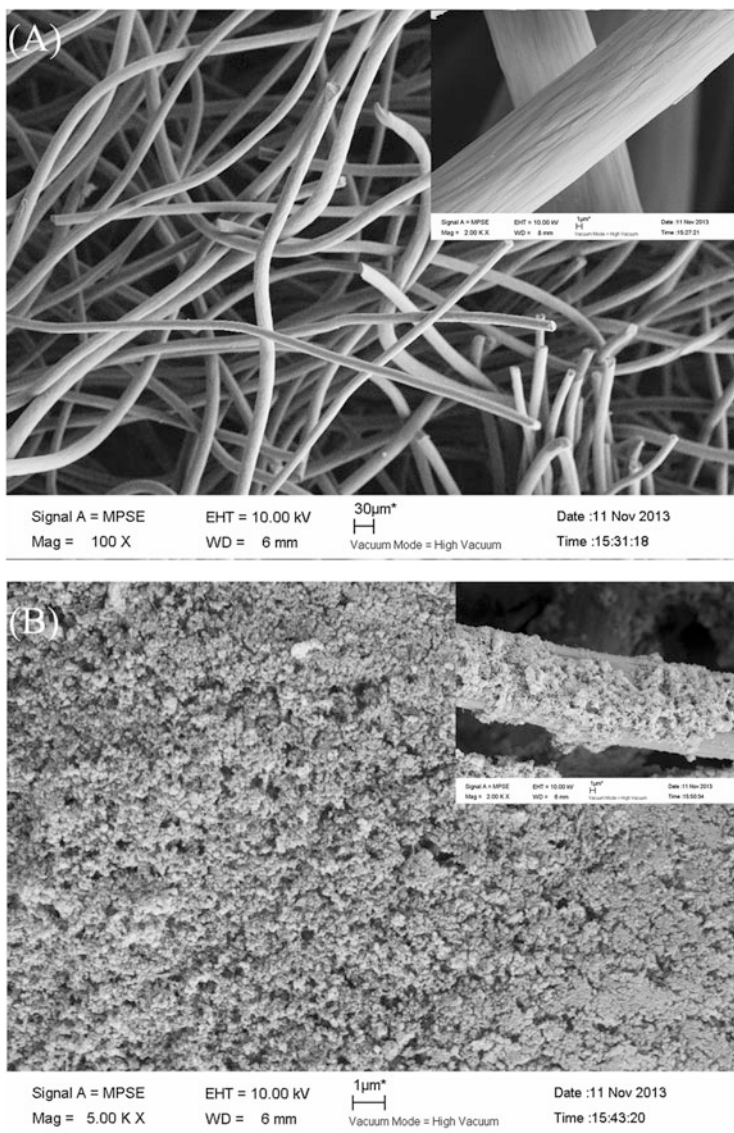


Fig. 11 The SEM of unmodified GF and GF-(1:5). Reproduced from Yu et al. [35], Copyright 2015, with permission from Elsevier

while it increased by 2.8 times to 0.258 s^{-1} ($R^2 = 0.991$) on the modified cathode. Similarly, at initial pH 7, the rate constant increased from 0.065 s^{-1} ($R^2 = 0.984$) to 0.169 s^{-1} ($R^2 = 0.989$).

During degradation, the solution pH was found dramatically decreased in 10 min to lower than 5, and kept constant between 4.5 and 4.0. It could be that due to the

Fig. 12 Linear sweep voltammetry (LSV) of GF with different mass ratios of the carbon black to PTFE. Conditions: scanning rate 10 mV s^{-1} , $0.05 \text{ M Na}_2\text{SO}_4$, and initial pH 7. Adapted from Yu et al. [35], Copyright 2015, with permission from Elsevier

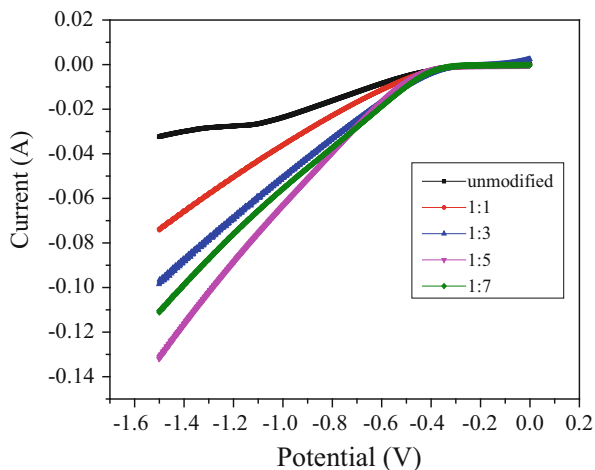
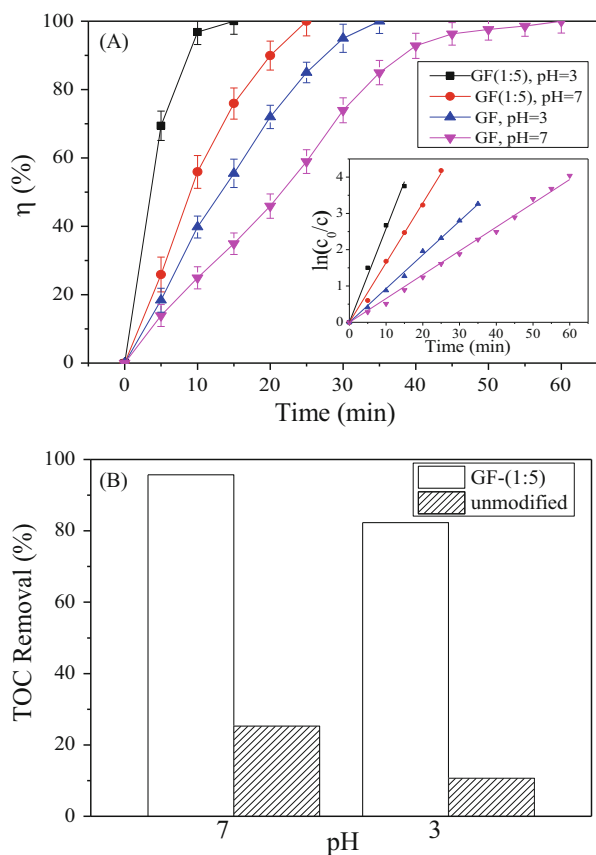


Fig. 13 The degradation of different concentrations of MO in EF system on decolorization (a) and total organic carbon (TOC) removal (b). Conditions: current density 50 A m^{-2} , initial pH 3 or 7, and $0.05 \text{ M Na}_2\text{SO}_4$. Adapted from Yu et al. [35], Copyright 2015, with permission from Elsevier



rapid transformation of Fe^{3+} , no iron precipitation was observed during degradation, indicating that the electro-Fenton reactions worked well. These results showed that the modified cathode possessed a much better performance on the degradation of MO by EF. Further, the energy consumption for the complete removal of MO was calculated to be 2.25 kWh m^{-3} at initial pH 3 on the unmodified cathode, but after modification, it significantly decreased to 0.75 kWh m^{-3} . Similarly, at initial pH 7, after cathode modification, the energy consumption significantly decreased from 4.5 to 1.26 kWh m^{-3} . The increased cost percentage for cathode modification was about 29.2%, compared with the unmodified GF. Account for the great enhancement in production of H_2O_2 by about 10.7 times and significant reduction in energy consumption, such a small increase in cathode modification cost was deserved. Therefore, the modified graphite felt was more efficient and cost-effective to be used as cathode in EF process.

The TOC removal efficiency after 2 h treatment on the modified cathode was 95.7% and 85.3% at initial pH 3 and 7, respectively, compared with that of 23.3% and 12.7% on the unmodified cathode (Fig. 13b). This overwhelming superiority should be attributed to the great improvement of H_2O_2 production on the modified cathode. After cathode modification, the current response under the same applied potential and the electron transfer process were obviously enhanced. Moreover, the increase of surface area and pore volume would also benefit the enhancement on H_2O_2 production, and thus improved the performance in EF process.

5 Heterogeneous EF

5.1 Cathode Preparation

Appropriate amounts of carbon black and metal nitrate (Fe, Co, Ce, and Cu) salts were mixed in an ultrasonic bath for 30 min and dried overnight at 70°C in an oven. The mixture was heated for 2 h in a ceramic tube furnace at 900°C under N_2 protection. Appropriate amounts of metal oxide (0.3 g), PTFE, distilled water (30 mL), and *n*-butanol (3%) were mixed in an ultrasonic bath for 10 min to create a highly dispersed mixture. The pretreated GF were immersed into the mixture and sonicated for 30 min and then dried at 80°C for 24 h. At last, the samples were annealed at 360°C for 30 min. The composite electrodes were marked as GF-C (with carbon black), GF-Fe, GF-Co, GF-Ce, and GF-Cu, respectively.

Since H_2O_2 production is very important for electro-Fenton process, it is necessary to identify the H_2O_2 production capacity of these transition metal-based cathodes. Figure 14a, b shows the accumulation of H_2O_2 with different metal loadings at pH 3 and 7, respectively. After 120 min electrolysis, the concentration of H_2O_2 reached 554.8, 474.7, 454.1, 440, 380.5, and 35.6 mg L^{-1} at pH = 3 using GF-Co, GF-Fe, GF-Ce, GF-Cu, GF-C, and GF, respectively. Accordingly, the concentration of H_2O_2 reached 516.8, 442.7, 404.1, 378.6, 315.2, and 25.5 mg L^{-1} at pH = 7.

Similarly, GF-Co had the highest CE for H_2O_2 production (Fig. 14c, d), which reached 41 and 38% in 2 h at pH 3 and 7, respectively. There was a slight increase of the H_2O_2 accumulation at pH 3 because a low pH was favorable to H_2O_2 production. In summary, the prepared GF-metal is a very good cathode material for H_2O_2 production and potential to be used in electro-Fenton process.

5.2 Cathode Characteristics

Figure 15 shows the SEM images of unmodified GF and modified GF. Before the transition metal was loaded, GF showed a clean fiber structure composed of an entangled network of carbon microfilaments with diameters around $15\ \mu\text{m}$ (Fig. 15a). After the transition metal was loaded, a large number of interconnected particles appeared on the fiber of GF (Fig. 15b–f). These carbon particles and porous structure on the electrode surface could promote O_2 electro-sorption and electro-reduction and pollutants degradation [46]. Figure 15c shows GF-Co had a more uniform surface with particles, which might render it has the highest catalytic activity.

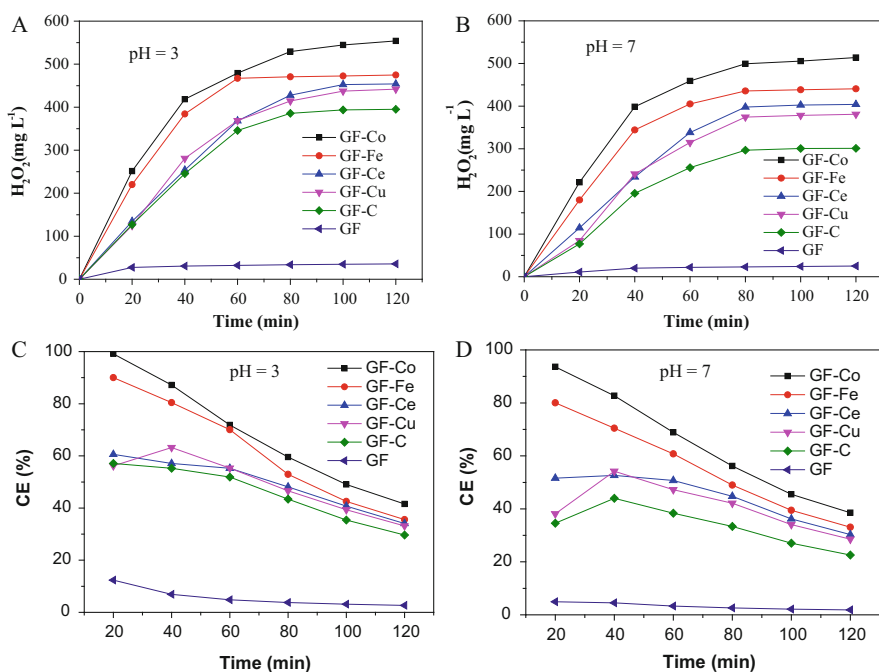


Fig. 14 Effect of metals loading on: (a, b) H_2O_2 production and (c, d) current efficiency. Conditions: $0.05\ \text{M}\ \text{Na}_2\text{SO}_4$, current density $50\ \text{A}\ \text{m}^{-2}$, air flow rate $0.5\ \text{L}\ \text{min}^{-1}$, $1.0\ \text{wt}\%$ Co, $1.0\ \text{wt}\%$ Fe, $1.0\ \text{wt}\%$ Ce, and $0.5\ \text{wt}\%$ Cu. Reproduced from Liang et al. [36], Copyright 2017, with permission from Springer

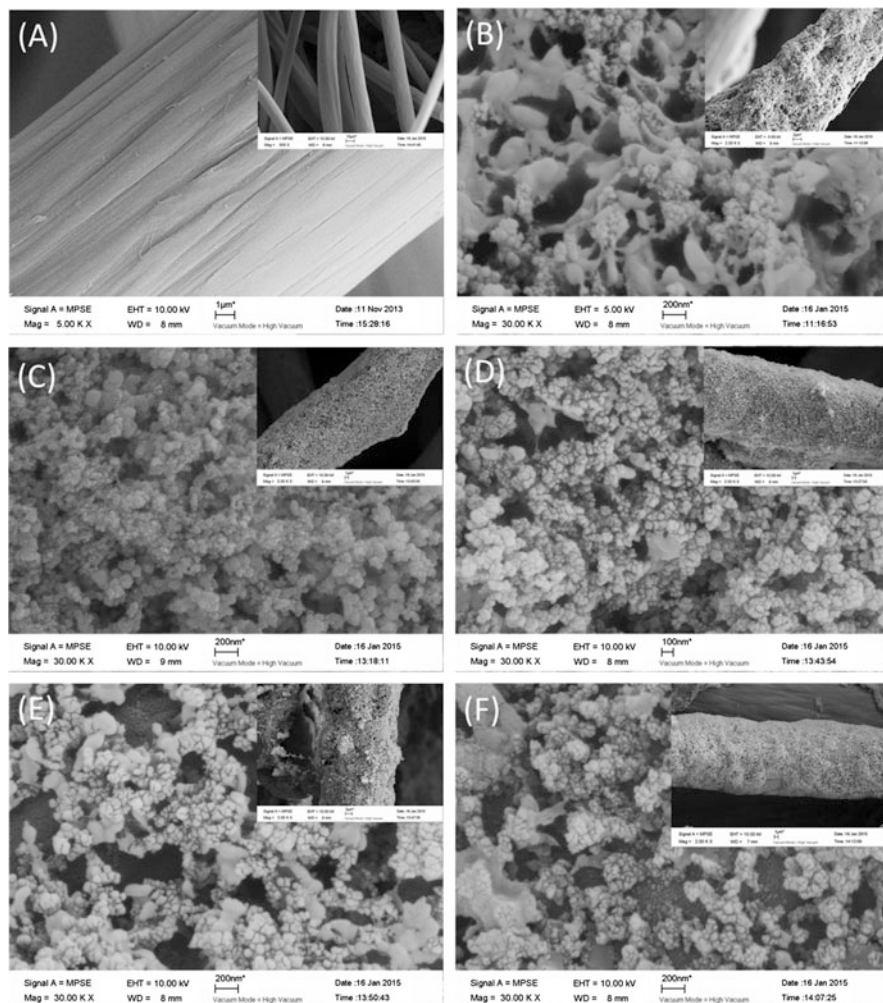


Fig. 15 SEM image of :**(a)** GF, **(b)** GF-C, **(c)** GF-Co, **(d)** GF-Fe, **(e)** GF-Ce, and **(f)** GF-Cu. Reproduced from Liang et al. [36], Copyright 2017, with permission from Springer

The surface element of GF-C and GF-Fe was studied by XPS analysis. Compared with GF-C (Fig. 16a), not only C and O elements but also Fe element was observed and the ratio between O and C (O/C) increased in GF-Fe (Fig. 16b), which indicated that the number of oxygen-containing functional groups increased. The F element was also detected, which was probably due to the addition of PTFE during modification.

For GF-Fe, peak fitting of C1s and O1s were carried out, and the results are shown in Fig. 16c, d. For C1s spectra, the main peak at 284.6–284.7 eV was attributed to graphitized carbon (C=C) [45]. The other three peaks should be attributed to the defects on

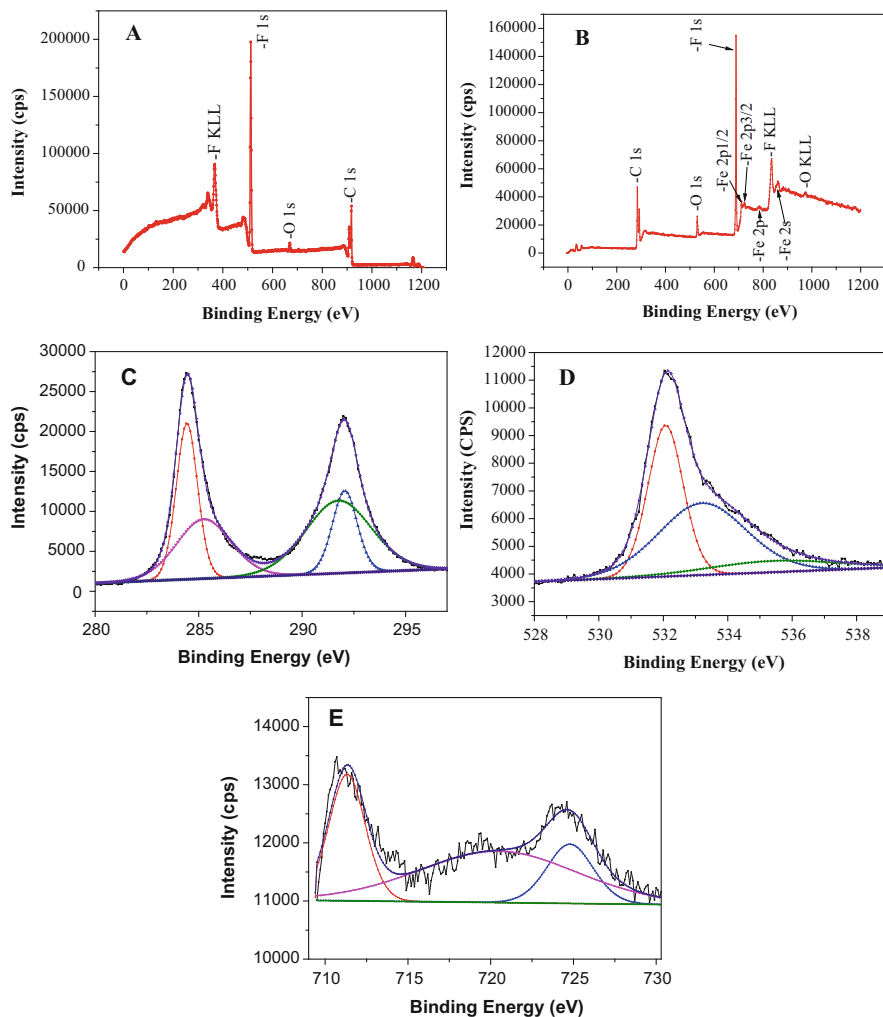


Fig. 16 XPS of: (a) GF-C and (b) GF-Fe; the high-resolution XPS spectrum of: (c) C1s region, (d) O1s region, and (e) Fe2p region for GF-Fe. Reproduced from Liang et al. [36], Copyright 2017, with permission from Springer

the GF structure (C=C, 285.1 eV), C–OH (286.0–286.3 eV), and C–O (286.8–287.0 eV) [46]. Regarding the O1s spectra, the split peaks were located at 532.2–532.7, 531.0–531.1, and 533.9–534.2 eV, which should be assigned to O–H and C–O [47].

Figure 16e presents the high-resolution spectra of Fe 2p. The peaks centered at 713.7 and 725.1 eV were assigned to Fe(III), and the peak centered at 722.0 eV was attributed to Fe⁰ [48]. Therefore, the iron species was mainly composed of Fe⁰ and Fe₂O₃. These oxygen-containing groups and ferrite-carbon black hybrid could be acted as the active sites capable of accelerating the electrochemical reactions and

make dissolved oxygen accessible to the cathode surface facilitating electro-generation of H_2O_2 [24].

5.3 EF Application

To optimize the optimal mass ratio of the transition metal to carbon black for GF-metal, the performance of methyl orange (MO) degradation was tested. As shown in Fig. 17, with the increasing of this mass ratio, the MO degradation improved, and then it decreased. The MO removal efficiency was found significantly increased after transition metals loaded. The degradation efficiency reached the maximum of 99.2, 94.2, 89.5, and 70.1% with 1 wt.% Co, 1 wt.% Fe, 1 wt.% Ce, and 0.5 wt.% Cu within 120 min, which was much higher than 35.5% and 12.6% on GF-C and GF, respectively. The GF-Co electrode showed the highest MO removal rate. This was mainly due to more $\cdot\text{OH}$ production with the dissolution of transition metal ions in the solution [49]. However, a further increase of the transition metals

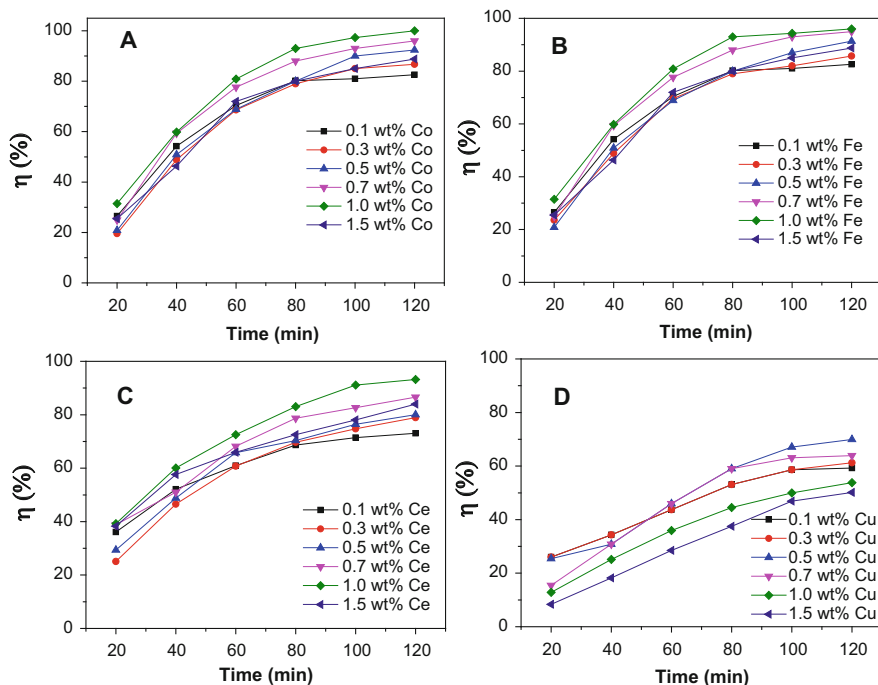


Fig. 17 Effect of metal loadings on the degradation of MO: (a) Co, (b) Fe, (c) Ce, and (d) Cu. Conditions: 0.05 M Na_2SO_4 , 50 mg L^{-1} MO, current density 50 A m^{-2} , pH = 3, and air flow rate 0.5 L min^{-1} . Reproduced from Liang et al. [36], Copyright 2017, with permission from Springer

content might cause an inhibition for MO degradation due to the loss of $\cdot\text{OH}$ by reaction with excess transition metal ion, taken Fe^{2+} , for example (Eq. 7) [50]:



6 Summary and Outlook

This chapter summarized our works on the modification of graphite felt by chemical, electrochemical, and composite hybrid method to improve EF performance. As demonstrated, these methods are simple but effective in enhancing hydrogen peroxide generation even more than ten times. Thus, they improved the EF performance with less energy consumption or more suitability in wider pH conditions. Also the transition metal doping on the composite graphite felt fulfilled in situ heterogeneous EF in near neutral pH conditions, which partly solved the problem of second pollution, for example, the disposal of iron sludge in conventional EF process.

It has to be noted that these methods are not only limited to graphite felt cathode, they are also effective for other carbon material cathode. For example, our results on active fiber felt by modification with carbon black and PTFE confirmed that the hydrogen peroxide generation could be much higher than that of the unmodified cathode. Of course, it needs more studies to extend these methods on other carbonaceous materials.

Our recent attempt with graphene may also reflect the future trend in cathode modification. A novel graphite felt cathode modified with graphene and carbon black was developed, presenting a very high H_2O_2 generation rate of $7.7 \text{ mg h}^{-1} \text{ cm}^{-2}$ with relatively low energy consumption ($9.7 \text{ kWh kg}^{-1} \text{ H}_2\text{O}_2$). Such graphene modified cathode demonstrated effectiveness for the degradation of four kinds of representative pollutants (Orange II, methylene blue, phenol, and sulfadiazine) by EF process, proving great potential practical application for organic wastewater treatment [51]. These results indicated that cathode modification with nanomaterial (e.g., carbon nanotube, and graphene) would be a potential hot research area in electrode modification. And more works need to be carried out deep into the modification mechanism to regulate the electrode preparation.

The other research direction might be the application of this cathode material in sound electrochemical reactor. For example, the rotation of disk cathode resulted in the efficient production of hydrogen peroxide without oxygen aeration, which solved the problem of low oxygen utilization ratio [52]. The use of graphite felt modified with carbon black was found to be cost-effective for flow-through EF, which was energy-efficient and potential for degradation of organic pollutants. The methyl blue and TOC removal efficiency of the effluents could keep above 90% and 50%, respectively, and the energy consumption was $23.0 \text{ kWh (kg TOC)}^{-1}$, which was much lower than conventional EF process ($50\text{--}1,000 \text{ kWh (kg TOC)}^{-1}$) [53].

Based on the modified graphite felt cathode with carbon black, an innovative design incorporated a Venturi-based jet aerator to supply atmospheric oxygen. Compared with a flow-by cell with a gas diffusion cathode under similar conditions, the CE toward hydrogen peroxide accumulation was even higher (72 vs 65% at 1 h), standing as a promising oxygen supply [54].

Finally, the last but not the least is the scale-up of the modification of the cathode, which would be vital to prepare a large-area cathode in view of EF application, especially to guarantee the good cathode performance which is as similar as that in small lab scale.

References

1. Oturan MA, Peiroten J, Chartrin P, Acher A (2000) Complete destruction of p-nitrophenol in aqueous medium by electro-Fenton method. *Environ Sci Technol* 34:3474–3479
2. Zhou M, Wu Z, Ma X, Cong Y, Ye Q, Wang D (2004) A novel fluidized electrochemical reactor for organic pollutant abatement. *Sep Purif Technol* 34:81–88
3. Wei L, Zhu H, Mao X, Gan F (2011) Electrochemical oxidation process combined with UV photolysis for the mineralization of nitrophenol in saline wastewater. *Sep Purif Technol* 77:18–25
4. Bo L, Quan X, Chen S, Zhao H, Zhao Y (2006) Degradation of p-nitrophenol in aqueous solution by microwave assisted oxidation process through a granular activated carbon fixed bed. *Water Res* 40:3061–3068
5. Sires I, Brillas E (2012) Remediation of water pollution caused by pharmaceutical residues based on electrochemical separation and degradation technologies: a review. *Environ Int* 40:212–219
6. Zhang C, Jiang YH, Li YL, Hu ZX, Zhou L, Zhou MH (2013) Three-dimensional electrochemical process for wastewater treatment: a general review. *Chem Eng J* 228:455–467
7. Brillas E, Sires I, Oturan MA (2009) Electro-Fenton process and related electrochemical technologies based on Fenton's reaction chemistry. *Chem Rev* 109:6570–6631
8. Wang CT, Hu JL, Chou WL, Kuo YM (2008) Removal of color from real dyeing wastewater by electro-Fenton technology using a three-dimensional graphite cathode. *J Hazard Mater* 152:601–606
9. Zhang GQ, Yang FL, Gao MM, Fang XH, Liu LF (2008) Electro-Fenton degradation of azo dye using polypyrrole/anthraquinonedisulphonate composite film modified graphite cathode in acidic aqueous solutions. *Electrochim Acta* 53:5155–5161
10. Scialdone O, Galia A, Sabatino S (2013) Electro-generation of H₂O₂ and abatement of organic pollutant in water by an electro-Fenton process in a microfluidic reactor. *Electrochem Commun* 26:45–47
11. Pimentel M, Oturan N, Dezotti M, Oturan MA (2008) Phenol degradation by advanced electrochemical oxidation process electro-Fenton using a carbon felt cathode. *Appl Catal Environ* 83:140–149
12. Panizza M, Oturan MA (2011) Degradation of alizarin red by electro-Fenton process using a graphite-felt cathode. *Electrochim Acta* 56:7084–7087
13. Zhou MH, Tan QQ, Wang Q, Jiao YL, Oturan N, Oturan MA (2012) Degradation of organics in reverse osmosis concentrate by electro-Fenton process. *J Hazard Mater* 215:287–293
14. Özcan A, Sahin Y, SavasKoparal A, Oturan MA (2008) Carbon sponge as a new cathode material for the electro-Fenton process: comparison with carbon felt cathode and application to degradation of synthetic dye basic blue 3 in aqueous medium. *J Electroanal Chem* 616:71–78

15. Wang AM, Qu JH, Ru J, Liu HJ, Ge JT (2005) Mineralization of an azo dye acid red 14 by electro-Fenton's reagent using an activated carbon fiber cathode. *Dyes Pigments* 65:227–233
16. Zhou MH, Yu QH, Lei LC (2007) Electro-Fenton method for the removal of methyl red in an efficient electrochemical system. *Sep Purif Technol* 57:380–387
17. Zarei M, Salari D, Niaei A, Khataee A (2009) Peroxi-coagulation degradation of C.I. Basic Yellow 2 based on carbon-PTFE and carbon nanotube-PTFE electrodes as cathode. *Electrochim Acta* 54:6651–6660
18. Brillas E, Calpe JC, Casado J (2000) Mineralization of 2,4-D by advanced electrochemical oxidation processes. *Water Res* 34:2253–2262
19. Loaiza-Ambuludi S, Panizza M, Oturan N, Ozcan A, Oturan MA (2013) Electro-Fenton degradation of anti-inflammatory drug ibuprofen in hydroorganic medium. *J Electroanal Chem* 702:31–36
20. Mousset E, Oturan N, van Hullebusch ED, Guibaud G, Esposito G, Oturan MA (2014) Treatment of synthetic soil washing solutions containing phenanthrene and cyclodextrin by electro-oxidation. Influence of anode materials on toxicity removal and biodegradability enhancement. *Appl Catal Environ* 160–161:666–675
21. Zhou L, Hu ZX, Zhang C, Bi ZH, Jin T, Zhou MH (2013) Electrogeneration of hydrogen peroxide for electro-Fenton system by oxygen reduction using chemically modified graphite felt cathode. *Sep Purif Technol* 111:131–136
22. Zhou L, Zhou MH, Zhang C, Jiang YH, Bi ZH, Yang J (2013) Electro-Fenton degradation of *p*-nitrophenol using the anodized graphite felts. *Chem Eng J* 233:185–192
23. Zhou L, Zhou MH, Hu ZX, Bi ZH, Serrano KG (2014) Chemically modified graphite felt as an efficient cathode in electro-Fenton for *p*-nitrophenol degradation. *Electrochim Acta* 140:376–383
24. Miao J, Zhu H, Tang Y, Chen YM, Wan PY (2014) Graphite felt electrochemically modified in H_2SO_4 solution used as a cathode to produce H_2O_2 for pre-oxidation of drinking water. *Chem Eng J* 250:312–318
25. Basova YV, Hatori H, Yamada Y, Miyashita K (1999) Effect of oxidation-reduction surface treatment on the electrochemical behavior of PAN-based carbon fibers. *Electrochem Commun* 1:540–544
26. Tammeveski K, Kontturi K, Nichols RJ, Potter RJ, Schiffrin DJ (2001) Surface redox catalysis for O_2 reduction on quinone-modified glassy carbon electrodes. *J Electroanal Chem* 515:101–112
27. Zhang X, Fu J, Zhang Y, Lei L (2008) A nitrogen functionalized carbon nanotube cathode for highly efficient electrocatalytic generation of H_2O_2 in electro-Fenton system. *Sep Purif Technol* 64:116–123
28. Alexeyeva N, Shulga E, Kisand V, Kink I, Tammeveski K (2010) Electroreduction of oxygen on nitrogen-doped carbon nanotube modified glassy carbon electrodes in acid and alkaline solutions. *J Electroanal Chem* 648:169–175
29. Segura Y, Martinez F, Melero JA, Molina R, Chand R, Bremner DH (2012) Enhancement of the advanced Fenton process (Fe^0/H_2O_2) by ultrasound for the mineralization of phenol. *Appl Catal Environ* 113:100–106
30. Liang L, An YR, Yu FK, Liu MM, Ren GB, Zhou MH (2016) Novel rolling-made gas-diffusion electrode loading trace transition metal for efficient heterogeneous electro-Fenton-like. *J Environ Chem Eng* 4:4400–4408
31. Dhakshinamoorthy A, Navalon S, Alvaro M, Garcia H (2012) Metal nanoparticles as heterogeneous Fenton catalysts. *ChemSusChem* 5:46–64
32. Ammar S, Oturan MA, Labiadh L, Guersalli A, Abdelhedi R, Oturan N, Brillas E (2015) Degradation of tyrosol by a novel electro-Fenton process using pyrite as heterogeneous source of iron catalyst. *Water Res* 74:77–87
33. Zhang C, Zhou MH, Ren GB, Yu XM, Ma L, Yang J, Yu FK (2015) Heterogeneous electro-Fenton using modified iron-carbon as catalyst for 2,4-dichlorophenol degradation: influence factors, mechanism and degradation pathway. *Water Res* 70:414–424

34. Zhao HY, Wang YJ, Wang YB, Cao TC, Zhao GH (2012) Electro-Fenton oxidation of pesticides with a novel $\text{Fe}_3\text{O}_4/\text{Fe}_2\text{O}_3$ /activated carbon aerogel cathode: high activity, wide pH range and catalytic mechanism. *Appl Catal Environ* 125:120–127
35. Yu FK, Zhou MH, Yu XM (2015) Cost-effective electro-Fenton using modified graphite felt that dramatically enhanced on H_2O_2 electro-generation without external aeration. *Electrochim Acta* 163:182–189
36. Liang L, Yu FK, An YR, Liu MM, Zhou MH (2017) Preparation of transition metal composite graphite felt cathode for efficient heterogeneous electro-Fenton process. *Environ Sci Pollut Res* 24:1122–1132
37. Sheng ZH, Shao L, Chen JJ, Bao WJ, Wang FB, Xia XH (2011) Catalyst-free synthesis of nitrogen-doped graphene via thermal annealing graphite oxide with melamin and its excellent electrocatalysis. *ACS Nano* 5:4350–4358
38. Liu SH, Wu MT, Lai YH, Chiang CC, Yu N, Liu SB (2011) Fabrication and electrocatalytic performance of highly stable and active platinum nanoparticles supported on nitrogen-doped ordered mesoporous carbons for oxygen reduction reaction. *J Mater Chem* 21:12489–12496
39. Gavrilov N, Pašti IA, Vujković M, Travas-Sejdic J, Ćirić-Marjanović G, Mentus SV (2012) High-performance charge storage by N-containing nanostructured carbon derived from polyaniline. *Carbon* 50:3915–3927
40. Khare B, Wilhite P, Tran B, Teixeira E, Fresquez K, Mvondo DN, Bauschlicher C, Meyyappan J, Meyyappan M (2005) Functionalization of carbon nano-tubes via nitrogen glow discharge. *J Phys Chem B* 109:23466–23472
41. Okpalugo TIT, Papakonstantinou P, Murphy H, McLaughlin J, Brown NMD (2005) High resolution XPS characterization of chemical functionalised MWCNTs and SWCNTs. *Carbon* 43:153–161
42. Sarapu A, Vaik K, Schiffrin DJ, Tammeveski K (2003) Electrochemical reduction of oxygen on anthraquinone-modified glassy carbon electrodes in alkaline solution. *J Electroanal Chem* 541:23–29
43. Kundu S, Wang Y, Xia W, Muhler M (2008) Thermal stability and reducibility of oxygen-containing functional groups on multiwalled carbon nanotube surfaces: a quantitative high-resolution XPS and TPD/TPR study. *J Phys Chem C* 112:16869–16878
44. Roldan L, Santos I, Armenise S, Fraile JM, García-Bordejé E (2011) The formation of a hydrothermal carbon coating on graphite microfiber felts for using as structured acid catalyst. *Carbon* 50:1363–1372
45. Wang Y, Zhao G, Chai S, Zhao H (2013) Three-dimensional homogeneous ferrite carbon aerogel: one pot fabrication and enhanced electro-Fenton reactivity. *Appl Mater Interfaces* 5:842–852
46. Wu MF, Jin YN, Zhao GH, Li MF, Li DM (2010) Electrosorption-promoted photodegradation of opaque wastewater on a novel TiO_2 /carbon aerogel electrode. *Environ Sci Technol* 44:1780–1785
47. Wang Y, Liu YH, Wang K, Song SQ, Tsiakaras P, Liu H (2015) Preparation and characterization of a novel KOH activated graphite felt cathode for the electro-Fenton process. *Appl Catal Environ* 165:360–368
48. Ai ZH, Lu LR, Li JP, Zhang LZ, Qiu JR, Wu MH (2007) $\text{Fe}@\text{Fe}_2\text{O}_3$ core-shell nanowires as the iron reagent. 2. An efficient and reusable sono-Fenton system working at neutral pH. *J Phys Chem C* 111:7430–7436
49. Ai ZH, Gao ZT, Zhang LZ, He WW, Yin JJ (2013) Core-shell structure dependent reactivity of $\text{Fe}@\text{Fe}_2\text{O}_3$ nanowires on aerobic degradation of 4-chlorophenol. *Environ Sci Technol* 47:5344–5352
50. Nidheesh PV, Gandhimathi R (2012) Trends in electro-Fenton process for water and wastewater treatment: an overview. *Desalination* 299:1–15
51. Yang W, Zhou MH, Cai JJ, Liang L, Ren GB (2017) Ultrahigh yield of hydrogen peroxide on graphite felt cathode modified with electrochemically exfoliated graphene. *J Mater Chem* 5:8070–8080

52. Yu F, Zhou MH, Zhou L, Peng R (2014) A novel electro-Fenton process with H₂O₂ generation in a rotating disk reactor for organic pollutant degradation. *Environ Sci Technol Lett* 1:320–324
53. Ma L, Zhou MH, Ren GB, Yang WL, Liang L (2016) A highly energy-efficient flow-through electro-Fenton process for organic pollutants degradation. *Electrochim Acta* 200:222–230
54. Perez JF, Llanos J, Saez C (2016) Electrochemical jet-cell for the in-situ generation of hydrogen peroxide. *Electrochem Commun* 71:65–68

Conventional Reactors and Microreactors in Electro-Fenton

Marco Panizza and Onofrio Scialdone

Abstract The cells used for electro-Fenton process look quite different, ranging from the simple open tanks, through the parallel-plate cells, to the sometimes complex designs with three-dimensional moving electrodes or microelectrodes. Recently, pressurized cells and microreactors have been used to improve the performance of the process. This chapter presents a general overview of the main cell configurations used in electro-Fenton process for the treatment of organic pollutants. A global perspective on the fundamentals and experimental setups is offered, and laboratory-scale and pilot-scale experiments are examined and discussed.

Keywords Electrochemical reactors, Micro-reactors, Moving three-dimensional electrodes, Parallel-plate flow cell, Pressurized reactors, Tank cell

Contents

1	Introduction	206
2	Tank Cell	207
3	Parallel-Plate Flow Cell	213
4	Moving Three-Dimensional Electrodes	217
5	Pressurized Reactors	220
6	Microreactors	222
7	Conclusions	230
	References	231

M. Panizza (✉)

Department of Civil, Chemical and Environmental Engineering, University of Genoa, P.le Kennedy 1, Genoa 16129, Italy
e-mail: marco.panizza@unige.it

O. Scialdone

Dipartimento dell'innovazione industriale e digitale, Ingegneria chimica, gestionale, informatica, meccanica, University of Palermo, Viale delle Scienze, Palermo 90144, Italy

1 Introduction

The choice of the electrode materials and the design of the electrochemical reactor are the key challenges for the development of any electrochemical processes. It requires the knowledge of many factors, including thermodynamics and kinetics of the reactions, the current and potential distribution, the type of electrolyte flow, mass transfer, and the costs of the various components. Electrochemical reactors share some modes of operation and characteristics with classical chemical engineering ones. For example, regarding the flow configuration, they can be classified in (1) simple batch reactor (Fig. 1, a), (2) single-pass continuous stirred tank reactor (CSTR, Fig. 1, b), (3) single-pass plug flow reactor (PFR, Fig. 1, b), and (4) batch-recycle mode (CSTR or PFR, Fig. 1, c).

However, a wide range of cell designs are commonly used in the electrochemical engineering and in particular in electro-Fenton, ranging from open tanks through parallel-plate cell to complex cell with moving packed bed electrodes. This is not unexpected because different type of electrode materials can be used in electro-Fenton. Furthermore, recently it has been shown that pressurized cells and

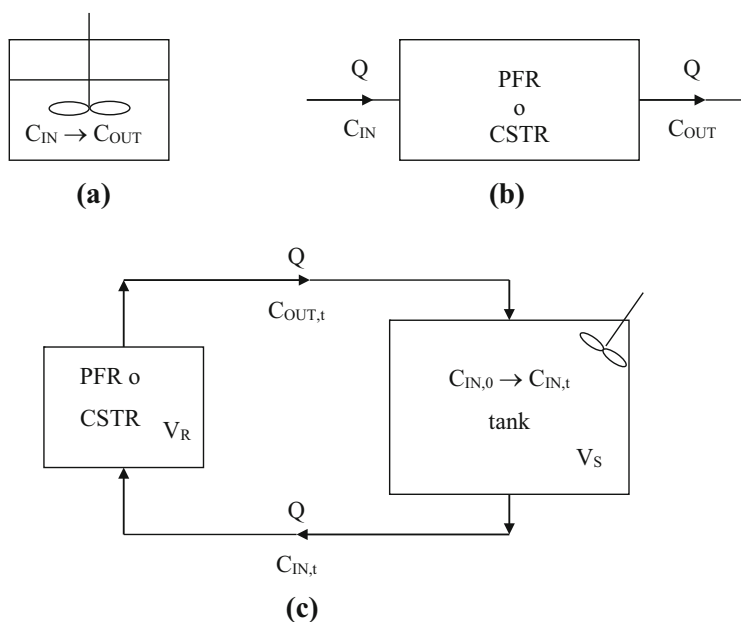


Fig. 1 Sketch of the common modes of operation: (a) simple batch reactor (SBR), (b) single-pass continuous stirred tank reactor (CSTR) or single-pass plug flow reactor (PFR) and (c) batch-recycle mode (CSTR or PFR). Adapted from Ref. [1]

microreactors can enhance the cathodic generation of hydrogen peroxide and the abatement of organic pollutants by electro-Fenton process allowing to use cheap compact graphite cathodes.

In this chapter, typical example of cell design used in the electro-Fenton process will be discussed, and some results obtained with these cells will be presented.

2 Tank Cell

The plate-in-tank cell is one of the most common reactors used on a laboratory scale because it offers an easy fabrication and it requires simple components. The cells can contain only one anode and one cathode or multiple electrodes, with monopolar or bipolar connection. In some processes, the cell can be also divided by a separator or a membrane. Despite the simplicity of construction and operation of this type of cell, it has the main drawback that the mass transport is limited even in the presence of mechanical means. This type of cell is used in industrial electrochemistry in many traditional processes such as water electrolysis, aluminum extraction, electrowinning and electrorefining, and electrogeneration of many organic and inorganic compounds.

Many laboratories use the tank cell for the electro-Fenton process with different types of electrodes including graphite felt, activated carbon fiber (ACF), reticulated vitreous carbon (RVC), gas diffusion electrodes (GDE) as cathode and platinum, mixed metal oxide, PbO_2 , and boron-doped diamond (BDD) as anode. Some examples are summarized in Table 1.

For example, the group of Panizza focused on the treatment of organic pollutants by electrogenerated Fenton's reagent utilized an undivided cell schematized in Fig. 2 [2]. The laboratory cell has a variable volume from 0.20 to 35 dm^{-3} , and it is equipped with a heat exchanger to control the temperature. They used a carbon felt with a thickness of 0.5 cm as cathode with a platinum wire isolated from the solution for the electric contact. The anode was either a Pt wire placed in front of the cathode or a Ti/RuO₂ net centered in the electrolytic cell, surrounded by the cathode, which covered the inner wall of the cell.

In this cell, $\cdot\text{OH}$ are produced in the bulk of the polluted solution using the electrogenerated Fenton's reagent (Eq. 1) where H_2O_2 is supplied in situ from the two-electron reduction of O_2 (Eq. 2) and Fe^{2+} is continually regenerated from Fe^{3+} reduction (Eq. 3):

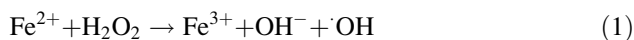


Table 1 Some examples of organic compounds treated by electro-Fenton using a tank reactor

Cathode	Anode	Compound	Comment	Ref.
Graphite felt	Pt	Industrial effluent	Complete removal of naphthalene and anthraquinone sulfonic acids	[2]
Graphite felt	Pt	Chlorophenols	99% of TOC removal for 4-CP and 87% of TOC removal for poly-CP	[3]
GDE or graphite felt	Pt	Alizarin red	95% of the initial TOC removal in 210 min	[4, 5]
Graphite felt	Ti/RuO ₂	p-Coumaric acid	Complete removal of coumaric acid and 95% of TOC removal	[6]
Graphite felt	Pt and BDD	Chlorobenzene	95% TOC removal	[7]
Graphite felt	Pt and BDD	Antibiotic levofloxacin	95% TOC removal of 0.23 mM antibiotic solution was degraded in 8 h	[8]
Graphite felt	Pt and BDD	Pharmaceutical ranitidine	Almost complete mineralization of the ranitidine using a BDD	[9]
Graphite felt	(RuO ₂ IrO ₂ , Pt and BDD)	Antibiotic tetracycline	TOC removal up to 98% with BDD anode	[10]
Graphite felt	Pt	Ibuprofen	Complete removal of ibuprofen in hydroorganic medium	[10]
Graphite felt	Pt	Reverse osmosis concentrate	62% COD removal in 3 h	[11]
Graphite felt	Pt	Herbicide diuron	Photo-Fenton process leads to 97.8% of TOC removal in 3 h of treatment.	[12]
Graphite felt	Pt	β-Blockers	Complete degradation of atenolol, metoprolol, and propranolol	[13]
Graphite felt	Pt	Acid orange 7 dye	92% Removal of TOC	[14]
Graphite felt and GDE	Pt and BDD	Antimicrobials triclosan and triclocarban	Decay rate: Pt/carbon felt > BDD/carbon felt > Pt/O ₂ diffusion > BDD/O ₂ diffusion	[15]
Graphite felt	Pt	Malachite green	Overall mineralization was reached at 540 min	[16]
Graphite felt and GDE	Pt and BDD	Antimicrobial chlorophene	Highest oxidizing power with BDD/carbon-felt cell	[17]
GDE	Pt	Methyl red	Methyl red concentration of 100 mg dm ⁻³ was degraded of 80% in 20 min	[18]
Graphite felt	Pt	p-Nitrophenol	Mineralization of p-nitrophenol was above 78%.	[19, 20]
GDE	Ti/IrO ₂ -RuO ₂	2,4-Dichlorophenol	The degradation efficiency of 2,4-DCP exceed 95% in 120 min	[21, 22]

(continued)

Table 1 (continued)

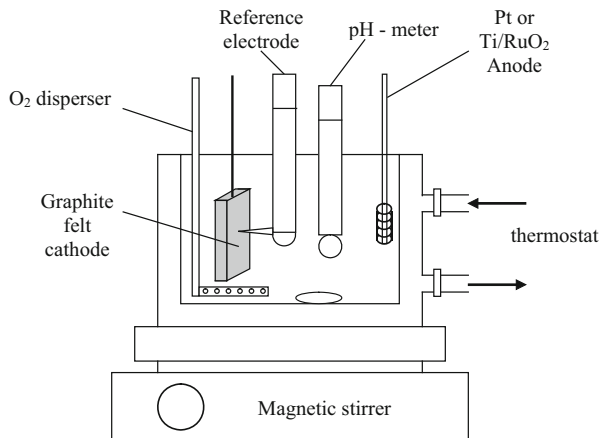
Cathode	Anode	Compound	Comment	Ref.
Graphite felt	BDD	Pesticides thiamethoxam	Complete degradation of thiamethoxam and 92% of TOC removal	[23]
Graphite felt	BDD	Imidacloprid	Imidacloprid removals of 80% and 90% in 2 and 4 h, respectively	[24]
Nickel foam	BDD	Winery wastewater	100% of decolorization, 92% of CI reduction, and 82% of COD reduction	[25]
GDE	PbO ₂ or Pt	Aniline	Photoelectron-Fenton process allows to destroy 92% of TOC after 6 h	[26, 27]
GDE	Pt or BDD	Chlorophenoxy herbicides	Total mineralization of as 4-CPA, MCPA, 2,4-D and 2,4,5-T, 2-DP and MCPP herbicides	[28–32]
GDE	Pt or BDD	Indigo carmine	Complete mineralization with a BDD anode and Fe ²⁺ and Cu ²⁺ catalysts	[33]
GDE	BDD	Azo dyes	Acid orange 7, acid red 151, direct blue 71, acid red 29, direct yellow	[34–39]
GDE	BDD or Pt	Pharmaceuticals	Enrofloxacin beta-blocker, ibuprofen, chloramphenicol	[40–47]
Graphite	Graphite	tetracycline	Tetracycline was degraded completely with a rotating disc electrode	[48]
Activated carbon fiber (ACF)	Ti/RuO ₂	Antibiotic cephalixin	Not complete COD removal but biodegradability enhancement	[49]
RVC	Ti/TiO ₂	Azo dye orange G	Complete orange G removal	[50]



Continuous saturation of the solution by O₂ at atmospheric pressure was ensured by bubbling of compressed air having passed through a frit at about 1 dm³ min⁻¹, starting 10 min before electrolysis. Solutions were vigorously stirred using a magnetic bar with a rotation rate of about 700 rpm to enhance mass transfer of dissolved oxygen and iron ions to the cathode. The cell is also equipped with a pH-meter that allowed the continuous control of the solution pH in order to maintain it in the range pH 3–5 that is recognized to be the optimum for Fenton's reagent [51].

The majority of researchers prefers to perform electrolysis working under galvanostatic conditions, but others study the electrogeneration of H₂O₂ under potentiostatic conditions. In the latter condition, it is possible to have a better control of the electrochemical reactions and thus results in higher current

Fig. 2 Sketch of the experimental setup utilized by the group of Panizza for the removal of organic pollutants from industrial wastewater by electrogenerated Fenton's reagent. Reprinted from Ref. [2], Copyright 2001, with permission from Elsevier



efficiency, but it is necessary to add a reference electrode in the cell. In order to reduce the errors due to ohmic drop, it is preferable to place the reference electrode in a glass-luggin capillary positioned near the cathode surface, as shown in Fig. 2.

Using this type of cell, Panizza and Oturan [5] investigated the removal of the anthraquinone dye alizarin red S (AR) under different experimental conditions. They reported that AR was completely removed by the reaction with $\cdot\text{OH}$ radicals generated from electrochemically assisted Fenton's reaction, and the decay kinetic always follows a pseudo-first-order reaction. Applying a current of 300 mA and with catalyst concentration of 0.2 mM Fe^{2+} , 95% of the initial total organic carbon (TOC) was removed in 210 min of electrolysis, meaning the almost complete mineralization of the organic content of the treated solution. The mineralization current efficiency (MCE) at the beginning of the electrolysis was about 50%.

A tank cell is also commonly used by the group of Oturan for the treatment of many organic pollutants. As schematized in Fig. 3, the cell is an open, undivided, and cylindrical glass cell of 0.25 dm^{-3} capacity. The continuous saturation of oxygen at atmospheric pressure was assured by bubbling compressed air through a frit at about $0.5 \text{ dm}^{-3} \text{ min}^{-1}$. During the electrolyses, the solution is continuously stirred by using a magnetic stirrer. They used either a cylindrical Pt mesh (4.5 cm height, i.d. = 3.1 cm) or a 25 cm^2 thin-film BDD electrode as anode and a 105 cm^2 piece of carbon felt ($17.5 \times 6 \text{ cm}$) as cathode. In all electrolyses, the anode was centered in the cell, surrounded by the carbon-felt cathode covering the totality of the inner wall of the electrochemical reactor.

Using this type of cell, they efficiently treated a great variety of pollutants, including pesticides [7, 52–55], drugs [56–65], and dyes [66–71]. They reported that the pollutants rapidly reacts with electrochemically produced hydroxyl radicals leading to their oxidative degradation and mineralization. The removal rate and the efficiency depends on the experimental conditions applied (e.g., applied current, iron concentration, pollutant type, and concentration) and on the nature of the anode. For example, during the degradation of carbaryl [52], the second most

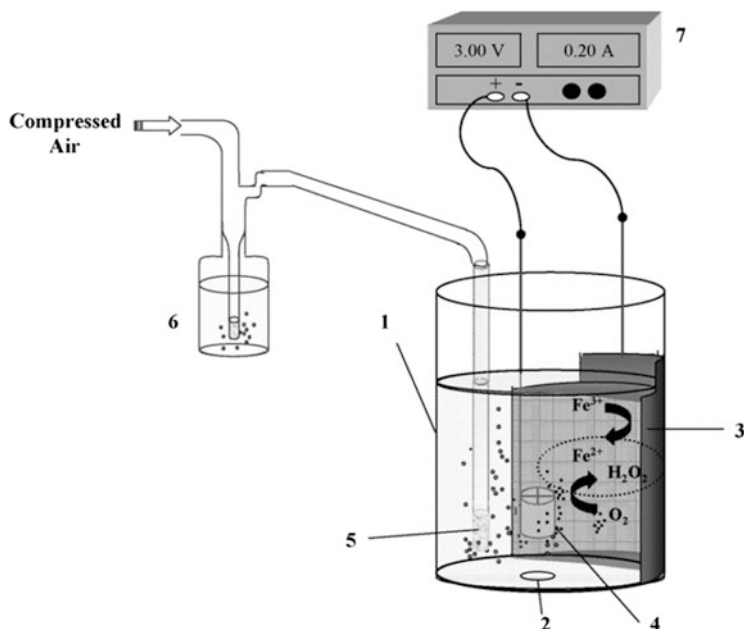
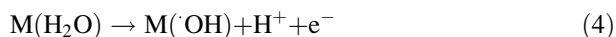


Fig. 3 Scheme of the experimental setup used. (1) Electrolytic cell, (2) magnetic stir bar, (3) carbon-felt cathode, (4) Pt anode, (5) air diffuser, (6) air drying solution, and (7) galvanostat. Reprinted from Ref. [16], Copyright 2008, with permission from Elsevier

frequently found insecticide in water, they reported that after 2 h of electrolysis, TOC removal was 73.7% with Pt anode and 90.2% with BDD anode. After 4 h of electrolysis, they achieved a mineralization of more than 85% with Pt electrode and almost total mineralization with BDD. This behavior is related to the nature of electrode material (M). In fact, during the electrolysis, together with the homogeneous $\cdot\text{OH}$ produced by the Fenton's reaction (Eq. 1), there is formation of heterogeneous hydroxyl radical on the anode surface by oxidation of water (Eq. 4) [51, 72]:



The amount and reactivity of heterogeneous $\cdot\text{OH}$ is strongly related to the nature of anode materials. It is well known [73, 74] that the amount of BDD($\cdot\text{OH}$) formed with BDD anode is largely higher than that Pt($\cdot\text{OH}$) generated with Pt anode [73, 75]. On the other hand, BDD($\cdot\text{OH}$) are physisorbed on the anode surface, while Pt($\cdot\text{OH}$) are chemisorbed. Consequently, the formers are more available and more reactive for oxidation of organics than the latter.

Many authors [11, 15, 70] observed that the hydrogen peroxide generation rate in an undivided cell increased at the beginning of the electrolysis, but after 50–60 min, the H_2O_2 accumulation rate was decreased and reached a steady-state value when

its generation at the cathode (Eq. 2) and decomposition at the anode became equal. This phenomenon can be attributed to the self-decomposition of hydrogen peroxide when it reached higher concentrations (Eq. 5) [76]:



Another reason may be hydrogen peroxide oxidation at the anode:

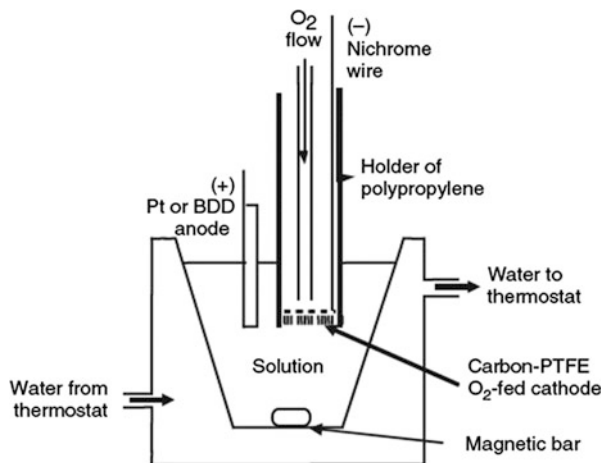


In order to prevent the decomposition of hydrogen peroxide at the anode, Sudoh et al. [77] proposed the use of H-type two-compartment cell with a graphite cathode. They reported a maximum current efficiency of 85% for H_2O_2 production, with a gradual increase in H_2O_2 concentration with prolonging electrolysis time.

Some papers [78, 79] reported that the efficiency of H_2O_2 production is highly dependent on the diffusion of oxygen of the gaseous phase into the liquid phase. Due to the low solubility of oxygen, most oxygen bubbled into the solution cannot reach the electrode surface, resulting in the low oxygen utilization efficiency. In order to increase the mass transport of the oxygen to the cathode surface, Zhang et al. [48] proposed the use of a rotating graphite disk electrode as cathode. They demonstrated that the H_2O_2 concentration increased from 15.6 to 45.3 mg dm^{-3} when the rotating speed increased from 100 to 400 rpm. However, a small decrease in H_2O_2 concentration was observed when the rotation speed increased further to 500 rpm. In addition, the CE at rotation rate of 100, 200, 300, 400, and 500 rpm were 10.5, 17.3, 17.5, 17.4, and 9.1%, respectively. The cathode rotation increased the contact area between oxygen and electrode, thus, improving the efficiency of oxygen mass transfer and the generation rate of H_2O_2 . However, when rotation speed was too high, the resistance of electrolyte solution increased with the excessive bubbles in the system, resulting in a drop in the yields of H_2O_2 . At a rotation speed of 400 rpm, 50 mg dm^{-3} of tetracycline was degraded completely within 2 h with the addition of ferrous ion (1.0 mM). A rotating RVC cylinder cathode was also used by Badellino et al. [80] for the degradation of the herbicide 2,4-dichlorophenoxyacetic acid, and they obtained a 69% of TOC removal.

Tank cells are also utilized with carbon-PTFE O_2 -fed cathode or gas diffusion electrode (GDE) because it is allowed to obtain a uniform and easy to control O_2 pressure in the back of the cathode. An example of an undivided electrolytic cell used by the group of Brillas for the mineralization of many organic pollutants [81–88] by electro-Fenton process is schematized in Fig. 4. The cell consists in a one-compartment vessel with a volume of 0.100 dm^{-3} containing a Pt or PbO_2 anode and the carbon-PTFE O_2 -fed cathode and operated at constant current between 30 and 750 mA. The cell also has a thermal jacket to maintain the temperature at a constant value of 25 °C during the experiments, and the solution was vigorously stirred with a magnetic bar to achieve an efficient transport of all species toward the electrodes.

Fig. 4 Sketch of the open undivided cell with an O₂-diffusion cathode used by the group of Brillas. Reprinted from Ref. [85], Copyright 1995, with permission from Electrochemical Society



A great advantage of this cell configuration is the possibility of adding a UV lamp tube at the top of the cell and compare the performance of electro-Fenton and photoelectro-Fenton processes [32, 33, 89–94]. For example, Brillas et al. [90] used this cell equipped with using a Pt anode and an O₂-diffusion cathode to study the mineralization of herbicide 3,6-dichloro-2-methoxybenzoic acid in aqueous medium by anodic oxidation, electro-Fenton, and photoelectro-Fenton. They reported that anodic oxidation enabled only 20% of mineralization, electro-Fenton yields 60–70% mineralization, and photoelectro-Fenton allows a fast and complete depollution of herbicide solutions, even at low currents, by the action of UV irradiation. During electro-Fenton and photoelectron-Fenton processes, herbicide degradation generated carboxylic acids such as formic, maleic, and oxalic. In electro-Fenton, formic acid was completely mineralized and all maleic acid is transformed into oxalic acid, but the last acid forms stable complexes with Fe³⁺, which remained in the electrolyzed solution as final products. On the contrary, in the presence of UV radiation, there was a fast photodecarboxylation of such complexes, and this explains the highest oxidative ability of photoelectro-Fenton.

3 Parallel-Plate Flow Cell

Most of the industrial electrochemical processes are based on the parallel-plate electrode configuration, which is generally constructed with many electrodes in a plate-and-frame arrangement and mounted on a filter press. An example of these cells can be found in the chlor-alkali industry.

The parallel-plate cells are convenient for many reasons [1]:

- Simplicity of construction with regard to features such as cell frames, electrode connection, and membrane sealing.

- Wide availability of electrode materials and separators in a suitable form.
- The potential distribution is reasonably uniform.
- Mass transport may be enhanced and adjusted using a variety of turbulence promoters.
- Scale-up readily achieved.
- Versatility, with respect to monopolar or bipolar operation and the possibility of modifying the fundamental unit cell
- Constructions and appearance of the filter-press cell has similarities with the known example of chemical engineering.

The success of the parallel-plate cells has been demonstrated for a wide range of application, such as chlor-alkali industry, potassium permanganate production, Monsanto adiponitrile synthesis, and other processes of organic electrosynthesis. At present, a number of cells are commercially available in different sizes and from various manufacturers.

For example, the group of Brillas, scaling up from the laboratory experiments to a pilot plant scale, changed the reactor from a tank cell, as mentioned above, to a parallel-plate cell, as presented in Fig. 5 [95–98]. The electrochemical cell was an undivided filter-press Electrocell AB containing electrodes of 100 cm² area in contact with the solution and separated 5 mm by a turbulence promoter. The oxygen diffusion cathode was GDE electrode. The feeding O₂ was supplied by a cylinder to a gas chamber in contact with the cathode. Thus, O₂ diffuses through this electrode until reaching the interface with the liquid, where it is reduced to H₂O₂ from reaction (2). A mesh of platinized titanium (Ti/Pt) or a DSA[®] plate or a BDD were used as anodes. The solution was introduced in the reservoir to be continuously recirculated by means of a pump at a constant rate ranging between 200 and 900 dm³ h⁻¹ measured by a flowmeter, corresponding to a mean linear velocity of 0.056–0.25 m s⁻¹. Its temperature was kept at 40 °C with a heat exchanger. Electrolyses were performed at constant current ranging between 2 and 20 A.

Furthermore, the parallel-plate cell in a recirculation mode has the advantage that the electro-Fenton process can be easily modified in photoelectro-Fenton (PEF) and solar photoelectro-Fenton (SPEF) irradiating the solution by a UV lamp or solar light when it is recirculated from the reactor to the reservoir.

As an example, in Fig. 6 there is a sketch of a pilot plant used by the group of Brillas for electro-Fenton and solar photoelectro-Fenton treatment of pharmaceuticals [96, 99–104], pesticides [98, 105–108], dyes [109–114], other compounds [115, 116].

The solution was introduced in the reservoir and continuously recirculated through the cell by a peristaltic pump at a liquid flow rate of 180 dm³ h⁻¹ adjusted by a flowmeter. The temperature was maintained at 30 °C by two heat exchangers. The solar photoreactor was a polycarbonate box of 240 mm × 240 mm × 25 mm, connected to the liquid outlet of the cell. Figure 6b shows a scheme of the one-compartment filter-press cell used as electrolytic reactor. All components were 80 mm × 120 mm in dimension, separated with Viton gaskets to avoid leakages. The liquid compartment and O₂ chamber were made of PVC and had a

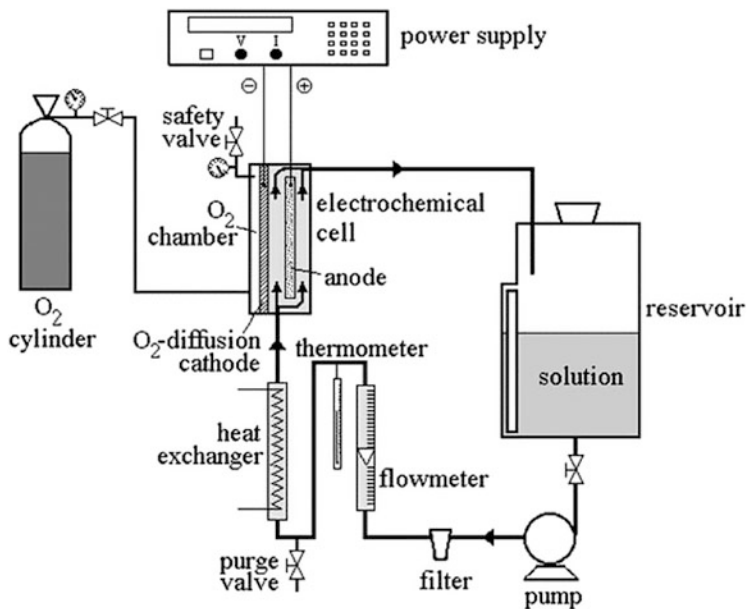


Fig. 5 Sketch of the experimental setup of the pilot flow reactor used for aniline degradation. Reprinted from Ref. [95], Copyright 2002, with permission from Elsevier

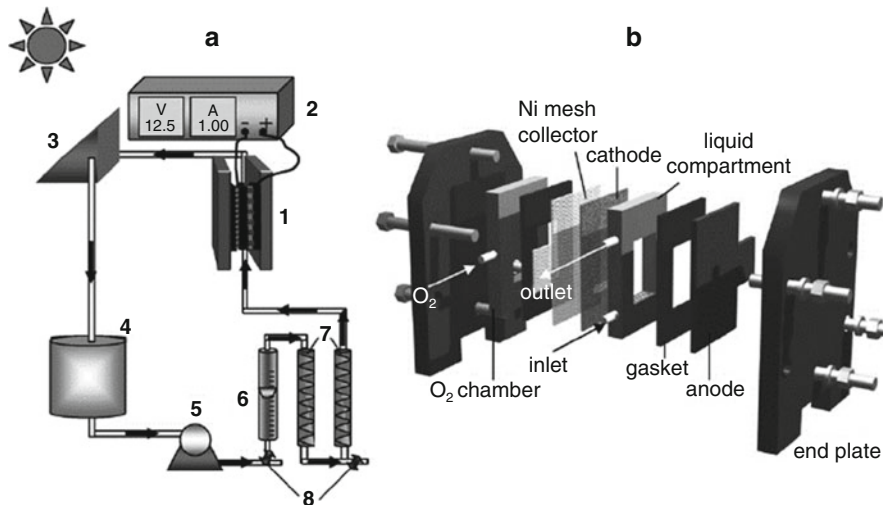


Fig. 6 Sketches of (a) the flow plant and (b) the filter-press electrochemical cell. In sketch (a), (1) flow cell, (2) power supply, (3) solar photoreactor, (4) reservoir, (5) peristaltic pump, (6) flowmeter, (7) heat exchangers, and (8) purge valves. Reprinted from Ref. [92], Copyright 2007, with permission from Elsevier

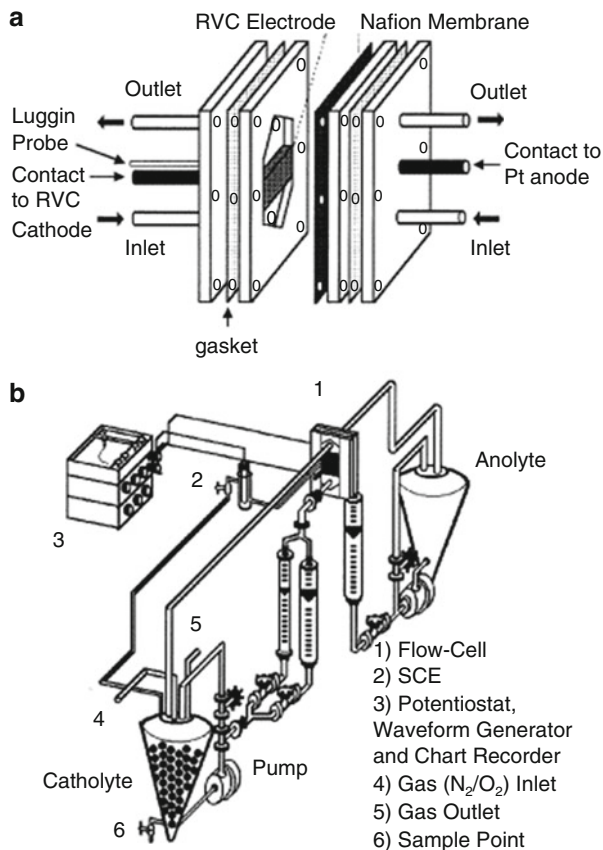
central window of 40 mm \times 50 mm to contact the effluent with the outer faces of both electrodes and to inject pure O₂ to the cathode by its inner face, respectively. The anode was a BDD and the cathode was a GDE electrode. O₂ gas was injected at 1.5 bar regulated with a back-pressure gage connected to the O₂ chamber. A Ni mesh between this chamber and the cathode acted as electrical connector. The interelectrode gap was 12 mm. In this type of process, pollutants are mainly oxidized by hydroxyl radical formed at the anode surface from water oxidation (Eq. 4) and in the medium from Fenton's reaction between Fe²⁺ and cathodically electrogenerated H₂O₂ (Eq. 1), giving rise to complexes of Fe³⁺ with final carboxylic acids that are rapidly photodecomposed by UV light supplied by solar irradiation.

For example, Flox et al. [92] demonstrated that the reactor schematized in Fig. 6 can effectively degrade *o*-cresol, *m*-cresol and *p*-cresol contained in 2.5 dm³ of electrolyte by solar photoelectro-Fenton. They obtained complete mineralization of all cresols up to ca. 0.5 g dm⁻³ with 1.0 mM Fe²⁺ as catalyst at pH 3.0 and 50 mA cm⁻² in 420 min with an energy consumption as low as 6.6 kWh m⁻³. Comparative electro-Fenton treatment leads to a much slower degradation, thus confirming the very positive action of UV light supplied by solar irradiation to photodecompose complexes of Fe³⁺ with final carboxylic acids.

The filter-press cell can also be used with three-dimensional electrodes, such as RVC [117–121], graphite felt [122], or graphite chips [123], in order to increase the electrode surface. Alvarez-Gallegos and Pletcher [117–119] used the flow divided three-electrode cell to generate H₂O₂ at a RVC cathode. The cell is sketched in Fig. 7. It was fabricated from four blocks of polypropylene, each 280 \times 100 \times 12 mm thick. The steel plate cathode current collector was sunk into one of the outer blocks. The inner polymer blocks were machined to form the electrolyte channels. Each had extended entry and exit lengths, while the RVC cathodes (50 \times 50 \times 12 mm thick) fitted tightly into the center of the catholyte channel and electrical contact with the current collector was made with conducting carbon cement. The anode was a platinum gauze (50 \times 50 mm) placed in the anolyte stream so that it faced the RVC cathode and electrical connection was made via a contact through the second outer polymer block. The separator was a Nafion[®] 417 cation permeable membrane. Typically, experiments were carried out with 2.5 dm³ of catholyte, and a similar volume of anolyte and the solutions were continuously recycled through the cell. The catholyte reservoir was fitted with a sparger and a fast stream air or oxygen was passed throughout each electrolysis. They demonstrated that electrogenerated H₂O₂ in the presence of Fe²⁺ is an aggressive oxidant in aqueous solutions at pH 2. They destroyed a number of aromatic molecules including phenol, cresol, catechol, quinone, hydroquinone, aniline, oxalic acid, and the azo dye present in solution. In all cases studied, the COD was reduced from 50–500 ppm to below 10 ppm, generally with a current efficiency >50%.

Fig. 7 Sketches of (a) the flow cell with RVC cathode and (b) the flow circuit.

Reprinted from Ref. [117], Copyright 1998, with permission from Elsevier



4 Moving Three-Dimensional Electrodes

A three-dimensional electrode is attractive in industrial applications over a two-dimensional electrode, for its larger active surface area per unit volume, even if not all the area is available for the electrochemical process. There are many types of three-dimensional electrodes, including graphite fiber and cloth, metal and carbon foams (reticulates), and particulate bed of carbon granules. When small particles are polarized in a three-dimensional electrode reactor, they form charged microelectrodes with a short distance between the reactant and the electrode thereby resulting in higher efficiency.

However, fluidized or moving-bed electrodes still present some problems of bed agglomeration, poor bed-feeder contact, and nonuniform current and potential distribution, and therefore only few works used these reactors for electro-Fenton oxidation [124–128].

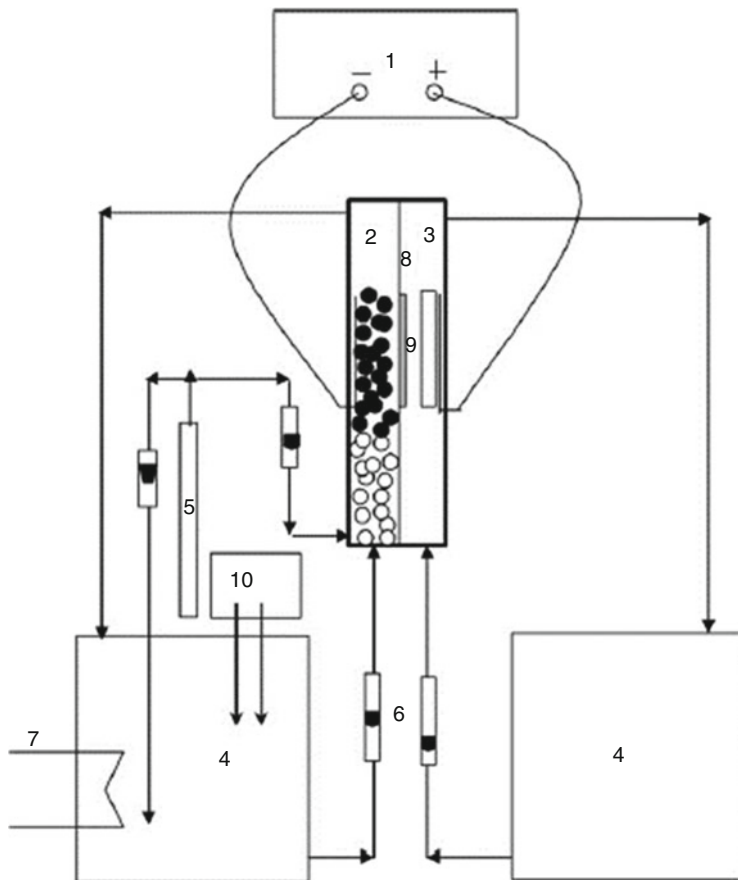


Fig. 8 Sketch of the experimental setup used for the removal of color. (1) Power supply, (2) cathodic chamber, (3) anodic chamber, (4) reservoir, (5) oxygen cylinder, (6) valves, (7) heat exchanger, (8) separator, (9) membrane, (10) pH controller, *filled circle* graphite rings, *open circle* glass beads. Reprinted from Ref. [125], Copyright 2008, with permission from Elsevier

Figure 8 schematically depicts the fluidized bed used by Wang et al. [125] for the removal of color from wastewater that contains low dyestuff concentrations by the electro-Fenton process.

The cell was made of 0.2 cm thick acrylic material ($15 \times 5 \times 5$ cm), and it was divided by a Nafion[®] 417 membrane. The cathodic chamber was packed randomly with 50 graphite Raschig rings with a total surface area of 220 cm^2 for use as the three-dimensional cathode, and the anode used was a Pt/Ti plate ($8 \times 2 \times 1$ cm). Two titanium plates were used as current feeders. Small glass beads were packed at the bottom of the cathodic chamber to increase the uniformity of the flow velocity distribution. The catholyte and anolyte solutions have a volume of 1.5 dm^3 , and they were introduced into the bottom of the cell, flowed out of the top, and returned to the reservoir. The oxygen was bubbled into the bottom of the cathodic. Using this

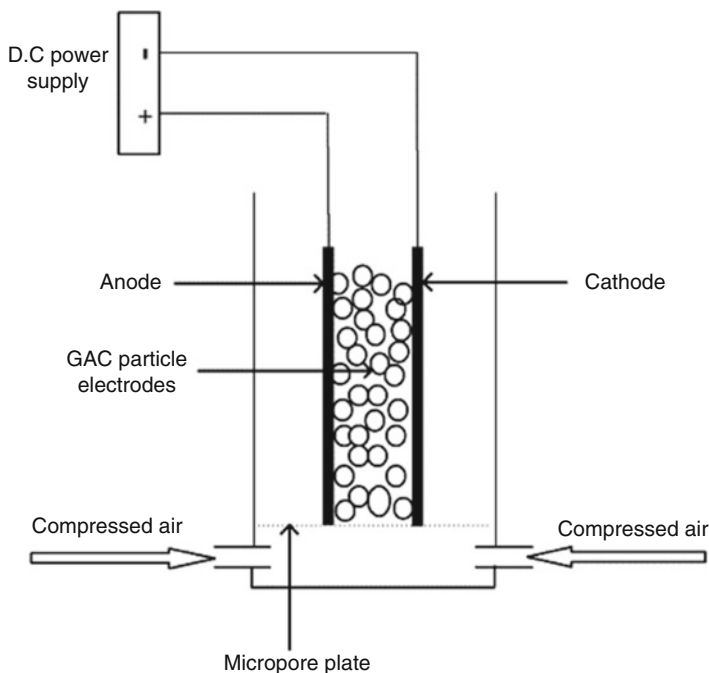


Fig. 9 Schematic diagram of the three-dimensional electrode reactor used for the treatment of C.I. acid orange 7. Reprinted from Ref. [126], Copyright 2008, with permission from Elsevier

reactor configuration, Wang et al. [125] reported that the removal efficiency of the color in the cathodic chamber reached 70.6% in 150 min working at the optimal applied current density of 68 A m^{-2} , adding 20 mM Fe^{2+} to the solution and at pH 3. In this case, the energy consumption was 20 kWh m^{-3} .

Another three-electrode configuration was proposed by Xu et al. [126] (Fig. 9). The reactor was made up of an undivided 1.0 dm^3 volume cylindrical glass tank with a stainless steel plate as anode and an activated carbon fiber (ACF) as cathode. Both anode and cathode were $7 \times 5 \text{ cm}$ in size and were situated 3 cm from each other. Granular activated carbon (50.0 g) with a specific surface area of $910 \text{ m}^2 \text{ g}^{-1}$ and an average pore diameter of 2.10 nm were packed between the cathode and anode to form a three-dimensional electrode.

A microporous plate attached to the lower part of the tank was used to support the particle electrode and disperse bubbles that arose from the compressed air sparged from the bottom. They used this cell for the treatment of a simulated wastewater containing the monoazo dye acid orange 7. After 180 min electrolysis at 20 V, almost the complete decolorization of the dye was secured, with a COD and TOC removal 80% and 72%, respectively. They reported that more hydroxyl radicals were generated in the three-dimensional electrode system than in the two-dimensional one, because of the formation of many microelectrodes, by means of which, the distance between the reactant and the electrode can be

shortened thereby increasing, greatly, the specific surface area of the electrode, resulting in higher electrolytic efficiency.

5 Pressurized Reactors

When an electrochemical process deals with gaseous reagents that present low solubility in the adopted solvent at atmospheric pressure, the performances of the process can be adversely affected by slow kinetics and mass transfer limitations. In these cases, the utilization of pressurized electrochemical reactors can be attractive for industrial applications, in order to enhance the solubility of the reagents. As an example, the reduction of carbon dioxide to formic acid at a tin cathode in water was dramatically improved using pressurized CO_2 in the range 3–30 bar [129–131]. In an undivided cell a maximum concentration lower than 50 mM (with a faradaic efficiency FE close to 30%) was achieved after 6 h at 1 bar [131]. The utilization of pressurized CO_2 allowed to increase drastically the operating current density, the faradic efficiency, and the final concentration of formic acid: as an example, a generation of formic acid of 0.42 M (with a FE close to 30%) was achieved at 30 bar and 75 mA cm^{-2} [131]. The utilization of pressurized reactors is particularly convenient from an economic point of view for pressures up to 20 bar. Indeed, for these values of the pressure, very small increases of operating and investment costs are expected at an industrial level with respect to that involved at atmospheric pressure [132].

In electro-Fenton, the performances of the process are affected by the very low solubility of oxygen in water (about 40 or 8 mg dm^{-3} in contact with pure oxygen or air, respectively, at 1 atm and $25 \text{ }^\circ\text{C}$ [133]). Thus, two-dimensional cheap graphite electrodes give slow generation of H_2O_2 , resulting in low H_2O_2 bulk concentrations. Hence, these electrodes were often considered not to be adequate for electro-Fenton process. As above mentioned, a possible strategy could be the adoption of three-dimensional or gas diffusion electrodes. An alternative strategy consists in the utilization of pressurized air or oxygen.

The group of Scialdone investigated the effect of air pressure on both the electrogeneration of hydrogen peroxide and the treatment of a synthetic wastewater contaminated by acid orange 7 (AO7), a largely used azoic dye [134], at cheap compact graphite cathodes. Electrolyses were performed in an undivided high-pressure AISI 316 stainless steel cell (that can be operated up to more than 100 bar) with a coaxial cylindrical geometry, equipped with a gas inlet, a $\text{Ti/IrO}_2\text{-Ta}_2\text{O}_5$ anode, a graphite cathode, and a magnetic stir bar (Fig. 10).

The electrolysis of 0.050 dm^{-3} of 35 mM Na_2SO_4 solutions (at pH 3.0 by addition of H_2SO_4) at $25 \text{ }^\circ\text{C}$ and 80 mA was performed at various pressures to evaluate the effect of the pressure on the generation of H_2O_2 in the absence of the iron catalyst and of pollutants. It was found that an enhancement of the air pressure gave rise to a drastic increase of the generation of hydrogen peroxide (Fig. 11): after 2 h, a concentration of H_2O_2 of about 1 and 12 mM was obtained at 1 and 12 bar,

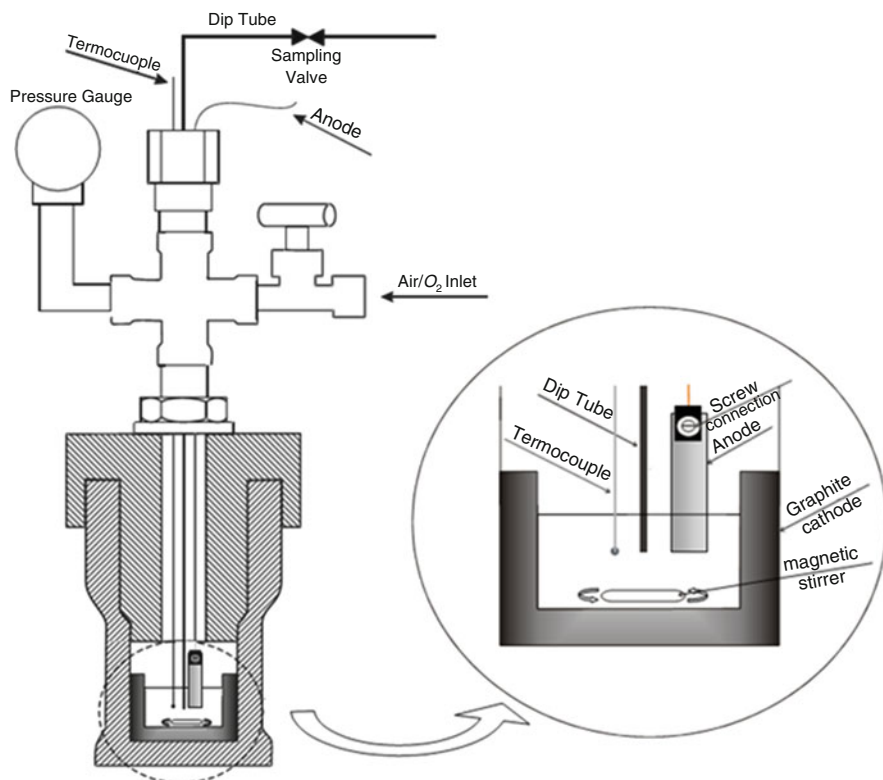


Fig. 10 Schematic diagram of the pressurized cell used for the electrogeneration of H_2O_2 and the treatment of acid orange 7. Reprinted from Ref. [134], Copyright 2015, with permission from Elsevier

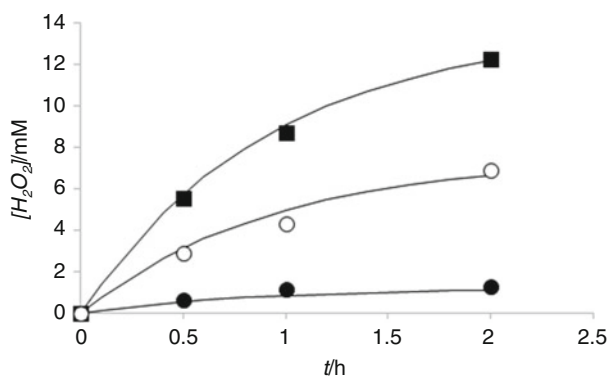
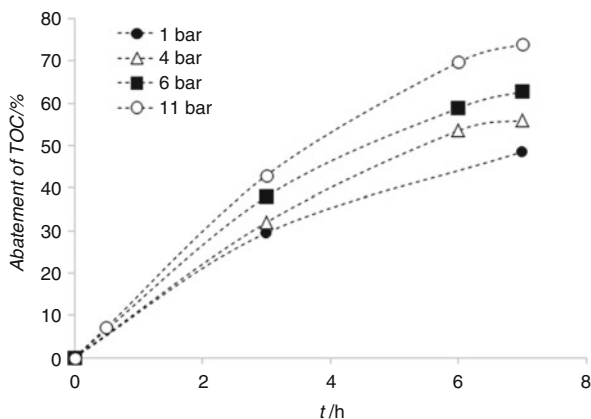


Fig. 11 Evolution of the concentration of H_2O_2 during the electrolysis of 0.050 dm^{-3} of $35 \text{ mM Na}_2\text{SO}_4$ solutions (pH 3.0) at 25°C and 80 mA and various air pressures: 1 (filled circle), 6 (o), and 11 (filled square) bar. Reprinted from Ref. [134], Copyright 2015, with permission from Elsevier

Fig. 12 Abatement of TOC during the electrolysis of 0.050 dm^{-3} of $35 \text{ mM Na}_2\text{SO}_4$, 0.5 mM FeSO_4 , and 0.43 mM AO7 aqueous solutions (pH 3.0) at 18°C and 100 mA at compact graphite cathode at various air pressures. Anode: $\text{Ti}/\text{IrO}_2\text{-Ta}_2\text{O}_5$. Reprinted from Ref. [134], Copyright 2015, with permission from Elsevier



respectively, because of the increase of the oxygen dissolved in water (close to 8 and 96 mg dm^{-3} at 1 and 12 bar, respectively).

To evaluate the effect of the pressure on electro-Fenton process, the electrolysis of aqueous solutions of $35 \text{ mM Na}_2\text{SO}_4$, 0.5 mM FeSO_4 , and 0.43 mM AO7 (pH 3.0) was performed at 18°C and 100 mA at compact graphite cathode at various air pressures (1, 4, 6, and 11 bar).

As shown in Fig. 12, the utilization of higher pressures allowed to achieve drastically higher abatements of TOC, reasonably because the enhanced H_2O_2 generation. In particular, an increase of the pressure from 1 to 6 bar allowed to enhance the abatement of the TOC after 7 h from 48 to 63%. A further increase of the pressure to 11 bar gave an abatement of the TOC of about 74%.

It is useful to observe that the applicative utilization of electrochemical processes for the treatment of wastewater is up to now often limited by the energetic costs. It is worth mentioning that the utilization of higher pressures allowed also to increase the current efficiency of the process and to decrease the cell potential. Hence, the energy consumptions of the electrolysis were strongly reduced. The overall energy consumptions, including both that of the electrolysis and of air compression, were estimated [134]. It was found that an increase of the pressure from 1 to 12 bar allowed to decrease the overall energy consumption from 3.8 to about $2 \text{ kWh g}^{-1} \text{ TOC}$ [134].

6 Microreactors

In the last years, microfluidic technology has been successfully adopted for analytical and synthetic purposes in various areas such as the food, the pharmaceutical, and the chemical industries [135]. In particular, chemical reactions performed in suitable microfluidic devices can benefit of enhanced heat and mass transfer, higher product yield, selectivity and purity, improved safety, access to new products, and

quite easy scale-up or modularization of the processes [135]. Electrochemical microfluidic devices were widely employed in the last years for analytical [136] and preparative purposes [137–140] or to evaluate chemical-physical parameters such as diffusion coefficients and kinetic rate constants. Furthermore, in the last years, electrochemical microfluidic cells were successfully used for the treatment of wastewaters contaminated by organic pollutants resistant to conventional biological processes, by various processes including direct electrochemical oxidation, direct cathode reduction, electro-Fenton, and coupled processes [141–148].

Microfluidic electrochemical devices are characterized by very small distances between electrodes of tens or few hundreds of micrometers. For analytical purposes, microfluidic channels with very low volumes are used, thus allowing to minimize the volume of the samples. This requires the minimization of both the distance between the electrodes and of the surface of the electrodes. In contrast, microfluidic electrochemical devices for preparative purposes and for wastewater treatment require normal surfaces of the electrodes (from cm^2 for studies in the lab to dm^2 – m^2 for real applications) in order to treat large volumes; hence, only the distance between the electrodes is minimized.

Various kinds of microfluidic devices can be used. As an example, the group of Scialdone used two different kinds of devices [139, 140].

The first microreactor (microreactor I in Fig. 13a) consists in a commercial undivided filter-press flow cell equipped with one or more PTFE spacers (with a nominal thickness of 50–250 μm). This device can be easily and quickly assembled and disassembled at the laboratory scale, thus allowing fast screening of the effect of operating parameters on the process, such as the interelectrode distance and the nature of the electrodes. This device can be assembled with very low interelectrode distances (e.g., 50 μm) and significant surface areas (e.g., 5 cm^2) and a large set of solvents and electrodes.

The second device (microreactor II in Fig. 13b) was prepared with a procedure, adapted in part from approaches used in microelectronics, involving micro-milled adhesive spacers to implement microchannels and a press to provide a good adhesion between the spacers and the electrodes, which could be easily scaled up on an industrial scale.

The utilization of microfluidic devices offers various advantages for the wastewater treatment with respect to conventional macro devices [140–148]:

- Very small distances between electrodes lead to a drastic reduction of the ohmic resistances, thus allowing electrochemical abatement of organic pollutants with lower cell potentials and without supporting electrolyte. This aspect is of particular importance for wastewater with low conductivity (e.g., aqueous solutions coming from soil vapor extraction) which would require in conventional cells the addition of a supporting electrolyte with a dramatic increase of the operative costs.
- The small interelectrode distance gives rise to the intensification of the mass transport of the pollutants to electrodes surfaces, which enhances the current efficiencies and decreases the durations of treatment, since mass transfer rates

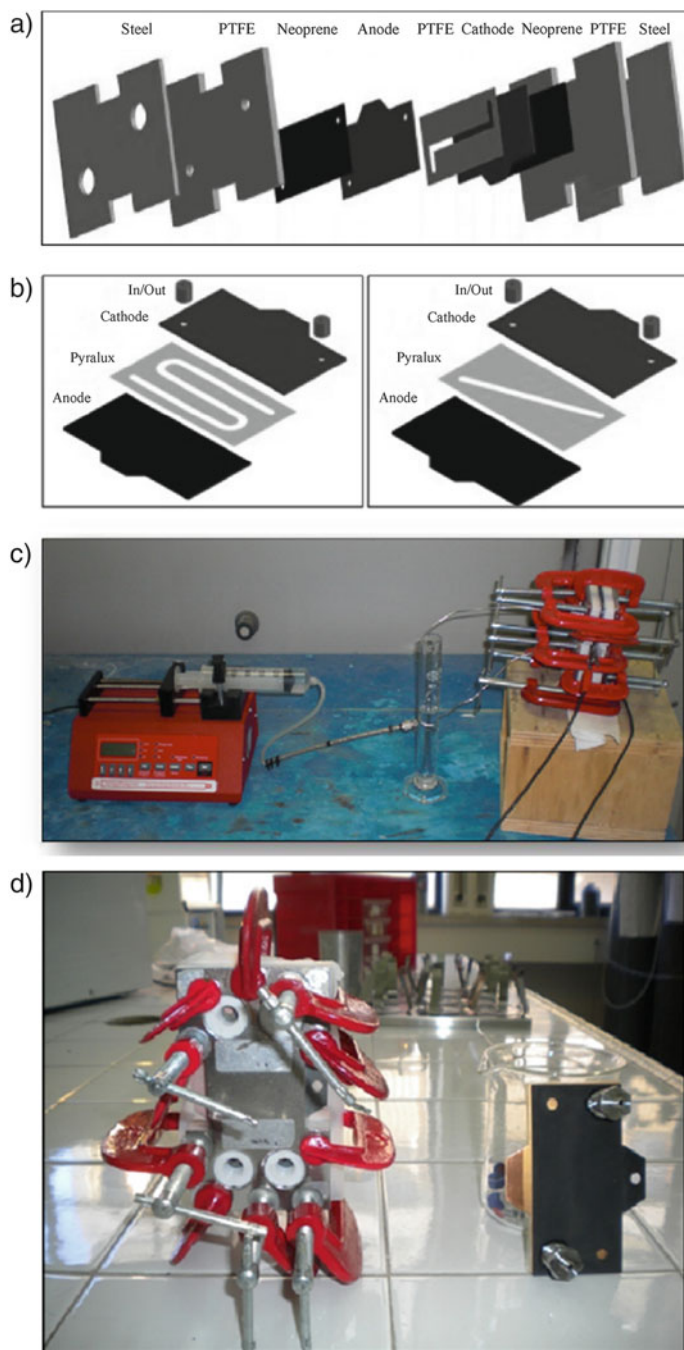


Fig. 13 Scheme and photos of two microreactors: (a) microreactor I; (b) microreactor II; (c) system with pump, microreactor I, and tubing; (d) photo of the devices (microreactor I on the *left* and microreactor II on the *right*). Reprinted from Ref. [139], Copyright 2014, with permission from Wiley

toward electrodes are usually extremely reduced at the low pollutant concentrations required by regulations [143].

- The small distances between electrodes allow very high conversions of the organic pollutants for a single passage of the water solution inside the cell, thus allowing continuous operations. The possibility to operate in a continuous mode potentially allows the utilization of a multistage system involving two or more cells operating in series with different processes and/or applied current densities in order to maximize the current efficiency and to minimize the treatment times [148].
- Fast screening of the effect of operative parameters. As a consequence of the very short treatment times, a screening of the effect of operative parameters on the performances of the process can be performed in short times by fast changing of the steady-state conditions in comparison to conventional macro-systems that must operate in batch recycling mode [145].
- Easier scale-up procedure through simple parallelization of many small units.

However, the utilization of microdevices presents also some potential drawbacks such as an easier fouling and clogging.

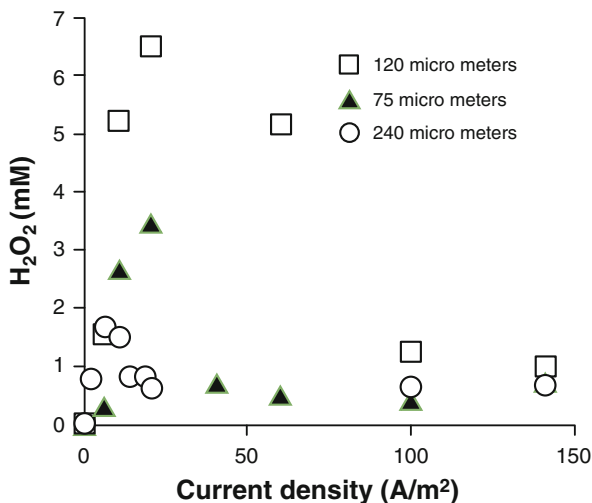
The electrogeneration of H_2O_2 and the abatement of the model organic pollutant acid orange 7 (AO7) in water by an electro-Fenton process were performed both in a microfluidic reactor (microreactor I in Fig. 13) and in a conventional undivided glass macro-cell (with magnetic stirring) for the sake of comparison [144]. The reduction of oxygen (with air at atmospheric pressure) at compact graphite in an aqueous solution of sodium sulfate resulted in the conventional lab glass cell in concentrations of H_2O_2 close to 0.6 mM. Under optimized operative conditions (interelectrode distance 120 μm , current density in the range 1–2 mA cm^{-2} , corresponding to 10–20 A m^{-2}), the micro-device gave rise to a concentration of H_2O_2 of about 6 mM, one order of magnitude higher than that achieved in the conventional macro-cell (Fig. 14).

To explain the higher concentrations of hydrogen peroxide achieved in the microreactor, one has to consider that in the micro-cell a large part of the oxygen formed at the anode is approximately uniformly distributed in the form of discrete bubbles in all the liquid phase [149, 150]. Hence, the concentration of oxygen should be close to its solubility also in the proximity of the cathode surface, thus giving rise to an overall faster mass transfer of oxygen to the cathode surface with respect to that achieved in a conventional cell.

It is worth mentioning that the microfluidic cell operated in the absence of a flux of air, using the oxygen naturally dissolved in water and that generated by the anodic oxidation of water.

Some experiments were performed in the micro-cell changing the interelectrode distance h (75, 120, and 240 μm). The maximum concentration of H_2O_2 was achieved for $h = 120 \mu\text{m}$. Lower h is expected to result in a more uniform distribution of oxygen in the cell, thus favoring the generation of H_2O_2 formation, and also in faster mass transport rate of H_2O_2 to the anode surface with consequent

Fig. 14 Concentration of H_2O_2 achieved by the electrolysis of a water solution of H_2SO_4 (pH 3.0) at 25 °C using a microreactor with a graphite cathode at various current densities and interelectrode distances h of 75 (filled triangle), 120 (open square) and 240 (open circle) μm . Reprinted from Ref. [144], Copyright 2013, with permission from Elsevier



faster consumption of H_2O_2 by its anodic oxidation to oxygen. Conversely, too high h result in a less effective mass transfer of oxygen to the cathode surface [144].

Experiments were repeated in the presence of iron (II) and of acid orange 7 (AO7) as model organic pollutant in order to evaluate the electro-Fenton process in both a conventional macro-lab cell and in a micro-device [144]. In the conventional macro-cell equipped with compact graphite or carbon-felt cathode and $\text{Ti}/\text{IrO}_2\text{-Ta}_2\text{O}_5$ anode, a slow abatement of COD took place during the electro-Fenton of the water solution of AO7 (Fig. 15). The utilization of a microreactor with $h = 120 \mu\text{m}$ with compact graphite cathode gave drastically higher abatements of COD (Fig. 15). As an example, after about 9 h, the abatement of COD was lower than 35% for the conventional cell and between 44 and 76% for the micro-cell depending on the adopted current density. Furthermore, the cell potential in the microreactor (2.1–2.5 V) in the presence of the sole H_2SO_4 (to have a pH of 3) was significantly lower than that recorded in the conventional cell with Na_2SO_4 (>3.0 V).

According to the literature, the degradation of organic compounds by electro-Fenton results in the formation of more resistant carboxylic acids. The higher resistance of carboxylic acid is due to the formation of complexes with the homogeneous iron catalyst. However, the utilization of microfluidic cells gives rise to a drastic reduction of the final concentration of carboxylic acids and of other oxidation by-products [145].

The electrochemical treatment of water solutions of AO7 was carried out in microdevices also using a BDD anode with a compact graphite cathode and Fe^{2+} catalyst in order to achieve the simultaneous degradation by anodic oxidation and EF. This coupled process gave higher abatements of COD with respect to the sole EF with $\text{DSA}^{\text{®}}$ anode or the sole anodic oxidation at BDD (in the absence of iron catalyst) at all adopted distances between the electrodes (50, 75, 120, and 240 μm).

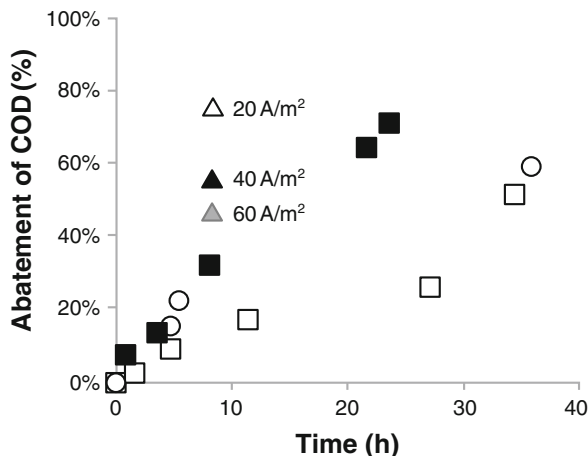


Fig. 15 Abatement of COD vs. time of treatment for a solution of 0.050 dm^{-3} of AO7 (0.43 mM) and 0.5 mM FeSO_4 at a $\text{pH} = 3$. Anode: $\text{Ti}/\text{IrO}_2\text{-Ta}_2\text{O}_5$. Experiments performed in conventional cell with Na_2SO_4 0.035 M at graphite [at 60 (open square) and 100 A m^{-2} (open circle)] and carbon-felt (filled square) cathode and in a micro-cell without supporting electrolyte at compact graphite cathode with $h = 120 \mu\text{m}$ at 20 (open triangle), 40 (filled triangle) and 60 (grey triangle) A m^{-2} . Reprinted from Ref. [144], Copyright 2013, with permission from Elsevier

As an example, for experiments performed with a nominal distance between the electrodes of $50 \mu\text{m}$ at flow rate of $0.3 \text{ dm}^{-3} \text{ min}^{-1}$ and at density current of 40 A/m^2 , the removal of COD was slightly higher than 80% for the sole anodic oxidation at BDD, close to 40% for EF and higher than 90% for the coupled process. However, the performances of the coupled processes strongly depended on the interelectrode distance: the higher abatements of COD were achieved at both 50 and $120 \mu\text{m}$, while lower ones were recorded at both 75 and $240 \mu\text{m}$ [145]. These results are due to the fact that the anodic oxidation at BDD is favored from the lower interelectrode distances, while EF process gave best results using an intermediate distance of $120 \mu\text{m}$. Quite interestingly, when experiments were carried out with $h = 50 \mu\text{m}$, best results were achieved at higher current densities that favor the direct anodic oxidation process; conversely, for $h = 120 \mu\text{m}$, higher abatements of COD were obtained by working with the low current densities that optimize the EF process (e.g., close to 40 A m^{-2}) [145].

Hence, it is possible to conclude that even if the coupling of EF and direct anodic oxidation at BDD gave better results than the single processes, the optimization of this coupled process is difficult because EF and direct anodic oxidation require different optimal operating conditions.

Another possible strategy to benefit from both EF and direct anodic oxidation consists in the utilization of microreactors in series, which offers the possibility to optimize the operating conditions for each adopted process. The utilization of reactors in series is facilitated by the adoption of microfluidic devices, which

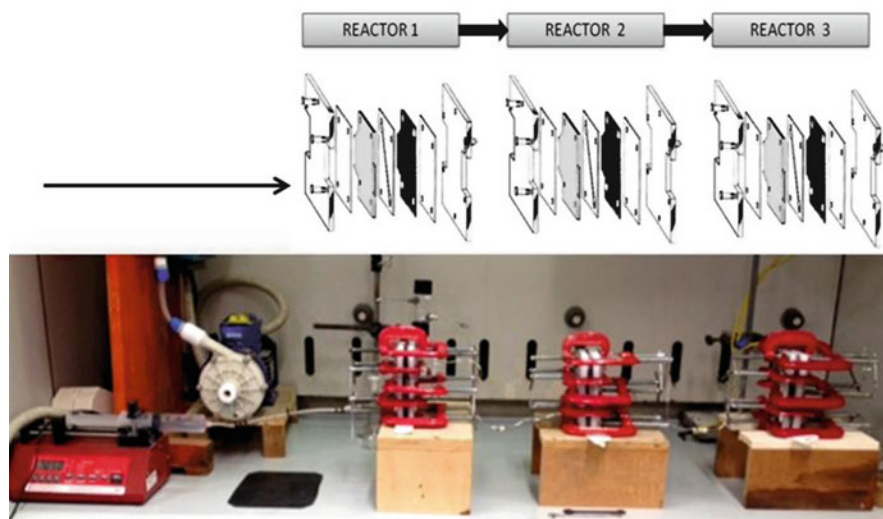


Fig. 16 Scheme and photo for the utilization of three micro-reactors in series. Reprinted from Ref. [148], Copyright 2016, with permission from Wiley

allow high removal of pollutants for a single passage inside the cell and, as a consequence, continuous operations.

EF is characterized by lower energetic consumptions (EC) and cheaper electrodes but lower mineralization of organic pollutants with respect to direct anodic oxidation (EO) at BDD. Hence, in order to synergize the different characteristics of these processes, Sabatino et al. [148] have studied the utilization of two (or three microreactors) in series (Fig. 16) with the following approach:

- In the first reactor (Fig. 16), the wastewater was treated by EF with the aim to reduce the TOC content with low EC and cheap electrodes.
- In the last reactor, the wastewater was treated by EO with the aim to achieve the degradation of organics formed in EF and complete the mineralization.

In particular, here for the sake of brevity, we will recall only the experiments performed with two reactors in series. Since these two processes are optimized under very different conditions (see above), different operating conditions were set for the two reactors (the first and the second put in series). In particular, a nominal distance between the electrodes of 120 and 50 μm was used for the reactors devoted to EF and EO, respectively. By a proper differentiation of current densities (2 and 20 mA cm^{-2} in the first and in the second reactor), it was possible to achieve both high TOC removal and moderate energetic consumptions (Fig. 17). Under these conditions, both processes were fully exploited:

- The first microreactor devoted to EF, equipped with cheap electrodes, presents low investment costs and operating ones, due to the low energetic consumptions,

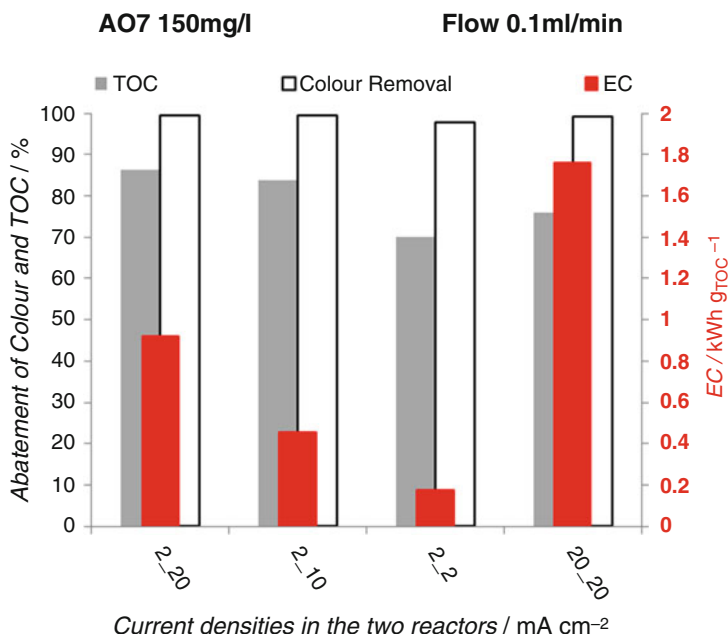


Fig. 17 Effect of current density on the abatement of color, TOC and energy consumptions (*EC*) for two microreactors in series. First reactor was devoted to EF at graphite cathode, with a nominal distance between the electrodes of 120 μm . Second reactor was devoted to the anodic oxidation at BDD anode, with a nominal distance between the electrodes of 50 μm . Reprinted from Ref. [148], Copyright 2016, with permission from Wiley

and allowed to reduce significantly the TOC content with the formation of some by-products, such as hydroquinone, oxalic, and maleic acids.

- Afterward, the solution passed in the second microreactor devoted to EO with BDD, which presents higher investment and operating costs, due to the high cost of BDD and to the higher cell potential. The second reactor allowed to increase the final abatement of TOC, since it was able to remove the by-products generated by EF.

The pretreatment with EF, reducing the TOC content, allowed to use limited BDD surfaces and passed charge, reducing the overall cost of EO. It is worth mentioning that the utilization of the two processes in series gave higher abatement and lower energetic consumptions than that achievable by each single process.

7 Conclusions

In recent years, a large variety of reactors and cells were used for the treatment of wastewater by electro-Fenton. The main kinds of cells used can be grouped as follows:

- Simple batch reactors were widely used for lab experiments and equipped with various kinds of three-dimensional and gas diffusion electrodes, thus allowing to evaluate the performances of EF process for the treatment of various wastewaters and a large number of organic pollutants and to evaluate the effect of various operating parameters.
- Since industrial electrochemical processes are usually based on the parallel-plate electrode configuration, many experiments were also performed using this kind of cells. The system based on the parallel-plate cell in a recirculation mode can be also slightly modified to perform photoelectro-Fenton and solar photoelectro-Fenton irradiating the solution by a UV lamp or solar light when it is recirculated from the reactor to the reservoir.
- Floating or rotating three-dimensional electrodes were sometimes used to increase the mass transfer kinetics. However, these electrodes still present some problems of poor bed-feeder contact, nonuniform current and potential distribution and therefore only few works used these reactors for electro-Fenton oxidation.
- Recently, it has been shown that using pressurized reactors, it is possible to increase drastically the generation of hydrogen peroxide from the cathodic reduction of oxygen and, therefore, the abatement of TOC in the treatment of wastewater by EF. In addition, the utilization of pressures up to 15–20 bar allows also to limit the investment and operating costs. Hence, the utilization of pressurized reactors seems very appealing from an applicative point of view. However, further studies are necessary to better characterize the utilization of such devices and in order to evaluate the adoption of both pressurized cells and cathodes with large surfaces.
- Micro-cells, characterized by very small distances between the electrodes, were also used for EF process. It was demonstrated that these kinds of cells can present various advantages, such as the possibility to work with wastewater with low conductivity, to enhance the H_2O_2 generation and the abatement of the TOC also using cheap compact graphite cathodes, and to work under continuous mode. However, these devices present the disadvantage of an easier fouling and clogging. Hence, their utilization could be particularly suggested for wastewater with low conductivity and low solid contents.

References

1. Pletcher D, Walsh FC (1990) Industrial electrochemistry. Chapman & Hall, London
2. Panizza M, Cerisola G (2001) Removal of organic pollutants from industrial wastewater by electrogenerated Fenton's reagent. *Water Res* 35:3987–3992
3. Oturan N, Panizza M, Oturan MA (2009) Cold incineration of chlorophenols in aqueous solution by advanced electrochemical process electro-Fenton. Effect of number and position of chlorine atoms on the degradation kinetics. *J Phys Chem A* 113:10988–10993
4. Panizza M, Cerisola G (2009) Electro-Fenton degradation of synthetic dyes. *Water Res* 43:339–344
5. Panizza M, Oturan MA (2011) Degradation of alizarin red by electro-Fenton process using a graphite-felt cathode. *Electrochim Acta* 56:7084–7087
6. Elaoud SC, Panizza M, Cerisola G, Mhiri T (2012) Coumaric acid degradation by electro-Fenton process. *J Electroanal Chem* 667:19–23
7. Zazou H, Oturan N, Sönmez-Çelebi M, Hamdani M, Oturan MA (2016) Mineralization of chlorobenzene in aqueous medium by anodic oxidation and electro-Fenton processes using Pt or BDD anode and carbon felt cathode. *J Electroanal Chem* 774:22–30
8. Barhoumi N, Labiadh L, Oturan MA, Oturan N, Gadri A, Ammar S, Brillas E (2015) Electrochemical mineralization of the antibiotic levofloxacin by electro-Fenton-pyrite process. *Chemosphere* 141:250–257
9. Olvera-Vargas H, Oturan N, Brillas E, Buisson D, Esposito G, Oturan MA (2014) Electrochemical advanced oxidation for cold incineration of the pharmaceutical ranitidine: mineralization pathway and toxicity evolution. *Chemosphere* 117:644–651
10. Loaiza-Ambuludi S, Panizza M, Oturan N, Özcan A, Oturan MA (2013) Electro-Fenton degradation of anti-inflammatory drug ibuprofen in hydroorganic medium. *J Electroanal Chem* 702:31–36
11. Zhou M, Tan Q, Wang Q, Jiao Y, Oturan N, Oturan MA (2012) Degradation of organics in reverse osmosis concentrate by electro-Fenton process. *J Hazard Mater* 215–216:287–293
12. Oturan MA, Oturan N, Edelahi MC, Podvorica FI, Kacemi KE (2011) Oxidative degradation of herbicide diuron in aqueous medium by Fenton's reaction based advanced oxidation processes. *Chem Eng J* 171:127–135
13. Sirés I, Oturan N, Oturan MA (2010) Electrochemical degradation of β -blockers. Studies on single and multicomponent synthetic aqueous solutions. *Water Res* 44:3109–3120
14. Özcan A, Oturan MA, Oturan N, Şahin Y (2009) Removal of acid orange 7 from water by electrochemically generated Fenton's reagent. *J Hazard Mater* 163:1213–1220
15. Sirés I, Oturan N, Oturan MA, Rodríguez RM, Garrido JA, Brillas E (2007) Electro-Fenton degradation of antimicrobials triclosan and triclocarban. *Electrochim Acta* 52:5493–5503
16. Oturan MA, Guivarch E, Oturan N, Sirés I (2008) Oxidation pathways of malachite green by Fe^{3+} -catalyzed electro-Fenton process. *Appl Catal B-Environ* 82:244–254
17. Sirés I, Garrido JA, Rodríguez RM, Brillas E, Oturan N, Oturan MA (2007) Catalytic behavior of the $\text{Fe}^{3+}/\text{Fe}^{2+}$ system in the electro-Fenton degradation of the antimicrobial chlorophene. *Appl Catal B-Environ* 72:382–394
18. Zhou M, Yu Q, Lei L, Barton G (2007) Electro-Fenton method for the removal of methyl red in an efficient electrochemical system. *Sep Purif Technol* 57:380–387
19. Zhou L, Zhou M, Zhang C, Jiang Y, Bi Z, Yang J (2013) Electro-Fenton degradation of p-nitrophenol using the anodized graphite felts. *Chem Eng J* 233:185–192
20. Zhou L, Zhou M, Hu Z, Bi Z, Serrano KG (2014) Chemically modified graphite felt as an efficient cathode in electro-Fenton for p-nitrophenol degradation. *Electrochim Acta* 140:376–383
21. Zhang C, Zhou M, Yu X, Ma L, Yu F (2015) Modified iron-carbon as heterogeneous electro-Fenton catalyst for organic pollutant degradation in near neutral pH condition: characterization, degradation activity and stability. *Electrochim Acta* 160:254–262

22. Zhang C, Zhou M, Ren G, Yu X, Ma L, Yang J, Yu F (2015) Heterogeneous electro-Fenton using modified iron-carbon as catalyst for 2,4-dichlorophenol degradation: influence factors, mechanism and degradation pathway. *Water Res* 70:414–424
23. Mejjide J, Gómez J, Pazos M, Sanromán MA (2016) Degradation of thiamethoxam by the synergetic effect between anodic oxidation and Fenton reactions. *J Hazard Mater* 319:43–50
24. Iglesias O, Gómez J, Pazos M, Sanromán MÁ (2014) Electro-Fenton oxidation of imidacloprid by Fe alginate gel beads. *Appl Catal B-Environ* 144:416–424
25. Iglesias O, Mejjide J, Bocos E, Sanromán MÁ, Pazos M (2015) New approaches on heterogeneous electro-Fenton treatment of winery wastewater. *Electrochim Acta* 169:134–141
26. Brillas E, Mur E, Sauleda R, Sánchez L, Peral J, Domènech X, Casado J (1998) Aniline mineralization by AOP's: anodic oxidation, photocatalysis, electro-Fenton and photoelectro-Fenton processes. *Appl Catal B-Environ* 16:31–42
27. Sauleda R, Brillas E (2001) Mineralization of aniline and 4-chlorophenol in acidic solution by ozonation catalyzed with Fe^{2+} and UVA light. *Appl Catal B-Environ* 29:135–145
28. Brillas E, Boye B, Sirés I, Garrido JA, RMa Rodríguez, Arias C, P-LS C, Comninellis C (2004) Electrochemical destruction of chlorophenoxy herbicides by anodic oxidation and electro-Fenton using a boron-doped diamond electrode. *Electrochim Acta* 49:4487–4496
29. Brillas E, P-LS C, RMa Rodríguez, Arias C, Garrido JA, Oliver R (2004) Degradation of the herbicide 2,4-DP by catalyzed ozonation using the $\text{O}_3/\text{Fe}^{2+}/\text{UVA}$ system. *Appl Catal B-Environ* 51:117–127
30. Brillas E, Calpe JC, Cabot P-L (2003) Degradation of the herbicide 2,4-dichlorophenoxyacetic acid by ozonation catalyzed with Fe^{2+} and UVA light. *Appl Catal B-Environ* 46:381–391
31. Brillas E, Baños MÁ, Skoumal M, Cabot PL, Garrido JA, Rodríguez RM (2007) Degradation of the herbicide 2,4-DP by anodic oxidation, electro-Fenton and photoelectro-Fenton using platinum and boron-doped diamond anodes. *Chemosphere* 68:199–209
32. Flox C, Garrido JA, Rodríguez RM, Cabot P-L, Centellas F, Arias C, Brillas E (2007) Mineralization of herbicide mecoprop by photoelectro-Fenton with UVA and solar light. *Catal Today* 129:29–36
33. Flox C, Ammar S, Arias C, Brillas E, Vargas-Zavala AV, Abdelhedi R (2006) Electro-Fenton and photoelectro-Fenton degradation of indigo carmine in acidic aqueous medium. *Appl Catal B-Environ* 67:93–104
34. Garcia-Segura S, Centellas F, Arias C, Garrido JA, Rodríguez RM, Cabot PL, Brillas E (2011) Comparative decolorization of monoazo, diazo and triazo dyes by electro-Fenton process. *Electrochim Acta* 58:303–311
35. Almeida LC, Garcia-Segura S, Arias C, Bocchi N, Brillas E (2012) Electrochemical mineralization of the azo dye acid red 29 (Chromotrope 2R) by photoelectro-Fenton process. *Chemosphere* 89:751–758
36. Garcia-Segura S, El-Ghenymy A, Centellas F, Rodríguez RM, Arias C, Garrido JA, Cabot PL, Brillas E (2012) Comparative degradation of the diazo dye direct yellow 4 by electro-Fenton, photoelectro-Fenton and photo-assisted electro-Fenton. *J Electroanal Chem* 681:36–43
37. Garcia-Segura S, Dosta S, Guilemany JM, Brillas E (2013) Solar photoelectrocatalytic degradation of acid orange 7 azo dye using a highly stable TiO_2 photoanode synthesized by atmospheric plasma spray. *Appl Catal B-Environ* 132–133:142–150
38. Florenza X, Solano AMS, Centellas F, Martínez-Huitle CA, Brillas E, Garcia-Segura S (2014) Degradation of the azo dye Acid Red 1 by anodic oxidation and indirect electrochemical processes based on Fenton's reaction chemistry. Relationship between decolorization, mineralization and products. *Electrochim Acta* 142:276–288
39. Pereira GF, El-Ghenymy A, Thiam A, Carlesi C, Eguiluz KIB, Salazar-Banda GR, Brillas E (2016) Effective removal of Orange-G azo dye from water by electro-Fenton and

- photoelectro-Fenton processes using a boron-doped diamond anode. *Sep Purif Technol* 160:145–151
40. Guinea E, Garrido JA, Rodríguez RM, Cabot P-L, Arias C, Centellas F, Brillas E (2010) Degradation of the fluoroquinolone enrofloxacin by electrochemical advanced oxidation processes based on hydrogen peroxide electrogeneration. *Electrochim Acta* 55:2101–2115
 41. Garcia-Segura S, Cavalcanti EB, Brillas E (2014) Mineralization of the antibiotic chloramphenicol by solar photoelectro-Fenton: From stirred tank reactor to solar pre-pilot plant. *Appl Catal B-Environ* 144:588–598
 42. Moreira FC, Garcia-Segura S, Boaventura RAR, Brillas E, Vilar VJP (2014) Degradation of the antibiotic trimethoprim by electrochemical advanced oxidation processes using a carbon-PTFE air-diffusion cathode and a boron-doped diamond or platinum anode. *Appl Catal B-Environ* 160–161:492–505
 43. Antonin VS, Santos MC, Garcia-Segura S, Brillas E (2015) Electrochemical incineration of the antibiotic ciprofloxacin in sulfate medium and synthetic urine matrix. *Water Res* 83:31–41
 44. Isarain-Chávez E, Arias C, Cabot PL, Centellas F, Rodríguez RM, Garrido JA, Brillas E (2010) Mineralization of the drug β -blocker atenolol by electro-Fenton and photoelectro-Fenton using an air-diffusion cathode for H_2O_2 electrogeneration combined with a carbon-felt cathode for Fe^{2+} regeneration. *Appl Catal B-Environ* 96:361–369
 45. Isarain-Chávez E, Rodríguez RM, Garrido JA, Arias C, Centellas F, Cabot PL, Brillas E (2010) Degradation of the beta-blocker propranolol by electrochemical advanced oxidation processes based on Fenton's reaction chemistry using a boron-doped diamond anode. *Electrochim Acta* 56:215–221
 46. Isarain-Chávez E, Cabot PL, Centellas F, Rodríguez RM, Arias C, Garrido JA, Brillas E (2011) Electro-Fenton and photoelectro-Fenton degradations of the drug beta-blocker propranolol using a Pt anode: identification and evolution of oxidation products. *J Hazard Mater* 185:1228–1235
 47. Skoumal M, Rodríguez RM, Cabot PL, Centellas F, Garrido JA, Arias C, Brillas E (2009) Electro-Fenton, UVA photoelectro-Fenton and solar photoelectro-Fenton degradation of the drug ibuprofen in acid aqueous medium using platinum and boron-doped diamond anodes. *Electrochim Acta* 54:2077–2085
 48. Zhang Y, Gao M-M, Wang X-H, Wang S-G, Liu R-T (2015) Enhancement of oxygen diffusion process on a rotating disk electrode for the electro-Fenton degradation of tetracycline. *Electrochim Acta* 182:73–80
 49. Ledezma Estrada A, Li Y-Y, Wang A (2012) Biodegradability enhancement of wastewater containing cefalexin by means of the electro-Fenton oxidation process. *J Hazard Mater* 227–228:41–48
 50. Xie YB, Li XZ (2006) Interactive oxidation of photoelectrocatalysis and electro-Fenton for azo dye degradation using TiO_2 -Ti mesh and reticulated vitreous carbon electrodes. *Mater Chem Phys* 95:39–50
 51. Brillas E, Sirés I, Oturan MA (2009) Electro-Fenton process and related electrochemical technologies based on Fenton's reaction chemistry. *Chem Rev* 109:6570–6631
 52. Çelebi MS, Oturan N, Zazou H, Hamdani M, Oturan MA (2015) Electrochemical oxidation of carbaryl on platinum and boron-doped diamond anodes using electro-Fenton technology. *Sep Purif Technol* 156(Part 3):996–1002
 53. Mbaye OMA, Gaye Seye MD, Coly A, Tine A, Oturan MA, Oturan N, Aaron JJ (2013) Photo-induced fluorescence properties of the propanil herbicide and analytical usefulness. *Microchem J* 110:579–586
 54. Abdessalem AK, Bellakhal N, Oturan N, Dachraoui M, Oturan MA (2010) Treatment of a mixture of three pesticides by photo- and electro-Fenton processes. *Desalination* 250:450–455

55. Oturan MA, Oturan N, Lahitte C, Trevin S (2001) Production of hydroxyl radicals by electrochemically assisted Fenton's reagent: application to the mineralization of an organic micropollutant, pentachlorophenol. *J Electroanal Chem* 507:96–102
56. Olvera-Vargas H, Oturan N, Buisson D, Oturan MA (2016) A coupled bio-EF process for mineralization of the pharmaceuticals furosemide and ranitidine: feasibility assessment. *Chemosphere* 155:606–613
57. Yahya MS, Oturan N, El Kacemi K, El Karbane M, Aravindakumar CT, Oturan MA (2014) Oxidative degradation study on antimicrobial agent ciprofloxacin by electro-fenton process: kinetics and oxidation products. *Chemosphere* 117:447–454
58. Oturan MA, Pinson J, Bizot J, Deprez D, Terlain B (1992) Reaction of inflammation inhibitors with chemically and electrochemically generated hydroxyl radicals. *J Electroanal Chem* 334:103–109
59. Sopaj F, Oturan N, Pinson J, Podvorica F, Oturan MA (2016) Effect of the anode materials on the efficiency of the electro-Fenton process for the mineralization of the antibiotic sulfamethazine. *Appl Catal B-Environ* 199:331–341
60. Sopaj F, Rodrigo MA, Oturan N, Podvorica FI, Pinson J, Oturan MA (2015) Influence of the anode materials on the electrochemical oxidation efficiency. Application to oxidative degradation of the pharmaceutical amoxicillin. *Chem Eng J* 262:286–294
61. Ganiyu SO, van Hullebusch ED, Cretin M, Esposito G, Oturan MA (2015) Coupling of membrane filtration and advanced oxidation processes for removal of pharmaceutical residues: a critical review. *Sep Purif Technol* 156(Part 3):891–914
62. El-Ghenymy A, Oturan N, Oturan MA, Garrido JA, Cabot PL, Centellas F, Rodríguez RM, Brillas E (2013) Comparative electro-Fenton and UVA photoelectro-Fenton degradation of the antibiotic sulfanilamide using a stirred BDD/air-diffusion tank reactor. *Chem Eng J* 234:115–123
63. Haidar M, Dirany A, Sirés I, Oturan N, Oturan MA (2013) Electrochemical degradation of the antibiotic sulfachloropyridazine by hydroxyl radicals generated at a BDD anode. *Chemosphere* 91:1304–1309
64. Wu J, Zhang H, Oturan N, Wang Y, Chen L, Oturan MA (2012) Application of response surface methodology to the removal of the antibiotic tetracycline by electrochemical process using carbon-felt cathode and DSA (Ti/RuO₂-IrO₂) anode. *Chemosphere* 87:614–620
65. Dirany A, Sirés I, Oturan N, Oturan MA (2010) Electrochemical abatement of the antibiotic sulfamethoxazole from water. *Chemosphere* 81:594–602
66. Le TXH, Bechelany M, Lacour S, Oturan N, Oturan MA, Cretin M (2015) High removal efficiency of dye pollutants by electron-Fenton process using a graphene based cathode. *Carbon* 94:1003–1011
67. Labiadh L, Oturan MA, Panizza M, Hamadi NB, Ammar S (2015) Complete removal of AHPS synthetic dye from water using new electro-fenton oxidation catalyzed by natural pyrite as heterogeneous catalyst. *J Hazard Mater* 297:34–41
68. Bouafia-Chergui S, Oturan N, Khalaf H, Oturan MA (2012) A photo-Fenton treatment of a mixture of three cationic dyes. *Procedia Eng* 33:181–187
69. Oturan MA, Sirés I, Oturan N, Pérocheau S, Laborde J-L, Trévin S (2008) Sono-electro-Fenton process: a novel hybrid technique for the destruction of organic pollutants in water. *J Electroanal Chem* 624:329–332
70. Özcan A, Şahin Y, Savaş Kopal A, Oturan MA (2008) Carbon sponge as a new cathode material for the electro-Fenton process: comparison with carbon felt cathode and application to degradation of synthetic dye basic blue 3 in aqueous medium. *J Electroanal Chem* 616:71–78
71. Hammami S, Oturan N, Bellakhal N, Dachraoui M, Oturan MA (2007) Oxidative degradation of direct orange 61 by electro-Fenton process using a carbon felt electrode: application of the experimental design methodology. *J Electroanal Chem* 610:75–84
72. Panizza M, Cerisola G (2005) Application of diamond electrodes to electrochemical processes. *Electrochim Acta* 51:191–199

73. Michaud P-A, Panizza M, Ouattara L, Diaco T, Foti G, Comminellis C (2003) Electrochemical oxidation of water on synthetic boron-doped diamond thin film anodes. *J Appl Electrochem* 33:151–154
74. Panizza M, Cerisola G (2003) Influence of anode material on the electrochemical oxidation of 2-naphthol. Part 1. Cyclic voltammetry and potential step experiments. *Electrochim Acta* 48:3491–3497
75. Foti G, Gandini D, Comminellis C, Perret A, Haenni W (1999) Oxidation of organics by intermediates of water discharge on IrO₂ and synthetic diamond anodes. *Electrochem Solid State* 2:228–230
76. Zhou M, Yu Q, Lei L (2008) The preparation and characterization of a graphite-PTFE cathode system for the decolorization of C.I. acid red 2. *Dyes Pigments* 77:129–136
77. Sudoh M, Kodera T, Sakai K (1986) Oxidative degradation of aqueous phenol effluent with electrogenerated Fenton's reagent. *J Chem Eng Jpn* 19:513–518
78. Petrucci E, Da Pozzo A, Di Palma L (2016) On the ability to electrogenerate hydrogen peroxide and to regenerate ferrous ions of three selected carbon-based cathodes for electro-Fenton processes. *Chem Eng J* 283:750–758
79. Zhou L, Hu Z, Zhang C, Bi Z, Jin T, Zhou M (2013) Electrogeneration of hydrogen peroxide for electro-Fenton system by oxygen reduction using chemically modified graphite felt cathode. *Sep Purif Technol* 111:131–136
80. Badellino C, Rodrigues CA, Bertazzoli R (2006) Oxidation of pesticides by in situ electrogenerated hydrogen peroxide: study for the degradation of 2,4-dichlorophenoxyacetic acid. *J Hazard Mater* 137:856–864
81. Brillas E, Calpe JC, Casado J (2000) Mineralization of 2,4-D by advanced electrochemical oxidation processes. *Water Res* 34:2253–2262
82. Boye B, Brillas E, Dieng MM (2003) Electrochemical degradation of the herbicide 4-chloro-2-methylphenoxyacetic acid in aqueous medium by peroxi-coagulation and photoperoxi-coagulation. *J Electroanal Chem* 540:25–34
83. Boye B, Marième Dieng M, Brillas E (2003) Electrochemical degradation of 2,4,5-trichlorophenoxyacetic acid in aqueous medium by peroxi-coagulation. Effect of pH and UV light. *Electrochim Acta* 48:781–790
84. Brillas E, Boye B, Baños MÁ, Calpe JC, Garrido JA (2003) Electrochemical degradation of chlorophenoxy and chlorobenzoic herbicides in acidic aqueous medium by the peroxi-coagulation method. *Chemosphere* 51:227–235
85. Brillas E, Bastida RM, Llosa E, Casado J (1995) Electrochemical destruction of aniline and 4-chloroaniline for wastewater treatment using a carbon-PTFE O₂-fed cathode. *J Electrochem Soc* 142:1733–1741
86. Brillas E, Mur E, Casado J (1996) Iron(II) catalysis of the mineralization of aniline using a carbon-PTFE O₂-fed cathode. *J Electrochem Soc* 143:49–53
87. Brillas E, Sauleda R, Casado J (1997) Peroxi-coagulation of aniline in acidic medium using an oxygen diffusion cathode. *J Electrochem Soc* 144:2374–2379
88. Brillas E, Sauleda R, Casado J (1999) Use of an acidic Fe/O₂ cell for wastewater treatment: degradation of aniline. *J Electrochem Soc* 146:4539–4543
89. Boye B, Morième Dieng M, Brillas E (2003) Anodic oxidation, electro-Fenton and photoelectro-Fenton treatments of 2,4,5-trichlorophenoxyacetic acid. *J Electroanal Chem* 557:135–146
90. Brillas E, Baños MÁ, Garrido JA (2003) Mineralization of herbicide 3,6-dichloro-2-methoxybenzoic acid in aqueous medium by anodic oxidation, electro-Fenton and photoelectro-Fenton. *Electrochim Acta* 48:1697–1705
91. Brillas E, Boye B, Dieng MM (2003) Peroxi-coagulation and photoperoxi-coagulation treatments of the herbicide 4-chlorophenoxyacetic acid in aqueous medium using an oxygen-diffusion cathode. *J Electrochem Soc* 150:148–154

92. Flox C, Cabot P-L, Centellas F, Garrido JA, Rodríguez RM, Arias C, Brillas E (2007) Solar photoelectro-Fenton degradation of cresols using a flow reactor with a boron-doped diamond anode. *Appl Catal B-Environ* 75:17–28
93. Sirés I, Arias C, Cabot PL, Centellas F, Garrido JA, Rodríguez RM, Brillas E (2007) Degradation of clofibrilic acid in acidic aqueous medium by electro-Fenton and photoelectro-Fenton. *Chemosphere* 66:1660–1669
94. Guinea E, Centellas F, Garrido JA, Rodríguez RM, Arias C, Cabot P-L, Brillas E (2009) Solar photoassisted anodic oxidation of carboxylic acids in presence of Fe^{3+} using a boron-doped diamond electrode. *Appl Catal B-Environ* 89:459–468
95. Brillas E, Casado J (2002) Aniline degradation by electro-Fenton® and peroxi-coagulation processes using a flow reactor for wastewater treatment. *Chemosphere* 47:241–248
96. Isarain-Chávez E, Rodríguez RM, Cabot PL, Centellas F, Arias C, Garrido JA, Brillas E (2011) Degradation of pharmaceutical beta-blockers by electrochemical advanced oxidation processes using a flow plant with a solar compound parabolic collector. *Water Res* 45:4119–4130
97. El-Ghenymy A, Garcia-Segura S, Rodríguez RM, Brillas E, El Begrani MS, Abdelouahid BA (2012) Optimization of the electro-Fenton and solar photoelectro-Fenton treatments of sulfanilic acid solutions using a pre-pilot flow plant by response surface methodology. *J Hazard Mater* 221–222:288–297
98. García O, Isarain-Chávez E, El-Ghenymy A, Brillas E, Peralta-Hernández JM (2014) Degradation of 2,4-D herbicide in a recirculation flow plant with a Pt/air-diffusion and a BDD/BDD cell by electrochemical oxidation and electro-Fenton process. *J Electroanal Chem* 728:1–9
99. Almeida LC, Garcia-Segura S, Bocchi N, Brillas E (2011) Solar photoelectro-Fenton degradation of paracetamol using a flow plant with a Pt/air-diffusion cell coupled with a compound parabolic collector: process optimization by response surface methodology. *Appl Catal B-Environ* 103:21–30
100. Olvera-Vargas H, Oturan N, Oturan MA, Brillas E (2015) Electro-Fenton and solar photoelectro-Fenton treatments of the pharmaceutical ranitidine in pre-pilot flow plant scale. *Sep Purif Technol* 146:127–135
101. Pérez T, Garcia-Segura S, El-Ghenymy A, Nava JL, Brillas E (2015) Solar photoelectro-Fenton degradation of the antibiotic metronidazole using a flow plant with a Pt/air-diffusion cell and a CPC photoreactor. *Electrochim Acta* 165:173–181
102. Sirés I, Brillas E (2012) Remediation of water pollution caused by pharmaceutical residues based on electrochemical separation and degradation technologies: a review. *Environ Int* 40:212–229
103. Garza-Campos B, Brillas E, Hernández-Ramírez A, El-Ghenymy A, Guzmán-Mar JL, Ruiz-Ruiz EJ (2016) Salicylic acid degradation by advanced oxidation processes. Coupling of solar photoelectro-Fenton and solar heterogeneous photocatalysis. *J Hazard Mater* 319:34–42
104. El-Ghenymy A, Cabot PL, Centellas F, Garrido JA, Rodríguez RM, Arias C, Brillas E (2013) Mineralization of sulfanilamide by electro-Fenton and solar photoelectro-Fenton in a pre-pilot plant with a Pt/air-diffusion cell. *Chemosphere* 91:1324–1331
105. Gozzi F, Sirés I, Thiam A, de Oliveira SC, Junior AM, Brillas E (2017) Treatment of single and mixed pesticide formulations by solar photoelectro-Fenton using a flow plant. *Chem Eng J* 310(Part 2):503–513
106. Pipi ARF, Sirés I, De Andrade AR, Brillas E (2014) Application of electrochemical advanced oxidation processes to the mineralization of the herbicide diuron. *Chemosphere* 109:49–55
107. Garza-Campos BR, Guzmán-Mar JL, Reyes LH, Brillas E, Hernández-Ramírez A, Ruiz-Ruiz EJ (2014) Coupling of solar photoelectro-Fenton with a BDD anode and solar heterogeneous photocatalysis for the mineralization of the herbicide atrazine. *Chemosphere* 97:26–33
108. Garcia-Segura S, Almeida LC, Bocchi N, Brillas E (2011) Solar photoelectro-Fenton degradation of the herbicide 4-chloro-2-methylphenoxyacetic acid optimized by response surface methodology. *J Hazard Mater* 194:109–118

109. Moreira FC, Garcia-Segura S, Vilar VJP, Boaventura RAR, Brillas E (2013) Decolorization and mineralization of sunset yellow FCF azo dye by anodic oxidation, electro-Fenton, UVA photoelectro-Fenton and solar photoelectro-Fenton processes. *Appl Catal B-Environ* 142–143:877–890
110. Garcia-Segura S, Brillas E (2014) Advances in solar photoelectro-Fenton: Decolorization and mineralization of the direct yellow 4 diazo dye using an autonomous solar pre-pilot plant. *Electrochim Acta* 140:384–395
111. Antonin VS, Garcia-Segura S, Santos MC, Brillas E (2015) Degradation of Evans Blue diazo dye by electrochemical processes based on Fenton's reaction chemistry. *J Electroanal Chem* 747:1–11
112. Solano AMS, Garcia-Segura S, Martínez-Huitle CA, Brillas E (2015) Degradation of acidic aqueous solutions of the diazo dye Congo Red by photo-assisted electrochemical processes based on Fenton's reaction chemistry. *Appl Catal B-Environ* 168–169:559–571
113. Thiam A, Sirés I, Centellas F, Cabot PL, Brillas E (2015) Decolorization and mineralization of Allura red AC azo dye by solar photoelectro-Fenton: identification of intermediates. *Chemosphere* 136:1–8
114. Garcia-Segura S, Brillas E (2016) Combustion of textile monoazo, diazo and triazo dyes by solar photoelectro-Fenton: Decolorization, kinetics and degradation routes. *Appl Catal B-Environ* 181:681–691
115. Garcia-Segura S, Salazar R, Brillas E (2013) Mineralization of phthalic acid by solar photoelectro-Fenton with a stirred boron-doped diamond/air-diffusion tank reactor: Influence of Fe^{3+} and Cu^{2+} catalysts and identification of oxidation products. *Electrochim Acta* 113:609–619
116. Moreira FC, Boaventura RAR, Brillas E, Vilar VJP (2015) Remediation of a winery wastewater combining aerobic biological oxidation and electrochemical advanced oxidation processes. *Water Res* 75:95–108
117. Alvarez-Gallegos A, Pletcher D (1998) The removal of low level organics via hydrogen peroxide formed in a reticulated vitreous carbon cathode cell, part 1. The electrosynthesis of hydrogen peroxide in aqueous acidic solutions. *Electrochim Acta* 44:853–861
118. Alvarez-Gallegos A, Pletcher D (1999) The removal of low level organics via hydrogen peroxide formed in a reticulated vitreous carbon cathode cell. Part 2: the removal of phenols and related compounds from aqueous effluents. *Electrochim Acta* 44:2483–2492
119. Leon CPD, Pletcher D (1995) Removal of formaldehyde from aqueous solutions via oxygen reduction using a reticulated vitreous carbon cathode cell. *J Appl Electrochem* 25:307–314
120. Fockedey E, Van Lierde A (2002) Coupling of anodic and cathodic reactions for phenol electro-oxidation using three-dimensional electrodes. *Water Res* 36:4169–4175
121. Hsiao Y-L, Nobe K (1993) Hydroxylation of chlorobenzene and phenol in a packed bed flow reactor with electrogenerated Fenton's reagent. *J Appl Electrochem* 23:943–946
122. Ma L, Zhou M, Ren G, Yang W, Liang L (2016) A highly energy-efficient flow-through electro-Fenton process for organic pollutants degradation. *Electrochim Acta* 200:222–230
123. Lei Y, Liu H, Shen Z, Wang W (2013) Development of a trickle bed reactor of electro-Fenton process for wastewater treatment. *J Hazard Mater* 261:570–576
124. Anotai J, C-C S, Tsai Y-C, M-C L (2010) Effect of hydrogen peroxide on aniline oxidation by electro-Fenton and fluidized-bed Fenton processes. *J Hazard Mater* 183:888–893
125. Wang C-T, J-L H, Chou W-L, Kuo Y-M (2008) Removal of color from real dyeing wastewater by electro-Fenton technology using a three-dimensional graphite cathode. *J Hazard Mater* 152:601–606
126. Xu L, Zhao H, Shi S, Zhang G, Ni J (2008) Electrolytic treatment of C.I. acid orange 7 in aqueous solution using a three-dimensional electrode reactor. *Dyes Pigments* 77:158–164
127. Xiong Y, He C, Karlsson HT, Zhu X (2003) Performance of three-phase three-dimensional electrode reactor for the reduction of COD in simulated wastewater-containing phenol. *Chemosphere* 50:131–136

128. Liu W, Ai Z, Zhang L (2012) Design of a neutral three-dimensional electro-Fenton system with foam nickel as particle electrodes for wastewater treatment. *J Hazard Mater* 243:257–264
129. Hara K, Kudo A, Sakata T (1995) Electrochemical reduction of carbon dioxide under high pressure on various electrodes in an aqueous electrolyte. *J Electroanal Chem* 391:141–147
130. Köleli F, Balun D (2004) Reduction of CO₂ under high pressure and high temperature on Pb-granule electrodes in a fixed-bed reactor in aqueous medium. *Appl Catal A-Gen* 274:237–242
131. Scialdone O, Galia A, Nero GL, Proietto F, Sabatino S, Schiavo B (2016) Electrochemical reduction of carbon dioxide to formic acid at a tin cathode in divided and undivided cells: effect of carbon dioxide pressure and other operating parameters. *Electrochim Acta* 199:332–341
132. Sabatino S, Galia A, Saracco G, Scialdone O (2017) Development of an electrochemical process for the simultaneous treatment of wastewater and the conversion of carbon dioxide to higher value products. *ChemElectroChem* 4:150–159
133. Do JS, Chen CP (1993) In situ oxidative degradation of formaldehyde with electrogenerated hydrogen peroxide. *J Electrochem Soc* 140:1632–1637
134. Scialdone O, Galia A, Gattuso C, Sabatino S, Schiavo B (2015) Effect of air pressure on the electro-generation of H₂O₂ and the abatement of organic pollutants in water by electro-Fenton process. *Electrochim Acta* 182:775–780
135. Kockmann N (2006) Advanced micro and nanosystems, micro process engineering. Fundamentals, devices, fabrication and application. Wiley-VCH Verlag GmbH & Co. KGaA, Weinheim
136. Erickson D, Li D (2004) Integrated microfluidic devices. *Anal Chim Acta* 507:11–26
137. Paddon CA, Pritchard GJ, Thiemann T, Marken F (2002) Paired electrosynthesis: micro-flow cell processes with and without added electrolyte. *Electrochem Commun* 4:825–831
138. Suga S, Okajima M, Fujiwara K, Yoshida J-i (2001) “Cation flow” method: a new approach to conventional and combinatorial organic syntheses using electrochemical microflow systems. *J Am Chem Soc* 123:7941–7942
139. Scialdone O, Galia A, Sabatino S, Vaiana GM, Agro D, Busacca A, Amatore C (2014) Electrochemical conversion of dichloroacetic acid to chloroacetic acid in conventional cell and in two microfluidic reactors. *ChemElectroChem* 1:116–124
140. Scialdone O, Galia A, Sabatino S, Mira D, Amatore C (2015) Electrochemical conversion of dichloroacetic acid to chloroacetic acid in a microfluidic stack and in a series of microfluidic reactors. *ChemElectroChem* 2:684–690
141. Scialdone O, Guarisco C, Galia A, Filardo G, Silvestri G, Amatore C, Sella C, Thouin L (2010) Anodic abatement of organic pollutants in water in micro reactors. *J Electroanal Chem* 638:293–296
142. Scialdone O, Guarisco C, Galia A (2011) Oxidation of organics in water in microfluidic electrochemical reactors: theoretical model and experiments. *Electrochim Acta* 58:463–473
143. Scialdone O, Galia A, Guarisco C, La Mantia S (2012) Abatement of 1,1,2,2-tetrachloroethane in water by reduction at silver cathode and oxidation at boron doped diamond anode in micro reactors. *Chem Eng J* 189–190:229–236
144. Scialdone O, Galia A, Sabatino S (2013) Electro-generation of H₂O₂ and abatement of organic pollutant in water by an electro-Fenton process in a microfluidic reactor. *Electrochem Commun* 26:45–47
145. Scialdone O, Galia A, Sabatino S (2014) Abatement of acid orange 7 in macro and micro reactors. Effect of the electrocatalytic route. *Appl Catal B-Environ* 148–149:473–483
146. Khongthong W, Jovanovic G, Yokochi A, Sangvanich P, Pavarajarn V (2016) Degradation of diuron via an electrochemical advanced oxidation process in a microscale-based reactor. *Chem Eng J* 292:298–307
147. Khongthong W, Pavarajarn V (2016) Effect of nitrate and sulfate contamination on degradation of diuron via electrochemical advanced oxidation in a microreactor. *Eng J* 20:25–34

148. Sabatino S, Galia A, Scialdone O (2016) Electrochemical abatement of organic pollutants in continuous-reaction systems through the assembly of microfluidic cells in series. *ChemElectroChem* 3:83–90
149. Kříšťál J, Kodým R, Bouzek K, Jiříčný V (2008) Electrochemical microreactor and gas-evolving reactions. *Electrochem Commun* 10:204–207
150. de Loos SRA, van der Schaaf J, Tiggelaar RM, Nijhuis TA, de Croon MHJM, Schouten JC (2010) Gas-liquid dynamics at low Reynolds numbers in pillared rectangular micro channels. *Microfluid Nanofluidics* 9:131–144

Cost-Effective Flow-Through Reactor in Electro-Fenton

Minghua Zhou, Gengbo Ren, Liang Ma, Yinqiao Zhang, and Sijin Zuo

Abstract In order to increase the degradation efficiency and reduce the treatment cost of electro-Fenton (EF) process, many aspects have been attempted, among which the design of cost-effective reactors is very important. Flow-through EF reactor, i.e., the solution flow through the anode and cathode, is able to increase mass and electron transfer, which is favorable to improve electrochemical conversion, current efficiency and reduce energy consumption. Carbon-based materials, for example, graphite felt, are desirable cathodic electrodes for the flow-through EF system because of their stability, conductivity, high surface area and chemical resistance, as well as the filtration characteristics. The effects of some important parameters including current density, pH, and flow rate on organic pollutant removal efficiency were discussed. Moreover, some new attempts on coupled flow-through EF with other water/wastewater treatment technology (e.g., coagulation, adsorption, and ozonation) were extended to reach a higher treatment efficiency. The perspective of this process was also summarized. In conclusion, compared with conventional EF reactor, flow-through EF reactor was more energy-efficient and potential for degradation of organic pollutants.

Keywords Adsorption, Coupled process, Electrochemical advanced oxidation processes (EAOP), Electro-Fenton, Flow-through, Graphite felt, Peroxi-coagulation

Contents

1	Introduction	242
2	The Mechanism of Flow-Through Reactor	244
	2.1 Mass Transfer	244

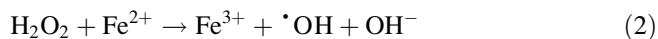
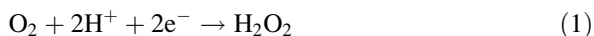
M. Zhou (✉), G. Ren, L. Ma, Y. Zhang, and S. Zuo

Key Laboratory of Pollution Process and Environmental Criteria, Ministry of Education,
College of Environmental Science and Engineering, Nankai University, Tianjin 300350, China
e-mail: zhoumh@nankai.edu.cn

2.2	Adsorption, Desorption, and Oxidation	245
2.3	Electron Transfer	245
3	Cathode Material	245
3.1	Carbon Nanotubes (CNTs)	246
3.2	Carbon Fiber	246
3.3	Graphite Felt	247
3.4	Carbonaceous Materials	247
4	The Application of Flow-Through EF System	248
4.1	The Advantages of Flow-Through EF	248
4.2	Stability of the Flow-Through EF	249
4.3	Influence of Operating Parameters	250
4.4	Combined Flow-Through EF Reactor	252
5	Coupling of Flow-Through EF with Other Water Treatment Technology	255
5.1	Flow-Through EF/Adsorption	255
5.2	Flow-Through Peroxi-Coagulation	256
5.3	Flow-Through EF + Ozone	257
6	Summary and Perspective	258
	References	259

1 Introduction

The electrochemical advanced oxidation processes (EAOPs) have shown to be a promising technology for degradation of refractory pollutants in wastewater because of the advantages including environmental compatibility, amenability of automation, high energy efficiency, versatility, and safe operation under mild conditions. Electro-Fenton (EF) based on Fenton's reaction chemistry is perhaps one of the most popular EAOPs, in which H_2O_2 is continuously generated in situ via cathodic reduction of O_2 (Eq. 1) and can be further converted into hydroxyl radicals ($\cdot\text{OH}$) (Eq. 2) in the presence of Fe^{2+} [1, 2]. The hydroxyl radicals, which have a high potential [2.8 V vs. standard hydrogen electrode (SHE)], can rapidly and nonselectively destroy refractory pollutants [1].



While EF is effective for the degradation of many organic pollutants, such as dyes, pesticides, phenols, and pharmaceuticals, the energy consumption is usually reported ranging from 87.7 to 275 kWh (kg TOC)⁻¹ [3–5]. In order to further improve EF efficiency, quite a few researches have focused on combined EF such as photoelectro-Fenton (PEF) [6, 7], solar photoelectron-Fenton (SPEF) [8], photoperoxi-coagulation (PPC), and sonoelectro-Fenton (SEF) processes [9–11]. Though hybrid synergism is observed in the combined EF processes, they are usually complicated or need additional energy input, when compared with single EF.

The design of cost-effective EF reactor is another important approach to promote the degradation efficiency and reduce the treatment cost. Basically, EF reactors are

divided into two main categories: undivided and divided reactor [1]. Undivided EF reactor is that both the anode and cathode are in the same electrolyte or contaminant solution. As for the divided reactors, the anode and cathode are located in the anodic and cathodic chambers separated by the glass plate, membrane, or cation exchange membrane. Sudoh et al. [12] designed a membrane reactor to test the production of hydrogen peroxide using a three-electrode system, which was much higher than the non-membrane system under the same conditions. It is noticeable that the shorter contact time between the generated hydrogen peroxide and the electrode is, the fewer electrode side reactions in the continuous-flow EF system take place. Therefore, continuous-flow EF is generally operated in a non-membrane reactor, which can simplify the design of EF reactor.

Over the past several decades, most of the continuous-flow EF reactors have been focusing on flow-by reactors, i.e., the pollutants flow parallel to the anode and cathode surface. Zhang et al. developed a Fered-Fenton system in a continuous stirred tank reactor (CSTR) using Ti/RuO₂-IrO₂-SnO₂-TiO₂ mesh anodes and Ti mesh cathodes to treat landfill leachate [13], proving that the complete mixing condition was fulfilled and the COD removal followed a modified pseudo-first order kinetic model. Rosales et al. designed a bubble EF reactor for the treatment of wastewater containing synthetic dyes [14], which followed an ideal continuous stirred tank reactor behavior. A pilot flow reactor in recirculation mode with a filter-press cell using an oxygen diffusion cathode was studied to degrade aniline solution [15]. Ling et al. designed a novel continuous multi-cell reactor using PbO₂/Ti anode and stainless steel cathode to treat 500 mg/L phenol wastewater, achieving the effluent COD of 242 mg/L with a current efficiency of 71.8% [16]. Moreira et al. reported a novel electrochemical filter-press cell with a BDD or Pt anode and a carbon-PTFE air-diffusion cathode to electro-generate H₂O₂, and nearly 50% TOC removal efficiency after 180 min could be achieved under the conditions of pH 3, current intensity of 5 mA/cm², and Fe²⁺ of 2 mg/L [17].

In summary, for these conventional continuous EF reactors, the pollutant removal efficiency is still unsatisfactory due to the low space-time treatment efficiency and mass transfer limitation. The mass transfer limitations arise since convection becomes negligible near the electrode-water interface, and the relatively slow molecular diffusion to the electrode surface cannot complete kinetically with electron transfer [18]. In this regard, it is very necessary to design an efficient EF reactor to overcome these weaknesses.

Flow-through reactor, i.e., the solution flow through the anode and cathode, are able to increase mass transfer to the electrode surface, which will not only increase the extent of electrochemical transformation, but will also result in improved current efficiency and reduced energy consumption [19]. This work summarized our works on flow-through EF reactor and its application for organic pollutants degradation. The effects of some important parameters including current density, pH, and flow rate on organic pollutant removal efficiency, as well as some coupled flow-through EF processes with other water/wastewater treatment technology (e.g., coagulation, adsorption, and ozonation) were presented. The perspective of this process was also summarized.

2 The Mechanism of Flow-Through Reactor

Figure 1 shows the possible enhanced mechanism of the flow-through reactor, which consists of three primary aspects [19, 20]: (1) mass transfer to the electrode, (2) adsorption, desorption, and oxidation on the electrode, and (3) electron transfer at the electrode.

2.1 Mass Transfer

Although electron transfer is responsible for electrochemical reaction, mass transfer to the electrode surface is often found to be the limiting step in the overall kinetics. As for conventional EF reactor, mass transfer limitations arise since convection becomes negligible near the electrode–water interface, and the relatively slow molecular (pollutant or oxygen) diffusion to the electrode surface cannot complete kinetically with electron transfer. And the reaction rate is usually determined by the diffusion of substrates through a thin stagnant boundary layer. Though high surface area electrode can help to increase the reaction rate, it is limited since the electrode roughness are smaller than the diffusion length. In contrast, the thickness of diffusion layer in the flow-through system is much lesser than the conventional system under the same experimental conditions due to the hydrodynamic compression of the diffusion layer. Yang et al. reported that in a flow-through electrochemical reactor, the mass transfer improved 1.6-fold, current efficiency improved threefold, and the energy consumption reduced 20% as compared to those of conventional bipolar reactors [20]. Therefore, flow-through EF reactors are able to increase mass transfer to the electrode surface, which will not only increase the extent of electrochemical reaction, but also result in improved current efficiency and reduced energy consumption.

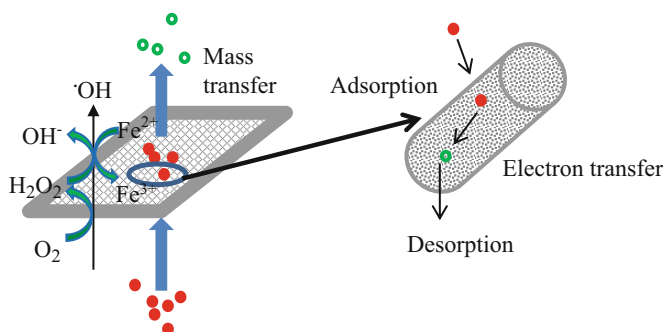


Fig. 1 The mechanism of flow-through EF

2.2 *Adsorption, Desorption, and Oxidation*

The flow-through electrode material, especially the adsorptive electrode, can enrich the pollutants when they flow through the electrode, resulting in increasing the concentration of local pollutants and accelerating the oxidation rate, especially for the low concentration of organic pollutants. As shown in Eqs. (1) and (2), the hydrogen peroxide generated on the suitable cathode would be catalyzed by Fe^{2+} in the solution, producing powerful hydroxyl radicals, which lead to the Fenton oxidation of organic pollutants. A fast adsorption of organic pollutants in the flow-through reactor would simultaneously promote such a Fenton oxidation since adsorption is very important for an interface reaction nearby the cathode. Moreover, physical and chemical adsorption of species to the flow-through cathode surface can significantly affect the electron transfer kinetics by altering its surface structure and chemistry, leading to a shift in the Gibbs free energy of reactants [21]. These reactions would decrease the interface pollutants concentration, resulting in desorption and adsorption capacity regeneration, which guarantee the continuous run of the performance.

2.3 *Electron Transfer*

While mass transfer and adsorption are important processes that affect the overall extent of oxidation during electrochemical oxidation, the target pollutant is ultimately transformed during the electron transfer step. The influent pollutants concentration and cathode potential were examined to determine the electron transfer kinetics and mechanism during electrochemical oxidation [22]. As expected, the electron transfer increase with the increase of potential, and at high influent pollutant concentrations when the adsorption sites are saturated, the overall reaction rate will be limited by the electron transfer kinetics in the conventional EF system. In the flow-through EF system, direct electron transfer can be enhanced due to the hydrodynamic compression on the electrode surface, resulting in a higher current response and efficiency.

3 **Cathode Material**

The cathode material determines the hydrogen peroxide production, which would affect the effectiveness of pollutants decontamination by EF. Therefore, suitable cathode is of great significance to the flow-through EF system. Carbon-based materials are desirable cathodic electrodes because of their stability, conductivity, high surface area, and chemical resistance.

3.1 Carbon Nanotubes (CNTs)

Carbon nanotubes (CNTs) or CNT-based materials have potential for application in EF system due to their combination of unique electronic, chemical, and mechanical properties, including small dimensions of the tubes and channels [22]. Therefore, compared with bare glass carbon, CNTs modified glass carbon electrode shows much lower over-potential and higher peak current [23, 24]. And the CNTs can strongly adsorb many chemical species because of a large specific surface area. For example, CNTs have been observed to adsorb aromatic compounds and natural organic matter via a combination of hydrophobic interactions and strong π - π interactions [25]. In addition, utilizing CNTs as either a bulk electrode or a modified working electrode has been observed to increase electron transfer rates [26].

CNTs were vacuum filtered onto a 5- μm polytetrafluorethylene (PTFE) membrane, which was adopted as the cathode in the flow-through EF reactor [27]. The undoped CNTs (C-CNT), nitrogen-doped CNTs (N-CNT), and boron-doped CNTs (B-CNT) were used to examine the H_2O_2 production as the function of cathode potential [28, 29]. The N-CNT cathode had a maximum H_2O_2 production of 3.0 mg/L, which was the lowest among the three CNT samples possibly due to reduction of H_2O_2 to $\cdot\text{OH}$ and H_2O . The C-CNT had the highest H_2O_2 production of 13.5 mg/L H_2O_2 at -0.3 V, while B-CNT had a moderate production of 8.5 mg/L. However, such a low H_2O_2 production on the CNT membrane was not sufficient to well satisfy the need of EF, which may attribute to the low concentration of dissolved oxygen (DO) though pumping air or pure oxygen was used to increase the DO in solution.

3.2 Carbon Fiber

Both large specific electrode areas and high mass transfer coefficients of dissolved oxygen can be obtained due to the flow-through hydrodynamic conditions inside the three-dimensional carbon fiber [30, 31]. Plakas et al. reported the CF-1371 (carbon fiber with a specific surface area 1,371 m^2/g and thickness 1 mm) and CF-1410 (carbon fiber with a specific surface area 1,410 m^2/g and thickness 2 mm) cathode used in flow-through EF system [32]. As for CF-1371, a linear increase of H_2O_2 concentration during the first 45 min of the electrolysis was observed, subsequently exhibiting a tendency for stabilization. On the CF-1410 cathode, the electro-generation of H_2O_2 was significantly higher, and thus an average current efficiency of 70% was observed, which was much higher than that on CF-1371 (<10%). Consequently, the CF-1410 was the desirable cathode in the flow-through EF system. Another significant advantage of the porous carbon fibers was their negligible effect on the water flux because of no pressure drop recorded during the experiments.

3.3 Graphite Felt

Graphite felts (GF) have been regarded as one of the most widely used cathode materials in EF process due to their large three-dimensional active surface, mechanical integrity, commercial availability, easy acquisition, and efficient cathodic regeneration of Fe^{2+} [33]. However, the productions of H_2O_2 on pristine GF was not so satisfactory [34, 35], thus considerable efforts on GF modification have been devoted to enhance its electrochemical activity by increasing surface oxygen content or specific surface area using different modification methods. A high performance of hydrogen peroxide production on GF modified by carbon black and PTFE was achieved, which was 35 mg/L in the flow-through EF system, much higher than that with the unmodified GF (6 mg/L) [36]. These results could be explained by the significant increase of micropore and mesoporous pore and the pore volume, as well as the enhancement of hydrophobic properties of the cathode surface [36].

Furthermore, it is vital to assemble the modified cathode and design a sound EF system that can satisfy the high production of H_2O_2 and take the advantage of flow-through process. In previous flow-through EF system, the solution was pretreated by pumping air or pure oxygen to increase the concentration of DO [27, 32, 37]. Unfortunately, the production of H_2O_2 was found rather low, which limited the Fenton oxidation rate due to the low DO in the solution. The modified GF has the properties of high porosity and hydrophobicity, and allows air or oxygen to cross the pore and contact with the active sites, providing lots of active surface sites for catalyzing O_2 reduction to H_2O_2 [1, 38]. Normally, modified GF is operated in a flow-by reactor [17, 39], in our previous work, a novel flow-through reactor using this modified GF was developed [19], in which the influent and pumped air flowed through the cathode. The energy consumption of H_2O_2 production in this reactor was only 5.2 kWh/(kg H_2O_2), which was much lower than other systems [40–42].

Recently, a novel Venturi-based jet reactor has been designed using the GF modified with the same method [43]. Higher H_2O_2 generation rate and lower energy consumption were obtained compared with the conventional system.

3.4 Carbonaceous Materials

The cathodic electrodes made of carbonaceous materials have been designed and constructed [32]. The “CCB-470” was made of powdered carbon obtained from a Coconut Carbon Black cartridge, which was compressed to form discs (diameter 4.2 cm, thickness 3.7 mm) with a specific surface area 470 m^2/g . The H_2O_2 production could only be measured at high potential, and the steady-state H_2O_2 concentration was about 3.7 mg/L. Thus the H_2O_2 concentration and current efficiency were very low and undesirable for the EF system. Moreover, the application of the less porous powdered carbon discs resulted in significant pressure drop, which was undesirable for EF practical applications.

4 The Application of Flow-Through EF System

A highly energy-efficient flow-through EF system was designed using a perforated DSA as anode and the GF modified by carbon black and PTFE as cathode [19], in which the influent and pumped air flowed through the cathode and the anode sequentially.

4.1 The Advantages of Flow-Through EF

The accumulation of H_2O_2 and the EF performance by the flow-through, flow-by, and regular system were compared, using methylene blue (MB) as the model organic pollutant. As shown in Fig. 2, the flow-through system had the best degradation performance among three systems, in which the MB removal efficiency reached 92% during 120 min treatment. However, in the flow-by system, it was about 64.9%. The MB removal efficiency reached 85% in the regular system.

In order to explain the above differences, the production of H_2O_2 in three systems was investigated under the comparable condition. The flow-through system had the highest production of H_2O_2 (57.8 mg/L), keeping stable during 120 min. By contrast, the flow-by and regular system were 51.9 and 37.2 mg/L, respectively. These results could be explained by the convection-enhanced transfer of O_2 and the

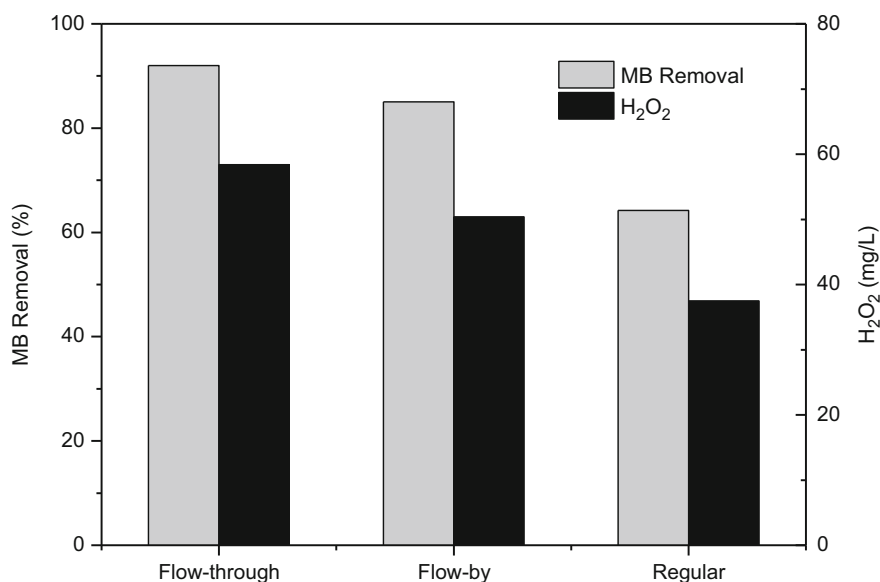


Fig. 2 The comparison of flow-through, flow-by, and regular EF system on the MB removal and H_2O_2 production [19]

Table 1 The comparison of energy consumption of TOC removal between flow-through EF and conventional EF

Method	Electrode (anode/cathode)	Pollutant	EEC (kWh/kg TOC)	References
Solar photoelectro-Fenton (SPEF)	Pt/ADE	4-Chloro-2-methylphenoxyacetic acid	87.7	[4]
SPEF	Pt/ADE-Pt/CF	Atenolol	84	[5]
SPEF	BDD/ SPEF	Food color additives (E122, E124 and E129)	290	[44]
SPEF	BDD/ADE	Acid yellow 36 azo dye	70	[8]
EF	BDD/ADE	Azo dye carmoisine	1,280	[10]
EF	Pt/ADE	Azo dye amaranth	370	[45]
Flow-through EF	Multiwalled carbon nanotube	Oxalate	46	[27]
SPEF	ADE/Pt	Salicylic acid	61	[44]
Flow-through EF	DSA/ADE	MB	23	[19]
		Orange II (OG)	29.6	
		Acetylsalicylic acid (ASA)	28.9	
		Tetracycline (TC)	83.3	
		2,4-Dichlorophen (2,4-DCP)	49.8	

pollutant molecule because of the solution flowing through the electrode, and the enhanced mass transfer would result in the higher current efficiency and lower energy consumption [20, 22].

Moreover, the energy consumption of TOC removal between this flow-through EF system and conventional EF system was also compared (Table 1). It was observed that the energy consumption was greatly reduced, which could be explained by the following two aspects. On the one hand, it had a high efficiency of H_2O_2 generation with a low energy consumption of $5.2 \text{ kWh}/(\text{kg } \text{H}_2\text{O}_2)$, therefore more $\cdot\text{OH}$ could be generated to mineralize the pollutant per energy consumption due to the convection-enhanced transfer of O_2 on the cathode. On the other hand, the filtration system enhanced the mass transfer and adsorption ability of pollutant molecule on the surface of the cathode, which increased the reaction chance of the pollutant molecule with $\cdot\text{OH}$.

4.2 Stability of the Flow-Through EF

The stability of the flow-through EF system was evaluated by five-times consecutive degradation operated under the same conditions. As shown in Fig. 3, both the

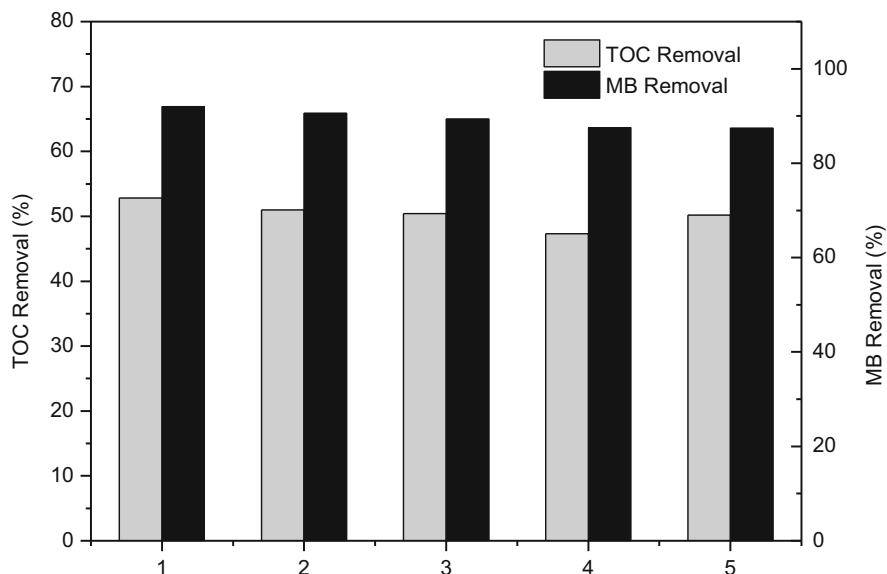


Fig. 3 The stability of flow-through EF system in five-times continuous runs [19]

MB removal efficiency and TOC removal were almost stable in all five runs. The TOC removal reached almost above 50% except the fourth time with a slight decrease with a value of 47.3%, and the MB removal of effluents kept all above 87%. The stability of both cathodic material and the flow-through EF system ensured good quality of effluent in all investigated runs. Therefore, this novel flow-through EF system had great potential for pollutant degradation due to its high stability and low energy consumption.

4.3 Influence of Operating Parameters

The degradation rate of target pollutant in the flow-through EF depends on operation parameters such as current, solution pH, and flow rate. Most of these parameters are optimized to achieve the best current efficiency and the lowest energy consumption.

4.3.1 Influence of Current

Figure 4 shows the effect of current on the MB removal and H_2O_2 production. It showed that when the current was higher than 30 mA, the MB removal efficiency reached 93%, but at the current of 30 mA, it was only 81.6% at 60 min. The H_2O_2 production was in the following sequence: 90 mA > 70 mA > 50 mA > 30 mA.

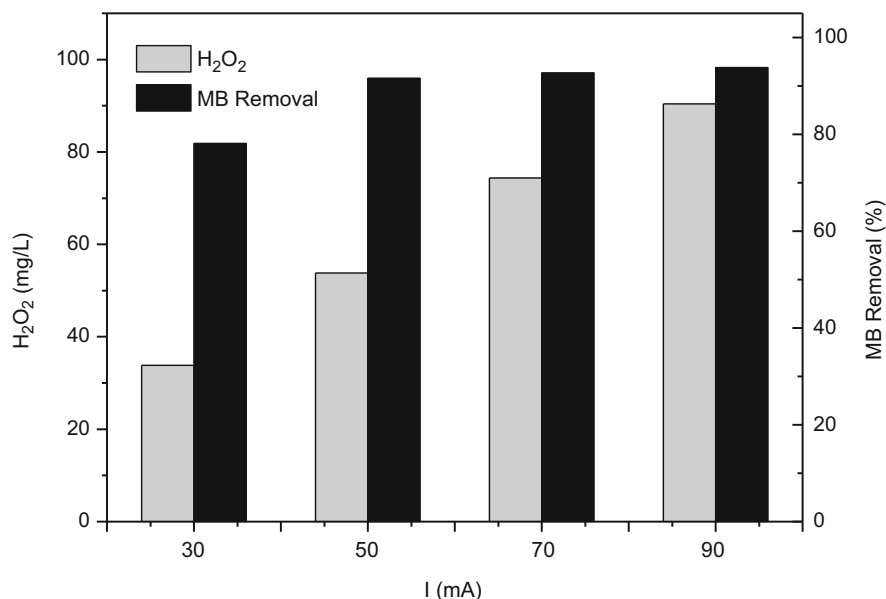


Fig. 4 Effect of current on the MB removal and H₂O₂ production [19]

The increased current could accelerate the electron transfer on the modified GF cathode that would promote two-electron reduction to H₂O₂. However, some side reactions might also occur when the current increased, such as hydrogen evolution reaction and four-electron reduction to H₂O. This could explain the result that why the current efficiency declined when the current density increased. At the current of 30 mA, the current efficiency was about 74.6%, but decreased to 66% at the current of 90 mA.

4.3.2 Influence of Initial pH

In EF process, pH mainly influences the production of H₂O₂ and the state of Fe²⁺ catalyst in the solution. Figure 5 shows the effect of initial pH ranged from 3 to 9 on the removal of MB, which performed in the following sequence: pH = 3 > 6.3 > 5 > 9. It was well known that the optimum pH value for EF reaction was about 3 [46], which was consistent with the result in this study.

However, the accumulation of H₂O₂ was 53.5, 56.3, 60.2, and 61.5 mg/L respectively, when the initial pH values were 3, 5, 6.3, and 9, increasing slightly with the increase of initial pH. This outcome might be attributed to the competitive side reactions of four-electron reduction to H₂O and H₂O₂ consumption which were reinforced in acid solution [46, 47]. However, at a high pH condition, Fe²⁺ would transform to iron hydroxides, which resulted in the declination of MB removal

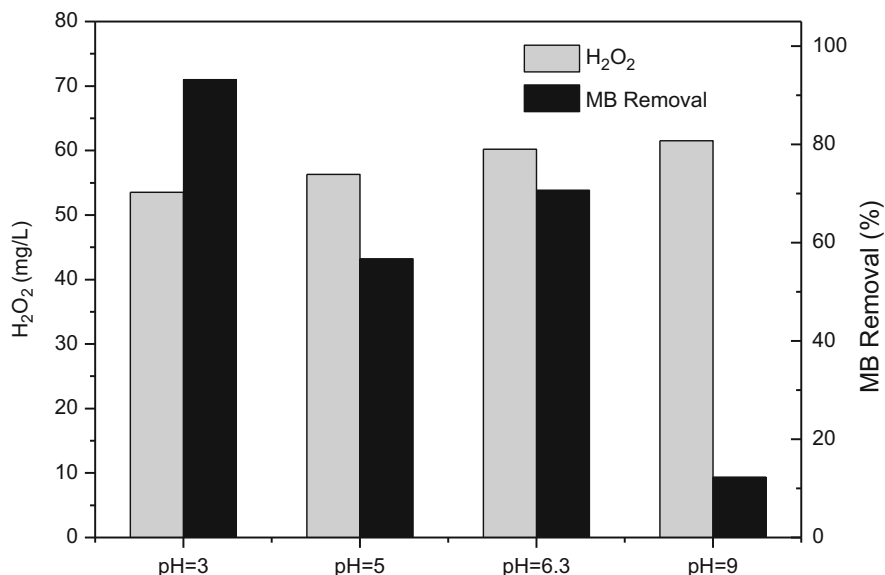


Fig. 5 Effect of pH on the MB removal and H₂O₂ production [19]

performance although the H₂O₂ production was increased slightly with the increase of initial pH.

4.3.3 Influence of Flow Rate

Both the accumulation of H₂O₂ in the EF process and the residence time of pollutants in the reactor are affected by the flow rate [27]. As shown in Fig. 6, when the flow rate varied from 3.5 to 10.5 mL/min, the MB removal efficiency were 95.0%, 92.7%, 92%, 84.9%, and 75.9%, respectively at 60 min, indicating that the MB removal efficiency increased with the reduction of flow rate. At the same time, the concentration of hydrogen peroxide was found decreased with the increase of flow rate. As shown in Fig. 6, when the flow rate varied from 3.5 to 10.5 mL/min, the concentration of H₂O₂ decreased from 92.8 to 34.4 mg/L. The higher concentration of H₂O₂ could induce more [•]OH generation, and the long residence time would increase the chance of the pollutant molecule reaction with [•]OH.

4.4 Combined Flow-Through EF Reactor

A novel combined flow-through EF reactor was designed, which consisted of ten cell compartments using PbO₂ mesh anode and modified GF cathode [36]. As shown in Fig. 7, the EF reactor consisted of ten small compartments with the

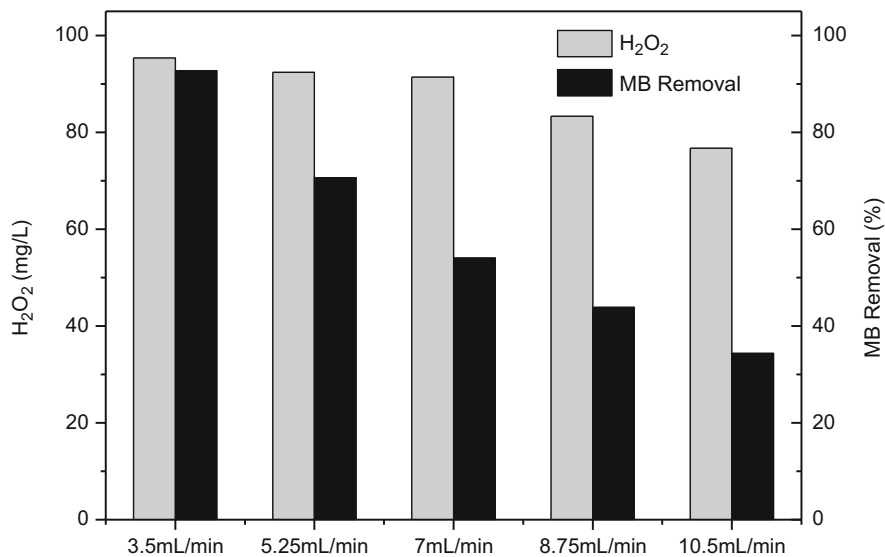


Fig. 6 Effect of flow rate on the MB removal and H₂O₂ production [19]

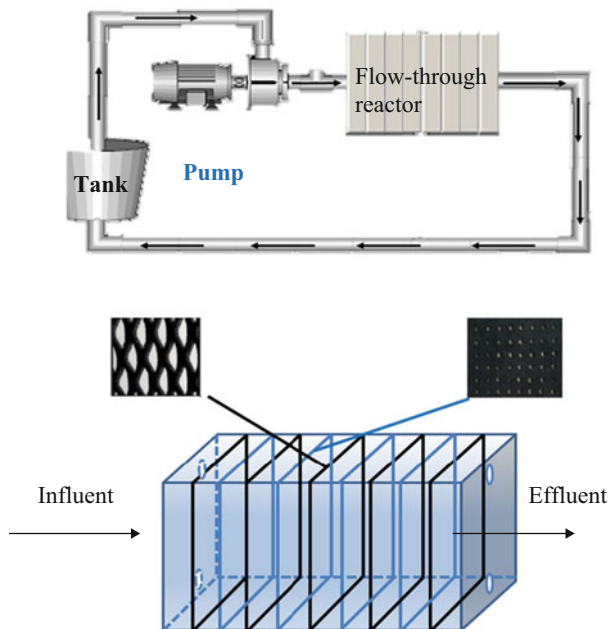


Fig. 7 The schematic diagram of the novel combined flow-through EF reactor

dimensions of $24 \times 10 \times 12$ cm and a total effective volume of 2,000 mL. The electrodes were fixed vertically along the flow direction in the reaction chamber, and the PbO_2 mesh anode and GF cathode alternately arranged. The performance on tartrazine degradation and mineralization efficiency in this EF reactor was further compared with the traditional parallel-flow reactor.

The TOC removal in the flow-through system was 64.47%, much higher than that in the flow-by (51.98%). It could thus conclude that flow-through EF advantaged over that flow-by one in term of removal efficiency. Therefore, it could be reasonably speculated that in the flow-through EF system the pollutants successively penetrated the cathode and anode surface, which enhanced the mass transfer rate and was beneficial to improve the removal efficiency to some extent.

Besides, the removal efficiency and energy consumption changes with the different compartments were investigated. As shown in Fig. 8, the TOC value was reduced with the flow direction from the first to the tenth cell compartment. The TOC removal was about 30% at the first cell, but it was larger than 60% at the eighth cell when steady-state conditions were achieved. It should also be noticed that the TOC removal could no longer be enhanced when the cell number was larger than 8. In addition, the energy consumption was found to decrease in the first six cell compartments but to increase with the further addition of chambers. In view of both removal efficiency and energy consumption, eight cell chambers would be an optimum.

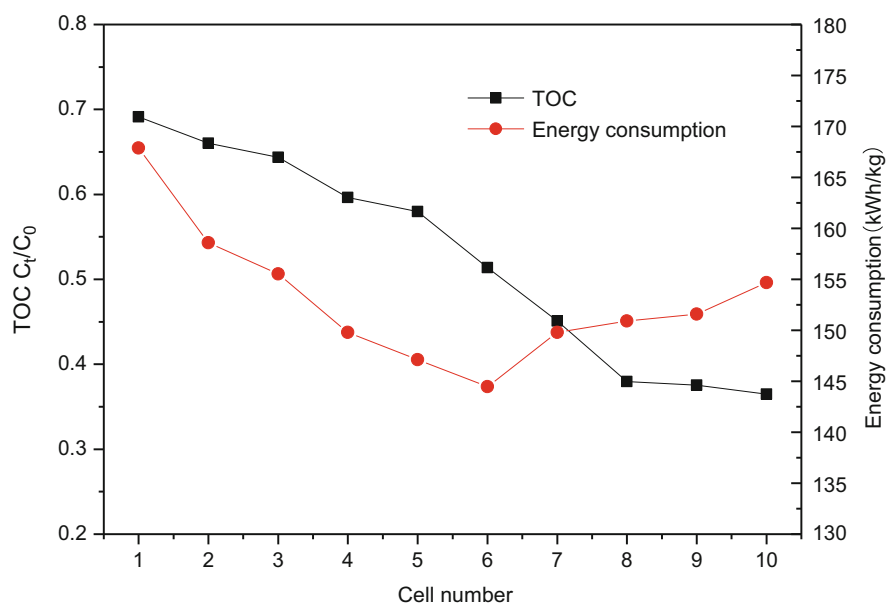


Fig. 8 The variation of TOC and energy consumption with the cell numbers [36]

5 Coupling of Flow-Through EF with Other Water Treatment Technology

It is well known that the optimum pH value for EF reaction is about 3 and EF is not cost-effective for the degradation of relatively high concentration pollutants [46]. Therefore, in order to overcome these drawbacks and meet the demand of the high removal efficiency of complex industrial wastewater, coupling of flow-through EF with other water treatment technology is very necessary.

5.1 Flow-Through EF/Adsorption

A flow-through EF/adsorption system was designed to remove tetracycline. The perforated DSA and the modified GF were used as the anode and the cathode in the EF system, and activated carbon fiber (ACF) was used as an adsorbent in flow-through adsorption system. It was observed from Fig. 9 that the tetracycline removal efficiency by the flow-through EF/adsorption, the flow-through EF, the flow-through adsorption, and regular adsorption system were 87.36%, 71.25%, 29.64%, and 15.68%, respectively. Compared with the single flow-through EF or adsorption system, flow-through EF/adsorption system showed the best performance. Moreover, the flow-through adsorption system demonstrated a higher removal efficiency than the regular adsorption system. Besides, five-times consecutive degradation tests were conducted to test the stability of the flow-through

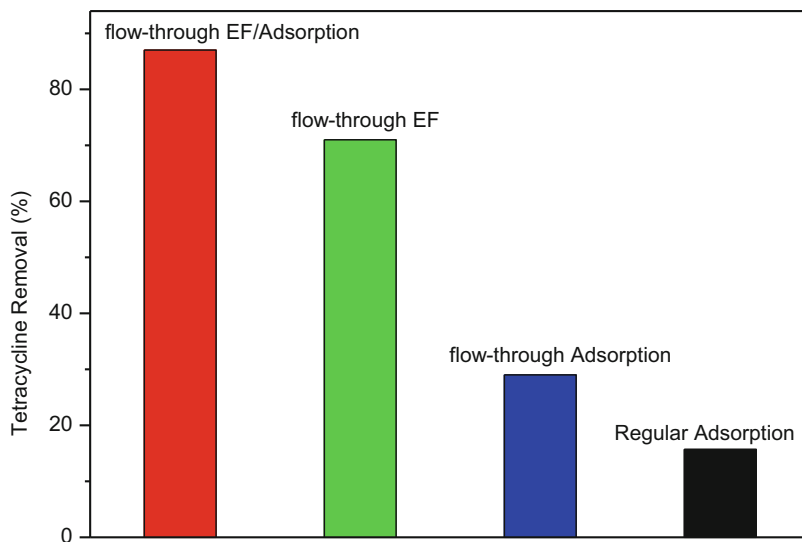


Fig. 9 The removal of tetracycline by four different systems

EF/adsorption system under the same condition. Both the tetracycline and TOC removal efficiency were almost stable. The tetracycline removal efficiency could reach above 85%, and the TOC removal efficiency kept above 30%. The above results illustrated that the flow-through EF/adsorption system can effectively remove tetracycline, and ACF was partially regenerated so that the system kept stable performance in five-times runs.

5.2 Flow-Through Peroxi-Coagulation

Peroxi-coagulation (PC) was carried out with a sacrificial Fe anode, which continuously supplies soluble Fe^{2+} to the solution. Fe^{2+} reacts with electrogenerated H_2O_2 to yield a concentrated Fe^{3+} solution, while the excess of such ion precipitates as $\text{Fe}(\text{OH})_3$. Target pollutants are then removed by their homogeneous degradation with $\cdot\text{OH}$ and their parallel coagulation with the $\text{Fe}(\text{OH})_3$ precipitate [46]. A flow-through PC system was designed to remove tetracycline. For the flow-through PC system, the anode was iron mesh and the cathodes were the modified GF. As shown in Fig. 10, the flow-through PC showed a better performance than the flow-through EF system in the comparable condition. The tetracycline removal efficiency was about 90% in the continuous flow-through PC system, while in the EF system was about 35%. The advantage of the flow-through PC system could be

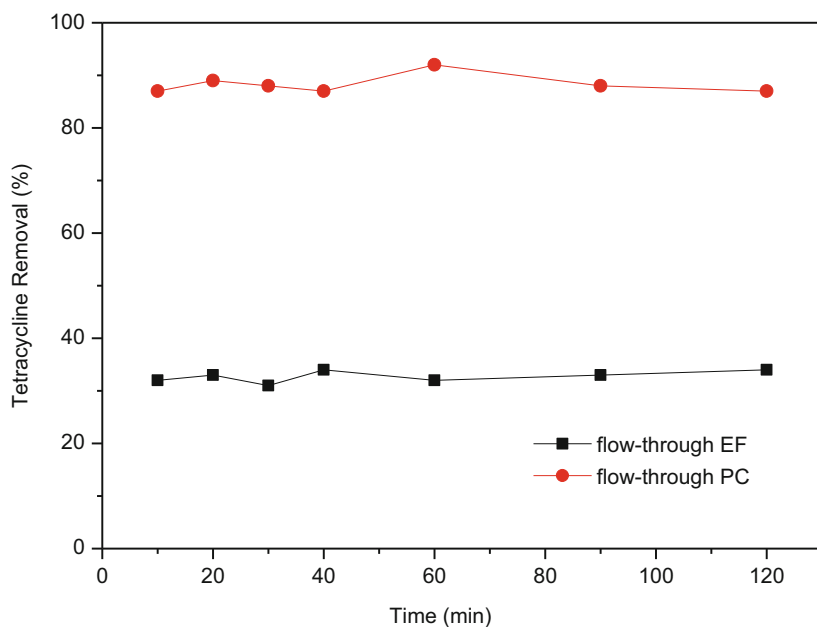


Fig. 10 The comparison of flow-through EF and flow-through PC on the tetracycline removal

attributed to the high production of $\cdot\text{OH}$ by the reaction of fast formation of H_2O_2 on the modified cathode and the continuous generation of Fe^{2+} from electrocoagulation, as well as the parallel coagulation with the $\text{Fe}(\text{OH})_3$ precipitate [48].

5.3 Flow-Through EF + Ozone

Ozonation is another widely used water treatment process for oxidation and disinfection. It has been demonstrated that it is capable of removing pharmaceutical compounds and steroids. In the flow-through EF/Ozone system, an ozone generator was used to generate ozone from pure oxygen. The O_2 and O_3 gas mixture from the ozone generator was then sparged into an electrochemical reactor, which could convert O_2 to H_2O_2 effectively by electrochemical reduction on the modified GF cathode. The in situ generated H_2O_2 then reacted with the sparged O_3 to produce hydroxyl radicals ($\cdot\text{OH}$), which is a very powerful oxidant and can degrade and mineralize organic pollutants effectively [45]. Compared with H_2O_2 (E^0 of 1.77 V/SHE) and O_3 (E^0 of 2.07 V/SHE), $\cdot\text{OH}$ (E^0 of 2.80 V/SHE) is a stronger oxidant. As shown in Fig. 11, the flow-through EF/ozone system showed a better performance than the flow-through EF and ozone system under the comparable conditions. The tetracycline removal efficiency was about 89% in the continuous flow-through EF/Ozone system, while by EF and ozone system they were about 30% and 45%, respectively. The results indicated that the flow-through EF/ozone process provided

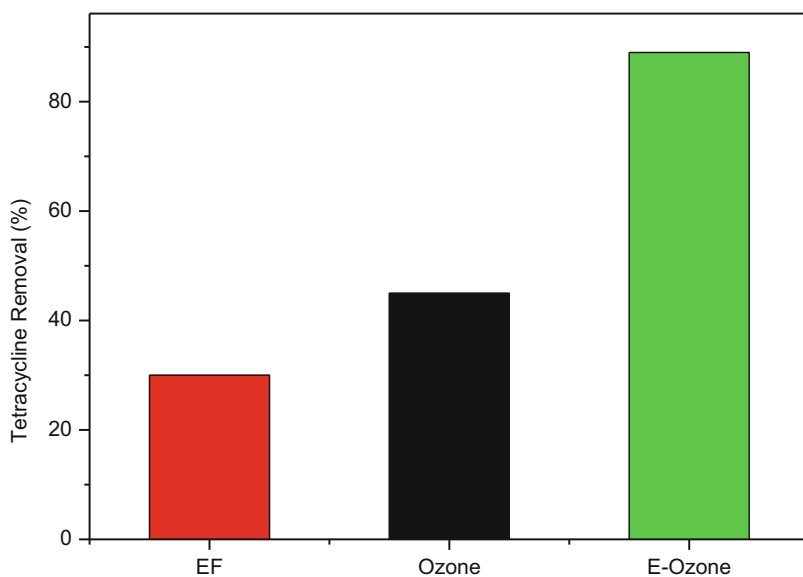


Fig. 11 The comparison of flow-through EF, ozone and flow-through EF/ozone system on the tetracycline removal

a convenient and effective alternative to conventional advanced oxidation processes for degrading refractory organic pollutants in wastewater.

6 Summary and Perspective

Flow-through EF reactor, has attracted much attention in recent years because of its unique properties and advantages, such as the fast mass and electron transfer to the electrode surface, which will not only increase the extent of electrochemical transformation, but also result in improved current efficiencies and reduced energy consumption. Moreover, coupling of flow-through EF with other water treatment technology is urgently necessary to meet the demand of the high removal efficiency of complex industrial wastewater. Compared with conventional EF, flow-through EF was more energy-efficient and potential for the degradation of organic pollutants. However, there are still many works to be done to improve the efficiency, reduce the cost, and expand the scale of application.

The following aspects need to be strengthened:

1. *Flow-through cathode material.* The cathode material determines the production of hydrogen peroxide in the EF system, thus affects the removal efficiency and energy consumption. Therefore, a high performance cathode is of great significance to the flow-through EF system. At present, the hydrogen peroxide production of flow-through EF cathode is still at a very low level, far from the level of air diffusion electrode. In addition, the pressure drop on the cathode should also be taken into consideration when the solution flow through. Therefore, the preparation or modification of cathode should be an appropriate trend to improve the performance of flow-through EF system.
2. *Expanding the scale of flow-through EF system.* The study of flow-through EF system is presently mainly focused on a laboratory scale. In order to test the feasibility of application, how to design a large-scale reactor and keep the high performance as that of lab scale is still need to explore. Also, a large area of electrode especially the cathode would be a big challenge.
3. *The combination of flow-through EF with other technologies for application.* As discussed above, the optimum pH value for EF reaction is about 3 and EF is not suitable to degrade relatively high concentration pollutants. In order to overcome the limitation of EF process and meet the demand of the high removal efficiency of complex industrial wastewater, coupling of flow-through EF with other water treatment technology, such as adsorption, electrocoagulation, and ozonation, is very necessary. Obviously, in viewpoint of environmental protection, this attempt is urgently required and needs reinforcement.

References

1. Brillas E, Sirés I, Oturan M (2009) Electro-Fenton process and related electrochemical technologies based on Fenton's reaction chemistry. *Chem Rev* 109:6570–6631
2. Yu X, Zhou M, Ren G, Ma L (2015) A novel dual gas diffusion electrodes system for efficient hydrogen peroxide generation used in electro-Fenton. *Chem Eng J* 263:92–100
3. Yavuz Y (2007) EC and EF processes for the treatment of alcohol distillery wastewater. *Sep Purif Technol* 53:135–140
4. Garcia-Segura S, Almeida L, Bocchi N, Brillas E (2011) Solar photoelectro-Fenton degradation of the herbicide 4-chloro-2-methylphenoxyacetic acid optimized by response surface methodology. *J Hazard Mater* 194:109–118
5. Isarain-Chávez E, Rodríguez R, Cabot P, Centellas F, Arias C, Garrido J, Brillas E (2011) Degradation of pharmaceutical beta-blockers by electrochemical advanced oxidation processes using a flow plant with a solar compound parabolic collector. *Water Res* 45:4119–4130
6. Peralta-Hernández J, Meas-Vong Y, Rodríguez F, Chapman T, Maldonado M, Godínez L (2006) In situ electrochemical and photo-electrochemical generation of the Fenton reagent: a potentially important new water treatment technology. *Water Res* 40:1754–1762
7. Moreira F, Garcia-Segura S, Vilar V, Boaventura R, Brillas E (2013) Decolorization and mineralization of Sunset Yellow FCF azo dye by anodic oxidation, electro-Fenton, UVA photoelectro-Fenton and solar photoelectro-Fenton processes. *Appl Catal B Environ* 142–143:877–890
8. Figueroa S, Vazquez L, Alvarez-Gallegos A (2009) Decolorizing textile wastewater with Fenton's reagent electrogenerated with a solar photovoltaic cell. *Water Res* 43:283–294
9. Garcia-Segura S, Garrido J, Rodríguez R, Cabot P, Centellas F, Arias C, Brillas E (2012) Mineralization of flumequine in acidic medium by electro-Fenton and photoelectro-Fenton processes. *Water Res* 46:2067–2076
10. Oturan M, Sirés I, Oturan N, Pérocheau S, Laborde J, Trévin S (2008) Sonoelectro-Fenton process: a novel hybrid technique for the destruction of organic pollutants in water. *J Electroanal Chem* 624:329–332
11. Li H, Lei H, Yu Q, Li Z, Feng X, Yang B (2010) Effect of low frequency ultrasonic irradiation on the sonoelectro-Fenton degradation of cationic red X-GRL. *Chem Eng J* 160:417–422
12. Sudoh M, Kodera T, Sakai K, Zhang J, Koide K (1986) Oxidative degradation of aqueous phenol effluent with electrogenerated Fenton's reagent. *J Chem Eng Jpn* 19:513–518
13. Zhang H, Ran X, Wu X (2012) Electro-Fenton treatment of mature landfill leachate in a continuous flow reactor. *J Hazard Mater* 241–242:259–266
14. Zhu R, Yang C, Zhou M, Wang J (2015) Industrial park wastewater deeply treated and reused by a novel electrochemical oxidation reactor. *Chem Eng J* 260:427–433
15. Vasconcelos V, Ponce-de-León C, Nava J, Lanza M (2016) Electrochemical degradation of RB-5 dye by anodic oxidation, electro-Fenton and by combining anodic oxidation–electro-Fenton in a filter-press flow cell. *J Electroanal Chem* 765:179–187
16. Ling Y, Xu H, Chen X (2015) Continuous multi-cell electrochemical reactor for pollutant oxidation. *Chem Eng Sci* 122:630–636
17. Moreira F, Garcia-Segura S, Boaventura R, Brillas E, Vilar V (2014) Degradation of the antibiotic trimethoprim by electrochemical advanced oxidation processes using a carbon-PTFE air-diffusion cathode and a boron-doped diamond or platinum anode. *Appl Catal B Environ* 160–161:492–505
18. Bard AJ, Faulkner LR (1983) *Electrochemical methods fundamentals and applications*. *J Chem Educ* 60:669–676
19. Ma L, Zhou M, Ren G, Yang W, Liang L (2016) A highly energy-efficient flow-through electro-Fenton process for organic pollutants degradation. *Electrochim Acta* 200:222–230
20. Liu H, Vecitis C (2012) Reactive transport mechanism for organic oxidation during electrochemical filtration: mass-transfer, physical adsorption, and electron-transfer. *J Phys Chem C* 116:374–383

21. Yang J, Wang J, Jia J (2009) Improvement of electrochemical wastewater treatment through mass transfer in a seepage carbon nanotube electrode reactor. *Environ Sci Technol* 43:3796–3802
22. Colmati F, Tremiliosi-Filho G, Gonzalez E, Berná A, Herrero E, Feliu J (2009) Surface structure effects on the electrochemical oxidation of ethanol on platinum single crystal electrodes. *Faraday Discuss* 140:379–397
23. Wang J, Li M, Shi Z, Li N, Gu Z (2002) Electrocatalytic oxidation of norepinephrine at a glassy carbon electrode modified with single wall carbon nanotubes. *Electroanalysis* 14:225–230
24. Britto P, Santhanam K, Ajayan P (1996) Carbon nanotube electrode for oxidation of dopamine. *Bioelectrochem Bioenerg* 41:121–125
25. Pan B, Xing B (2008) Adsorption mechanisms of organic chemicals on carbon nanotubes. *Environ Sci Technol* 42:9005–9013
26. Wang J, Musameh M (2003) Carbon nanotube/teflon composite electrochemical sensors and biosensors. *Anal Chem* 75:2075–2079
27. Gao G, Zhang Q, Hao Z, Vecitis C (2015) Carbon nanotube membrane stack for flow-through sequential regenerative electro-Fenton. *Environ Sci Technol* 49:2375–2383
28. Chen Z, Higgins D, Chen Z (2010) Nitrogen doped carbon nanotubes and their impact on the oxygen reduction reaction in fuel cells. *Carbon* 48:3057–3065
29. Chen Z, Higgins D, Tao H, Hsu R, Chen Z (2009) Highly active nitrogen-doped carbon nanotubes for oxygen reduction reaction in fuel cell applications. *J Phys Chem C* 113:21008–21013
30. Schnoor M, Vecitis C (2013) Quantitative examination of aqueous ferrocyanide oxidation in a carbon nanotube electrochemical filter: effects of flow rate, ionic strength, and cathode material. *J Phys Chem C* 117:2855–2867
31. Lannoy C, Jassby D, Gloe K, Gordon A, Wiesner MR (2013) Aquatic biofouling prevention by electrically charged nanocomposite polymer thin film membranes. *Environ Sci Technol* 47:2760–2768
32. Plakas K, Karabelas A, Sklari S, Zaspalis V (2013) Toward the development of a novel electro-Fenton system for eliminating toxic organic substances from water. Part I. In situ generation of hydrogen peroxide. *Ind Eng Chem Res* 52:13948–13956
33. Panizza M, Oturan M (2011) Degradation of Alizarin Red by electro-Fenton process using a graphite-felt cathode. *Electrochim Acta* 56:7084–7087
34. Zhou L, Zhou M, Hu Z, Bi Z, Serrano K (2014) Chemically modified graphite felt as an efficient cathode in electro-Fenton for p-nitrophenol degradation. *Electrochim Acta* 140:376–383
35. Zhou L, Zhou M, Zhang C, Jiang Y, Bi Z, Yang J (2013) Electro-Fenton degradation of p-nitrophenol using the anodized graphite felts. *Chem Eng J* 233:185–192
36. Ren G, Zhou M, Liu M, Ma L, Yang H (2016) A novel vertical-flow electro-Fenton reactor for organic wastewater treatment. *Chem Eng J* 298:55–67
37. Sklari S, Plakas K, Pesti P, Zaspalis V, Karabelas A (2015) Toward the development of a novel electro-Fenton system for eliminating toxic organic substances from water. Part 2. Preparation, characterization, and evaluation of iron-impregnated carbon felts as cathodic electrodes. *Ind Eng Chem Res* 54:2059–2073
38. Zhang C, Jiang Y, Li Y, Hu Z, Zhou L, Zhou M (2013) Three-dimensional electrochemical process for wastewater treatment: a general review. *Chem Eng J* 228:455–467
39. Forti J, Nunes J, Lanza M, Bertazzoli R (2007) Azobenzene-modified oxygen-fed graphite/PTFE electrodes for hydrogen peroxide synthesis. *J Appl Electrochem* 37:527–532
40. Barros W, Reis R, Rocha R, Lanza M (2013) Electrogeneration of hydrogen peroxide in acidic medium using gas diffusion electrodes modified with cobalt (II) phthalocyanine. *Electrochim Acta* 104:12–18

41. Reis R, Beati A, Rocha R, Assumpção M, Santos M, Bertazzoli R (2012) Use of gas diffusion electrode for the in situ generation of hydrogen peroxide in an electrochemical flow-by reactor. *Ind Eng Chem Res* 51:649–654
42. Pérez J, Llanos J, Sáez C, López C, Cañizares P, Rodrigo M (2016) Electrochemical jet-cell for the in-situ generation of hydrogen peroxide. *Electrochem Commun* 71:65–68
43. Panizza M, Cerisola G (2009) Electro-Fenton degradation of synthetic dyes. *Water Res* 43:339–344
44. Guinea E, Arias C, Cabot P, Garrido J, Rodriguez R, Centellas F (2008) Mineralization of salicylic acid in acidic aqueous medium by electrochemical advanced oxidation processes using platinum and boron-doped diamond as anode and cathodically generated hydrogen peroxide. *Water Res* 42:499–511
45. Li Z, Yuan S, Qiu C, Wang Y, Pan X, Wang J (2013) Effective degradation of refractory organic pollutants in landfill leachate by electro-peroxone treatment. *Electrochim Acta* 102:174–182
46. Nidheesh P, Gandhimathi R (2014) Electrolytic removal of Rhodamine B from aqueous solution by peroxicoagulation process. *Environ Sci Pollut Res* 21:8585–8594
47. Thiam A, Sires I, Brillas E (2015) Treatment of a mixture of food color additives (E122, E124 and E129) in different water matrices by UVA and solar photoelectro-Fenton. *Water Res* 81:178–187
48. Barros W, Franco P, Steter J, Rocha R, Lanza M (2014) Electro-Fenton degradation of the food dye amaranth using a gas diffusion electrode modified with cobalt (II) phthalocyanine. *J Electroanal Chem* 722–723:46–53

Reactor Design for Advanced Oxidation Processes

José L. Nava and Carlos Ponce de León

Abstract Electrochemical reactor design for oxidation processes follows similar engineering principles used for typical electrosynthesis reactors and include considerations of the components materials, electrode and cell geometries, mass transport conditions, rate of reactions, space–time yield calculations, selectivity, modeling, and energy efficiencies. It is common practice to optimize these characteristics at laboratory scale level followed by more practical considerations to build a larger reactor able to accomplish a required performance that can be easily assembled and requires low maintenance and monitoring. The scaling-up process should involve testing a variety of electrode configurations and cell designs to maximize the degradation of a particular pollutant. In this chapter, we describe the general principles of reactor design and list the most typical reactor configurations and performance followed by some recent advances in modeling and further developments.

Keywords Computational fluid dynamics, Current distributions, Electrochemical reactor, Filter-press flow cell, Mass transport, Non-ideal electrolyte flow, Packed bed electrode, Parallel plate electrodes, Rotating cylinder electrode, Wastewater treatment

J.L. Nava (✉)

Departamento de Ingeniería Geomática e Hidráulica, Universidad de Guanajuato, Av. Juárez 77, Guanajuato 3600, Mexico

e-mail: jlmm@ugto.mx

C. Ponce de León

Electrochemical Engineering Laboratory, Energy Technology Research Group, Faculty of Engineering and the Environment, University of Southampton, Highfield, Southampton SO17 1BJ, UK

e-mail: capla@soton.ac.uk

Contents

1	Introduction	264
2	Design and Basic Considerations	265
2.1	Electrode Materials	268
2.2	Cell Potential	269
2.3	Performance	270
3	Design and Characterization of Electrochemical Reactors	271
3.1	Experimental Characterization	271
3.2	Theoretical Characterization (Modeling and Simulation)	276
4	Further Developments and Perspectives	283
	References	284

1 Introduction

Electrochemical engineering uses the principles of chemical engineering and electrochemical sciences in order to develop an interdisciplinary field that nowadays is very diversified and extensive, covering aspects of design and performance of electrochemical processes that might involve non-electrochemical aspects. Well-known electrochemical engineering processes include the chlor-alkali industry, inorganic synthesis, electrowinning, refining and recovering metals, redox flow batteries for energy storage, batteries, and fuel cells, and in recent years, the field has established new and effective methodologies for environmental remediation and pollution control. Electrochemical technologies have been typically used for metal recovery; however, advances also include electrochemical oxidation process for recalcitrant organic materials and the electrocoagulation process that has also been used for organic removal. This has been forced by government regulations to clean households and industrial wastewaters before disposal and the urgent need to include green and sustainable processes into the existing industrial manufacturing. This chapter considers the advances of cell design and architecture and electrode materials and analyzes current trends and developments.

Electrochemical advanced oxidation processes (EAOPs) are well-established technologies characterized by the production of highly active hydroxyl radicals ($\cdot\text{OH}$) that can be divided into heterogeneous and homogenous processes. Typically, boron-doped diamond electrodes or photocatalytic surfaces such as TiO_2 generate the radical in the heterogeneous process, while in the homogeneous process, the radical is formed by the Fenton's Reaction by electro-generated hydrogen peroxide and Fe^{2+} ions in solution. The electrochemical cell is the center of the EAOPs and requires careful consideration of suitable designs, electrodes, and whether or not a separator material between anode and cathode is necessary [1–3]. In most cases, the cell design should provide uniform current and potential distribution that promotes the optimization of parameters such as energy consumption and increases the oxidation rate and the selectivity.

2 Design and Basic Considerations

Typical electrochemical cell design includes the parallel plate electrode geometry which offers uniform current and potential distributions and is by far the most popular cell design used. This particular design allows easy control of the distance between the electrodes and high rates of mass transport when used in a flow cell. In addition, parallel plate electrodes cells can be scaled-up relatively easily into modules of up to 200 bipolar parallel plates. However, it is common to find the use of parallel plates or rod electrodes immersed in rounded beakers at laboratory scale reactors with nonuniform stirring patterns that generally provide poor current and potential distribution and the flow regime cannot be easily determined. In these works, mass transport effects cannot be quantified and are not conducive to scale up the systems. A typical example of a parallel plate reactor is shown in Fig. 1a, and some examples for the degradation of organic materials include the treatment of municipal solid waste leachate [4] and removal of pharmaceutical clofibric acid and dyes [5, 6] and reactive yellow [7]. Other reactor designs are also popular due to their versatility although they are not so easy to scale up as the parallel plate geometry includes rotating cylindrical electrodes (RCE). A typical configuration is presented in Fig. 1b, and some examples include the reduction of ferric ions for the removal of benzene sulfonic acid [8]. Another type of reactor less frequently used is the bipolar trickle tower containing three-dimensional electrodes layers (see Fig. 1c [9, 10]), the fluidized bed (see Fig. 1d [11–13]), and the H-type cells for the degradation of herbicide diquat dibromide [14] (see Fig. 1e) and rotating anodes to evaluate the perchlorate formation in drinking water disinfected by direct electrolysis [15]. In all these configurations, it is desirable that the reactors have the following characteristics [2]:

- Low cost of materials for construction, maintenance, and operation together with easy installation and simplicity during the scaling-up
- Low cell potential difference
- Low-pressure drop including manifolds and electrolyte compartment
- An undivided cell is preferred for simplicity and to keep costs low
- Large surface area electrodes working at uniform current density and potential
- High conversion rates that could be achieved with high rates of mass transport

The factors above are closely associated with the selection of electrode materials, membranes, flow regime, and type of operation. The following section outlines some of the materials used for advanced oxidation processes.

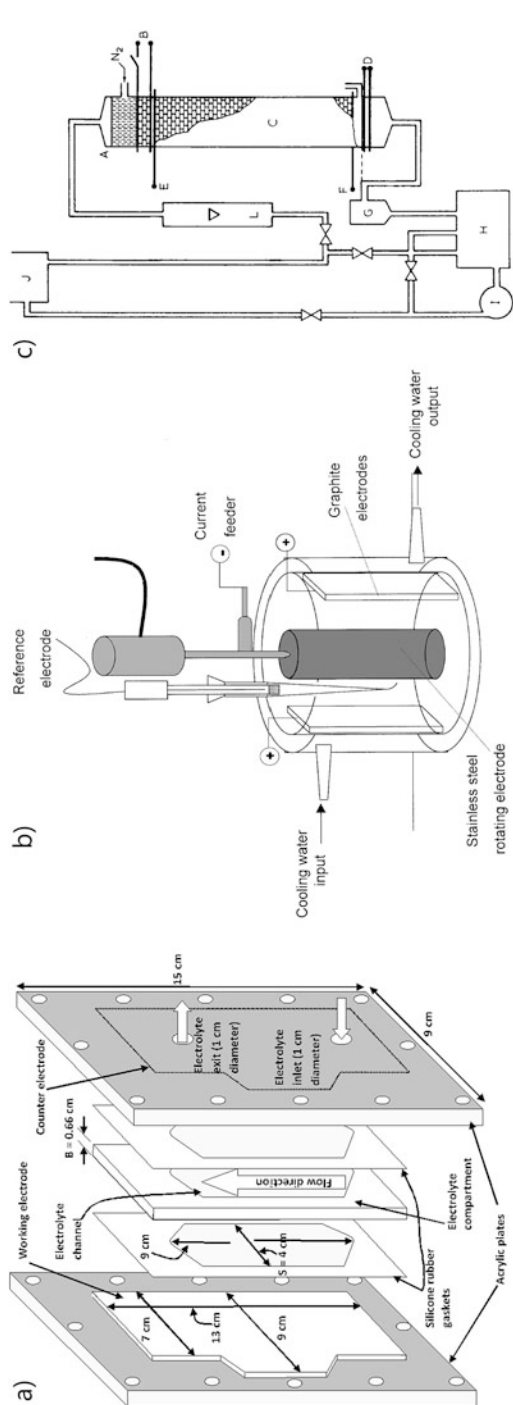


Fig. 1 Reactor configurations. (a) Parallel plate reprinted from [16], Copyright 2011, with permission from Elsevier, (b) rotating cylinder reprinted from [17], Copyright 2001, with permission from Elsevier, (c) bipolar trickle tower reprinted from [18], Copyright 1980, with permission from Springer, (d) fluidized bed reprinted from [11], Copyright 2010, with permission from Elsevier, and (e) H-type, reprinted from [14], Copyright 2017, with permission from Springer

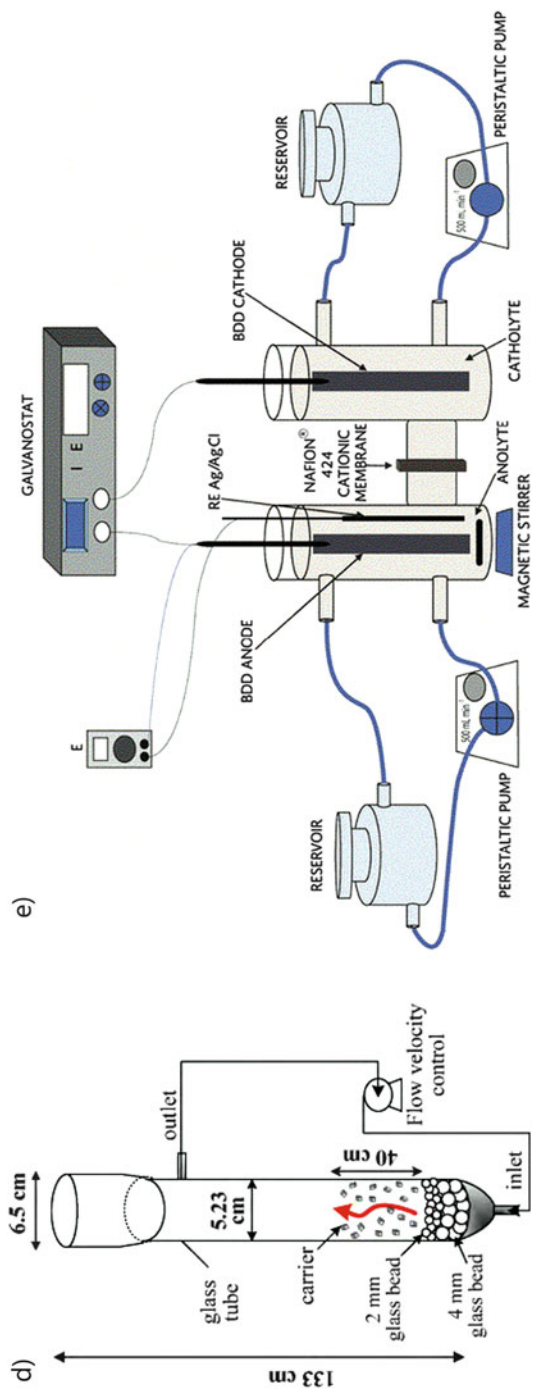


Fig. 1 (continued)

2.1 *Electrode Materials*

The selectivity and efficiency of the oxidation process is strongly dependent on the electrode material. Two types of anode materials have been generally accepted, which include electrodes with low overpotential for the oxygen evolution Reaction (OER) (active) and those with high overpotential for the OER (non-active) [19]. The active electrodes include most carbons and platinum, iridium, and ruthenium oxides based electrodes whereas those with high overpotential for OER are mainly antimony doped tin oxide, lead dioxide, and boron-doped diamond (BDD) electrodes. Carbon electrodes are used as cathodes for the generation of hydrogen peroxide to form the Fenton reagent for an indirect electrochemical oxidation. Many forms of carbon have been used and these include 3D electrodes such as reticulated vitreous carbon, felts, cloths, or gas diffusion electrodes (GDE) [20]. The manufacture of the GDE should pay attention to the hydrophobicity in order to avoid flooding the electrode while providing a 3-phase point of contact for electrolyte, gas, and catalyst. These electrodes overcome the problem of low solubility of oxygen in aqueous electrolytes by continuously supplying oxygen for the production of hydrogen peroxide and thus generate the Fenton reagent [21]. The most important characteristic of the electrode is the electroactive area. In a flat planar electrode fitted into a flow cell, the geometrical area is generally taken as the active electrode area whereas it is more difficult to determine the electroactive area for three-dimensional electrodes obtained from depositing nano-structured materials on a flat plate [22] or from using reticulated, meshed, or felt materials. The electroactive area should be as high as possible but avoiding high-pressure drops of the electrolyte flow or poor potential distribution generally encountered in 3D electrodes. Since the sections of the 3D electrodes are located at dissimilar distances from the counter electrode causing different surface potential and current densities, thin electrodes are preferred to minimize uneven distribution. The use of 3D BDD electrodes demonstrates the advantages of three-dimensional structures. For example, [23] recently demonstrated that using a 3D BDD electrode, organic pollutants such as phenols, aspirin, paracetamol, xylene, and methyl orange and alizarin red S can be mineralized completely at higher rates compared to flat BDD electrodes, using the same electrical charge. A typical problem in three-dimensional electrodes is to achieve a good electrical contact with the current collector. Conductive glue or pressure is used, but the point of contact is always prone to corrosion and increases the overpotential.

The current intensity (I) on the electrode depends on the concentration gradient of the electroactive species between the bulk (c_b) and the surface (c_0) and the mass transport coefficient k_m :

$$I = n F A k_m (c_b - c_0) \quad (1)$$

where n , F , and A are the number of electrons exchanged, the Faraday constant, and the electroactive surface, respectively. At the mass transport limiting conditions, i.e., when $c_0 = 0$, the equation can be simplified to:

$$I_L = n F A k_m c_b \quad (2)$$

where I_L is the limiting current. In porous 3D electrodes operating under complete mass transport control such as reticulated materials, stack meshes, and packed beds, the area of the electrode can be considered as the area per unit volume $A_e (=A/V_e)$ where V_e is the electrode volume. High values for the k_m and A_e are desirable to improve the reactor performance.

2.2 Cell Potential

In electrochemical reactors used for EAOPs, the ideal thermodynamic energy input is related to the Gibbs free energy change for the cell Reaction, ΔG_{cell} , which relates to the cell potential, E_{cell} , at the equilibrium:

$$\Delta G_{\text{cell}} = -nFE_{\text{cell}} \quad (3)$$

When the current or potential is applied at the limiting current conditions, the potential difference for any electrochemical cell is a complicated quantity with several contributions that depend on the electrolyte, electrode materials, and the equilibrium potentials of the anodic and cathodic reactions:

$$E_{\text{cell}} = E_c^0 - E_a^0 - \sum |\eta| - \sum |IR| \quad (4)$$

The first and second terms on the right-hand side of Eq. (4) are the cathodic and anodic standard potentials, whereas the third and fourth terms correspond to the overpotentials and the electrical resistance of the components. These last two terms represent the inefficiencies of the system and lead to a higher cell voltage requiring additional energy to drive the Reaction. While there is some freedom to select the anodic and cathodic reactions, it is more common to minimize the last two terms. The overpotentials depend on the activation and mass transport polarization, which can be minimized by operating the reactor at high temperatures and by selecting an appropriate catalyst for the desired Reaction together with high rates of mass transport. The term can be expanded as:

$$\sum |\eta| = |\eta_{c,act}| + |\eta_{a,act}| + |\eta_{c,conc}| + |\eta_{a,conc}| \quad (5)$$

where $\eta_{c,act}$ and $\eta_{a,act}$ represent the electron transfer limitations and dominate at low currents, whereas the terms $\eta_{c,conc}$ and $\eta_{a,conc}$ are the mass transport limitations due to lack of supply of electroactive species and it is generally observed at high currents when the current being withdrawn is larger than the rate at which the electroactive species reach the electrode surface. The IR term can be expanded to:

$$\sum |IR| = |IR_{c,circuit}| + |IR_{a,circuit}| + |IR_{catholyte}| + |IR_{anolyte}| + |IR_{membrane}| \quad (6)$$

The equation clearly shows the need to minimize the resistance of the components of the electrochemical reactor, including electrolytes, electrodes, electrical components, current collectors, and the membrane in the case of divided cells.

2.3 Performance

One of the most relevant parameters to evaluate the reactor performance which is rarely reported in AOP is the space–time yield, ρ_{ST} , which represents the amount of material w , reacted per unit reactor volume V per unit time:

$$\rho_{ST} = \frac{1}{V} \frac{dw}{dt} = \frac{\phi I}{nFV} \quad (7)$$

where w is the mass of materials (kg), and ϕ is the current efficiency. Typical values of this parameter for electrochemical processes are in the order of 0.08–0.1 kg h⁻¹ dm⁻³, whereas for non-electrochemical processes the values range between 0.1 and 1 kg h⁻¹ dm⁻³. The challenge for electrochemical engineers is to increase this value and recent academic studies have tried to develop changes in cell design and electrodes.

In electrochemical process under kinetic control, the rate of electron transfer prevails and the Reaction rate depends on the electrode potential and the choice of catalyst; the electrode area should be high. Under these conditions, the current varies exponentially with the overpotential [24]:

$$I = nFAk_c \exp\left(\frac{\alpha_a n F \eta}{RT}\right) \quad (8)$$

High surface area and active electrocatalyst promote high rate constants, k , which is related to the exchange current density j_0 ; α_a is the anodic charge transfer coefficient. Under these conditions, the secondary reactions are minimized. On the contrary, under full mass transport conditions the electroactive species are consumed immediately when they reach the electrode surface and the rate of reactant

supply or product removal dominates, the system operates at the maximum limiting current I_L . At these conditions, the convective-diffusion regime and the relative mean linear velocity u , of the electrolyte in a flow channel or the peripheral velocity of a rotating cylinder, to the electrode surface control the limiting current, where Eq. (2) is transformed into Eq. (9) [25]:

$$I_L = K u^\omega \quad (9)$$

where K is a constant given by the properties of the electrolyte composition and temperature while ω depends on geometry. Laminar flows are observed at $\omega = 0.33$ while turbulent flows at $\omega > 0.5$. The equation shows the importance of having large surface electrode area, high rates of mass transport k_m , and high concentration.

3 Design and Characterization of Electrochemical Reactors

The need for characterizing and modeling electrochemical reactors for EAOPs resides on the intensification of the wastewater treatment process taking into account the kinetic and mass transport conditions mentioned in the previous section. Modeling helps to achieve the optimal design of the electrochemical reactor, its understanding, and the design of compact technologies with rapid degradation rates, high mineralization current efficiencies (MCEs), and low electric energy consumptions (E_c). In order to achieve high MCEs, the desirable electrochemical reactions need to be controlled, avoiding as much as possible any parasitic side reactions. In this context, the experimental characterization and theoretical modeling of electrochemical reactors plays a crucial role, because it helps to design the correct shape and size of the reactor components, such as type and length of electrodes, nature and form of the turbulent promoters, electrolyte distributors, frames, and current feeders. In addition, the combination of the experimental characterization and modeling of transport phenomena, such as hydrodynamics, mass transport, heat transfer, and potential and current distributions, allows determining the optimal operational conditions to be applied to the electrochemical reactor.

3.1 Experimental Characterization

3.1.1 Pressure Drop and Non-ideal Flow Dispersion

In electrochemical reactors, the experimental characterization of flow pattern is widely explored by researchers because it offers mathematical simplicity, compared with those CFD predictions, and their contribution from the design of

electrochemical cells, flow, and pressure expressions is well described by empirical correlations and simple mathematical functions. The residence time distribution and pressure drop measurements are the typical techniques to characterize experimentally fluid flow patterns and pressure drops within electrochemical flow cells.

Pressure drop measurements are employed to determine the pumping energy requirements necessary to allow passage of the electrolyte streams within the electrochemical cell. The empirical pressure drop (ΔP) is typically described by a logarithmic function of the dimensionless Reynolds number:

$$\Delta P = a\text{Re}^b \quad (10)$$

where the Reynolds relates to the inertial and viscous forces of the electrolyte flow and is described as:

$$\text{Re} = \frac{ud}{\nu} \quad (11)$$

The coefficient a and exponent b are typically associated with geometric factors and flow patterns (i.e., laminar and turbulent flow in empty channels), respectively. The variables u , d , and ν are the mean linear flow rate, characteristic length of the electrochemical reactor, and kinematic viscosity. The characteristic length in rectangular flow cells is equal to the hydraulic diameter, while in rotating cylinder cells, d is defined as the diameter of the inner rotating cylinder. In packed bed electrochemical reactors, filled with particulate material as electrodes, the diameter of the spheroid type material employed takes the role of the characteristic length.

Several authors also report the mass transport coefficients as a function of the pressure drop (Eq. 12), which is realized considering that the mass transport parameter depends on the electrode geometry and the flow pattern (Eq. 13).

$$k_m A = a\Delta P^b \quad (12)$$

$$k_m A = a\text{Re}^b \quad (13)$$

Table 1 shows the experimental correlations of pressure drop over the well-known FM01-LC reactor extensively employed in EAOPs. In the case of the single-cell configuration, the a and b parameters increase in the filled channel (with turbulence promoter) with respect to the empty channel. This is attributed to the obstruction of the transversal area by the plastic net (turbulence promoter), where the electrolyte flows, which demands higher energy from the pumps. Meanwhile, the pressure drop increases in the stack of three empty undivided cells, indicating that this configuration demands higher energy pump consumption. The mass transport for 3D electrodes indicates that the metal foam electrodes present a higher $k_m A$ for a similar pressure drop across the expanded metal electrodes. The presence of porous electrodes demands higher pumps power, although mass transport is enhanced.

Table 1 Experimental values of pressure drop over the FM01-LC reactor

Configuration	$a \times 10^2$	b	Correlation	Ref.
Empty single cell	0.69	1.39	$\Delta P = aRe^b$	[26]
Filled single cell with PTFE turbulence promoter	1.69	1.54	$\Delta P = aRe^b$	[26]
Stack of three empty undivided cells	0.028	2.88	$\Delta P = aRe^b$	[27]
Expanded metal configuration (single cell)	0.29	0.44	$k_{nr}A = a\Delta P^b$	[28]
Metal foam (single cell)	0.38	0.47	$k_{nr}A = a\Delta P^b$	[28]

On the other hand, in filter press type reactors the ideal plug flow model is expected, although this cannot be guaranteed since the electrolyte kinetic energy losses, attributed to the friction of the liquid on the walls, induce plug flow deviations. Several models have been developed to describe these plug flow variations, which are typically obtained by means of experiments of the residence time distribution (RTD). The most common model used to describe plug flow deviations is the dispersion plug flow (DPF) model:

$$\frac{\partial C}{\partial \theta} = \frac{1}{Pe} \frac{\partial^2 C}{\partial x^2} - \frac{\partial C}{\partial x} \quad (14)$$

where C is the dimensionless tracer concentration ($=c/c_0$), θ is the dimensionless time ($=t/\tau$), Pe is the dimensionless Peclet number ($=uL_x/D_{ax}\xi$), and x is the dimensionless axial length ($=X/L_x$). Here, c is the tracer concentration at any time, c_0 is the initial tracer concentration, X is the axis coordinate along the FM01-LC reactor length, L_x is the axial length, u is average mean linear liquid velocity in an empty channel, ξ is the bed void fraction (in empty channels, $\xi = 1$), and D_{ax} is the dispersion coefficient.

RTD experiments allow obtaining D_{ax} , which accounts for the plug flow deviations. Figure 2 shows the experimental and adjusted RTD curves in an empty flow channel of a filter press electrolyzer. Close agreement between simulation and experimental data was attained. The dispersion coefficient tends to increase with flow velocity.

The RTD impacts directly to the conversion because the fluid elements have different residence times. These fluctuations create variations of the concentration at the exit of the cell. In the ideal plug flow model, where there is no dispersion degree of the electrolyte, the concentration of the electroactive species leaves the reactor at $\theta = 1$.

Other models of RTD applied to filter-press flow reactors have been extensively investigated [29]. CFD techniques have been extensively performed to model and simulate the RTD showing excellent agreement between experiments and simulations; the latter will be discussed below.

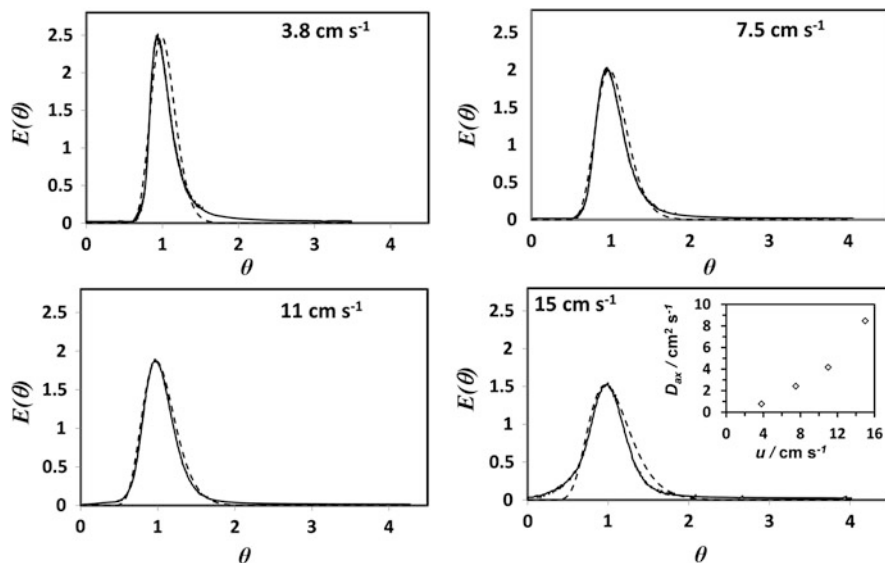


Fig. 2 Comparisons of experimental (—) and theoretical (----) RTD curves in the empty channel of the FM01-LC reactor at different flow velocities. The simulation was performed by the DPF model. Inset shows the axial dispersion coefficient versus flow velocity

3.1.2 Mass Transport Characterization

The experimental mass transport characterization is an important tool for evaluating the performance of an electrochemical reactor under mass transport control. The global mass transport coefficient is directly related to the global limiting current, as derived from (Eq. 2), and the electrolyte flow rate. The mass transport coefficient can be expressed in two types of correlations, the former, in terms of mean linear flow rates according to Eq. (15), and the second, by means of the dimensionless numbers, through Eq. (16).

$$k_m = au^b \quad (15)$$

$$\text{Sh} = a\text{Re}^b\text{Sc}^{0.33} \quad (16)$$

where a and b are empirical constants. The Sherwood number ($\text{Sh} = k_m u / D$) relates the convective mass transport to molecular diffusion, and the Schmidt number ($\text{Sc} = \nu / D$) correlates momentum diffusivity and molecular diffusion; the variable D is the diffusion coefficient. It is worth mentioning that the mass transport coefficient depends on the geometry of electrochemical reactor, electrolyte properties, and electrochemical systems [29]. Table 2 summarizes the mass transport correlations of different electrochemical reactors.

From the analysis of Table 2, we can observe that the a and b parameters vary depending on the type of reactor. In the case of the FM01-LC reactor, the mass

Table 2 Mass transport correlations ($Sh = aRe^bSc^c$) for the reduction of ferricyanide, for type of reactors

Channel configuration	Re and Re_p range	a	b	Cathode material	Ref.
<i>Filter-press type reactors</i>					
FM01-LC					
Empty channel	$200 < Re < 1,000$	0.22	0.71	Stainless steel	[32]
Channel with turbulence promoter	$200 < Re < 1,000$	0.74	0.62	Stainless steel	[32]
3-D electrode: reticulated metal	$264 < Re_p < 1,065$	3.81	0.68	Nickel foam	[33]
DIACELL™					
Empty channel	$25 < Re < 100$	0.69	0.36	BDD	[34]
Empty channel	$100 < Re < 2,500$	0.14	0.45	BDD	[34]
ElectroSyn™					
3-D electrode: reticulated metal	$300 < Re < 2,300$	0.32	0.61	Nickel foam	[35]
<i>Stirred type reactor</i>					
Rotating cylinder					
Inner rotating cylinder	$112 < Re < 1.62 \times 10^5$	0.079	0.7	Nickel	[36]

The parameter c is equal to 0.33 and 0.356 for filter-press type and rotating cylinder reactor
 Re_p is the particle Reynolds number

transport enhances in the following order: empty channel < channel with turbulence promoter < channel with reticulated electrode. In the empty rectangular channel, the laminar flow is developed between $100 < Re < 2,300$, while the turbulent flow is achieved at $Re > 2,300$. In smooth rotating cylinder electrodes, the turbulent flow is achieved at $Re > 100$. In this latter type of reactor, the turbulent mass transport predominates.

Recently, the characterization of mass transport during the reduction of dissolved oxygen to yield hydrogen peroxide was reported using graphite felt (GF), reticulated vitreous carbon (RVC), and planar BDD as cathodes [30]. The empirical law of mass transport described by Eq. (15) revealed a chaotic flow pattern within the porous structures of GF and RVC, which favored the mass transport. Mass transport was especially enhanced in the cell with GF due to its larger volumetric area, resulting in greater limiting current values.

On the other hand, in many papers about the anodic oxidation (AO) on BDD electrodes several authors use the Eq. (2), for the ferri/ferricyanide electrochemical system, to calculate the mass transport value k_m , and subsequently the limiting current is evaluated and applied to the BDD–electrolyte interface by means of the following equation [31]:

$$I_L = 4AFk_mCOD \quad (17)$$

This expression considers that all the organic compounds, present in the electrolyte, can be completely oxidized to CO_2 . Here, $n = 4$ and COD is the chemical oxygen demand. This methodology has been extended to PbO_2 electrodes.

The experimental evaluation of electrochemical reactors used in EAOPs requires the analysis of RTD to avoid undesirable flow patterns that impact on the performance of the electrochemical cell. Following this analysis, the experimental mass transport characterization is essential to find the operational conditions that include the electrolyte flow rate and the limiting current density being applied to the electrochemical reactor. The empirical mass transport correlations are helpful for scaling-up purposes.

3.2 *Theoretical Characterization (Modeling and Simulation)*

The modeling of hydrodynamics, mass transport, and current distribution in electrochemical reactors can be performed by CFD techniques, which allow measuring local variables and parameters such as velocity, concentration, mass transport coefficients, potential, and current. The CFD simulations with commercial and open access software which employ mesh methods in 2D and 3D are common practice. In the first instances, the electrochemical reactor is used to establish the domain of the numerical simulation. The numerical methods typically employed are the finite element and volume element methods, among others. The numerical methods provide a similar result if a sensitivity analysis of the mesh is performed. Taking the latter into account, a systematic study of the calculations of hydrodynamics, mass transport, and current and potential distribution, emphasizing their usefulness to guarantee acceptable mineralization current efficiencies and energy consumptions, is presented below.

3.2.1 **Simulation of Hydrodynamics in a Filter-Press Type Electrolyzer**

Figure 3a, b shows the simulation domain in the empty and filled channels used for the computational analysis. The cell dimensions are shown elsewhere [29].

The mean linear flow rates studied were comprised in the range between (0.038 and 0.15 m s^{-1}) giving Reynolds number between 300 and 1,500, characteristic of a laminar flow for the empty channel. Thus, the solution of the Navier–Stokes (NS) and diffusion-convection equations were used for the velocity field and RTD determinations. On the other hand, the same flow rates for the channel in the presence of the net plastic were used. However, since the net plastic creates high velocity streams causing 3D flow instabilities and eddy formations, we solve the Reynolds averaged Navier–Stokes (RANS) and the averaged diffusion-convection equations for the simulations.

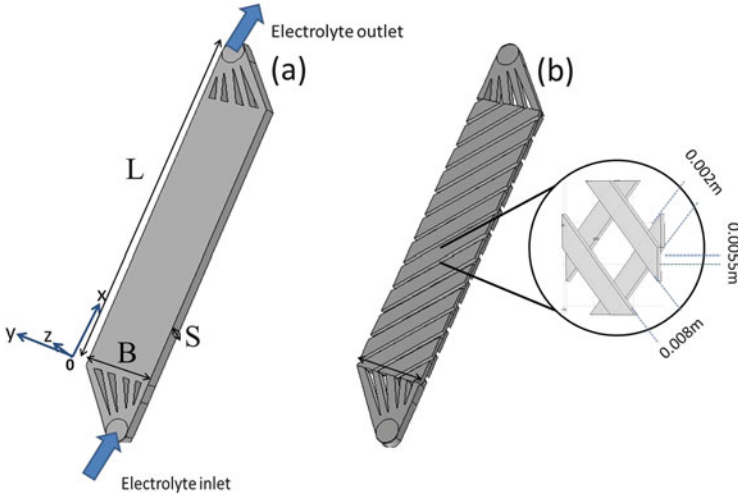


Fig. 3 Simulation domain established to implement the CFD simulation: (a) empty channel and (b) turbulence promoter-filled channel. The inset enlarges the turbulence promoter. Adapted from [37]

Laminar Flow (Empty Channel)

Under laminar flow conditions, the equations of the model for an incompressible fluid flow can be stated as follows. The Navier–Stokes and the continuity equations in steady state are:

$$\rho(\mathbf{u} \cdot \nabla)\mathbf{u} = \nabla \cdot [-P + \mu(\nabla \cdot \mathbf{u})] \tag{18}$$

$$\nabla \cdot (\rho\mathbf{u}) = 0 \tag{19}$$

where μ denotes the dynamic viscosity of the fluid, \mathbf{u} is the velocity vector, P is the pressure, and ρ is the density of the fluid. To solve Eqs. (18) and (19), the corresponding boundary conditions are considered as follows:

1. At the inlet, a normal inflow velocity was used, $\mathbf{u} = -\mathbf{n}U_0$, where \mathbf{n} is the unit normal vector,
2. A value of pressure at the outlet, $\rho(\mathbf{u} \cdot \nabla)\mathbf{u} = \nabla \cdot [-P + \mu(\nabla \cdot \mathbf{u})] = -\mathbf{n}P_0$,
3. In the walls, no slip consideration was set: $\mathbf{u} = 0$,

where U_0 is the inflow velocity and P_0 is the pressure at the exit of the cell.

Turbulent Flow (Filled Channel)

The net plastic used as a turbulence promoter usually performs a chaotic hydrodynamic flow pattern. Then, the fluid flow must be stated with a turbulence model. In this case, the RANS equations are applied:

$$\rho(\mathbf{u} \cdot \nabla)\mathbf{u} = -\nabla P + \nabla \cdot \left((\mu + \mu_T) \left(\nabla \cdot \mathbf{u} + (\nabla \cdot \mathbf{u})^T \right) \right) \quad (20)$$

where the so-called Reynolds stresses can be expressed in terms of a turbulent viscosity μ_T , according to the standard k - ε turbulence model:

$$\mu_T = \rho C_\mu \frac{k^2}{\varepsilon} \quad (21)$$

where k is the turbulent kinetic energy, and ε is the turbulent energy dissipation rate. A detailed description of the typical boundary conditions to solve Eqs. (20) and (21) can be consulted elsewhere [38].

Results and Discussion

Figure 4a, b shows the velocity field profile plots for an inflow velocity of 0.11 m s^{-1} in the empty and filled channels. The effect of inlet flow distributor on the velocity can be observed in the empty channel, which develops a jet flow. This flow deviation is avoided by the net-like spacer (classical turbulence promoter type D) because it homogenizes the velocity field inside the channel. This last effect is a desirable condition to guarantee an acceptable fluid flow dispersion, mass transport enhancement, and uniform current distribution during the scaling-up.

Comparisons of the experimental and simulated RTD in the empty and filled channel as a function of the dimensionless residence time (not shown) demonstrated excellent agreement between the theoretical and experimental RTD curves. Recently, the RTD in a multi-electrode stack has been modeled. The results demonstrate the powerful potential of CFD simulation to predict non-ideal flow deviations in very complex geometries [27].

The use of CFD techniques leads to visualize the fluid pattern within the electrode gap in electrochemical reactors. CFD visualizations are a powerful tool to prevent undesirable flow deviations such as stagnant zones, back mixing, and recirculation of electrolyte. These numerical models can be extended to design novel 3D electrodes, such as BDD or DSA[®] foams, expanded metal electrodes, and granular packed bed structures, among others. In addition, the CFD tools are useful in the design of net-like spacers used as turbulence promoters and during the scale-up of electrochemical reactors.

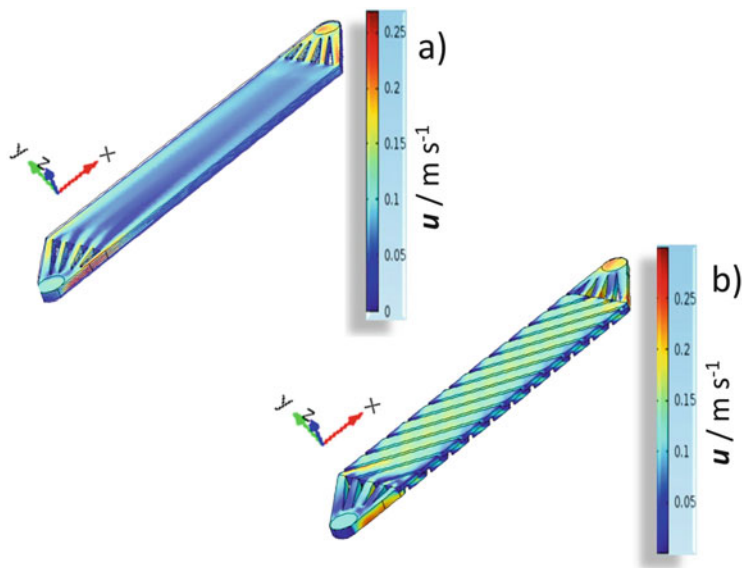


Fig. 4 Simulated velocity field magnitude at characteristic inflow velocity of 0.11 m s^{-1} . (a) Empty channel, (b) turbulence promoter-filled channel. Adapted from [37]

3.2.2 Simulations of the Secondary Current Distribution Along the BDD Plate During the Formation of Hydroxyl Radicals from the Water Discharge

In electrolytic cells containing large extended electrode area, the control of the potential and current is mandatory to guarantee the selectivity of the desired electrochemical reactions and to avoid undesirable side reactions. Here, we present the primary and secondary current distribution along a BDD plate fitted into the FM01-LC reactor. Oxidation of water to yield BDD($\cdot\text{OH}$) in acidic sulfate electrolyte was used as an example of an electrochemical system.

Formulation of the Numerical Simulation

The domain was considered inside the cell as a parallelepiped shape similar to that shown in Fig. 3a, and it was assumed that the potential drop along the conductive BDD material was negligible. In dilute solutions, the current density, j , at any point inside the parallelepiped cell is determined by the gradient of the local potential, ϕ , by means of the Ohm's Law of the ionic conductance:

$$j = -\kappa \nabla \phi \quad (22)$$

Table 3 Boundary conditions to solve the Laplace Eq. (23)

	Primary current distribution	Secondary current distribution
At BDD anode	$\phi = \phi_a$	$-\kappa \frac{\partial \phi}{\partial \xi} = j_0 \exp\left(\frac{\eta}{b_a}\right)$
At platinized cathode	$\phi = \phi_c$	$-\kappa \frac{\partial \phi}{\partial \xi} = j_{ave}$
At isolants	$-\kappa \frac{\partial \phi}{\partial \xi} = 0$	$-\kappa \frac{\partial \phi}{\partial \xi} = 0$

where κ is the ionic conductivity of the electrolyte. While the potential distribution in the electrolyte is described by the Laplace equation:

$$\nabla^2 \phi = 0 \quad (23)$$

Equation (23) is resolved first with corresponding boundary conditions, which are shown in Table 3, for the primary and secondary problem. Then, the current distribution is determined using Eq. (22).

In Table 3, ϕ_a , ϕ_c are surface potentials adjacent to anode and cathode; in practice, these are equal to the open circuit potentials, ξ is the normal component to the surface, j_0 is the exchange current density, η is the potential difference between the applied potential, and $\phi_a (=V - \phi_a)$, b_a is the anodic Tafel slope, and j_{ave} is the averaged current density at the cathode.

The numerical solution of transport equations was solved by the finite element software (COMSOL Multiphysics[®]). More details of the methodology used in the numerical simulations can be consulted in [39].

Results and Discussion

Figure 5 shows the normalized primary current distribution on the BDD surface (at $z = 0$) versus the normalized BDD length, x/L , at heights (y) of 0, 0.25, 0.8, and 2 cm. Border edges are located close to $x/L = 0$ and $x/L = 1$, being more important near the curved corners. However, these edge effects differ with a magnitude order of 1×10^{-5} ; therefore, the primary current distribution at BDD anode in the FM01-LC reactor can be considered uniform. This figure also shows the secondary current distribution evaluated at an overpotential, $\eta = 1.7$ V, where the hydroxyl radical formation occurs. A clear homogeneous current distribution, as predicted, was observed. The disappearance of the border effects in the secondary current distribution is related to the charge transfer resistance of water discharge on the BDD surface.

The homogeneous primary and secondary current distributions in the FM01-LC were developed considering the absence of isolated walls in the plane $x - y$, where the BDD is fitted, and by the 90° angle, forming by the polypropylene frame and the electrodes. The latter confirms the appropriateness of the engineered cell design and is consistent with several studies performed by our group where current efficiencies

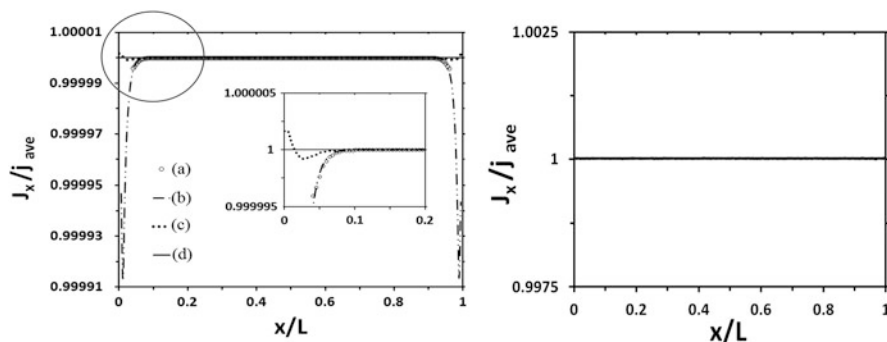


Fig. 5 Normalized primary (*left*) and secondary (*right*) current distribution profiles along the BDD working electrode at different heights: (a) $y = 0$ cm, (b) $y = 0.25$ cm, (c) $y = 0.8$ cm, and (d) $y = 2$ cm. Secondary simulations were performed at $\eta = 1.7$ V. Adapted from Ref. [39], Copyright 2013, with permission from Elsevier

during electrochemical incineration of cresols, indigo dye, and diclofenac using BDD as anode achieved current efficiencies greater than 80% [40–42].

The simulation of the tertiary current distribution along the BDD electrode during the anodic oxidation of organic compounds might be described by means of the limiting current density Eq. (17). The local mass transport coefficient, k_m , can be numerically evaluated via the empirical correlation described by Eq. (15), where the local velocity magnitude in this equation should come from the solution of NS or RANS equations. The simulation of the tertiary current distribution during anodic oxidation of organics has not yet been reported; however, for the purpose of visualizing the pattern of this tertiary distribution, readers can consult a paper published by our groups [38].

3.2.3 The Modeling of a Solar Photoelectro-Fenton Flow Plant

Figure 6 presents a schematic diagram of a pre-pilot solar photoelectron-Fenton (SPEF) flow plant in recirculation mode of operation that has been used for modeling. This plant couples a filter-press flow cell (the FM01-LC) in series with a compound parabolic collector (CPC) photoreactor. The mineralization of 10 dm^3 of the antibiotic erythromycin (ERY) was used as a model to test the system.

Mathematical Model

A parametric model including the mass balance in the electrochemical reactor and the CPC reservoir tank in one dimension was implemented. The model considers that the potential distribution on the GF is small, which avoids the side hydrogen evolution Reaction (HER).

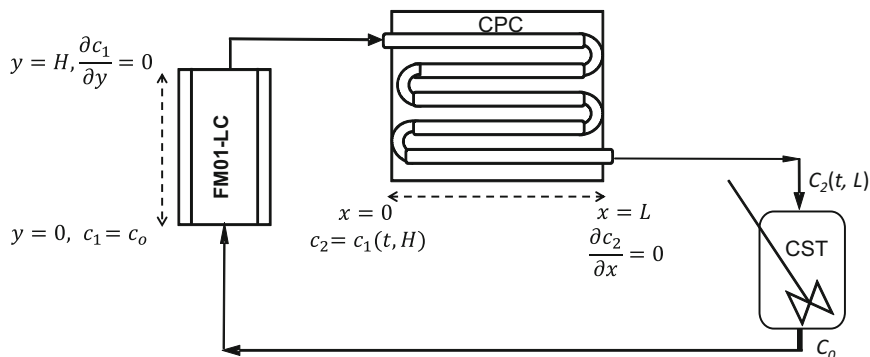


Fig. 6 Setup of the SPEF flow plant in pre-pilot scale. Reprinted from Ref. [43], Copyright 2017, with permission from Elsevier

The dissolved organic carbon (DOC) decay from ERY solutions treated here involves several Reaction steps and kinetic constants such as the electrogeneration of H_2O_2 , the Fenton's Reaction, photocatalytic reactions, and hydroxylation/dehydrogenation of the compounds leading to the formation of complex organic by-products and radicals during the degradation [44–46]. In order to construct a working model that follows the gradual depletion of DOC over time in recirculation mode, the following strategy was utilized: (1) the dispersion model expression for the FM01-LC, (2) the dispersion model with a global Reaction rate term for the CPC, and (3) the mass balance equation in the continuous stirred tank (CST) in transient regime. The abovementioned conservation equations were solved via finite element method using the boundary conditions shown in Fig. 6. In this parametric model, the Reaction order that better fitted the experimental DOC–time curves was zero, as determined after several simulation trials. A detailed description of the considerations of this model can be consulted in Ref. [43].

Results and Discussion

Figure 7 depicts the simulated DOC–time plots, as solid lines determined from the proposed parametric model, and as symbols from experimental data, obtained for 50, 100, 150 mg dm^{-3} ERY solution with $0.50 \times 10^{-3} \text{ mol dm}^{-3} \text{ Fe}^{2+}$ at pH 3.0 and $j = 0.16 \text{ mA cm}^{-2}$ at $Q = 3.0 \text{ dm}^3 \text{ min}^{-1}$. Close agreement between theoretical and experimental data was obtained. The model predicts well the experiments if the oxygen reduction to yield H_2O_2 is favored, avoiding HER; in other words, the applied current density to favor the oxygen reduction Reaction (ORR) should give a cathodic potential between $-0.4 < E < 0.1 \text{ V}$ versus SHE, because at $E < -0.4 \text{ V}$ versus SHE, the parasitic HER occurs [30] and inhibits the SPEF process. Additional simulations including, i.e., the influence of current density, Fe (II) concentration, and electrode potential on ERY degradation, can be found in [43].

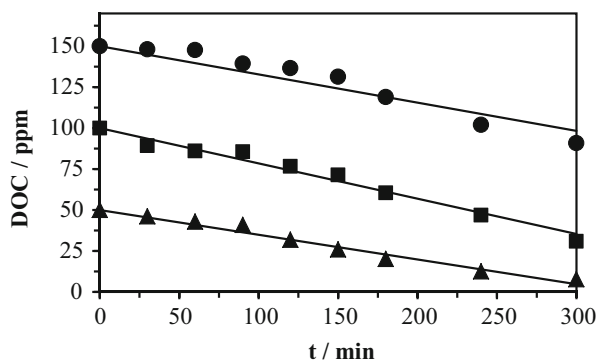


Fig. 7 DOC removal with electrolysis time for the SPEF experiments with initial DOC of (filled triangles) 50 mg dm^{-3} , (filled squares) 100 mg dm^{-3} , and (filled circles) 150 mg dm^{-3} , at $Q = 3.0 \text{ dm}^3 \text{ min}^{-1}$. Solid lines (—) are the theoretical data determined from the parametric model taking $C_0 = \text{DOC}$. Electrolyte: $0.050 \text{ mol dm}^{-3} \text{ Na}_2\text{SO}_4$ with $0.50 \times 10^{-3} \text{ mol dm}^{-3} \text{ Fe}^{2+}$ at $\text{pH} = 3.0$. The cathodic current density was 0.16 mA cm^{-2} . Reprinted from Ref. [43], Copyright 2017, with permission from Elsevier

It is important to remark that the parametric model developed here was designed to understand and correlate the experimental DOC decay with time. In other words, this model allowed determining the global apparent Reaction term, without the contribution of the non-ideal flow deviations in the FM01-LC and CPC reactors. In this global apparent Reaction term, $\cdot\text{OH}$ is presupposed as the most powerful oxidant, although slower Reactions with other weaker oxidizing species like H_2O_2 and $\text{HO}_2\cdot$ are feasible.

Modeling strategy is a basic tool for scaling-up of EAOPs, since if the theoretical approach (in pre-pilot scale) reproduces the experimental data the electrochemical engineer can extend the model to design a pilot plant. A very important factor to mention is the fact the scale-up process should satisfy the similarities of geometry, momentum, chemical reaction and mass transport, electric field, and heat transfer; the latter analysis was out of the scope of this chapter, but interested readers should consult Ref. [47].

4 Further Developments and Perspectives

In order to design electrochemical reactors for EAOPs, CFD simulations with the experimental characterization help to (1) develop novel electrochemical cells involved in EAOPs and (2) characterize the Reaction environment of existing reactors. These models can be extended to design novel 3D electrodes, such as BDD or DSA[®] foams, expanded metal electrodes, and granular packed bed structures; in addition, CFD techniques can be used to design novel net-like spacers used as turbulence promoters that favor mass transport. The characterization of the

Reaction environment such as hydrodynamics, mass transport, heat transfer, and potential and current distributions, allows determining the optimal operational conditions to be applied to the reactors.

The optimal design of the electrochemical reactors allows developing compact volumes with rapid degradation rates, high mineralization current efficiencies, and low electric energy consumptions. One of the most valuable parameters, not often considered in the design and evaluation of advanced oxidation processes, is the space–time yield.

The challenges reside on the modeling of biphasic systems (including gas H_2/O_2 release), which have not been yet characterized, even when it is well known that gas bubbling increases the electrolytic energy consumption. The modeling of flow plants (containing several reactors and unit operations) also deserves special attention. The mathematical modeling is crucial during the scale-up of EAOPs.

References

1. Wendt H, Kreysa G (2010) *Electrochemical engineering: science and technology in chemical and other industries*. Springer, Berlin
2. Pletcher D, Walsh FC (1990) *Industrial electrochemistry*, 2nd edn. Chapman and Hall, London
3. Bebelis S, Bouzek K, Cornell A, Kelsall GH, Ferreira MGS, Lapicque F, Ponce de León C, Rodrigo MA, Walsh FC (2013) Highlights during the development of electrochemical engineering. *Chem Eng Res Des* 91:1998–2020
4. Quan X, Cheng Z, Chen B, Zhu X (2013) Electrochemical oxidation of recalcitrant organic compounds in biologically treated municipal solid waste leachate in a flow reactor. *J Environ Sci* 25:2023–2030
5. Brillas E, Garrido JA, Rodríguez RM, Arias C, Cabot PL, Centellas F (2008) Wastewaters by electrochemical advanced oxidation processes using a BDD anode and electrogenerated H_2O_2 with Fe(II) and UVA light as catalysts. *Port Electrochim Acta* 26:15–46
6. Vasconcelos VM, Ponce-de-León C, Nava JL, Lanza MRV (2016) Electrochemical degradation of RB-5 dye by anodic oxidation, electro-Fenton and by combining anodic oxidation-electro-Fenton in a filter-press flow cell. *J Electroanal Chem* 765:179–187
7. Bedolla-Guzman A, Feria-Reyes R, Gutierrez-Granados S, Peralta-Hernández JM (2017) Decolorization and degradation of reactive yellow HF aqueous solutions by electrochemical advanced oxidation processes. *Environ Sci Pollut Res* 24:12506–12514
8. Ting WP, Lu MC, Huang YH (2008) The reactor design and comparison of Fenton, electro-Fenton and photoelectro-Fenton processes for mineralization of benzene sulfonic acid (BSA). *J Hazard Mater* 156:421–427
9. Koparal AS, Yavuz Y, Gürel C, Ögütveren UB (2007) Electrochemical degradation and toxicity reduction of C.I. Basic Red 29 solution and textile wastewater by using diamond anode. *J Hazard Mater* 145:100–108
10. Yavuz Y, Shahbazi R (2012) Anodic oxidation of reactive black 5 dye using boron doped diamond anodes in a bipolar trickle tower reactor. *Separ Purif Tech* 85:130–136
11. Anotai J, Su CC, Tsai YC, Lu MC (2010) Effect of hydrogen peroxide on aniline oxidation by electro-Fenton and fluidized-bed Fenton processes. *J Hazard Mater* 183:888–893
12. Hussain SN, Roberts EPL, Asghar HMA, Campen AK, Brown NW (2013) Oxidation of phenol and the adsorption of breakdown products using a graphite adsorbent with electrochemical regeneration. *Electrochim Acta* 92:20–30

13. Cusick RD, Ullery ML, Dempsey BA, Logan BE (2014) Electrochemical struvite precipitation from digestate with a fluidized bed cathode microbial electrolysis cell. *Water Res* 54:297–306
14. Valenzuela AL, Vázquez-Medrano R, Ibáñez JB, Frontana-Uribe BA, Prato-García D (2017) Remediation of diquat-contaminated water by electrochemical advanced oxidation processes using boron-doped diamond (BDD) anodes. *Water Air Soil Pollut* 228:67
15. Bergmann MEH, Rollin J, Iourtchouk T (2009) The occurrence of perchlorate during drinking water electrolysis using BDD anodes. *Electrochim Acta* 54:2102–2107
16. Recio FJ, Herrasti P, Vazquez L, Ponce de León C, Walsh FC (2013) Mass transfer to a nanostructured nickel electrodeposition of high surface area in a rectangular flow channel. *Electrochim Acta* 90:507–513
17. Nava-M de Oca JL, Sosa E, Ponce de León C, Oropeza MT (2001) Effectiveness factors in an electrochemical reactor with rotating cylinder electrode for the acid-cupric/copper cathode interface process. *Chem Eng Sci* 56:2695–2702
18. Fleischmann M, Ibrisagić Z (1980) Electrical measurement in bipolar trickle reactors. *J Appl Electrochem* 10:151–156
19. Cominellis C (1994) Electrocatalysis in the electrochemical conversion/combustion of organic pollutants for waste water treatment. *Electrochim Acta* 39:1857–1862
20. Pletcher D, Walsh FC (1992) Three-dimensional electrodes. In: Genders JD, Weinberg NL (eds) *Electrochemical technology for a cleaner environment*. The Electrosynthesis Company Inc, Lancaster, NY
21. Harrington T, Pletcher D (1999) The removal of low levels of organics from aqueous solutions using Fe(II) and hydrogen peroxide formed in situ at gas diffusion electrodes. *J Electrochem Soc* 146:2983–2989
22. Recio FJ, Herrasti P, Sirés I, Kulak AN, Bavykin DV, Ponce de León C, Walsh FC (2011) The preparation of PbO₂ coatings on reticulated vitreous carbon for the electro-oxidation of organic pollutants. *Electrochim Acta* 56:5158–5165
23. He Y, Lin H, Wang X, Huang W, Chen R, Li H (2016) A hydrophobic three-dimensionally networked boron-doped diamond electrode towards electrochemical oxidation. *Chem Commun* 52:8026–8029
24. Bard AJ, Faulkner LR (2001) *Electrochemical methods; fundamentals and applications*, 2nd edn. Wiley, Hoboken, NJ
25. Walsh FC (1993) *A first course in electrochemical engineering*. The Electrochemical Consultancy, Romsey
26. Trinidad P, Walsh FC (1996) Hydrodynamic behaviour of the FM01-LC reactor. *Electrochim Acta* 41:493–502
27. Sandoval MA, Fuentes R, Walsh FC, Nava JL, Ponce de León C (2016) Computational fluid dynamics simulations of single-phase flow having a stack of three cells. *Electrochim Acta* 216:490–498
28. Bengoa C, Montillet A, Legentilhomme P, Legrand J (2000) Characterization and modeling of the hydrodynamic behaviour in the filter-press-type FM01-LC electrochemical cell by direct flow visualization and residence time distribution. *Ind Eng Chem Res* 29:2199–2206
29. Rivera FF, Ponce de León C, Walsh FC, Nava JL (2015) The reaction environment in a filter-press laboratory reactor: the FM01-LC cell. *Electrochim Acta* 161:436–452
30. Coria G, Pérez T, Sirés I, Nava JL (2015) Mass transport studies during dissolved oxygen reduction to hydrogen peroxide in a filter-press electrolyzer using graphite felt, reticulated vitreous carbon and boron-doped diamond as cathodes. *J Electroanal Chem* 257:225–229
31. Gherardini L, Michaud PA, Panizza M, Cominellis C, Vatisias N (2001) Electrochemical oxidation of 4-chlorophenol for wastewater treatment. *J Electrochem Soc* 148:D78–D82
32. Brown CJ, Pletcher D, Walsh FC, Hammond JK, Robinson D (1992) Local mass transport effects in the FM01 laboratory electrolyser. *J Appl Electrochem* 22:613–619
33. Griffiths M, Ponce de León C, Walsh FC (2005) Mass transport in the rectangular channel of a filter-press electrolyzer (the FM01-LC reactor). *Am Int Chem Eng J* 51:682–687

34. Santos JLC, Geraldés V, Velizarov S, Crespo JG (2010) Characterization of fluid dynamics and mass-transfer in an electrochemical oxidation cell by experimental and CFD studies. *Chem Eng J* 157:379–392
35. Montillet A, Comiti J, Legrand J (1994) Application of metallic foams in electrochemical reactors of filter-press type. Part II: mass transfer performance. *J Appl Electrochem* 24:384–389
36. Eisenberg M, Tobias CW, Wilke CR (1954) Ionic mass transfer and concentration polarization at rotating electrode. *J Electrochem Soc* 101:306–320
37. Castañeda LF (2016) Evaluation of the performance of the FM01-LC reactor in the regeneration of H_2SO_4 from depleted baths by the electro dialysis process: theoretical and practical study. Dissertation, Centro de Investigación y Desarrollo Tecnológico en Electroquímica S.C.
38. Pérez T, Ponce de León C, Walsh FC, Nava JL (2015) Simulation of current distribution along a planar electrode under turbulent flow conditions in a laboratory filter-press flow cell. *Electrochim Acta* 154:352–360
39. Pérez T, León MI, Nava JL (2013) Numerical simulation of current distribution along the boron-doped diamond anode of a filter-press-type FM01-LC reactor during the oxidation of water. *J Electroanal Chem* 707:1–6
40. Butrón E, Juárez ME, Solís M, Teutli M, González I, Nava JL (2007) Electrochemical incineration of indigo textile dye in filter-press-type FM01-LC electrochemical cell using BDD electrodes. *Electrochim Acta* 52:6888–6894
41. Coria G, Nava JL, Carreño G (2014) Electrooxidation of diclofenac in synthetic pharmaceutical wastewater using an electrochemical reactor equipped with a boron doped diamond electrode. *J Mex Chem Soc* 58:303–308
42. Nava JL, Núñez F, González I (2007) Electrochemical incineration of *o*-cresol and *p*-cresol in the filter-press-type FM01-LC electrochemical cell using BDD electrodes in sulphate media at pH 0. *Electrochim Acta* 52:3229–3235
43. Pérez T, Sirés I, Brillás E, Nava JL (2017) Solar photoelectron-Fenton flow plant modelling for the degradation of the antibiotic erythromycin in sulphate medium. *Electrochim Acta* 228:45–56
44. Brillás E, Martínez-Huitle CA (2015) Decontamination of wastewaters containing synthetic organic dyes by electrochemical methods. An updated review. *Appl Catal Environ* 166–167:603–643
45. Martínez-Huitle CA, Rodrigo MA, Sirés I, Scialdone O (2015) Single and coupled electrochemical processes and reactors for the abatement of organic water pollutants: a critical review. *Chem Rev* 115:13362–13407
46. Sirés I, Brillás E, Oturan MA, Rodrigo MA, Panizza M (2014) Electrochemical advanced oxidation processes: today and tomorrow. A review. *Environ Sci Pollut Res* 21:8336–8367
47. Goodridge F, Scott K (1995) *Electrochemical process engineering: a guide to the design of electrochemical plant*. Plenum Press, New York

Modeling of Electro-Fenton Process

A.A. Alvarez-Gallegos and S. Silva-Martínez

Abstract From the conventional Fenton process (H_2O_2 and Fe^{2+}), the electro-Fenton process was derived to improve the hydroxylation method (partial organic oxidation). Thereafter, electro-Fenton was adapted to water remediation. Since then, this approach has received much attention for wastewater treatment because it is an eco-friendly process and its technological implementation is simple. Although electro-Fenton involves a few and very simple chemical species (H_2O_2 , Fe^{2+} , Fe^{3+} , O_2), the interactions among them produce one of the most difficult set of chemical reactions. Therefore, the predictions of the main chemical reactions are a challenging task. The aim of this chapter is to propose a methodology for developing a general, practical, simple, semiempirical chemical model to predict organic pollutant abatement in a reliable electrochemical reactor by electro-Fenton process. The main outputs of this chemical model include the rate of H_2O_2 generation and its activation by Fe^{2+} to produce a strong oxidant. The organic pollutant degradation rate and the energy and time required to carry out the organic degradation are also included. Although under this approach it is not possible to follow a detailed evolution of concentration profiles of some by-products during the degradation time, this procedure is less complicated than others already available. Moreover, it can fulfil the main requirements of wastewater treatment: abatement of the organic pollutant.

Keywords Decolorization kinetic model, Electro-Fenton process, Low-cost electrodes for wastewater treatment, Unmodified carbon cathode for H_2O_2 generation, Wastewater treatment prediction

A.A. Alvarez-Gallegos (✉) and S. Silva-Martínez
CIICAp, UAEM, Cuernavaca, Morelos, Mexico
e-mail: aalvarez@uaem.mx

Contents

1	Introduction	288
1.1	The Technological Challenge of Wastewater Treatment	288
2	Fenton Process	289
2.1	Hydroxylation	290
2.2	Wastewater Treatment	291
2.3	Kinetic Modeling	293
3	Electro-Fenton Processes	296
3.1	Wastewater Treatment	296
3.2	Activation of H ₂ O ₂ by Iron Ions	297
3.3	Degradation of Organics by Fenton and EF Process	299
4	Modeling of Electro-Fenton Process	300
4.1	Multistep Mechanistic Rate Laws	300
4.2	Empirical Kinetic Modeling	301
5	Conclusions	308
	References	309

1 Introduction

Since the beginning of synthetic dyestuff production, its manufacture was linked to unfriendly chemistry. Under this scenario, the textile industry has been always linked with a huge pollution problem, and it is considered the second (agriculture is the first one) most important polluter of clean water.

1.1 The Technological Challenge of Wastewater Treatment

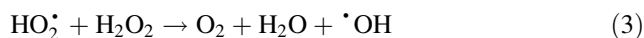
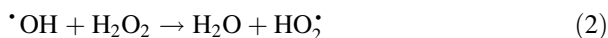
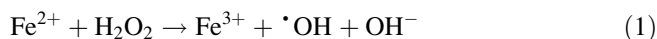
Daily textile mill productions of 8,000 kg of fabric require 1,600 m³ of water as well. More than 8,000 chemicals (some of them are dosed at a rate of several tons per month) are needed in various processes of textile manufacture [1]. As a consequence, mills discharge thousands of m³ of hazardous wastewater containing different concentrations of heavy metals, inorganic compounds, organic compounds, and dyes, among other toxic chemicals. Although the integral treatment of textile wastewaters is a challenging task, the main contamination source is coming from the most obvious indicator of water pollution: the color [2]. Many of these synthetic dyestuffs cannot be treated successfully by the conventional methods. Hence, removal of effluent color has become the integral part of textile wastewater treatment. Advanced oxidation processes (AOPs) are between the promising techniques for the environmental destruction organic dyes. A broad list of technological approaches such as supercritical water oxidation, sonolysis, electron beams γ -ray irradiation, ultraviolet (UV)-based processes, photocatalytic redox processes, O₃-based processes, and Fenton's reactions comes under advanced oxidation techniques [3].

From the conventional Fenton process, a mixture of H_2O_2 and Fe^{2+} (Fenton 1,894), the electro-Fenton process (EF) was derived to improve the hydroxylation process: the partial benzene oxidation to phenol [4]. Thereafter, EF process was adapted to water remediation [5]. Since then, EF process has received much attention for wastewater treatment because it is an eco-friendly process and its technological implementation is simple. Although both process, conventional Fenton and EF, involve a few and very simple chemical species (H_2O_2 , Fe^{2+} , Fe^{3+} , O_2), the interactions among them produce one of the most difficult set of chemical reactions. Therefore, the predictions of the main chemical reactions are a challenging task.

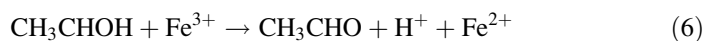
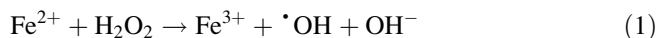
The aim of this chapter is to discuss the conceptual and technological problems involved in the development of a chemical model to predict organic pollutant abatement. In this way it is discussed, in a chronological way, how Fenton and EF processes were evolving from an academic activity to a technological application focused to solve a pollution problem. Then, a simple methodology for developing a general, practical, and simple semiempirical chemical model to predict organic pollutant abatement by EF is proposed.

2 Fenton Process

The first Fenton process was documented more than a century ago by Fenton [6] when he demonstrated a rapid and strong oxidation of tartaric acid in mildly acidic condition by H_2O_2 in the presence of a small amount of Fe^{2+} . Afterward, the $\text{Fe}^{2+}/\text{H}_2\text{O}_2$ mixture was known as Fenton's reagent. The first kinetic studies were published, and the first intermediate product was identified as an instable high oxidation species: H_2FeO_4 [7]. In 1932, through a catalytic mechanism developed by Bray and Gorin [8], a second strong oxidant produced in the Fenton process was identified as FeO^{2+} . A couple of years later, a third chemical species ($\cdot\text{OH}$) was proposed, by Haber and Weiss [9], as the strong oxidant. Nowadays, both main mechanisms are accepted to theoretically describe the H_2O_2 activation in the presence of Fe^{2+} . The Haber-Weiss mechanism is:

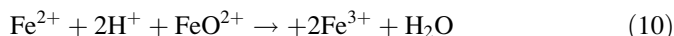
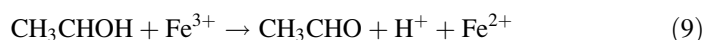
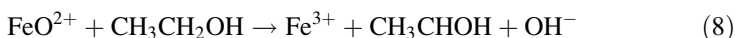
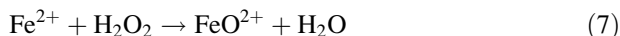


The active intermediate ($\cdot\text{OH}$) can react with Fe^{2+} , H_2O_2 , and other organic compounds. In this way, the oxidation of a simple organic molecule (ethanol to acetaldehyde) may be described by the Haber-Weiss mechanism [10]:



H_2O_2 activation is described by Eq. (1), the rate-determining step [11]. Equations (5 and 6) represent the oxidation and induced oxidation of ethanol, respectively. Equation (4) represents the end of the chain mechanism.

The ethanol oxidation may also be described as well by the Bray-Gorin mechanism [10]:

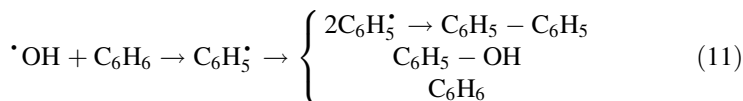


In a similar form, Eq. (7) represents the strong oxidant produced through a catalytic decomposition of H_2O_2 . Equations (8 and 9) represent the oxidation and induced oxidation of ethanol, respectively. Finally, the end of the chain mechanism is described by Eq. (10). As we can expect, both mechanisms give the same conclusions. The chemistry behind both main mechanisms is extremely complicated and might involve tens of consecutive and/or parallel reactions. During the last 70 years, a voluminous literature has been generated to describe both mechanisms, the ferryl [12, 13] and radical [14, 15] species. However, the identification and exact formation sequence of the strong oxidant are far from been clear, and it still remains controversial.

2.1 Hydroxylation

At the end of the 1940s, it was found that an aqueous solution of acrylonitrile showed polymerization if it were irradiated by X-rays or γ -rays. The chemical process was explained by the hydroxyl radical formation during the irradiation process because some similar results were obtained by the action of hydroxyl radicals produced by Fenton's reagent [16]. The active participation of $\cdot\text{OH}$ radicals during the hydroxylation was just inferred from the results obtained.

A clear description of the chemical mechanism of the first oxidation products obtained during benzene oxidation and induced benzene oxidation was a challenging task; Eq. (11) describes benzene oxidation and induced benzene oxidation. In a simplified form, at least three main parallel reactions can occur in the aqueous solution [17]:



A mixture of diphenyl and phenol are obtained with large amounts of oxidants. However, at low concentration of oxidants, most of the first oxidation products form back benzene. A controlled simultaneous addition of slightly acidified FeSO_4 and diluted H_2O_2 to a homogeneous emulsion of benzene will produce a large amount of diphenyl. Total yields are considerably below 100% because several parameters (strongly linked among them) control the benzene and benzene induced oxidations. As a result, the yield of the synthesized chemicals varied from experiment to experiment indicating a weak control during the radical production [17].

2.2 Wastewater Treatment

The application of Fenton process to wastewater treatment started at the end of the 1960s [18]. It was demonstrated that the abatement of organic pollutants was carried out in mildly, environment-friendly conditions. Therefore, Fenton process was viewed as a feasible wastewater treatment solution. Since then, the main interest was focused to explain that a broad type of organics (mainly contaminants) can be degraded at lab scale by the Fenton conventional approach: commercial H_2O_2 is added (its quantity was determined by a series of trial and error experiments) to a flask reactor (0.1–2 L) containing an aqueous solution of an organic molecule (homogenized by a magnetic stir), Fe^{2+} addition at suitable pH. Under this experimental approach, a general kinetic degradation path can be obtained from a set of optimal operational parameters: background electrolyte, temperature, and concentration of the target organic. Most of the authors consider that the degradation rate follows a pseudo-first-order kinetic, with respect to organic pollutant [19–21]. The complexity of the Fenton process can be visualized by the following idealized ethanol oxidation by Fenton process (Fig. 1). The ethanol degradation mechanism strongly depends on the short time life of main key active species (i.e., $\cdot\text{OH}$, $\text{HO}_2\cdot$, $\text{R}\cdot$, FeO^{2+} , among others) formed during the oxidation. The Fenton conventional approach cannot discern between both main mechanisms. Therefore, Fenton mechanisms, Haber-Weiss (Eqs. 1–6), and Bray-Gorin (Eqs. 7–10) give the same conclusions.

From a practical point of view, the idealized ethanol degradation can be fitted to a first-order kinetic reaction, according to:

$$[\text{Eth}]_t = a(e^{-kt}) \quad (12)$$

where $[\text{Eth}]_t$ is the ethanol concentration (mM), at any time t during the electrolysis time, a (mM) is a constant but does not represent the initial Eth concentration, and

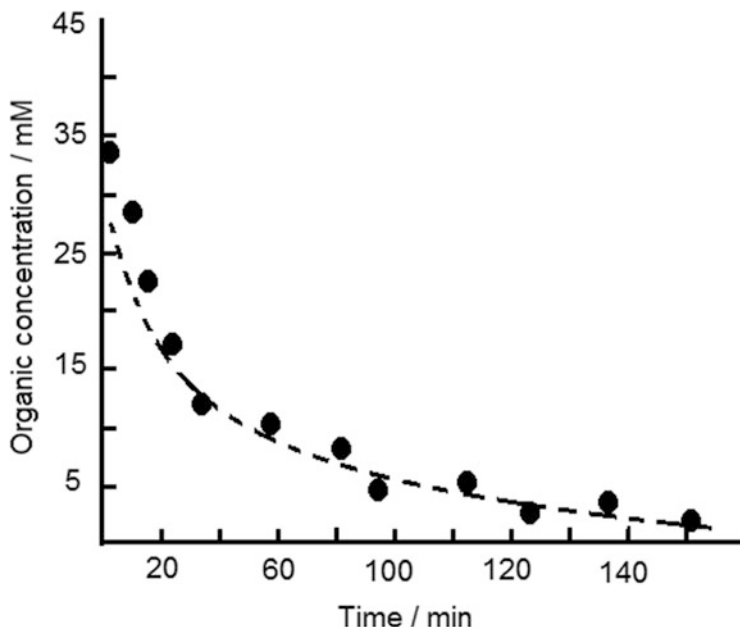


Fig. 1 Idealized ethanol degradation by Fenton process. Full circles represent experimental data. Dotted line represents the numerical evaluation from a pseudo-first-order kinetic model

k (min^{-1}) is the rate constant of the reaction. Hence, the academic attractiveness of the Fenton process is its simplicity. As a result, the academic attention in such subject was grown almost exponentially.

However, from the beginning, the application of Fenton's reagent to wastewater treatment faced similar problems to that described during Fenton hydroxylation: A controlled organic oxidation can be obtained only by a careful H_2O_2 addition/activation. Among the main technological problems that limit the application of Fenton's reagent to wastewaters treatment are the following:

- (a) Stoichiometric. It was recognized that an excess of H_2O_2 was needed to oxidize organics [22–25].
- (b) The complexity of Fenton chemistry. It is very difficult to develop a kinetic path of the organic and induced organic oxidation [18, 26].
- (c) The ambiguity of the nature of the strong oxidant. An additional problem arises when a detailed organic degradation needs to be represented by a set of kinetic reactions.

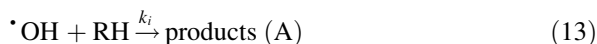
Indeed, organic degradation may be partially explained either Haber-Weiss or Bray-Gorin mechanism. While organics undergo a feasible degradation at lab scale, the standard Fenton's procedure is impractical for a real wastewater treatment capable of sustaining at variable pollutant organic loading.

2.3 Kinetic Modeling

2.3.1 Multistep Mechanistic Rate Laws

When wastewater was one of the most important applications of the Fenton process, the kinetic studies were focused to develop detailed kinetic models for better understanding H_2O_2 activation, including the organic oxidation mechanism under the Fenton traditional laboratory approach. Under this approach, it is necessary to describe the organic oxidation by a series of chemical reactions including its kinetic constants. Then a set of differential equations describing the concentration changes, as a function of time, for the main chemical species is defined. Consequently, this kind of kinetic models is able to predict the evolution of concentration profiles of some by-products as a function of degradation time. Nowadays, more than 1,700 rate constants for Fenton process are available. Therefore, at least in theory, from a mechanistic standpoint, it is possible to describe a complex Fenton process by a set of chemical equations based on the radical mechanism.

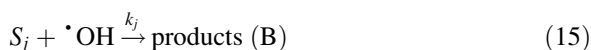
For developing such kinetic models, the following main assumptions are taken into account: (a) the $\cdot\text{OH}$ is nearly stoichiometric generated from reaction (1); (b) normally $\cdot\text{OH}$ is considered the unique strong oxidant responsible for the organic degradation mechanism; (c) organic degradation by different oxidants such as $\text{R}\cdot$, $\text{RO}\cdot$, and $\text{ROO}\cdot$ (i.e., Eq. 6) is minimized; and (d) as $\cdot\text{OH}$ is a very reactive species, its concentration is considered constant. In general, the degradation of the organic compounds (RH) by Fenton process can be expressed as [27, 28]:



And its reaction rate may be expressed as:

$$-d[\text{RH}]/dt = k_i [\cdot\text{OH}] [\text{RH}] \quad (14)$$

where products (A) are one set of products and k_i is a global rate coefficient. During the abatement of the target organic pollutant, their degradation products can alter the redox potential of iron ion and thereby affecting the most important reaction rates [29–32]. Scavenger species such as intermediates and excess of H_2O_2 , Fe^{2+} , $\cdot\text{OH}$, and $\text{HO}_2\cdot$, among others, are produced and consumed during the Fenton process through a series of parallel and consecutive reactions (i.e., Eqs. 2–4, Eqs. 28–33), changing its concentration and the rest of by-product concentrations. Therefore, the reaction rate can be more complicated if other oxidants are present. In this case, additional terms must be added to Eq. (14) [27, 28]. In a simplified form, all of them can be represented by S_j and their degradation products:



$$d[\cdot\text{OH}]/dt = k_1[\text{H}_2\text{O}_2][\text{Fe}^{2+}] - k_i[\text{RH}][\cdot\text{OH}] - \sum_j k_j[S_j][\cdot\text{OH}] \quad (16)$$

where products (B) are a second set of products and k_j is a global rate coefficient. Taking into account the assumption (d), the Eq. (16) is simplified:

$$[\cdot\text{OH}] = \frac{k_1[\text{H}_2\text{O}_2][\text{Fe}^{2+}]}{k_i[\text{RH}] + \sum_j k_j[S_j]} \quad (17)$$

Consequently, Eq. (14) is transformed to:

$$-d[\text{RH}]/dt = k_i \frac{k_1[\text{H}_2\text{O}_2][\text{Fe}^{2+}]}{k_i[\text{RH}] + \sum_j k_j[S_j]} [\text{RH}] \quad (18)$$

Consequently:

$$-d[\text{RH}]/dt = k_{\text{ap}}[\text{RH}] \quad (19)$$

where k_{ap} takes into account $k_1 k_i [\text{H}_2\text{O}_2][\text{Fe}^{2+}]/\sum_j k_j[S_j]$ and represent the pseudo-first-order reaction rate with respect to HR. Most of the authors agree with this fact [19, 21, 28, 33]. Therefore, $k_{\text{ap}} = f([\text{Fe}^{2+}], [\text{H}_2\text{O}_2], S_j, \text{pH}, \text{background electrolyte}, \text{temperature}, \text{among other parameters})$ [34]. For developing a Fenton process model, a set of experimental degradations are necessary to adjust k_{ap} .

Based on the above multistep mechanistic rate laws (or one adaptation of it), commercial kinetic software or kinetic models developed by the researchers (including from 10 to 54 chemical reactions) were tested for oxidation of different organic molecules by Fenton process. The best kinetic models are able to predict the evolution of concentration profiles of some by-products as a function of degradation time. Although most of the numerical results reasonably agree with the experimental data, some over- and underestimations of main chemical species concentrations and important differences were also spotted among them [20, 21, 35, 36].

The main drawbacks of these approaches are the use of (a) flask ranging from 100 to 2000 mL used as chemical reactors; (b) a magnetic stir to keep the working solution homogenized; (c) commercial H_2O_2 (including the cost and hazards associated with the transport and handling of concentrated H_2O_2); (d) the required H_2O_2 to oxidize a known amount of organics was determined by a series of trial and error experiments; (e) low organic concentration; (f) HO^\bullet that is usually regarded as the only powerful species for the oxidation/degradation of organic compounds; (g) except for a few cases, solution ion strength was kept by salts very unlikely to be found in real wastewater effluents (i.e., $\text{HClO}_4/\text{NaClO}_4$); and (h) the kinetic model uses reaction rates that do not necessarily represent the same chemical conditions at which the organic degradation was carried out.

Accordingly, some authors have focused to obtain a practical, less difficult kinetic model (similar to that depicted in Fig. 1), representing the kinetics of the overall reaction. From such a model, it is possible to obtain valuable information (a set of optimal operational parameters, cost-efficient operating conditions) for potential application of Fenton conventional approach to treat wastewaters containing an organic pollutant. However, this method does not give detailed information about the evolution of concentration profiles of some by-products as a function of degradation time [37].

2.3.2 Empirical Kinetic Modeling

From Eq. (19) versatile kinetic model can be developed to simulate a broad range of experiments within a given experimental framework. Once the experimental setup is defined (including chemical reactor, target organic, pH, background electrolyte, temperature, among others), the organic degradation by Fenton process can be studied systematically inside a selected experimental framework. Its boundaries will be defined by a set of key (minimum/maximum) concentration parameters. As a result, for a selected set of experiments, organic degradation (RH) will follow pseudo-first-order reaction rate with respect to RH. A k_{ap} can be estimated for all degradations. Therefore, experiments can be predicted within the selected experimental framework. This methodology can provide valuable information on the organic degradation as a function of key parameters.

Under this approach, a semiempirical kinetic model was developed for the bisphenol A (BPA) degradation by a heterogeneous Fenton-like catalyst [38]. Based on one of the main assumptions, the BPA degradation can be described as:



where k_{obs} is the observed rate coefficient defined in terms of key parameters:

$$k_{\text{obs}} = \frac{1}{C_0} k_{\text{ap}} ([\text{H}_2\text{O}_2]_0)^a ([\text{BPA}]_0)^b ([\text{Catal}]_0)^c \quad (21)$$

where a , b , and c represent the apparent rate orders of $[\text{H}_2\text{O}_2]_0$, $[\text{BPA}]_0$, and the loading amount of catalyst, respectively. C_0 is an arbitrary standard concentration; k_{ap} is the apparent rate coefficient defined in terms of the temperature:

$$k_{\text{ap}} = (A) \exp\left(-\frac{E_a}{RT}\right) \quad (22)$$

where A is the pre-exponential coefficient and E_a is the apparent activation energy for this reaction. For a given standard concentration (C_0), the effect of key

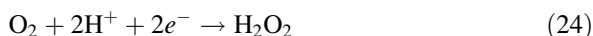
parameters on k_{obs} can be evaluated experimentally by keeping constant all parameters except one of them. In this way, the effect of the H_2O_2 on BPA degradation can be evaluated from several experiments in which H_2O_2 varies, but the temperature, initial load of BPA, and catalyst remain constant. From a bi-logarithmic plot of $\ln(k_{\text{obs}})$ vs $\ln([\text{H}_2\text{O}_2])$, a straight line is obtained; from its slope, the constant a is determined. The rest of the constants (b and c) are evaluated following the same procedure [34], and Eq. (21) is useful for the prediction of BPA degradation in the reactor.

3 Electro-Fenton Processes

Although EF process can be developed under different technological approaches [39, 40], the main basic configurations are briefly described as follows: First, H_2O_2 is continuously electro-generated on a suitable cathodic surface in the presence of Fe^{2+} (externally added) [5]. Second, Fe^{3+} is externally added, and both H_2O_2 and Fe^{2+} are electro-generated on a suitable cathodic surface [41]. Third, H_2O_2 is externally added, but Fe^{2+} is electro-generated via the reduction of Fe^{3+} on a suitable cathodic surface [42]. However, several combined EF processes (peroxi-coagulation) are as well feasible: H_2O_2 is externally added, while Fe^{2+} is electro-produced by a sacrificial iron anode [43]. Both species, H_2O_2 and Fe^{2+} , are electro-generated, the first one at the cathode and the second one at sacrificial anode [40].

3.1 Wastewater Treatment

One of the first works that demonstrated the feasibility to oxidize the 71% of 2.5 mM phenol by the EF process was documented at the middle of the 1980s [5]. Fenton's reagent was formed from the simultaneously cathodic O_2 and Fe^{3+} reduction on a carbon surface in the presence of 2 mM Fe^{2+} , in the pH interval of $2 < \text{pH} < 3$, according to:



During the electrolysis, cathodic reactions (23) and (24) took place. However, at least the following two electrochemical simultaneous reactions were expected to occur:

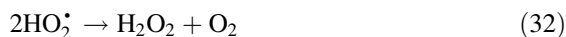
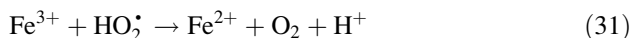
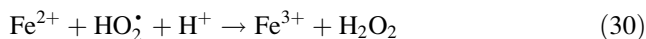
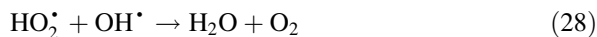
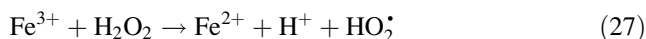




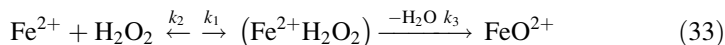
As a result, the electrolysis was carried out at 60% of current efficiency for the phenol degradation in mildly conditions. Phenol degradation can be explained by the mechanism proposed by Walling [29]. This novel process demonstrated that a controlled generation of $\cdot\text{OH}$ minimizes the H_2O_2 waste in unwanted parallel and consecutive reactions. During the last three decades, the EF process has been gradually emerging as a new environmental wastewater treatment technology. As a result, a massive amount of technical literature has been published in such subject. Main goals were focused on the elaboration of a detailed mechanistic chemical path during the oxidation of a given organic pollutant. A representative example is the methyl parathion degradation through 13 by-products [44].

3.2 Activation of H_2O_2 by Iron Ions

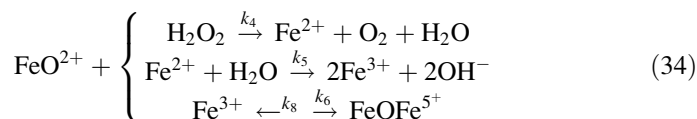
The first set of equations, the most accepted, is the Haber-Weiss mechanism [14, 45] represented by Eqs. (1–4). The efficiency of the $\cdot\text{OH}$ generation strongly depends on $\text{H}_2\text{O}_2/(\text{Fe}^{\text{II}} + \text{Fe}^{\text{III}})$ ratio. If H_2O_2 concentration is high, a series of unwanted reactions take place, and H_2O_2 is wasted through reaction Eqs. (2 and 27), producing a less reactive radical. Moreover, the strong oxidant is quenched by reaction (4), scavenged by reaction (28), and lost by reaction (29). Additionally, the available Fe^{2+} concentration is diminished by reaction (14) and reaction (30). The possible regeneration of Fe^{2+} is carried out by a series of parallel reactions; among the most important are reactions (27) and (31). Some of the H_2O_2 available can be regenerated by the following set of competitive reactions (30) and (32):



It has been accepted that it is not possible to give a solid proof (experimental/theoretical) that $\cdot\text{OH}$ is the strong oxidant produced from the mixture of iron ions and H_2O_2 [46, 47]. The second set of equations is the generation of the strong oxidant by Bray-Gorin mechanism represented by Eq. (7). However experimental results, based on the time dependence of the O_2 quantity evolved during the Fenton's reaction, suggest that the generation of the FeO^{2+} (initiation step) is more complex [12, 48]:



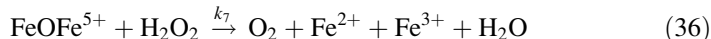
Fenton process starts with the reversible formation of the complex $\text{Fe}^{2+}\text{H}_2\text{O}_2$. From it the strong oxidant is formed by losing H_2O . At this point, FeO^{2+} may oxidize suitable substrates, if they are present in the solution, but it can simultaneously react with H_2O_2 and both iron ions according to:



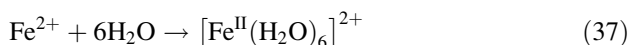
From this set of equations, the catalyst is regenerated by the reaction located at the top. The reaction in the middle represents a possible catalyst termination reaction. Additionally a binuclear species (FeOFe^{5+}) can be formed by the interactions between FeO^{2+} and Fe^{3+} , represented by the bottom reaction (34). The course of the above set of reactions can be influenced by the pH:



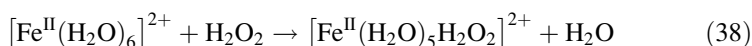
Furthermore, the complex (FeOFe^{5+}) can react with H_2O_2 to form O_2 and a mixture of $\text{Fe}^{2+}/\text{Fe}^{3+}$, according to:



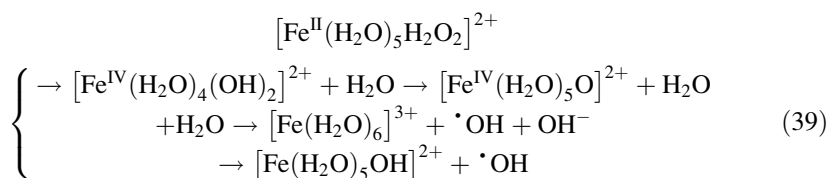
Main mechanisms based on experimental results are limited by the short time life of the main species considered above. However, such limitation can be minimized, and several complex mechanisms taking into account the water solvent and different intermediates can be analyzed by using density functional theory. Under this approach, the formation of the FeO^{2+} can be rewritten as follows [49, 50]: Fenton process starts with the formation of the hexa-aqua- Fe^{2+} complex:



The exchange of a water molecule in the hydration shell of the hexa-aqua- Fe^{2+} by H_2O_2 gives the first intermediate:



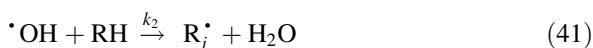
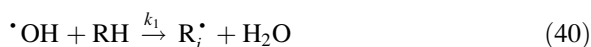
The first intermediate follows a very complicated chemistry. At least three parallel pathways are expected, and it might produce both strong oxidants [51]: $\cdot\text{OH}$ and FeO^{2+} :



Under some unknown experimental conditions, $\cdot\text{OH}$ may be the major product, while FeO^{2+} may be the main product under different conditions. Therefore, it is not a surprise that different active species can be produced in different experimental setups [49]. However, the formation of $[\text{Fe}^{\text{IV}}(\text{H}_2\text{O})_5\text{O}]^{2+}$ has been as well questioned [52].

3.3 Degradation of Organics by Fenton and EF Process

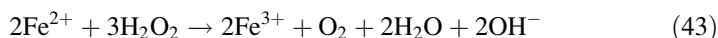
In the presence of organic molecules, both $\cdot\text{OH}$ and iron ions start a series of parallel, reversible, and consecutive reactions that lead to its oxidation. The prediction of the reaction paths that describes a detailed organic degradation by Fenton process is a very challenging task. The oxidation of alcohols by Fenton's reagent offers a good insight about the Fenton chemistry complexity when it is described by the Haber-Weiss mechanism. Once the $\cdot\text{OH}$ is produced (Eq. (1)), it can oxidize an organic molecule (RH) producing three different hydroxyalkyl radicals through a series of consecutive and parallel reactions according to [29, 31, 53]:



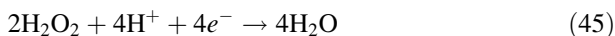
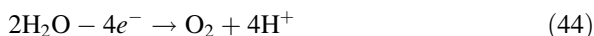
The rate constants ($k_{i,j,k}$) are between 10^7 and $10^9 \text{ L mol}^{-1} \text{ s}^{-1}$. Therefore, the quantity of each hydroxyalkyl radicals produced is very different, and they will further react following three main scenarios: (a) if R^\cdot is a carbonyl-conjugated radical and reacts with Fe^{2+} , the oxidation stops giving RH; (b) if R^\cdot is a primary or secondary alkyl radical and reacts with a similar alkyl radical, the oxidation chain stops giving a dimer R-R; and (c) if R^\cdot is a tertiary radical and reacts with Fe^{3+} , it can undergo further oxidation, regenerating Fe^{2+} and propagating the redox chain. If the identification list of main by-products is not available, the theoretical inference of a particular degradation pathway is always a risky task.

4 Modeling of Electro-Fenton Process

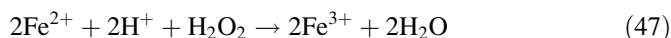
According to the Haber-Weiss mechanism Eqs. (1–14), electrons are transferred from Fe^{2+} to H_2O_2 converting it in molecular O_2 and H_2O , according to the global reaction:



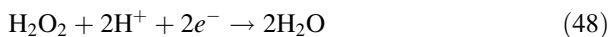
The above reaction may be as well represented as:



Something equivalent can be obtained if Fenton process is interpreted by the Bray-Gorin mechanism Eqs. (7 and 10):



In both cases, each H_2O_2 mole is gaining $2e^-$ moles according to:



Equation (48) should be the basis to evaluate the EF efficiency. Modeling wastewater treatment by EF process can be performed by two different approaches: multistep mechanistic rate laws and empirical kinetic modeling.

4.1 Multistep Mechanistic Rate Laws

This approach was already discussed (see Sect. 2.3). An application of this method is illustrated with the degradation of 200 mg L^{-1} 4-nitrophenol (4-NP) by EF. It was investigated in an electrochemical flow reactor (5 L) in batch recirculation mode [54]. It was found that a controlled $\cdot\text{OH}$ production improved the Fenton process. The 4-NP degradation in terms of COD decay followed pseudo-first-order kinetics. The final COD-removed efficiency (during 120 min electrolysis) was 92% against 54% when Fenton's reagent alone was applied under the same experimental condition. From experimental COD data, the electrochemical reactor was mathematically modeled as a plug flow reactor and its reservoir as a continuous stirred tank reactor. The pseudo-first-order rate constant was obtained from the model. Although, the model does not give information about the main concentration profiles of some by-products during 4-NP mineralization path, it gives valuable general

information focused to a wastewater treatment: an acceptable abatement of COD for a given electrolysis time.

4.2 *Empirical Kinetic Modeling*

Modeling wastewater treatment by EF process is a challenging task because it involves complex mechanisms and the rate constants are very difficult to evaluate. However, once they are evaluated, they should not be used to simulate the Fenton process in different experimental conditions. As a result, the design and scale-up of electrochemical reactors to be used in an industrial setting became a very difficult task. The problem can be circumvented by using an empirical model methodology based on experimental design methodology, artificial neural networks (ANN), and semiempirical kinetic model. All of them are useful when the process in question is not well understood and depends on several parameters.

4.2.1 **Experimental Design Methodology**

This method is an important tool of experimental design for developing complex processes and optimizing their performance. Based on statistical and mathematical methods, an empirical model can be built, by performing a set of minimum experiments, to predict targeted responses [55]. The experimental design is adapted according to the complexity of the target process. Among them, complete and fractional factorial design, central composite design, and Doehlert matrix, among others, can be mentioned. It is important to divide the main variables into two groups: independents (processing conditions) and dependents (experimental response of interest). The set of independent variables may include a large number of parameters interacting among them. In the case of Fenton process, the set of independent variables (x) could be pH, temperature, background electrolyte, and concentrations of target organic, H_2O_2 , and Fe^{2+} , among others. While the set of dependent variables (y) could include apparent rate constants, pollutants degradation rates (expressed as COD, TOC, etc.), and energy required to abate organic pollutants, among others. The experimental design can be developed by commercial software [56]. The experimental response is not going to allow the researcher to understand detailed mechanistic rate laws of the EF process; rather its goal is to determine a set of key parameters (or experimental conditions) needed to achieve the objectives of a wastewater treatment: abatement of the contamination. The experimental response of interest (y) is associated to the experimental design by a polynomial (quadratic or lineal) model [56, 57], for example:

$$y = \beta_0 + \sum_{j=1}^k \beta_j x_j + \sum_{j=1}^k \beta_{jj} x_j^2 + \sum_i \sum_{<j=2}^k \beta_{ij} x_i x_j + e_i \quad (49)$$

where y is the experimental response of interest; x_i, x_j are independent variables; β_0 is a constant coefficient; $\beta_j, \beta_{jj}, \beta_{ij}$ are interaction coefficients of linear, quadratic, and second-order terms, respectively; and the error is e_i . Equation (49) can be solved by commercial software. The effect of operational parameters (independent variables) is shown in the response surface graphs.

Experimental design methodology has been applied to wastewater treatment by EF process; as an example, a kinetic model developed to oxidize 150 mL of 0.05–0.2 mM chlortoluron solutions can be mentioned [57]. The electrochemical reactor was a cylindrical cell (500 mL) with a carbon-felt cathode and a cylindrical Pt-grid anode. The background electrolyte was 50 mM Na₂SO₄. During the electrolysis time, the interactions of $\cdot\text{OH}$ with chlortoluron give the typical exponential behavior (interpreted as a pseudo-first-order kinetic reaction) of the organic degradation, expressed as TOC. The optimal experimental parameters (cell current, chlortoluron concentration, electrolysis time) were obtained from a factorial experimental design combined with Doehlert matrix. The main by-products of the EF oxidation were identified as a function of the electrolysis time. This model allows the prediction/sets the best experimental condition for an effective EF oxidation in a wide variety of chlortoluron concentrations, from 0.05 mM (60 mA, 4 min) to 0.125 mM (300 mA, 8 h).

4.2.2 Artificial Neural Networks

ANN is a tool for modeling complex systems presenting nonlinearities. The method is detailed elsewhere [58]; however, a brief description is given here. One of its characteristics is that it does not require a kinetic description of the EF process and no global parameters (such as apparent rate constant of the reaction, k_{ap}) are needed. However, the pollutant degradation can be predicted. ANN is built up with several layers interacting among them. Normally three parallel interconnected structures (layers) could be enough for an EF process [59]. The strength of these interconnections is determined by a given weight. Independent variables (e.g., pollutant concentration, applied voltage/current, pH, background electrolyte, electrolysis time, among others) are located in the first (neuron) layer. The second structure consists of a hidden layer (feature detectors); its neuron number is determined iteratively and depends on the desired accuracy in the neural predictions. In this layer, each neuron is defined as follows:

$$n_1 = (W_{1,1})(In_1) + (W_{1,2})(In_2) + \dots (W_{1,k})(In_k) + b_1 \quad (50)$$

where n_1 is the first neuron, In_1 is the input one, $W_{1,1}$ is the weight corresponding to neuron one and input one, and b_1 is the bias corresponding to neuron one. The inputs (independent variables) are transformed by carrying out a weighted

summation (Eq. (50)), and then they are transferred to the hidden layer where they are transformed using an activation function. The sum Eq. (50) is the argument of the sigmoid transfer function f . The coefficients associated with the hidden layer are organized as matrices W (weights) and b_1 (biases). Dependent variables (pollutant degradation in terms of COD, TOC, among others) are located in the final output layer. The output of this hidden layer is the input to the last layer where it undergoes a further transformation. The output layer computes the weighted sum of the signals provided by the hidden layer, and the associated coefficients are arranged as matrices W_0 and b_2 . Using the matrix notation, the output layer can be given by:

$$\text{Out} = g[(W_0 f(W \cdot \text{In} + b_1) + b_2)] \quad (51)$$

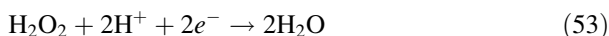
where f and g are any differentiable transfer function to generate their output. The system modifies the weights using an iterative technique to minimize errors between the calculated and the experimental values of the response variables. The number of inputs and outputs depends on the problem to be solved, and they are related to both variables: dependents and independents. The topology of ANN is related to the numbers of layers, number of neurons in each layer, and the transfer function. One of the most important tasks is the optimization of the ANN topology. The ANN prediction accuracy is a function of the set of experimental available values, and this condition can be regarded as one of the main drawback of this approach. Indeed, the larger the experimental values set, the better ANN prediction is obtained. In general, ANN has been applied to wastewater treatment by electrochemical process [60], sonophotocatalysis process [58], and light-enhanced Fenton process [61, 62], but a few works have been published on wastewater treatment by EF process. Among them it can be mentioned in the following work.

The oxidation of an aqueous solution of Basic Yellow 2 (20 mg L^{-1}) in a $0.05 \text{ M Na}_2\text{SO}_4$ medium (pH 3) was performed by a combined EF process (peroxi-coagulation). The electrochemical reactor was an open, undivided cylindrical glass cell (600 mL), and it was working at constant current (100 mA); working solutions were stirred magnetically. The cathode was a gas diffusion electrode, and the anode was an iron sheet. The cathodic reaction expected was electro-production of H_2O_2 , and the anodic reaction was iron oxidation to form ferrous ion. The Basic Yellow 2 degradation followed a pseudo-first-order reaction, and its rate constant was determined. An ANN model was developed to predict the performance of the Basic Yellow 2 degradation by the combined EF process. The independent variables (input layer) were electrolysis time, pH, applied current, and dye concentration. The dependent variable (output layer) was discoloration efficiency. The hidden layer was built with 16 nodes after several series of topology designs were tested. The sigmoid function was used as transfer function in the hidden layer. All experimental results were divided in three sample groups: training (70), validation (24), and test subsets (23). The validation of ANN can be represented as graph of predicted against experimental discoloration efficiency values. In this work, it was found that such a graph is a straight line with a correlation coefficient of 0.9713.

4.2.3 Semiempirical Kinetic Models

An alternative to experimental design methodology and ANN is semiempirical models. From wastewater treatment point of view, the target organic degradation by Fenton process may be visualized as a pseudo-first-order reaction rate [38]. The proposed kinetic model is based on the following assumptions: (a) both main mechanisms that explain the Fenton process give same theoretical results, (b) the activation of H_2O_2 is carried out very fast in the presence of Fe^{2+} , and (c) during the Fenton process, 1 mol of activated H_2O_2 may react as a two-equivalent reducing agent (Eq. (48)).

As a simple illustration, the oxidation of ethanol to acetaldehyde by the Fenton process may be described by several sets of equations: in the first one, the Haber-Weiss mechanism through the sequenced equations, Eq. (1, 4–6); in the second one, the Bray-Gorin mechanism through the sequenced equations, Eqs. (7–10); and in the third one, the following simple, clear mechanism through the following sequenced equations:



Therefore, the ethanol degradation can be fitted to a pseudo-first-order reaction rate (Eq. (12)). The advantage of this approach is the straightforward evaluation of the right H_2O_2 amount needed to oxidize the target organic. This fact allows to electro-generate the stoichiometric Fenton's reagent for a given quantity of organic and assess the EF process efficiency.

From the above kinetic model, a general, simple semiempirical chemical model can be developed to predict pollutant abatement for a wastewater treatment capable of sustaining at variable pollutant organic loading [63]. The chemical model is illustrated for Acid Orange 7 (AO7) abatement at room temperature in a catholyte continuously saturated with O_2 consisting of 1.5 L of 0.05 M Na_2SO_4 , pH 2 (H_2SO_4), and 1 mM Fe_2SO_4 . The anolyte was 1.5 L of 0.8 M H_2SO_4 . The organic degradation was performed by EF process using an electrochemical reactor divided by a Nafion[®] cation membrane, fully described elsewhere [63–66]. The cathode was a piece of unidirectional carbon fabric, and the electrochemical reaction expected was, first, electro-generation and then activation of H_2O_2 . The anode was a mesh of commercial stainless steel (SS), and the electrochemical reactions expected were SS oxidation to produce Fe^{2+} and then its oxidation to produce Fe^{3+} . Both electrodes were placed parallel to each other with an interelectrode gap of 6 mm. Electrodes were connected to a DC power supply. Catholyte and anolyte were separated by a Nafion[®] cation membrane, and they were pumped at constant flow rate (7 L min^{-1}). Figures 2 and 4 were adapted from [63].

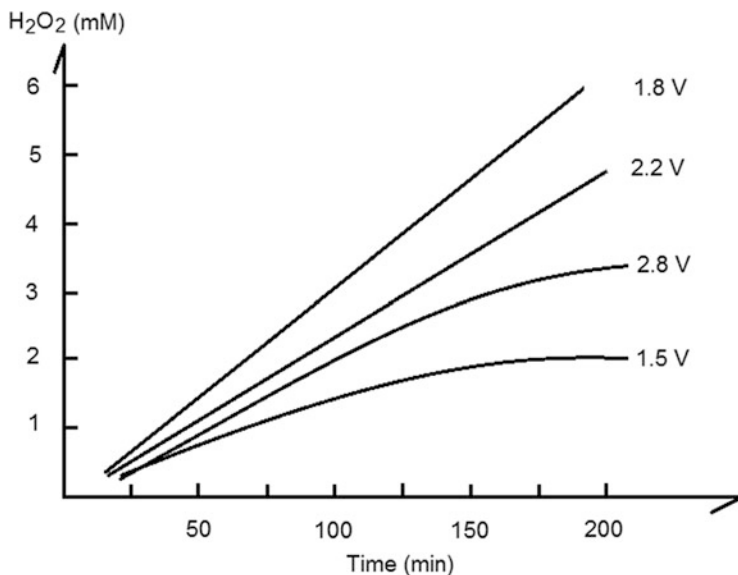
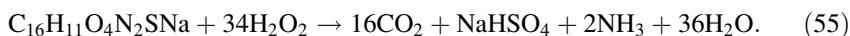


Fig. 2 Four different electrolyses to reduce O_2 as a function of the applied cell voltage. Catholyte continuously saturated with O_2 , 1.5 L of 0.05 M Na_2SO_4 , pH 2. Anolyte, 1.5 L of 0.8 M H_2SO_4 . Flow velocity, $7 L min^{-1}$. Adapted from [63]

The AO7 mineralization by H_2O_2 may be represented as the stoichiometric 68-electron AO7 oxidation reaction, if sulfur and nitrogen are transformed in H_2SO_4 and NH_3 , respectively, then:



A series of H_2O_2 production as a function of applied voltage was carried out in the electrochemical reactor by the oxygen reduction reaction (24) on a carbon surface. The best energetic condition (cell voltage, 1.8 V, 96% current efficiency for H_2O_2) was experimentally found: Fig. 2. At the best experimental conditions, the amount of electro-generated H_2O_2 is a linear function of the electrical charge passed during the O_2 reduction, following Faraday's law. Therefore, the H_2O_2 electro-production can be fitted to:

$$[H_2O_2] = a(ET) + b \quad (56)$$

where ET is the electrolysis time (min) and a and b are constants to be determined from the best experimental H_2O_2 electro-production, by a graph of $[H_2O_2]$ vs electrolysis time. Figure 3 (adapted from [66]) shows the data from two electrolyses to reduce O_2 , carried out in the flow cell at the best experimental conditions.

In absence of Fe^{2+} , see curve (a); H_2O_2 electro-production can accumulate in the catholyte following a straight line Eq. (56). In contrast, when 1 mM Fe^{2+} is added to

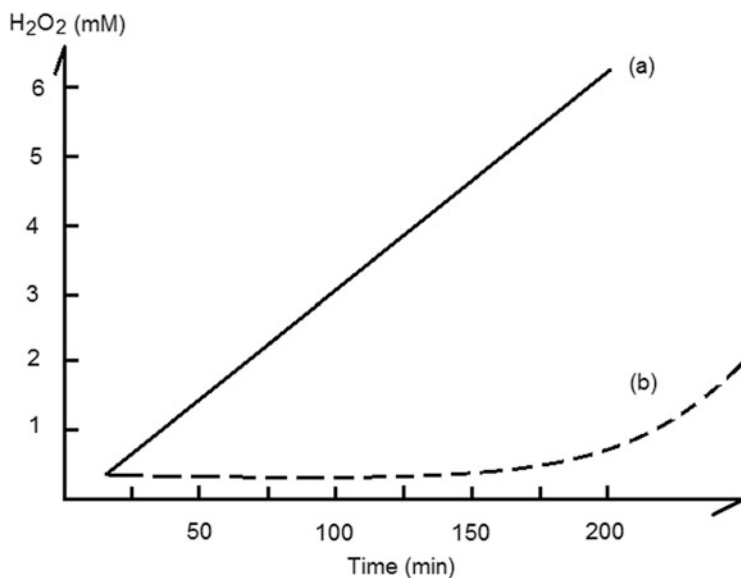


Fig. 3 Plots of electrolysis time vs H_2O_2 formed with addition of (a) 0 mM Fe^{2+} and (b) 1 mM Fe^{2+} added. Catholyte continuously saturated with O_2 , 1.5 L of 0.05 M Na_2SO_4 , pH 2. Anolyte, 1.5 L of 0.8 M H_2SO_4 . Flow velocity, 7 L min^{-1} . Adapted from [66]

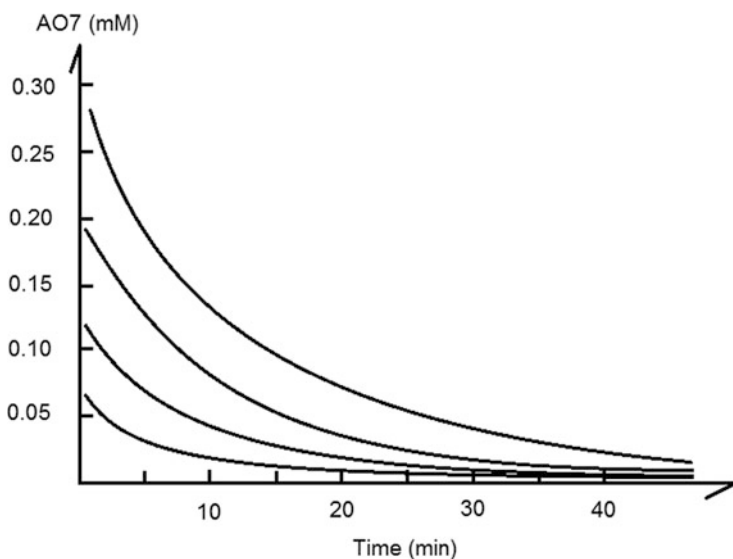


Fig. 4 Degradation of four AO7 concentrations. Catholyte continuously saturated with O_2 , 1.5 L of AO7 + 1 mM Fe^{2+} + 0.05 M Na_2SO_4 , pH 2. Anolyte, 1.5 L of 0.8 M H_2SO_4 . Flow velocity, 7 L min^{-1} . Adapted from [63]

the catholyte, during the first 200 min of electrolysis, the current efficiency of H_2O_2 electro-production is close to 0%. This suggests that a strong oxidant or a mixture of them (FeO^{2+} and/or $\cdot\text{OH}$) are formed when the H_2O_2 produced reacts with iron ions in the bulk solution. This experimental fact supports the assumption (b) for this kinetic model. After 200 min, Fenton process stops because the rate of ferrous ion consumption is higher than its regeneration and due to iron ions speciation. At the best experimental conditions, a series of AO7 degradation by EF process was carried out in the electrochemical reactor.

Several AO7 concentrations can be studied; the maximum AO7 concentration would be limited by the maximum H_2O_2 electro-generation and the stoichiometric reaction (55). The minimum AO7 concentration was arbitrarily determined.

Figure 4 shows an idealized set of several AO7 concentrations, while they were abated by EF process in the electrochemical reactor. Except for the beginning of the oxidation (≈ 1 min), AO7 abatement followed an apparent first-order kinetic equation:

$$[\text{AO7}]_t = a(e^{-kt}) \quad (57)$$

where a (mM) is a constant but does not represent the initial AO7 concentration; $[\text{AO7}]_t$ is the AO7 concentration (mM), at any time t during the electrolysis time; and $k(\text{min}^{-1})$ is the rate constant of the reaction.

For each AO7 concentration, a pair of a and k values was obtained. In the experimental framework, these parameters are functions of the AO7 concentration, and they can be described by means of the following equations:

$$a = c_1[\text{AO7}] + c_2 \quad (58)$$

$$k = c_3[\text{AO7}]^2 + c_4[\text{AO7}] + c_5 \quad (59)$$

where c_1 and c_2 are constants to be evaluated from a graph of a vs $[\text{AO7}]$ and c_3 to c_5 are constants to be evaluated from a graph of k vs $[\text{AO7}]$. The energy (E in kWh m^{-3}) required for the degradation of each AO7 concentration can be evaluated from the following equation:

$$E = \frac{(I_{\text{Cell}})(\Delta E_{\text{Cell}})(\text{ETh})}{V} \quad (60)$$

where ETh is the electrolysis time (h), V is the aqueous volume (L) to be treated, I_{cell} is the observed current (A) of the electrochemical reactor, and ΔE_{Cell} is the applied potential.

As we can expect, the energy required to abate AO7 by EF process is a function of its concentration and can be represented by the following equation:

$$E (\text{kWh m}^{-3}) = c_6([\text{AO7}]) + c_7 \quad (61)$$

where c_6 and c_7 are constants to be evaluated from a graph of E vs [AO7]. Once the experimental domain is established by a few experiments (4–5), good AO7 oxidation predictions can be made by combining Eqs. (57–59). As an example, the predictions of the AO7 degradation rates were predicted for the following different concentrations: 0.24, 0.16, and 0.12 mM. In all cases, simulated degradation rates agreed very well with experimental degradation rates. For all cases studied, the COD abatement was almost 80%. Although under this approach it is not possible to follow the evolution of concentration profiles of some by-products during the degradation time, this procedure is less complicated than the others, and it can fulfil the main requirements of wastewater treatment: abatement of the organic pollutant. Additionally, this approach provides a simple mathematical description of the main chemical process. This includes several important issues: (1) the rate of H_2O_2 generation and its fraction that is activated by Fe^{2+} to produce a strong oxidant (Eq. (56)), (2) the organic pollutant concentration range and its rate of degradation (Eq. (57)), and (3) the energy and time required to carry out the organic degradation (Eq. (57 and 61), respectively). This approach could be attractive to wastewater designers since it requires few experiments and minimal physical parameters to define an experimental domain representative of a target wastewater treatment.

5 Conclusions

Although, wastewater treatment by means of EF process is a feasible approach, the development of a chemical model to predict organic pollutant abatement is a challenging task. The following approaches were discussed: multistep mechanistic rate laws and empirical kinetic models.

While, the 1 kinetic model to predict the organic oxidation by EF process is possible and gives valuable information (about the evolution of concentration profiles of some by-products as a function of degradation time), its application to a real wastewater treatment is limited by the following assumptions: (1) reactions rates are considered to be constants and (2) $\cdot OH$ is usually regarded as the only species for the oxidation/degradation of organic compounds.

Based on statistical and mathematical empirical models (experimental design methodology and artificial neural networks), a model can be developed based on a set of minimum experiments, to predict the organic oxidation by EF process. Although these approaches are not going to give detailed mechanistic rate laws during the EF process, they will determine a set of experimental conditions to achieve the objectives of a wastewater treatment: abatement of the contamination. The main drawbacks of both approaches are the huge quantity of experiments that are needed to accurately predict the EF process.

In this context, a semiempirical kinetic model can be visualized as an alternative EF procedure to predict organic pollutant abatement. Under this approach, the following assumptions are taken into account: (1) the organic pollutant degradation

follows a pseudo-first-order reaction rate during the EF process and (2) both main mechanisms that explain the Fenton process can be ignored and just consider that 1 mol of activated H_2O_2 react as two-equivalent reducing agent. From a few organic degradation experiments (4 or 5), it is possible to evaluate their main kinetic parameters and express them as a function of the organic concentration. Therefore, a semiempirical chemical model can be developed to predict H_2O_2 electro-produced, oxidation rate, energy required, and electrolysis time to treat a textile effluent with a variable pollutant organic load in the studied range. A major feature of this approach is the minimal time and number of physical parameters needed for a rapid reliability test to simulate a wastewater treatment.

References

1. Kant R (2012) Textile dyeing industry an environmental hazard. *Nat Sci* 4:22–26. doi:[10.4236/ns.2012.41004](https://doi.org/10.4236/ns.2012.41004)
2. Chatzisymeon E, Xekoukoulotakis NP, Coz A et al (2006) Electrochemical treatment of textile dyes and dyehouse effluents. *J Hazard Mater* 137:998–1007. doi:[10.1016/j.jhazmat.2006.03.032](https://doi.org/10.1016/j.jhazmat.2006.03.032)
3. Thirugnanasambandham K, Sivakumar V, Maran JP (2014) Modeling and optimization of biogas production from rice mill effluent using up flow anaerobic sludge blanket reactor. *J Renew Sustain Energy*. doi: [Artn 023129rDoi 10.1063/1.4873400](https://doi.org/10.1063/1.4873400)
4. Tomat R, Vecchi E (1971) Electrocatalytic production of OH radicals and their oxidative addition to benzene. *J Appl Electrochem* 1:185–188. doi: [10.107/BF00616941](https://doi.org/10.107/BF00616941)
5. Sudoh M, Kodera T, Sakai K (1986) Oxidative degradation of aqueous phenol effluent with electrogenerated Fenton's reagent. *J Chem Eng Jpn* 19:513–518. doi:[10.1252/kakoronbunshu.11.70](https://doi.org/10.1252/kakoronbunshu.11.70)
6. Fenton HJH (1894) LXXIII – oxidation of tartaric acid in presence of iron. *J Chem Soc Trans* 65:899–910. doi:[10.1039/CT8946500899](https://doi.org/10.1039/CT8946500899)
7. Van BY (1920) The catalytic decomposition of hydrogen peroxide by ferric salts. *J Phys Chem* 32:270–284
8. Bray WC, Gorin MH (1932) Ferryl ion, a compound of tetravalent iron. *J Am Chem Soc* 54:2124–2125. doi:[10.1021/ja01344a505](https://doi.org/10.1021/ja01344a505)
9. Haber F, Weiss J (1934) The catalytic decomposition of hydrogen peroxide by iron salts. *Proc R Soc A* 147:332–351. doi:[10.1098/rspa.1934.0221](https://doi.org/10.1098/rspa.1934.0221)
10. Kolthoff IM, Medalia AI (1949) The reaction between ferrous iron and peroxides. II. Reaction with hydrogen peroxide, in the presence of oxygen. *J Am Chem Soc* 71:3784–3788. doi:[10.1021/ja01179a058](https://doi.org/10.1021/ja01179a058)
11. Baxendale JH, Evans MG, Park G (1946) Ation of polymerisation by systems. *Trans Faraday Soc* 42:155–169. doi:[10.1039/TF9464200155](https://doi.org/10.1039/TF9464200155)
12. Kremer ML (2003) The Fenton reaction. Dependence of the rate on pH. *J Phys Chem A* 107:1734–1741. doi:[10.1021/jp020654p](https://doi.org/10.1021/jp020654p)
13. Bataineh H, Pestovsky O, Bakac A (2012) pH-induced mechanistic changeover from hydroxyl radicals to iron(IV) in the Fenton reaction. *Chem Sci* 3:1594. doi:[10.1039/c2sc20099f](https://doi.org/10.1039/c2sc20099f)
14. Walling C, El-Taliawi GM (1973) Fentons' Reagent. II. Reactions of carbonyl compounds and α,β -unsaturated acids. *J Am Chem Soc* 95:844–847
15. Liu X, Qiu M, Huang C (2011) Degradation of the reactive black 5 by Fenton and Fenton-like system. *Procedia Eng* 15:4835–4840. doi:[10.1016/j.proeng.2011.08.902](https://doi.org/10.1016/j.proeng.2011.08.902)
16. Stein G, Weiss J (1948) Chemical effects of ionizing radiations. *Nature* 161:650–650. doi:[10.1038/161650a0](https://doi.org/10.1038/161650a0)

17. Merz JH, Waters WA (1949) The oxidation of aromatic compounds by means of the free hydroxyl radical. *J Chem Soc* 2427:2427–2433
18. Bishop DF, Stern G, Fleischman M, Marshal LS (1968) Hydrogen peroxide catalytic oxidation of refractory organics in municipal waste waters. *Ind Eng Chem Proc Des Dev* 7:110–117. doi:[10.1021/i260025a022](https://doi.org/10.1021/i260025a022)
19. Solozhenko EG, Soboleva NM, Goncharuk VV (1995) Decolourization of azodye solutions by Fenton's oxidation. *Water Res* 29:2206–2210. doi:[10.1016/0043-1354\(95\)00042-J](https://doi.org/10.1016/0043-1354(95)00042-J)
20. Tang WZ, Huang CP (1997) Stoichiometry of Fenton's reagent in the oxidation of chlorinated aliphatic organic pollutants. *Environ Technol* 18:13–23. doi:[10.1080/09593331808616508](https://doi.org/10.1080/09593331808616508)
21. Gallard H, Laat JDE (2000) Kinetic modelling of Fe (III)/H₂O₂ oxidation reactions in dilute aqueous solution using atrazine as a model organic compound. *Water Res* 34:3107–3116
22. Barbeni M, Minero C, Pelizzetti E (1987) Chemical degradation of chlorophenols with Fenton's reagent (Fe²⁺ + H₂O₂). *Chemosphere* 16:2225–2237. doi: [doi.org/10.1016/0045-6535\(87\)90281-5](https://doi.org/10.1016/0045-6535(87)90281-5)
23. Murphy AP, Boegli WJ, Price MK, Moody CD (1989) A fenton-like reaction to neutralize formaldehyde waste solutions. *Environ Sci Technol* 23:166–169. doi:[10.1021/es00179a004](https://doi.org/10.1021/es00179a004)
24. Zazo J, Casas J, Mohedano A et al (2005) Chemical pathway and kinetics of phenol oxidation by Fenton's reagent. *Environ Sci Technol* 39:9295–9302
25. Pham ALT, Doyle FM, Sedlak DL (2012) Kinetics and efficiency of H₂O₂ activation by iron-containing minerals and aquifer materials. *Water Res* 46:6454–6462. doi:[10.1016/j.watres.2012.09.020](https://doi.org/10.1016/j.watres.2012.09.020)
26. Zhu N, Gu L, Yuan H et al (2012) Degradation pathway of the naphthalene azo dye intermediate 1-diazo-2-naphthol-4-sulfonic acid using Fenton's reagent. *Water Res* 46:3859–3867. doi:[10.1016/j.watres.2012.04.038](https://doi.org/10.1016/j.watres.2012.04.038)
27. Pignatello JJ, Oliveros E, MacKay A (2006) Advanced oxidation processes for organic contaminant destruction based on the Fenton reaction and related chemistry. *Crit Rev Environ Sci Technol* 36:1–84. doi:[10.1080/10643380500326564](https://doi.org/10.1080/10643380500326564)
28. Sun JH, Sun SP, Fan MH et al (2007) A kinetic study on the degradation of p-nitroaniline by Fenton oxidation process. *J Hazard Mater* 148:172–177. doi:[10.1016/j.jhazmat.2007.02.022](https://doi.org/10.1016/j.jhazmat.2007.02.022)
29. Walling C (1975) Fenton's reagent revisited. *Acc Chem Res* 8:125–131. doi:[10.1021/ar50088a003](https://doi.org/10.1021/ar50088a003)
30. Chen R, Pignatello JJ (1997) Role of quinone intermediates as electron shuttles in Fenton and photoassisted Fenton oxidations of aromatic compounds. *Environ Sci Technol* 31:2399–2406. doi:[10.1021/es9610646](https://doi.org/10.1021/es9610646)
31. Gozzo F (2001) Radical and non-radical chemistry of the Fenton-like systems in the presence of organic substrates. *J Mol Catal A Chem* 171:1–22. doi:[10.1016/S1381-1169\(01\)00099-1](https://doi.org/10.1016/S1381-1169(01)00099-1)
32. Duesterberg CK, Cooper WJ, Waite TD (2005) Fenton-mediated oxidation in the presence and absence of oxygen. *Environ Sci Technol* 39:5052–5058. doi:[10.1021/es048378a](https://doi.org/10.1021/es048378a)
33. Ramirez JH, Duarte FM, Martins FG et al (2009) Modelling of the synthetic dye Orange II degradation using Fenton's reagent: from batch to continuous reactor operation. *Chem Eng J* 148:394–404. doi:[10.1016/j.cej.2008.09.012](https://doi.org/10.1016/j.cej.2008.09.012)
34. Zhang R, Yang Y, Huang CH et al (2016) Kinetics and modeling of sulfonamide antibiotic degradation in wastewater and human urine by UV/H₂O₂ and UV/PDS. *Water Res* 103:283–292. doi:[10.1016/j.watres.2016.07.037](https://doi.org/10.1016/j.watres.2016.07.037)
35. Zazo JA, Casas JA, Mohedano AF, Rodriguez JJ (2009) Semicontinuous Fenton oxidation of phenol in aqueous solution. A kinetic study. *Water Res* 43:4063–4069. doi:[10.1016/j.watres.2009.06.035](https://doi.org/10.1016/j.watres.2009.06.035)
36. Pontes RFF, Moraes JEF, Machulek A, Pinto JM (2010) A mechanistic kinetic model for phenol degradation by the Fenton process. *J Hazard Mater* 176:402–413. doi:[10.1016/j.jhazmat.2009.11.044](https://doi.org/10.1016/j.jhazmat.2009.11.044)
37. Sun SP, Li CJ, Sun JH et al (2009) Decolorization of an azo dye Orange G in aqueous solution by Fenton oxidation process: effect of system parameters and kinetic study. *J Hazard Mater* 161:1052–1057. doi:[10.1016/j.jhazmat.2008.04.080](https://doi.org/10.1016/j.jhazmat.2008.04.080)

38. Yang X, Xu X, Xu X et al (2016) Modeling and kinetics study of Bisphenol A (BPA) degradation over an FeOCl/SiO₂ Fenton-like catalyst. *Catal Today* 276:85–96. doi:[10.1016/j.cattod.2016.01.002](https://doi.org/10.1016/j.cattod.2016.01.002)
39. Brillas E, Sirés I, Oturan MA (2009) Electro-Fenton process and related electrochemical technologies based on Fenton's reaction chemistry. *Chem Rev* 109:6570–6631. doi:[10.1021/cr900136g](https://doi.org/10.1021/cr900136g)
40. Li J, Ai Z, Zhang L (2009) Design of a neutral electro-Fenton system with Fe@Fe₂O₃/ACF composite cathode for wastewater treatment. *J Hazard Mater* 164:18–25. doi:[10.1016/j.jhazmat.2008.07.109](https://doi.org/10.1016/j.jhazmat.2008.07.109)
41. Oturan MA, Peirotten J, Chartrin P, Acher AJ (2000) Complete destruction of p-Nitrophenol in aqueous medium by electro-fenton method. *Environ Sci Technol* 34:3474–3479. doi:[10.1021/es990901b](https://doi.org/10.1021/es990901b)
42. Chou S, Huang YH, Lee S-N et al (1999) Treatment of high strength hexamine-containing wastewater by electro-Fenton method. *Science* 33:751–759. doi: [doi.org/10.1016/S0043-1354\(98\)00276-0](https://doi.org/10.1016/S0043-1354(98)00276-0)
43. Kalpana PLAT (1994) Electrochemical peroxide treatment of aqueous herbicide solutions. *J Agric Food Chem* 42:209–215. doi:[10.1021/jf00037a038](https://doi.org/10.1021/jf00037a038)
44. Diagne M, Oturan N, Oturan MA (2007) Removal of methyl parathion from water by electrochemically generated Fenton's reagent. *Chemosphere* 66:841–848. doi:[10.1016/j.chemosphere.2006.06.033](https://doi.org/10.1016/j.chemosphere.2006.06.033)
45. Bokare A, Choi W (2014) Review of iron-free Fenton-like systems for activating H₂O₂ in advanced oxidation processes. *J Hazard Mater* 275:121–135. doi: doi.org/10.1016/j.jhazmat.2014.04.054
46. Walling C (1998) Intermediates in the reactions of Fenton type reagents. *Acc Chem Res* 31:155–157. doi:[10.1021/ar9700567](https://doi.org/10.1021/ar9700567)
47. Goldstein S, Meyerstein D (1999) Commentary: comments on the mechanism of the "Fenton-like" reaction. *Acc Chem Res* 32:547–550. doi:[10.1021/ar9800789](https://doi.org/10.1021/ar9800789)
48. Kremer ML (1999) Mechanism of the Fenton reaction. Evidence for a new intermediate. *Phys Chem Chem Phys* 1:3595–3605. doi:[10.1039/a903915e](https://doi.org/10.1039/a903915e)
49. Buda F, Ensing B, Gribnau MCM, Baerends EJ (2001) DFT study of the active intermediate in the Fenton reaction. *Chem Eur J* 7:2775–2783
50. Ensing B, Buda F, Blöchl P, Baerends EJ (2001) Chemical involvement of solvent water molecules in elementary steps of the Fenton oxidation reaction we gratefully acknowledge the helpful discussions with Michiel Gribnau (Unilever-Vlaardingen) and we thank the Netherlands Organization for Scientific Res. *Angew Chem Int Ed Engl* 40:2893–2895. doi:[10.1002/1521-3773\(20010803\)40:15<2893::AID-ANIE2893>3.0.CO;2-B](https://doi.org/10.1002/1521-3773(20010803)40:15<2893::AID-ANIE2893>3.0.CO;2-B)
51. Rachmilovich-Calis S, Masarwa A, Meyerstein N et al (2009) New mechanistic aspects of the fenton reaction. *Chem Eur J* 15:8303–8309. doi:[10.1002/chem.200802572](https://doi.org/10.1002/chem.200802572)
52. Pestovsky O, Stoian S, Bominaar EL et al (2005) Aqueous FeIV=O: spectroscopic identification and oxo-group exchange. *Angew Chemie Int Ed* 44:6871–6874. doi:[10.1002/anie.200502686](https://doi.org/10.1002/anie.200502686)
53. Walling C, Kato S (1971) Oxidation of alcohols by Fenton's reagent. Effect of copper ion. *J Am Chem Soc* 93:4275–4281. doi:[10.1021/ja00746a031](https://doi.org/10.1021/ja00746a031)
54. Zhang H, Lemley AT (2007) Evaluation of the performance of flow-through anodic Fenton treatment in amide compound degradation. *J Agric Food Chem* 55:4073–4079. doi:[10.1021/jf070104u](https://doi.org/10.1021/jf070104u)
55. Chau YK, Wong PTS (1998) Environmental analysis. *Environ Anal.* doi:[10.1016/B978-0-12-245250-5.50020-6](https://doi.org/10.1016/B978-0-12-245250-5.50020-6)
56. Körbahti BK (2007) Response surface optimization of electrochemical treatment of textile dye wastewater. *J Hazard Mater* 145:277–286. doi:[10.1016/j.jhazmat.2006.11.031](https://doi.org/10.1016/j.jhazmat.2006.11.031)
57. Abdessalem AK, Oturan N, Bellakhal N et al (2008) Experimental design methodology applied to electro-Fenton treatment for degradation of herbicide chlortoluron. *Appl Catal B Environ* 78:334–341. doi:[10.1016/j.apcatb.2007.09.032](https://doi.org/10.1016/j.apcatb.2007.09.032)

58. Hamzaoui YE, Hernández JA, Silva-Martínez S et al (2011) Optimal performance of COD removal during aqueous treatment of alazine and gesaprim commercial herbicides by direct and inverse neural network. *Desalination* 277:325–337. doi:[10.1016/j.desal.2011.04.060](https://doi.org/10.1016/j.desal.2011.04.060)
59. Salari D, Niaei A, Khataee A, Zarei M (2009) Electrochemical treatment of dye solution containing C.I. Basic yellow 2 by the peroxi-coagulation method and modeling of experimental results by artificial neural networks. *J Electroanal Chem* 629:117–125. doi:[10.1016/j.jelechem.2009.02.002](https://doi.org/10.1016/j.jelechem.2009.02.002)
60. Ahmed Basha C, Soloman PA, Velan M et al (2010) Electrochemical degradation of specialty chemical industry effluent. *J Hazard Mater* 176:154–164. doi:[10.1016/j.jhazmat.2009.10.131](https://doi.org/10.1016/j.jhazmat.2009.10.131)
61. Salari D, Daneshvar N, Aghazadeh F, Khataee AR (2005) Application of artificial neural networks for modeling of the treatment of wastewater contaminated with methyl tert-butyl ether (MTBE) by UV/H₂O₂ process. *J Hazard Mater* 125:205–210. doi:[10.1016/j.jhazmat.2005.05.030](https://doi.org/10.1016/j.jhazmat.2005.05.030)
62. Aleboyeh A, Kasiri MB, Olya ME, Aleboyeh H (2008) Prediction of azo dye decolorization by UV/H₂O₂ using artificial neural networks. *Dyes Pigments* 77:288–294. doi:[10.1016/j.dyepig.2007.05.014](https://doi.org/10.1016/j.dyepig.2007.05.014)
63. Ramírez B, Rondán V, Ortiz-Hernández L et al (2016) Semi-empirical chemical model for indirect advanced oxidation of acid Orange 7 using an unmodified carbon fabric cathode for H₂O₂ production in an electrochemical reactor. *J Environ Manag* 171:29–34. doi:[10.1016/j.jenvman.2016.02.004](https://doi.org/10.1016/j.jenvman.2016.02.004)
64. De Leon CP, Pletcher D (1995) Removal of formaldehyde from aqueous solutions via oxygen reduction using a reticulated vitreous carbon cathode cell. *J Appl Electrochem* 25:307–314. doi:[10.1007/BF00249648](https://doi.org/10.1007/BF00249648)
65. Alvarez-Gallegos A, Pletcher D (1998) The removal of low level organics via hydrogen peroxide formed in a reticulated vitreous carbon cathode cell, part 1. The electrosynthesis of hydrogen peroxide in aqueous acidic solutions. *Electrochim Acta* 44:853–861. doi:[10.1016/S0013-4686\(98\)00242-4](https://doi.org/10.1016/S0013-4686(98)00242-4)
66. Figueroa S, Vázquez L, Alvarez-Gallegos A (2009) Decolorizing textile wastewater with Fenton's reagent electrogenerated with a solar photovoltaic cell. *Water Res* 43:283–294. doi:[10.1016/j.watres.2008.10.014](https://doi.org/10.1016/j.watres.2008.10.014)

Solar-Assisted Electro-Fenton Systems for Wastewater Treatment

Enric Brillas

Abstract Herein, an overview over the performance of emerging electrochemical advanced oxidation processes (EAOPs) such as solar photoelectro-Fenton (SPEF) and related solar-assisted methods to remove organic pollutants from acidic wastewaters is presented. These procedures generate $\cdot\text{OH}$ at the anode surface from water oxidation and in the bulk from Fenton's reaction between added Fe^{2+} and H_2O_2 generated at a gas diffusion electrode (GDE) fed with pure O_2 or compressed air, similarly to the electro-Fenton (EF) process. SPEF involves the additional irradiation of the effluent with sunlight, which causes a synergistic effect on organic destruction due to the formation of more $\cdot\text{OH}$ from the photolysis of $\text{Fe}(\text{OH})^{2+}$ species and/or the photolysis of complexes of Fe(III) with generated carboxylic acids. Fundamentals of SPEF are explained to better clarify its characteristics on the removal of industrial chemicals, pesticides, dyes, pharmaceuticals, and real wastewaters. Examples with stirred tank reactors and pre-pilot flow plants equipped with electrochemical reactors containing a Pt or a boron-doped diamond anode and a GDE as cathode, coupled to a solar planar or CPC photoreactor, are given. The use of an autonomous flow plant powered by sunlight is examined. Coupled methods of SPEF with solar photocatalysis, photoelectrocatalysis, and biological treatment are described. The effect of experimental variables on the mineralization, current efficiency, and energy consumption is detailed. The decay kinetics of pollutants and the evolution of intermediates and released inorganic ions are discussed. SPEF is more efficient and less expensive than EAOPs like anodic oxidation and EF.

Keywords Coupled methods with solar photoelectro-Fenton, Degradation of dyes, Destruction of pharmaceuticals, Oxidative action of hydroxyl radicals and sunlight, Photolysis of Fe(III)-carboxylate complexes, Removal of pesticides, Solar

E. Brillas (✉)

Departament de Química Física, Facultat de Química, Universitat de Barcelona, Martí i Franquès 1-11, 08028 Barcelona, Spain
e-mail: brillas@ub.edu

photoelectro-Fenton treatment of wastewaters, Solar pilot plants with electrolytic cell and CPC photoreactor

Contents

1	Introduction	314
2	Fundamentals of the SPEF Method	315
3	Operation Parameters	317
4	Degradation of Pure Organic Pollutants	318
	4.1 Industrial Chemicals	318
	4.2 Pesticides	324
	4.3 Dyes	326
	4.4 Pharmaceuticals	330
5	Autonomous Solar Flow Plant	332
6	Coupled Solar-Assisted Electro-Fenton Treatments	334
7	Conclusions	339
	References	339

1 Introduction

Water pollution with organic and inorganic compounds remains a pervasive threat. A high number of synthetic organics like industrial chemicals, pesticides, dyes, and pharmaceuticals are released daily into many wastewaters and accumulated in the aquatic environment [1]. This pollution cannot be significantly removed by means of conventional wastewater treatment plants because most compounds are recalcitrant, showing a high stability to sunlight irradiation and resistance to microbial attack and temperature. As a result, low amounts of many synthetic organics, usually in $\mu\text{g L}^{-1}$, have been detected in rivers, lakes, oceans, and even drinking water in all over the world [2].

Over the past two decades, a large variety of powerful advanced oxidation processes (AOPs) have attracted increasing interest for the efficient removal of toxic and/or biorefractory pollutants from waters. These methods are considered environmentally friendly and are based on the in situ production of hydroxyl radical ($\cdot\text{OH}$) as the main oxidant. The high standard reduction potential of this radical ($E^\circ(\cdot\text{OH}/\text{H}_2\text{O}) = 2.80 \text{ V/SHE}$) allows its nonselective reaction with organics yielding dehydrogenated or hydroxylated derivatives, which can be in turn mineralized to CO_2 , water, and inorganic ions [3, 4]. The simplest and most typical chemical AOP is the Fenton's reagent in which a mixture of Fe^{2+} and H_2O_2 is used to degrade organics. Its oxidation power is significantly improved upon illumination of the treated effluent with UV light (photo-Fenton method) or sunlight (solar photo-Fenton method) [5]. The coupling of these methods with electrochemistry is another way to enhance its decontamination efficiency.

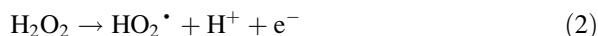
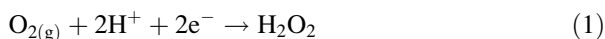
Several electrochemical AOPs (EAOPs) have been recently developed, presenting environmental compatibility, versatility, high efficiency, amenability of automation, and safety because they operate under mild conditions [1]. In

these treatments, organics can be oxidized at the anode and/or using the Fenton's reagent partially or completely generated from electrode reactions. The most ubiquitous EAOP is the electrochemical oxidation or anodic oxidation (AO) method [6, 7]. When the Fenton's reagent is electrogenerated, EAOPs based on Fenton's reaction chemistry are utilized, being useful for the treatment of acidic wastewaters. The most popular of these methods is the electro-Fenton (EF) process in which an iron catalyst (Fe^{2+} , Fe^{3+} , or iron oxides) is added to the effluent and H_2O_2 is produced at the cathode with O_2 or air feeding. The degradation power of EF on organic pollutants can be improved by combining it with other oxidizing processes [4]. The most effective methods have been found when the effluent treated by EF is simultaneously exposed to UV or solar radiation, corresponding to the so-called UV photoelectro-Fenton (PEF) and solar PEF (SPEF) methods. The latter procedure is most interesting in practice because it uses an inexpensive and renewable energy source as sunlight [5]. SPEF is an emerging EAOP developed in our laboratory since 2007.

The aim of this chapter is to present a general overview on the performance of SPEF and related methods over the destruction of organic pollutants from waters and wastewaters, including industrial chemicals, pesticides, dyes, pharmaceuticals, and real effluents. Fundamentals of SPEF are initially described to better analyze its characteristics and oxidation ability. Coupled systems of SPEF and related methods with heterogeneous solar photocatalysis (SPC), photoelectrocatalysis (PEC), and biological treatment are also described.

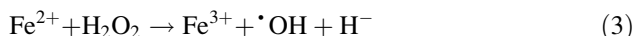
2 Fundamentals of the SPEF Method

It has been well established that H_2O_2 can be accumulated in aqueous medium from the cathodic two-electron reduction of dissolved O_2 gas at carbonaceous electrodes with high surface area [2]. Upon acidic conditions, this electrode reaction with $E^\circ = 0.68 \text{ V/SHE}$ can be written as reaction (1), being easier than the four-electron reduction of O_2 to water ($E^\circ = 1.23 \text{ V/SHE}$). The accumulation of H_2O_2 depends on cell configuration, cathode material, and operating conditions. In an undivided cell, the loss of this species is preeminently due to its electrochemical oxidation to O_2 at the anode surface from reaction (2) yielding the hydroperoxyl radical (HO_2^\bullet) as intermediate [3, 8].

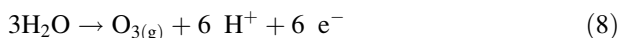
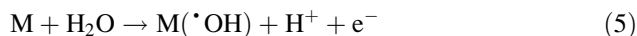


The SPEF treatment of acidic aqueous solutions of organic contaminants involves the continuous generation of H_2O_2 from O_2 directly injected as pure gas or compressed air. It has been developed in our laboratory using an efficient gas diffusion electrode (GDE) composed of a 3D carbon-polytetrafluoroethylene

(PTFE) sheet [5, 8]. A small catalytic quantity of Fe^{2+} , usually <1 mM, is added to the acidic effluent to react with electrogenerated H_2O_2 giving Fe^{3+} and $\cdot\text{OH}$ in the bulk according to the classical Fenton's reaction (3) with optimum pH near 2.8. A key advantage of SPEF compared to the chemical photo-Fenton method is that Fe^{2+} is continuously regenerated from the electroreduction of Fe^{3+} at the cathode according to reaction (4), with $E^\circ = 0.77$ V/SHE:

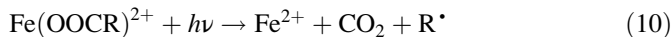


In undivided cells, the quicker destruction of organics in SPEF is achieved at pH near 3, and they are not only attacked by reactive oxygen species (ROS) such as $\cdot\text{OH}$ and to smaller extent by H_2O_2 and $\text{HO}_2\cdot$ but also by physisorbed $\cdot\text{OH}$ produced at a high O_2 overvoltage anode (M) from water oxidation by reaction (5) [4]. While the degradation action of $\text{M}(\cdot\text{OH})$ is very ineffective for active electrodes like Pt, it is much more efficient using a non-active boron-doped diamond (BDD) thin layer anode. At high current, reactive BDD($\cdot\text{OH}$) is produced in much greater amount than Pt($\cdot\text{OH}$) and can mineralize completely aromatics and unsaturated compounds such as carboxylic acids [1]. Several parasitic reactions cause the consumption of oxidant hydroxyl radical, more extensively the anodic oxidation of $\text{M}(\cdot\text{OH})$ to O_2 via reaction (6), also being feasible the dimerization of $\cdot\text{OH}$ in the bulk and its reaction with H_2O_2 and Fe^{2+} . Moreover, when a sulfate medium is employed, the generation of other weaker oxidizing agents like $\text{S}_2\text{O}_8^{2-}$ ion from the oxidation of the electrolyte by reaction (7) and ozone by reaction (8) is also feasible [5, 8].



Apart from the electrogeneration of ROS, the SPEF process involves the simultaneous illumination of the acidic treated effluent with sunlight. This is the difference with the PEF process, where UVA ($\lambda = 315\text{--}400$ nm), UVB ($\lambda = 285\text{--}315$ nm), or UVC ($\lambda < 285$ nm) light supplied by artificial lamps as energy sources is employed. The mineralization action of a UV irradiation is due to (1) higher Fe^{2+} regeneration and production of additional $\cdot\text{OH}$ from photoreduction of $\text{Fe}(\text{OH})^{2+}$, the predominant Fe^{3+} species at pH 2.8–3.5, from reaction (9) and (2) photodecarboxylation of Fe(III)-carboxylate complexes, like of oxalic acid, also allowing Fe^{2+} regeneration as shown in the general reaction (10) [8].





The main drawback of PEF in practice is the high electrical cost of the artificial UV lamps utilized. The use of SPEF in which the solution is directly irradiated with sunlight as a cheap and renewable energy source with $\lambda > 300$ nm represents a good alternative for industrial application. The higher intensity of UV radiation of sunlight and the additional absorption at $\lambda > 400$ nm, e.g., for the photolysis of Fe(III)-carboxylate complexes, lead to higher degradation rate for SPEF than for EF.

3 Operation Parameters

Several experimental parameters are determined during the SPEF treatment of an organic pollutant in water, including the absorbance (A) at the λ_{max} of the UV-Vis spectrum, typically for dyes, the concentration (c) of the pollutant obtained by reversed-phase HPLC, and the total organic carbon (TOC) of the solution. The effect of operation variables like solution pH, applied current, and concentration of catalyst and pollutants, among others, over the above parameters is typically assessed to know the process performance. Detection of intermediates by GC-MS and LC-MS, final carboxylic acid by ion exclusion HPLC, and released inorganic ions by chromatographic techniques allows clarifying the routes of pollutant mineralization.

Results obtained for A , c , and TOC decay are depicted as a function of electrolysis time, as well as plots of the percentage of color removal and percentage of TOC removal. The kinetic analysis of concentration decay allows a better analysis of the performance of the degradative process. For example, the percentage of TOC removal is determined as follows [1]:

$$\text{TOC removal (\%)} = \frac{\Delta(\text{TOC})}{\text{TOC}_0} 100 \quad (11)$$

where $\Delta(\text{TOC})$ is the experimental TOC decay (mg L^{-1}) at electrolysis time t and TOC_0 is the initial value before treatment. From TOC measurements, the mineralization current efficiency (MCE) for treated solutions at a given time t (h) is estimated from Eq. (12) [3, 9]:

$$\text{MCE (\%)} = \frac{n F V_s \Delta(\text{TOC})}{4.32 \times 10^7 m I t} 100 \quad (12)$$

where n is the number of electrons exchanged in the mineralization of the compound, F is the Faraday constant ($96,485 \text{ C mol}^{-1}$), V_s is the solution volume (L), 4.32×10^7 is a conversion factor ($=3,600 \text{ s h}^{-1} \times 12,000 \text{ mg carbon mol}^{-1}$), m is the number of carbon atoms of the compound, and I is the applied current (A). It is

noteworthy that MCE can attain a maximum value of 200% because oxidants $\cdot\text{OH}$ are produced from anode and cathode reactions. Nevertheless, even superior MCE values can be determined because the oxidative action of sunlight is not taken into account in Eq. (12).

Energetic parameters are essential figures of merit to assess the viability of the process for industrial application. At constant I , the energy consumption per unit volume (EC) and unit TOC mass (EC_{TOC}) are calculated from Eqs. (13) and (14), respectively [10–12]:

$$\text{EC} \text{ (kWh m}^{-3}\text{)} = \frac{E_{\text{cell}} I t}{V_s} \quad (13)$$

$$\text{EC}_{\text{TOC}} \text{ (kWh (g TOC)}^{-1}\text{)} = \frac{E_{\text{cell}} I t}{V_s \Delta(\text{TOC})} \quad (14)$$

where E_{cell} is the average potential difference of the cell (V).

An important parameter in SPEF and other solar-assisted procedures is the intensity of the UV light supplied by sunlight over the treated solution. In our laboratory, the SPEF trials were made during clear and sunny days of summer months, running 360 min as maximal from the noon. The solar photoreactor was tilted an angle of 42° corresponding to the latitude of Barcelona (latitude, $41^\circ 21' \text{ N}$; longitude, $2^\circ 10' \text{ E}$) to perpendicularly collect the direct solar rays in order to better absorb the incident photons. An average UV intensity of $30\text{--}32 \text{ W m}^{-2}$ was measured using a Kipp & Zonen CUV 5 global UV radiometer [13].

4 Degradation of Pure Organic Pollutants

Several industrial chemicals, pesticides, dyes, and pharmaceuticals have been degraded using SPEF since 2007. The assays were made at two levels, with stirred tank reactors and with recirculation pre-pilot plants as a first step for its possible application at industrial scale. This section describes the degradative characteristics of this procedure, as well as of related methods. Table 1 collects the good percent of TOC removal, MCE, and specific energy consumption obtained for several pollutants under selected conditions operating with 2.5 and 10 L solar flow plants [10–12, 14–22].

4.1 Industrial Chemicals

The first research over SPEF was performed with a 2.5 L pre-pilot flow plant equipped with a BDD/GDE reactor of 20 cm^2 electrode area and a solar planar photoreactor of 600 mL irradiation volume operating under batch recirculation

Table 1 Percentage of TOC removal, mineralization current efficiency, and energy consumption per unit TOC mass determined for the SPEF degradation of organic pollutant solutions in 0.05M Na₂SO₄ of pH 3.0 using a recirculation pre-pilot plant coupled to a solar photoreactor submitted to an average UV irradiation of about 30–32 W m⁻² under selected conditions

Pollutant	Anode	Solution	% TOC removal	% MCE	EC _{TOC} (kWh (g TOC) ⁻¹)	Reference
<i>Industrial chemicals</i>						
Cresols ^a	BDD	128 mg L ⁻¹ , 1 mM Fe ²⁺ , pH 3.0, 1 A, and 35°C for 180 min	98	122	0.155	[10]
Sulfanilic acid ^a	Pt	108 mg L ⁻¹ , 0.50 mM Fe ²⁺ , pH 4.0, 2 A, and 35°C for 120 min	76	52	0.275	[14]
<i>Pesticides</i>						
MCPA ^b	Pt	186 mg L ⁻¹ , 1 mM Fe ²⁺ , pH 3.0, 5 A, and 35°C for 120 min	75	71	0.088	[15]
Mecoprop ^a	BDD	634 mg L ⁻¹ , 0.50 mM Fe ²⁺ , pH 3.0, 1 A, and 35°C for 540 min	97	93	0.129	[11]
Tebuthiuron ^a	BDD	0.18 mM each, 0.50 mM Fe ²⁺ , pH 3.0, 0.5 A, and 35°C for 360 min	53	20	0.93	[16]
Ametryn ^a			51	21	0.86	
<i>Dyes</i>						
Acid Red 88 ^a	BDD	50 mg L ⁻¹ TOC, 0.50 mM Fe ²⁺ , pH 3.0, 1 A, and 35°C for 360 min ^c	98	20	0.490	[12]
Acid Yellow 9 ^a			95	20	0.390	
Allura Red AC ^a	Pt	460 mg L ⁻¹ , 0.50 mM Fe ²⁺ , pH 3.0, 1 A, and 35°C for 360 min	95	81	0.045	[17]
Disperse Red 1 ^a	BDD	100 mg L ⁻¹ TOC, 0.50 mM Fe ²⁺ , pH 3.0, 1 A, and 35°C for 240 min ^c	97	82	0.151	[18]
Disperse Yellow 9 ^a			96	80	0.155	
Evans Blue ^b	Pt	0.245 mM, 0.50 mM Fe ²⁺ , pH 3.0, 5 A, and 35°C for 300 min	88	42	2.13	[19]

(continued)

Table 1 (continued)

Pollutant	Anode	Solution	% TOC removal	% MCE	EC _{TOC} (kWh (g TOC) ⁻¹)	Reference
<i>Pharmaceuticals</i>						
Enrofloxacin ^a	Pt	158 mg L ⁻¹ , 0.20 mM Fe ²⁺ , pH 3.0, 1 A, and 35°C for 300 min	69	34	0.226	[20]
	BDD	0.20 mM Fe ²⁺ , pH 3.0, 1 A, and 35°C for 300 min	86	42	0.246	
Paracetamol ^b	Pt	157 mg L ⁻¹ , 0.40 mM Fe ²⁺ , pH 3.0, 5 A and 35°C for 120 min	75	71	0.093	[21]
Sulfanilamide ^a	Pt	239 mg L ⁻¹ , 0.50 mM Fe ²⁺ , pH 3.0, 1 A, and 35°C for 180 min	91	78	0.120	[22]

^a2.5 L treated in pre-pilot plant with a filter-press cell of 20 cm² electrodes coupled to a solar planar photoreactor of 600 mL irradiated volume

^b10 L degraded in a pre-pilot flow plant with a filter-press cell of 90.3 cm² electrodes coupled to a solar CPC of 1.57 L irradiated volume

^c0.10M Na₂SO₄

mode at constant current density (j). Figure 1a, b illustrates a scheme of the setup of the plant and the electrochemical reactor, respectively [10, 11]. Figure 1c depicts the evolution of H₂O₂ concentration during the electrolysis of a 0.05M Na₂SO₄ solution at pH 3.0 in the above system. In the absence of organic matter and iron ions (anodic oxidation with electrogenerated H₂O₂ (AO-H₂O₂)), a gradual accumulation of H₂O₂ can be observed to attain a steady concentration, which increased linearly to 17, 35, and 54 mM with rising j at 50 mA cm⁻² (curve *c*), 100 mA cm⁻² (curve *b*), and 150 mA cm⁻² (curve *a*). This tendency suggests that all electrode reactions involved are faradaic and a steady H₂O₂ concentration was reached exactly when its generation rate from reaction (1) became equal to its decomposition one, primarily from reaction (2). In contrast, when 100 mg L⁻¹ of the herbicide mecoprop and 0.50 mM Fe²⁺ were added to the solution operating under SPEF conditions, the H₂O₂ content decreased strongly up to near 2 mM at $j = 50$ mA cm⁻² (curve *d*), as a result of organic mineralization by [•]OH formed from Fenton's reaction (3), also induced by reaction (9). These findings indicate that H₂O₂ can be produced at high enough rate under SPEF conditions to remove organic contaminants at relatively high concentration.

The above system was applied to remove cresol isomers using the same electrolyte with 0.25 mM Fe²⁺ [10]. As shown in Fig. 2a, 128 mg L⁻¹ of *o*-, *m*-, or *p*-cresols were not practically photodecomposed upon direct solar radiation and disappeared completely in about 80 min at $j = 50$ mA cm⁻², at similar rate for EF and SPEF. This means that BDD([•]OH) produced from reaction (5) and [•]OH originated by Fenton's reaction (3) are the main oxidants of pollutants, with small

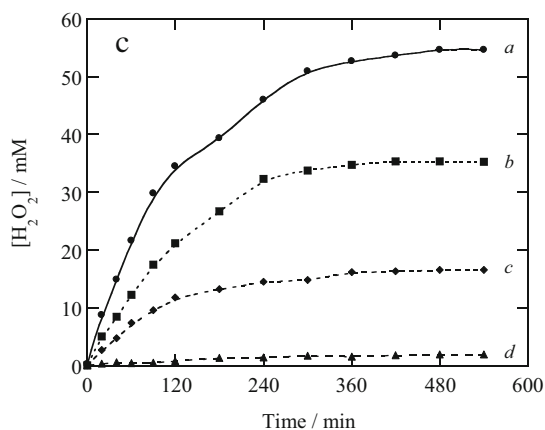
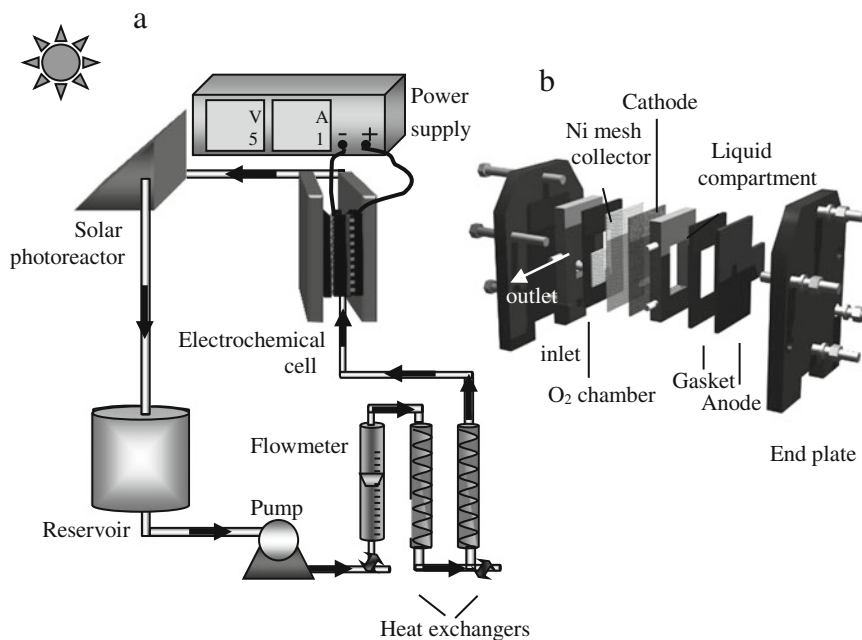


Fig. 1 Schemes of (a) the 2.5 L pre-pilot plant and (b) the one-compartment filter-press electrochemical reactor with a BDD anode and an O₂ diffusion (GDE) cathode, both of 20 cm² area, used for solar photoelectro-Fenton (SPEF). (c) Concentration of accumulated H₂O₂ vs. time during the electrolysis of 2.5 L of a 0.05M Na₂SO₄ solution at pH 3.0 in the plant at (a) 150 mA cm⁻², (b) 100 mA cm⁻², and (c) 50 mA cm⁻², 25°C, and liquid flow rate of 180 L h⁻¹. In curve d, 100 mg L⁻¹ mecoprop solution with 0.50 mM of Fe²⁺ was degraded under the same conditions at 50 mA cm⁻² by SPEF. Adapted from [10, 11]. Copyright 2007 Elsevier

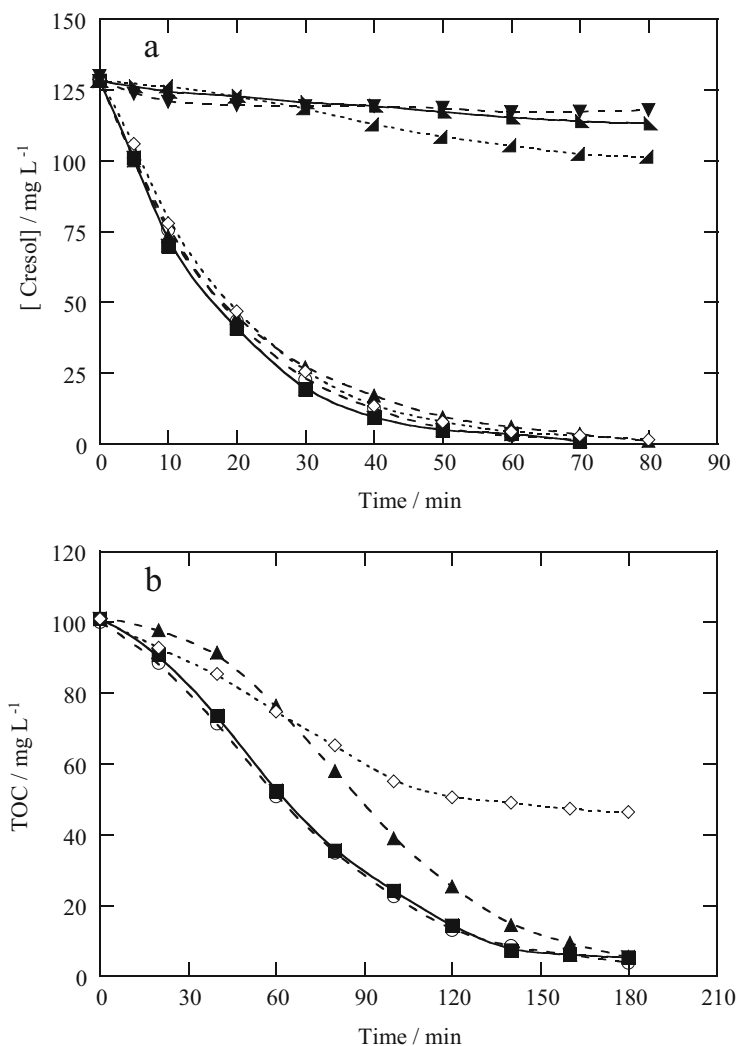


Fig. 2 (a) Time course of the concentration of cresols and (b) TOC removal with electrolysis time for the degradation of 2.5 L of solutions containing 128 mg L⁻¹ cresol solutions in 0.05M Na₂SO₄ with 0.25 mM Fe²⁺ of pH 3.0 using the flow plant of Fig. 1a at 50 mA cm⁻², 30°C, and liquid flow rate of 180 L h⁻¹. (inverted triangle) *o*-Cresol, (lower left triangle) *m*-cresol, and (lower right triangle) *p*-cresol solutions under solar illumination, but without current. (diamond) Electro-Fenton with a BDD anode of *o*-cresol. SPEF with a BDD anode of (circle) *o*-cresol, (square) *m*-cresol, and (triangle) *p*-cresol. Adapted from [10]. Copyright 2007 Elsevier

participation of reaction (9). The concentration decays always followed a pseudo-first-order kinetics, suggesting a constant content of generated oxidants to attack the pollutants. In contrast, Fig. 2b evidences a rapid TOC removal for all cresols by SPEF, attaining almost total mineralization with 98% TOC reduction in 180 min,

whereas only ca. 50% TOC was abated by EF, indicating a powerful degradative action of sunlight over intermediates. The optimum pH 3.0 for all mineralizations, related to Fenton's reaction (3), was confirmed, and similar degradation rates were found between 0.25 and 1 mM Fe^{2+} . The increase in j from 25 to 100 mA cm^{-2} enhanced the mineralization process due to the generation of more $\cdot\text{OH}$, but with lower MCE and greater EC_{TOC} . Conversely, the rise in substrate concentration from 128 to 1,024 mg L^{-1} yielded lesser TOC reduction with greater amount of TOC removed and MCE, along with lower EC_{TOC} , because of the deceleration of parasitic reactions by the quicker reaction of $\cdot\text{OH}$ with higher quantities of organics. For the lower pollutant content, a current mineralization as high as 122% and an EC_{TOC} of 0.155 kWh (g TOC)^{-1} were found after 180 min of electrolysis at $j = 50 \text{ mA cm}^{-2}$ (see Table 1). GC-MS analysis of electrolyzed solutions revealed that the initial hydroxylation of *o*-cresol and *m*-cresol gave 2-methyl-*p*-benzoquinone via 2-methylhydroquinone, whereas dihydroxylation of *p*-cresol led to 5-methyl-2-hydroxy-*p*-benzoquinone. Further destruction of these intermediates yielded a mixture of carboxylic acids, being oxalic and acetic acids the most persistent final by-products, as detected by ion exclusion HPLC. Large mineralization was attained by the efficient photodecarboxylation of Fe(III)-oxalate complexes.

Further, El-Ghenymy et al. [14] optimized the EF and SPEF treatments of 240 mg L^{-1} sulfanilic acid in 0.05M Na_2SO_4 using the flow plant of Fig. 1a with a Pt/GDE reactor by response surface methodology (RSM). The large superiority of SPEF was evidenced again. Optimum variables of $j = 100 \text{ mA cm}^{-2}$, 0.50 mM Fe^{2+} , and pH 4.0 were determined after 240 min of EF and 120 min of SPEF. EF only gave 47% of mineralization, and the powerful SPEF yielded 76% TOC reduction with MCE = 52% and $\text{EC}_{\text{TOC}} = 0.275 \text{ kWh (g TOC)}^{-1}$ (see Table 1). As expected, sulfanilic acid dropped at similar rate in both treatments following a pseudo-first-order kinetics. The final solution treated by EF contained a stable mixture of tartaric, acetic, oxalic, and oxamic acids, which formed Fe(III) complexes that underwent a quick photolysis by UV light of sunlight in SPEF. NH_4^+ in larger proportion than NO_3^- were the inorganic nitrogen ions released in both processes.

The excellent oxidation power of SPEF was also confirmed by Serra et al. [23, 24], who studied the treatment of 250 mL of 500 mg L^{-1} of α -methylphenylglycine, an amino acid precursor of many pharmaceuticals, in 0.05M Na_2SO_4 with 10 mg L^{-1} Fe^{2+} at pH 2.9. A stirring BDD/GDE tank reactor with electrodes of 3 cm^2 area was used for EF and SPEF. Comparative trials were performed with chemical Fenton degradations, concluding that the oxidation ability of processes increased in the sequence Fenton < EF < solar photo-Fenton < SPEF. Again, the potent action of sunlight favored strongly the mineralization of organics. This was due to the photodecomposition of Fe(III) complexes of the most persistent carboxylic acids, preferentially oxalic, upon sunlight, which accounts for by the best performance of solar-assisted processes with iron ions.

Several works centered their attention to remove by-products detected during aromatic degradation such as phthalic acid, formed from naphthalene derivatives

[25] and final oxalic and oxamic acids [26]. The trials were conducted in stirring BDD/GDE tank reactors containing 100 mL of solutions in 0.10M Na₂SO₄ of pH 3.0. Different Fe³⁺/Cu²⁺ mixtures were tested as cocatalysts to enhance the SPEF process with only iron ions. For 2.0 mM phthalic acid, it was found an acceleration of mineralization by combination of both ions, because Cu(II)-carboxylate complexes were also removed with [•]OH. The best SPEF process was found for 0.125 mM Cu²⁺ +0.375 mM Fe³⁺, giving rise to 99% mineralization with MCE = 40% and EC_{TOC} = 0.294 kWh (g TOC)⁻¹ after 240 min of electrolysis at $j = 33.3 \text{ mA cm}^{-2}$. The same conclusions were reached by degrading 2.08 mM of oxalic and oxamic acids under the same conditions. The former acid was more rapidly removed with 0.50 mM Cu²⁺ +0.50 mM Fe³⁺ than only with 0.50 mM Fe³⁺ because of the synergistic effect of the photolysis of Fe(III)-oxalate complexes and the oxidation of competitive Cu(II)-oxalate ones with [•]OH. Oxamic acid was more recalcitrant since it was preeminently removed by [•]OH oxidation of its Cu(II) complexes because of the low photoactivity of its Fe(III) species.

4.2 Pesticides

The first investigation on the degradation of pesticides by SPEF was made with the herbicide mecoprop (2-(4-chloro-2-methylphenoxy)propionic acid) with the same pre-pilot flow plant and electrochemical reactor as shown in Fig. 1a, b, respectively [11]. Experiments were performed with 0.05M Na₂SO₄ at pH 3.0, and a similar behavior to that described above for cresols was found by varying operation variables like j up to 150 mA cm⁻², Fe²⁺ content up to 5 mg L⁻¹, and pollutant content up to near saturation (634 mg L⁻¹) over TOC removal, MCE, and EC_{TOC}. The best performance was then obtained for the most concentrated solution with 0.50 mM Fe²⁺ and $j = 50 \text{ mA cm}^{-2}$ (see Table 1). High MCE values were determined at short electrolysis time as a result of the large destruction of Fe(III)-carboxylate complexes by UV photolysis from sunlight. Nevertheless, MCE always decayed drastically at long electrolysis time because of the loss of organic load and the formation of more recalcitrant by-products, a common feature for all EAOPs. It was also found an oxidative enhancement in the order AO-H₂O₂ < EF < SPEF. This trend is expected for these processes, because BDD([•]OH) only acts as oxidant in AO-H₂O₂, whereas [•]OH in the bulk is additionally originated in EF. The combination of these radicals with sunlight explains the superior power of SPEF.

More recently, the pre-pilot flow plant of Fig. 1a was applied to the SPEF treatment of 0.186 mM of the herbicide diuron [27] and single and mixed herbicides of tebuthiuron and ametryn [16], always in 0.05M Na₂SO₄ and 0.50 mM Fe²⁺ solutions of pH 3.0. For diuron, 70% of mineralization was achieved after 360 min at $j = 50 \text{ mA cm}^{-2}$. Lower mineralization was obtained for 0.18 mM solutions of tebuthiuron or ametryn, with small MCE and high EC_{TOC} values, under the same conditions (see Table 1) due to their higher recalcitrance. RSM has also been utilized for the optimization of the SPEF process of the herbicide 4-chloro-2-

methylphenoxyacetic acid (MCPA) in 0.05M Na_2SO_4 by varying the applied I , Fe^{2+} content, and pH [15]. Trials were performed with the 10 L pre-pilot plant schematized in Fig. 3a, which was equipped with a Pt/GDE cell, similar to that of Fig. 1b but with electrodes of 90.3 cm^2 area, and a compound parabolic collector (CPC) of 1.57 L irradiated volume as solar photoreactor, much more efficient for photon caption than a planar one. 75% of TOC reduction with 71% of MCE and $0.088 \text{ kWh (g TOC)}^{-1}$ of EC_{TOC} were determined after only 120 min of treatment under the best operation conditions (see Table 1).

Kinetic analysis of the concentration decays of mecoprop, diuron, and MCPA revealed that they obeyed a pseudo-first-order kinetics. In contrast, tebuthiuron and ametryn underwent a very rapid pseudo-first-order abatement kinetics at short time, related to the oxidation of the Fe(II) complexes of each herbicide, followed by a much slower pseudo-first-order kinetics associated with the decay of their Fe(III)

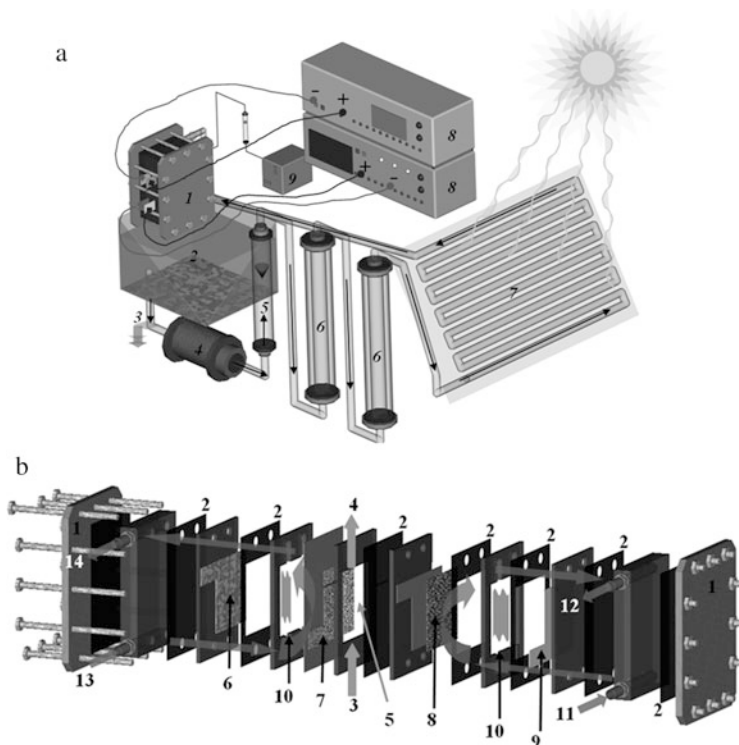


Fig. 3 (a) Experimental setup of a 10 L recirculation pre-pilot plant for the SPEF treatment of organic pollutants. (1) Flow electrochemical cell, (2) reservoir, (3) sampling, (4) peristaltic pump, (5) flowmeter, (6) heat exchanger, (7) solar CPC (photoreactor), (8) power supply, and (9) air pump. (b) Sketch of a combined filter-press electrochemical cell. (1) End plate, (2) gasket, (3) air inlet, (4) air outlet, (5) air chamber, (6) 90.3 cm^2 BDD anode, (7) 90.3 cm^2 GDE cathode, (8) 90.3 cm^2 carbon felt (CF) cathode, (9) 90.3 cm^2 Pt anode, (10) liquid compartment, (11) liquid inlet in the cell, (12) liquid outlet of the Pt/CF pair connected to 13, (13) liquid inlet in the BDD/air diffusion pair, and (14) liquid outlet of the cell. Adapted from [31]. Copyright 2011 Elsevier

complexes. GC-MS and HPLC of electrolyzed solutions allowed identifying primary by-products like 4-chloro-*o*-cresol, methylhydroquinone, and methyl-*p*-benzoquinone for mecoprop; 4-chloro-2-methylphenol, methylhydroquinone, and methyl-*p*-benzoquinone for MCPA; and several heterocycles for tebuthiuron and ametryn. Several final carboxylic acids were identified during the treatment of mecoprop, diuron, and MCPA. While Fe(III)-oxalate complexes were well photolyzed by sunlight from reaction (10), it was found that Fe(III) species of acetic and oxamic acid were much less photoactive and their oxidation was rather due to their reaction with BDD(\cdot OH). The heteroatoms of herbicides were mineralized to Cl^- , SO_4^{2-} , NO_3^- , and NH_4^+ ions, with further slow oxidation of Cl^- to Cl_2 .

On the other hand, it is interesting to remark the work of Peng et al. [28], who used a simulated solar-assisted heterogeneous EF for the degradation of 100 mL of 200 mg L⁻¹ of the neonicotinoid insecticide imidacloprid (1-(6-chloronicotiny)-2-nitroimino-imidazolidine) in 0.10M Na₂SO₄ at pH 6.8. The stirred tank reactor contained a BDD anode and a 3D-ordered macroporous Fe₂O₃/carbon aerogel cathode and was illuminated with simulated sunlight (500 W He lamp). Upon continuous air injection to the solution and without organic matter, a steady H₂O₂ concentration of 18 mg L⁻¹ was produced from reaction (1) at $j = 10 \text{ mA cm}^{-2}$ and times >120 min. Total disappearance of the insecticide was achieved in 180 min as a result of its reaction with \cdot OH formed from Fenton's reaction between Fe(II) at the cathode surface (formed by reduction of Fe(III)) and generated H₂O₂. The main drawback of the cathode was the continuous leaching of Fe³⁺ ion, making doubtful its short lifetime for long electrolysis at industrial level.

4.3 Dyes

The dyes Sunset Yellow FCF [29], Evans Blue [19], and Congo Red [30] were degraded by SPEF using a stirred BDD/GDE tank reactor with 100 mL solutions and further, the 2.5 or 10 L pre-pilot flow plant of Figs. 1a and 3a [31], equipped with a Pt/GDE cell. Fast decolorization and dye removal, along with excellent mineralization, were found in all cases (see Table 1). In the stirred tank cell, for example, a 290 mg L⁻¹ Sunset Yellow FCF solution in 0.05M Na₂SO₄ and 0.50 mM Fe²⁺ of pH 3.0 was totally mineralized in only 120 min of electrolysis at $j = 33.3 \text{ mA cm}^{-2}$. In the 10 L plant with a Pt/GDE reactor, the rise in j from 33.3 to 77.6 mA cm⁻² enhanced the decolorization rate and TOC removal by the production of more physisorbed Pt(\cdot OH) and homogeneous \cdot OH and the quicker photolysis of Fe(III)-carboxylate species because they are more rapidly generated from the cleavage of aromatic intermediates. The most economic process was attained at $j = 33.3 \text{ mA cm}^{-2}$, with 0.060 kWh (g TOC)⁻¹ at 180 min upon colorless solution and 80% TOC reduction. Dye removal was more rapid than decolorization in which colored by-products were also destroyed, although pseudo-first-order kinetics were determined in both cases. For the 10 L plant with a Pt/GDE cell, it was also found that the mineralization rate of azo dyes depended on their

number of azo bonds, decreasing in the order monoazo Acid Orange 7 > diazo Acid Red 151 > triazo Disperse Blue 71, due to the growing difficulty of breaking more azo groups [32]. A high number of aromatic by-products were identified by GC-MS and LC-MS analysis of all treated dyes. Figure 4 exemplifies the reaction sequence proposed for Congo Red degradation from the 21 aromatic intermediates detected [30]. Further degradation of these compounds gave a mixture of oxalic, tartaric, oxamic, tartronic, and acetic acids, which formed Fe(III) complexes that were quickly mineralized preferentially by the UV radiation of sunlight. This can be observed in Fig. 5, where the evolution of these five carboxylic acids for a 0.260 mM Congo Red solution in the 2.5 L solar flow plant with a Pt/GDE reactor at $j = 100 \text{ mA cm}^{-2}$ is depicted, disappearing in 240 min. The initial N was released as NH_4^+ and NO_3^- ions, but in many cases, it was partially lost as volatile N-products.

The characteristics of the 2.5 L solar flow plant of Fig. 1a with the electrochemical reactor of Fig. 1b for the treatment of dyeing solutions have been investigated for Acid Yellow 36 [9]; Acid Red 88, and Acid Yellow 9 [12]; Disperse Red 1 and Yellow 9 [18]; the food azo dyes E122, E124, and E129 [13]; and Allura Red AC [17]. The degradation of 50–460 mg L^{-1} TOC of these dyes in 0.05–0.10M Na_2SO_4 showed the quickest total decolorization and almost total TOC removal for 0.50 mM Fe^{2+} and pH 3.0 (see Table 1). Higher j always caused the destruction of more organic matter, but with loss of MCE due to the acceleration of parasitic reactions of BDD($\cdot\text{OH}$) and $\cdot\text{OH}$. In contrast, greater dye content was more slowly

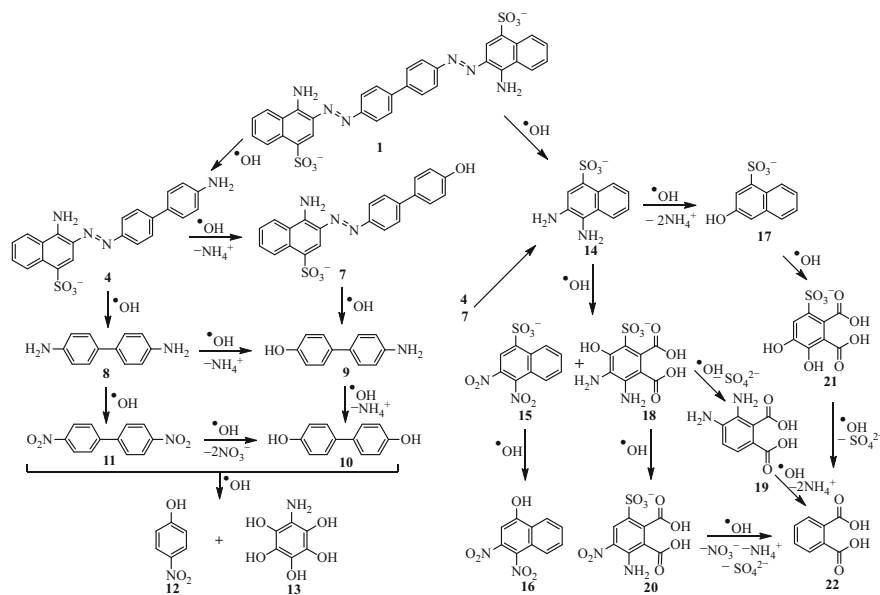


Fig. 4 Proposed reaction sequence for the initial degradation of Congo Red diazo dye (1) by SPEF process. Reproduced from [30]. Copyright 2015 Elsevier

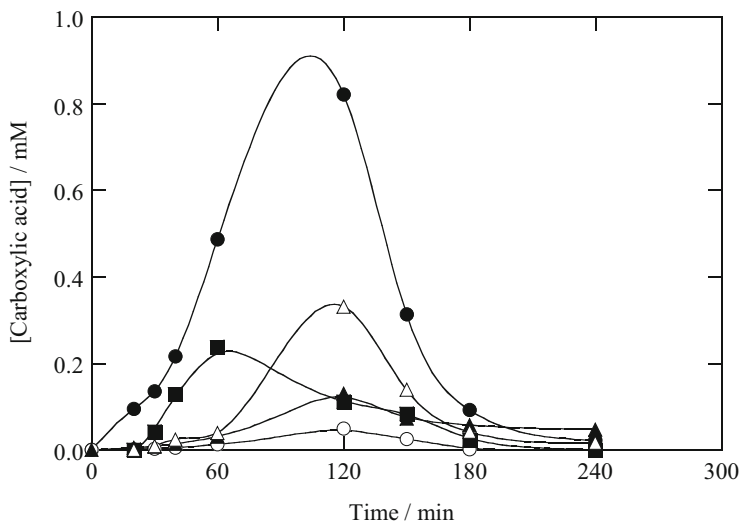


Fig. 5 Evolution of the concentration of (*filled circle*) oxalic, (*square*) tartaric, (*filled triangle*) oxamic, (*open circle*) tartronic, and (*open triangle*) acetic acids detected as final carboxylic acids during the SPEF degradation of 2.5 L of a 0.260 mM Congo Red, 0.05M Na₂SO₄, and 0.50 mM Fe²⁺ solution of pH 3.0 using the flow plant of Fig. 1a with a Pt anode at 100 mA cm⁻², 35°C, and liquid flow rate of 200 L h⁻¹. Adapted from [30]. Copyright 2015 Elsevier

removed in percentage, but with higher MCE because of the faster reaction of the above radicals with the greater quantity of organics present in the effluent. Quicker dye removal than decolorization was always found. The solution was always decolorized at similar rate under comparable EF and SPEF conditions owing to the attack of dyes and its colored by-products by [•]OH mainly formed from Fenton's reaction (3). Conversely, the EF treatment led to poor decontamination since Fe(III)-oxalate and Fe(III)-oxamate complexes were slowly destroyed by BDD([•]OH), whereas the quick photolytic removal of these species yielded the higher mineralization degree in SPEF. For the food azo dyes E122, E124, and E129 [13], a fast decolorization and almost total mineralization in the presence of either a sulfate, perchlorate, nitrate, or sulfate + chloride electrolyte were found. In chloride medium, however, the formation of recalcitrant chloroderivatives decelerated the degradation process. Greater MCE and lower EC_{TOC} were attained in sulfate medium at low current density and high azo dye content. This means that sulfate is the best electrolyte to enhance the power of oxidants generated in SPEF.

The study made in the 2.5 L flow plant for 200 mg L⁻¹ Disperse Blue 3 solutions with 0.10M Na₂SO₄ and 0.50 mM Fe²⁺ or 0.50 mM Fe²⁺ + 0.10 mM Cu²⁺ as catalyst at $j = 50$ mA cm⁻² is remarkable [33]. Figure 6a depicts the quicker mineralization of SPEF compared to EF for both catalysts, although the use of the mixed catalyst slightly improved the performance of both processes. The EC_{TOC} values determined for these trials usually increased with prolonging electrolysis. At 210 min, about 0.150 kWh (g TOC)⁻¹ were spent to remove more than 95% TOC regardless

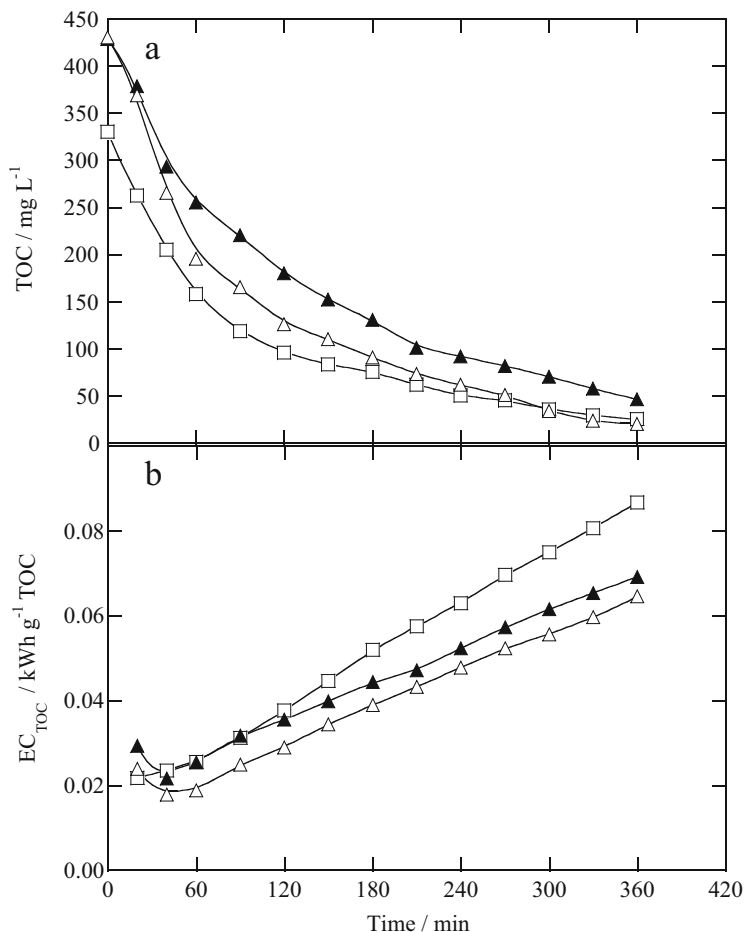


Fig. 6 Variation of (a) TOC and (b) energy consumption per unit TOC mass with electrolysis time for the SPEF treatment of 2.5 L of a simulated textile dyeing wastewater (330 mg L^{-1} TOC from additives) with $0.10 \text{ M Na}_2\text{SO}_4$ of pH 3.0 in the flow plant of Fig. 1a at 1.0 A , 35°C , and liquid flow rate of 200 L h^{-1} . Solutions: (*square*) $0.50 \text{ mM Fe}^{2+} + 0.10 \text{ mM Cu}^{2+}$, (*filled triangle*) 0.50 mM Fe^{2+} and 200 mg L^{-1} Disperse Blue 3, and (*open triangle*) $0.50 \text{ mM Fe}^{2+} + 0.10 \text{ mM Cu}^{2+}$ and 200 mg L^{-1} dye. Adapted from [33]. Copyright 2012 Elsevier

of the catalyst utilized (see Fig. 6b). GC-MS analysis allowed the identification of 15 aromatic by-products coming from $\cdot\text{OH}$ oxidation. Maleic, oxalic, oxamic, pyruvic, and acetic acids proceeding from the cleavage of the above aromatics disappeared more quickly in the presence of $0.50 \text{ mM Fe}^{2+} + 0.10 \text{ mM Cu}^{2+}$. This was ascribed to the competitive formation of Cu(II)-carboxylate species that are destroyed much more rapidly with BDD($\cdot\text{OH}$) than the analogous Fe(III)-carboxylate ones. The N of the dye was released in large extent as NO_3^- than NH_4^+ .

Espinoza et al. [34] constructed an 8 L solar flow plant similar to that of Fig. 3a with an electrochemical BDD/GDE filter-press reactor similar to that of Fig. 1b of 50 cm² electrode active area and a solar CPC photoreactor of 0.70 L. For 284 mg L⁻¹ of the diazo dye Acid Yellow 42 in 0.05M Na₂SO₄ with 1.0 mM Fe²⁺ at pH 3.0 and $j = 80 \text{ mA cm}^{-2}$, total dye removal and decolorization were achieved at 60 and 150 min, respectively, whereas 83% mineralization with MCE = 35% and an energy cost of US \$6.5/m³ were obtained after 270 min of electrolysis. The decolorization of the solution was enhanced in the order AO-H₂O₂ < EF < SPEF. Complete disappearance of the Fe(III) complexes of citric, maleic, malic, acetic, formic, oxalic, and oxamic acids as final carboxylic acids at the end of the latter process was found. NO₃⁻ was released in larger proportion than NH₄⁺, but a balance of total N showed a loss of this heteroatom in the form of N₂ and N_xO_y.

On the other hand, Zhao et al. [35] treated 100 mL of 20 mg L⁻¹ of rhodamine B under the same experimental conditions as explained in Sect. 4.2 for the imidacloprid treatment of Peng et al. [28], but using a (Fe/Co) carbon aerogel cathode. The simulated solar-assisted heterogeneous EF at $j = 10 \text{ mA cm}^{-2}$ and pH 3.0 led to 100% color removal in 45 min and 91% mineralization in 600 min. It was found that the cathode showed an efficient degradation for rhodamine B in the pH range 3–9 and good reusability with very low iron and cobalt leaching (<0.5 ppm) even in an acidic medium.

4.4 Pharmaceuticals

The first studies to show the excellent performance of the SPEF process to degradation pharmaceuticals were made for salicylic acid [36], ibuprofen [37], and enrofloxacin [20] using a stirred tank reactor with a Pt or BDD anode and a GDE cathode, all of 3 cm² area. In the case of ibuprofen, for example, a saturated solution with 41 mg L⁻¹ drug, 0.05M Na₂SO₄, and 0.50 mM Fe²⁺ of pH 3.0 electrolyzed at $j = 33.3 \text{ mA cm}^{-2}$ was mineralized to a larger extent using a BDD anode instead of a Pt one owing to the greater oxidizing power of BDD(•OH) than Pt(•OH) to remove the contaminants. The concentration decay for both electrodes followed a pseudo-first-order kinetics. Similar results were found for the other organics tested, showing that SPEF was more powerful with BDD. In all cases, pH 3.0 was found optimal, near the optimum pH of 2.8 for Fenton's reaction (3), as expected if •OH is the main oxidant of organic pollutants. Moreover, higher amounts of TOC were removed with increasing j and drug concentration, the same behavior as described above for the other kinds of organic pollutants. Analysis of treated solutions revealed the formation of aromatic intermediates like 2,3-, 2,5-, and 2,6-dihydroxybenzoic acids for salicylic acid; 4-ethylbenzaldehyde, 4-isobutylacetophenone, 4-isobutylphenol, and 1-(1-hydroxyethyl)-4-isobutylbenzene for ibuprofen; and polyols, ketones, and *N*-derivatives for enrofloxacin. Ion exclusion HPLC allowed identifying and quantifying generated carboxylic acids. Oxalic acid was accumulated to a larger extent, and the quick photodecomposition of Fe(III)-oxalate complexes under sunlight exposition

explained the greatest mineralization degree attained in SPEF compared to EF. The initial F of enrofloxacin was totally transformed into F^- ion, and its initial N was primordially converted into NH_4^+ ion and in smaller proportion into NO_3^- ion.

The treatment of 158 mg L^{-1} of enrofloxacin was extended to the 2.5 L solar pre-pilot plant of Fig. 1a containing BDD/GDE and Pt/GDE cells like of Fig. 1b [20]. Table 1 shows that better mineralization and MCE were found for BDD, but lower EC_{TOC} was obtained when using Pt. It was also confirmed for each anode the superiority of SPEF over other EAOPs, their oxidation power raising in the sequence $AO-H_2O_2 < EF < SPEF$, as found in most compounds studied by these methods. Further researches with the same system with a Pt anode were focused in the degradation of the antibiotics sulfanilamide [22] and ranitidine [38] in 0.05M Na_2SO_4 and 0.50 mM Fe^{2+} solutions of pH 3.0. Good mineralization with 91% TOC decay was obtained when treating 239 mg L^{-1} of sulfanilamide in only 180 min at $j = 50 \text{ mA cm}^{-2}$ (see Table 1). In contrast, ranitidine was much more recalcitrant, and 16 mg L^{-1} of this antibiotic electrolyzed at $j = 100 \text{ mA cm}^{-2}$ only underwent 37% TOC reduction with $MCE = 8.7\%$ and $EC_{\text{TOC}} = 0.94 \text{ kWh (g TOC)}^{-1}$ in 360 min. The decay kinetics of both antibiotics obeyed a pseudo-first-order reaction. Catechol, resorcinol, hydroquinone, and *p*-benzoquinone were detected as products of the attack of sulfanilamide by $Pt(OH)$ and mainly $\cdot OH$. In both cases, the preponderant generated Fe(III)-oxalate complexes were efficiently photolyzed by UV radiation of sunlight, and NH_4^+ , NO_3^- , and SO_4^{2-} ions were released from their N and S heteroatoms.

The research with the 10 L solar pre-pilot plant of Fig. 3a was initially centered in the optimization of the treatment of 157 mg L^{-1} of paracetamol with 0.05M Na_2SO_4 by RSM [21]. A Pt/GDE cell was chosen for these trials since less energy consumption than using a BDD anode was required, because of its lower E_{cell} . The best operation variables were $I = 5 \text{ A}$, 0.40 mM Fe^{2+} , and pH 3.0 leading to 75% TOC removal, 71% current efficiency, and $0.093 \text{ kWh (g TOC)}^{-1}$ energy consumption ($EC = 7.2 \text{ kWh m}^{-3}$) at 120 min (see Table 1). From the HPLC analysis of electrolyzed solutions, hydroquinone, *p*-benzoquinone, 1,2,4-trihydroxybenzene, 2,5-dihydroxy-*p*-benzoquinone, and tetrahydroxy-*p*-benzoquinone were detected as aromatic by-products, preeminently removed by $\cdot OH$ in the bulk. Final carboxylic acids such as maleic, fumaric, succinic, lactic, formic, oxalic, and oxamic acids were mainly destroyed via photolysis of their Fe(III) complexes. The viability of the SPEF process was also confirmed for chloramphenicol [39] and metronidazole [40] using the same arrangement of the 10 L solar pre-pilot plant. For a 245 mg L^{-1} chloramphenicol solution in 0.05M Na_2SO_4 with 0.50 mM Fe^{2+} at pH 3.0, 89% mineralization with $MCE = 36\%$ and $EC = 30.8 \text{ kWh m}^{-3}$ were obtained after 180 min of electrolysis at $j = 100 \text{ mA cm}^{-2}$. The best process for a 1.39 mM metronidazole solution in 0.10M Na_2SO_4 with 0.50 mM Fe^{2+} at pH 3.0 was found at $j = 55.4 \text{ mA cm}^{-2}$ giving rise to 53% mineralization, $MCE = 36\%$, and $EC_{\text{TOC}} = 0.339 \text{ kWh (g TOC)}^{-1}$ in 300 min.

Isarain-Chávez et al. [31] studied the SPEF degradation of 10 L of 100 mg L^{-1} TOC of the β -blockers atenolol, metoprolol tartrate, and propranolol hydrochloride in 0.10M Na_2SO_4 with 0.50 mM Fe^{2+} at pH 3.0 using single Pt/GDE and BDD/GDE

cells and their combination with a Pt/CF cell to enhance Fe^{2+} regeneration from Fe^{3+} reduction via reaction (4). Figure 3b shows a sketch of the combined BDD/GDE-Pt/CF cell used. Figure 7a–c exemplifies the superiority of combined cells over single ones, BDD over Pt, and SPEF over EF regarding the normalized drug decay, TOC abatement, and MCE, respectively, for a 0.246 mM metoprolol tartrate solution. This can be accounted for by the greater production of $\cdot\text{OH}$ from Fenton's reaction (3) in the combined cells, the higher oxidizing power of BDD($\cdot\text{OH}$), and the photolytic action of sunlight in SPEF, as can also be deduced from the pseudo-first-order decay for tartrate concentration shown in the inset panel of Fig. 7a for the different cells checked. Nevertheless, the combined Pt/GDE-Pt/CF cell allowed the lowest EC_{TOC} of $0.080 \text{ kWh (g TOC)}^{-1}$ for 88–93% mineralization, thereby being the most viable system for industrial application. This indicates that the oxidation power of the anode is less significant in SPEF, suggesting the use of Pt and even cheaper dimensionally stable anodes due to the efficient degradation by $\cdot\text{OH}$ in the bulk combined with sunlight.

The aforementioned suggestion was also confirmed by Moreira et al. [41], who tested the degradative behavior of 20 mg L^{-1} of trimethoprim in $7.0 \text{ g L}^{-1} \text{ Na}_2\text{SO}_4$ and $2.0 \text{ mg L}^{-1} \text{ Fe}^{2+}$ of pH 3.5 using a 2.2 L solar flow plant similar to that Fig. 1a containing a filter-press BDD/GDE or Pt/GDE cell of 10 cm^2 electrode area connected to a CPC photoreactor of 0.694 L irradiated volume. It is noteworthy that at $j = 5 \text{ mA cm}^{-2}$ and liquid flow rate of 40 L h^{-1} , the influence of the anode in SPEF was almost negligible. After 420 min of electrolysis, 77 and 73% mineralization with 30 and 26% current efficiency and 1.2 and 0.9 kWh m^{-3} energy consumption were obtained for BDD and Pt, respectively. Up to 18 aromatic products and 19 hydroxylated derivatives were detected from trimethoprim degradation by LC-MS, and a high content of hardly oxidizable *N*-derivatives, containing the major part of *N*, was finally produced, along with small losses of NH_4^+ and NO_3^- ions.

5 Autonomous Solar Flow Plant

Despite the more cost-effective treatment of organic pollutants from wastewaters by SPEF than other EAOPs, as pointed out above, the electrolytic reactor used in this process spends energy since it needs the electrical current provided by a power supply. This still represents an economical problem for its possible application to water remediation at industrial level. To solve this problem, our group designed an autonomous solar flow plant in which the electrical energy required by the electrolytic cell was supplied by a solar photovoltaic panel, thereby making an energetically free SPEF process. A sketch of this autonomous plant is shown in Fig. 8 [42]. It consisted of the solar flow plant of Fig. 3 powered by a photovoltaic panel of 50 W, providing $I = 5.0 \text{ A}$ as maximum when a Pt/GDE reactor ($E_{\text{cell}} = 10.0 \text{ V}$) was used. The operation characteristics of this plant were assessed by studying the removal and mineralization of the diazo dye Direct Yellow 4 in a $0.05 \text{ M Na}_2\text{SO}_4$

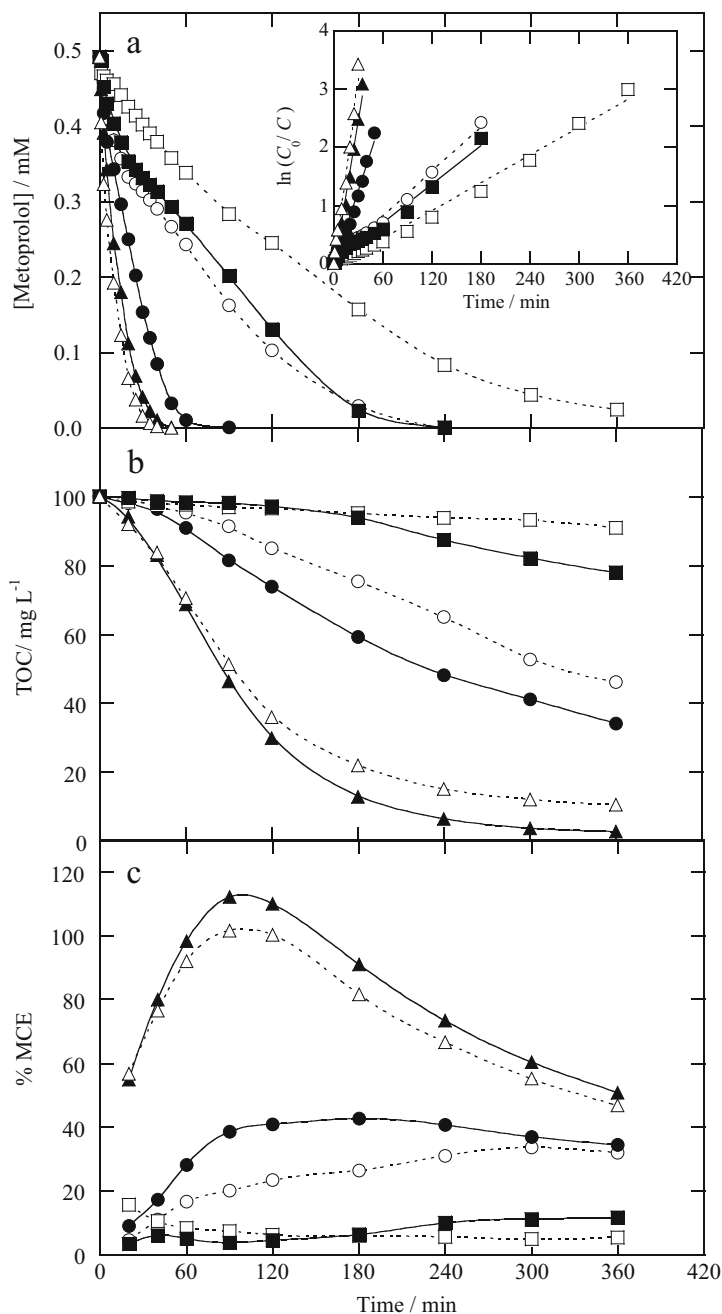


Fig. 7 (a) Concentration of metoprolol decay during the EF and SPEF treatments of 10 L of 0.492 mM drug in 0.10M Na₂SO₄ with 0.50 mM Fe²⁺ at pH 3.0 and 35°C in the pre-pilot plant of Fig. 3 with single and combined cells. The inset panel depicts the kinetic analysis assuming a pseudo-first-order reaction for the drug. (b) TOC removal and (c) mineralization current efficiency for the degradation of 0.246 mM metoprolol tartrate under the same conditions. (*open square*) EF in Pt/GDE cell at 3.0 A, (*filled square*) EF in Pt/GDE-Pt/CF cell at 3.0–0.4 A, (*open circle*) EF in

solution of pH 3.0. As illustrated in Fig. 9, 0.16 mM of the dye with 0.50 mM Fe^{2+} underwent about 96–97% mineralization in 180 min at 5.0 A, whereas a longer time of 240 min, but with higher MCE values, was required for a lower current of 3.0. This means that the free SPEF process is feasible to be used with much high currents to shorten the operation time. In all cases, Direct Yellow 4 was removed following a pseudo-first-order kinetics. LC-MS and ion exclusion HPLC revealed the presence of 11 aromatic products, 22 hydroxylated derivatives, and 9 short-linear carboxylic acids as intermediates. The Fe(III) complexes of most acids were quickly removed, preeminently photolyzed by UV radiation of sunlight, except those of acetic and oxamic acids that were more slowly destroyed. The N atoms of the dye were mainly released as NH_4^+ ion, and its S atoms were lost as SO_4^{2-} ion.

6 Coupled Solar-Assisted Electro-Fenton Treatments

The coupling of solar-assisted EF process with other methods including SPC, PEC, and biological treatment has been recently checked to obtain a more effective decontamination of wastewaters. It is noteworthy that coupled SPEF with biological treatment has been applied to real wastewaters, thereby opening the door for its use at industrial scale.

Garza-Campos et al. [43] constructed the 3 L solar pre-pilot plant of Fig. 10 useful for a coupled SPEF-SPC process. The system was composed of the flow plant of Fig. 1a with a Pt/GDE filter-press electrochemical reactor and an additional solar planar photocatalytic photoreactor connected between the solar photoreactor and the reservoir. The photocatalytic photoreactor was filled with TiO_2 deposited on small borosilicate glass spheres of 5 mm diameter in average to generate extra $\cdot\text{OH}$. This occurs when TiO_2 is illuminated with UV photons of $\lambda < 380$ nm, since an electron from the filled valence band is promoted to the empty conduction band (e^-_{cb}) with an energy gap of 3.2 eV, generating a positively charged vacancy or hole (h^+_{vb}) by reaction (15). The holes thus produced at the TiO_2 surface can oxidize either organics or water giving adsorbed $\cdot\text{OH}$ from reaction (16), which can subsequently attack also the organic species. However, a strong loss of efficiency occurs due to the recombination of promoted electrons either with unreacted holes by reaction (17) or with adsorbed $\cdot\text{OH}$ by reaction (18) [5].

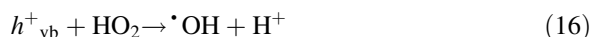
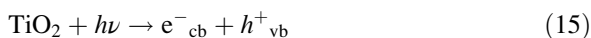


Fig. 7 (continued) BDD/GDE cell at 3.0 A, (*filled circle*) EF in BDD/GDE-Pt/CF cell at 3.0–0.4 A, (*open triangle*) SPEF in Pt/GDE-Pt/CF cell at 3.0–0.4 A, and (*filled triangle*) SPEF in BDD/GDE-Pt/CF cell at 3.0–0.4 A. Adapted from [31]. Copyright 2011 Elsevier

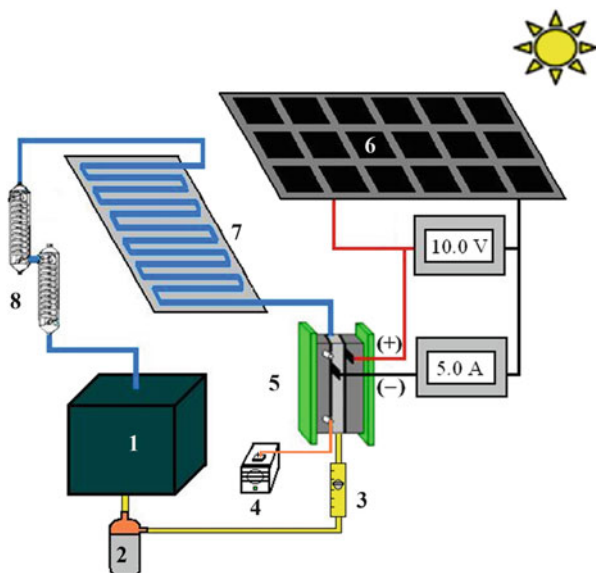


Fig. 8 Sketch of the autonomous solar pre-pilot plant used for the SPEF treatment of 10 L of Direct Yellow 4 solutions. (1) Reservoir, (2) magnetic drive centrifugal pump, (3) flowmeter, (4) air pump, (5) electrochemical filter-press reactor with a Pt anode and an air diffusion cathode of 90.3 cm² area, (6) solar photovoltaic panel of 50 W maximum power with the corresponding ammeter and voltmeter, (7) solar compound parabolic component (CPC) photoreactor of 1.57 L irradiation volume, and (8) heat exchangers. Adapted from [42]. Copyright 2014 Elsevier

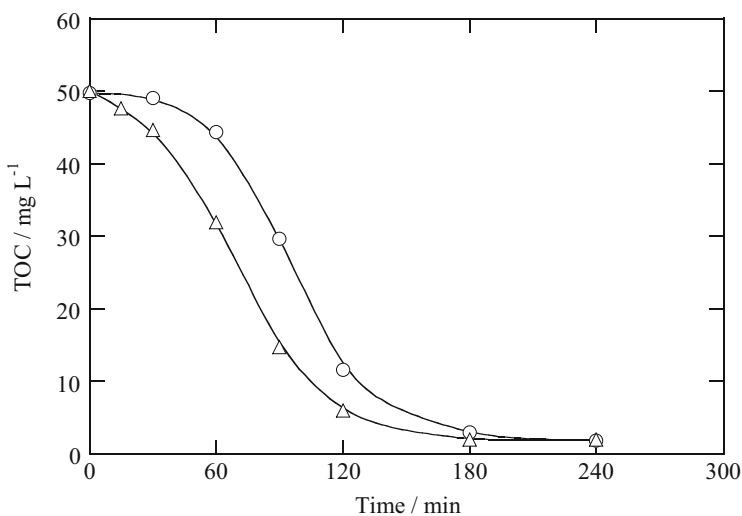


Fig. 9 Influence of current over TOC removal for the treatment of 10 L of a 0.16 mM Direct Yellow 4 solution in 0.05M Na₂SO₄ with 0.50 mM Fe²⁺ at pH 3.0 and 35°C by SPEF in the autonomous solar pre-pilot plant of Fig. 8 at a liquid flow rate of 200 L h⁻¹. Average applied current: (circle) 3.0 A and (triangle) 5.0 A. Adapted from [42]. Copyright 2014 Elsevier

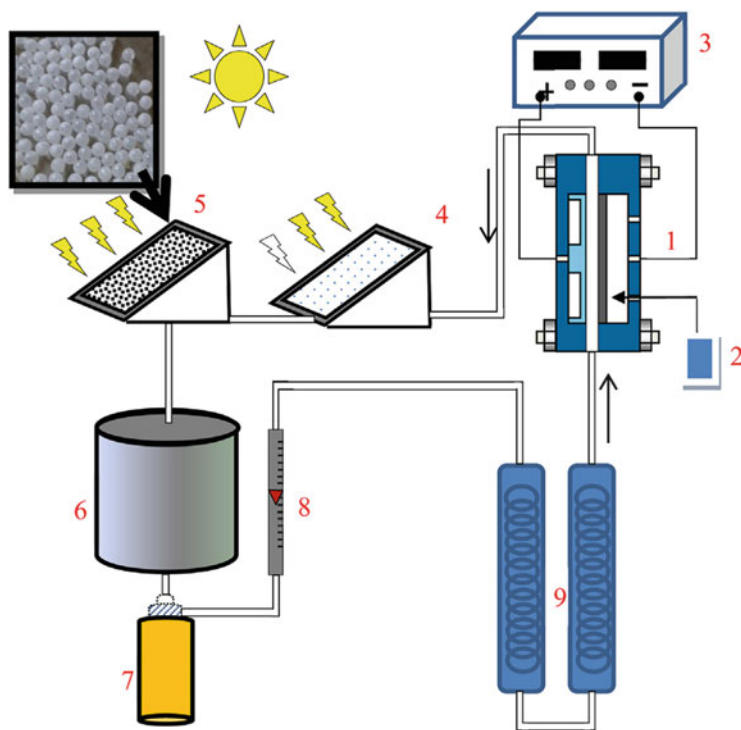
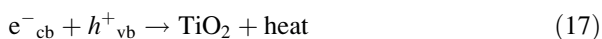


Fig. 10 Experimental setup for the degradation of 3.0 L of salicylic acid solutions by coupled SPEF and solar photocatalysis (SPC). (1) One-compartment filter-press cell with a 20 cm² Pt anode and a 20 cm² air diffusion cathode, (2) air pump, (3) power supply, (4) solar photoreactor, (5) solar photocatalytic photoreactor with TiO₂-coated spheres, (6) reservoir, (7) centrifugal pump, (8) rotameter, and (9) heat exchangers. Reproduced from [43]. Copyright 2016 Elsevier



The viability of the coupled process was assessed with 165 mg L⁻¹ of salicylic acid in 0.05M Na₂SO₄ of pH 3.0. After 360 min at $j = 50 \text{ mA cm}^{-2}$, the percentage of mineralization for individual and coupled processes grew as follows: AO-H₂O₂ (16%) < AO-H₂O₂-SPC (24%) < EF (29%) < SPEF (59%) < SPEF-SPC (66%). The latter process was the best one with MCE = 29% and EC_{TOC} = 0.249 kWh (g TOC)⁻¹. Figure 11a, b highlights the negligible degradation by SPC and the growing destruction of the drug at higher j by SPEF and SPEF-SPC from the normalized concentration decay and TOC removal, respectively. Under all these conditions, the coupled SPEF-SPC process led to better performance, thanks to the combined oxidation action of Pt(*OH) formed at the anode from reaction (5); *OH produced by Fenton's reactions (3), (9), and (16); photogenerated holes from

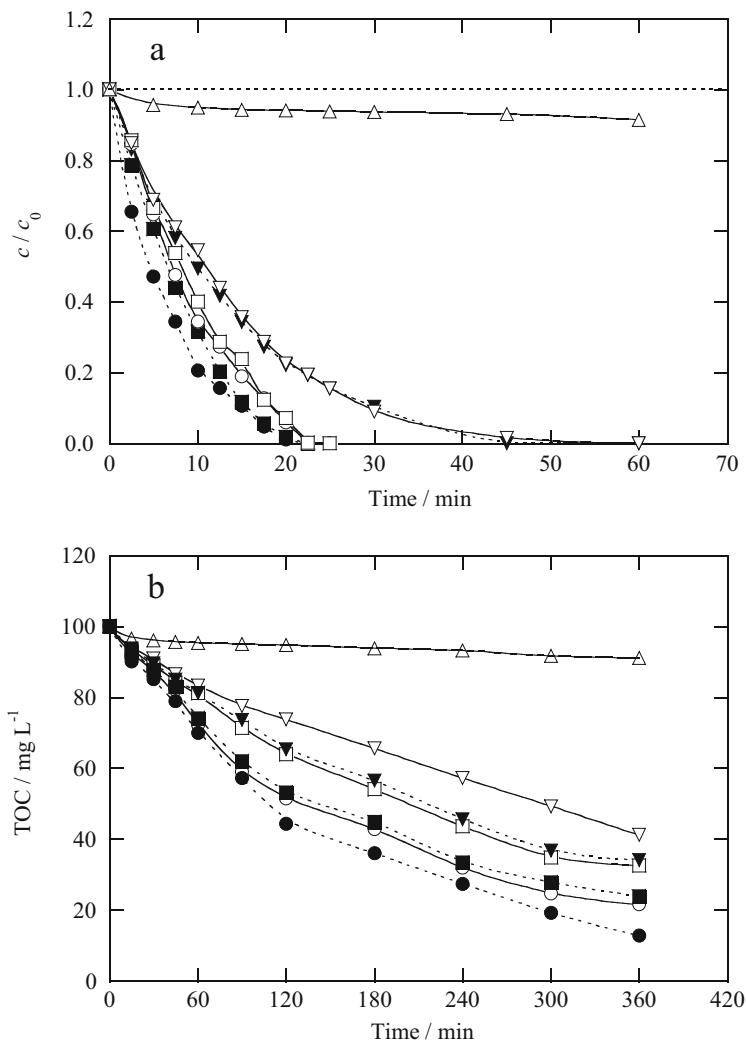


Fig. 11 (a) Normalized salicylic acid concentration decay and (b) TOC removal with time for the degradation of 3.0 L of 165 mg L⁻¹ drug solution in 0.05M Na₂SO₄ at pH 3.0 and 35°C using the flow plant of Fig. 10. Method: (open triangle) SPC; SPEF at (open inverted triangle) 50 mA cm⁻², (open square) 100 mA cm⁻², and (open circle) 150 mA cm⁻²; SPEF-SPC at (filled inverted triangle) 50 mA cm⁻², (filled square) 100 mA cm⁻², and (filled circle) 150 mA cm⁻². Adapted from [43]. Copyright 2016 Elsevier

reaction (15); and sunlight. For the highest j of 150 mA cm⁻², it gave 87% mineralization, MCE = 13%, and EC_{TOC} = 1.133 kWh (g TOC)⁻¹.

The power of the SPC process can be strongly enhanced by using the alternative PEC in which a TiO₂ film acts as photoanode, and the electrons promoted to the

conduction band are continuously extracted to the cathode through the circulating electrical current, avoiding their loss by reactions (17) and (18). The feasibility of using a SPEF-PEC process has been tested by Peng et al. [44], who prepared a photoanode composed of TiO₂ nanotubes of 40–50 nm modified with Fe₂O₃ and treated an O₂-saturated rhodamine B solution in a cell containing an activated carbon fiber cathode for H₂O₂ production from reaction (1). Upon optimum conditions, 96% of color removal was obtained in 60 min with a rate constant of 0.055 min⁻¹. Hydroxyl radicals and photogenerated holes contributed in 76.6% and 16.6%, respectively, to the rhodamine B decolorization.

The good coupling of SPEF with biological treatment has been investigated for winery [45], landfill leachate [46–48], and slaughterhouse [49] wastewaters. In the case of a winery wastewater, for example, the biological oxidation led to above 97% removals of TOC, chemical oxygen demand (COD), and 5-day biochemical oxygen demand (BOD₅), but it resulted inefficient on a bioresistant fraction corresponding to 130 mg L⁻¹ of TOC, 380 mg O₂ L⁻¹ of COD, and 8.2 mg caffeic acid equivalent L⁻¹ of total dissolved polyphenols. In a subsequent SPEF process with the 2.2 L solar pre-pilot plant with a BDD/GDE cell stated in Sect. 4.4, using 35 mg L⁻¹ Fe²⁺ at pH 2.8 and applying $j = 25 \text{ mA cm}^{-2}$, additional removals of 86% TOC and 68% COD in 240 min were obtained, with EC = 5.1 kWh m⁻³ and EC_{TOC} = 0.045 kWh (g TOC)⁻¹. The resulting water complied with all legislation targets, including a total dissolved polyphenol content of 0.35 mg caffeic acid equivalent L⁻¹.

Landfill leachates previously digested by anaerobic-aerobic systems were further treated by different solar-assisted processes. Ye et al. [48] utilized a 1.7 L solar Fered-Fenton pre-pilot plant with an electrochemical tank reactor containing a Ti/IrO₂-RuO₂-TiO₂ plate anode and a Ti plate cathode of 150 cm² area coupled to a solar CPC photoreactor of 0.70 L irradiation volume, at liquid flow rate of 13.6 L h⁻¹. Trials conducted upon optimum conditions by adding 47 mM H₂O₂ and 0.29 mM Fe²⁺ at pH 3.0 yielded 66% COD removal with respect to the biologically treated water and EC_{TOC} = 0.074 kWh (g TOC)⁻¹ after 120 min at $j = 60 \text{ mA cm}^{-2}$. The coupled treatment led to more than 98% removals of COD, ammonium, nitrate, nitrite, total nitrogen, and total phosphorous.

Vidal et al. [49] treated a slaughterhouse effluent by anaerobic oxidation during 30 days to obtain a wastewater with 52, 137, and 183 mg L⁻¹ of TOC, COD, and BOD₅, respectively. Further degradation of 100 mL of this wastewater with 1.0 mM Fe²⁺ by SPEF using a BDD/GDE stirred tank reactor of 2.5 cm² electrode area at $j = 50 \text{ mA cm}^{-2}$ allowed the reduction of the above parameters up to 2, 10, and 6 mg L⁻¹. These excellent results were accompanied by total loss of odor and suspended and volatile solids as well as a strong reduction of dissolved organic nitrogen.

7 Conclusions

The recent development of SPEF and related solar-assisted processes has corroborated the viability of these EAOPs to remove toxic and refractory aromatic pollutants such as industrial chemicals, pesticides, dyes and pharmaceuticals, as well as real wastewaters, upon acidic conditions. However, their use is limited by the weather and disposal of sunlight. High mineralization with good current efficiency was found for these environmentally friendly methods, which are simple, are safe, and can be easily scaled up to industrial level using recirculation flow plants. Very stable anodes like BDD or Pt and GDE cathodes for an efficient H_2O_2 generation can be utilized in SPEF. The main drawback for industrial application is the electrical consumption for running the electrochemical cell, even using inexpensive sunlight as photon source. The coupling of photovoltaic panels to power the electrochemical reactor allows the application of autonomous solar flow plants as an excellent free alternative way for SPEF. The coupling of the reactor with an efficient solar CPCs photoreactor represents an interesting arrangement for enhancing the degradation process. The SPEF treatment of organic pollutants with a BDD anode was more efficient and less expensive than other EAOPs like AO- H_2O_2 , EF, and PEF operating under comparable conditions, because of the potent degradation action of sunlight. Similar results were obtained with a Pt anode, being less significant the use of the expensive BDD one in SPEF. The coupling with SPC, PEC, or biological treatment can enhance the oxidation power of the method. The mineralization rate slowed down as applied current dropped, but with greater MCE and lower energy consumption. This trend was also found when pollutant concentration increased due to the inhibition of parasitic reactions of oxidant $\cdot\text{OH}$ by its quicker reaction with higher organic load. The kinetics of contaminant decay obeyed a pseudo-first-order reaction. Aromatic intermediates were oxidized to short-linear aliphatic carboxylic acids that extensively form Fe(III) complexes, most of which are rapidly photolyzed by the potent UV radiation of sunlight. Heteroatoms present in organics are released as inorganic ions such as F^- , Cl^- , SO_4^{2-} , NH_4^+ , and NO_3^- .

References

1. Brillas E, Martinez-Huitle CA (2015) Decontamination of wastewaters containing synthetic organic dyes by electrochemical methods. An updated review. *Appl Catal B Environ* 166–167:603–643
2. Oturan N, Sirés I, Oturan MA, Brillas E (2009) Degradation of pesticides in aqueous medium by electro-Fenton and related methods. A review. *J Environ Eng Manage* 19:235–255
3. Sirés I, Brillas E, Oturan MA, Rodrigo MA, Panizza M (2014) Electrochemical advanced oxidation processes: today and tomorrow. A review. *Environ Sci Pollut Res* 21:8336–8367
4. Moreira FC, Boaventura RAR, Brillas E, Vilar VJP (2017) Electrochemical advanced oxidation processes: a review on their application to synthetic and real wastewaters. *Appl Catal B Environ* 202:217–261

5. Brillas E (2014) Electro-Fenton, UVA photoelectro-Fenton and solar photoelectro-Fenton treatments of organics in waters using a boron-doped diamond anode: a review. *J Mex Chem Soc* 58:239–255
6. Sirés I, Brillas E (2012) Remediation of water pollution caused by pharmaceutical residues based on electrochemical separation and degradation technologies: a review. *Environ Int* 40:212–229
7. Yu X, Zhou M, Hu Y, Groenen-Serrano K, Yu F (2014) Recent updates on electrochemical degradation of bio-refractory organic pollutants using BDD anode: a mini review. *Environ Sci Pollut Res* 21:8417–8431
8. Brillas E (2014) A review on the degradation of organic pollutants in waters by UV photoelectro-Fenton and solar photoelectro-Fenton. *J Braz Chem Soc* 25:393–417
9. Ruiz EJ, Arias C, Brillas E, Hernández-Ramírez A, Peralta-Hernández JM (2011) Mineralization of Acid Yellow 36 azo dye by electro-Fenton and solar photoelectro-Fenton processes with a boron-doped diamond anode. *Chemosphere* 8:495–501
10. Flox C, Cabot PL, Centellas F, Garrido JA, Rodríguez RM, Arias C, Brillas E (2007) Solar photoelectro-Fenton degradation of cresols using a flow reactor with a boron-doped diamond anode. *Appl Catal B Environ* 75:17–28
11. Flox C, Garrido JA, Rodríguez RM, Cabot PL, Centellas F, Arias C, Brillas E (2007) Mineralization of herbicide mecoprop by photoelectro-Fenton with UVA and solar light. *Catal Today* 129:29–36
12. Ruiz EJ, Hernández-Ramírez A, Peralta-Hernández JM, Arias C, Brillas E (2011) Application of solar photoelectro-Fenton technology to azo dyes mineralization: effect of current density, Fe^{2+} and dye concentration. *Chem Eng J* 171:385–392
13. Thiam A, Sirés I, Brillas E (2015) Treatment of a mixture of food color additives (E122, E124 and E129) in different water matrices by UVA and solar photoelectro-Fenton. *Water Res* 81:178–187
14. El-Ghenymy A, Garcia-Segura S, Rodríguez RM, Brillas E, El Begrani MS, Abdelouahid BA (2012) Optimization of the electro-Fenton and solar photoelectro-Fenton treatments of sulfanilic acid solutions using a pre-pilot flow plant by response surface methodology. *J Hazard Mater* 221–222:288–297
15. Garcia-Segura S, Almeida LC, Bocchi N, Brillas E (2011) Solar photoelectro-Fenton degradation of the herbicide 4-chloro-2-methylphenoxyacetic acid optimized by response surface methodology. *J Hazard Mater* 194:109–118
16. Gozzi F, Sirés I, Thiam A, de Oliveira SC, Machulek Jr A, Brillas E (2017) Treatment of single and mixed pesticide formulations by solar photoelectro-Fenton using a flow plant. *Chem Eng J* 310:503–513
17. Thiam A, Sirés I, Centellas F, Cabot PL, Brillas E (2015) Decolorization and mineralization of Allura Red AC azo dye by solar photoelectro-Fenton: identification of intermediates. *Chemosphere* 136:1–8
18. Salazar R, Garcia-Segura S, Ureta-Zañartu MS, Brillas E (2011) Degradation of disperse azo dyes from waters by solar photoelectro-Fenton. *Electrochim Acta* 56:6371–6379
19. Antonin VS, Garcia-Segura S, Santos MC, Brillas E (2015) Degradation of Evans Blue diazo dye by electrochemical processes based on Fenton's reaction chemistry. *J Electroanal Chem* 747:1–11
20. Guinea E, Garrido JA, Rodriguez RM, Cabot PL, Arias C, Centellas F, Brillas E (2010) Degradation of the fluoroquinolone enrofloxacin by electrochemical advanced oxidation processes based on hydrogen peroxide electrogeneration. *Electrochim Acta* 55:2101–2115
21. Almeida LC, Garcia-Segura S, Bocchi N, Brillas E (2011) Solar photoelectro-Fenton degradation of paracetamol using a flow plant with a Pt/air-diffusion cell coupled with a compound parabolic collector: process optimization by response surface methodology. *Appl Catal B Environ* 103:21–30

22. El-Ghenymy A, Cabot PL, Centellas F, Garrido JA, Rodríguez RM, Arias C, Brillas E (2013) Mineralization of sulfanilamide by electro-Fenton and solar photoelectro-Fenton in a pre-pilot plant with a Pt/air-diffusion cell. *Chemosphere* 91:1324–1331
23. Serra A, Domènech X, Arias C, Brillas E, Peral J (2009) Oxidation of α -methylphenylglycine under Fenton and electro-Fenton conditions in the dark and in the presence of solar light. *Appl Catal B Environ* 89:12–21
24. Serra A, Domenech X, Peral J, Arias C, Brillas E (2008) Electrochemical advanced oxidation treatments of acidic aqueous solutions containing the amino acid α -methylphenylglycine using a boron-doped diamond anode. *J Environ Eng Manage* 18:173–181
25. Garcia-Segura S, Salazar R, Brillas E (2013) Mineralization of phthalic acid by solar photoelectro-Fenton with a stirred boron-doped diamond/air-diffusion tank reactor: influence of Fe^{3+} and Cu^{2+} catalysts and identification of oxidation products. *Electrochim Acta* 113:609–619
26. Garcia-Segura S, Brillas E, Cornejo-Ponce L, Salazar R (2016) Effect of the $\text{Fe}^{3+}/\text{Cu}^{2+}$ ratio on the removal of the recalcitrant oxalic and oxamic acids by electro-Fenton and solar photoelectro-Fenton. *Sol Energy* 124:242–253
27. Pipi ARF, Sirés I, De Andrade AR, Brillas E (2014) Application of electrochemical advanced oxidation processes to the mineralization of the herbicide diuron. *Chemosphere* 109:49–55
28. Peng Q, Zhao H, Qian L, Wang Y, Zhao G (2015) Design of a neutral photoelectro-Fenton system with 3D-ordered macroporous Fe_2O_3 /carbon aerogel cathode: high activity and low energy consumption. *Appl Catal B Environ* 174–175:157–166
29. Moreira FC, Garcia-Segura S, Vilar VJP, Boaventura RAR, Brillas E (2013) Decolorization and mineralization of Sunset Yellow FCF azo dye by anodic oxidation, electro-Fenton, UVA photoelectro-Fenton and solar photoelectro-Fenton processes. *Appl Catal B Environ* 142–143:877–890
30. Solano AMS, Garcia-Segura S, Martínez-Huitle CA, Brillas E (2015) Degradation of acidic aqueous solutions of the diazo dye Congo Red by photo-assisted electrochemical processes based on Fenton's reaction chemistry. *Appl Catal B Environ* 168:559–571
31. Isarain-Chávez E, Rodríguez RM, Cabot PL, Centellas F, Arias C, Garrido JA, Brillas E (2011) Degradation of pharmaceutical beta-blockers by electrochemical advanced oxidation processes using a flow plant with a solar compound parabolic collector. *Water Res* 45:4119–4130
32. Garcia-Segura S, Brillas E (2016) Combustion of textile monoazo, diazo and triazo dyes by solar photoelectro-Fenton: decolorization, kinetics and degradation routes. *Appl Catal B Environ* 181:681–691
33. Salazar R, Brillas E, Sirés I (2012) Finding the best $\text{Fe}^{2+}/\text{Cu}^{2+}$ combination for the solar photoelectro-Fenton treatment of simulated wastewater containing the industrial textile dye Disperse Blue 3. *Appl Catal B Environ* 115–116:107–116
34. Espinoza C, Romero J, Villegas L, Cornejo-Ponce L, Salazar R (2016) Mineralization of the textile dye Acid Yellow 42 by solar photoelectro-Fenton in a lab.-pilot plant. *J Hazard Mater* 319:24–33
35. Zhao H, Chen Y, Peng Q, Wang Q, Zhao G (2017) Catalytic activity of MOF(2Fe/Co)/carbon aerogel for improving H_2O_2 and $\cdot\text{OH}$ generation in solar photoelectro-Fenton process. *Appl Catal B Environ* 203:127–137
36. Guinea E, Arias C, Cabot PL, Garrido JA, Rodriguez RM, Centellas F, Brillas E (2008) Mineralization of salicylic acid in acidic aqueous medium by electrochemical advanced oxidation processes using platinum and boron-doped diamond as anode and cathodically generated hydrogen peroxide. *Water Res* 42:499–511
37. Skoumal M, Rodríguez RM, Cabot PL, Centellas F, Garrido JA, Arias C, Brillas E (2009) Electro-Fenton, UVA photoelectro-Fenton and solar photoelectro-Fenton degradation of the drug ibuprofen in acid aqueous medium using platinum and boron-doped diamond anodes. *Electrochim Acta* 54:2077–2085

38. Olvera-Vargas H, Oturan N, Oturan MA, Brillas E (2015) Electro-Fenton and solar photoelectro-Fenton treatments of the pharmaceutical ranitidine in pre-pilot flow plant scale. *Sep Purif Technol* 146:127–135
39. Garcia-Segura S, Cavalcanti EB, Brillas E (2014) Mineralization of the antibiotic chloramphenicol by solar photoelectro-Fenton. From stirred tank reactor to solar pre-pilot plant. *Appl Catal B Environ* 144:588–598
40. Pérez T, Garcia-Segura S, El-Ghenemy A, Nava JL, Brillas E (2015) Solar photoelectro-Fenton degradation of the antibiotic metronidazole using a flow plant with a Pt/air-diffusion cell and a CPC photoreactor. *Electrochim Acta* 165:173–181
41. Moreira FC, Garcia-Segura S, Boaventura RAR, Brillas E, Vilar VJP (2014) Degradation of the antibiotic trimethoprim by electrochemical advanced oxidation processes using a carbon-PTFE air-diffusion cathode and a boron-doped diamond or platinum anode. *Appl Catal B Environ* 160–161:492–505
42. Garcia-Segura S, Brillas E (2014) Advances in solar photoelectro-Fenton: decolorization and mineralization of the Direct Yellow 4 diazo dye using an autonomous solar pre-pilot plant. *Electrochim Acta* 140:384–395
43. Garza-Campos B, Brillas E, Hernández-Ramírez A, El-Ghenemy A, Guzmán-Mar JL, Ruiz-Ruiz J (2016) Salicylic acid degradation by advanced oxidation processes. Coupling of solar photoelectro-Fenton and solar heterogeneous photocatalysis. *J Hazard Mater* 319:34–42
44. Peng Z, Yu Z, Wang L, Liu Y, Xiang G, Chen Y, Sun L, Huang J (2016) Synthesis of Fe₂O₃/TiO₂ nanotube and its application in photoelectrocatalytic/photoelectro-Fenton decolorization of rhodamine B. *J Adv Oxide Technol* 19:34–42
45. Moreira FC, Boaventura RAR, Brillas E, Vilar VJP (2015) Remediation of a winery wastewater combining aerobic biological oxidation and electrochemical advanced oxidation processes. *Water Res* 75:95–108
46. Moreira FC, Soler J, Fonseca A, Saraiva I, Boaventura RAR, Brillas E, Vilar VJP (2015) Incorporation of electrochemical advanced oxidation processes in a multistage treatment system for sanitary landfill leachate. *Water Res* 81:375–387
47. Moreira FC, Soler J, Fonseca A, Saraiva I, Boaventura RAR, Brillas E, Vilar VJP (2016) Electrochemical advanced oxidation processes for sanitary landfill leachate remediation: evaluation of operational variables. *Appl Catal B Environ* 182:161–171
48. Ye Z, Zhang H, Yang L, Wu L, Qian Y, Geng J, Chen M (2016) Effect of a solar Fered-Fenton system using a recirculation reactor on biologically treated landfill leachate. *J Hazard Mater* 319:51–60
49. Vidal J, Huiliner C, Salazar R (2016) Removal of organic matter contained in slaughterhouse wastewater using a combination of anaerobic digestion and solar photoelectro-Fenton processes. *Electrochim Acta* 210:163–170

Electro-Fenton Applications in the Water Industry

Konstantinos V. Plakas and Anastasios J. Karabelas

Abstract In this chapter critical discussion is provided on the recent innovations and the potential of the Electro-Fenton (EF) and EF-related processes as eco-engineered technologies in the field of water treatment. Emphasis is placed on the treatment of water and wastewater to eliminate a wide variety of synthetic organic pollutants, such as pesticides, pharmaceuticals, and dyes, the refractory nature of which requires the application of strong oxidants for their total elimination. In comparison to the general public acceptance of traditional and/or advanced water treatment technologies (e.g., activated carbon, membrane technologies, etc.), there is ambiguity or skepticism regarding EF adaptation. This is due to the lack of technology certification, the limited large-scale applications, or even the small number of demonstrations in realistic operational environments. In view of this state of technology, the parameters involved in designing and operating EF systems are discussed together with the appropriate engineering rules that can support optimal system design and operation so that these systems can be used at an efficient, effective, and profitable manner at industrial scale.

Keywords Applications in water and wastewater treatment, Design and operation aspects, Electrochemical advanced oxidation, Electro-Fenton related patents, Electro-Fenton technology, Optimization of operation, Refractory organic pollutants, Scale-up

Contents

1	Electro-Fenton: A “Newcomer” in the Water Industry	344
2	Electro-Fenton Applications in the Water and Wastewater Sector	349
	2.1 Purification of Potable Water Sources	351

K.V. Plakas (✉) and A.J. Karabelas

Laboratory of Natural Resources and Renewable Energies, Chemical Process and Energy Resources Institute, Centre for Research and Technology Hellas, Thessaloniki, Greece
e-mail: kplakas@cperi.certh.gr

2.2	Treatment of Secondary Municipal Effluents	353
2.3	Chemical Industry Wastewater	355
2.4	Treatment of Agro-Industrial Wastewater	358
2.5	Remediation of Landfill Leachate	359
2.6	Other Applications	360
3	Patent Survey	361
4	Design and Operation Aspects Towards EF Optimization	367
4.1	Design of EF Reactors	367
4.2	Optimization of EF Operation	370
5	Recommendations for Future Research	373
	References	375

1 Electro-Fenton: A “Newcomer” in the Water Industry

More than 120 years ago, when Henry John Horstman Fenton published his fundamental work on the strong oxidation effects of the Fe(II)–H₂O₂ system to some organic acids [1], he could not imagine that this mixture, later called Fenton reagent, would open visionary research in the field of water science and technology. Beyond the synthesis of hydroxylated organic compounds or the analysis of tartaric acid in the early 1900s, Fenton reagent proved to be an efficient oxidation agent for various organic substrates [2]; later connected with radical reactions that promote the formation of highly reactive hydroxyl radicals ($\cdot\text{OH}$) [3]. The $\cdot\text{OH}$ is the strongest oxidant species known after fluorine with $E^\circ(\cdot\text{OH}/\text{H}_2\text{O}) = 2.80\text{ V}$ and is capable of completely mineralizing non-selectively most organic pollutants to CO₂, water, and inorganic ions.

The widespread interest in Fenton’s reagent potential to oxidize organics appeared in the mid-1960s [4], while in 1990s commercial reactors became available for wastewater treatment and for in situ groundwater treatment. Most of the original utilization of Fenton’s reagent was in relatively low concentrations in wastewater applications and the main criteria was to have a sufficient quantity of H₂O₂ in respect of the target organic chemical. The distinct drawbacks of Fenton reactions, such as the generation of significant amount of iron sludge [Fe(OH)₃ precipitate] that needs further treatment, separation and disposal, and the wastage of oxidants due to the radical scavenging effect of hydrogen peroxide and its self-decomposition [5, 6], motivated scientists to investigate new alternatives of Fenton process that allow an efficient use of H₂O₂ and the recovery/regeneration of iron ions for their subsequent recycle and reuse.

The Electro-Fenton (EF) process, which can be defined as an electrochemically assisted Fenton process, was the first method proposed among the so-called electrochemical advanced oxidation processes (EAOPs) and laid the foundation for a large variety of related processes [7]. It is an emerging technology that has been successfully applied to the treatment mostly of acidic aqueous solutions containing organic pollutants including pesticides, organic synthetic dyes, pharmaceuticals and personal care products (PPCPs), as well as a great deal of industrial pollutants.

EF uses electricity and special electrodes towards the in situ generation of the Fenton reagent, thereby avoiding (1) the cost of reagents and risks related to their transport and storage, (2) the formation of sludge, and (3) side reactions due to the maintaining of small reagent concentrations in the medium. Other advantages of the EF process are as follows:

- Like Fenton, the EF process can be carried out at room temperature and atmospheric pressure.
- Electricity as a clean energy source is used in the process, so the overall process does not create secondary pollutants.
- The hydrogen peroxide and radicals produced are “green” because the only by-products are water and oxygen.
- The oxidation process is faster than the classic electrochemical oxidation.
- EF has the advantage of allowing better control of the process [the electrical variables used, electric current (I), cell electric potential (E_{cell}), are particularly suited for facilitating data acquisition, process control, and automation].
- EF continuous processes are robust since the reaction can be terminated easily by cutting off the power and it can be also readily restarted after an operation problem.
- EF processes can cope with many organic pollutants while a complete mineralization is feasible at relatively low cost under optimum operation.

The origins, fundamentals, and the reaction mechanisms of EF process have been discussed in detail in chapter “Electro-Fenton Process: Fundamentals and Reactivity.” However, for the reader’s convenience, the different types of EF processes examined in literature are summarized here. Similar to Fenton, the EF process can be *homogeneous* or *heterogeneous* depending on where the catalytic reactions occur. In the homogeneous system, the catalytic process occurs in the bulk of the liquid phase, while in the heterogeneous system the catalysis process always occurs on the surface of the catalyst. In general, the homogeneous EF can be classified into five process schemes (Table 1), depending on Fenton reagent addition or formation. It is noted that EF processes III and IV (Table 1), which induce the in situ generation of H_2O_2 and the external addition of iron catalyst (preferably Fe^{2+}), are the original EF processes examined in literature. In contrast, the heterogeneous EF process is relatively simple; i.e., the heterogeneous catalyst is provided externally or has the form of an electrode while H_2O_2 is in situ electrogenerated on the surface of cathode by bubbling oxygen/air. In both homogeneous and heterogeneous systems, the destruction of organic pollutants can take place in the bulk by the action of Fenton reagent, as well as at anodes with high oxidation power, like boron-doped diamond (BDD) or dimensionally stable anodes (DSA[®]), with anodic oxidation (AO).

In order to overcome the shortcomings of the usage of iron catalysts in EF processes, such as the limited optimum pH range (at around pH 3) for avoiding the production of iron sludge, the difficulties in recycling the iron ions (Fe^{2+}) and the fact that the required concentration of the iron ion varies from 50 to 80 mg/L for batch processes [6], which is clearly above the 0.2 mg/L and 2 mg/L limits imposed

Table 1 Classification of EF process depending on Fenton's reagent addition or formation

EF process	H ₂ O ₂	Fe (II)	Comments
I	–	–	Electrogeneration of hydrogen peroxide and ferrous ion by means of O ₂ or air sparging or a gas-diffusion cathode, and a sacrificial anode, respectively [peroxi-coagulation (PC) process]
II	+	–	External addition of hydrogen peroxide and electrogeneration of ferrous ion by using a sacrificial anode [electrochemical peroxidation (ECP) process/anodic Fenton treatment (AFT) process. The difference between them simply arises from either using or not using a salt bridge, i.e., the use of undivided or divided cells]
III	–	+	External addition of ferrous ion and electrogeneration of hydrogen peroxide by means of O ₂ or air sparging or a gas-diffusion cathode
IV	–	+	Electrogeneration of hydrogen peroxide by means of O ₂ or air sparging or a gas-diffusion cathode, and ferrous ion is externally added and regenerated by reduction at the cathode
V	+	+	External addition of both hydrogen peroxide and ferrous ion with in situ regeneration of ferrous ion through the reduction of ferric ions on the cathode (Fered-Fenton process)

by the European Union (EU) for drinking water (98/83/EC) and direct discharge of wastewater into the environment (75/440/EEC), respectively, a great research effort has been devoted to developing alternative hetero-/homogeneous catalysts (except for Fe²⁺), including Cu²⁺/Cu⁺, Mn²⁺, Co²⁺, schorl, pyrite, and nano-zero-valent iron [8]. These established systems are called *hetero-/homogeneous electro-Fenton-like* processes.

It is understood that the “heart” of the EF process are the electrodes used, and more specifically the cathode, with the respective advances reviewed in the preceding chapters. The significant evolution of novel carbon-based cathodes along with the new reactor designs has boosted the successful development of EF technology towards its application in dilute aqueous solutions, e.g., potable water purification (groundwater, surface water), municipal wastewater treatment for safe disposal and/or reuse, as well as for the treatment of industrial effluents of heavy organic load including chemical, textile, agro-industry, tannery, food industry, and landfill leachate. This is evident by the results of a quick search in Scopus database illustrated in Fig. 1a, in which the tremendous growth of EF research observed in the last two decades is related mostly to the EF elimination of organic pollutants in different water and wastewater matrices. The vast majority of the published research work originates from China and Spain (Fig. 1b), including the extensive work by the groups of Brillas (from Spain) on carbon-PTFE O₂-diffusion cathode and boron-doped diamond (BDD) anode, of Oturan (from France) on carbon-felt electrodes, and Zhou group (from China) on the development of 3-dimensional electrochemical reactors.

Further to electrode materials research, significant effort has been made to improve the EF process by combining it with the simultaneous illumination of the solution by UVA light or sunlight or even treatment with ultrasonic waves,

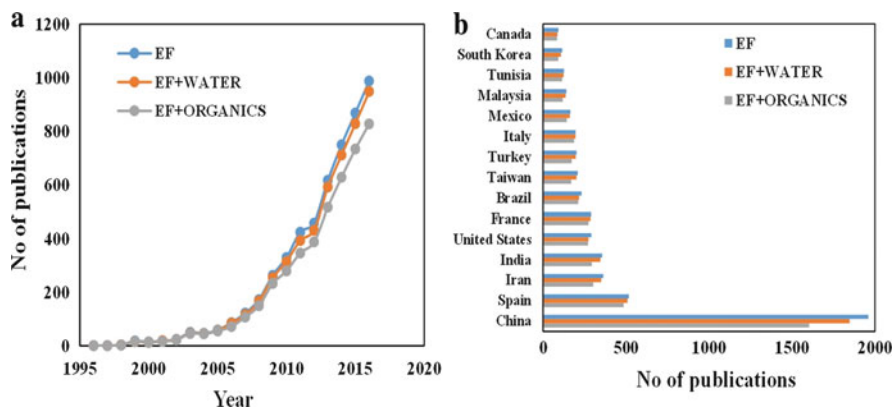


Fig. 1 Scopus results of publications for selected keywords

corresponding to the so-called UVA photoelectro-Fenton (PEF), solar PEF (SPEF), and sonoelectro-Fenton (SEF) methods, respectively [7]. Major review works have been published in the last decade, including a rather exhaustive analysis of the existing literature on the application of EF and the aforementioned EF-hybrid processes to water purification and wastewater treatment. Table 2 includes a list of recent reviews, as a source of information regarding the type of the equipment used along with the experimental conditions and important findings of previous publications and patents in the field. A common characteristic of all these reviews is the application of EF technologies for the purification of water and wastewater by removing non-biodegradable organic pollutants. The major drivers for such a research work were identified: (1) the fast disappearing of freshwater supplies that lead to the use of water from less desirable sources, (2) the increasing number of new man-made chemicals released to the aquatic environment, many of which are recalcitrant to conventional biological and chemical treatments and toxic to the human health and the aquatic environment, (3) the stringent environmental regulations for drinking water supply, wastewater discharge, and/or reuse, and (4) the reported low elimination rates of various organic pollutants by traditional water treatment processes.

Given such an extensive research, the question then arises as to why EF-based technologies have not found widespread application in the water industry? One reason may be that EF has displayed certain shortcomings which, until recently, have proved strong enough to hinder their wide usage. Specifically, the mechanical reliability and plant performance have not been evaluated extensively at a large scale and in realistic operational environments. Moreover, the oxidation capability of EF tends to be considerably diminished when treating high organic matter contents, thereby requiring high energy consumption that renders the treatment far less affordable. Pretreatment of wastewater is often required to ensure reliable performance, which could be potentially costly and technically demanding. For instance, presence of suspended and/or dissolved solids may foul/block the

Table 2 List of recent review studies on EF and EF-related processes

Reference	Scope/content
[9]	A critical review on the most promising electrochemical tools for the treatment of wastewater contaminated by organic pollutants. The review is focused on the direct electrochemical oxidation (EO), anodic oxidation (AO), indirect EO mediated by electrogenerated active chlorine, the use of cathodic processes and their promising coupling with anodic processes, and a critical assessment of the reactors that can be used to put these technologies into practice
[10]	A general overview on application of membrane filtration as well as combined membrane filtration and AOPs such as ozonation, Fenton oxidation, photocatalysis, and EAOPs for the removal of pharmaceutically active compounds (PhACs) from different water systems (including AO, EF, PEF, and hybrids)
[11]	The goal of this review is to present cutting-edge research for treatment of three common and problematic pollutants and effluents: dyes and textile wastewater, olive processing wastewater, and pharmaceuticals and hospital wastewater by EAOPs (including EF, PEF, Bio-EF, SPEF)
[12]	Applications of key EAOPs including anodic oxidation (AO), electro-Fenton (EF), photoelectro-Fenton (PEF), and sonoelectrochemistry (SE) are discussed in this review. A global perspective on the fundamentals and experimental setups is offered, and laboratory-scale and pilot-scale experiments are examined and discussed
[13]	Review of publications and patents dealing with water contaminated with different recalcitrant pollutants by photo-assisted Fenton, electro-Fenton, and photo-assisted electro-Fenton processes
[6]	Fundamentals and main applications of typical methods such as Fenton, electro-Fenton, photo-Fenton, sono-Fenton, sonophoto-Fenton, sono-electro-Fenton, and photo-electro-Fenton are discussed. This review also highlights the application of nano-zero-valent iron in treating refractory compounds
[14]	A general review over the application of the EF, PEF, and SPEF methods to the degradation of organic pollutants in waters using potent BDD anodes. Examples on the treatments of industrial chemicals, pesticides, dyes, and pharmaceuticals are examined to show the high oxidation ability of these EAOPs
[15]	Review and critical discussion of the effectiveness of EAOPs for the removal of anti-inflammatory and analgesic pharmaceuticals from aqueous systems, including anodic oxidation processes, EF process, and EF-related processes (PEF, SPEF, peroxi-coagulation – PC, photoperoxi-coagulation – PPC, SEF, electrochemical peroxidation – ECP, anodic Fenton treatment – AFT)
[16]	This review reports on the most recent experimental studies and developments in the field of electro-Fenton process. Fundamentals, experimental setups, main reactions, the parameters that affect these processes, and various applications are discussed in detail. Different cathodes and anodes used for electro-Fenton process are also analyzed
[17]	A general review of lab and pilot-plant experiments related to the most relevant applications of several electrochemical and photoassisted electrochemical methods, including electrocoagulation (EC), EO, EF, PEF
[7]	A largely cited review paper on the origins of Fenton's reaction chemistry for wastewater treatment and Fenton-based EAOPs developed until 2008. Fundamentals, experimental setups, and lab and pilot-plant experiments related to the major applications of EAOPs to synthetic and real effluents are described and thoroughly discussed

electrode surfaces, while bicarbonate ions (HCO_3^-) can appreciably reduce the concentration of $\cdot\text{OH}$ due to scavenging processes that yield H_2O and much less reactive species (e.g., $\text{CO}_3^{\cdot-}$). Moreover, there is a need to minimize the formation of toxic by-products and the loss of efficiency caused by mass transfer limitations and undesirable side reactions. The robustness (service life time), the scale-up, and the cost of the special electrodes applied are also a matter of concern. Recognition of the situations where these limitations pose potential health risks is a necessary step in the design and operation of EF systems. At the same time, existing, competing techniques, such as nanofiltration, ultra-low pressure reverse osmosis, or adsorption on composite materials, have improved in performance. This means that EF has to catch and overtake a moving target.

In view of the above considerations, the scope of this chapter is to review our current understanding and knowledge gained from the extensive research on the mineralization by EF-based processes of biorefractory organic contaminants from water and wastewater. Particular attention is paid to the parameters affecting the design and the performance of the systems, along with scale-up and optimization issues. The results of a patent search are also included. Finally, future R&D needs are discussed, both at the scientific and the technological level that would facilitate the development and penetration of EF-based systems into the water/wastewater treatment market.

2 Electro-Fenton Applications in the Water and Wastewater Sector

Considering the scope of this chapter, an effort is made in this section to summarize the applications of the EF-based processes in water and wastewater treatment. The objective of this summary is not the replication of the lab-, pilot-scale studies already reviewed by previous researchers (Table 2), but rather the description of the target wastewaters that can be effectively treated by EF and other related electrochemical technologies. Figure 2 illustrates the source of the water and wastewater investigated in literature, along with typical examples of organic pollutants contained in the respective effluents. According to Fig. 2, the efficiency and flexibility of EF technology has been proven with a wide diversity of effluents from municipal, chemical, and other related industries or activities, including pharmaceutical, pulp and paper, textile, food, cork processing, and landfilling among others. These wastewaters contain a cocktail of pollutants in a wide range of concentrations. The development of cost-effective technical solutions based on EF processes has been proven by several researchers, although the conclusions drawn are in many cases based on laboratory-scale results and with feedwater compositions that are not necessarily realistic, e.g., high organic concentrations (especially in the case of experiments with pure water solutions simulating potable

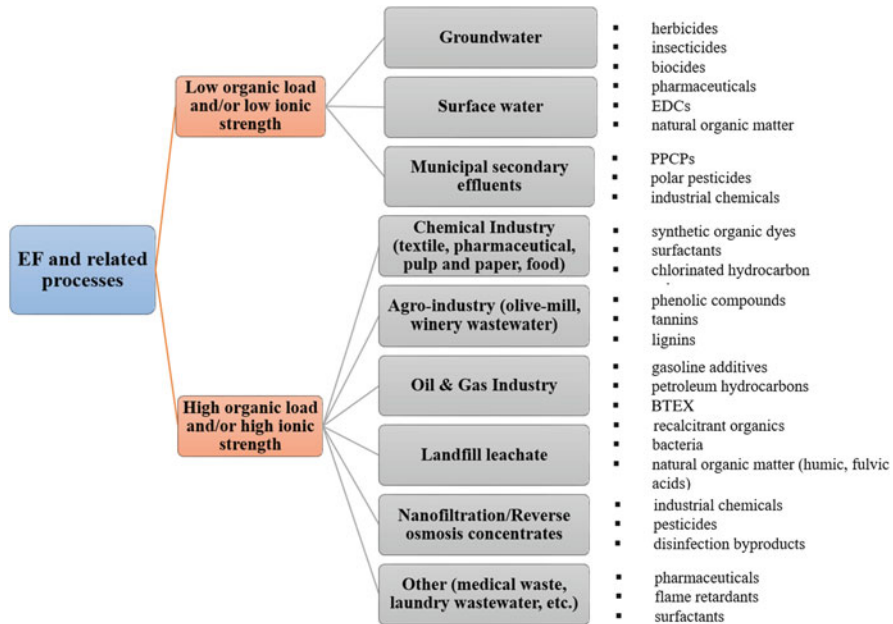


Fig. 2 Types of wastewater examined in literature for their treatment by EF-based processes

water), low pH, and high ionic strength (adjusted usually with the dilution of sodium sulfate at a concentration of 50 mM).

It is understood that there is a great variety of water types, spanning a continuous spectrum that goes from potable water, to “gray water,” to “black” water, to water of impaired quality that is not fit for any use. The concentration of the synthetic organic compounds detected in these waters can vary from few ng/L in drinking water sources (e.g., groundwater, surface water) to hundreds of mg/L in industrial effluents. Moreover, the ionic strength of the water may also vary significantly, being low in secondary municipal effluents (equal to an electrical conductivity of 1.5–3.0 mS/cm) and extremely high in saline effluents (e.g., electrical conductivity of 5–40 mS/cm in textile wastewater). These characteristics are important for the EF process, since the higher concentration of the dissolved ions results in lower cell voltages for a given current density. Unfortunately, not all waste streams have sufficient conductivity and the addition of an electrolyte is often necessary. For this reason, EF treatment is supposed to be more convenient and cost effective when the wastewater to be treated already has a moderate to high salinity.

In accordance with the applications of EF presented in Fig. 2, examples of real wastewater treatment from different sites for the elimination of non-biodegradable organic pollutants are discussed next. The elimination of inorganic species (e.g., As^{3+} , Zn^{2+}) from wastewater has also been studied, although to a lesser extent.

2.1 Purification of Potable Water Sources

The findings of a literature search on EF application for potable water treatment showed that the majority of the experimental studies have been performed with small stirred tank reactors (electrochemical cells) at laboratory scale using synthetic organic solutions of varying composition (solutions prepared usually with deionized water), without considering their viability for industrial application. Moreover, the feed concentrations of the target pollutants were many orders of magnitude higher than the actual concentrations identified in potable water sources (groundwater, surface water). It is understood that the achievement of high mass transfer rates in the EF reactors for such low concentrations is of paramount importance and it is one of the main issues that needs to be tackled before electrochemical oxidation can be applied successfully for potable water purification. In the last 5 years, however, several research groups orientate their research activities to pilot-scale experiments, taking advantage of the knowledge gained from the basic research carried out over the past 20 years.

Garcia et al. made a first step to demonstrate the efficiency of EO and EF processes with 3 L recirculation flow plants as a first step for the further scale-up of both EAOPs at industrial level [18, 19]. The undivided filter-press reactors consisted of (1) a Pt sheet anode and a carbon-PTFE air-diffusion cathode and (2) a BDD anode and cathode supported on niobium. In the first one, large amounts of $\cdot\text{OH}$ are produced by Fenton reaction owing to the high H_2O_2 generation at the air-diffusion cathode, whereas a small participation of $\text{Pt}(\cdot\text{OH})$ produced during the mineralization process is also expected. In contrast, in the latter, much lower H_2O_2 is generated at the BDD cathode, yielding smaller quantities of $\cdot\text{OH}$, but organics can also be mineralized by the more reactive $\text{BDD}(\cdot\text{OH})$ formed by the anode. In this work it has been demonstrated that the decontamination of a herbicide solution (92 mg/L 2,4-D) at pH 3.0 was more efficient in the case of a single BDD/BDD cell instead of a single Pt/air-diffusion one, obviously due to the higher ability of $\cdot\text{OH}$ at the BDD surface to mineralize organic intermediates. The most potent EF process with this cell gave 59% mineralization with 23% efficiency and 0.42 kWh/g TOC specific energy after 300 min at 0.5 A. It is noticed that the final solution of the EO process with a BDD/BDD cell contained a mixture of carboxylic acids as major component.

An undivided electrochemical reactor with a volume capacity of 1.5 L and a fixed bed of glassy carbon pellets three-dimensional cathode that was developed in the past by EDF (Électricité de France) to treat aqueous effluent containing heavy metal was used by Chmayssem et al. [20] for the application of EF at semi-pilot-plant scale. Experiments with Bisphenol A (BPA) demonstrated the high efficiency of the system to degrade the specific molecule (an absolute rate of BPA degradation was determined as $4.3 \times 10^9 \text{ M}^{-1} \text{ s}^{-1}$) at an applied current intensity 0.8 A and acidic pH. Considering that the system does not achieve a total TOC mineralization

(small organic acids present in the effluent, regardless the initial BPA concentration), a subsequent biological treatment is necessary prior to the discharge of the final effluent.

El-Ghenymy et al. [21] performed a comparative study of sulfanilamide degradation (drug frequently detected in surface water) by EF and SPEF using a 2.5 L pre-pilot plant equipped with a Pt/air-diffusion cell. The solar photoreactor was a polycarbonate box (600 mL irradiated volume), with a mirror at the bottom and an inclination of 41° to better collect the sun rays [the average UV irradiation intensity (300–400 nm) supplied by sunlight was measured 30–32 W/m²]. A mineralization up to 94% was achieved using SPEF, whereas EF yielded much poorer degradation.

Recent studies suggested that flow-through EF reactors (i.e., the feedwater flows through and not by the anode and cathode) tend to improve the degradation rate and efficiency due to the enhanced convective transfer of the pollutants to the electrode surface [22–24]. In these works, the solution was either pretreated by pumping air/oxygen to increase the concentration of the dissolved oxygen in solution [22] or electrolysis was taking place relying only on the dissolved oxygen of the feedwater (approx. 8–9 mg/L in tap water at room temperature) [24]. The novel electrochemical device developed by Plakas et al. [24] has the form of a “filter” that consists of a stack of carbon anodic and cathodic electrode pairs for operation in continuous mode. This “filter”-type design facilitates the scale-up of the device and promotes the uniform distribution of the water throughout the electrodes, thus ensuring the effective fluid contact with the in situ produced oxidants. Bench-scale tests with one pair of anode/cathode electrodes, using the pharmaceutical diclofenac as a model micropollutant [25], resulted in optimized cathodic electrodes (employing carbon felts and optimum procedures of iron nanoparticle impregnation), “filter” design, and operating conditions (cathodic potential, feed flow). These results paved the way for the design and construction of a fully automated laboratory-scale pilot system [26], which was tested under real operating conditions (continuous treatment of tap water, without the addition of electrolyte or the sparging of air/O₂), as a necessary step towards applications. Pilot studies with the pharmaceutical diclofenac, with three pairs of anode/cathode electrodes made of carbon felt (of total geometric area 175 cm² and effective surface area of approx. 4,000 m²) and with cathodes impregnated with iron nanoparticles (γ -Fe₂O₃/F₃O₄), various feedwater flow rates (10–40 L/h), and applied potentials (1.4–3.2 V), showed that the best “filter” performance was obtained at applied potential of 2 V per pair of electrodes, and low water superficial velocities (\sim 0.09 cm/s), i.e., the overall mineralization current efficiency (MCE) was $>20\%$, during continuous steady state treatment of tap water with low DCF concentrations (16 μ g/L DCF, TOC of tap water 0.56 mg/L). It is noteworthy that the EF “filter” exhibited satisfactory stability regarding both electrode integrity (no iron leaching) and removal efficiency, even after multiple filtration/oxidation treatment cycles, achieving (under steady conditions) DCF and TOC removal 85% and 36%, respectively. This performance is considered satisfactory because the EF process took place under rather unfavorable conditions, such as neutral pH, low dissolved O₂ concentration, low electrical conductivity (\sim 700 μ S/cm), and presence of natural organic matter and inorganic ions in tap water.

Progress on the aforementioned flow-through EF reactors was made in the work of Ma et al. [27]. Specifically, an energy-efficient flow-through EF reactor was designed, whereas the feed solution passed through a modified graphite felt cathode and a perforated Dimensionally Stable Anode (DSA[®]) anode sequentially, accompanying the pumped air. The flow-through EF system was compared to the flow-by and regular one, and confirmed to be best for the removal of the model organic pollutant used (methylene blue-MB) and TOC degradation. The MB and TOC removal efficiency of the effluents were kept above 90% and 50%, respectively, and the energy consumption was 23.0 kWh/kg TOC at current of 50 mA, pH 3, 0.3 mM Fe²⁺, and flow rate of 7 mL/min. It is noticed that the flow rate in flow-through cells has a great impact not only on the residence time of pollutants but also on the accumulation of H₂O₂ in the EF process. The choice of a suitable flow rate is thus, critical for the process efficiency, which in turn can be limited by the cross-sectional area of the inlet/outlet tubing.

In an effort to improve oxygen utilization efficiency, Xu et al. [28] fabricated a novel dual tubular membrane electrodes reactor which consists of a tubular membrane Ti/IrO₂-Ta₂O₅ anode and a carbon black polytetrafluoroethylene (CB-PTFE) modified graphite membrane as cathode. It was demonstrated that Ti/IrO₂-Ta₂O₅ anode provided enough oxygen to electrogenerate H₂O₂, up to 1,586 mg/m² h, at 10 A/m² without aeration in acidic solution. Experiments with the pesticide tricyclazole showed a stable removal of 79% after 20 min of treatment without recirculation.

Motivated by the pollution of drinking water sources by arsenic and organo-arsenic compounds such as monomethylarsinate (MMA) and dimethylarsinate (DMA), Lan et al. [29] developed a FeC_x/N-doped carbon fiber composite (FeC_x/NCNFs) as a catalyst for the degradation of DMA, and as an absorbent of the produced inorganic arsenic (As(V)), with degradation and adsorption occurring simultaneously, in an EF process. For an initial concentration of DMA 5 mg/L, 96% was degraded after reaction time of 360 min, with TOC efficiently removed at the same time. The residual As(V) concentration in solution was below the allowable limit of 0.01 mg/L under the optimum treatment conditions.

2.2 Treatment of Secondary Municipal Effluents

A large part of synthetic organic compounds (SOCs) identified into the aquatic environment are in their original form or metabolite due to the low removal efficiency of standard wastewater treatment plants (WWTPs) on such compounds. This fact combined with the special effects of specific organics (e.g., pharmaceuticals, pesticides, nonylphenols) on target even unintended organisms at low doses makes it urgent to develop more efficient technologies for their elimination. EF and related electrochemical technologies have been investigated as an advanced oxidation process to address a variety of objectives including the preliminary reduction of high percentages of organic load in terms of COD or TOC and removal of

recalcitrant and toxic pollutants, thus allowing for further conventional biological treatment (pretreatment) or for the final polishing of the secondary effluent (posttreatment) [11].

Xu et al. [30] investigated the feasibility of removing trace estrogens that are frequently detected in municipal wastewaters [17 β -estradiol (E2) and 17 α -ethynyl-estradiol (EE2)] by a bio-electro-Fenton (BEF) system equipped with a Fe@Fe₂O₃/non-catalyzed carbon felt composite cathode. The system consisted of two similar chambers of 75 mL separated by proton exchange membrane while the anodic chamber was filled with granular graphite to enhance the anodic power density. Under closed-circuit condition, 81% of E2 and 56% of EE2 were removed within 10 h in the system, in which the highest concentration of total iron ions and H₂O₂ reached 81 and 1.2 mg/L, respectively. The reported maximum power density of BEF system was 4.35 W/m³.

Kishimoto et al. [31] examined two combined processes, namely an activated sludge process followed by the EF with an oxidation–reduction potential (ORP) control (AS-EF process) and the EF process with an ORP control followed by an activated sludge process (EF-AS process), by using 1,4-dioxane contaminated municipal wastewater. The reactor comprised of a glass beaker with 300 mL of wastewater content, two electrochemical flow cells, two direct current power supplies, an ORP controller, an interflow cell, and a peristaltic pump (to feed the wastewater to the two electrochemical flow cells at a flow rate of 6.17 mL/s for each cell). The function of one flow cell was the onsite generation of HOCl, while that of the other was the onsite generation of Fe²⁺. The former cell had a plate DSE[®] anode and a plate cathode made of stainless steel, with an effective surface area of 42 cm² for both electrodes. The latter had a plate anode made of titanium, coated with ruthenium oxide and a plate cathode made of stainless steel, with an effective surface area of 63 cm² for both electrodes. AS-EF process was found to be superior to the EF-AS process in respect of both energy consumption and the performance of COD removal, as well as removal of 1,4-dioxane. Specifically, in the AS-EF process, the activated sludge process mainly contributed to the COD and BOD removal, whereas the EF process was responsible for 1,4-dioxane removal.

Recently, significant research effort was focused on the application of EF for wastewater disinfection. It was found that microorganisms can be inactivated electrochemically directly on a BDD anode or via the generation of [•]OH [32]. The combined elimination of refractory pollutants with microbial disinfection of wastewater in a single treatment step constitutes an attractive compact alternative, especially in the field of water reclamation and reuse where effective elimination of pathogens is crucial to protect public health. Many experimental studies have been carried out in this field, but the majority have been performed at laboratory scale and only lately have investigations begun at pilot scale by electrooxidation and peroxi-coagulation [33].

2.3 Chemical Industry Wastewater

The chemical industry is a major contributor to problem of industrial wastewaters, not only in terms of discharge volumes, but also regarding the hazardous nature of many of the pollutants found in the effluents. The increasingly stringent regulations have prompted the application of advanced technologies for complying with discharge regulations and allowing for water recycling. Considerable study of the application of EF process in industrial wastewater treatment has been undertaken to date. The process efficiency has been experimentally confirmed by different authors for the treatment of media containing pharmaceuticals, dyes, pesticides, surfactants, and other recalcitrant organics.

2.3.1 Pharmaceutical Industry

Treatment of pharmaceutical wastewaters has always been problematic owing to the wide variety of chemicals used in drug manufacturing, which leads to wastewaters of variable composition and fluctuations in pollutant concentrations. The substances synthesized by the pharmaceutical industry are in most cases structurally complex organic chemicals that are resistant to biological degradation. EF oxidation has proved to be a suitable pretreatment for pharmaceutical wastewaters, leading to an improvement of the wastewater biodegradability and a reduction of the toxicity of these effluents. Considering recent researches, the most frequently removed non-steroidal anti-inflammatory drugs (NSAIDs) by EF-based processes are ibuprofen, paracetamol, and diclofenac.

A hybrid process coupling EF and a biological degradation-step was investigated by Mansour et al. [34] in order to mineralize synthetic and industrial pharmaceutical effluents containing trimethoprim (TMP), a bacteriostatic antibiotic. The effluent contained a high TMP concentration (3.56 g/L; diluted to 58 mg/L for the scope of the experiments), it was characterized by a conductivity of 4.36 mS/cm, COD of 438.50 g/L, and TOC of 125.40 g/L. EF using an undivided two electrode Pt/carbon felt cylindrical glass cell of 1 L exhibited at optimum operational conditions (0.69 mM Fe^{2+} , pH 3, 466 mA, and 2 L/min recirculation flow rate) an almost total removal of TMP after 180 min of electrolysis. Although TOC removal was low, the biodegradability of the treated industrial effluent was improved. Overall removal yields were 80 and 89% for 180 and 300 min of EF pretreatment followed by 15 days activated sludge culture, respectively.

2.3.2 Pulp and Paper Industry

More than 250 chemicals may be present in the effluents resulting from the different stages of papermaking. Some of these pollutants are naturally occurring wood extractives (tannins, resin acids, lignin, etc.) while others are xenobiotic compounds

formed mostly in pulp manufacture (polyphenols, chlorinated organic compounds, aromatic compounds, dioxins and furans, cyanide, etc.) [35]. The latter are resistant to biological treatment, and therefore, strong oxidation processes in the form of integrated schemes with other physical and biological methods are usually considered for achieving the discharge standards. In a recent study by Jaafarzadeh et al. [36] the integration of permanganate (PM) (oxidation/precipitation), EF, and $\text{Co}_3\text{O}_4/\text{UV}/\text{peroxymonosulfate}$ (sulfate radical, $\text{SO}_4^{\bullet-}$) was investigated for COD removal from a real wastewater collected from a pulp and paper industry. The authors measured a COD reduction from 1,450 to 62 mg/L (~95%) as well as an enhanced biodegradability of the final effluent by employing the integrated process. The EF process was carried out by means of an electrochemical cell consisting of two iron sheets as anode and cathode (effective surface area 60 cm^2) which was immersed in the acidic effluent of the PM process (pH 2.7). After 60 min of electrolysis at 0.5 mA/cm^2 current density, and addition of 12 mM H_2O_2 , a COD removal of 57.8% was observed. The sludge produced during the PM and EF process included a considerable amount of organic pollutants which means that coagulation mechanism contributed to the overall performance. In such a process, the obtained sludge should be considered for remediation and recovery of manganese and iron.

2.3.3 Textile Industry

Textile industry is particularly known for its high water consumption as well as the amount and variety of chemicals used throughout the different operations. The environmental issues in the textile industry are associated with the bio-refractory nature of the wastewaters produced from the dyeing and finishing stages, including various dyestuffs and chemical additives (such as polyvinyl alcohol and surfactants). Estimates indicate that approximately, 7×10^5 tons of dyestuffs are produced annually and 280,000 tons of the textile dyes are discharged into water sinks through textile effluents [37]. That explains why textile effluent is characterized by high COD (150–10,000 mg/L), BOD (100–4,000 mg/L), pH (6–10), and color content (50–2,500) [38]. Fenton-based EAOPs have been largely investigated for the efficient mineralization of dyestuff [11, 14, 16, 38]. Among the different techniques examined, SPEF proved to be the most promising one achieving almost total mineralization and higher degradation compared to UVA-illuminated PEF due to the higher UV intensity of sunlight, which can quickly photolyze Fe(III)–carboxylate complexes that could not be destroyed by $\cdot\text{OH}$ in traditional EF processes.

Pilot-scale experiments by Garcia-Segura and Brillas [39] with an autonomous SPEF flow plant with a Pt/air-diffusion cell coupled to a compound parabolic collector (CPC) photoreactor showed the viability of the process for the combustion of acidic solutions of textile monoazo, diazo, and triazo dyes. Comparative trials were made by electrolyzing 10 L of 50 mg/L of dissolved organic carbon of each azo dye in 50 mM Na_2SO_4 with 0.50 mM Fe^{2+} of pH 3.0. The monoazo Acid

Orange 7 solution underwent the faster decolorization, azo dye decay, and DOC removal, attaining an almost total mineralization with 97% DOC abatement in about 180 min. The diazo Acid Red 151 solution was degraded more slowly than the triazo Disperse Blue 71 one, but in both cases the final solution still contained 8–10% of residual DOC due to the formation of very recalcitrant products. Ren et al. [40] developed recently a novel vertical-flow EF reactor of total effective volume of 2 L, comprised of 10 cell compartments using PbO_2 anode (10×12 cm), and modified graphite felt mesh cathode (10×12 cm); the latter was found to be more complete and efficient in organic pollutants degradation when comparing with the traditional parallel-flow reactor, using a model azo dye (tartrazine). The optimal operating conditions for this reactor were pH 3, voltage 4.0 V, flow rate 40 mL/min, Fe^{2+} of 0.4 mM, aeration rate 80 mL/min. Within 120 min of treatment tartrazine degradation efficiency could reach near 100% and the TOC removal efficiency was higher than 60%. According to the authors, the novel vertical-flow EF is versatile, since the cell numbers can be easily controlled to adapt to different concentration of pollutants to achieve an ideal treatment performance in practical applications.

The degradation of different dyes by EF oxidation was carried out also successfully in a continuous two electrode stainless steel/graphite bubble reactor by Rosales et al. [41]. The EF bubble reactor had a working volume of 0.675 L, and was operated in batch mode with total reflux or continuous mode. Steel or graphite bars were employed as electrodes. Each bar was 100 mm long with a diameter of 6.35 mm for graphite and 10 mm for stainless steel, resulting in a total contact surface area of 1.27 cm^2 for graphite and 3.14 cm^2 for stainless steel. A constant potential difference (15 V) was applied and a continuous saturation of air at atmospheric pressure was ensured by bubbling compressed air near the cathode at about 1 L/min. Under continuous treatment and an operating residence time of 21 h the reactor achieved a high decoloration efficiency (dyes tested Methyl Orange, Reactive Black 5 and Fuchsin Acid) close to 43% which is squared with a TOC reduction around 46%. El-Desoky et al. [42] employed an optimized EF system successfully, using a reticulated vitreous carbon cathode (60 PPI, dimensions 5×7 cm and thickness of 0.9 cm) and a platinum gauze anode (of an area 3.8 cm^2 placed at the center of the electrochemical cell), for complete degradation and significant mineralization (approx. 85–90%) of Levafix blue and red reactive azo dyes in real industrial wastewater samples of a textile dyeing house. Experiments were carried out in a three-electrode undivided glass electrochemical cell (reactor) containing 250 mL of the supporting electrolyte of pH 3.0, 50 mg (200 mg/L) of the investigated azo dye, and a catalyst quantity (0.5 mM) of Fe^{2+} or Fe^{3+} ions. The optimized cathode applied potential was -1.0 V vs. SCE. Wang et al. [43] studied the efficiency of COD removal from real dyeing wastewater (COD: 1,224 mg/L, TOC: 394.6 mg/L) by using Fe^{2+} in combination with electrogenerated hydrogen peroxide at a polyacrylonitrile-based activated carbon fiber cloth cathode. In this study a platinum wire (with a diameter of 0.05 cm) was used as anode while the cathode was designed as a hollow cylindrical structure with a diameter of 2.9 cm and height of 7 cm. Oxygen gas from an oxygen cylinder was dispensed directly at the bottom of the hollow cylindrical cathode at a rate ranging from 50 to 250 mL/min. The highest

COD removal efficiency (75.2%) was achieved at an applied current density 3.2 mA/cm², oxygen sparging rate 150 mL/min, pH 3, and the addition of 2 mM Fe²⁺.

Recently, bio-electro-Fenton (Bio-EF) has been successfully applied to degrade organic pollutants (i.e., *p*-nitrophenol and azo dyes) in a microbial fuel cell catholyte at neutral pH [44]. In such a system, electrons are released from the bio-reactions at the anode and transported to the cathode via an external load circuit. H₂O₂ is continuously generated by the two-electron reduction of oxygen on a carbon felt in the cathode chamber. Simultaneously, the Fe²⁺ ions can be generated in situ at neutral pH by direct electro-reduction of iron oxide in the cathode chamber. The feasibility of using such a system, consisting of a carbon felt/ γ -FeOOH composite cathode, to oxidize As(III) in aqueous solutions at neutral pH was also investigated by Wang et al. [45]. The results indicated that the process was capable of inducing As(III) oxidation with an apparent As(III) depletion first-order rate constant of 0.208 h⁻¹ and an apparent oxidation current efficiency as high as 73.1%. According to the authors, the γ -FeOOH dosage in the cathode was determined to be an important factor in the system performance while there is place for the operational parameters, such as the composition of the cathode or anode chamber and retention time, to be optimized.

2.4 Treatment of Agro-Industrial Wastewater

The EF technology, alone or in form of an integrated process, has also proved to be effective for the treatment of wastewaters generated by the food industry. This includes wastewaters from olive oil extraction plants, commonly named olive mill wastewaters (OMW) [46, 47] and winery wastewaters [48]. The composition of these wastewaters is heterogeneous including various contaminants, such as nitrogen or phenolic compounds, ethanol, sugars, organic acids, aldehydes in addition to some recalcitrant compounds. Moreover, the chelating character of some compounds present in these effluents leads to the presence of some toxic heavy metals in solution. In a recent work of Flores et al. [47] 100 mL of OMW solution (TOC 598 ± 42 mg/L, COD 2,368 ± 1 mg/L) was treated by AO (3 cm² BDD anode and a 3 cm² air-diffusion cathode at 16.7 mA/cm²), EF (with 0.5 mM Fe²⁺), and PEF (with 0.5 mM Fe²⁺ and 6 W UVA radiation). The oxidation capability of the processes increased in the order AO-H₂O₂ < EF < PEF with PEF exhibiting a maximum efficiency of up to 80% mineralization. A new two sequential column reactor design based on PEF technology combined with light emitting diode (LED) radiation has been also demonstrated by Díez et al. [48] as a viable alternative for the treatment of winery wastewaters (named LED-EF2CR). The sequential treatment was carried out in two-column reactors (glass columns of 40 mL capacity each) connected in series. The first column was equipped with two electrodes of different size: anode (18 cm²: 12 × 1.5 cm) and cathode (24 cm²: 12 × 2 cm) with an electrode gap of 1 cm. Graphite sheet was used as anode and various materials were used as cathode (graphite sheet, niquel foam, handmade activated carbon

polytetrafluoroethylene). Air was pumped on the cathode surface (0.5 L/min), permitting the generation of H_2O_2 and the homogenization of the fluid into the column. The LED irradiation was carried out in the second glass column by placing the LED lamp of 40 W (λ max 365 nm) 1 cm from the column wall. A slight agitation was provided in this column by bubbling air at a flow rate of 0.1 L/min. The experiments were carried out at different voltage drops (1, 3, and 5 V). The degradation of simulated and real winery wastewater was efficiently accomplished in this work; i.e., TOC removal between 50 and 70% was achieved, depending on the sample initial TOC (simulated: 4,427 and 33,200 mg/L, real: 60,100 mg/L). Furthermore, the new designed reactor was proved to be cost effective, since the energy consumption was found to be 1 kWh/g TOC removed.

2.5 Remediation of Landfill Leachate

Landfill leachate is a polluting liquid which can have harmful effects on the groundwater and surface water surrounding a landfill site, unless returned to the environment in a carefully controlled manner. The volumetric flow and chemical composition of the leachate may vary significantly while the most significant factor affecting leachate nature is the age of the landfill. Generally, “young” leachate with less than 5 years of landfilling is recalcitrant but readily biodegradable, while “old” leachate with more than five or 10 years of landfilling is non-biodegradable [49]. To treat these aged or refractory landfill leachates, different methods have been used such as flocculation–precipitation, adsorption on activated carbon, evaporation, chemical oxidation, and incineration. Among them, growing interest has been focused on EAOPs, which can achieve a substantial reduction of COD and improve the biodegradability.

Studies on the capacity of EF process to treat mature landfill leachate date back to 2000 [50–54]. The majority of the EF processes investigated involve the external addition of hydrogen peroxide rather than its continuous electrogeneration. This is due to the fact that a long treatment time is required for high strength wastewater such as mature leachate (the COD value is as high as several thousand mg/L) when H_2O_2 is electrogenerated in situ. Mohajeri et al. [53] used Fered-Fenton process where both H_2O_2 and ferrous ion were applied into the electrolytic cell. Experiments were carried out at laboratory scale using 500 mL beakers with a pair of anodic and cathodic aluminum electrodes, each 3×5 cm (active electrode area dipped in leachate). Optimized conditions under specified constraints were obtained at pH 3, $\text{H}_2\text{O}_2/\text{Fe}^{2+}$ molar ratio 1, current density 49 mA/cm², and reaction time 43 min. At these conditions 94% of COD (of initial average COD 2,950 mg/L) was removed from the leachate. The Fered-Fenton method has also been examined by Zhang et al. [51, 55] in rectangular plexiglass electrolytic reactors (containing 200 mL of leachate) with one pair of 5×11.9 cm anodic (Ti/RuO₂–IrO₂) and cathodic (Ti mesh) electrodes. For an initial COD of 5,000 mg/L, removal of 87.2% and 68.8% was achieved when batch and batch recirculation modes were employed,

respectively, under optimum $\text{H}_2\text{O}_2/\text{Fe}^{2+}$ molar ratio and current. Considering that landfill leachate is produced continuously, Zhang et al. [49] investigated the treatment of a mature landfill leachate by Fered-Fenton in a continuous stirred tank reactor (CSTR) using $\text{Ti}/\text{RuO}_2\text{--IrO}_2\text{--SnO}_2\text{--TiO}_2$ mesh anodes and Ti mesh cathodes. Out of the 73 organics detected in the leachate, 52 were completely removed by the Fered-Fenton process.

Beyond the removal of recalcitrant organics from landfill leachate, the EF process could potentially be applied for the removal of bacteria and other pathogenic microorganisms. The superiority of EF process over the simple Fenton, to remove coliform bacteria from two different leachates, was exhibited by Aziz et al. [56]. The optimum amounts of ferrous sulfate heptahydrate and hydrogen peroxide for both Fenton and EF treatments were determined in this study; 1,700 mg/L H_2O_2 and 2,800 mg/L Fe^{2+} with $\text{H}_2\text{O}_2/\text{Fe}^{2+}$ molar ratio 1:3. Disinfection efficiency was higher in the case of EF due to the synergistic anodic deactivation of the coliform bacteria and the destruction induced by the H_2O_2 and the electro-peroxidation. However, further treatment is necessary after the EF process in order for the final effluent to satisfy the maximum permissible limits of organic (COD) and iron content for direct discharge.

2.6 Other Applications

EF and EF-related technologies have been examined in literature for the decontamination of special wastewaters such as thin film transistor-liquid crystal display (TFT-LCD) wastewater [57], petrochemical wastewater [58], coal gasification wastewater [59], reverse osmosis concentrates [60], wastewater from liquid organic fertilizer plant [61], leather tanning industry wastewater [62], slaughterhouse effluent [63], tissue paper wastewater [64], spent caustic from ethylene plant [65].

Except from liquid effluents, the performance of EF was also assessed as an *ex situ* technique for the treatment of soils contaminated by petroleum hydrocarbons [66]. Authors implemented for the first time an innovative combination of soil column washing with Tween[®] 80 and EF treatment on a genuinely diesel-contaminated soil. Results showed that the EF treatment of the extracted eluates using an undivided two electrode BDD/carbon felt electrochemical reactor at 1,000 mA resulted to a quasi-complete mineralization (>99.5%) of the hydrocarbons within 32 h. However, the complete mineralization of the hydrocarbons in solution was not related to the toxicity of the solution, which increased throughout the degradation. The biodegradability (BOD_5/COD ratio) reached a maximum of 20% after 20 h of EF treatment, which is not enough to implement a combined treatment with a biological treatment process. Further improvement of the overall process is feasible and could pave the way for a new application of EF technique.

A novel system integrating three-dimensional catalytic electro-Fenton (3DCEF, catalyst of sewage sludge-based activated carbon loaded with Fe_3O_4) with membrane bioreactor (3DCEF-MBR) was recently developed by Jia et al. [59] as a

promising technology for advanced treatment in engineering applications. Laboratorial-scale results with biologically pretreated coal gasification wastewater indicated that 3DCEF–MBR can achieve significant enhancement on the COD and TOC removal, giving the efficiencies of 80% and 75%, respectively with 6 mA/cm² current density and 2 g/L catalyst dosage. 3DCEF significantly increased the enzymatic activities and promoted the membrane fouling mitigation thus, allowing the hybrid system to be operated for a long term.

3 Patent Survey

In this section a non-exhaustive list of patents in the field of electro-Fenton is presented. Table 3 lists 18 inventions published the last decade, related to processes and apparatus/devices that implement EF reactions. The list does not include equipment, devices, or methods where EF or other Fenton oxidation processes are only coupled to other installation arrangements (e.g., vortex diodes, high centrifugal forces, etc.). As with most water/wastewater treatment technologies, patents related to EF process have evolved from a direction to broader, more general concepts (for example, WO2016056994 which is directed to decomposing organic chemical compounds in a multitude of wastewater matrices) to another direction to more specific applications (for example, CN101844822 A which is directed to the treatment of heavy organic load wastewater or CN1629083 A patent which provides an electro-Fenton method and apparatus for removing multi-algae toxins from water). From Table 3 it is obvious that Chinese inventors have been very active in seeking patent protection in this field. However, based on the number of recently issued patents, it appears that patent activity in this field is increasing, and that this activity is worldwide. Given this increased activity, entities conducting research and development in this field should be mindful of the potential patent-related pitfalls which may await them in the future.

It is worth mentioning in this section the patent on “Electrolytic purification of contaminated waters by using oxygen diffusion cathodes” by J. Casado, E. Brillas, R.M. Bastida, M. Vandermeiren (US6224744) (Applicant: Sociedad Española De Carburos Metálicos, S.A.) issued in 2001, which was previously published as EP694501 in January 1996. The specific invention has also been protected in several national patent organizations [EP0694501 (B1); PT694501 (E); ES2144915 (A1); ES2144915 (B1); WO9522509 (A1); ES2080686 (A1); ES2080686 (B1); CA2160578 (A1); CA2160578 (C); AU1707695 (A); AT210604 (T)].

Patents that describe the preparation of cathode electrodes for use in EF were not included in Table 3. Examples of patents in this direction are as follows:

CN 105110423 A issued in December 2, 2015 discloses a method for preparing carbon-aerogel-carried bimetal organic framework as electro-Fenton cathode.

US 20150376817 issued in August 4, 2015 discloses a method for preparing an oxygen and nitrogen co-doped polyacrylonitrile-based carbon fiber for EF

Table 3 List of patents in the field of electro-Fenton set in inverse chronological order

Patent no	Published date	Description
WO2016097601 (A1) FR3030480 (A1)	23.06.2016	The invention relates to a process for treating a liquid effluent comprising an organic pollutant, with a pH in the range extending from 2 to 4, containing aqueous H ₂ O ₂ solution, at least one anode being capable of generating Fe ²⁺ ions by galvanic corrosion and one cathode being made of a material more noble than the constituent material of the anode, connected to one another by an electrical circuit. The electrical energy generated in the device is recovered
WO2016056994 (A1) SG10201406499S (A)	14.04.2016	An apparatus for conducting an electro-Fenton reaction for decomposing organic, preferably aromatic, chemical compounds in polluted wastewater, comprising at least one electrochemical cell having a cathode, and an anode, wherein at least the area of the cathode which comes into contact with the polluted wastewater when in use, is covered by at least one graphene layer having a nanoporous structure
CN105329991 A	17.02.2016	The invention provides a novel penetrating type electro-Fenton reactor and a method for treating organic wastewater. The novel electro-Fenton reactor comprises a reactor shell, the reactor shell is internally provided with multiple porous cathodes and porous anodes which are arranged sequentially and alternately, the reaction shell is divided into several small reaction compartments, and an aerating device is arranged at the lower end of each small reaction compartment to supply air to an electro-Fenton reaction
CN105036260 A	11.11.2015	According to the method, a metal oxide electrode is used as a positive pole, a high-efficiency hydrogen peroxide-producing electrode is used as a negative pole, and the distance between the two poles is 1–10 mm; after pH value regulation, ferrous sulfate is added into the organic wastewater, the obtained mixture is pumped into the negative pole of a reactor, and air is introduced into the negative pole at the same time; and then a reaction is carried out with current controlled, and the organic wastewater flows out from the positive pole, thereby realizing purifying of the organic wastewater

(continued)

Table 3 (continued)

Patent no	Published date	Description
WO2015110967 (A1) FR3016625 (A1) US2017008779 (A1) EP3097055 (A1)	30.07.2015	A device for injecting, into the liquid containing an oxygenated constituent, microbubbles; the oxygenated constituent being capable of reacting with the ferrous cations Fe^{2+} so as to generate hydroxyl radicals and hydrogen peroxide. The device includes a cavitation generator capable of generating bubbles, a bubble implosion chamber and a generator of ferrous cations Fe^{2+}
CN104773888 A	15.07.2015	The invention relates to an iron-carbon inner electrolysis-Fenton oxidation-electrolytic, electrocatalytic oxidation combined wastewater treatment method and device. Wastewater is subjected to iron-carbon inner electrolysis in an iron-carbon inner electrolysis filling material tower, and is subjected to Fenton-method treatment, such that residual Fe^{2+} in the solution obtained after iron-carbon inner electrolysis is subjected to a sufficient oxidation reaction; an electrolytic electrocatalytic oxidation reaction is carried out, such that heterocyclic organics in the wastewater are thoroughly decomposed
CN203938548 U	12.11.2014	The equipment is characterized in that a pulse power supply controller is arranged outside a box body, an electrode set electrically connected with the pulse power supply controller is arranged in the sewage region, and a dissolved gas releaser is arranged below the electrode set. The equipment integrating air flotation, electric flocculation, and Electro-Fenton can effectively treat grease and soluble organic pollutants in the sewage. Meanwhile, the equipment solves the problem that the existing polar plate of an electrode set for electric flocculation and electro-Fenton is easy to passivate and hard to operate continuously and stably
CN104030414 A CN104030414 B	19.09.2014	The device comprises an electrolytic cell, electrode slots, a multi-metal composite anode, a three-dimensional porous cathode plate, granular activated carbon, a baffle, a gas distribution plate, a gas inlet pipe, wires, a stabilized power supply, a stirring shaft, stirring blades, and a stirring motor

(continued)

Table 3 (continued)

Patent no	Published date	Description
CN103951018 A CN103951018B	30.07.2014	The multi-dimensional electro-Fenton device comprises a reactor shell, a water inlet pipe, and a water outlet pipe, wherein the reactor shell is internally provided with a plurality of reaction chambers which are communicated in sequence; the electro-Fenton device also comprises electro-Fenton units arranged in all the reaction chambers, wherein each electro-Fenton unit comprises a power source, an anode, a cathode, and packing arranged between the anode and the cathode
CN103496764 A	08.01.2014	A high oxygen evolution over-potential electrode is used as a positive pole, an air-diffusion electrode which efficiently produces hydrogen peroxide is used as a negative pole, and a polytetrafluoroethylene modified ferric-carbon is used as a heterogeneous catalyst, so as to construct an efficient heterogeneous Electro-Fenton system. The method is integrated with a plurality of functions such as ferric-carbon micro-electrolysis, adsorbing, electro-oxidization, and Electro-Fenton. The method is specially characterized in that the treatment effect on the nearly neutral organic wastewater is preferable, and in addition, the service life of the catalyst is long, and the leaching rate of ferrite is low
CN102765783 A	07.11.2012	Under the action of microwave, a boron-doped diamond film electrode is used as an anode material for electrochemical degradation processing. According to the invention, the boron-doped diamond film electrode is utilized to continuously generate hydroxyl radical with strong oxidation capacity in a wastewater system containing divalent iron ions, and in situ activation of the boron-doped diamond film electrode is carried out by means of thermal effect and non-thermal effect of microwave so as to increase activity of the electrode and promote mass transfer process during the degradation process of organic pollutants
US20120234694 US20120211367	20.09.2012	The filtration apparatuses and methods of the invention can separate at least one contaminant from an aqueous fluid and/or oxidize at least one contaminant. In

(continued)

Table 3 (continued)

Patent no	Published date	Description
		operation, an aqueous fluid is flowed through a filtration apparatus comprising a porous carbon nanotube filter material at an applied voltage. Further, hybrid electrooxidation technologies such as microwave-assisted BDD electrooxidation, photoelectrocatalysis, and electro-Fenton processes can be integrated into the filtration apparatus of the invention
CN102139938 A	04.07.2012	The invention relates to electro-Fenton reaction wastewater treatment equipment which is internally provided with a first anode plate, a cathode plate, and a second anode plate which are horizontally opposite, wherein both sides of the cathode plate are provided with extending cathodes; the first anode is a dimensionally stable anode with a titanium-based surface coated with a stannum–antimony–iridium–tantalum composite oxide catalyst, and the second anode is a steel plate
CN201932937 U	18.08.2011	The main device is provided with a first anode plate, a cathode plate, and a second anode plate which are horizontally parallel to and faced with each other, extending cathodes are arranged on two sides of the cathode plate, and a water outlet pipe connected with the depth reactor is arranged on the upper portion of the main device. A water inlet pump, a refluxing pump, and an air blower provide water and air from the bottom of the device. The first anode is a dimensionally stable anode with a stannum, antimony, iridium, and tantalum composite oxide catalyst plated on a titanium surface, and the second anode plate is a steel plate
CN101844822 A	29.09.2010	The invention discloses a three-dimensional electrode/electro-Fenton reactor, comprised by a main reaction tank and an organic wastewater which is hard to be degraded. The main reaction tank is provided with a net-like annular anode and a hollow columnar cathode, and adopts round design to cause material in the reactor to be evenly mixed without the blind angle

(continued)

Table 3 (continued)

Patent no	Published date	Description
CN101798130 A	11.08.2010	The invention discloses a wastewater treatment method based on electro-Fenton reaction, comprising the following steps of: applying a power supply to an electrode containing iron in wastewater so that the iron of the electrode loses electrons to form ferrous ions, reducing dissolved oxygen in the wastewater on the surface of a stainless steel cathode to generate hydrogen peroxide, and then reacting the hydrogen peroxide with the ferrous ions in the water to generate hydroxyl radicals for oxidizing and degrading organic matters in the wastewater
CN101538078 A	23.09.2009	A micro-multiphase electro-Fenton oxidation–reduction reactor consists of a shell, an electrolytic anode, an electrolytic cathode, an insulation layer, a cathode filling particle, an anode filling particle, an induction electrode, a water and gas distribution device, and a high-frequency pulse power supply. The reactor is characterized in that the reactor is different from a two-dimensional electrolytic electrode; and the induction electrode is added in the reactor simultaneously
CN1629083 A	22.06.2005	The invention provides an electro-Fenton method and apparatus for removing multi-algae toxins from water, wherein the method comprises, using the shape stabilized electrode as the anode for the reactor, using activated carbon fiber as the cathode, letting in quantitative oxygen to the cathode surface, charging small amount of ferrous salt into the algae-containing toxin solution with pH = 3 as catalyst, galvanizing electrolyzation to remove the algae toxin

applications [also published as EP2960361; JP2016510367 (A); CN104838051 (A); CN104838051 (B); WO2014127501 (A1)].

CN 104805682 A issued in July 29, 2015 discloses a method for preparing a material that is composed of carbon fibers and carbon hollow nanospheres that are loaded in-site on the surface of the carbon fibers.

CN 102887567 B issued in January 15, 2014 discloses a method for modifying graphite felt material applied to electro-Fenton system (also published as CN102887567A).

4 Design and Operation Aspects Towards EF Optimization

One of the key obstacles that have to be overcome before the full-scale implementation of EF-based processes is the development of sustainable process schemes that couple the attributes of more than one efficient technology(ies). When it comes to assess the sustainability of such an integrated EF process, the water industry (engineers, technologists, and managers of water/wastewater treatment plants) considers most often the total capital investment, the total product cost, the energy consumption, and to a lesser extent the discharge of pollutants. This stands from the viewpoint that sustainability resembles the viability of the plant in terms of an energetic efficient, economic, and reliable water production. However, it has long been recognized by experts in the field that the main challenges to more effective and sustainable long-time operation of an EF plant (of medium or large size) are largely technical, since environmental compliance and social acceptance are closely interconnected with the optimum design and construction of technologically advanced EF facilities (including pre- and post-treatment installations) of zero- or low-waste footprint, of minimum energy consumption, and of high economic feasibility. To this end, an effort will be made next to critically assess the key issues in respect of design and operation, that can be improved or optimized, towards the enhanced sustainability of the EF-based technologies in water/wastewater treatment applications.

4.1 Design of EF Reactors

The design of EF-type reactors and the respective engineering rules followed by the EF research community have been already discussed in chapter “Reactor Design for Advanced Oxidation Processes.” However, it is essential in this section to debate the critical issues that affect the process design and the respective optimization, according to the conclusions drawn by the various research groups working on the development of EF in the water industry.

It is generally believed that it is a challenge to design efficient and cost-effective EF systems without compromising the integrity of the system. The design optimization should start with identifying parameters affecting process efficiency. This is often the purpose of a research effort aiming to establish models able to represent oxidation capability in various EF cells/reactors. Such effort should focus on addressing how to represent the influence of a number of parameters on process

efficiency (both in terms of performance and cost). As shown in Fig. 3, these parameters can be divided into four groups:

- Parameters related to the feedwater
- Parameters related to the operating conditions
- Parameters related to the EF reactor configuration and electrodes
- Parameters related to the product water.

Once the design variables are identified (in relation to the above parameters) the designer should take into consideration (a) the cost function to be minimized (e.g., cost of electric energy per order of contaminant removal or unit volume treated), and (b) the constraints that must be satisfied. The constraints are normally the parameters representing the feedwater quality, influent quality, treatment efficiency, operating limits, and EF treatment characteristics. Next, data should be collected through targeted lab- and pilot-scale experiments to describe the EF system. These will help to obtain an initial design estimate that is subsequently analyzed to check the constraints. If the design satisfies the criteria originally set, then the design process stops. If not, the design should be modified using an optimization method. It is understood that design is an iterative process; iterative implies analyzing several trial designs one after another until an acceptable design is obtained. This is particularly true in EF design, since many bench-scale reactors in literature have been modified repeatedly (in terms of cell configuration, flow mode, electrode characteristics/geometry, etc.) before stepping to larger-scale setups. When an EF system is well defined, and the engineering parameters are known, an optimum design can be achieved in terms of performance, cost efficiency, and ease of maintenance and operation.

4.1.1 Towards Scale-Up

As an EF system increases in size, system properties that depend on quantity of matter might change. The chemical and physical properties of the EF system affect each other and create varying results. A good example of such a property is the surface area to liquid ratio. On a lab-scale, in an undivided cell, there is a relatively large surface area to liquid ratio. However, if the reaction in question is scaled up to fit in a multi-liter tank, the surface area to liquid ratio becomes much smaller. As a result of this difference in surface area to liquid ratio, the exact nature of the thermodynamics and the reaction kinetics of the process changes in a non-linear fashion. This is why a reaction in a stirred tank can behave vastly differently from the same reaction in a large-scale process. Other factors that change in the transition to a production scale include the fluid dynamics, the chemical equilibrium as well as the selection of equipment and materials. For this reason it is recommended to conduct pilot research in conjunction to computer simulations. Various modeling tools and methods can be used today for scale-up such as Aspen Plus/Aspen HYSYS modeling, Finite Elemental Analysis, and Computational Fluid Dynamics

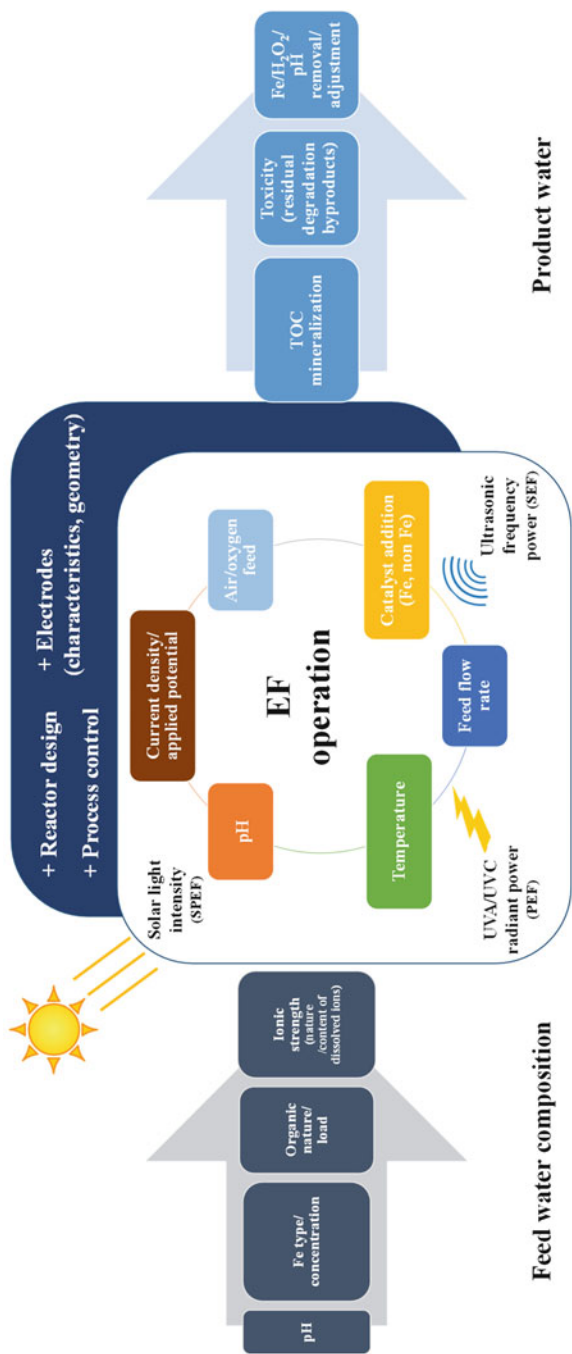


Fig. 3 Illustration of parameters affecting process design and operation in EF-based electrochemical technologies

(CFD). These modeling tools could lead to finalized mass and energy balances, prediction of pollutant behavior, optimized system design and capacity, equipment requirements, and system limitations. Moreover, the progress in the development of consistent mathematical models that describe the complex scenarios and reactions involved in the electrooxidation of multicomponent mixtures of various pollutants, and its integration with knowledge about reactor hydrodynamics, will undoubtedly contribute to the scale-up.

4.2 Optimization of EF Operation

The improvements in EF reactor design are closely interconnected with the optimization of the operating conditions so that the process can be used at an efficient, effective, and profitable industrial scale. Indeed, when designing an EF process it is crucial to have a good understanding of the effect of the operating conditions on process performance, such as the electric potential, the water flux, the pH, the air/oxygen feed, the catalyst dosage rate (where applicable), the UV radiant power per unit volume (in photo-induced EF processes), the ultrasonic frequency power (in case of SEF), and to a lesser extent of the operating temperature (Fig. 3). An effort is made next to summarize the knowledge gained from the substantive research carried out at lab- and pilot-scale on this direction.

4.2.1 Operating pH

As a chemical component of the water/wastewater, pH has direct influence on its treatability by EF since acidity has a profound effect on the iron and hydrogen peroxide speciation, and consequently on the type of oxidizing species available in the reaction medium; it is reported that superoxide radical $O_2^{\bullet-}$ is dominant at alkaline pH while $\bullet OH$ is dominant at acidic condition [67]. The efficiency of the Fenton reagent to degrade organic compounds is reduced both at high and low pH, with the optimum value being around 3, regardless of the target wastewater. Specifically, at alkaline pH the activity of Fenton reagent is reduced due to the presence of relatively inactive iron oxohydroxides and formation of ferric hydroxide precipitate. It is reported also that the oxidation potential of $\bullet OH$ decreases with increasing pH [68] while H_2O_2 can be auto-decomposed to water and O_2 [69]. On the other hand, at very low pH values, iron complex species $[Fe(H_2O)_6]^{2+}$ may prevail, which reacts more slowly with hydrogen peroxide than other species [70]. Fe^{2+} regeneration by the reaction of Fe^{3+} with H_2O_2 is also inhibited by excessive H^+ ions in the solution, while H_2O_2 can be solvated to form stable oxonium ion $[H_3O_2]^+$. Oxonium ions make H_2O_2 more stable and reduce its reactivity with Fe^{2+} [6].

The importance of pH on process efficiency makes its control a necessity. This adds of course to the complexity of the system, increases the operating cost (for

acidification and subsequent neutralization), while the corrosivity hazard requires the selection of resistant to corrosion materials. For a continuous process, pH should be controlled throughout the process by adding appropriate amounts of acid (sulfuric, acetic, phosphoric) or caustic (sodium hydroxide). The selection of the acid/base agents may also affect the oxidation efficiency as noted by several researchers. In the work of Benitez et al. [71] acetic acid/acetate buffer gave maximum oxidation efficiency whereas a decreased oxidation was observed with phosphate and sulfate buffers. This can be attributed to the formation of stable Fe^{3+} complexes that are formed under those conditions [72].

The pH adjustment is feasible in the case of wastewaters; however, it is not recommended for drinking water treatment. In the latter case, great research effort is devoted to the development of systems and catalysts to overcome the low pH requirement. One approach is the development of heterogeneous EF processes in which iron can be supported on various materials (carbon, resin, or nafion) or on the working electrodes to promote the presence of the Fenton mixture in the solution, thus avoiding the use of dissolved Fe salts and the operation at low pH values. The progress in this field is discussed in detail in chapter "Heterogeneous Electro-Fenton Process." Another approach proposed by Wang et al. [73] was a novel Electro-Fenton-Like (EFL) system that can be applied to neutral water treatment without any pH adjustment. Such system uses the Keggin-type iron-substituted heteropolytungstate anion $\text{PW}_{11}\text{O}_{39}\text{Fe(III)(H}_2\text{O)}^{4-}$ to substitute for Fe^{3+} in the conventional EF system.

4.2.2 Applied Potential or Electric Current

The importance of the applied potential or electric current is directly related to the electrogeneration of H_2O_2 or the degradation rate of organics under galvanostatic electrolysis, respectively [7]. One would expect that high current densities are beneficial to the EF process. However, this is not true, since significant decrease of the current efficiency is usually observed due to the production of oxygen, the activation of side reactions, and the polarization. Moreover, current efficiency is low at the acidic operating pH (≤ 3) due to the low solubility of O_2 . These facts should be taken into consideration by the operator before deciding on the applied voltage/electric current, since electricity does not only affect the oxidation of pollutants but also the operating expenses of the treatment.

4.2.3 Air/ O_2 Addition

An excessive air or pure O_2 aeration is usually leading to a high production rate of H_2O_2 , especially in divided electrochemical cells where the separator (glass frits, diaphragms, cationic membranes) prevents the mixing of the cathodically produced H_2O_2 , avoiding its destruction at the anode. In the case of undivided cells the sparging of air/ O_2 is necessarily accompanied with an appropriate agitation of the

feed solution in order to increase the oxygen utilization efficiency (the fraction of oxygen consumed for the production of H_2O_2 over the total amount of oxygen added) and the effective mass transfer of the organic pollutants to the electrodes surface. However, the agitation may induce a lot of H_2O_2 transferring on the anode surface where it can be oxidized to O_2 .

Except from the sparging rate, the air pressure has been proved to greatly affect the electrogeneration of H_2O_2 and the EF abatement of organic pollutants in water [74]. Specifically an increase of the pressure may drastically enhance the concentration of H_2O_2 . In systems pressurized with air at 11 bar, the electro-reduction of oxygen at a graphite cathode gave rise to a concentration of H_2O_2 of about 12 mM, i.e., one order of magnitude higher than that achieved at atmospheric pressure. This result is attributed to the mass transfer intensification induced by the higher local concentration of molecular oxygen dissolved in the aqueous phase [74].

Considering that air/ O_2 sparging adds to the complexity and the cost of the system, especially for small-scale drinking water systems, it is important to fabricate EF reactors/cells without the need for an external aeration device. Recently the feasibility of H_2O_2 production without aeration was demonstrated in a flow-through “filter” type device [24, 26], in a novel dual tubular membrane electrodes reactor [28], a rotating disk reactor [75], as well as with the usage of modified graphite felt electrodes [76].

The importance of O_2 control on the efficiency of the EF process was recently examined by Yu et al. [77]. These researchers studied the potential of on-line monitoring of Oxidation Reduction Potential (ORP) and Dissolved Oxygen (DO) as key parameters for controlling the EF process in treating textile wastewater. Their results showed that the DO and ORP profiles have high correlation with the variations in H_2O_2 , Fe^{2+} , and Fe^{3+} , which can help identify over-dosing of H_2O_2 . They concluded that monitoring DO and ORP has great potential to effectively control the EF process and could result in chemical cost savings.

4.2.4 Catalyst Addition

The catalyst dose (in form of iron or non-iron species) is a critical operating parameter since Fenton or Fenton-like reactions are strongly affected by the type and the concentration of the catalyst in the bulk. The optimal dose range can vary between wastewaters depending on the organic load and the presence of other constituents (e.g., inorganic ions) that scavenge the Fenton-type reactions. Obviously, there should be flexibility regarding the catalyst dose, which should be easily altered to be adapted to any variation of the feedwater composition. In case of iron the rate of organics degradation remains the same above a certain concentration. Typical ranges are 1 part Fe per 5–25 parts H_2O_2 (wt/wt). For most applications, it does not matter whether Fe^{2+} or Fe^{3+} salts are used to catalyze the reaction; the catalytic cycle begins quickly if H_2O_2 and organic material are in abundance. However, ferrous iron may be preferred in case of negligible cathodic reduction of Fe^{3+} , even if the cathode is capable of producing large quantities of H_2O_2 .

Neither does it matter whether a chloride or sulfate salt of the iron is used, although with the former, chlorine may be generated at high rates of application.

4.2.5 Feed Flow Rate

The feed flow rate defines the hydraulic residence time (HRT) of the wastewater in the EF system. This is of great significance in continuous processes where feedwater is continuously treated and discharged. In determining HRT it is important to know the actual reaction kinetics which again are influenced by the variables already discussed (Fig. 3), most notably the $\text{H}_2\text{O}_2/\text{Fe}^{2+}$ ratio and the wastewater composition (concentration and refractory nature of the organics). Values of HRT from several minutes to few hours can be determined depending on the treatment targets set (e.g., compliance with discharge standards or BOD_5/COD limit for subsequent biological posttreatment).

4.2.6 Operating Temperature

The effect of temperature on the overall efficiency of the electrooxidation process has not been widely studied. Most studies have been performed at ambient temperature and to a lesser extent at fixed temperatures (regulated with the aid of thermostatic baths). Considering that chemical reactions are greatly affected by temperature, it is assumed that Fenton reaction will be also influenced by the temperature in an EF system. In principle, higher temperatures can provide more energy to overcome the reaction activation energy [78] and then accelerate the reaction by increasing the reaction rate constant according to the Arrhenius equation [79]. On the other hand, an increase in operating temperature can favor the decomposition of H_2O_2 towards O_2 and H_2O , whose rate increases around 2.2 times each 10°C in the range $20\text{--}100^\circ\text{C}$ [80]. Moreover, the solubility of oxygen in water decreases as temperature increases, which in turn may negatively affect the in situ electrogeneration of H_2O_2 .

5 Recommendations for Future Research

Following successful proof-of-concept work, significant progress has been made during the last decade on EF-based electrochemical technologies, regarding the development of new electrode materials, the design and construction of lab-scale pilot plants, and finally the investigation of process performance with synthetic or real wastewaters. The variants EF, PEF, SPEF, Fered-Fenton as well as integrated processes with other physical, chemical, and biological methods have generally proven to be efficient and versatile, capable of degrading/mineralizing a wide variety of synthetic organic compounds present in wastewater. However, more

research effort is needed towards the development of larger-scale systems that will aid the scientific/research community to assess the dynamic potential of these technologies to address the water treatment challenges. Moreover, while patent activity has been rather intensive in pursuing commercialization of the EF technology, there appears to be little progress in licensing and sale of intellectual property. However, the literature suggests that there is potential in the EF technology, which may eventually pave the way towards substantial improvements in the water treatment sector, regarding cost and sustainable process performance. Along these lines, the following recommendations for future research are suggested towards the development of efficient, cost competitive, and sustainable processes.

- Development of high-performance and cost-effective (low cost/life ratio) anodes and cathodes with enhanced electrocatalytic properties (long service time) which will result in smaller operating and capital costs. Emphasis on 3-D electrode technology.
- Further development of promising hybrid technologies, such as Bio-EF and (SP) EF followed by membrane bioreactor (MBR) or biological activated carbon.
- Use of renewable energy sources (photovoltaic modules, wind turbines) as a cheap source of electrical power (energy self-sufficient processes).
- Process modeling and pollutant behavior prediction. Studies on the degradation mechanisms, comprising the parent compounds and the possible by-products in a broader and more comprehensive approach.
- Detailed toxicological assessment of the treated water/wastewater. This will assist in the environmental verification of the developed technologies.
- Application of optimization strategies to the design of large-scale reactors in order to overcome the technical shortcomings (leading to reduced capital and energy costs) which have hindered the widespread commercialization of the EF reactors.
- Application of computer simulations and modeling tools towards optimized EF reactor design and scale-up.
- Extensive investigation of the robustness and feasibility (validation) of full-scale EF technologies in a real operating environment.
- Detailed studies on economic assessment of EF-based technologies, considering operating and investment costs that enable comparison with other conventional or advanced water treatment technologies, currently used.

Once the practical and economic constraints of the final application are appropriately factored in, it will become possible to set a rational design of an effective EF technology. This is verified by examples of successful EAOPs developments, some of which are commercially available by the Swiss RedElec Technologie S.A., Ever-Clear Co. from Taiwan, Global Advantech from UK, E. Elgressy Ltd. from Israel, Xh2o Solutions Pvt. Ltd. from India, AQUALOGY S.A. from Spain, and VentilAQUA S.A. from Portugal. EAOPs based on diamond electrodes (AO) are also marketed by CONDIAS GmbH from Germany and Advanced Diamond Technologies Inc. from the USA.

References

1. Fenton HJH (1894) Oxidation of tartaric acid in presence of iron. *J Chem Soc* 65:899–910
2. Wieland H, Franke W (1927) Mechanism of the oxidation process. XII. The activation of hydrogen peroxide by iron. *Justus Liebig's Ann Chem* 457:1–70
3. Haber F, Willstätter R (1931) Unpaarigkeit und radikalketten im reaktion-mechanismus organischer und enzymatischer vorgänge. *Chem Ber* 64:2844–2856
4. Brown RF, Jamison SE, Pandit K et al (1964) The reaction of Fenton's reagent with phenoxyacetic acid and some halogen-substituted phenoxyacetic acids. *J Org Chem* 29:146–153
5. Pignatello JJ, Oliveros E, MacKay A (2006) Advanced oxidation processes for organic contaminant destruction based on the Fenton reaction and related chemistry. *Crit Rev Environ Sci Technol* 36:1–84
6. Babuponnusami A, Muthukumar K (2014) A review on Fenton and improvements to the Fenton process for wastewater treatment. *J Environ Manage* 2:557–572
7. Brillas E, Sirés I, Oturan MA (2009) Electro-Fenton process and related electrochemical technologies based on Fenton's reaction chemistry. *Chem Rev* 109:6570–6631
8. Wang N, Zheng T, Zhang G et al (2016) A review on Fenton-like processes for organic wastewater treatment. *J Environ Chem Eng* 4:762–787
9. Martínez-Huitle CA, Rodrigo MA, Sirés I et al (2015) Single and coupled electrochemical processes and reactors for the abatement of organic water pollutants: a critical review. *Chem Rev* 115(24):13362–13407
10. Ganiyu SO, van Hullebusch ED, Cretin M et al (2015) Coupling of membrane filtration and advanced oxidation processes for removal of pharmaceutical residues: a critical review. *Sep Purif Technol* 156:891–914
11. Ganzenko O, Huguenot D, van Hullebusch ED et al (2014) Electrochemical advanced oxidation and biological processes for wastewater treatment: a review of the combined approaches. *Environ Sci Pollut Res* 21:8493–8524
12. Sirés I, Brillas E, Oturan MA et al (2014) Electrochemical advanced oxidation processes: today and tomorrow. A review. *Environ Sci Pollut Res* 21:8336–8367
13. Bañuelos JA, Rodríguez FJ, Manríquez J et al (2014) A review on arrangement and reactors for Fenton-based water treatment processes. In: Peralta-Hernández JM, Rodrigo MA, Martínez-Huitle CA (eds) *Evaluation of electrochemical reactors as a new way to environmental protection*, Kerala, India, pp 97–137
14. Brillas E (2014) Electro-Fenton, UVA photoelectro-Fenton and solar photoelectro-Fenton treatments of organics in waters using a boron-doped diamond anode: a review. *J Mex Chem Soc* 58(3):239–255
15. Feng L, van Hullebusch ED, Rodrigo MA et al (2013) Removal of residual anti-inflammatory and analgesic pharmaceuticals from aqueous systems by electrochemical advanced oxidation processes. A review. *Chem Eng J* 228:944–964
16. Nidheesh PN, Gandhimathi R (2012) Trends in electro-Fenton process for water and wastewater treatment: an overview. *Desalination* 299:1–15
17. Martínez-Huitle CA, Brillas E (2009) Decontamination of wastewaters containing synthetic organic dyes by electrochemical methods: a general review. *Appl Catal Environ* 87:105–145
18. García O, Isarain-Chávez E, El-Ghenymy A et al (2014) Degradation of 2,4-D herbicide in a recirculation flow plant with a Pt/air-diffusion and a BDD/BDD cell by electrochemical oxidation and electro-Fenton process. *J Electroanal Chem* 728:1–9
19. García O, Isarain-Chávez E, Garcia-Segura S et al (2013) Degradation of 2,4-dichlorophenoxyacetic acid by electro-oxidation and electro-Fenton/BDD processes using a pre-pilot plant. *Electrocatalysis* 4:224–234
20. Chmayssem A, Taha S, Hauchard D (2017) Scaled-up electrochemical reactor with a fixed bed three-dimensional cathode for electro-Fenton process: application to the treatment of bisphenol A. *Electrochim Acta* 225:435–442

21. El-Ghenymy A, Cabot PL, Centellas F et al (2013) Mineralization of sulfanilamide by electro-Fenton and solar photoelectro-Fenton in a pre-pilot plant with a Pt/air-diffusion cell. *Chemosphere* 91:1324–1331
22. Khataee AR, Safarpour M, Zarei M et al (2012) Combined heterogeneous and homogeneous photodegradation of a dye using immobilized TiO₂ nanophotocatalyst and modified graphite electrode with carbon nanotubes. *J Mol Catal A Chem* 363–364:58–68
23. Liu H, Vecitis CD (2012) Reactive transport mechanism for organic oxidation during electrochemical filtration: mass-transfer, physical adsorption, and electron transfer. *J Phys Chem C* 116:374–383
24. Plakas KV, Karabelas AJ, Sklari SD et al (2013) Toward the development of a novel electro-Fenton system for eliminating toxic organic substances from water. Part 1. In situ generation of hydrogen peroxide. *Ind Eng Chem Res* 52:13948–13956
25. Sklari SD, Plakas KV, Petsi PN et al (2015) Toward the development of a novel electro-Fenton system for eliminating toxic organic substances from water. Part 2. Preparation characterization, and evaluation of iron-impregnated carbon felts as cathodic electrodes. *Ind Eng Chem Res* 54:2059–2073
26. Plakas KV, Sklari SD, Yiankakis DA et al (2016) Removal of organic micropollutants from drinking water by a novel electro-Fenton filter: pilot-scale studies. *Water Res* 91:183–194
27. Ma L, Zhou M, Ren G et al (2016) A highly energy-efficient flow-through electro-Fenton process for organic pollutants degradation. *Electrochim Acta* 200:222–230
28. Xu A, Han W, Li J (2016) Electrogeneration of hydrogen peroxide using Ti/IrO₂-Ta₂O₅ anode in dual tubular membranes electro-Fenton reactor for the degradation of tricyclazole without aeration. *Chem Eng J* 295:152–159
29. Lan H, Li J, Sun M et al (2016) Efficient conversion of dimethylarsinate into arsenic and its simultaneous adsorption removal over FeC_x/N-doped carbon fiber composite in an electro-Fenton process. *Water Res* 100:57–64
30. Xu N, Zhang Y, Tao H et al (2013) Bio-electro-Fenton system for enhanced estrogens degradation. *Bioresour Technol* 138:136–140
31. Kishimoto N, Hatta M, Kato M et al (2017) Effects of oxidation–reduction potential control and sequential use of biological treatment on the electrochemical Fenton-type process. *Process Saf Environ* 105:134–142
32. Polcaro AM, Vacca A, Mascia M et al (2007) Characterization of a stirred tank electrochemical cell for water disinfection processes. *Electrochim Acta* 52:2595–2602
33. Cotillas S, Llanos J, Rodrigo MA et al (2015) Use of carbon felt cathodes for the electrochemical reclamation of urban treated wastewaters. *Appl Catal B Environ* 162:252–259
34. Mansour D, Fourcade F, Soutrel I et al (2015) Mineralization of synthetic and industrial pharmaceutical effluent containing trimethoprim by combining electro-Fenton and activated sludge treatment. *J Taiwan Inst Chem Eng* 53:58–67
35. Kamali M, Khodaparast Z (2015) Review on recent developments on pulp and paper mill wastewater treatment. *Ecotoxicol Environ Saf* 114:326–342
36. Jaafarzadeh N, Ghanbari F, Ahmadi M et al (2017) Efficient integrated processes for pulp and paper wastewater treatment and phytotoxicity reduction: permanganate, electro-Fenton and Co₃O₄/UV/peroxymonosulfate. *Chem Eng J* 308:142–150
37. Eren Z (2012) Ultrasound as a basic and auxiliary process for dye remediation: a review. *J Environ Manage* 104:127–141
38. Asghar A, Abdul Raman AA, Ashri Wan Daud WM (2015) Advanced oxidation processes for in-situ production of hydrogen peroxide/hydroxyl radical for textile wastewater treatment: a review. *J Clean Prod* 87:826–838
39. Garcia-Segura S, Brillas E (2016) Combustion of textile monoazo, diazo and triazo dyes by solar photoelectro-Fenton: decolorization, kinetics and degradation routes. *Appl Catal B Environ* 181:681–691
40. Ren G, Zhou M, Liu M et al (2016) A novel vertical-flow electro-Fenton reactor for organic wastewater treatment. *Chem Eng J* 298:55–67

41. Rosales E, Pazos M, Longo MA et al (2009) Electro-Fenton decoloration of dyes in a continuous reactor: a promising technology in colored wastewater treatment. *Chem Eng J* 155(1–2):62–67
42. El-Desoky HS, Ghoneim MM, El-Sheikh R et al (2010) Oxidation of Levafix CA reactive azo-dyes in industrial wastewater of textile dyeing by electrogenerated Fenton's reagent. *J Hazard Mater* 175:858–865
43. Wang CT, Chou WL, Chung MH et al (2010) COD removal from real dyeing wastewater by electro-Fenton technology using an activated carbon fiber cathode. *Desalination* 253:129–134
44. Feng C, Li F, Liu H et al (2010) A dual-chamber microbial fuel cell with conductive film-modified anode and cathode and its application for the neutral electro-Fenton process. *Electrochim Acta* 55:2048–2054
45. Wang X-Q, Liu C-P, Yuan Y et al (2014) Arsenite oxidation and removal driven by a bio-electro-Fenton process under neutral pH conditions. *J Hazard Mater* 275:200–209
46. Khoufi S, Aloui F, Sayadi S (2006) Treatment of olive oil mill wastewater by combined process electro-Fenton reaction and anaerobic digestion. *Water Res* 40:2007–2016
47. Flores N, Cabot PL, Centellas F, Garrido JA, Rodríguez RM, Brillas E, Sirés I (2017) 4-Hydroxyphenylacetic acid oxidation in sulfate and real olive oil mill wastewater by electrochemical advanced processes with a boron-doped diamond anode. *J Hazard Mater* 321:566–575
48. Díez AM, Rosales E, Sanromán MA et al (2017) Assessment of LED-assisted electro-Fenton reactor for the treatment of winery wastewater. *Chem Eng J* 310:399–406
49. Zhang H, Ran X, Wu X (2012) Electro-Fenton treatment of mature landfill leachate in a continuous flow reactor. *J Hazard Mater* 241–242:259–266
50. Lin SH, Chang CC (2000) Treatment of landfill leachate by combined electro-Fenton oxidation and sequencing batch reactor method. *Water Res* 34:4243–4249
51. Zhang H, Zhang DB, Zhou JY (2006) Removal of COD from landfill leachate by electro-Fenton method. *J Hazard Mater* 135:106–111
52. Atmaca E (2009) Treatment of landfill leachate by using electro-Fenton method. *J Hazard Mater* 163:109–114
53. Mohajeri S, Aziz HA, Isa MH et al (2010) Statistical optimization of process parameters for landfill leachate treatment using electro-Fenton technique. *J Hazard Mater* 176:749–758
54. Orkun MO, Kuleyin A (2012) Treatment performance evaluation of chemical oxygen demand from landfill leachate by electro-coagulation and electro-Fenton technique. *Environ Prog Sustain Energy* 31:59–67
55. Zhang H, Cheng ZH, Zhang DB (2007) Treatment of landfill leachate by electro-Fenton process. *Fresen Environ Bull* 16:1216–1219
56. Aziz HA, Othman OM, Abu Amr SS (2013) The performance of electro-Fenton oxidation in the removal of coliform bacteria from landfill leachate. *Waste Manag* 33:396–400
57. Colades JI, de Luna MDG, Su C-C et al (2015) Treatment of thin film transistor-liquid crystal display (TFT-LCD) wastewater by the electro-Fenton process. *Sep Purif Technol* 145:104–112
58. Cho SH, Lee HJ, Moon SH (2008) Integrated electroenzymatic and electrochemical treatment of petrochemical wastewater using a pilot scale membraneless system. *Process Biochem* 43:1371–1376
59. Jia S, Han H, Hou B et al (2015) Advanced treatment of biologically pretreated coal gasification wastewater by a novel integration of three-dimensional catalytic electro-Fenton and membrane bioreactor. *Bioresour Technol* 198:918–921
60. Zhou M, Tan Q, Wang Q et al (2012) Degradation of organics in reverse osmosis concentrate by electro-Fenton process. *J Hazard Mater* 215–216:287–293
61. Akyol A, Can OT, Demirbas E (2013) A comparative study of electrocoagulation and electro-Fenton for treatment of wastewater from liquid organic fertilizer plant. *Sep Purif Technol* 112:11–19
62. Kurt U, Apaydin O, Gonullu MT (2007) Reduction of COD in wastewater from an organized tannery industrial region by electro-Fenton process. *J Hazard Mater* 143:33–40

63. Paramo-Vargas J, Camargo AME, Gutierrez-Granados S et al (2015) Applying electro-Fenton process as an alternative to a slaughterhouse effluent treatment. *J Electroanal Chem* 754:80–86
64. Un UT, Topal S, Oduncu E et al (2015) Treatment of tissue paper wastewater: application of electro-Fenton method. *Int J Environ Sci Develop* 6(6):415–418
65. Gameel A, Malash G, Mubarak AA et al (2015) Treatment of spent caustic from ethylene plant using electro-Fenton technique. *Am J Environ Eng Sci* 2(4):37–46
66. Huguenot D, Mousset E, van Hullebusch ED (2015) Combination of surfactant enhanced soil washing and electro-Fenton process for the treatment of soils contaminated by petroleum hydrocarbons. *J Environ Manage* 153:40–47
67. Fang G-D, Zhou D-M, Dionysiou DD (2013) Superoxide mediated production of hydroxyl radicals by magnetite nanoparticles: demonstration in the degradation of 2-chlorobiphenyl. *J Hazard Mater* 250–251:68–75
68. Bossmann SH, Oliveros E, Gob S et al (1998) New evidence against hydroxyl radicals as reactive intermediates in the thermal and photochemically enhanced Fenton reaction. *J Phys Chem* 102:5542–5550
69. Szpyrkowicz L, Juzzolino C, Kaul SN (2001) A comparative study on oxidation of disperse dye by electrochemical process, ozone, hypochlorite and Fenton reagent. *Water Res* 35:2129–2136
70. Xu XR, Li XY, Li XZ et al (2009) Degradation of melatonin by UV, UV/H₂O₂, Fe²⁺/H₂O₂ and UV/Fe²⁺/H₂O₂ processes. *Sep Purif Technol* 68:261–266
71. Benitez FJ, Acero JL, Real FJ et al (2001) The role of hydroxyl radicals for the decomposition of p-hydroxy phenylacetic acid in aqueous solutions. *Water Res* 35:1338–1343
72. Pignatello JJ (1992) Dark and photoassisted Fe³⁺-catalyzed degradation of chlorophenoxy herbicides by hydrogen peroxide. *Environ Sci Technol* 26:944–951
73. Wang C, Hua Y, Tong Y (2010) A novel electro-Fenton-like system using PW₁₁O₃₉Fe³⁺(H₂O)⁴⁻ as an electrocatalyst for wastewater treatment. *Electrochim Acta* 55(22):6755–6760
74. Scialdone O, Galia A, Gattuso A et al (2015) Effect of air pressure on the electro-generation of H₂O₂ and the abatement of organic pollutants in water by electro-Fenton process. *Electrochim Acta* 182:775–780
75. Liu H (2007) A novel electro-Fenton process for water treatment: reaction-controlled pH adjustment and performance assessment. *Environ Sci Technol* 41:2937–2942
76. Yu F, Zhou M, Yu X (2015) Cost-effective electro-Fenton using modified graphite felt that dramatically enhanced on H₂O₂ electro-generation without external aeration. *Electrochim Acta* 163:182–189
77. Yu R-F, Lin C-H, Chen H-W et al (2013) Possible control approaches of the electro-Fenton process for textile wastewater treatment using on-line monitoring of DO and ORP. *Chem Eng J* 218:341–349
78. Xu HY, Liu WC, Qi SY et al (2014) Kinetics and optimization of the decoloration of dyeing wastewater by a schorl-catalyzed Fenton-like reaction. *J Serb Chem Soc* 79:361–377
79. Ifelebuegu AO, Ezenwa CP (2011) Removal of endocrine disrupting chemicals in wastewater treatment by Fenton-like oxidation. *Water Air Soil Pollut* 217:213–220
80. Bautista P, Mohedano AF, Casas JA et al (2008) An overview of the application of Fenton oxidation to industrial wastewaters treatment. *J Chem Technol Biotechnol* 83:1323–1338

The Application of Electro-Fenton Process for the Treatment of Artificial Sweeteners

Heng Lin, Nihal Oturan, Jie Wu, Mehmet A. Oturan, and Hui Zhang

Abstract This chapter presents the degradation and mineralization of emerging trace contaminants artificial sweeteners (ASs) in aqueous solution by electro-Fenton process in which hydroxyl radicals were formed concomitantly by $\cdot\text{OH}$ formed from electrocatalytically generated Fenton's reagent in the bulk solution and $\text{M}(\cdot\text{OH})$ from water oxidation at the anode surface. Experiments were performed in an undivided cylindrical glass cell with a carbon-felt cathode and a Pt or boron-doped diamond (BDD) anode. The effect of catalyst (Fe^{2+}) concentration and applied current on the degradation and mineralization kinetics of ASs was evaluated. The absolute rate constants for the reaction between ASs and $\cdot\text{OH}$ were determined. The formation and evolution of short-chain carboxylic acids as well as released inorganic ions, and toxicity assessment during the electro-Fenton process have been reported and compared.

Keywords Artificial sweeteners, Electro-Fenton, Hydroxyl radicals, Mineralization, Wastewater treatment

Contents

1	Introduction	380
2	Treatment of ASs by Electro-Fenton Process	384
2.1	Oxidation Kinetics of ASs	384

H. Lin and H. Zhang (✉)

Department of Environmental Engineering, Wuhan University, Wuhan 430079, China
e-mail: eeng@whu.edu.cn

N. Oturan and M.A. Oturan (✉)

Laboratoire Géomatériaux et Environnement (EA 4605), Université Paris-Est, 5 Bd. Descartes,
77454 Marne-la-Vallée Cedex 2, France
e-mail: mehmet.oturan@univ.paris-est.fr

J. Wu

Fuzhou Environmental Monitoring Center, Fuzhou 350011, China

M. Zhou et al. (eds.), *Electro-Fenton Process: New Trends and Scale-Up*,
Hdb Env Chem (2018) 61: 379–398, DOI 10.1007/698_2017_59,

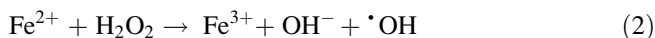
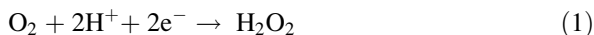
© Springer Nature Singapore Pte Ltd. 2017, Published online: 21 July 2017

2.2	Determination of the Rate Constants for ASs by $\cdot\text{OH}$	387
2.3	Mineralization of ASs in Electro-Fenton Process	387
2.4	Evaluation of Mineralization Current Efficiency (MCE) and Energy Consumption (EC)	389
2.5	Identification and Evolution of Short-Chain Carboxylic Acids and Inorganic Ions	390
2.6	Toxicity Assessment During Treatment	393
3	Conclusions	394
	References	394

1 Introduction

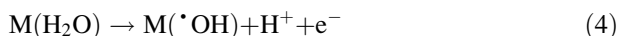
Advance oxidation processes (AOPs) have been proved to be effective for the degradation of many toxic/persistent organic contaminants from aqueous medium such as coloring matters, pesticides, and pharmaceuticals and personal care products (PPCPs) [1–6]. The most commonly used AOPs for the removal of organic pollutants from aqueous medium is based on the Fenton's reagent (an aqueous mixture of Fe^{2+} and H_2O_2 which can produce hydroxyl radicals ($\cdot\text{OH}$)) [7–9]. Fenton's reaction has been used as an attractive and effective technology for the degradation of various organic pollutants [10–13] due to the lack of toxicity of the reagents, eventually leaving no residues and the simplicity of the technology [14, 15]. However, the conventional Fenton process has the disadvantages of high Fe^{2+} concentration addition and Fe sludge formation which limit its application [16].

Electro-Fenton process, in which H_2O_2 is produced electrochemically and Fe^{2+} can be regenerated at the same time, overcomes these disadvantages of conventional Fenton's process. H_2O_2 is generated by the 2-electron reduction of the dissolved oxygen on the cathode surface (Eq. 1) in an electrolytic cell. H_2O_2 can then react with the externally added Fe^{2+} to produce $\cdot\text{OH}$ according to the well-known Fenton's reaction (Eq. 2). Moreover, Fe^{2+} , consumed in Fenton's reaction, is regenerated at the cathode by the reduction of Fe^{3+} generated in Fenton's reaction (Eq. 3). This electrocatalysis allows reducing significantly the initial Fe^{2+} concentration to a catalytic amount. This low Fe^{2+} concentration also prevents the formation of process sludge contrarily to the classical Fenton's process [17].



The cathode materials favoring electrogeneration of H_2O_2 are gas diffusion electrodes (GDEs) [18–21], graphite [22, 23], and three-dimensional electrodes such as carbon-felt [24–26], activated carbon fiber (ACF) [27–29], reticulated vitreous carbon (RVC) [30, 31], and carbon sponge [32]. Recently, boron-doped diamond (BDD) electrode is also reported as a cathode material favoring H_2O_2

generation [33]. The commonly used anode materials in electro-Fenton process are high oxygen overvoltage anodes (M), such as dimensionally stable anodes (DSA), Pt, PbO₂, BDD, and recently reported sub-stoichiometric titanium oxide [34]. The higher the value of oxygen evolution overvoltage, the higher the possibility of generation of heterogeneous hydroxyl radicals M([•]OH) at the surface of the anode (Eq. 4) [17].



The simultaneous production of [•]OH in the bulk of solution and M([•]OH) at the anode surface enhances oxidation power of the process [35].

As sugar substitutes in food, beverages, and sanitary products, artificial sweeteners (ASs) have been used considerably all over the world [36]. They provide negligible energy and thus are ingredients of dietary products [37]. The most popular ASs are aspartame (ASP), saccharin (SAC), sucralose (SUC), acesulfame (ACE), and its potassium salt acesulfame K (ACE-K). The chemical structure and main characteristics of the commonly used ASs were presented in Table 1.

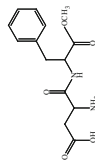
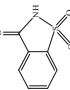
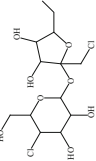
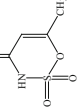
ASs are water contaminants that are highly specific to wastewater. Different from other emerging trace contaminants, such as PPCPs, ASs have been considered in environmental sciences only recently [36, 38–41]. Excretion after human consumption is one of the major sources of ASs in the environment [42]. ASs can also enter into wastewater treatment plants from households and industrial effluents and they eventually reside in the receiving environmental bodies [43].

Since they are used as food additives [37, 44, 45], ASs are extensively tested for potential adverse health effects on humans. Although the measured concentrations of some ASs range up to microgram per liter levels in surface water, groundwater, and drinking water, there is a huge safety margin regarding potential adverse health effects [36]. Acceptable daily intake value of ASs is 5 mg kg⁻¹ of body weight per day and is thus three to four orders of magnitude above the maximum possible daily human intake by drinking water. Adverse human health effects for the application of ASs have been reported in several studies [36, 46]. However, the long-term health effects resulting from the chronic exposure to low levels of these compounds are largely unknown [47].

Some of the ASs are difficult to degrade by conventional wastewater treatments processes [48]. Consequently, different AOPs have been proposed as an alternative method to degrade ASs effectively [49]. Toth et al. [46] studied the reaction kinetics for [•]OH reaction with some ASs. The rate constants for ACE-K, ASP, SAC, and SUC with [•]OH were $(3.87 \pm 0.27) \times 10^9$, $(2.28 \pm 0.02) \times 10^9$, $(1.85 \pm 0.01) \times 10^9$, and $(1.50 \pm 0.01) \times 10^9$ M⁻¹ s⁻¹, respectively.

Soh et al. [50] degraded 1 μM ASs by applying 100 μM ozone. Six percent SUC remained after 60 min and ACE-K was not detected in a 5-min reaction. Oxidation by ozone can occur through direct reaction with ozone and radical mediated oxidation [51]. When adding 0.5 mM *t*-butanol as a radical quench, the degradation of SUC was completely hindered while ACE-K was still completely degraded,

Table 1 The chemical structure and main characteristics of some commonly used ASs

Name	Chemical structure	Molecular formula	Molecular weight (g/mol)	CAS number	Water solubility (g/L)	Number of times sweeter than sucrose
Aspartame		$C_{14}H_{18}N_2O_5$	394.31	22839-47-0	~10 (25°C)	200
Saccharin		$C_7H_5NO_3S$	183.18	81-07-2	4	200–700
Sucralose		$C_{12}H_{19}Cl_3O_8$	397.63	56038-13-2	283 (20°C)	600
Acesulfame		$C_4H_5NO_4S$	163.15	33665-90-6	270 (20°C)	200

though at slower rates [50]. Since SUC does not have any evident sites for direct oxidation by ozone, the removal of SUC was mainly caused by hydroxyl radicals generated in the oxidative system [49, 50]. It can be concluded that the harsher and less selective degradation pathway of radical mediated oxidation is necessary for the breakdown of sucralose. Hollender et al. [52] treated a secondary effluent containing SUC at the scale of a municipal WWTP by ozonation. The elimination efficiency of SUC was only 31%, which confirmed ozonation was not an effective technology for SUC elimination.

The study of Soh et al. indicated SUC was not degraded after 5 h UV exposure [50]. Therefore, UV was combined with oxidant (H_2O_2 and peroxydisulfate) or catalyst to degrade SUC. In UV/ H_2O_2 process, 0.5 mg L^{-1} SUC was able to be efficiently degraded at high irradiation intensity, i.e., $4,000 \text{ mJ cm}^{-2}$ [53]. Xu et al. [54] investigated the mineralization of SUC by UV/peroxydisulfate (PDS) and UV/ H_2O_2 process. The results indicated the UV/PDS system can completely mineralize 0.126 mM SUC in a 60-min reaction using a 30-fold excess of PDS over SUC molar concentration. The study of Calza et al. [55] suggested that both heterogeneous TiO_2 and homogeneous photo-Fenton photocatalytic treatments are suitable for the elimination of SUC from the aqueous medium. In TiO_2 photocatalytic process, 15 mg L^{-1} SUC can be completely degraded in a 30-min reaction and be totally mineralized after 240 min of irradiation. Calza et al. [56] also investigated the degradation of ACE using cerium doped ZnO as a solar light photocatalyst. The rate constant of ACE decomposition using ZnO doped with cerium as photocatalyst under solar was 0.011 min^{-1} .

Except for ozonation and UV-based AOPs, other AOPs also began to be applied in the degradation of ASs, e.g., ferrate(VI) and electrochemical advanced oxidation processes (EAOPs). Ferrate(VI) is a potential water treatment chemical due to its dual functions as an oxidant and a subsequent coagulant/precipitant as ferric hydroxide [57]. Sharma et al. [58] oxidized SUC by ferrate(VI) at neutral pH. Comparison of the reactivity of ferrate(VI) with other oxidants showed that free radical species such as $\cdot\text{OH}$ have much higher reactivity than Fe(VI) towards SUC. Therefore, ferrate(VI) may not be feasible to degrade sucralose in water, similar to ozonation [49]. Punturat et al. [59] degraded ACE-K by electro-oxidation in aqueous solution. At current density of 100 mA cm^{-2} and 25°C , the degradation of ACE-K on tested anodes followed the order $\text{BDD} > \text{PbO}_2 > \text{Pt}$.

Due to the successful application of electro-Fenton process to the degradation of various organic compounds, it can be estimated that ASs can be mineralized by this process. Therefore, in this chapter, electro-Fenton process was employed to treat ASs in aqueous medium. The oxidation kinetics and mineralization behavior of ASs during electro-Fenton process were assessed. The absolute rate constants for the reaction between ASs and $\cdot\text{OH}$ were determined. The formation and evolution of aliphatic short-chain carboxylic acids, formed as end-products before complete mineralization, the evolution of inorganic ions released into the solution, and toxicity assessment were monitored during treatment.

2 Treatment of ASs by Electro-Fenton Process

Bulk experiments were carried out at room temperature in a 250 mL undivided cylindrical glass cell of 6 cm diameter containing 220 mL ASs solution. DSA (24 cm², mixed metal oxide Ti/RuO₂–IrO₂, Baoji Xinyu GuangJiDian Limited Liability Company, China), Pt (4.5 cm height, i.d. = 3.1 cm, Platecxis, France), and BDD (24 cm², COMDIAS GmbH, Germany) anodes, which were centered in the cell, were used in electro-Fenton process to degrade ASs [60]. Carbon-felt (17.5 × 5 cm) was used as cathode which covered the inner wall of the 250 mL capacity glass cell.

2.1 Oxidation Kinetics of ASs

Figure 1a shows that 0.2 mM SAC could be completely removed in a 25-min reaction for all the anode materials. SAC concentration decay followed pseudo-first-order kinetics. The apparent rate constant (k_{app}) values for SAC degradation with DSA, Pt, and BDD anodes were 0.18, 0.19, and 0.21 min⁻¹, respectively. However, when it comes to mineralization, BDD anode showed its great superiority. In a 360-min treatment time, the TOC removal efficiencies for SAC were 55.8%, 76.1%, and 96.2% for DSA, Pt, and BDD anodes, respectively (Fig. 1b). On the one hand, the BDD(·OH) radicals can effectively mineralize short chain carboxylic acids generated in electro-Fenton process, which are relatively recalcitrant to homogeneous ·OH produced in the bulk solution from Fenton's reaction (Eq. 2) [61]. On the other hand, the loosely bound BDD(·OH) could readily react with organic pollutant, in contrast to the chemisorbed Pt(·OH) (Eq. 4) which limited the oxidation ability of Pt anode [6, 62, 63].

It is well known that catalyst (Fe²⁺) concentration and applied current are significant parameters affecting the performance of electro-Fenton process [17]. The generation rate of ·OH from Fenton's reaction (Eq. 2) is dependent on the availability of free Fe²⁺ [64, 65]. On the other hand, an excess of Fe²⁺ can harm process efficiency because of enhancement of its reaction with ·OH [6, 9]. The applied current controls the production of hydroxyl radicals both at the anode surface via Eq. (4) and in the bulk solution through Eqs. (1)–(3) [64]. Moreover, the value of applied current is crucial for the operational cost and process efficiency [66].

The effect of catalyst concentration and applied current on SAC oxidation during electro-Fenton process was investigated by using BDD as anode and carbon-felt as cathode (Fig. 2) [60]. The degradation of SAC followed pseudo-first-order kinetics and the apparent rate constants (k_{app}) calculated from insets were given in Table 2. SAC disappeared in a 30-min reaction at all operating conditions. The optimal Fe²⁺ concentration for SAC removal was 0.2 mM. When Fe²⁺ concentration increased from 0.2 to 0.5 mM, SAC removal efficiency decreased evidently (Fig. 2). The

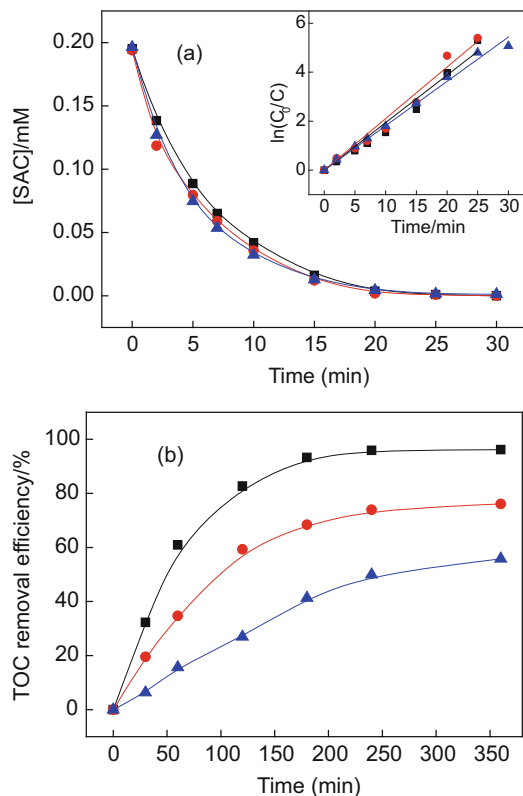


Fig. 1 Comparison of different anodes on the degradation (a) and mineralization (b) of 0.2 mM SAC solutions at 200 mA constant current electrolysis with BDD (*filled square*), Pt (*filled circle*), and DSA (*filled triangle*). $[SAC]_0 = 0.2$ mM, $[Fe^{2+}] = 0.2$ mM, $[Na_2SO_4] = 50$ mM, $pH_0 = 3.0$. The *inset* of (a) shows the kinetic analysis of SAC degradation following a pseudo-first order kinetics and points out close apparent rates values for all anode materials. Reprinted with permission from [60]. Springer Science + Business Media

negative influence of higher Fe^{2+} concentration might be attributed to the role of Fe^{2+} as scavenger of hydroxyl radicals (Eq. 5) which occurred with a large rate constant ($k = 3.20 \times 10^8 \text{ M}^{-1} \text{ s}^{-1}$) [17, 67]. Therefore, this reaction became competitive for consuming $\cdot OH$ radicals at higher Fe^{2+} concentration and consequently inhibited the oxidation of SAC.



Table 2 showed that the apparent rate constant for SAC oxidation increased from 0.09 to 0.19 min^{-1} when the applied current increased from 50 to 200 mA. High currents could promote both the Fe^{2+} regeneration (Eq. 3) and the production of H_2O_2 (Eq. 1) [1]. However, further increasing current intensity to 500 mA, the

Fig. 2 Effect of catalyst (Fe^{2+}) concentration (a) (in mM): 0.05 (filled square), 0.1 (filled circle), 0.20 (filled triangle), 0.3 (filled inverted triangle), 0.5 (left mounted triangle) and applied current (b) (in mA): 50 (filled square), 100 (filled circle), 200 (filled inverted triangle), 300 (filled inverted triangle), 500 (left mounted triangle) on the oxidative degradation of 0.2 mM SAC during electro-Fenton process with BDD anode versus carbon-felt cathode. Experimental conditions: (a), $I = 200$ mA, $\text{pH}_0 = 3.0$, $[\text{Na}_2\text{SO}_4] = 50$ mM. (b), $[\text{Fe}^{2+}] = 0.2$ mM, $\text{pH}_0 = 3.0$, $[\text{Na}_2\text{SO}_4] = 50$ mM. Reprinted with permission from [60]. Springer Science + Business Media

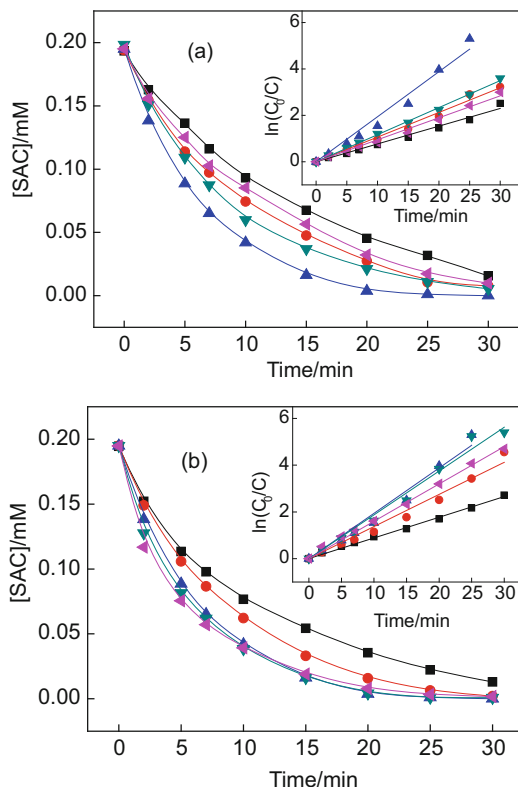


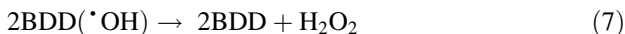
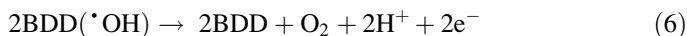
Table 2 Apparent rate constants (k_{app}) obtained in electro-Fenton processes for SAC degradation, assuming pseudo-first order kinetic model under different operating conditions

$[\text{Fe}^{2+}]$ (mM)	I (mA)	k_{app} (min^{-1})	R^2
0.05	200	0.08 ± 0.01	0.994
0.1	200	0.11 ± 0.01	0.995
0.2	200	0.19 ± 0.01	0.988
0.3	200	0.12 ± 0.01	0.999
0.5	200	0.09 ± 0.01	0.996
0.2	50	0.09 ± 0.01	0.998
0.2	100	0.14 ± 0.01	0.991
0.2	300	0.19 ± 0.01	0.993
0.2	500	0.16 ± 0.01	0.998

Operating conditions: I and $[\text{Fe}^{2+}]$ variable, pH: 3.0, BDD anode and carbon felt cathode. Reprinted with permission from [60]. Springer Science + Business Media

apparent rate constant decreased slightly to 0.16 min^{-1} . The decrease of oxidation efficiency at higher current could be due to the increase of side reactions consuming $\cdot\text{OH}$ such as the oxidation (Eq. 6) or recombination (Eq. 7) of BDD($\cdot\text{OH}$) [18]. Additionally, the decrease of SAC oxidation efficiency at applied current

above 200 mA could be related to the increase of parasitic reactions such as H₂ evolution reaction (Eq. 8) [68] and the promotion of 4-electron reduction of O₂ to water (Eq. 9), which is detrimental to H₂O₂ formation (Eq. 1).



2.2 Determination of the Rate Constants for ASs by $\cdot\text{OH}$

The absolute rate constant (k_{abs}) for the second order kinetics of the reaction between ASs and $\cdot\text{OH}$ was determined by using the competition kinetics method [67]. Benzoic acid (BA) was employed as the standard competitor with a well-known absolute rate constant, $k_{\text{abs,BA}} = 4.30 \times 10^9 \text{ M}^{-1} \text{ s}^{-1}$ [17]. Experiments were performed using a Pt anode with 0.1 mM ASs and BA concentrations in the presence of 0.2 mM Fe²⁺ at 50 mA current. The initial pH was 3.0. The hydroxylation absolute rate constants for oxidation reaction of ASs by hydroxyl radicals were then calculated according to Eq. (10).

$$\ln \left(\frac{[\text{ASs}]_0}{[\text{ASs}]_t} \right) = \left(\frac{k_{\text{abs,ASs}}}{k_{\text{abs,BA}}} \right) \ln \left(\frac{[\text{BA}]_0}{[\text{BA}]_t} \right) \quad (10)$$

Based on Fig. 3, the absolute rate constant for the oxidation reaction of ASP and SAC by $\cdot\text{OH}/\text{M}(\cdot\text{OH})$ was determined as $(5.23 \pm 0.02) \times 10^9 \text{ M}^{-1} \text{ s}^{-1}$ and $(1.85 \pm 0.01) \times 10^9 \text{ M}^{-1} \text{ s}^{-1}$, respectively. For ASP, the obtained $k_{\text{abs,ASP}}$ values is close to that reported in literature $(6.06 \pm 0.05) \times 10^9 \text{ M}^{-1} \text{ s}^{-1}$ by direct observation of the formation of the cyclohexadienyl radical adduct using a pulsed radiolysis technique [46]. Interesting, the rate constant value of SAC is the same as that reported by Toth et al. [46].

2.3 Mineralization of ASs in Electro-Fenton Process

The mineralization behavior of ASs ASP, SAC, and SUC during electro-Fenton process was investigated [60, 69, 70]. Figure 4 showed the mineralization efficiency of three ASs under constant current (200 mA) using Pt and BDD anode versus carbon felt cathode. In Pt/carbon-felt cell, the mineralization efficiency of ASP,

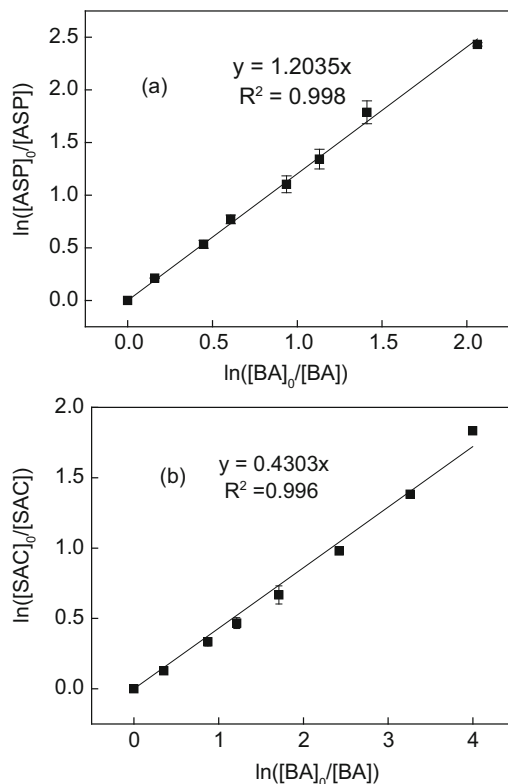


Fig. 3 Determination of the absolute rate constant of the reaction between ASs (ASP (a) and SAC (b)) and $\cdot\text{OH}$ by using competition kinetics method. Benzoic acid (BA) was selected as standard competitor. Experimental conditions: $[\text{ASs}]_0 = 0.1 \text{ mM}$, $[\text{BA}]_0 = 0.1 \text{ mM}$, $[\text{Fe}^{2+}] = 0.2 \text{ mM}$, $[\text{Na}_2\text{SO}_4] = 50 \text{ mM}$, $I = 50 \text{ mA}$, $\text{pH}_0 = 3.0$. Reprinted with permission from [60, 69]. Springer Science + Business Media and Elsevier

SAC, and SUC in 360-min electrolysis were 81.7%, 76.1%, and 95.2%, respectively, indicating the mineralization of SUC was under a much faster reaction rate in electro-Fenton process using Pt as anode. The mineralization efficiency in BDD/carbon-felt cell for ASP, SAC, and SUC were 97.5%, 96.2%, and 98.9%, respectively, which was higher than that in Pt/carbon-felt cell, confirming the great superiority of BDD anode on mineralization.

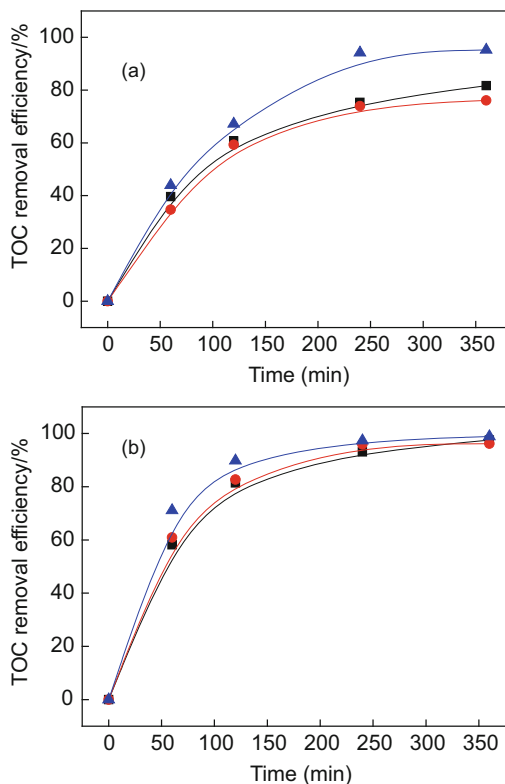


Fig. 4 Mineralization of ASs ASP (filled square), SAC (filled circle), and SUC (filled triangle) by electro-Fenton process with Pt (a) and BDD (b) anode versus carbon-felt cathode. Experimental conditions: $[ASP]_0 = [SAC]_0 = [SUC]_0 = 0.2$ mM, $I = 200$ mA, $[Fe^{2+}] = 0.2$ mM, $pH_0 = 3.0$, $[Na_2SO_4] = 50$ mM. Reprinted with permission from [60, 69, 70]. Springer Science + Business Media and Elsevier

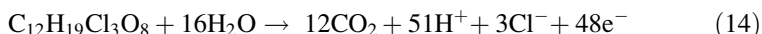
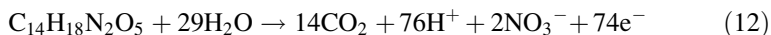
2.4 Evaluation of Mineralization Current Efficiency (MCE) and Energy Consumption (EC)

From the TOC removal data, the mineralization current efficiency (MCE) for each treated ASs solution at constant current I (in A) and a given electrolysis time t (in h) was estimated by Eq. (11) [17, 71, 72]:

$$MCE = \frac{nFV_s \Delta(\text{TOC})_{\text{exp}}}{4.32 \times 10^7 mIt} \quad (11)$$

where n is the number of electrons consumed per ASs molecule according to Eqs. (12)–(14), F is the Faraday constant ($=96,487$ C mol $^{-1}$), V_s is the solution volume (L), $\Delta(\text{TOC})_{\text{exp}}$ is the experimental TOC decay (mg L $^{-1}$), 4.32×10^7 is the

conversion factor to homogenize units ($=3,600 \text{ s h}^{-1} \times 12,000 \text{ mg of C mol}^{-1}$), and m is the number of carbon atoms of ASs molecule.



The energy consumption (EC) is essential for the viability of EAOPs (including electro-Fenton process) at industrial scale. In order to determine the energy consumption, the value energy consumption per unit TOC (EC_{TOC}) was calculated according to Eq. (15) [17, 61].

$$\text{EC}_{\text{TOC}} (\text{kWh g TOC}^{-1}) = \frac{E_{\text{cell}} I t}{\Delta(\text{TOC})_{\text{exp}} V_s} \quad (15)$$

where E_{cell} is average cell voltage.

The MCE and EC_{TOC} values for mineralization of ASP, SAC, and SUC during electro-Fenton process were calculated according to the TOC values shown in Fig. 4 and the results were illustrated in Fig. 5 [60, 69, 70]. The order of MCE and EC_{TOC} for three ASs during electro-Fenton process was in the following sequence: $\text{ASP} > \text{SUC} > \text{SAC}$ in both Pt/carbon-felt and BDD/carbon-felt cells. By comparing Fig. 5a, b, it can be seen that the MCE of Pt/carbon-felt cell was lower over the whole treatment time than that of BDD/carbon-felt cell. This result can be attributed to the low oxidation power of Pt anode compared to BDD [73]. In agreement with MCE values, the EC_{TOC} is particularly lower for ASP while it increases quickly with treatment time for SAC. Figure 5 also showed that the MCE values decreased continuously from the beginning to the end of the electrolysis for every trial in both cells. This was due to the gradual formation of intermediates such as carboxylic acids that are more difficult to be destroyed by $\cdot\text{OH}/\text{BDD}(\cdot\text{OH})$ and the mass transport limitations on account of the low concentration of organic matter [74, 75].

2.5 Identification and Evolution of Short-Chain Carboxylic Acids and Inorganic Ions

Generally, oxidation of organic compounds by AOPs leads to the formation of short-chain carboxylic acids as ultimate step before mineralization [17]. The carboxylic acids released by ASP, SAC, and SUC during electro-Fenton process were identified by ion-exclusion HPLC. For three ASs, carboxylic acids were generated from the beginning of the electrolysis, followed by an accumulation-destruction cycle. In addition, mineralization of organics results in release of inorganic ions corresponding heteroatoms present in the mother molecules. Therefore, the

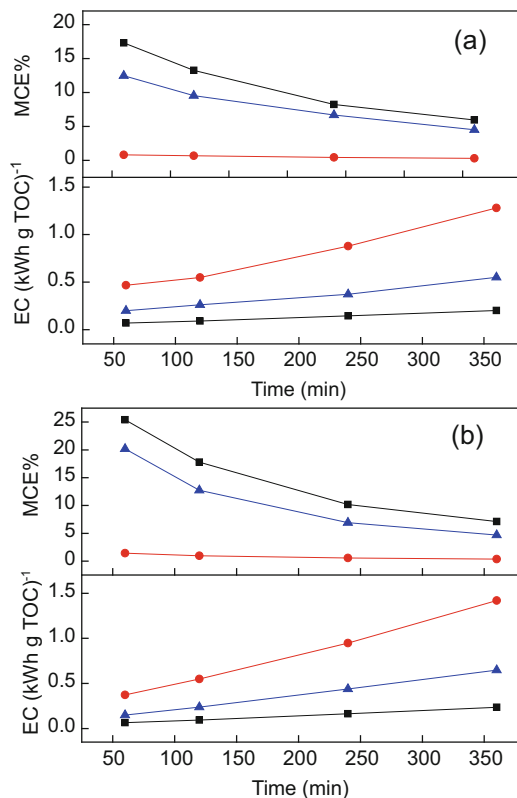


Fig. 5 Evolution of mineralization current efficiency (MCE) and energy consumption per unit TOC (EC_{TOC}) of ASs ASP (filled square), SAC (filled circle), and SUC (filled triangle) calculated from Eq. (11) on the electrolysis time with Pt (a) and BDD (b) anode versus carbon-felt cathode. Experimental conditions: $[ASP]_0 = [SAC]_0 = [SUC]_0 = 0.2$ mM, $[Fe^{2+}] = 0.2$ mM, $I = 200$ mA, pH₀ 3.0, $[Na_2SO_4] = 50$ mM. Reprinted with permission from [60, 69, 70]. Springer Science + Business Media and Elsevier

released mineral ions such as NO_3^- , NH_4^+ , SO_4^{2-} , and Cl^- were monitored by ion chromatography [60, 69, 70]. Figure 6 showed the evolution of short-chain carboxylic acids and inorganic ions detected when 0.2 mM ASP was degraded at 200 mA using BDD as anode. Oxalic and oxamic acids were present in the medium during the electrolysis. Moreover, carboxylic acids nearly disappeared at the end of electrolysis (360 min) in the BDD/carbon-felt cell, which is in agreement with the higher mineralization degree shown in Fig. 4a. Their accumulation reached maximum concentration at about 90 min (0.14 mM for oxalic acid and 0.45 mM for oxamic acids, respectively) before undertaking a gradual decrease until the mineralization to CO_2 was almost complete at the end of the treatment showing the great mineralization power of the process.

The release of NO_3^- and NH_4^+ during the mineralization can be seen in Fig. 6b. The concentrations of NO_3^- and NH_4^+ rose gradually to reach 0.12 and 0.18 mM, respectively, in a 360-min reaction, which account to 75.0% of the total nitrogen. This gradual rise is probably due to the slow mineralization of oxamic acid. The concentration of NH_4^+ predominates on longer treatment time which can be related to the reduction of NO_3^- to NH_4^+ at the cathode. Since TOC was nearly removed completely in BDD/carbon-felt cell at 360-min reaction, the non-equilibrating of the nitrogen mass balance could be attributed to the partial transformation of nitrogen into other nitrogen species such as N_2 , NO_2 , N_2O_4 , ..., mainly by electro-reduction of NO_3^- at carbon-felt cathode [76]. These reactions are promoted from 3D structure of carbon-felt cathode and its very large surface area. Despite the presence of NH_4^+ in the effluent, 2.5 mg/L of ammonia-nitrogen is still below the

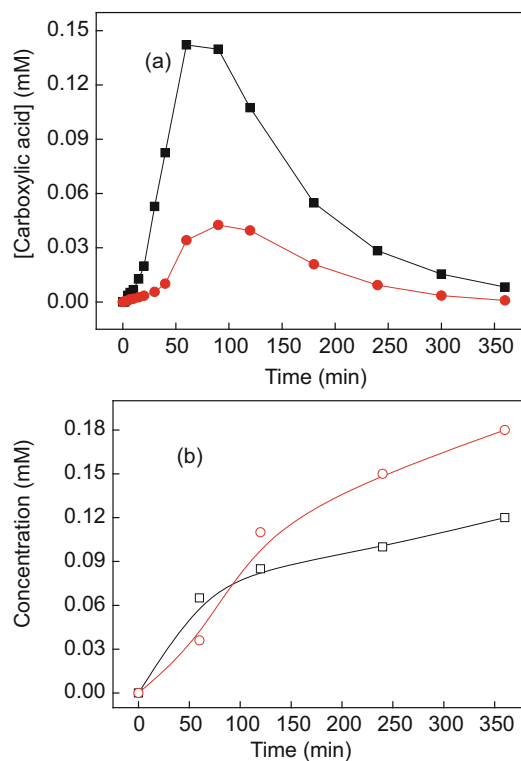


Fig. 6 Evolution of carboxylic acids (a) and inorganic ions (b) detected during the oxidative degradation of 0.2 mM ASP by electro-Fenton process with BDD anode versus carbon-felt cathode ($I = 200$ mA, $[\text{Fe}^{2+}] = 0.2$ mM, $\text{pH}_0 = 3.0$, $[\text{Na}_2\text{SO}_4] = 50$ mM): (a) (filled square) oxalic acid and (filled circle) oxamic acid; (b) (open square) NO_3^- and (open circle) NH_4^+ . Reprinted with permission from [60, 69, 70]. Springer Science + Business Media and Elsevier

first level A criteria (5 mg/L) of the Discharge Standard of Pollutants for Municipal Wastewater Treatment Plant (GB 18918-2002). Therefore, NH_4^+ formed during degradation would be acceptable.

2.6 Toxicity Assessment During Treatment

The toxicity of treated ASs solutions was assessed by Microtox[®] method in terms of inhibition of the bioluminescence of bacteria *V. fischeri*. As can be seen from Fig. 7, the toxicity of all the ASs (ASP, SAC, and SUC) solutions increased significantly and attained the maximum luminescence inhibition peak at 20-min electrolysis [60, 69, 70]. The strong augmentation of toxicity during treatment highlights the formation of cyclic/aromatic oxidation intermediates which are significantly more toxic compared to target pollutants. When the reaction time was extended to 120 min, the toxicity of all the ASs solutions decreased significantly, showing the disappearance of toxic intermediate products. Thereafter, the percentage of bacteria luminescence inhibition in the SUC solution still exhibited a pronounced drop, which reached a minus value at the end of the treatment. It indicates that the SUC effluent even favors the growth of bacteria *V. fischeri*, compared with the blank sample. But for the ASP or SAC solution, the percentage of inhibition changed insignificantly with reaction time ranging from 120 to 360 min. The value of the ASP effluent was minus, which is similar to that of the SUC effluent. Although the inhibition percentage of the SAC effluent is 12.4%, it is acceptable considering the similar value to the original SAC solution (9.0%).

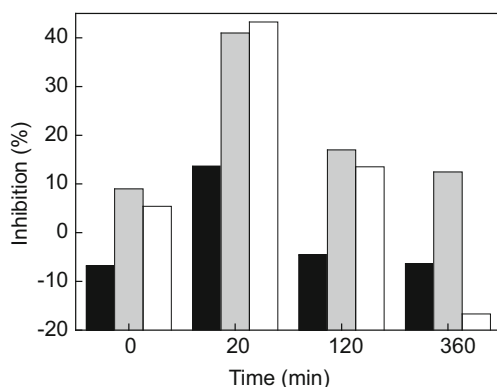


Fig. 7 Evolution of the inhibition of marine bacteria *Vibrio fischeri* luminescence (Microtox method) of ASP (filled bars), SAC (grey bars), and SUC (open bars) during electro-Fenton processes with BDD anode. Experimental conditions: $[\text{ASP}]_0 = [\text{SAC}]_0 = [\text{SUC}]_0 = 0.2$ mM, $[\text{Fe}^{2+}] = 0.2$ mM, $I = 200$ mA, $\text{pH}_0 = 3.0$, $[\text{Na}_2\text{SO}_4] = 50$ mM. Reprinted with permission from [60, 69, 70]. Springer Science + Business Media and Elsevier

3 Conclusions

Electro-Fenton process was proved to be an effective method on the degradation of ASs in aqueous medium. The ASs under study (ASP, SAC, and SUC) were quickly oxidized in about 25 min. When initial ASs concentration was 0.2 mM, Fe^{2+} concentration was 0.2 mM, applied current was 200 mA, pH_0 was 3.0, and Na_2SO_4 concentration was 50 mM, all the treated ASs (ASP, SAC, and SUC) can be totally mineralized in a 360-min reaction by electro-Fenton process using BDD as anode and carbon-felt as cathode. Short-chain carboxylic acids and inorganic ions were generated during the mineralization of ASs but they can be mineralized under longer treatment time. The toxicity of treated ASs solutions was assessed using a Microtox method showing the formation of toxic intermediates during the initial stage of the treatment. The toxic intermediates were effectively destroyed with the progress of the reaction and the percentage of bacteria luminescence inhibition in the effluent was close to or even lower than that in the original solution.

Acknowledgments Lin H. would like to acknowledge the financial support by the Fundamental Research Funds for the Central Universities (No. 2042016kf0060) and Natural Science Foundation of Hubei Province, China (Grant No. 2016CFB112).

References

1. Lin H, Zhang H, Wang X, Wang L, Wu J (2014) Electro-Fenton removal of Orange II in a divided cell: reaction mechanism, degradation pathway and toxicity evolution. *Sep Purif Technol* 122:533–540
2. El-Ghenymy A, Centellas F, Garrido JA, Rodríguez RM, Sirés I, Cabot PL, Brillas E (2014) Decolorization and mineralization of Orange G azo dye solutions by anodic oxidation with a boron-doped diamond anode in divided and undivided tank reactors. *Electrochim Acta* 130:568–576
3. Rodrigo MA, Oturan N, Oturan MA (2014) Electrochemically assisted remediation of pesticides in soils and water: a review. *Chem Rev* 114(17):8720–8745
4. Wu J, Zhang H, Oturan N, Wang Y, Chen L, Oturan MA (2012) Application of response surface methodology to the removal of the antibiotic tetracycline by electrochemical process using carbon-felt cathode and DSA ($\text{Ti}/\text{RuO}_2\text{--IrO}_2$) anode. *Chemosphere* 87(6):614–620
5. Kim I, Tanaka H (2009) Photodegradation characteristics of PPCPs in water with UV treatment. *Environ Int* 35(5):793–802
6. Sirés I, Brillas E, Oturan M, Rodrigo M, Panizza M (2014) Electrochemical advanced oxidation processes: today and tomorrow. A review. *Environ Sci Pollut Res* 21(14):8336–8367
7. Pignatello JJ, Oliveros E, MacKay A (2006) Advanced oxidation processes for organic contaminant destruction based on the Fenton reaction and related chemistry. *Crit Rev Environ Sci Technol* 36(1):1–84
8. Neyens E, Baeyens J (2003) A review of classic Fenton's peroxidation as an advanced oxidation technique. *J Hazard Mater* 98(1–3):33–50
9. Oturan MA, Aaron J-J (2014) Advanced oxidation processes in water/wastewater treatment: principles and applications. A review. *Crit Rev Environ Sci Technol* 44(23):2577–2641

10. Zazo JA, Casas JA, Mohedano AF, Rodriguez JJ (2009) Semicontinuous Fenton oxidation of phenol in aqueous solution. A kinetic study. *Water Res* 43(16):4063–4069
11. Kuo WG (1992) Decolorizing dye wastewater with Fenton's reagent. *Water Res* 26(7):881–886
12. Zhang H, Choi HJ, Huang C-P (2005) Optimization of Fenton process for the treatment of landfill leachate. *J Hazard Mater* 125(1–3):166–174
13. Bautista P, Mohedano AF, Casas JA, Zazo JA, Rodriguez JJ (2008) An overview of the application of Fenton oxidation to industrial wastewaters treatment. *J Chem Technol Biotechnol* 83(10):1323–1338
14. Sun J-H, Sun S-P, Fan M-H, Guo H-Q, Qiao L-P, Sun R-X (2007) A kinetic study on the degradation of p-nitroaniline by Fenton oxidation process. *J Hazard Mater* 148(1–2):172–177
15. Zhang H, Choi HJ, Huang C-P (2006) Treatment of landfill leachate by Fenton's reagent in a continuous stirred tank reactor. *J Hazard Mater* 136(3):618–623
16. Zhang H, Zhang D, Zhou J (2006) Removal of COD from landfill leachate by electro-Fenton method. *J Hazard Mater* 135(1–3):106–111
17. Brillas E, Sirés I, Oturan MA (2009) Electro-Fenton process and related electrochemical technologies based on Fenton's reaction chemistry. *Chem Rev* 109(12):6570–6631
18. Garcia-Segura S, Brillas E (2011) Mineralization of the recalcitrant oxalic and oxamic acids by electrochemical advanced oxidation processes using a boron-doped diamond anode. *Water Res* 45(9):2975–2984
19. Panizza M, Cerisola G (2009) Electro-Fenton degradation of synthetic dyes. *Water Res* 43(2):339–344
20. Yu X, Zhou M, Ren G, Ma L (2015) A novel dual gas diffusion electrodes system for efficient hydrogen peroxide generation used in electro-Fenton. *Chem Eng J* 263:92–100
21. Bedolla-Guzman A, Sirés I, Thiam A, Peralta-Hernández JM, Gutiérrez-Granados S, Brillas E (2016) Application of anodic oxidation, electro-Fenton and UVA photoelectro-Fenton to decolorize and mineralize acidic solutions of reactive yellow 160 azo dye. *Electrochim Acta* 206:307–316
22. Yuan S, Tian M, Cui Y, Lin L, Lu X (2006) Treatment of nitrophenols by cathode reduction and electro-Fenton methods. *J Hazard Mater* 137(1):573–580
23. Nidheesh PV, Gandhimathi R, Sanjini NS (2014) NaHCO₃ enhanced Rhodamine B removal from aqueous solution by graphite-graphite electro Fenton system. *Sep Purif Technol* 132:568–576
24. Pimentel M, Oturan N, Dezotti M, Oturan MA (2008) Phenol degradation by advanced electrochemical oxidation process electro-Fenton using a carbon felt cathode. *Appl Catal B Environ* 83(1–2):140–149
25. Diagne M, Sharma V, Oturan N, Oturan M (2014) Depollution of indigo dye by anodic oxidation and electro-Fenton using B-doped diamond anode. *Environ Chem Lett* 12(1):219–224
26. Olvera-Vargas H, Oturan N, Aravindakumar CT, Paul MMS, Sharma V, Oturan M (2014) Electro-oxidation of the dye azure B: kinetics, mechanism, and by-products. *Environ Sci Pollut Res* 21(14):8379–8386
27. Wang A, Qu J, Ru J, Liu H, Ge J (2005) Mineralization of an azo dye Acid Red 14 by electro-Fenton's reagent using an activated carbon fiber cathode. *Dyes Pigments* 65(3):227–233
28. Wang C-T, Chou W-L, Chung M-H, Kuo Y-M (2010) COD removal from real dyeing wastewater by electro-Fenton technology using an activated carbon fiber cathode. *Desalination* 253(1–3):129–134
29. Lei H, Li H, Li Z, Li Z, Chen K, Zhang X, Wang H (2010) Electro-Fenton degradation of cationic red X-GRL using an activated carbon fiber cathode. *Process Saf Environ Prot* 88(6):431–438
30. Xie YB, Li XZ (2006) Interactive oxidation of photoelectrocatalysis and electro-Fenton for azo dye degradation using TiO₂-Ti mesh and reticulated vitreous carbon electrodes. *Mater Chem Phys* 95(1):39–50

31. Martínez SS, Bahena CL (2009) Chlorbromuron urea herbicide removal by electro-Fenton reaction in aqueous effluents. *Water Res* 43(1):33–40
32. Özcan A, Şahin Y, Savaş Kopal A, Oturan MA (2008) Carbon sponge as a new cathode material for the electro-Fenton process: comparison with carbon felt cathode and application to degradation of synthetic dye basic blue 3 in aqueous medium. *J Electroanal Chem* 616 (1–2):71–78
33. Cruz-González K, Torres-López O, García-León A, Guzmán-Mar JL, Reyes LH, Hernández-Ramírez A, Peralta-Hernández JM (2010) Determination of optimum operating parameters for acid yellow 36 decolorization by electro-Fenton process using BDD cathode. *Chem Eng J* 160 (1):199–206
34. Ganiyu SO, Oturan N, Raffy S, Cretin M, Esmilaire R, van Hullebusch E, Esposito G, Oturan MA (2016) Sub-stoichiometric titanium oxide (Ti_4O_7) as a suitable ceramic anode for electrooxidation of organic pollutants: a case study of kinetics, mineralization and toxicity assessment of amoxicillin. *Water Res* 106:171–182
35. Oturan N, Wu J, Zhang H, Sharma VK, Oturan MA (2013) Electrocatalytic destruction of the antibiotic tetracycline in aqueous medium by electrochemical advanced oxidation processes: effect of electrode materials. *Appl Catal B Environ* 140–141:92–97
36. Lange F, Scheurer M, Brauch H-J (2012) Artificial sweeteners – a recently recognized class of emerging environmental contaminants: a review. *Anal Bioanal Chem* 403(9):2503–2518
37. Kroger M, Meister K, Kava R (2006) Low-calorie sweeteners and other sugar substitutes: a review of the safety issues. *Compr Rev Food Sci Food Saf* 5(2):35–47
38. Richardson SD, Ternes TA (2011) Water analysis: emerging contaminants and current issues. *Anal Chem* 83(12):4614–4648
39. Richardson SD (2010) Environmental mass spectrometry: emerging contaminants and current issues. *Anal Chem* 82(12):4742–4774
40. Loos R, Gawlik BM, Locoro G, Rimaviciute E, Contini S, Bidoglio G (2009) EU-wide survey of polar organic persistent pollutants in European river waters. *Environ Pollut* 157(2):561–568
41. Mead RN, Morgan JB, Avery Jr GB, Kieber RJ, Kirk AM, Skrabal SA, Willey JD (2009) Occurrence of the artificial sweetener sucralose in coastal and marine waters of the United States. *Mar Chem* 116(1–4):13–17
42. Kokotou MG, Asimakopoulos AG, Thomaidis NS (2012) Artificial sweeteners as emerging pollutants in the environment: analytical methodologies and environmental impact. *Anal Methods* 4(10):3057–3070
43. Houtman CJ (2010) Emerging contaminants in surface waters and their relevance for the production of drinking water in Europe. *J Integr Environ Sci* 7(4):271–295
44. Schiffman SS, Gatlin CA (1993) Sweeteners: state of knowledge review. *Neurosci Biobehav Rev* 17(3):313–345
45. Rodero AB, de Souza Rodero L, Azoubel R (2009) Toxicity of sucralose in humans: a review. *Int J Morphol* 27(1):239–244
46. Toth JE, Rickman KA, Venter AR, Kiddle JJ, Mezyk SP (2012) Reaction kinetics and efficiencies for the hydroxyl and sulfate radical based oxidation of artificial sweeteners in water. *J Phys Chem A* 116(40):9819–9824
47. Mawhinney DB, Young RB, Vanderford BJ, Borch T, Snyder SA (2011) Artificial sweetener sucralose in U.S. drinking water systems. *Environ Sci Technol* 45(20):8716–8722
48. Bernardo EC, Fukuta T, Fujita T, Ona EP, Kojima Y, Matsuda H (2006) Enhancement of saccharin removal from aqueous solution by activated carbon adsorption with ultrasonic treatment. *Ultrason Sonochem* 13(1):13–18
49. Sharma V, Oturan M, Kim H (2014) Oxidation of artificial sweetener sucralose by advanced oxidation processes: a review. *Environ Sci Pollut Res* 21(14):8525–8533
50. Soh L, Connors KA, Brooks BW, Zimmerman J (2011) Fate of sucralose through environmental and water treatment processes and impact on plant indicator species. *Environ Sci Technol* 45(4):1363–1369

51. Hoigné J, Bader H (1983) Rate constants of reactions of ozone with organic and inorganic compounds in water – I. *Water Res* 17(2):173–183
52. Hollender J, Zimmermann SG, Koepke S, Krauss M, McArdell CS, Ort C, Singer H, von Gunten U, Siegrist H (2009) Elimination of organic micropollutants in a municipal wastewater treatment plant upgraded with a full-scale post-ozonation followed by sand filtration. *Environ Sci Technol* 43(20):7862–7869
53. Keen OS, Linden KG (2013) Re-Engineering an artificial sweetener: transforming sucralose residuals in water via advanced oxidation. *Environ Sci Technol* 47(13):6799–6805
54. Xu Y, Lin Z, Zhang H (2016) Mineralization of sucralose by UV-based advanced oxidation processes: UV/PDS versus UV/H₂O₂. *Chem Eng J* 285:392–401
55. Calza P, Sakkas VA, Medana C, Vlachou AD, Dal Bello F, Albanis TA (2013) Chemometric assessment and investigation of mechanism involved in photo-Fenton and TiO₂ photocatalytic degradation of the artificial sweetener sucralose in aqueous media. *Appl Catal B Environ* 129:71–79
56. Calza P, Gionco C, Giletta M, Kalaboka M, Sakkas VA, Albanis T, Paganini MC (2017) Assessment of the abatement of acesulfame K using cerium doped ZnO as photocatalyst. *J Hazard Mater* 323:471–477
57. Lee Y, Zimmermann SG, Kieu AT, von Gunten U (2009) Ferrate (Fe(VI)) application for municipal wastewater treatment: a novel process for simultaneous micropollutant oxidation and phosphate removal. *Environ Sci Technol* 43(10):3831–3838
58. Sharma VK, Sohn M, Anquandah GAK, Nesnas N (2012) Kinetics of the oxidation of sucralose and related carbohydrates by ferrate(VI). *Chemosphere* 87(6):644–648
59. Punturat V, Huang K-L (2016) Degradation of acesulfame in aqueous solutions by electro-oxidation. *J Taiwan Inst Chem Eng* 63:286–294
60. Lin H, Wu J, Oturan N, Zhang H, Oturan MA (2016) Degradation of artificial sweetener saccharin in aqueous medium by electrochemically generated hydroxyl radicals. *Environ Sci Pollut Res* 23(5):4442–4453
61. Mhemdi A, Oturan MA, Oturan N, Abdelhédi R, Ammar S (2013) Electrochemical advanced oxidation of 2-chlorobenzoic acid using BDD or Pt anode and carbon felt cathode. *J Electroanal Chem* 709:111–117
62. Panizza M, Cerisola G (2009) Direct and mediated anodic oxidation of organic pollutants. *Chem Rev* 109(12):6541–6569
63. Rodrigo MA, Cañizares P, Sánchez-Carretero A, Sáez C (2010) Use of conductive-diamond electrochemical oxidation for wastewater treatment. *Catal Today* 151(1–2):173–177
64. Barhoumi N, Oturan N, Olvera-Vargas H, Brillas E, Gadri A, Ammar S, Oturan MA (2016) Pyrite as a sustainable catalyst in electro-Fenton process for improving oxidation of sulfamethazine. Kinetics, mechanism and toxicity assessment. *Water Res* 94:52–61
65. Özcan A, Şahin Y, Koparal AS, Oturan MA (2008) Degradation of picloram by the electro-Fenton process. *Environ Sci Technol* 153(1–2):718–727
66. Özcan A, Şahin Y, Koparal AS, Oturan MA (2009) A comparative study on the efficiency of electro-Fenton process in the removal of propham from water. *Appl Catal B Environ* 89(3–4):620–626
67. Oturan MA, Edelahe MC, Oturan N, El Kacemi K, Aaron J-J (2010) Kinetics of oxidative degradation/mineralization pathways of the phenylurea herbicides diuron, monuron and fenuron in water during application of the electro-Fenton process. *Appl Catal B Environ* 97(1–2):82–89
68. Dirany A, Sirés I, Oturan N, Özcan A, Oturan MA (2012) Electrochemical treatment of the antibiotic sulfachloropyridazine: kinetics, reaction pathways, and toxicity evolution. *Environ Sci Technol* 46(7):4074–4082
69. Lin H, Oturan N, Wu J, Zhang H, Oturan MA (2017) Cold incineration of sucralose in aqueous solution by electro-Fenton process. *Sep Purif Technol* 173:218–225

70. Lin H, Oturan N, Wu J, Sharma VK, Zhang H, Oturan MA (2017) Removal of artificial sweetener aspartame from aqueous media by electrochemical advanced oxidation processes. *Chemosphere* 167:220–227
71. Hamza M, Abdelhedi R, Brillas E, Sirés I (2009) Comparative electrochemical degradation of the triphenylmethane dye methyl violet with boron-doped diamond and Pt anodes. *J Electroanal Chem* 627(1–2):41–50
72. Skoumal M, Arias C, Cabot PL, Centellas F, Garrido JA, Rodríguez RM, Brillas E (2008) Mineralization of the biocide chloroxyleneol by electrochemical advanced oxidation processes. *Chemosphere* 71(9):1718–1729
73. Oturan N, Hamza M, Ammar S, Abdelhédi R, Oturan MA (2011) Oxidation/mineralization of 2-nitrophenol in aqueous medium by electrochemical advanced oxidation processes using Pt/carbon-felt and BDD/carbon-felt cells. *J Electroanal Chem* 661(1):66–71
74. Özcan A, Şahin Y, Oturan MA (2008) Removal of protham from water by using electro-Fenton technology: kinetics and mechanism. *Chemosphere* 73(5):737–744
75. Sirés I, Arias C, Cabot PL, Centellas F, Garrido JA, Rodríguez RM, Brillas E (2007) Degradation of clofibrac acid in acidic aqueous medium by electro-Fenton and photoelectro-Fenton. *Chemosphere* 66(9):1660–1669
76. Li M, Feng C, Zhang Z, Sugiura N (2009) Efficient electrochemical reduction of nitrate to nitrogen using Ti/IrO₂-Pt anode and different cathodes. *Electrochim Acta* 54(20):4600–4606

Soil Remediation by Electro-Fenton Process

Emmanuel Mousset, Clément Trellu, Nihal Oturan, Manuel A. Rodrigo, and Mehmet A. Oturan

Abstract Soil remediation by electro-Fenton (EF) process has been recently proposed in literature. Being applied for solution treatment, EF is mainly combined with soil washing (SW)/soil flushing (SF) separation techniques to remove the organic pollutants. The main criteria influencing the combined process have been identified as (1) operating parameters (electrode materials, current density, and catalyst (Fe^{2+}) concentration), (2) the matrix composition (nature and dose of extracting agent, pH, complexity of SW/SF solutions), and (3) the environmental impact (acute ecotoxicity and biodegradability of effluent as well as impact on soil microbial activity). The influence of these parameters on the SW/EF and SF/EF integrated processes has been reviewed. Energy consumption calculations have been finally considered as it constitutes the main source of operating cost in EF process.

Keywords Bioassays, Cyclodextrins, Electrode materials, Hydrocarbons, Soil washing, Surfactant

Contents

1	Introduction	400
2	Influence of Operating Parameters	403

E. Mousset (✉)

Laboratoire Réactions et Génie des Procédés, CNRS – Université de Lorraine (UMR 7274),
1 rue Grandville, Nancy, Cedex 54001, France
e-mail: emmanuel.mousset@univ-lorraine.fr

C. Trellu, N. Oturan, and M.A. Oturan

Université Paris-Est, Laboratoire Géomatériaux et Environnement (EA 4508), UPEM, 77454
Marne-la-Vallée, France

M.A. Rodrigo

Department of Chemical Engineering, University of Castilla-LaMancha, Enrique Costa
Novella Building, Campus Universitario s/n, 13071 Ciudad Real, Spain

M. Zhou et al. (eds.), *Electro-Fenton Process: New Trends and Scale-Up*,
Hdb Env Chem (2018) 61: 399–424, DOI 10.1007/698_2017_38,

© Springer Nature Singapore Pte Ltd. 2017, Published online: 24 May 2017

2.1	Influence of Electrode Materials	403
2.2	Influence of Current Density	406
2.3	Influence of Catalyst (Fe^{2+}) Concentration	408
3	Effect of the Matrix	409
3.1	Influence of Nature of Extracting Agent and Possibility of Recovery	410
3.2	Influence of pH	412
3.3	Synthetic vs. Real Effluent	413
4	Impacts on Ecotoxicity, Biodegradability, and Soil Respirometry	415
5	Energy Considerations and Concluding Remarks	419
	References	421

1 Introduction

Nowadays, soil pollution is a topic of the major importance not only because of the direct consequences of this pollution on ecosystems but also because it may lead to the pollution of supply water reservoirs and, consequently, prevent their use. This is especially important in regions that traditionally lack water and in areas where periodic droughts (now intensified with the climate change) make water a very valuable resource, which may even limit its economic and social subsistence. One of the types of pollution, which is gaining more and more attention in the scientific community because of its relevance, is the pollution with organic compounds, in particular with non-biodegradable anthropogenic organic species such as solvents, hydrocarbons, and pesticides. It is not a simple problem because these species can have very different characteristics in terms of hazardousness, biodegradability, solubility in water, and volatility, and, hence, there is not a unique efficient treatment that can be successfully applied for their depletion [1–3].

Instead, there are many types of competing technologies that can be applied to solve this important problem, and, nowadays, scientists are trying to shed light on the choice of the best for each type of pollutant and soil. Some of them, like soil washing (SW) or vapor extraction, transfer the pollutant from the soil to a different phase (liquid or gas), which is later treated *ex situ* in a more efficient way, removing rapidly the pollution from soil and avoiding its dispersion. They are very important, in fact, key technologies in the solution of the problem, because treatment of a large volume of soil affected by diffuse pollution is more difficult and, overall, more expensive than the treatment of a much lower volume of soil highly polluted with the same contaminant.

Regarding the transport of pollution from soil to a liquid, there are two main technologies: SW (*ex situ*) or soil flushing (SF) (*in situ*). The first needs the excavation of the soil and its transport to a washing unit, in which pollutants are removed in the best operation conditions by selecting the optimal washing fluid composition and volume, mixing rate, temperature, and contact time [2, 4, 5]. It may attain a very good removal of pollutants from the chemical point of view, but other soil characteristics like compaction are dramatically modified during this treatment, and special care should be taken after the treatment to try to come

back to the pristine properties, once the soil is cleaned and placed again in the zone that it occupied before the pollution event. The composition of the SW fluid is rather important and in case of removal of low-solubility pollutants, the addition of extracting agents is key to extract them in efficient conditions [1, 2, 6]. Treatment of the SW wastes produced becomes a very important point to have an integrated solution to the problem, because it typically consists of highly loaded wastewater containing the soil pollutant, extracting agents, and many other species extracted from soil. Selective removal of pollutant in order to try to regenerate the SW fluid for reuse is the optimum solution looked for, because it may lead to a very efficient treatment technology from the viewpoint of sustainability and economy.

The other alternative consists of flushing a fluid throughout the soil to drag the pollutants contained and to collect this fluid into a special zone, where the flushing fluid is pumped to a subsequent liquid treatment [7–9]. This alternative modifies much less importantly soil characteristics, but it is more difficult to select the best extraction operation conditions because soil remains in its position during the treatment. In case of high permeability soil, the flushing fluid is pumped and collected directly without further requirements, using the gradient of hydrostatic pressure (pump and treat technology) as driving force for the transport of fluid. For low-permeability soils, this driving force is not efficient, and, here, the application of an electric field between pairs of anode-cathode may activate more complex transport processes such as electroosmosis, electromigration, and electrophoresis, commonly known as electrokinetic treatment. As in the SW technologies, these processes can be combined with an efficient composition of flushing fluid, which helps to drag efficiently pollutants that cannot be dragged directly by water. At this point, extracting agents may play a very important role as in the SW processes, although in SF, interactions are much more complex. These treatments also produce a polluted flushing fluid which should be treated once produced and the ideal final point of this treatment is to remove pollutants without affecting extracting agents and other possible additives in order to regenerate the flushing fluid and recycle it to the treatment.

There are many technologies that can be used to treat the SW and SF wastes. Initially, biological process should be the primary election because of their lower cost. However, it is important to remind that SW and SF are applied when in situ bioremediation technologies are not efficient and this means that pollutant should be hardly removed by microorganisms either in soil or in a liquid waste. In this context, advanced physicochemical technologies become the target for the treatment of these types of wastes. Among them, electrochemical advanced oxidation processes (EAOPs) are very promising [10], and one of them is going to be widely described in this chapter, i.e., the electro-Fenton (EF) process. In parallel, there have been many work carried out in the recent years in the development of other EAOPs such as anodic oxidation, photoelectrolysis, and sonoelectrolysis [11–15]. EF has the advantages (1) to generate in situ Fenton's reagent leading to the formation of $\cdot\text{OH}$, (2) to be less dependent on the mass transport of the pollutants thanks to homogeneous catalysis, (3) to avoid sludge formation and $\cdot\text{OH}$ wasting reactions thanks to controlled generation of H_2O_2 and Fe^{2+} , and (4) to favor some selective oxidation as discussed later in this chapter.

Table 1 Published studies on the EF treatment of contaminated soil

Kind of process SW/EF	SW/SF		EF		Studied parameters	Ref.
	Nature of soil	Nature of SW/SF solution	Cathode (surface)	Anode (surface)		
SW/EF	–	Synthetic solution ^a	Carbon felt (60 cm ²)	Pt grid (3 cm diameter, 4.5 cm height)	Current density	[20]
SW/EF	–	Synthetic solution ^b	Carbon felt (150 cm ²)	Pt grid (3 cm diameter, 5 cm height)	[Fe ²⁺], current density, biodegradability, and toxicity of solution	[21]
SW/EF	–	Synthetic solution ^c	Carbon felt (150 cm ²)	Pt grid (3 cm diameter, 5 cm height), DSA (40 cm ²), BDD (40 cm ²)	Anode materials, current density, biodegradability, and toxicity of solution	[22]
SW/EF	Spiked soil; real uncontaminated soil ^d	Synthetic and real SW solution ^e	Carbon felt (10 cm ²)	Pt sheet (1 cm ²)	Current density, toxicity of solution	[23]
SW/EF	Spiked soil; kaolinite clay or real uncontaminated soil	Real SW solution ^f	Graphite (1.27 cm ²) or stainless steel (3.14 cm ²)	Graphite (1.27 cm ²) or stainless steel (3.14 cm ²)	Electrodes materials, initial pollutant concentration	[18]
SW/EF	Historically contaminated soil ^g	Real SW solution ^h	Carbon felt (150 cm ²)	Pt grid (3 cm diameter, 5 cm height)	Number of SW cycles; pH, soil respirometry	[16]
SF/EF	Historically contaminated soil ⁱ	Real SW solution ^j	Carbon felt (150 cm ²)	BDD (40 cm ²)	pH, biodegradability, and toxicity of solution	[9]

^aBeta-cyclodextrin (BCD) (1 mM) in 150 mL undivided cell, pH 3, [Na₂SO₄] = 50 mM, [Fe²⁺] = 0.2 mM, current density: 1.0–4.2 mA cm⁻²

^bTween 80 (0.75 g L⁻¹) and HPCD (10 g L⁻¹) in 400 mL undivided cell, pH 3, [Na₂SO₄] = 150 mM, [Fe²⁺] = 0.05–10 mM, current density: 3.3–13.3 mA cm⁻²

^cHPCD (9 g L⁻¹) in 400 mL undivided cell, pH 3, [Na₂SO₄] = 150 mM, [Fe²⁺] = 0.2 mM, current density: 3.3–13.3 mA cm⁻²

^dClay: 22.6%; silt, 23%; sand, 54.4%. The soil also had these additional characteristics: pH_{water}: 8.3; organic matter content, 6.5%; cation exchange capacity (CEC), 23.5 meq kg⁻¹

^eHPCD (5 mM) in 125 mL undivided cell, pH 3, [Fe²⁺] = 0.5 mM, current density: 4.0–20.0 mA cm⁻²

^f150 mL undivided cell, cell potential: 5 V, pH 3, Na₂SO₄ (100 mM), Fe²⁺ = 0.2 mM

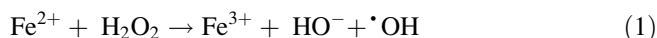
^gClay (< 2 mm): 19.7%; fine silt (2–20 mm), 23.3%; coarse silt (20–50 mm), 7.5%; fine sand (50–200 mm), 12.3%; coarse sand (200–2,000 mm), 37.1%. The soil also had these additional characteristics: pH_{water}: 8.3; organic matter content, 4.7%; CEC, 203 meq kg⁻¹; saturation of clay-humic complex, 100%

^hTween 80 (7.5 g L⁻¹) or HPCD (7.5 g L⁻¹) in 400 mL undivided cell, no pH adjustment, [Na₂SO₄] = 150 mM, no Fe²⁺ added, current density: 6.7 mA cm⁻²

ⁱSandy loam soil with sand: 60%; loam, 25%; clay, 15%. Additional soil characteristics are as follows: pH_(H2O): 8.4; organic matter content, 44.6 g kg⁻¹ dry weight; CEC, 15.7 cmol kg⁻¹ dry weight

^jTween 80 (11 g L⁻¹) in 400 mL undivided cell, no pH adjustment, [Na₂SO₄] = 150 mM, no Fe²⁺ added, current density: 6.7 mA cm⁻²

EF treatment has been conventionally applied *ex situ* for SW/SF solutions [1, 2, 16] or a mixture of solutions with solid particles [17, 18], by generating hydroxyl radicals ($\cdot\text{OH}$) through Fenton reaction in bulk solution [19] (Eq. 1):



A synthetic table (Table 1) summarizes the different research articles studying the combination between SW/SF and EF treatment for soil remediation.

All the SW/EF and SF/EF studies have been focused on hydrophobic organic contaminants (HOCs) such as petroleum hydrocarbons [9], polycyclic aromatic hydrocarbons (PAHs) including phenanthrene (PHE) and the 16 PAHs from US Environmental Protection Agency (USEPA) list [16, 18, 21, 22], pesticides [pentachlorophenol (PCP)] [23], explosives [trinitrotoluene (TNT)] [20], and dyes (Lissamine Green B) [18].

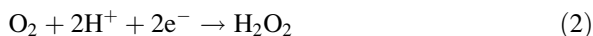
Three main criteria have been identified to be crucial in the cost-effectiveness of EF treatment of contaminated soil (Table 1): (1) the influence of operating parameters, (2) the matrix composition, and (3) the environmental impact. The significance of these parameters is discussed in the following sections.

2 Influence of Operating Parameters

In EF process, the main operating parameters playing a role at laboratory scale are (1) the nature of electrode materials, (2) the applied current density, and (3) the catalyst (ferrous iron) concentration, whose respective impacts on SW effluent degradation and mineralization efficiency are discussed in the three following subsections.

2.1 Influence of Electrode Materials

The electrode materials play a major role in EF process. According to the cathode materials employed, hydrogen peroxide (H_2O_2) can be electro-generated through the two-electron reduction of dissolved O_2 (Eq. 2) along with simultaneous ferrous ion (Fe^{2+}) regeneration through Fe^{3+} reduction (Eq. 3). Both reagents react to form hydroxyl radicals ($\cdot\text{OH}$) in bulk solution through the Fenton reaction (Eq. 1).



Carbon-based materials are preferentially employed for their high hydrogen (H_2) evolution overvoltage and their low catalytic activity for H_2O_2 decomposition.

Carbon felt has especially shown good performance for its high specific surface area and its mesoporous structure, facilitating the O₂ diffusion and its subsequent adsorption [24, 25]. This material was therefore used in EF treatment of SW solutions [16, 21, 22]. However, the use of porous carbon sponge cathode has shown to easily adsorb HOCs such as humic substances [26] – a fraction of soil organic matter – that are typically present in real SW solutions. Hydroxyl radicals produced homogeneously in the electrochemical cell could also oxidize these substances into more hydrophilic by-products leading to a rebound effect of the total organic carbon in bulk solution. To avoid this phenomena, non-porous cathode such as graphite or stainless steel could be used [18], though the H₂O₂ electro-generation at their surface is poor [27]. In that case, the amount of [•]OH generated through the Fenton reaction is limited.

Alternatively, adequate anode materials can be combined to such cathode materials. Two kinds of anode materials have been used in EAOPs: (1) active anodes such as platinum (Pt), carbon (e.g., graphite), and mixed metal oxides [e.g., dimensionally stable anode (DSA)] and (2) non-active anodes such as lead dioxide (PbO₂), doped tin dioxide (e.g., F-SnO₂ and Sb-SnO₂), and boron-doped diamond (BDD). The first category is dedicated to materials that have a low O₂ evolution overpotential, e.g., around 1.5 V vs. SHE with DSA, 1.6 V vs. SHE with Pt, and 1.7 V vs. SHE with graphite. In these conditions, [•]OH are chemisorbed at the anode surface, being barely available for pollutant oxidation. Contrastingly, the non-active anodes exhibit a high O₂ evolution overpotential, e.g., 1.9 V vs. SHE with SnO₂ and PbO₂ and 2.3 V vs. SHE with BDD. As a consequence, [•]OH are generated in a large potential window and are physisorbed at the anode surface, resulting in the mineralization of the organic pollutants. Unlike [•]OH that are produced from the Fenton's reaction in the bulk, these [•]OH are generated in a heterogeneous way on the anode surface. Therefore, their reaction is limited to the anode surface.

The influence of anode materials, i.e., Pt, DSA, and BDD, has been studied in the EF treatment of SW solutions containing PHE as representative pollutant and hydroxypropyl-beta-cyclodextrin (HPCD) as representative washing agent (Fig. 1). The kinetics rates of PHE and HPCD degradation are displayed in Fig. 1a.

Interestingly, the pollutant is more quickly degraded with active anode such as Pt and DSA than with BDD anode. Inversely, the extracting agent is faster degraded with BDD than with Pt and DSA. This difference is attributed to the ways of oxidation of [•]OH from the bulk in the presence of cyclodextrin (Sect. 3.1) and the nature of electrode material as explained below. This trend further highlights the competitive oxidation between PHE and HPCD, which can be further underlined by the degradation kinetics ratio between the pollutant and the washing agent. It was noticed that the HPCD degradation rates were inversely correlated to the pollutant decay rates, i.e., when the kinetics rate of HPCD increased, the kinetics rate of PHE decreased inversely. Moreover, PHE was quicker degraded than HPCD whatever the anode employed, which is interesting if a recirculation loop is considered by reusing the solubilizing agent present in the partially oxidized SW solution as discussed in Sect. 3.1.

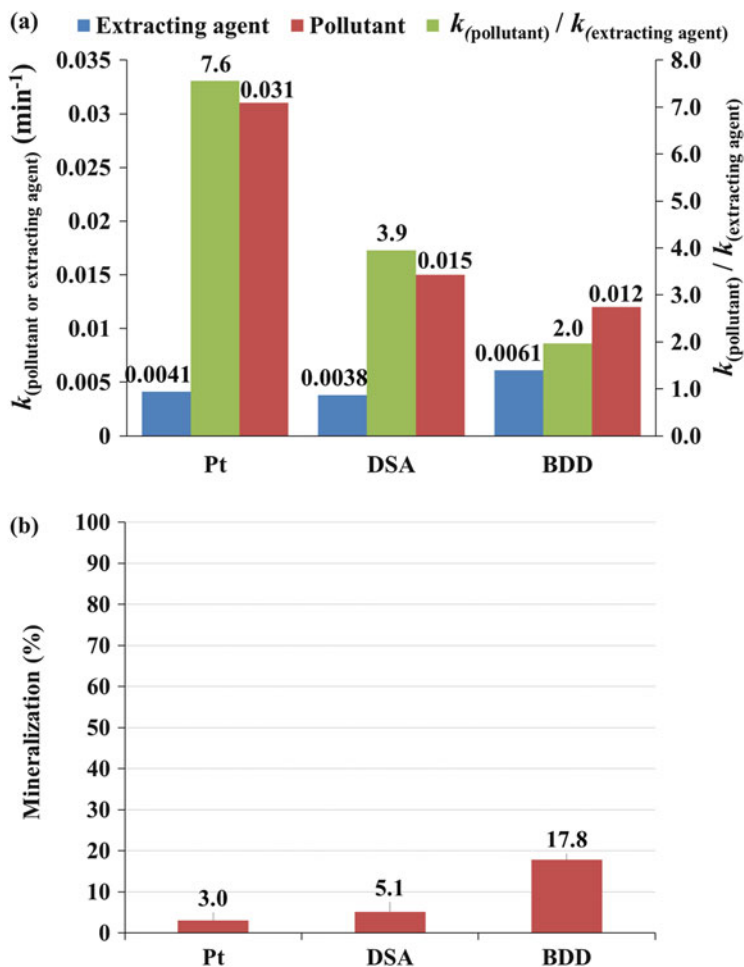
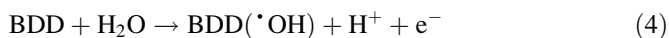
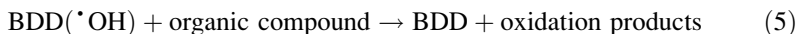


Fig. 1 Influence of anode materials during EF treatment of SW solution: (a) kinetics rate constant of pollutant (PHE) and extracting agent (HPCD) degradation and (b) mineralization. *Operating conditions:* current density, 6.7 mA cm^{-2} ; catalyst concentration, $[\text{Fe}^{2+}] = 0.2 \text{ mM}$; treatment time in mineralization graph (b), 4 h. (adapted with permission from [21, 22]) (Copyright 2014 Elsevier)

Looking at the comparison of mineralization power (Fig. 1b), the superiority of BDD is clear as compared to Pt and DSA. It was attributed to the high amount of heterogeneous $\cdot\text{OH}$ formed at BDD surface and their availability (physisorption) and the subsequent oxidation of organic compounds (Eqs. 4 and 5) [28]:



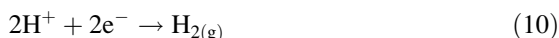
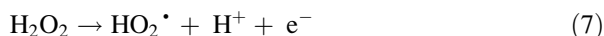
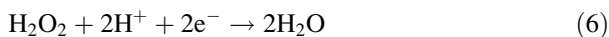


Thus, the involvement of two sources of $\cdot\text{OH}$ in the EF process using BDD anode implies higher degradation yield of extracting agent that predominate in washing solution as well as higher mineralization degree.

2.2 Influence of Current Density

The current density is another important parameter that plays a role on the electrochemical reaction rates and on the yield of electro-generated oxidants. Increasing the current density amplifies the in situ generation of Fenton reagent (H_2O_2 and Fe^{2+}) at the cathode (Eqs. 2 and 3) and generation rate of heterogeneous hydroxyl radical ($\text{M}(\cdot\text{OH})$) at the anode. In this way, the current density is usually determined by normalizing the current intensity with the cathode surface area that is the working electrode in traditional EF process in which an active anode is employed as counter electrode. In the aim at comparing all the EF processes whatever the anode employed (active or non-active), the cathode area was considered in the current density values given in this chapter.

Figure 2a illustrates an increase of the kinetics rates of the washing agent when the current density increased from 3.3 to 6.7 mA cm^{-2} . In this range of current density, the kinetics rates of the pollutant remain constant, the oxidation being mainly focused on the solubilizing agent. Besides, raising the current density until 13.3 mA cm^{-2} could not improve the degradation efficiency of both pollutant and extracting agent. This is due to the increase of reaction rate of parasitic reactions such as the H_2O_2 decomposition at the cathode (Eq. 6), at the anode (Eqs. 7 and 8), and in a lesser extent in bulk solution (Eq. 9) as well as hydrogen (H_2) formation (Eq. 10):



These reactions are in competition with H_2O_2 electro-generation (Eq. 2) at the cathode.

In addition, the slight decrease of the degradation kinetics ratio between the pollutant and the washing agent at high current intensity indicates that current intensity may modify oxidation mechanisms in the electrochemical cell. For example, mediated oxidation is favored at high current intensity due to the generation of other strong oxidants such as persulfates, sulfate radicals, or ozone [10].

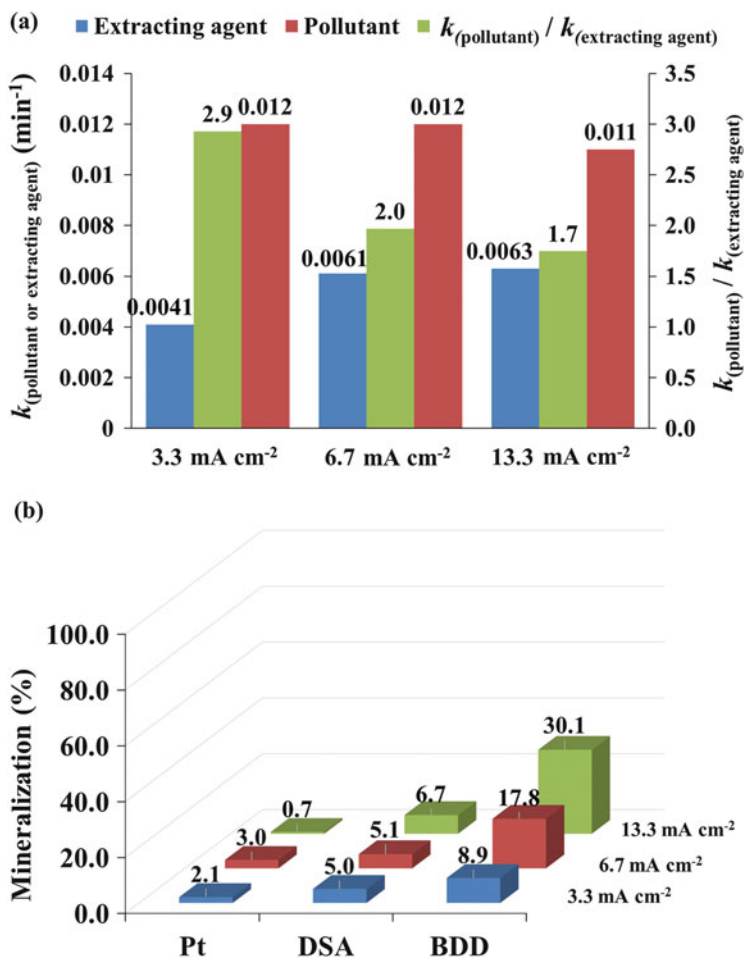


Fig. 2 Influence of current density during EF treatment of SW solution: (a) kinetics rate constant of pollutant (PHE) and extracting agent (HPCD) degradation and (b) mineralization. *Operating conditions:* catalyst concentration, [Fe²⁺] = 0.2 mM; anode material in kinetic constants graph (a), BDD; treatment time in mineralization graph (b), 4 h (adapted with permission from [21, 22]) (Copyright 2014 Elsevier)

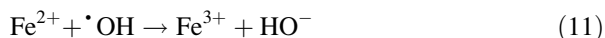
Considering the mineralization (Fig. 2b), the yields were increasing when the current density increased from 3.3 to 13.3 mA cm⁻² with BDD anode material, while the yields remained quasi-constant with Pt and DSA anodes (considering standard deviations around ±1.4%). Still, BDD depicted much higher mineralization performance due to the paired electro-catalysis process.

2.3 Influence of Catalyst (Fe^{2+}) Concentration

Ferrous ion acts as a catalyst in the EF process and is therefore added at a catalytic amount in the solution.

By varying the concentration of Fe^{2+} from 0.05 to 10 mM in a synthetic SW solution containing PHE and HPCD (Fig. 3a), the decay rate of the pollutant increased until a ferrous ion concentration of 0.2 mM. Increasing the catalyst concentration makes increase the amount of hydroxyl radicals formed through the Fenton reaction (Eq. 1).

Remarkably, higher Fe^{2+} concentration did not improve the kinetics rate of the pollutant degradation. It can be explained by the progressive inhibition of the oxidant generation, because of the greater extent of the waste reaction between Fe^{2+} and $\cdot OH$ (Eq. 11):



In these conditions, 0.2 mM was defined as the optimal Fe^{2+} concentration, which is in the range of concentration (0.1–0.2 mM) usually employed in EF processes at lab scale in batch experiments [18, 21, 22, 29].

The difference of the presence or absence of Fe^{2+} has been tested by Rosales et al. [18] in a soil slurry batch reactor. It is noticed that the dye decoloration rates was 1.35-fold higher with ferrous ion (2.3 h^{-1}) than without addition of Fe^{2+} (1.7 h^{-1}) by using graphite material as cathode and anode. It highlights the high oxidation efficiency of $\cdot OH$ formed by Fenton reaction (Eq. 1) as compared to the direct electro-oxidation treatment. In addition, the comparison between a BDD anode treatment in synthetic SW solution without the addition of Fe^{2+} – namely, anodic oxidation (AO) – and the mineralization efficiency of EF is displayed in Fig. 3b. By treating the same synthetic SW solution (PHE and HPCD), EF process gave 1.3 times higher efficiency as compared to AO process, and the mineralization yield was higher whatever the applied current density. This again emphasized the superiority of EF due to the double source of $\cdot OH$ production, by the additional presence of Fe^{2+} leading to $\cdot OH$ generation in the bulk.

More excitingly, the combination between SW/SF and EF treatment remains interesting since the presence of iron extracted from soil in SW/SF solution can be used as an iron source for the electrochemical treatment. This was evidenced by treating real SF solution [9] and real SW solution [16] by EF process without any addition of iron, since dissolved iron was present initially in the SW/SF solution at a concentration ranging from 0.02 to 0.06 mM. These amounts of concentration are sufficient to involve the Fenton reaction (Eq. 1). Thus, this parameter also strongly depends on the nature of the soil treated (particularly the concentration and availability of iron in the soil).

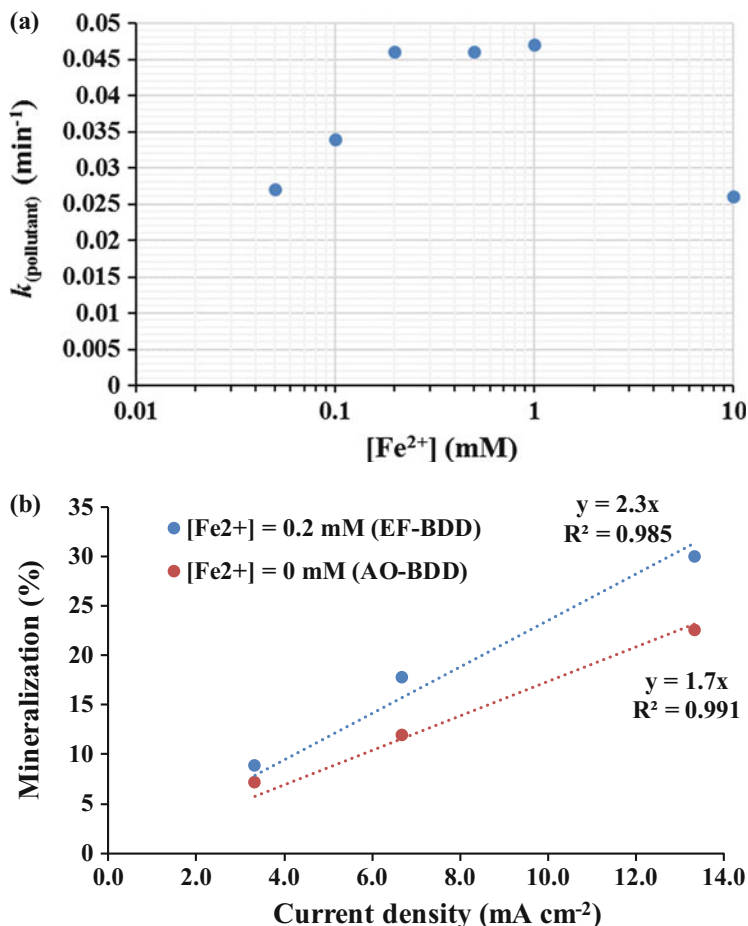


Fig. 3 Influence of ferrous ion concentration during EF treatment of SW solution: (a) kinetics rate constant of pollutant (PHE) degradation and (b) mineralization yield (adapted with permission from [21, 22]) (Copyright 2014 Elsevier)

3 Effect of the Matrix

Apart from the EF parameters, the matrix composition has a great influence on the process efficiency, especially the washing agent, the pH of SW/SF solution, and the degree of complexity of the SW/SF solution (presence of soil organic matter, inorganic ions, etc.). The impacts of those parameters are discussed hereafter.

3.1 *Influence of Nature of Extracting Agent and Possibility of Recovery*

In SW- and SF-pollution transfer, technologies extracting agents are used to enhance the pollutant extraction by a two-step mechanism: (1) the desorption of the contaminant from the binding site in the solid matrix and (2) the elution from the solid phase into the extraction fluid [2, 6]. Several families of agents have been used in literature in SW/SF techniques such as surfactants, cyclodextrins, co-solvents, dissolved organic matter, deoxyribonucleic acid, chelating agents, fatty acid methyl esters, and vegetable oil [2]. In the case of surfactants, the pollutant extraction occurs when the agent is added in solution at concentrations higher than their critical micelle concentration (CMC) [30]. There are several criteria that prevail in the selection of these agents: low or even absence of CMC, low adsorption onto soil, and high pollutant extraction efficiency.

Nonionic surfactants correspond to these criteria, especially Tween 80 that possesses higher PAHs extraction capacity than Brij 35, Tergitol NP10, Tween 20, Tyloxapol, Igepal CA-720, and Triton X-100 [31, 32]. Tween 80 is therefore often selected as representative surfactant in literature, especially for combination with an electrochemical treatment [4, 15, 16, 21, 31, 33, 34]. Surfactants are amphiphilic molecules whose hydrophilic heads constitute a first barrier between $\cdot\text{OH}$ and the pollutant (HOC) (Fig. 4a). Before the oxidation of pollutant, the surfactant needs to be degraded first as it has been observed that the size of micelles decreases with treatment time [35]. In addition, the ratio between the pollutant and the surfactant is key in the size of these micelles and hence on the time course of a later treatment technology. The higher the dose of surfactant, the lower the size of the micelles and the higher is the resulting organic load in the SW fluid [35]. Therefore, the soil/liquid ratio determines not only the concentration of pollutant in the washing/flushing fluid but also the speciation that is particularly important in terms of the occurrence of micelles. Furthermore, steric hindrance of large micelles could prevent direct oxidation of micelles on the BDD anode surface [12], which could underscore the significant oxidation role of homogeneous $\cdot\text{OH}$ formed by Fenton reaction (Eq. 1) in bulk solution as well as other oxidant species leading to mediated oxidation of organic compounds in the bulk.

Alternatively, cyclodextrins have been used as washing agent since they do not have CMC and they do not form high viscosity emulsions [23]. These semi-natural molecules have a toroidal shape that allows trapping the pollutant inside their cavity (Fig. 4b). On the contrary to surfactant, in the case of HPCD, the HOC is trapped into the hydrophobic cavity, and the formation of a ternary complex between Fe^{2+} , pollutant (HOC), and HPCD ($\text{Fe}^{2+}:\text{HPCD}:\text{HOC}$) – evidenced by UV spectrophotometry measurements (formation constant of 56 mM^{-1} ; [21]) – allows the $\cdot\text{OH}$ to directly react with the pollutant (Eqs. 12 and 13) [21, 23]:

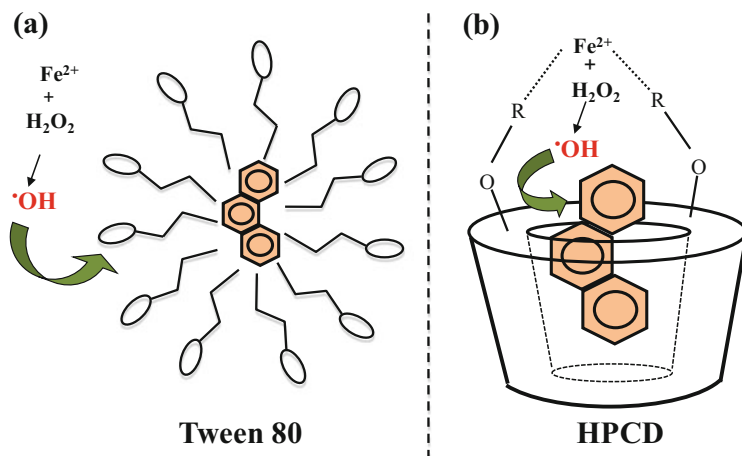
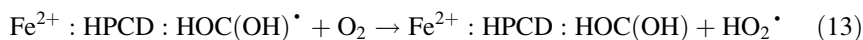
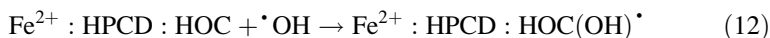


Fig. 4 Schematic representation of two different ways of $\cdot\text{OH}$ oxidative degradation of hydrophobic organic pollutant in the presence of (a) surfactant (Tween 80) or (b) cyclodextrin (HPCD) in aqueous solution (adapted with permission from [21]) (Copyright 2014 Elsevier)



The binding between Fe^{2+} and the cyclodextrin depends on the functional group. In the case of HPCD, Fe^{2+} is likely coordinated with the hydroxyl group present on the rim of the molecule [36].

Thus, two different mechanisms have been highlighted according to the way to form cyclodextrin/HOC and surfactant/HOC complexes [21]. However, when considering a treatment of SW/SF solutions, the recycling abilities of the extracting agent are another important criterion to take into account aiming at reducing both the operating cost of reagents for the SW/SF step and energy requirements during the EF treatment of SW solution. Therefore, a synthetic solution containing Tween 80 (0.75 g L^{-1}) or HPCD (10 g L^{-1}) and PHE at the same initial concentration (17 mg L^{-1}) has been treated by EF using a carbon felt cathode (150 cm^2) and a Pt grid anode in a 400 mL undivided cell (Fig. 5) [21]. After 4 h of treatment, 95% of PHE was degraded with a pseudo-first order rate constant of 0.013 min^{-1} , while 50% of Tween 80 was removed. In the case of cyclodextrin, the pollutant was completely removed after 4 h at a rate of 0.026 min^{-1} though HPCD was barely degraded at a 10% yield. The two times higher degradation rate of PHE in the presence of HPCD could be explained by the ternary complex as abovementioned. However, it is important to note that 13.3 times higher HPCD concentration was required to solubilize the same amount of PHE as compared to Tween 80. Therefore, after the removal of more than 90% of PHE, 1 g L^{-1} of HPCD was removed, while 0.375 g L^{-1} of Tween 80 was only degraded. Thus, considering the amount of extracting agent removed per quantity of pollutant degraded, Tween 80 has better

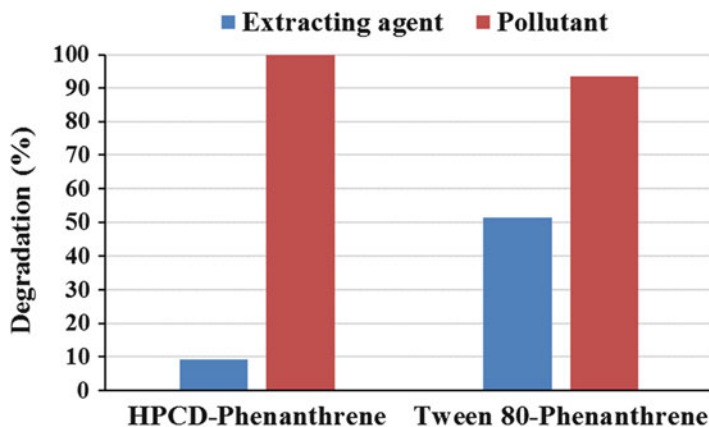


Fig. 5 Influence of nature of extracting agent [HPCD (10 g L^{-1}) or Tween 80 (0.75 g L^{-1})] on pollutant [PHE (17 mg L^{-1})] degradation. *Operating conditions:* current density, 13.3 mA cm^{-2} ; catalyst concentration, $[\text{Fe}^{2+}] = 0.05 \text{ mM}$; anode material, Pt (Reprinted with permission from [21]) (Copyright 2014 Elsevier)

recycling abilities compared to HPCD, because of the less solubilization power of the cyclodextrin.

All these statements therefore emphasize the importance of two main criteria in the recycling abilities of extracting agent: (1) the shape of extracting agents and their functional groups, i.e., the toroidal shape of cyclodextrins allowing making selective the $\cdot\text{OH}$ degradation unlike the micelles shape, and (2) the concentration of the washing agent required to solubilize the pollutant, i.e., more than ten times with cyclodextrins as compared to surfactants. It is also important to mention that the oxidation by-products and the extracting agent would be in contact with the soil during the reuse of the agent, which means that the solution pH and the ecotoxicity of soil and solution are other parameters to monitor as discussed in Sects. 3.2 and 4, respectively.

3.2 Influence of pH

The pH of solution is determinant in processes involving Fenton reaction, due mainly to the pH dependency of iron ion species. At pH below 2, there is formation of peroxonium ion (H_3O_2^+) that is less reactive with Fe^{2+} which makes a decrease in the rate of Fenton's reaction [19]. At pH higher than 4, the precipitation of ferric hydroxide ($\text{Fe}(\text{OH})_3$) occurs [29]. Thus, most of the EF studies are performed at an optimal pH of 3 [18, 20–22]. However, adjusting the pH requires acid reagents that increase the operating costs. That is why some efforts have been devoted to operate at circumneutral pH. Interestingly, in an experiment at an initial pH of 6 of PHE polluted-SW HPCD solution, the pollutant removal rate (0.026 min^{-1}) was very

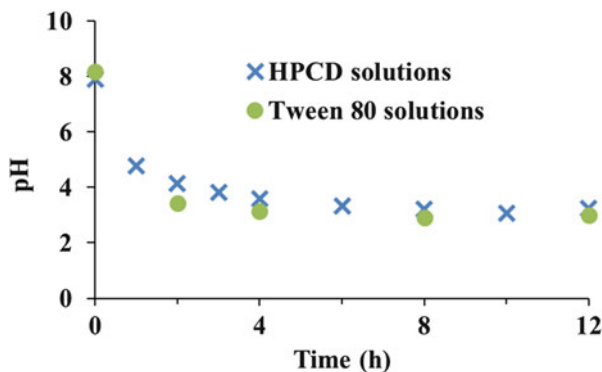


Fig. 6 Evolution of solution pH during EF treatment of SW solutions containing either HPCD or Tween 80 as washing agent. *Operating conditions:* current density, 6.7 mA cm^{-2} ; anode material, BDD

similar to the one obtained at pH 3 (0.027 min^{-1}) [21]. Additionally, when degrading by EF a PAHs contaminated SW-HPCD or Tween 80 solution with an initial pH of 8, the pH decreased quickly until a plateau around 3 after only 1 h of treatment (Fig. 6) [37]. In addition, the drop of pH occurs whatever the kind of anode material employed, e.g., active anode (Pt) [16] and non-active anode (BDD) [37]. This phenomenon is due to the formation of carboxylic acids that can be formed very quickly, especially from the opening of aromatic rings during the oxidative degradation of pollutants. The presence of carboxylic acids and aromatics molecules in organic matter – much more present in Tween 80 solutions (due to its higher extraction capacity) – can also contribute to the acidification of solutions.

Interestingly, recycling the partially treated SW solution for a second SW step did not affect the soil pH, as the pH value equaled the initial one (pH = 8) [16]. This is due to the strong buffering capacity of the soil with the presence of clay minerals and organic matter. Ionic exchange between the protons from SW solutions and the clay-humic complex saturated in Ca^{2+} , K^+ , and Mg^{2+} , and Na^+ restores the alkaline soil pH.

3.3 Synthetic vs. Real Effluent

Synthetic effluents are usually preferred as a first experimental approach at laboratory scale. However, these treated solutions do not contain all the components that can be found in real SW/SF effluents such as inorganic ions (Ca^{2+} , Na^+ , Mg^{2+} , K^+ , etc.) and organic matter.

The potential presence of iron in soil can positively influence the electrochemical process efficiency as discussed in Sect. 2.3. During SW/SF extraction, iron can be solubilized and can then be involved in the Fenton reaction as demonstrated by

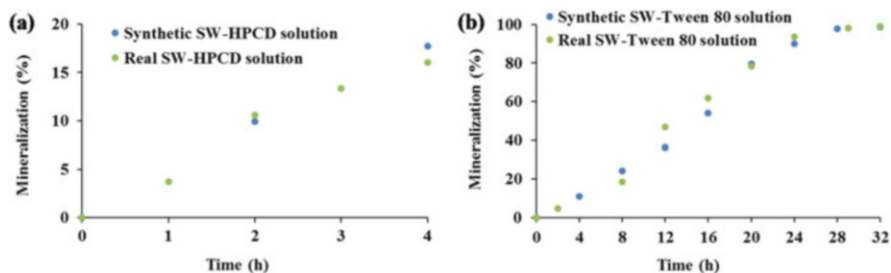


Fig. 7 Influence of synthetic vs. real SW effluent using (a) HPCD or (b) Tween 80 as washing agent. *Operating conditions:* current density, 6.7 mA cm^{-2} ; anode material, BDD (adapted with permission from [22]) (Copyright 2014 Elsevier)

our previous reports [9, 16]. In that case, the addition of ferrous iron – as traditionally performed in synthetic solutions – is useless.

The presence of organic matter is a parameter impacting the process efficiency by being easily adsorbed on porous carbon electrodes due to hydrophobic interactions [26] as abovementioned in Sect. 2.1. Dissolved organic matter (DOM) is also well known to decrease process efficiency (1) by decreasing the pollutant availability and (2) by increasing the competition with the pollutant since fulvic acids from DOM react very quickly with $\cdot\text{OH}$ [38, 39]. In addition, synthetic SW solutions are usually spiked with only one pollutant or several compounds from a contaminant family, whereas in real SW solutions, mixed pollutions are commonly found including numerous pollutants that are even not analyzed. This also makes rise the $\cdot\text{OH}$ consumption by wasting reactions.

To clarify the above statements, the EF treatments using BDD anode at a constant current density (6.7 mA cm^{-2}) of synthetic and real SW solutions polluted by PAHs have been compared in Fig. 7 [16, 22, 37].

Interestingly, whatever the extracting agent employed (HPCD or Tween 80), the mineralization rates and yields are very similar for the treatment of synthetic and real SW solutions. This result is attributed to the negligible organic carbon fraction [4–5% of total organic carbon (TOC)] coming from the pollutants and organic matter as compared to the fraction from the washing agent itself (95–96% of TOC). It is important to keep in mind that the organic matter content as well as the level of organic pollution in soil could still have a role on the mineralization efficiency. In the presented data, an organic matter content of 4.7% was present in the studied soil with PAHs content of $1,000 \text{ mg kg}^{-1}$ [16]. Higher concentration of pollution along with higher organic matter content would have implied lower mineralization efficiency as compared to studies in synthetic media.

4 Impacts on Ecotoxicity, Biodegradability, and Soil Respirometry

The environmental impact is a critical issue that needs to be assessed especially if successive washings are considered after EF treatment of partially oxidized SW solutions and/or if a pre-/post-biological treatment is performed.

Two kinds of bioassays have been mainly performed with SW solutions: (1) acute ecotoxicity tests of EF-treated SW solutions have been performed by monitoring the bioluminescence of *Vibrio fischeri* marine bacteria as representative eco-organism and (2) biodegradability tests represented by the BOD₅/COD ratio, BOD₅ being the biochemical oxygen demand after 5 days and COD being the chemical oxygen demand [21, 22, 37]. The influence of three parameters on ecotoxicity and biodegradability could be reviewed: (1) the nature of extracting agent (Fig. 8), (2) the nature of pollutant and matrix composition (Fig. 9), and (3) the anode material (Fig. 10).

Figure 8 compares the bioassays evolution during EF treatment of real SW solutions using HPCD or Tween 80 extracting agent in the same following conditions [37]: (1) both agents at the same initial concentration ($7.5 \pm 0.2 \text{ g L}^{-1}$), considering that less than 2% of extracting agent adsorb onto the soil, (2) in the same operating conditions (BDD anode, 6.7 mA cm^{-2}), and (3) from the same historically PAHs-contaminated soil. With both solubilizing agents, the ecotoxicity was high during the first hours of treatment. At this time, oxidation by-products are formed and can be more toxic than the initial molecule [21, 22, 40]. After 12 h of EF treatment, the toxicity of HPCD solutions starts decreasing until the end of treatment, due to the transformation of toxic intermediates to short-chain carboxylic. Contrastingly, experiments with Tween 80 do not show any drop of toxicity. It could be explained by the higher solubilization power of Tween 80 that extracted more toxic and recalcitrant pollutants [9] and/or by the lower ability of cyclodextrins to generate toxic intermediates [21]. Biodegradability assays corroborate these trends by highlighting a lag phase during the first 4 h of EF treatment whatever the

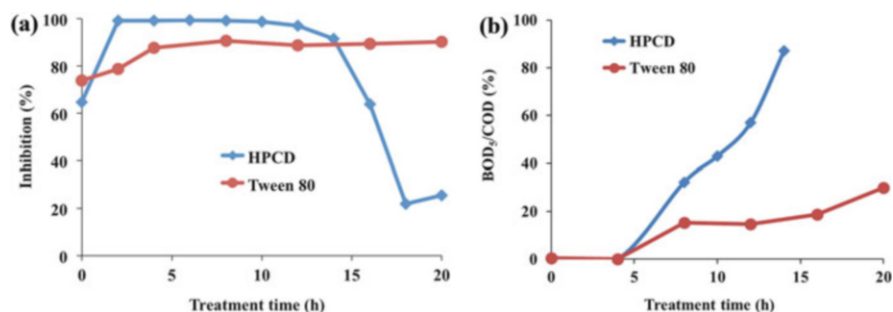


Fig. 8 Influence of extracting agent (HPCD or Tween 80) on (a) *Vibrio fischeri* inhibition and (b) biodegradability (BOD₅/COD) evolution during EF treatment of SW solutions. Operating conditions: current density, 6.7 mA cm^{-2} ; anode material, BDD

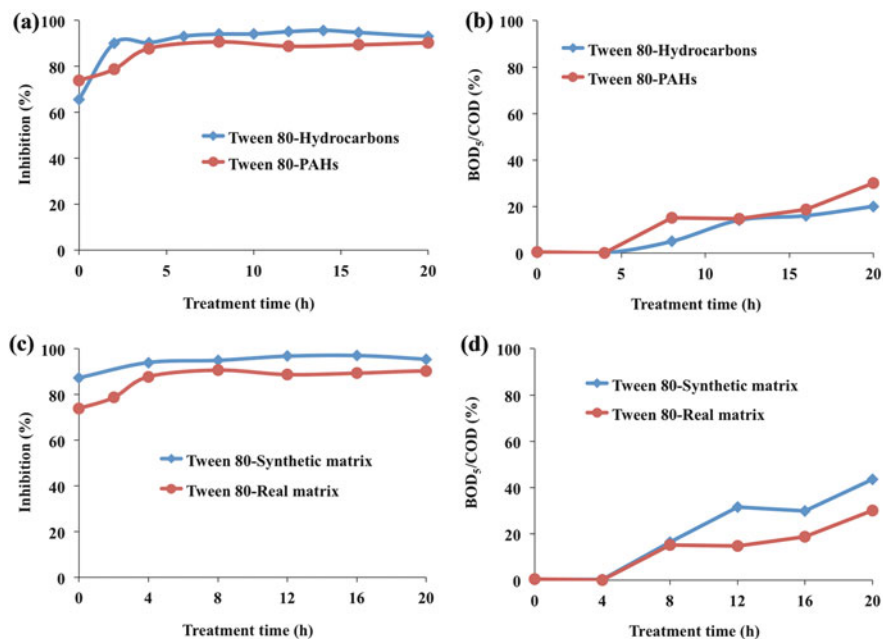


Fig. 9 Influence of (a, b) pollutants and (c, d) matrix composition on (a, c) *Vibrio fischeri* inhibition and (b, d) biodegradability (BOD₅/COD) evolution during EF treatment of SW-Tween 80 solutions. *Operating conditions:* current density, 6.7 mA cm⁻²; anode material, BDD; [Tween 80]_{hydrocarbons} = 11 g L⁻¹; [Tween 80]_{PAHs} = 7.5 g L⁻¹; [Tween 80]_{synthetic matrix} = 9 g L⁻¹; [Tween 80]_{real matrix} = 7.5 g L⁻¹ (adapted with permission from [9]) (Copyright 2015 Elsevier)

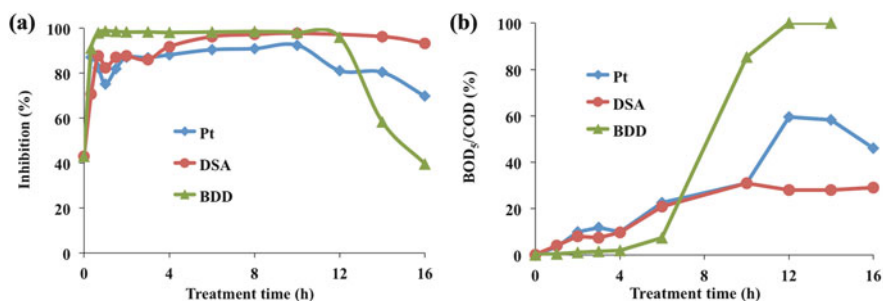


Fig. 10 Influence of anode materials on (a) *Vibrio fischeri* inhibition and (b) biodegradability (BOD₅/COD) evolution during EF treatment of SW-HPCD solutions. *Operating conditions:* current density, 6.7 mA cm⁻² (adapted with permission from [22]) (Copyright 2014 Elsevier)

agents employed, followed by a great increase of BOD₅/COD ratio with HPCD solutions and slight rise with Tween 80 matrix. Considering that a threshold BOD₅/COD ratio value of 33% is the acceptable level to consider a biological posttreatment [41], it could be considered after 8.5 and 20 h for HPCD solutions

and Tween 80 solutions, respectively. Though the required treatment time was 2.3 times longer with Tween 80 solutions, the COD was 2.1-fold lower ($2,900 \text{ mg-O}_2 \text{ L}^{-1}$) compared to HPCD solution ($6,200 \text{ mg-O}_2 \text{ L}^{-1}$), meaning that a shorter biological treatment time would be then needed with Tween 80 effluent. It is further interesting to note that the initial biodegradability of SW solutions was very low ($\text{BOD}_5/\text{COD} < 0.5\%$) whatever the extracting agent employed (Tween 80 or HPCD). However, the biodegradability enhancement factor (Eq. 14) reached more than 98% in all the cases after 8 h of treatment proving the high ability of EF process to increase the biodegradability of SW solutions.

$$E_{\text{biodeg}} = 100 \times (1 - R_i/R) \quad (14)$$

Where R and R_i are the BOD_5/COD ratio and BOD_5/COD initial ratio, respectively.

Figure 9a, b compare the EF experiments performed with Tween 80 present in two different kinds of matrix: (1) one is coming from a historically PAHs-contaminated soil [37] and (2) the second comes from a genuinely hydrocarbon-contaminated soil [9]. It is clearly shown that the influence of pollutants does not play a great role in EF treatment of SW solutions as similar trends in bioluminescence inhibition and biodegradability evolution are observed whatever the nature of pollutant. When considering the TOC ratio (%) between the TOC of pollutants and the TOC of surfactant, i.e., 4.8% in PAHs solutions and 3.2% in hydrocarbons solutions, it could be the reason why the contaminants have a negligible impact on the bioassay results. Similarly, the influence of the matrix composition (Fig. 9c, d) has a negligible impact on acute ecotoxicity when comparing synthetic SW solution (PHE, surfactant) with real SW solution (PAHs, surfactant, organic matter, and inorganic compounds). However, the biodegradability was lower with real effluent, with a BOD_5/COD ratio of 33% reached after 12 and 20 h for EF treatment of synthetic and real solutions, respectively. The presence of organic matter and numerous pollutants induced the formation of less biodegradable compounds. Though it is noticeable that the initial biodegradability was very low, the biodegradability enhancement factors reached more than 97% after 8 h of EF treatment whatever the composition of the SW matrix.

Considering the influence of Pt, DSA, and BDD anode materials on bioassay results (Fig. 10), it is noticed that active anodes (Pt and DSA) had worse trend than non-active anode (BDD) when studying the EF treatment of synthetic SW-HPCD solutions [22]. The lag phase appearing at the beginning of all the treatments might be due to the production of hydroxylated degradation by-products such as, for example, hydroxylated PHEs, well known to be more toxic than the pristine compound [42].

The combination between EF process and a biological posttreatment has been proposed successfully for the mineralization of pharmaceuticals [43, 44] and pesticides [45]. Still, it has never been suggested for the treatment of SW/SF solutions. Recently, a combination between AO and an aerobic biological treatment was implemented to treat synthetic SW solution containing PHE and Tween 80 [15]. A synergistic effect was observed with a 3-h pretreatment by AO at

21 mA cm⁻², leading to 80% overall COD removal after the biological treatment. The addition of Fe²⁺ and the use of a cathode allowing H₂O₂ generation should even increase the process efficiency in an EF setup, upon validation with supplementary experiments.

When considering a recirculation loop in SW/SF combined to EF treatment, the impact on the general soil microbial activity has to be considered since by-products are present in acidic SW solutions as abovementioned. It can be assessed by soil respirometry tests [16]. Interestingly, after a second SW cycle with EF-treated SW solution, the oxygen consumption rates were higher (0.81 µg-O₂ (gh)⁻¹ with Tween 80 and 0.34 µg-O₂ (gh)⁻¹ with HPCD) than a second fresh washing cycle (0.70 µg-O₂ (gh)⁻¹ with Tween 80 and 0.20 µg-O₂ (gh)⁻¹ with HPCD) (Fig. 11) [16]. It was also noticed that the oxygen consumption rates decreased when the number of successive washings increased, whatever the washing agent employed, even with only ultrapure water [16]. This could be assumed to be the result of the decrease in nutrient concentration, since nutrients are solubilized in each step of SW extraction [16]. It further highlighted that the oxidation of SW solutions did not affect the general soil microbial activity, which is corroborated by the quite similar oxygen consumption rates between the first SW cycle (0.93 µg-O₂ (gh)⁻¹ with Tween 80 and 0.37 µg-O₂ (gh)⁻¹ with HPCD) and the second cycle with treated SW solution. This trend would be explained by the hydrophilicity properties of oxidation by-products due to the formation of hydroxylated products (by ·OH addition reactions), which makes the interactions negligible between the intermediates and soil particles.

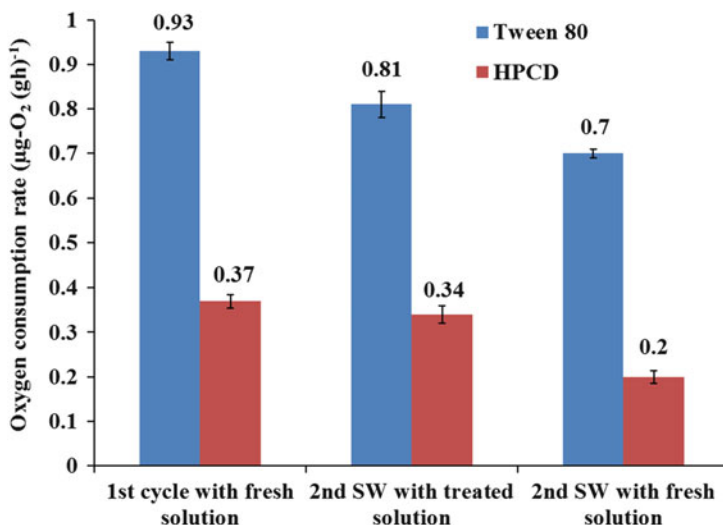


Fig. 11 Soil respirometry rates obtained after successive washings with different extracting agents (Tween 80 and HPCD) (adapted with permission from [16]) (Copyright 2016 Elsevier)

5 Energy Considerations and Concluding Remarks

Energy requirement represents the main part in operating cost of such electrochemical process. Therefore, authors try to reduce as much as possible the energy consumption in order to be competitive. The energy ($E_{\text{consumption}}$) is usually calculated as follows (Eq. 15) [29]:

$$E_{\text{consumption}} (\text{kWh m}^{-3}) = \frac{E_{\text{cell}} I t}{V_s} \quad (15)$$

where E_{cell} is the average cell voltage (V), I is the applied current intensity (A), t is the electrolysis time (h), and V_s is the solution volume (L).

The energy requirements are compared according to the washing agent employed, the degree of complexity of the treated SW solution, and the mineralization time [partial mineralization or quasi-complete (>99%)] (Table 2) [9, 22, 37].

EF treatment of SW-HPCD solutions required between 1.4 and 2.8 times less energy than SW-Tween 80 solutions [37]. However, in such combined process, the solubilization efficiency of the extracting agent needs to be also taken into account in the calculations. Considering that ten more SW cycles are required with HPCD to extract the same PAHs concentration than with Tween 80, the energy required to treat the SW solutions would be ten times more, by assuming a linear relation between the initial organic load and the EF treatment time [37]. Another interesting feature would be to estimate the energy consumed per amount of pollutant degraded, so that the energy efficiency comparison could be more reliable. However, at the time to reach 33% of biodegradability or quasi end of mineralization, all the pollutants are already degraded. It means that global parameter such as COD or TOC of pollutant removed needs to be taken into account. The challenge will be

Table 2 Energy consumption calculations comparison

Kind of soil remediation process	SW/EF ^a		SW/EF ^a		SF/EF ^a
Kind of washing agent	HPCD		Tween 80		Tween 80
Degree of solution complexity	Synthetic ^b	Real ^c	Synthetic ^d	Real ^e	Real ^f
$E_{\text{consumption}}$ (kWh m ⁻³) after reaching 33% of biodegradability ^g	96	112	182	316	nd
$E_{\text{consumption}}$ (kWh m ⁻³) after complete mineralization	275	320	425	443	508

nd not determined since biodegradability was lower than 33% all along the treatment

^aOperating conditions of EF: carbon felt cathode; BDD anode; applied current density, 6.7 mA cm⁻²

^bContain PHE (0.09 mM) and HPCD (9 g L⁻¹)

^cReal PAHs-contaminated SW solutions with HPCD (7.5 g L⁻¹)

^dContain PHE (0.09 mM) and Tween 80 (9 g L⁻¹)

^eReal PAHs-contaminated SW solutions with Tween 80 (7.5 g L⁻¹)

^fReal hydrocarbon-contaminated SF solution with Tween 80 (11 g L⁻¹)

^gConsidering the ratio BOD₅/COD

then to estimate the TOC coming from the washing agent and its intermediates as well as the TOC coming from the pollutants and their oxidation by-products.

The SF/EF treatment of real Tween 80 solution required more energy (508 kWh m^{-3}) than the EF treatment of SW-Tween 80 solutions (443 kWh m^{-3}). Considering the pollutant removal efficiency, SW could extract around 41% of PAHs pollutant ($1,090 \text{ mg kg}^{-1}$ initially) after one cycle (24 h), while SF could extract only 1% of hydrocarbons ($3,900\text{--}6,100 \text{ mg kg}^{-1}$ initially) in 24 h. Further experiments would be required to compare the efficiency of SW with SF techniques in similar conditions as the energy calculation only takes into account the EF treatment and not the whole process.

Furthermore, achieving an EF treatment until quasi-complete mineralization with BDD anode material was less energy efficient per volume of treated effluent than reaching 33% of biodegradability whatever the washing agent employed and the degree of complexity of solution. Thus, the EF combination with a biological treatment has to be considered and experimented for the treatment of SW/SF solutions as only biodegradability assays have been performed for now. An optimal EF treatment time could be determined at a minimal energy consumed.

In addition, the energy required to completely degrade PHE from a synthetic HPCD solution was around 41 kWh m^{-3} with BDD anode [22]. Interestingly, it was around 60 times less than the energy consumed in another electrochemical setup developed to treat a synthetic SW-HPCD solution spiked with 35 mg L^{-1} of PHE [11]. The superiority of the EF process was imputed to the electrocatalytic formation of $\cdot\text{OH}$ radicals.

Though EF treatment of SW/SF solutions was efficient, the electric energy devoted to the pollutant degradation itself is low as compared to the energy devoted to the waste reactions and washing agent oxidation, which makes the energy strongly depend on the concentration of extracting agent used. Still, the possibility to implement an EF process allowing to reuse SW/SF solution and to recycle extracting agent is an interesting research area in order to improve the cost-effectiveness of the whole integrated process (SW/EF or SF/EF) and needs further development. In parallel, experiments could be performed to optimize EF treatment of soil slurry without addition of solubilizing agent or at concentration close to their CMC (ranging from 10 to 200 mg L^{-1}) as proposed by Rosales et al. [18]. In such conditions, appropriate electrode materials would be required to avoid electrode fouling while keeping a high oxidant generation efficiency by minimizing the adverse effect on soil integrity due to strong oxidizing conditions. It could be an alternative to the in situ electrokinetic-Fenton proposed in literature. Finally, EF treatment can be a good alternative to replace or improve existing soil remediation technologies as it is clean (electron reagent), safe (mild conditions), easy to handle (simple equipment required), and versatile (adaptable to wide ranges of flow rates and organic load). The next step would be to scale up the suggested integrated processes by combining kinetics, hydrodynamics, and modeling studies to optimize the reactor design, the removal rates, and the energy efficiency. It will bring EF closer to industrial development.

References

1. Trellu C, Mousset E, Pechaud Y, Huguenot D, Van HED, Esposito G, Oturan MA (2016) Removal of hydrophobic organic pollutants from soil washing/flushing solutions: a critical review. *J Hazard Mater* 306:149–174
2. Mousset E, Oturan MA, Van Hullebusch ED, Guibaud G, Esposito G (2014) Soil washing/flushing treatments of organic pollutants enhanced by cyclodextrins and integrated treatments: state of the art. *Crit Rev Environ Sci Technol* 44:705–795
3. Rodrigo MA, Oturan N, Oturan MA (2014) Electrochemically assisted remediation of pesticides in soils and water: a review. *Chem Rev* 114:8720–8745
4. Sáez C, López-Vizcaíno R, Canizares P, Rodrigo MA (2010) Conductive-diamond electrochemical oxidation of surfactant-aided soil-washing effluents. *Ind Eng Chem Res* 49:9631–9635
5. López-Vizcaíno R, Sáez C, Cañizares P, Rodrigo MA (2012) The use of a combined process of surfactant-aided soil washing and coagulation for PAH-contaminated soils treatment. *Sep Purif Technol* 88:46–51
6. Paria S (2008) Surfactant-enhanced remediation of organic contaminated soil and water. *Adv Colloid Interface Sci* 138:24–58
7. Risco C, Rubí-juárez H, Rodrigo S, López-vizcaíno R, Saez C, Cañizares P, Barrera-díaz C, Navarro V, Rodrigo MA (2016) Removal of oxyfluorfen from spiked soils using electrokinetic soil flushing with the surrounding arrangements of electrodes. *Sci Total Environ* 559:94–102
8. dos Santos EV, Souza F, Saez C, Canizares P, Lanza MRV, Martínez-huitle CA, Rodrigo MA (2016) Application of electrokinetic soil flushing to four herbicides: a comparison. *Chemosphere* 153:205–211
9. Huguenot D, Mousset E, van Hullebusch ED, Oturan MA (2015) Combination of surfactant enhanced soil washing and electro-Fenton process for the treatment of soils contaminated by petroleum hydrocarbons. *J Environ Manage* 153:40–47
10. Sirés I, Brillas E, Oturan MA, Rodrigo MA, Panizza M (2014) Electrochemical advanced oxidation processes: today and tomorrow. A review. *Environ Sci Pollut Res Int* 21:8336–8367
11. Gómez J, Alcántara MT, Pazos M, Sanromán MÁ (2010) Soil washing using cyclodextrins and their recovery by application of electrochemical technology. *Chem Eng J* 159:53–57
12. dos Santos EV, Sáez C, Martínez-Huitle CA, Cañizares P, Rodrigo MA (2015) The role of particle size on the conductive diamond electrochemical oxidation of soil-washing effluent polluted with atrazine. *Electrochem Commun* 55:26–29
13. dos Santos EV, Sáez C, Martínez-huitle CA, Cañizares P, Rodrigo MA (2016) Removal of oxyfluorfen from ex-situ soil washing fluids using electrolysis with diamond anodes. *J Environ Manage* 171:260–266
14. dos Santos EV, Sáez C, Cañizares P, Martínez-huitle CA, Rodrigo MA (2017) Treating soil-washing fluids polluted with oxyfluorfen by sono-electrolysis with diamond anodes. *Ultrason Sonochem* 34:115–122
15. Trellu C, Ganzenko O, Papirio S, Pechaud Y, Oturan N, Huguenot D, van Hullebusch ED, Esposito G, Oturan MA (2016) Combination of anodic oxidation and biological treatment for the removal of phenanthrene and Tween 80 from soil washing solution. *Chem Eng J* 306:588–596
16. Mousset E, Huguenot D, Van Hullebusch ED, Oturan N, Guibaud G, Esposito G, Oturan MA (2016) Impact of electrochemical treatment of soil washing solution on PAH degradation efficiency and soil respirometry. *Environ Pollut* 211:354–362
17. Pazos M, Iglesias O, Gómez J, Rosales E, Sanromán MA (2013) Remediation of contaminated marine sediment using electrokinetic-Fenton technology. *J Ind Eng Chem* 19:932–937
18. Rosales E, Pazos M, Longo MA, Sanroman MA (2009) Influence of operational parameters on electro-Fenton degradation of organic pollutants from soil. *J Environ Sci Health A Tox Hazard Subst Environ Eng* 44:1104–1110

19. Oturan MA, Aaron J-J (2014) Advanced oxidation processes in water/wastewater treatment: principles and applications. A review. *Crit Rev Environ Sci Technol* 44:2577–2641
20. Murati M, Oturan N, van Hullebusch ED, Oturan MA (2009) Electro-Fenton treatment of TNT in aqueous media in presence of cyclodextrin. Application to ex-situ treatment of contaminated soil. *J Adv Oxid Technol* 12:29–36
21. Mousset E, Oturan N, van Hullebusch ED, Guibaud G, Esposito G, Oturan MA (2014) Influence of solubilizing agents (cyclodextrin or surfactant) on phenanthrene degradation by electro-Fenton process – study of soil washing recycling possibilities and environmental impact. *Water Res* 48:306–316
22. Mousset E, Oturan N, van Hullebusch ED, Guibaud G, Esposito G, Oturan MA (2014) Treatment of synthetic soil washing solutions containing phenanthrene and cyclodextrin by electro-oxidation. Influence of anode materials on toxicity removal and biodegradability enhancement. *Appl Catal Environ* 160–161:666–675
23. Hanna K, Chiron S, Oturan MA (2005) Coupling enhanced water solubilization with cyclodextrin to indirect electrochemical treatment for pentachlorophenol contaminated soil remediation. *Water Res* 39:2763–2773
24. Sirés I, Garrido JA, Rodríguez RM, Brillas E, Oturan N, Oturan MA (2007) Catalytic behavior of the $\text{Fe}^{3+}/\text{Fe}^{2+}$ system in the electro-Fenton degradation of the antimicrobial chlorophene. *Appl Catal Environ* 72:382–394
25. Hu J, Sun J, Yan J, Lv K, Zhong C, Deng K, Li J (2013) A novel efficient electrode material: activated carbon fibers grafted by ordered mesoporous carbon. *Electrochem Commun* 28:67–70
26. Trellu C, Péchaud Y, Oturan N, Mousset E, Huguenot D, van Hullebusch ED, Esposito G, Oturan MA (2016) Comparative study on the removal of humic acids from drinking water by anodic oxidation and electro-Fenton processes: mineralization efficiency and modelling. *Appl Catal Environ* 194:32–41
27. Sopaj F (2013) Study of the influence of electrode material in the application of electrochemical advanced oxidation processes to removal of pharmaceutical pollutants from water. University of Paris-Est
28. Panizza M, Cerisola G (2009) Direct and mediated anodic oxidation of organic pollutants. *Chem Rev* 109:6541–6569
29. Brillas E, Sirés I, Oturan MA (2009) Electro-Fenton process and related electrochemical technologies based on Fenton's reaction chemistry. *Chem Rev* 109:6570–6631
30. Rosen MJ (2004) *Surfactants and interfacial phenomena*, 3rd edn. Wiley, New York
31. Alcántara MT, Gómez J, Pazos M, Sanromán MA (2008) Combined treatment of PAHs contaminated soils using the sequence extraction with surfactant-electrochemical degradation. *Chemosphere* 70:1438–1444
32. Dhenain A, Mercier G, Blais J-F, Bergeron M (2006) PAH removal from black sludge from Aluminium industry by flotation using non-ionic surfactants. *Environ Technol* 27:1019–1030
33. Gómez J, Alcántara MT, Pazos M, Sanromán MA (2010) Remediation of polluted soil by a two-stage treatment system: desorption of phenanthrene in soil and electrochemical treatment to recover the extraction agent. *J Hazard Mater* 173:794–798
34. Mousset E, Oturan N, van Hullebusch ED, Guibaud G, Esposito G, Oturan MA (2013) A new micelle-based method to quantify the Tween 80[®] surfactant for soil remediation. *Agron Sustain Dev* 33:839–846
35. dos Santos EV, Saez C, Martínez-Huitle CA, Canizares P, Rodrigo MA (2015) Combined soil washing and CDEO for the removal of atrazine from soils. *J Hazard Mater* 300:129–134
36. Lindsey ME, Xu G, Lu J, Tarr MA (2003) Enhanced Fenton degradation of hydrophobic organics by simultaneous iron and pollutant complexation with cyclodextrins. *Sci Total Environ* 307:215–229
37. Mousset E (2013) Integrated processes for removal of persistent organic pollutants: soil washing and electrochemical advanced oxidation processes combined to a possible biological

- post-treatment. University of Paris-Est – University of Cassino and The Southern Lazio – UNESCO-IHE for Water Education
38. Westerhoff P, Aiken G, Amy G, Debroux J (1999) Relationships between the structure of natural organic matter and its reactivity towards molecular ozone and hydroxyl radicals. *Water Res* 33:2265–2276
 39. Lindsey ME, Tarr MA (2000) Inhibited hydroxyl radical degradation of aromatic hydrocarbons in the presence of dissolved fulvic acid. *Water Res* 34:3–7
 40. Dirany A, Sirés I, Oturan N, Ozcan A, Oturan MA (2012) Electrochemical treatment of the antibiotic sulfachloropyridazine: kinetics, reaction pathways, and toxicity evolution. *Environ Sci Technol* 46:4074–4082
 41. Rodier J, Legube B, Merlet N (2009) *Analyse de l'eau (water analysis)*, 9th edn. Dunod, Paris, (in French)
 42. Fernandes D, Porte C (2013) Hydroxylated PAHs alter the synthesis of androgens and estrogens in subcellular fractions of carp gonads. *Sci Total Environ* 447:152–159
 43. Mansour D, Fourcade F, Huguet S, Soutrel I, Bellakhal N, Dachraoui M, Hauchard D, Amrane A (2014) Improvement of the activated sludge treatment by its combination with electro Fenton for the mineralization of sulfamethazine. *Int Biodeter Biodegr* 88:29–36
 44. Olvera-Vargas H, Oturan N, Buisson D, Oturan MA (2016) A coupled bio-EF process for mineralization of the pharmaceuticals furosemide and ranitidine: feasibility assessment. *Chemosphere* 155:606–613
 45. Fontmorin J-M, Fourcade F, Geneste F, Floner D, Huguet S, Amrane A (2013) Combined process for 2,4-dichlorophenoxyacetic acid treatment – coupling of an electrochemical system with a biological treatment. *Biochem Eng J* 70:17–22

Index

A

Acesulfame (ACE), 381, 382
Acesulfame K (ACE-K), 381
Acetic acid, 45, 159, 323, 326–330, 334, 371
Acid Blue 92, 118
Acid Orange 7 (AO7), 126, 157, 162, 208–225, 304, 327, 356
Acid Orange II, 19, 50
Acid Red 14, 118
Acid Red 88, 319, 327
Acid Red 151, 327, 357
Acid Yellow 9, 319, 327
Acid Yellow 36 (AY36), 120, 249, 327
Acid Yellow 42, 165, 330
Activated carbon fiber (ACF), 7, 76, 113, 132
Adsorption, 21, 51, 76, 85, 106, 164, 241, 349, 359, 404
Advanced oxidation processes (AOPs), 3, 29, 32, 85, 207, 209, 219, 255, 263, 380
Aerobic biological treatment (ABT), 36
Alginate, 19, 85, 99–103, 107, 161
Alizarin Red S (AR), 157, 210
Allura Red AC, 327
Ametryn, 319, 324–326
4-Amino-3-hydroxy-2-p-tolylazo-naphthalene-1-sulfonic acid (AHPS), 94, 160
Aniline, 153, 209, 215, 216, 243
Anthraquinone, 6, 59, 157, 210
Anthraquinone-2,6-disulfonate/polypyrrole (AQDS/PPy), 159
Anthraquinone monosulfonate (AQS), 128
Aromatics, 21, 44, 65, 70, 316, 329, 413
Arsenic, 353, 358

Arsenic(V), 353
Arsenic(III), oxidation, 50
Artificial neural networks (ANN), 302
Artificial sweeteners, 379, 381
Aspartame (ASP), 381
Aspirine, 268
Atrazine, 60
Autonomous solar flow plant, 332
Average oxidation state (AOS), 33

B

Basic Yellow 2, 116, 303
Benzene, 2, 68, 289–291
Benzene sulfonic acid, 265 2
 ρ -Benzoquinone, 331
Beta-blockers, 31, 38, 208, 331
Bicarbonate, 349
Bioassays, 399, 415
Biodegradability, 29, 33, 60, 355, 399, 415
 indicators, 33
Bio-electro-Fenton (Bio-EF), 29, 36
Biological treatment, 29
Bioluminescence-based toxicity test, 33, 97, 393, 415
Bisphenol A (BPA), 130, 157, 295, 351
Boron-doped diamond (BDD), 7, 34, 70, 113, 207, 264, 268, 316, 345, 380, 404
Bray-Gorin mechanism, 289, 290, 297, 300, 304
Brilliant Red X3B (X3B), 132
Bromate, 60, 62, 67
Bromide, 60, 62, 67
tert-Butylhydroquinone, 101

C

Caffeic acid, 338
Caffeine, 39, 44
Carbamazepine, 31
Carbaryl, 210
Carbon, 85
 cathode, unmodified, 287
 felt, 113, 145, 156, 159
 fiber, 113, 146, 176, 207, 219, 246
 iron-loaded, 101
 mesoporous, 111, 130
 nanomaterials, 111
 sponge, 7, 15, 113, 147, 176, 380, 404
Carbon nanotubes (CNTs), 7, 50, 111–115, 152, 176, 246
 boron-doped (B-CNTs), 246
 multiwalled (MWCNTs), 8, 115, 152
 single-walled (SWCNTs), 115, 152
Carboxylic acids, 6, 21, 32, 37, 45, 70, 86, 97, 159, 226, 313–339, 351, 379, 390, 413
Carmoisine, 22
Catalysts, concentration, 408
 iron, 18
 solid, 85
Catechol, 216, 331
CCB-470, 247
Cell potential, 222, 229, 269
CF-1371, 246
CF-1410, 246
Chalcopyrite, 161
Chemical oxygen demand (COD), 33, 157, 276, 338, 415
Chloramphenicol, 165, 209, 331
Chloride, 5, 21, 80, 328, 373
Chlorine, 21–24, 67, 80, 373
Chlorobenzene, 68, 69, 73, 208
 ρ -Chlorobenzoic acid (ρ -CBA), 65, 66
4-Chloro-2-methylphenol, 157, 326
4-Chloro-2-methylphenoxyacetic acid (MCPA), 249, 319, 325
Chlorophene, 159
Chlorophenols, 208
Chlorophenoxy acid, 157, 209
Chlorpyrifos, 102
Chlortoluron, 157, 302
Citric acid, 100, 330
Clay minerals, 413
Clofibrac acid, 265
CoFe-layered double hydroxide (CoFe-LDH), 161
Combined process, 29

Conductivity, 7, 37, 113, 145, 175, 191, 241, 350, 355
Congo Red, 326–328
Copper, 2, 92
 ρ -Coumaric acid (4-hydroxycinnamic acid), 157
Coupled process, 241
Coupled solar-assisted electro-fenton treatments, 334
CPC photoreactor, 281, 313, 330, 356
Cresols, 101, 106, 216, 319, 322
Crystal violet, 157
Current density, 8, 18, 63, 151, 219, 241, 406
Current distribution, 263, 271, 281
Cyanides, 3, 356
Cyclodextrins, 399, 404, 410–412, 415

D

2,4-D, 101, 107, 124, 157, 351
Decolorization, kinetic model, 287
Degradation kinetics, 1, 16, 70, 93, 404
2,4-Dichlorophenol, 101, 107, 124, 157, 351
Diclofenac, 74, 75, 78, 93, 162, 164, 281, 352, 355
Dicyandiamide, 132
Di-2-ethylhexyl phthalate, 100
3,4-Dihydroxybenzoic acid, 106
Dimensionally stable anodes (DSA), 381
Dimethylarsinate (DMA), 353
Dimethyl phthalate (DMP), 124, 134, 136
1,4-Dioxane, 60, 70–73, 354
Dioxins, 356
Diphenyl, 291
Diquat dibromide, 265
Direct Yellow 4, 165, 332, 334, 335
Disordered mesoporous carbon (DMC), 132
Disperse Blue 71, 327, 357
Dissolved organic carbon (DOC), 33, 66, 75, 282, 356
Diuron, 157, 324
Drinking water, 60, 75, 164, 265, 314, 346, 371, 381
Dyes, degradation, 15, 30, 47, 100, 120, 157, 176, 210, 214, 242, 265, 288, 313, 326, 343, 403

E

E122, 249, 327, 328
E124, 249, 327, 328
E129, 249, 327, 328

- Ecotoxicity, 399, 412, 415
Effluent organic matter (EfOM), 75
Electrochemical activity, 145
Electrochemical advanced oxidation processes (EAOPs), 29, 32, 57, 59, 241, 264, 314, 383, 401
Electrochemical reactors, 205
Electrodes, low-cost, 287
 materials, 399
 packed bed, 263
 parallel plate, 263
 rotating cylinder, 263, 271, 275
 three-dimensional, moving, 205, 217
Electro-Fenton, 1, 15, 29, 34, 59, 85, 111, 145, 175, 241, 296, 343
 catalyst source, 1
 heterogeneous, 85
Electrolyte flow, non-ideal, 263
Electrolytic cells, 1, 313
Electron transfer, 3, 5, 105, 152, 179, 245, 251, 270
Electro-peroxone, 57
Emerging contaminants, 31
Energy requirements, 419
Enoxacin (ENXN), 161
Enrofloxacin, 209, 320, 330
E-peroxone process, 57, 61
Estrogens, 163, 354
Ethanol, 101, 149, 159, 179, 180, 289–292, 304, 358
Ethylene, 360
Evans Blue, 326
- F**
Fast green, 157
Fe(III)-carboxylate complexes, 313
Fenton's reagent, 2, 3, 22, 34, 49, 94, 207, 289, 314, 344, 379, 401
FeOOH, 50, 99, 128, 161, 177, 358
Fered-Fenton, 3, 243, 338, 346, 359, 373
Ferrate(VI), 32, 383
Ferric chloride, 87
Ferric hydroxide, 370, 383
Ferric ions, 86–92, 99, 104, 129, 265
Ferric-salicylic acid, 104
Ferrous iron (Fe²⁺), 58, 90, 212, 303, 307, 346, 359, 372, 403, 414
Ferrous sulfate, 87, 360, 362
Ferryl ions, 2–5, 290
Filter-press flow cell, 263
Flow cell, parallel-plate, 205
Flow-through, 241
- Fluid dynamics, computational, 263
5-Fluorouracil, 44
Formic acid, 33, 97, 220
Fuchsin Acid, 357
Furosemide, 43, 45
- G**
Gas diffusion electrode (GDE), 6, 113, 207, 313, 380
Gemfibrozil, 74, 75, 78
Geosmin, 74, 75, 79
Goethite, 105
Graphene, 111, 120
Graphene oxide, 111, 113, 122
 reduced, 111
Graphite felt, 175, 241, 247
- H**
Haber-Weiss mechanism, 289, 297
Heavy metals, 101, 288, 351, 358
Herbicides, 157, 213, 265, 320, 324
Hierarchically porous carbon (HPC), 130
Hydrocarbons, 159, 399, 420
Hydrogen peroxide, 1, 6, 57, 111, 145, 287
Hydrophilicity, 115, 122, 150, 177, 181, 418
Hydrophobicity, 165, 247, 268
Hydrophobic organic contaminants (HOCs), 403
Hydroquinone, 229, 331
Hydroxyalkyl radicals, 299
Hydroxylation, 3, 97, 282, 290, 323, 387
Hydroxyl radicals, 29, 85, 104, 111, 379
Hydroxypropyl-beta-cyclodextrin (HPCD), 404
Hypochlorous acid, 21
- I**
Ibuprofen, 31, 60, 72, 75, 78, 208, 330, 355
Imidacloprid, 100, 102, 161, 209, 326, 330
Indole, 99
Iron, 2, 18
 zero-valent (ZVI), 90
Iron alginate gel beads (FeAB), 161
Iron hydroxides, 177, 251
Iron oxides, 85, 89, 104, 177, 315, 358
Iron sludge, 6, 19, 60, 128, 177, 199, 344
- K**
Ketones, 330
Ketoprofen, 31

L

Landfill leachate, 30, 47, 163, 243, 338, 346, 359
Lead dioxide, 404
Levafix blue, 357
Levofloxacin, 40, 96, 160, 208
Lipid peroxidation, 2
Lissamine Green B, 100, 161, 403
Luminescence inhibition, 33, 97, 393, 415

M

Magnetite, 89, 104, 107, 128
Malachite green, 157
Maleic acid, 45, 213, 229, 329–331
Manganese, 92, 100, 152, 356
Mass transfer/transport, 7, 64, 70, 111, 162, 180, 206, 220, 244, 263, 349, 372
MCPA, 319, 325
Mecoprop (2-(4-chloro-2-methylphenoxy) propionic acid), 324
Metal-organic frameworks (MOFs), 130
Methanol, 2, 152
Methylene blue (MB), 126, 199, 248, 353
Methyl green, 157
5-Methyl-2-hydroxy-p-benzoquinone, 323
2-Methylisoborneol (MIB), 75
Methyl orange (MO), 117, 135, 162, 191, 198, 268, 357
Methylparaben, 22
Methyl parathion, 157, 297
2-Methyl-p-benzoquinone, 323
 α -Methylphenylglycine, 323
Metoprolol, 38, 46
Metronidazole, 331
Microbial fuel cell (MFC), 49, 155, 163, 358
Micropollutants, 30, 57, 164, 352
Microreactors, 205–229
Mineralization, 30, 379, 417
Mineralization current efficiency (MCE), 35, 95, 210, 271, 317, 352, 389
Monomethylarsinate (MMA), 353

N

Nafion 324, 8, 9
Nafion 417, 10, 216–218
Nafion 424, 9
Naproxen, 31
Nitrate, 5, 21, 159, 194, 328, 338
Nonsteroidal anti-inflammatory drugs (NSAIDs), 31, 355

O

Ordered mesoporous carbons (OMC), 130
Oxalic acid, 33, 45, 72, 97, 159, 213, 216, 229, 316, 323, 391
Oxamic acid, 45, 323–331, 334, 391, 392
Oxoiron, 2, 5
Oxygen evolution reaction (OER), 268
Oxygen reduction reactions (ORRs), 120, 160, 179, 282, 305
Ozonation, 32, 51, 57, 241, 257, 383
Ozone, 21, 57–80, 257, 316, 381, 406

P

Packed bed electrode, 263
Palladium, 129
Paracetamol, 160, 163, 268, 320
Parallel plate electrodes, 213, 263
Parathion, 157, 297
Patents, 343, 361
Pentachlorophenol (PCP), 157, 403
Perfluorooctanoate (PFOA), 137
Permanganate, 356
Peroxicoagulation, 241, 256, 303
Peroxidation, lipids, 2
Peroxydisulfate, 21
Peroxone, 58
Peroxonium ion, 412
Persistent organic pollutants (POPs), 147, 156
Persulfates, 153, 406
Pesticides, 15, 30, 102, 313, 319, 324
Petroleum hydrocarbons, 360, 403
pH, 412
Pharmaceuticals and personal care products (PPCPs), 344, 381
Pharmaceuticals, degradation, 15, 30, 47, 70, 159, 176, 242, 313, 343, 380
mineralization, 417
Phenanthrene, 36, 403
Phenol(s), 2, 70, 73, 91, 101, 122, 176, 242, 268, 297
Photoelectro-Fenton (PEF), 47
Photoelectro-peroxone (PE-peroxone) process, 67
Photolysis, 5, 58, 69, 313, 317, 331
Photoreactors, 214, 281, 313–339, 352
Phthalic acid, 323, 324
Platinum, 156, 207, 216, 268, 357, 404
 p -Nitrophenol (PNP), 75, 80, 100, 118, 159, 163, 181, 300, 358
Polyaniline (PANi), 153
Polycyclic aromatic hydrocarbons (PAHs), 159, 403

- Polyphenols, 338, 356
Polypyrrole (PPy), 153
Polytetrafluoroethylene (PTFE), 101, 113, 246
Prussian blue (ferric hexacyanoferrate), 155
Pulp and paper industry, 6, 349, 355
Pyrite, 19, 85, 92–98, 107, 160, 161, 346
Pyrrhotite, 162
- Q**
Quinone-functionalized graphene,
 electrochemical exfoliation approach
 (QEEG), 130
- R**
Ranitidine, 35, 43, 45, 208, 331
Reactive Black 5, 100, 103, 357
Reactive oxygen species (ROS), 4, 20, 316
Reactive Yellow, 265
Reactors, electrochemical, 263
 flow-through, 241
 pressurized, 205, 220
Reduced graphene oxide (rGO), 113, 120, 151
Refractory organic pollutants, 343
Resorcinol, 331
Reticulated vitreous carbon (RVC), 7, 59, 113,
 147, 207, 268, 275, 357, 380
Rhodamine B, 90, 103, 163, 330, 338
Rotating cylinder electrode, 263, 271, 275
- S**
Saccharin (SAC), 381
Salicylic acid, 92, 104, 249, 330, 336
Sepiolite, iron-loaded, 103
Slaughterhouse effluent, 42, 338, 360
Sludge, iron, 6, 19, 60, 128, 177, 199, 344
Sodium sulfate, 222, 302
Soil flushing (SF), 400
Soil respirometry, 415
Soil washing, 36, 93, 159, 400
Solar photoelectro-Fenton (SPEF), 47, 165, 313
Solar photoreactor, 214, 281, 318, 334, 338, 352
Solar pilot plants, 313
Sucralose (SUC), 381
Sulfamethazine, 41, 49, 96, 97
Sulfanilamide, 165, 320, 331, 352
Sulfanilic acid, 319, 323
Sunlight, 3, 165, 313, 339, 346, 356
Sunset Yellow FCF, 326
Surface area, 3, 19, 89, 101, 111, 145, 177, 191,
 217, 241, 315, 352, 368, 406
Surface characteristics, 175, 191
Surface water, 11, 30, 65, 74, 79, 346
- Surfactants, 130, 355, 399, 412
 nonionic, 410
Synthetic organic compounds (SOCs), 353
- T**
Tank cells, 205, 207, 326
Tartaric acid, 2, 289, 323, 327, 344
Tartrazine, 162, 254, 357
Tebuthiuron, 324
Tetracycline, 37, 208, 209, 212, 249,
 255–257
Textile industry, 288, 356
Tissue paper wastewater, 360
Total organic carbon (TOC), 22, 33,
 57, 60, 120, 157, 181, 193, 210,
 317, 414
 mineralization, 57
Toxicity, 29
 ecotoxicity, 399, 412, 415
 tests, 38
Transition metals, 19, 58, 67, 89, 155,
 194, 198
 doping, 175, 177
Triclocarban, 159
Triclosan, 159, 208
Trimethoprim, 332, 355
Trinitrotoluene (TNT), 403
Triton X-100, 410
Tween 80, 36, 410–420
Tyloxapol, 410
Tyrosol, 96–98, 160
- U**
Ultraviolet, 58, 288
UVA, 3, 316, 346, 358
UVB/UVC, 316
UV/H₂O₂ processes, 58
- W**
Wastewater, acidic, 315
 chemical industry, 355
 domestic, 163
 industrial, 255, 258, 264, 355
 leather tanning industry, 360
 medicinal herbs, 163
 soil pollutants, 401
 textile, 288, 350, 372
 winery, 209, 338, 358
Wastewater treatment, 57, 85, 147, 156, 263,
 291, 296, 343, 379
 agro-industrial, 358
 prediction, 287

Wastewater treatment plants (WWTPs),
30, 75, 353
Water treatment, 29, 57, 85, 343

X

Xylenol, 268

Z

Zahn-Wellens assays, 33
Zeolite-modified electrodes (ZMEs), 155
Zeolites, 6, 85, 102, 155–158
 iron-supported, 85, 102
Zeolitic imidazolate framework
 (ZIF-8), 156